METABOLIC CONSEQUENCES OF MALNUTRITION: HOW TO BALANCE NUTRIENTS AND GENES

EDITED BY: Demin Cai, Haoyu Liu, Hui-Xin Liu and Ju-Sheng Zheng

PUBLISHED IN: Frontiers in Nutrition

frontiers Research Topics

ISSN 1664-8714
ISBN 978-2-83250-697-4
DOI 10.3389/978-2-83250-697-4

About Frontiers

Frontiers is more than just an open-access publisher of scholarly articles: it is a pioneering approach to the world of academia, radically improving the way scholarly research is managed. The grand vision of Frontiers is a world where all people have an equal opportunity to seek, share and generate knowledge. Frontiers provides immediate and permanent online open access to all its publications, but this alone is not enough to realize our grand goals.

Frontiers Journal Series

The Frontiers Journal Series is a multi-tier and interdisciplinary set of open-access, online journals, promising a paradigm shift from the current review, selection and dissemination processes in academic publishing. All Frontiers journals are driven by researchers for researchers; therefore, they constitute a service to the scholarly community. At the same time, the Frontiers Journal Series operates on a revolutionary invention, the tiered publishing system, initially addressing specific communities of scholars, and gradually climbing up to broader public understanding, thus serving the interests of the lay society, too.

Dedication to Quality

Each Frontiers article is a landmark of the highest quality, thanks to genuinely collaborative interactions between authors and review editors, who include some of the world's best academicians. Research must be certified by peers before entering a stream of knowledge that may eventually reach the public - and shape society; therefore, Frontiers only applies the most rigorous and unbiased reviews.
Frontiers revolutionizes research publishing by freely delivering the most outstanding research, evaluated with no bias from both the academic and social point of view. By applying the most advanced information technologies, Frontiers is catapulting scholarly publishing into a new generation.

What are Frontiers Research Topics?

Frontiers Research Topics are very popular trademarks of the Frontiers Journals Series: they are collections of at least ten articles, all centered on a particular subject. With their unique mix of varied contributions from Original Research to Review Articles, Frontiers Research Topics unify the most influential researchers, the latest key findings and historical advances in a hot research area! Find out more on how to host your own Frontiers Research Topic or contribute to one as an author by contacting the Frontiers Editorial Office: frontiersin.org/about/contact

METABOLIC CONSEQUENCES OF MALNUTRITION: HOW TO BALANCE NUTRIENTS AND GENES

Topic Editors:
Demin Cai, Yangzhou University, China
Haoyu Liu, Yangzhou University, China
Hui-Xin Liu, China Medical University, China
Ju-Sheng Zheng, Westlake University, China

Citation: Cai, D., Liu, H., Liu, H.-X., Zheng, J.-S., eds. (2022). Metabolic Consequences of Malnutrition: How to Balance Nutrients and Genes. Lausanne: Frontiers Media SA. doi: 10.3389/978-2-83250-697-4

Table of Contents

05 ***Editorial: Metabolic Consequences of Malnutrition: How to Balance Nutrients and Genes***
Hao-Yu Liu, Hui-Xin Liu, Ju-Sheng Zheng and Demin Cai

09 ***COVID-19 Outcome Relates With Circulating BDNF, According to Patient Adiposity and Age***
Luciele Guerra Minuzzi, Marília Seelaender, Bruna Spolador De Alencar Silva, Eduardo del Bosco Brunetti Cunha, Marina De Castro Deus, Franciane Thais Falcão Vasconcellos, Luis Felipe Beltrão Marqueze, Ana Carolina Gadotti, Cristina Pellegrino Baena, Telmo Pereira, Karsten Krüger, Andréa Novais Moreno Amaral, Ricardo Aurino Pinho and Fábio Santos Lira

24 ***Aberrant Cholesterol Metabolic Genes Regulation in a Negative Feedback Loop Induced by an Alphacoronavirus***
Hao-Yu Liu, Haotian Gu, Huan Qu, Wenbin Bao, Yanhua Li and Demin Cai

35 ***Hepatic PPARα Is Destabilized by SIRT1 Deacetylase in Undernourished Male Mice***
Ji Ho Suh, Kang Ho Kim, Margaret E. Conner, David D. Moore and Geoffrey A. Preidis

45 ***Identification and Spatial Visualization of Dysregulated Bile Acid Metabolism in High-Fat Diet-Fed Mice by Mass Spectral Imaging***
Qi Zhang, Zhen-Hua Wu, Shan-Shan Zhao, Jing Yang, Lei Chen, Xiao-Yu Wang, Zhan-You Wang and Hui-Xin Liu

57 ***Maternal High-Fat Diet Impairs Placental Fatty Acid β-Oxidation and Metabolic Homeostasis in the Offspring***
Ling Zhang, Ziwei Wang, Honghua Wu, Ying Gao, Jia Zheng and Junqing Zhang

70 ***Different Interactive Effects of Metformin and Acarbose With Dietary Macronutrient Intakes on Patients With Type 2 Diabetes Mellitus: Novel Findings From the MARCH Randomized Trial in China***
Yu An, Yinhui Li, Nannan Bian, Xiaoyu Ding, Xiaona Chang, Jia Liu and Guang Wang

87 ***A New Way of Investigating the Relationship Between Fasting Blood Sugar Level and Drinking Glucose Solution***
Muhammad Aslam and Mohammed Albassam

92 ***Protective Effect of Oyster Peptides Derived From* Crassostrea gigas *on Intestinal Oxidative Damage Induced by Cyclophosphamide in Mice Mediated Through Nrf2-Keap1 Signaling Pathway***
Hui Chen, Huizhen Zheng, Tiejun Li, Qihong Jiang, Shulai Liu, Xuxia Zhou, Yuting Ding and Xingwei Xiang

103 ***Nutrition, Epigenetics, and Major Depressive Disorder: Understanding the Connection***
Miguel A. Ortega, Óscar Fraile-Martínez, Cielo García-Montero, Miguel Angel Alvarez-Mon, Guillermo Lahera, Jorge Monserrat, Maria Llavero-Valero, Fernando Mora, Roberto Rodríguez-Jiménez, Sonia Fernandez-Rojo, Javier Quintero and Melchor Alvarez De Mon

117 ***Short-Term High-Fat Diet Fuels Colitis Progression in Mice Associated With Changes in Blood Metabolome and Intestinal Gene Expression***
Zhen-Hua Wu, Jing Yang, Lei Chen, Chuang Du, Qi Zhang, Shan-Shan Zhao, Xiao-Yu Wang, Jing Yang, Yang Liu, Demin Cai, Jian Du and Hui-Xin Liu

130 ***The Protective Effect of Sulforaphane on Dextran Sulfate Sodium-Induced Colitis Depends on Gut Microbial and Nrf2-Related Mechanism***
Canxia He, Mingfei Gao, Xiaohong Zhang, Peng Lei, Haitao Yang, Yanping Qing and Lina Zhang

145 ***Applications of Machine Learning Models to Predict and Prevent Obesity: A Mini-Review***
Xiaobei Zhou, Lei Chen and Hui-Xin Liu

152 ***The Role of Branched-Chain Amino Acids and Branched-Chain α-Keto Acid Dehydrogenase Kinase in Metabolic Disorders***
Chuang Du, Wen-Jie Liu, Jing Yang, Shan-Shan Zhao and Hui-Xin Liu

162 ***Fructose Metabolism and Its Role in Pig Production: A Mini-Review***
Jiahao Xie, Shiyi Shi, Yucheng Liu, Shaoshuai Wang, Shahid Ali Rajput and Tongxing Song

frontiers | Frontiers in Nutrition

TYPE Editorial
PUBLISHED 20 October 2022
DOI 10.3389/fnut.2022.1028502

OPEN ACCESS

EDITED AND REVIEWED BY
Anne Marie Minihane,
University of East Anglia,
United Kingdom

*CORRESPONDENCE
Demin Cai
demincai@yzu.edu.cn

SPECIALTY SECTION
This article was submitted to Nutrition and Metabolism, a section of the journal Frontiers in Nutrition

RECEIVED 26 August 2022
ACCEPTED 12 October 2022
PUBLISHED 20 October 2022

CITATION
Liu H-Y, Liu H-X, Zheng J-S and Cai D (2022) Editorial: Metabolic consequences of malnutrition: How to balance nutrients and genes. *Front. Nutr.* 9:1028502. doi: 10.3389/fnut.2022.1028502

Editorial: Metabolic consequences of malnutrition: How to balance nutrients and genes

Hao-Yu Liu[1], Hui-Xin Liu[2], Ju-Sheng Zheng[3] and Demin Cai[1]*

[1]College of Animal Science and Technology, Yangzhou University, Yangzhou, China, [2]Institute of Life Sciences, China Medical University, Shenyang, China, [3]Key Laboratory of Growth Regulation and Translational Research of Zhejiang Province, School of Life Sciences, Westlake University, Hangzhou, China

KEYWORDS

malnutrition, metabolic disorders, NAFLD, oxidative stress, dietary intervention, coronavirus, epigenetics

Editorial on the Research Topic
Metabolic consequences of malnutrition: How to balance nutrients and genes

Introduction

A healthy diet and exercise reduce the risk of chronic metabolic diseases. Nutrient intake and diet composition can have immediate and long-term beneficial or detrimental consequences on health. In this regard, maternal nutrition deficiencies may also impact the metabolic programming and health of the child. Malnutrition refers to imbalances of energy, protein, and other nutrients. Currently, the issues due to insufficient food availability have been largely overcome in developed countries. However, these countries begin to face the other side of malnutrition, i.e., overnutrition, which brought about high rates of chronic metabolic diseases. The interaction between nutrition, metabolism, and gene expression is crucial for the maintenance of whole-body homeostasis. The interplays between nutrition and the human genome can define and mark the gene expression and metabolic response. This in turn may affect the individual's health and susceptibility to disease. With the exponential increase of nutrition-related diseases, targeted approaches are needed to provide balanced diets in parallel with the development of national preventive health systems and screening programs adapted to local needs. Dietary intake is an essential factor, however, there is a marked inter-personal variation in metabolic disease onset, underpinning the significance of the complexity of interactions between genetic and environmental factors. This Research Topic "*Metabolic Consequences of Malnutrition: How to Balance Nutrients and Genes*" in Frontiers in Nutrition collected

14 scientific contributions from highly qualified research groups focusing on nutrition and metabolism-related diseases. This Research Topic is to clarify the basic knowledge about the vital role of nutrition-related genes in various disease states and to identify new concepts that could highlight the relation between nutrition and gene expression. Based on these studies, we hope to provide a better understanding of the mechanism and pathogenesis of metabolic disorders caused by a hyper-glucose, under-nourish, high-fat diet, micronutrient deficiency, oxidative stress, major depressive disorder, and even coronavirus diseases.

Metabolic consequences of malnutrition

In particular, the nutrient-sensing nuclear receptor peroxisome proliferator-activated receptor-α (PPARα) is critical for the host response to short-term fasting and modifies the transcriptional programs of ketogenesis, fatty acid oxidation and transport, and autophagy in the liver. This regulation is ineffective in chronically undernourished individuals, often causing dyslipidemia and hepatic steatosis. Meanwhile, sirtuin-1 (SIRT1), a NAD-dependent deacetylase, is a regulator of nuclear receptors, decreasing their expression levels by proteasome-mediated degradation. Moore and Preidis' group revealed that PPARα is a novel target for Sirt1-mediated deacetylation, ubiquitination, and proteasomal degradation, and demonstrated that hepatic PPARα protein levels can be rescued in undernourished mice. These results pointed to a potential therapy targeting SIRT1 inhibition for undernutrition-induced liver and metabolic dysfunction (Suh et al.). Given SIRT1 is a mediator for AMPK-peroxisome proliferator activated receptor gamma coactivator 1-alpha (PGC1α) pathway, Zhang L. et al. revealed that the reduced AMPK-SIRT1-PGC1α signaling pathway caused by maternal high-fat diet (HFD), blunted the fatty acid β-oxidation in the placenta, leading to abnormal glucose and lipid metabolism of offspring at weaning. These findings indicate that fatty acid β-oxidation related gene profiles exert vital roles in modulating maternal overnutrition and metabolic health in the offspring (Zhang L. et al.).

In addition to metabolic diseases, overnutrition is also linked to intestinal inflammation. In a preclinical model of inflammatory bowel disease (IBD), Wu et al. have demonstrated that mice under short-term HFD exposure exhibited more severe clinical symptoms and colonic ulceration. In the intestinal mucosa of these animals, higher gene expressions of proinflammatory cytokines were observed (Wu et al.). In this study, the authors adopted new methodologies for identification and visualization of the spatial organization of bile acids (BAs) metabolism in the intestine of HFD-fed mice using mass spectrometry imaging (MSI). They demonstrated the application of MSI with a high spatial resolution (3 μm) plus mass accuracy matrix-assisted laser desorption ionization (MALDI) to identify BAs and N-1-naphthylphthalamic acid (NPA). This method could clearly determine the zonation patterns and regional difference characteristics of BAs on mouse liver, ileum, and colon tissue sections. The relative content of BAs based on NPA could also be ascertained (Zhang Q. et al.). In another mouse model of colitis, the core genes including nuclear factor (erythroid-derived 2)-like2 (Nrf2), signal transducer and activator of transcription 3 (STAT3), and phase II enzyme UDP-glucuronosyltransferase (UGT) were shown to be involved in the protective effects against colitis when treated with sulforaphane.

The effects of dietary interventions against malnutrition and inflammation are also explored. He et al. showed that an isothiocyanate, present in cruciferous vegetables such as broccoli and brussels sprouts, displays a therapeutic potential against ulcerative colitis. Nrf2 is one of the predominant factors to control oxidative stress by regulating the genes involved in the peroxidation pathway. Chen et al. found that oyster peptide (OP), a multi-nutritional food, substantially improves cyclophosphamide-induced intestinal oxidative stress in mice *via* the simulation of the antioxidant Nrf2-Keap1 signaling pathway. This study supports the potential application of peptide nutrients in the protection against oxidative stress and other metabolic disorders (Chen et al.). A review article summarized the important roles of branched-chain amino acids (BCAAs) in different metabolic disorders. BCAAs composed of leucine, isoleucine, and valine, account for about 35% of essential amino acids in most mammals and are critical in health and diseases. Lacking BCAAs may cause severe neurological disorders and growth retardation, while insulin resistance, obesity, heart failure, and even cancer are all associated with the accumulation of excess BCAAs. This review has also offered information about a series of novel methods for BCAAs measurement, facilitating researchers in the field to get a comprehensive picture of metabolic studies in BCAAs (Du et al.). It is worth mentioning that machine learning (ML) models have been successfully used in many obesity studies to predict obesity rates and identify risk factors in samples of interest. Because of that considerable current effort has been made by the computer science community and industry to apply artificial intelligence technology in the field of biology and biomedicine. A mini-review collected several ML algorithms or platforms, particularly focusing on nutrition, environment, and social factors, genetics or genomics, and microbiome research (Zhou et al.). This article also included detailed information on 23 open-source ML algorithms and related databases, including the project name, the linked website, applicable data types, and a simplified description of usage. ML algorithms are useful analytic tools that help us to conceptualize and study metabolic disorders within a fundamentally novel framework. So far, most ML algorithms used in metabolic research are in a single field. Whereas in the close future, the algorithms should be put together across platforms or data types.

Fructose is a pivotal nutrient that has been suggested to be strongly linked to metabolic diseases. Low dietary fructose increases the length of the intestine and the height of intestinal villi, contributing to weight gain and fat accumulation, which suggests the potential and beneficial role of fructose with appropriate concentration. Animal models are widely employed for studying fructose-induced metabolic changes. The anatomical and physiological similarities between pigs and humans suggest that a pig model is an important tool for biomedical research. In addition, pig production plays an important role in farming systems worldwide and the large-scale pig industry is developing rapidly all over the world to satisfy the requirement of growing consumers. The application of fructose in pig biomedical models and pig production needs further progress to production methods majorization and study of human diseases more accurately. A mini-review concluded the characteristics and metabolism of fructose in pig reproduction, growth, development, and as a human biomedical model (Xie et al.). This review addresses fructose metabolism in several key organs and its related functions in the intestine and blood cycle, benefiting new strategies for maintaining blood glucose balance and curbing metabolic diseases in humans and animals. Disagreeing with the existing *t*-test of a correlation coefficient, Aslam and Albassam provide a new way of investigating the relationship between fasting blood glucose level and drinking glucose solution. In this perspective article, the authors performed the test on data obtained from diabetes patients. The proposed method of a correlation coefficient was demonstrated to be effective for studying the significance of correlation in an indeterminate environment. It is anticipated that this new method could be applied to investigate correlations in a wide field involving economics, business, medicine, and industry in future. Till today, anti-diabetic oral agents and nutritional management are frequently used together as first-line therapies for type 2 diabetes mellitus (T2DM). However, their interaction is still unclear. Serving as the classic anti-diabetic medications, the interactive effect of acarbose and metformin with dietary intakes of macronutrients on glycemic control and cardiometabolic risk factors in a Chinese cohort was investigated as the initial hypoglycemic treatment (MARCH) randomized clinical trial (An et al.). Metformin and acarbose mainly exerted divergent interactive effects with dietary macronutrients on GLP-1 secretion, insulin release, and SBP, implying the distinct benefits for glycemic control due to the complexities of drug-diet therapies. The novel findings from the MARCH trial highlight the complicated nature of combining drug and diet therapies, and concomitant use of drug and diet with an expectation of additive may further benefit different hypoglycemic medications.

Higher adiposity is tightly linked to the aggravation of COVID symptoms, and the white adipose tissue (WAT) exerts a positive response to the infection by SARS-CoV-2. Moreover, adipokines like adiponectin are demonstrated to be associated with lipid metabolism and inflammatory factor secretion in patients with SARS-CoV-2. This adipokine may thus influence COVID-19 severity directly and indirectly. In a prospective study by Minuzzi et al., 145 hospitalized patients with COVID-19 were evaluated. They showed a robust linkage between brain-derived neurotrophic factor (BDNF) levels and COVID-19 severity (Minuzzi et al.). While adiponectin and leptin do not predict disease severity, the ratio of BDNF/adiponectin is informative of patient status and is sex-specific. These results reveal that serum BDNF content and BDNF/adiponectin ratio may serve as tools for predicting worsened prognosis in COVID-19, especially for male patients. Given that cholesterol is required for coronavirus infection *in vitro*, the role of endogenous cholesterol metabolism in regulating coronavirus infection and the mechanism behind it should be elucidated. With a mechanistic study in an animal model, Liu et al. demonstrate that a porcine coronavirus triggers an aberrant regulation of cholesterol metabolic genes *via* epigenetic inhibition of SREBP2/FXR-mediated transcription, offering a novel antiviral strategy against PEDV and other coronaviruses. Since the outbreak of COVID-19, numerous studies from around the world have reported declines in mental health such as major depressive disorder (MDD), which is a complex, multifactorial disorder of rising prevalence and incidence worldwide. The link between nutritional epigenetics and MDD composes a new field of research. A deep understanding of these diet-related epigenetic shifts becomes necessary highlighting complementary branches such as nutritional neuroscience and nutritional psychology for the integrative study of MDD. Thus, Ortega et al. present a critical review to integrate different areas of research to serve as a link between malnutrition-related epigenetic changes involved in MDD pathophysiology. They have discussed metabolic changes derived from an impairment in cellular processes owing to lacking some essential nutrients in the diet and therefore in the organism. Finally, aspects related to nutritional interventions and recommendations are also discussed.

Conclusions and perspectives

The epigenetic actions of nutrition suggest that it can modulate numerous metabolic pathways which have been investigated in the context of metabolic disorder pathophysiology. Novel advances in clinical trials have generated promising results in the ability of nutrition intervention to reverse or attenuate these epigenetic marks. There are still large gaps in the understanding of the pathophysiology of metabolic diseases and the associated epigenetic drivers, signature genes, and functional pathways, even more in the knowledge of the connection between malnutrition and consequent epigenetic marks involved in metabolic disease pathophysiology.

Author contributions

DC wrote the introduction and the conclusion. H-YL wrote the central part with comments on the cited papers and references. H-XL and J-SZ contributed to the review and editing. All authors contributed to the article and approved the submitted version.

Funding

This work was supported by the Natural Science Foundation of Jiangsu Province (BK20200932 and BK20220582), Natural Science Foundation of the Higher Education Institutions of Jiangsu Province (20KJB230001), and the Priority Academic Program Development of Jiangsu Higher Education Institutions (PAPD).

Conflict of interest

The authors declare that the research was conducted in the absence of any commercial or financial relationships that could be construed as a potential conflict of interest.

Publisher's note

frontiers in Nutrition

ORIGINAL RESEARCH
published: 10 December 2021
doi: 10.3389/fnut.2021.784429

COVID-19 Outcome Relates With Circulating BDNF, According to Patient Adiposity and Age

Luciele Guerra Minuzzi[1], Marília Seelaender[2], Bruna Spolador De Alencar Silva[1], Eduardo del Bosco Brunetti Cunha[3], Marina De Castro Deus[3], Franciane Thais Falcão Vasconcellos[3], Luis Felipe Beltrão Marqueze[3], Ana Carolina Gadotti[3], Cristina Pellegrino Baena[3], Telmo Pereira[4,5], Karsten Krüger[6], Andréa Novais Moreno Amaral[3], Ricardo Aurino Pinho[3] and Fábio Santos Lira[1]*

[1] Exercise and Immunometabolism Research Group, Postgraduation Program in Movement Sciences, Department of Physical Education, Universidade Estadual Paulista (UNESP), Presidente Prudente, Brazil, [2] Cancer Metabolism Research Group, LIM26-HC, FMUSP, University of São Paulo, São Paulo, Brazil, [3] Graduate Program in Health Sciences, School of Medicine, Pontificia Universidade Catolica do Parana, Curitiba, Brazil, [4] Polytechnic Institute of Coimbra, Coimbra Health School, Coimbra, Portugal, [5] Laboratory for Applied Health Research (LabinSaúde), Coimbra, Portugal, [6] Department of Exercise Physiology and Sports Therapy, Institute of Sports Science, Justus-Liebig-University Giessen, Giessen, Germany

OPEN ACCESS

Edited by:
Ju-Sheng Zheng, Westlake University, China

Reviewed by:
Isabelle Wolowczuk, INSERM U1019 Centre d'Infection et Immunité de Lille (CIIL), France
Joseph S. Marino, University of North Carolina at Charlotte, United States

***Correspondence:**
Luciele Guerra Minuzzi
lucielegm@gmail.com
orcid.org/0000-0002-9342-5563

Specialty section:
This article was submitted to Nutrition and Metabolism, a section of the journal Frontiers in Nutrition

Received: *27 September 2021*
Accepted: *11 November 2021*
Published: *10 December 2021*

Citation:
Minuzzi LG, Seelaender M, Silva BSDA, Cunha EdBB, Deus MDC, Vasconcellos FTF, Marqueze LFB, Gadotti AC, Baena CP, Pereira T, Krüger K, Amaral ANM, Pinho RA and Lira FS (2021) COVID-19 Outcome Relates With Circulating BDNF, According to Patient Adiposity and Age. Front. Nutr. 8:784429. doi: 10.3389/fnut.2021.784429

Background and Aims: We evaluated adipose tissue-derived hormones, body composition, serum metabolic profile, levels of brain-derived neurotrophic factor (BDNF), and the association of these parameters with the clinical outcome in patients with COVID-19. We sought to examine whether obesity, sex, and age influence the adipose tissue endocrine response to the disease.

Methods: This prospective study investigated 145 hospitalized patients with COVID-19. Patients were categorized based on their body mass index (BMI), sex and age, and were also classified regarding their outcome after hospitalization as: (a) Non-ICU: patients hospitalized who did not receive intensive care; (b) ICU-survivor: patients admitted to the intensive care unit and discharged; (c) ICU-death: patients who died. Blood samples were collected by the hospital staff between the first and third day of hospitalization. Serum leptin, adiponectin and BDNF concentrations, triglycerides, total cholesterol and cholesterol fractions were performed following the manufacturer's guidelines.

Results: We demonstrate that BDNF levels predict intensive care (IC) need ($p < 0.01$). This association was found to be stronger in patients >60y ($p = 0.026$). Neither leptin nor adiponectin concentration was associated with IC requirement or with patient's outcome, while the BDNF/adiponectin ratio was closely associated with worsened outcomes ($p < 0.01$). BDNF concentration was similar between sexes, however tended to be lower in male patients ($p = 0.023$). In older patients, BDNF concentration was lower than that of younger patients ($p = 0.020$). These age and sex-specific differences should be considered when employing these potential markers for prognosis assessment. While appetite and body composition regulating hormones secreted by the white adipose

tissue are not reliable predictors of disease severity, the ratio BDNF/adiponectin was indicative of patient status.

Conclusion: Thus, we propose that serum BDNF content and BDNF/adiponectin ratio may serve as tools predicting worsened prognosis in COVID-19, especially for male patients.

Keywords: adiponectin, leptin, BDNF, COVID-19 severity, adipose tissue hormones

INTRODUCTION

According to the WHO report of April 27th, 2021, the total number of confirmed patients with COVID-19 has risen sharply to 148,797,483, and 3,138,200 (2.1%) deaths were reported. A conspicuously higher mortality rate in overweight/obese patients is observed (1). It seems true, that higher adiposity is closely related to the aggravation of covid symptoms (2), and that the white adipose tissue (WAT) plays an active role in the response to the infection by SARS-CoV-2. The WAT is involved in the pathophysiology of various diseases (3–5), and by secreting a myriad of factors, it exerts influence on different compartments of the body, modulating an ample specter of physiological and pathological responses. Of particular interest is the capacity of WAT to actively express and secrete hormones and inflammatory factors. The likely contribution of the adipose tissue for covid-19-related "cytokine storm," and hence, to the aggravated form of the disease and worsened prognosis, has been recently proposed (6–8).

Dugail et al. (2020) (9) and others (8, 10) have postulated that the infection of the adipose tissue by SARS-CoV-2 *via* angiotensin-converting enzyme 2 (ACE2) receptor expression and transmembrane protease serine 2 (TMPRSS2) might be involved with virus replication in WAT, increased lipolysis (releasing fatty acids into the circulation, including the inflammation-inducing saturated fatty acids), production and secretion of lipid active metabolites, cytokines, and dysregulation of WAT endocrine function. Indeed, individuals with higher adiposity and diabetes show augmented vulnerability to infectious diseases, especially those of the respiratory tract (11–13). Furthermore, the severity of various infectious respiratory diseases caused by viruses is increased in obese patients (14, 15).

Growing attention has been given to the inflammatory (mainly cytokine actions) contribution of WAT to the severity of COVID-19, while little (on 03/24/20, only 5 results could be retrieved in PubMed under the entry: adipose tissue hormone AND covid) information is available regarding the appetite and body composition regulating hormones secreted by the tissue. The hormones secreted by WAT, leptin, and adiponectin have, however, an important role in the regulation of the immune system (16, 17), which could be of relevance for patient outcome in covid-19, as hypothesized by De Bandt and Monin (18). Immune cells present leptin receptors, which, upon binding of the hormone, elicit changes in intracellular metabolism, translating the information about the nutritional status of the organism (19). Leptin receptors of immune cells have also been linked to the extent of the respiratory tract response to inflammatory factors such as INF-gamma, to virus clearance capacity and survival upon infection (20).

Adiponectin has been very recently (21) found to be associated with the regulation of lipid metabolism and inflammatory factor secretion in patients with SARS-CoV-2. This adipokine may thus influence both in direct and indirect form COVID-19 severity. Bearing in mind that adiponectin and leptin secretion is markedly altered in obesity (22), it seems plausible to put forth the proposition that these hormones may present a role in the aggravation of COVID-19 in overweight patients.

However, actual data on the association of these hormones and COVID-19 pathophysiology are missing in the literature. Another potential effect of leptin is regulating brain-derived neurotrophic factor (BDNF) presence and actions in WAT (23). BDNF is an agent that regulates lipolysis and many other WAT functions, by warranting the integrity and optimal function of sympathetic activity in the tissue. BDNF is known to be expressed by visceral adipose tissue in mammals (24). We sought therefore, to examine in COVID-19 patients with different severity of the disease, the adiponectin/leptin ratio as a predictor of outcome and the association of these hormones with BDNF concentration in the circulation.

MATERIALS AND METHODS

Study Design

One hundred forty-five hospitalized patients diagnosed with COVID-19 admitted at the Marcelino Champagnat Hospital, Curitiba, Paraná, Brazil, between June and November 2020, were included in a prospective study. Patients were admitted only after signing the fully informed consent. The study was approved by the research ethics committee approval (number 31558020.8.0000.0103).

Inclusion and Exclusion Criteria

Patients of both sexes were included when meeting the following criteria: being over 18 years old and showing clinical symptoms and positive RT-PCR for COVID-19. Sars-CoV-2 infection was confirmed by the clinical-radiological exam and nasopharyngeal swab polymerase chain reaction (PCR). Patients diagnosed with other viral infections or other common respiratory viruses were excluded as were those who underwent solid organ or hematological transplantation in the past.

Patient Groups

In this study, we included 145 patients with COVID-19. Patients were categorized based on their body mass index (BMI) as: Non-obese = BMI < 29.9 kg/m^2 (n = 78); Obese = BMI >30 kg/m^2

(n = 67); Sex: Female (n = 59) and male (n = 86); Age: < 60 years old (n = 93) and ≥60 years old (n = 52). BMI was calculated based on the following formula: bodyweight in kilograms divided height in meters squared. COVID-19 patients were also classified regarding their outcome after hospitalization as: (a) Non-ICU: patients hospitalized who did not receive intensive care; (b) ICU-survivor: patients admitted to the intensive care unit and discharged; (c) ICU-death: patients who died. The statistical power of the sample size was calculated after sample analysis based on the linear regression between BDNF and outcome (death) observed in the study ($r^2 = 0.09$, $\rho^2 = 0.101$) and 95% confidence level using G*Power version 3.1.9.6. The power of the sample size of this study is 0.915.

Patient Clinical Data and Blood Collection

The medical records of the patients provided the data on sex, age, body weight, height, coexisting diseases, clinical symptoms, peripheral oxygen saturation, continuous medication, and COVID-19-specific medication assessment, as well as the length of the hospital (ICU or ward) stay. Non-fasting blood samples (10 mL) were collected by the hospital staff between the first and third day of hospitalization. Peripheral blood was collected in vacutainer tubes without additives, containing separating gel, and kept at room temperature for 30 min to induce clotting. Samples were then centrifuged at 1500 rpm for 10 min at 4°C. The tubes remained at rest for 60 min in a vertical position and the serum was aliquoted and stored at −70°C until the biochemical tests were performed. Hemolyzed serum samples were discarded.

Blood Parameters

The tubes were refrigerated for 1 h before centrifugation for 15 min at 3,000 rpm at 4°C (Centrifuge 5430 R, Eppendorf, Hamburg, Germany) for serum separation. Next, the serum content was stored at −20°C until frozen and stored at −80°C until analysis. Serum leptin, adiponectin and BDNF concentrations were assessed employing enzyme-linked immunosorbent assay (ELISA) (R&D System, Minneapolis, MN, USA). The assays were performed following the manufacturer's guidelines. Triglycerides (TAG), total cholesterol and cholesterol fractions (TC, HDL-c) were analyzed with commercial colorimetric kits (Labtest, Brazil) and Non-HDL cholesterol was calculated by subtracting HDL-c concentration from Triacylglycerol. The concentration of insulin and cortisol were analyzed with ELISA commercial kits (Monobind Inc., USA) and glucose content was assessed with a colorimetric kit (Labtest®, Brazil). The homeostatic model assessment of insulin resistance (HOMA-IR) index was calculated according to the formula: (glucose [mmol/L] × insulin [μIU/mL]/22.5) (25).

Statistical Analysis

Data normality was tested using the Shapiro-Wilk test. Continuous values were expressed as medians and interquartile range (IQR) and categorical variables as counts and percentages. The comparisons among groups (non-obese vs. obese; female vs. male; < 60 years vs. ≥60 years) were performed with Mann-Whitney for non-parametric continuous variables. Categorical variables were compared using the Chi-square test. For the values of adipose-derived hormones and BDNF levels for patients with COVID-19 regarding their clinical outcome, data are mean ± Standard Error of the Mean. To compare the values from patients that were hospitalized without intensive care (Non-ICU), patients admitted to the intensive care unit and discharged (ICU-survivor), and patients who died (ICU-death), ANOVA was performed, followed by the Tukey test (normal distribution). For non-parametric data, Kruskal-Wallis test was performed, followed by the Dunn test. Linear regression was used to examine the associated factors. Then, binary logistic regression analysis was employed to identify factors associated with ICU admission and outcome—survivor or death. Univariate and multivariate binary logistic regression were performed to test the association between the dependent and the independent variables. The statistical significance was set at $p < 0.05$.

RESULTS

Characteristics of the Study Cohort

Characteristics of the total of 145 hospitalized patients with confirmed COVID-19 at the Marcelino Champagnat Hospital, Curitiba, Paraná, Brazil are illustrated in (**Table 1**). Among the patients, 86 (59.3%) were male, and the median age was 53 (IQR 43–68) years. Patients were classified as obese or non-obese, considering BMI clusters = non-obese <29.9 kg/m^2; obese >30 kg/m^2. A total of 67 (46.2%) of these patients were obese. The median BMI in the Obese group and the Non-obese group were 32.9 (IQR 31–35) and 26.3 (IQR 24–27) kg/m^2 ($p < 0.001$), respectively. There were no significant differences between the two subgroups in respect to sex ($p = 0.669$), age ($p = 0.481$), and use of medication ($p = 0.120$). Obese group showed a higher frequency of comorbidities (76.1%), when compared to the non-obese group (57.7%), $p = 0.019$. There were additionally, significant differences between these two subgroups in regard to diseases, as the former (obese group) showed a higher incidence of hypertension ($p = 0.001$), and dyslipidemia ($p = 0.017$) (**Table 1**).

We further divided the patients according to the requirement or not of intensive care (ICU). A total of 56 patients (38.6%) were admitted to the ICU, followed by discharge (26.9%, ICU-survivor subgroup) or death (11.7%, ICU-death subgroup). COVID-19 patients receiving intensive care were on average older (58.5, IQR 46–73 years), when compared to the Non-intensive care group (50, IQR 40–63 years) ($p = 0.006$) (**Table 1**).

Patients who needed intensive care were more frequently obese (64.3%, $p < 0.001$) and presented more comorbidities (78.6 %, $p = 0.013$). The mean BMI of critically ill patients admitted to ICU was around 31.5 kg/m^2 at admission. In fact, in our sample, 75% of all SARS-CoV-2 positive patients that required IC had a BMI of 30 kg/m^2 or higher (mean 31.8 kg/m^2). The other 25% had a mean BMI of 26.9 kg/m^2. Among the non-survivors, 94.1% were under chronic medication for comorbidities, mainly for arterial hypertension (64.7%) or multiple diseases (76.5%) (**Table 1**).

TABLE 1 | Characteristics of patients with Covid-19.

	All patients	Non-Obese	Obese	P value	Non-ICU	ICU-survivor	ICU-death	P value
N (%)	145 (100)	78 (53.8)	67 (46.2)		89 (61.4)	39 (26.9)	17 (11.7)	
Age, years	53 (43–68)	54 (42–68)	56 (43–69)	0.976	53 (43–65)[c]	58 (42–69)[c]	72 (50–78)	<0.0001
Body weight, kg	85 (73–98)	75 (69–85)	98 (88–108)	<0.001	83 (71–90)	90 (72–108)	90 (71–104)	0.145
BMI, kg·m^2	29.4 (26–32)	26.3 (24–27)	32.9 (31–35)	<0.001	28.3 (25–30)	31.5 (27–34)[a]	31.9 (26–34)	0.001
Sex								
Female, *n* (%):	59 (40.7)	33 (42.3)	26 (38.8)	0.669	38 (42.7)	16 (41.0)	5 (29.4)	0.593
Male, *n* (%):	86 (59.3)	45 (57.7)	41 (61.2)		51 (57.3)	23 (59.0)	12 (70.6)	
Age range								
Age, <60 years, *n* (%):	93 (64.1)	48 (61.5)	45 (67.2)	0.481	63 (70.8)	27 (69.2)	3 (17.6)	<0.0001
Age, ≥ 60 years, *n* (%)	52 (35.9)	30 (38.5)	22 (32.8)		26 (29.2)	12 (30.8)	14 (82.4)	
Comorbidities								
No, *n* (%):	49 (33.8)	33 (42.3)	16 (23.9)	0.019	37 (41.6)	11 (28.2)	1 (5.9)	0.012
Yes, *n* (%):	96 (66.2)	45 (57.7)	51 (76.1)		52 (58.4)	28 (71.8)	16 (94.1)	
Hypertension, *n* (%):	53 (36.6)	19 (24.4)	34 (50.7)	0.001	25 (28.1)	17 (43.6)	11 (64.7)	0.009
Diabetes, *n* (%):	33 (22.8)	16 (20.5)	17 (25.4)	0.553	16 (18.0)	11 (28.2)	6 (35.3)	0.189
Dyslipidemia, *n* (%):	21 (14.5)	6 (7.7)	15 (22.4)	0.017	10 (11.2)	6 (15.4)	5 (29.4)	0.146
Respiratory diseases„ *n* (%):	13 (9.0)	5 (6.4)	8 (11.9)	0.383	5 (5.65)	6 (15.4)	2 (11.8)	0.187
Other, *n* (%):	66 (45.5)	34 (43.6)	32 (47.8)	0.621	34 (38.2)	19 (48.7)	13 (76.5)	0.013
Medication								
No, *n* (%):	53 (36.6)	33 (42.3)	20 (29.9)	0.120	36 (40.4)	16 (41.0)	1 (5.9)	0.020
Yes, *n* (%)	92 (63.4)	45 (57.7)	47 (70.1)		53 (59.6)	23 (59.0)	16 (94.1)	

Values are reported as a number (%) or median and interquartile range (Q1–Q3). Mean difference: Chi-square (Categorical variables) and Mann-Whitney test (Continuous variables). Body mass index classes: non-obese <29.9 kg·m^2; obese > 30 kg·m^2.

Biochemical and Metabolic Profiles

The baseline biochemical and metabolic profile results of all patients and the comparison between the subgroups stratified within the criteria of obesity and need for intensive care are presented in **Table 2**. The patients from the Obese group showed higher concentration of TAG, non-HDL cholesterol and cortisol, compared to the Non-obese patients ($p < 0.05$). In the patients who needed intensive care, triglyceride levels were also higher ($p = 0.001$). Thus, we observed that the patients who went to the ICU showed higher TAG, compared to the non-ICU group; while we failed to find differences in total cholesterol content among groups. HDL-c was higher in female, when compared to male patients ($p = 0.027$, 29.8 (IQR 25–35) and 27.1 (IQR 24–32), respectively) (**Supplementary Table 1**).

Only 11.2% of the COVID-19 patients did not present insulin resistance, as indicated by the index based on fasting blood insulin and glucose concentrations (HOMA-IR) (**Table 2**). Although there was no statistical difference in HOMA-IR between Obese and non-obese groups, as all mean values were quite high (median 8.4), when we compared these with normal values (under 2.5).

Adipose-Derived Hormones Concentration in Patients With COVID-19 in the Different Subgroups

We analyzed and compared the results for adiponectin, leptin, and the adiponectin/leptin ratio, to understand the endocrine physiology of adipose tissue response in COVID-19, considering the effect of the factors: obesity, sex, and age.

BMI

Obesity caused leptin to be higher when compared to non-obese individuals ($p < 0.001$) (**Figure 1B**). The leptin values may be associated with the lower adiponectin/leptin ratio found in the obese individuals in the study (0.159, IQR = 0.09–0.27), when compared to non-obese patients ($p < 0.001$, **Figure 1C**), as the adiponectin levels are similar (**Figure 1A**). Adiponectin/leptin ratio is an important clinical parameter that reflects the functionality of the adipose tissue and may be employed to identify those subjects more susceptible to developing cardiometabolic diseases (ratio > 1.0 = normal, between 0.5 and 1.0 = moderate-medium increased risk, < 0.5 = severe increase in cardiometabolic risk) (22). In this regard, we analyzed the profile of the adipose tissue-secreted hormones and the adiponectin/leptin ratio, as the BMI increases, by linear regression analyses (**Figures 1G–I**). With the increment of BMI (suggested increased adiposity), the level of leptin increases, as expected ($r^2 = 0.197$; $p < 0.0001$, **Figure 1H**). We also found that the adiponectin/leptin ratio decreases as BMI increases, and from 30 kg/m^2 the ratio was below 0.4 (suggesting cardiometabolic risk) ($r^2 = 0.075$, $p < 0.01$, **Figure 1I**).

There was no significant difference in BDNF levels between the obese and non-obese groups ($p = 0.847$) (**Figure 1D**). In the present study, the ratio of BDNF to leptin was significantly lower in obese individuals than non-obese ($p = 0.0001$, **Figure 1F**),

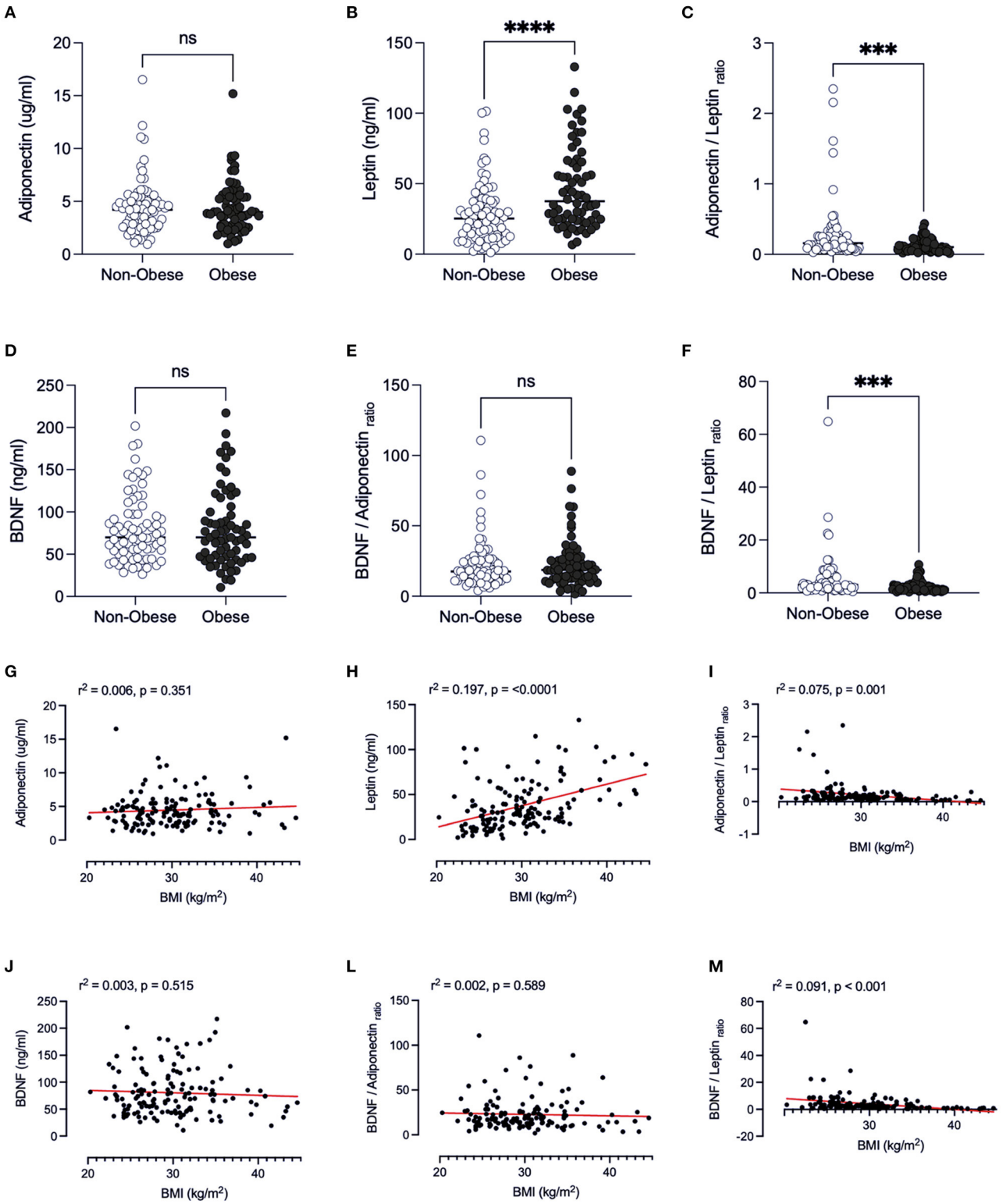

FIGURE 1 | Comparison of adipose-derived hormones levels between non-obese and obese patients with Covid-19. Values expressed as median of adiponectin (ug/ml) **(A)**, leptin (ng/ml) **(B)**, adiponectin/leptin ratio **(C)**, BDNF (ng/ml) **(D)**, BDNF/Adiponectin ratio **(E)**, BDNF/Leptin ratio **(F)**, BDNF / Adiponectin/Leptin ratio **(G)** were compared between two groups. Dashed box presents Linear regression curve of adiponectin **(G)**, leptin **(H)**, adiponectin/leptin ratio **(I)**; BDNF **(J)**, BDNF/Adiponectin ratio **(L)**, BDNF/Leptin ratio **(M)** as dependent variable (Y axis) with body index mass (BMI) as independent variable (X axis). Significance: $^{***}p < 0.001$; $^{****}p < 0.0001$.

TABLE 2 | Biochemical and metabolic profiles of patients with COVID-19.

	All Patients (n = 145)	Non-Obese (n = 78)	Obese (n = 67)	P value	Non-ICU (n = 89)	ICU-survivor (N = 39)	ICU-Death (N = 17)	P value
Cholesterol, mg·dL^{-1}	184.2 (156–216)	182.0 (157–206)	188.6 (154–226)	0.157	183.6 (157–209)	200.5 (156–232)	183.8 (155–212)	0.435
Triglyceride, mg·dL^{-1}	136.2 (111–185)	125.4 (106–156)	177.0 (121–223)	<0.001	130.7 (110–175)[b]	181.2 (131–211)	125.0 (102–137)[b]	0.001
HDL-c, mg·dL^{-1}	28.1 (24–33)	28.3 (24–33)	28.0 (24–33)	0.818	28.5 (25–35)	27.2 (24–32)	25.6 (20–33)	0.137
Non-HDL-c, mg·dL^{-1}	153.4 (125–186)	147.4 (122–178)	160.5 (126–195)	0.140	148.0 (123–177)	175.1 (125–201)	160.5 (129–185)	0.217
Insulin, μU·mL^{-1}	32.4 (20–46)	32.3 (22–45)	34.5 (18–48)	0.530	34.3 (21–46)	35.0 (19–47)	25.4 (15–44)	0.551
Glucose, mg·dL^{-1}	90.9 (79–109)	88.5 (80–106)	96.5 (79–113)	0.295	88.8 (80–103)	98.2 (79–120)	97.5 (83–111)	0.187
HOMA-IR	7.7 (4–12)	7.2 (5–12)	9.1 (4–12)	0.986	7.3 (4–12)	9.4 (5–13)	6.2 (3–11)	0.417
Cortisol nmol·L^{-1}	6.6 (2–16)	5.7 (2–10)	10.2 (6–49)	<0.001	6.7 (3–12)	8.3 (3–48)	48.9 (4–50)	0.065

Values are presented as median and interquartile range (Q1–Q3). Mean difference: Mann-Whitney test.
Intensive care contained discharged and dead patients.

whilst the BDNF/adiponectin ratio was similar (**Figure 1E**). This finding was reinforced by the demonstration that there is a decrease in this ratio as BMI increases (**Figure 1M**) which can be pointed out as an indicator of endocrine physiology of the adipose tissue depots.

Sex

By examining the factor sex (**Figures 2A–M**), we found that male patients presented lower concentration of adiponectin [3.60 (IQR 2.57–4.52)] (**Figure 2A**), and of leptin [24.07 (IQR 14.76–33.25)] (**Figure 2B**) and therefore, higher adiponectin/leptin ratio [0.14 (IQR 0.09–0.24)] (**Figure 2C**), when compared to female counterparts ($p < 0.05$) (4.47 (IQR 3.58–6.10), 48.67 (IQR 28.52–77.81) and 0.09 (IQR 0.05–0.19), respectively). BDNF content was similar between sexes (**Figure 2D**), however linear regression showed that BDNF concentration was lower in male patients ($r^2 = 0.035$, $p = 0.023$, **Figure 2J**).

Age

When considering the effect of age (**Figures 3A–M**), the values of the above-mentioned hormones were similar in individuals <60 years vs. ≥60 years ($p > 0.05$) (**Figures 3A–C**). In patients ≥60 years, BDNF concentrations were lower than those of younger patients <60 years old ($p = 0.020$) (**Figure 3D**). We examined whether adipose-derived tissue hormones and BDNF levels were related to age by a series of linear regression analyses. A significant effect of age was found for adiponectin, BDNF and all BNDF-calculated ratios. These findings suggest that an age-related decline in BDNF levels partially contributes to the adverse outcome with advancing age.

Clinical Outcome

In the entire cohort of 145 patients with COVID-19, a total of 17 patients died (mortality 11.7%). Individuals who did not require ICU spent a shorter interval in the hospital (6.0 days (IQR 3–10), when compared to those who were under intensive care who were discharged [ICU-survivor, 18 days of hospitalization (IQR 13–28)] or who died (ICU-death, 21 days of hospitalization [IQR 13–25)] ($p < 0.01$) (**Table 3**). When dividing the patients according to sex, age, and obesity, the same was observed (**Table 3**). Intubation (36 patients, 24.8%) was a clear indicator of COVID-19 progression and severity in hospitalized patients, as expected (**Table 3**).

Regarding WAT-derived hormones (**Figures 4A–M**), neither leptin nor adiponectin levels were factors linked with admission to ICU, regardless of the outcome of obese patients (**Figures 4A,D**). Despite the finding that leptin plasma content was higher in obese individuals when compared to non-obese individuals (**Figure 1B**), only for the Non-ICU subgroup, this difference was significant ($p = 0.016$) (**Figure 4D**). A higher concentration of leptin was found in females compared to male patients (**Figure 1H**), independent of the type of hospitalization (Non-ICU $p < 0.001$; ICU-survivor $p < 0.001$ and ICU-death $p = 0.048$) (**Figure 4E**).

Curiously, in non-obese individuals who required ICU and died (7.7%), the adiponectin/leptin ratio was higher, when compared to non-obese individuals in the subgroups Non-ICU and ICU-survivor ($p = 0.018$, $p = 0.008$, respectively) (**Figure 4G**). This suggests the results be associated with the tendency for lower leptin concentration and higher adiponectin values in non-obese individuals who passed ($p = 0.09$; **Figure 4D**).

When we consider WAT-derived hormones according to sex and age (≥60 years and <60 years), no differences were detected when comparing the Non-ICU, ICU-survivor, and ICU-death subgroups ($p < 0.05$) (**Figures 4B,C,E,F**). Nevertheless, an increased adiponectin/leptin ratio was detected in patients ≥60 years who did not survive (**Figure 4I**).

Considering BDNF concentration (**Figures 5A–M**), besides having found that BDNF levels are related to sex and age (**Figures 2J**, **3J**), we also observed that in the obese individuals who did not require IC, these were higher, when compared with the group's ICU-survivor and ICU-death ($p = 0.007$; $p = 0.009$, respectively) (**Figure 5A**). The under 60 y patients who did not survive, showed a tendency to present lower BDNF levels than the non-ICU subgroup ($p = 0.0698$, **Figure 5C**). The ratio of BDNF/ adiponectin varies in parallel with different severities and outcomes (**Figure 5L**),

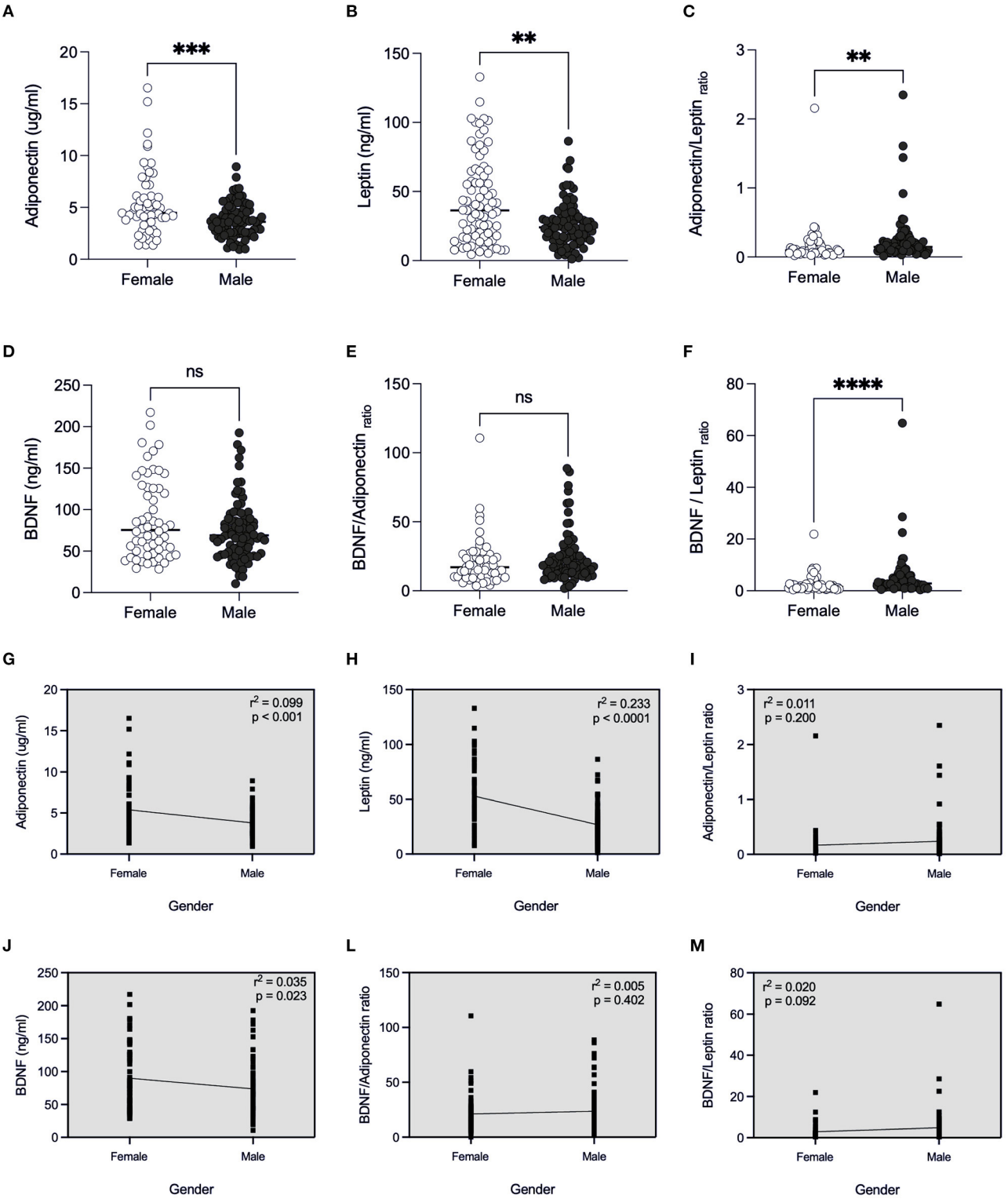

FIGURE 2 | Comparison of adipose-derived hormones levels between female and male patients with Covid-19. Values expressed as median of adiponectin (ug/ml) **(A)**, leptin (ng/ml) **(B)**, adiponectin/leptin ratio **(C)**, BDNF (ng/ml) **(D)**, BDNF/Adiponectin ratio **(E)**, BDNF/Leptin ratio **(F)**, BDNF / Adiponectin/Leptin ratio **(G)** were compared between two groups. Dashed box presents linear regression curve of adiponectin **(G)**, leptin **(H)**, adiponectin/leptin ratio **(I)**; BDNF **(J)**, BDNF/Adiponectin ratio **(L)**, BDNF/Leptin ratio **(M)** as dependent variable (Y axis) with sex (female or male) as independent variable (X axis). Significance: $^{**}p < 0.01$; $^{***}p < 0.001$; $^{****}p < 0.0001$.

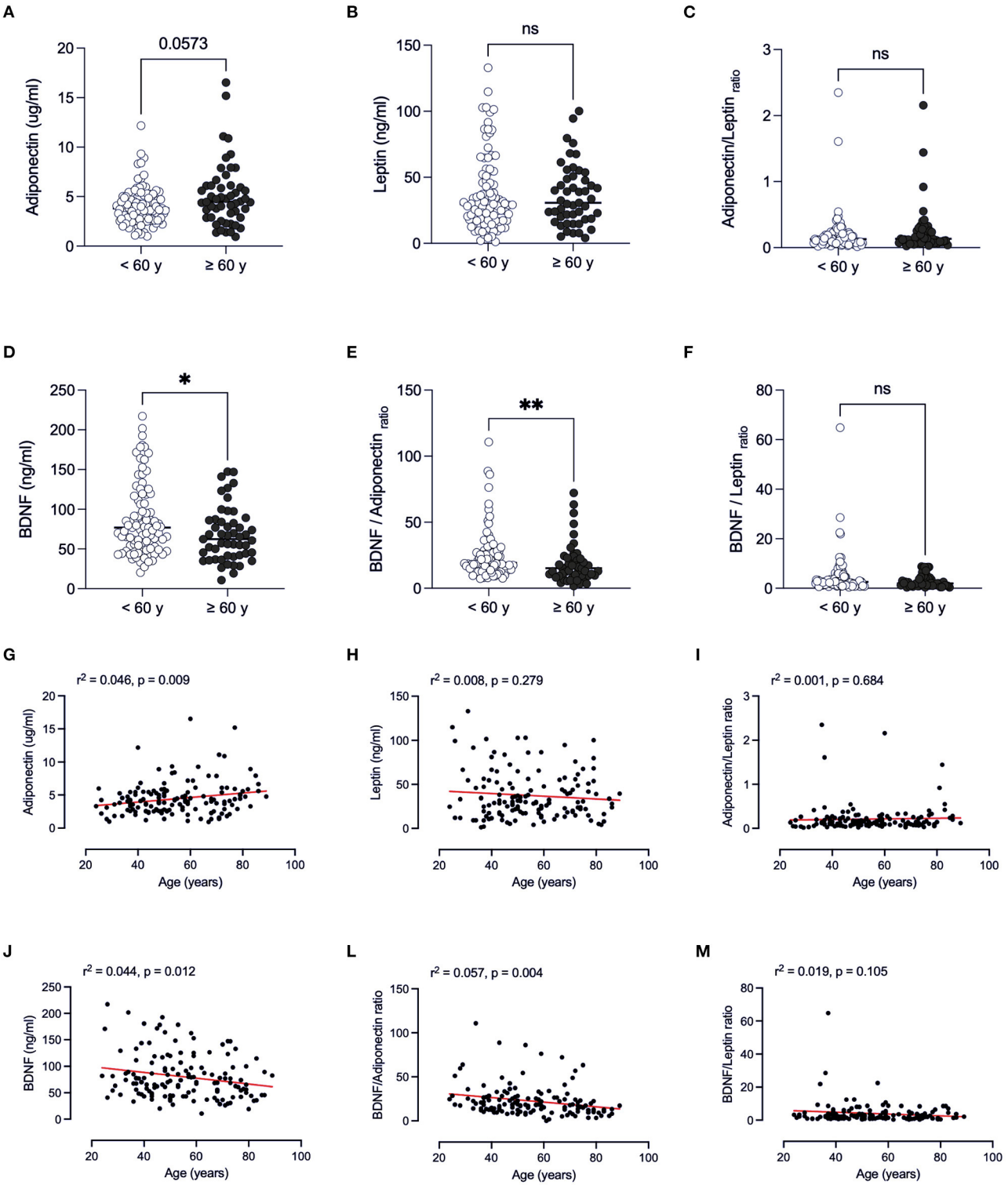

FIGURE 3 | Comparison of adipose-derived hormone levels between age ranges (<60 years vs. ≥60 years) of patients with Covid-19. Values expressed as median of adiponectin (ug/ml) **(A)**, leptin (ng/ml) **(B)**, adiponectin/leptin ratio **(C)**, BDNF (ng/ml) **(D)**, BDNF/Adiponectin ratio **(E)**, BDNF/Leptin ratio **(F)**, BDNF / Adiponectin/Leptin ratio **(G)** were compared between two groups. Dashed box presents linear regression curve of adiponectin **(G)**, leptin **(H)**, adiponectin/leptin ratio **(I)**; BDNF **(J)**, BDNF/Adiponectin ratio **(L)**, BDNF/Leptin ratio **(M)** as dependent variable (Y axis) with age as independent variable (X axis). Significance: $^{*}p < 0.05$; $^{**}p < 0.01$.

TABLE 3 | Comparison of the Clinical Outcomes of Patients between the Non-obese vs. Obese, Female vs. Male, and by age range groups.

Clinical outcome	Non-ICU		ICU-survivor		ICU-death		
Obese X non-obese	**Non-obese (*n* = 58)**	**Obese (*n* = 31)**	**Non-obese (*n* = 14)**	**Obese (*n* = 25)**	**Non-obese (*n* = 6)**	**Obese (*n* = 11)**	***P* value**
Hospitalization time (days)	5 (3–10)	6 (3–10)	17.5 (12–24)[a]	18 (12–28)[a]	18 (13–22)[a]	22 (11–27)[a]	<0.0001
Intubation,*n* (%)			6 (42.8)	13 (52.0)	6 (100.0)	11 (100.0)	
In-hospital mortality, *n* (%)					6 (35.3)	11 (64.7)	
Female X Male	Female (*n* = 38)	Male (*n* = 51)	Female (*n* = 16)	Male (*n* = 23)	Female (*n* = 5)	Male (*n* = 12)	P value
Hospitalization time (days)	4.5 (3–10)	6 (4–10)	19.5 (13–27)[a]	17 (11–28)[a]	22 (14–27)[a]	20 (9–25)[a]	<0.0001
Intubation,*n* (%)			8 (50)	11 (47.8)	5 (100)	12 (100)	
In-hospital mortality, *n* (%)					5 (29.4)	12 (70.6)	
<60 y vs. >60 y	<60 y (*n* = 63)	≥60 y (*n* = 26)	<60 y (*n* = 27)	≥ 60 y (*n* = 12)	<60 y (*n* = 3)	≥ 60 y (*n* = 14)	P value
Hospitalization time (days)	5 (3–10)	6 (3–10)	17 (11–21) [a]	25 (16–29)[a]	11 (>8)	21 (15–25)[a]	< 0.0001
Intubation,n (%)			11 (40.7)	8 (66.7)	3 (100)	14 (100)	
In-hospital mortality, *n* (%)					3 (17.6)	14 (82.4)	

Values are reported as a number (%) or median and interquartile range (Q1–Q3).
Body mass index classes: non-obese <29.9 kg·m^2; obese >30 kg·m^2.
Kruskal-Wallis test for differences between clinical results within groups, with statistical significance represent by symbols: [a] compared to Non-IC.

pointing out that adipose endocrine function is important in COVID-19.

Linear regression revealed that higher BDNF levels are negatively correlated with disease severity, with BDNF values being lower in patients who died ($r^2 = 0.092$, $p < 0.001$; **Figure 5J**). A beta coefficient of $b = -18.34$ was found for this correlation, indicating that for patients requiring IC (both survivor and death groups) we can expect a decrease in BDNF in 18.34 ng/ml each condition. This leads us to infer BDNF to be a possible marker of adverse clinical outcomes for COVID-19 patients.

In univariable logistic regression, Age, BMI, BDNF, BDNF/Adip ratio, hospitalization days, hypertension and respiratory diseases were significantly associated with ICU admission (all $p < 0.05$), whilst in-hospital death was significantly associated with age, BDNF, hospitalization days, hypertension and respiratory diseases, and ongoing pharmacological treatment (see **Supplementary Table 2**).

In multivariable regression analysis, designed to test the possibility of confounding relations of BDNF with other clinically relevant independent variables, BDNF hold a significant association with ICU admission (OR = 0.987; 95%IC:0.977 to 998; $p = 0.018$) in a model including Age (OR = 1.038, 95%IC: 1.011 to 1.065, $p = 0.005$), BMI (OR = 1.142, 95%IC: 1.058 to 1.232, $p = 0.001$), and Sex (0.779; 95%IC:0.352 to 1.727; $p = 0.539$). With Death as the dependent variable, BDNF lost the significant association (OR:0.985; 95%IC:0.966 to 1.005; $p = 0.146$) in a model also adjusted for Age, BMI and Sex, in which only Age maintained a significant association with Death (OR: 1.098; 95%IC: 1.048 to 1.151; $p < 0.001$). Similar results were depicted for the BDNF/Adip ratio, as portrayed in **Supplementary Table 3**. In additional multivariable logistic regression models, BDNF, BDNF/Adip ratio, hypertension and respiratory diseases were shown to be predictors of ICU admission, while hypertension and respiratory diseases were independent predictors of patients' risk of death (**Supplementary Table 4**). However, after adjusting for BDNF, BDNF/Adip ratio, Age, and BMI, logistic regression showed that hypertension and respiratory diseases are not predictors of death, being Age the only independent variable holding significant association with Death in either multivariable models considered (**Supplementary Table 5**).

DISCUSSION

In this prospective study, we examined adipose tissue-derived hormones involved in the control of appetite and body composition, the metabolic profile, and the levels of BDNF in the circulation, and the association of these parameters with disease severity and outcome in patients with COVID-19. The original findings show that (a) BDNF serum concentration is associated with disease outcome; (b) appetite and body composition regulating hormones secreted by WAT are not reliable predictors of disease severity, while the ratio BDNF/adiponectin was informative of patient status; (c) there are age and sex-specific changes that should be considered when employing these potential markers for prognosis assessment.

We report a linear and inverse relationship between BDNF and adverse outcomes in patients with COVID-19. The results also show that circulating BDNF declines with advancing age. In a COVID-19 condition, a hypothetical model suggested that the down-regulation of ACE-2 in the brain by SARS-CoV-2 inhibits the release of neurotropic factors such as BDNF (26). Recently, Azoulay and coll. (2020) showed that COVID-19 patients with moderate to severe disease showed decreased circulating content of BDNF when compared with those presenting milder symptoms (–∼15%) (27). In this small study,

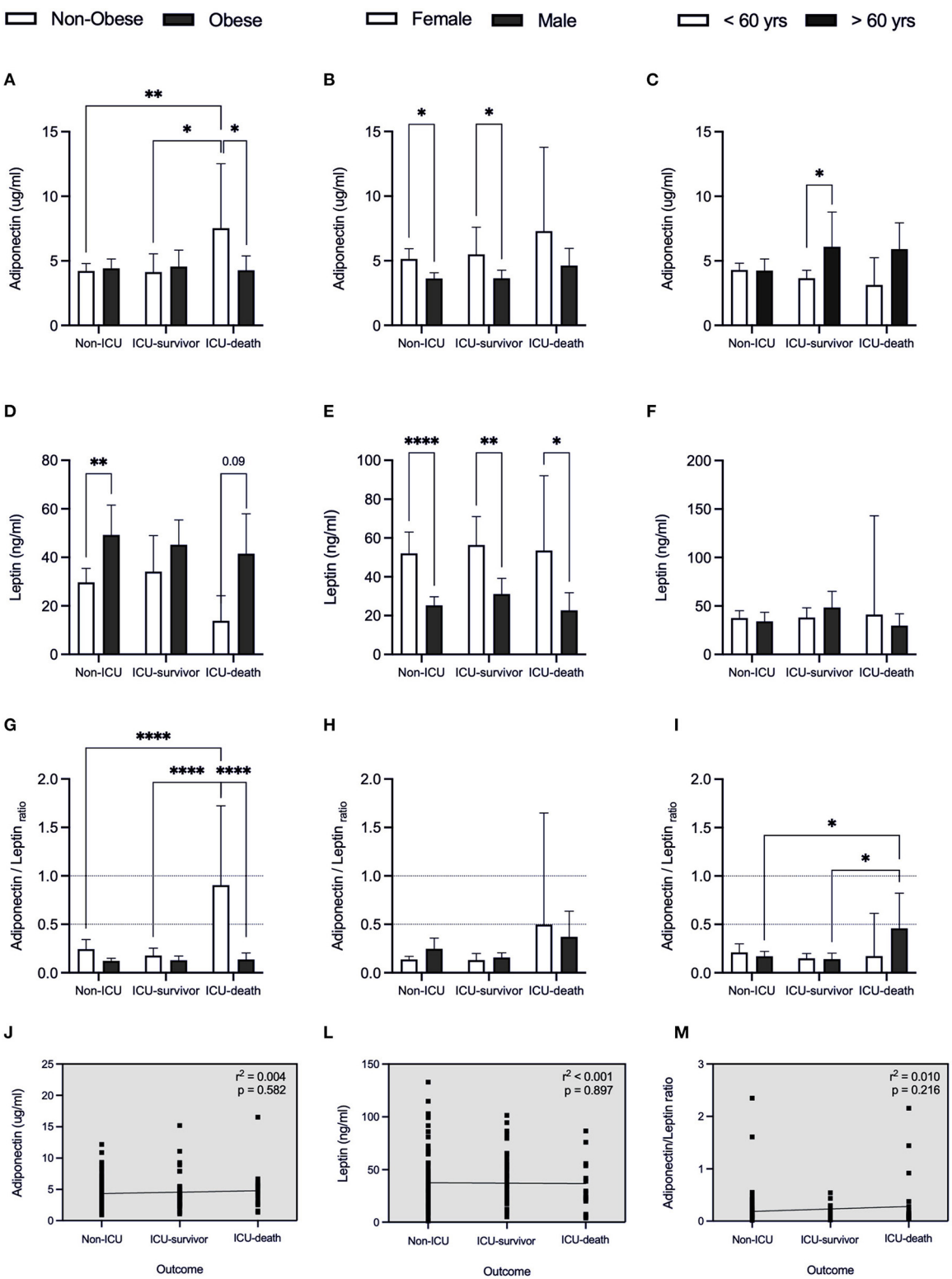

FIGURE 4 | Adipose-derived hormones for patients with COVID-19 in relation to clinical outcome. Values expressed as mean with 95% Confidence Interval for patients that were hospitalized without intensive care (Non-ICU), patients admitted to the intensive care unit and discharged (ICU-survivor) and patients who died (ICU-death), including: adiponectin **(A–C)**, leptin **(D–F)**, and adiponectin/leptin ratio **(G–I)** related to body index mass (BMI), sex and age, respectively. Dashed box presents linear regression curve of adiponectin **(J)**, leptin **(L)**, and adiponectin/leptin ratio **(M)** as dependent variable (Y axis) with outcome as independent variable (X axis). Significance: $^{*}p < 0.05$; $^{**}p < 0.01$; $^{****}p < 0.0001$.

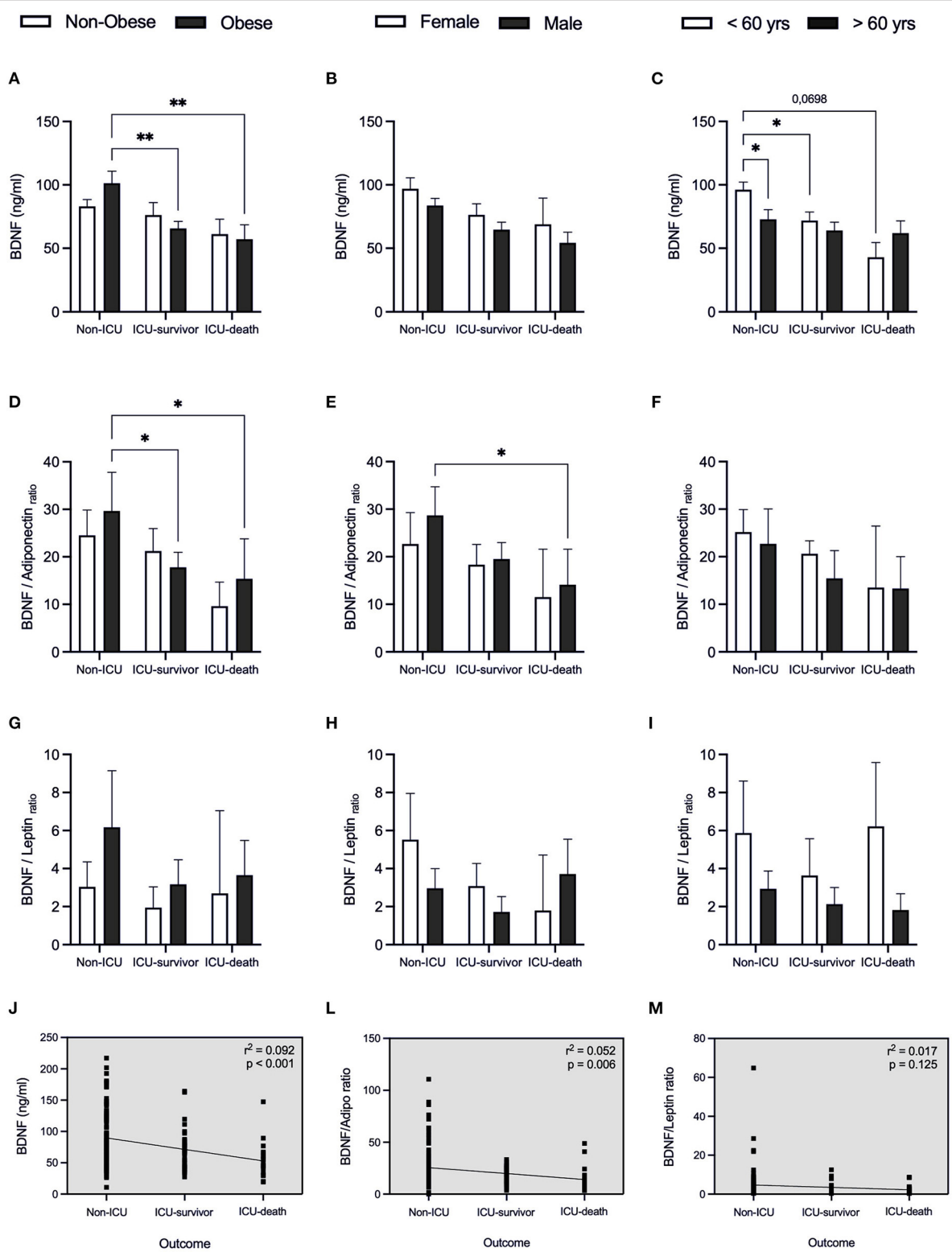

FIGURE 5 | BDNF and BDNF-related ratios for patients with COVID-19 in relation to clinical outcome. Values expressed as mean with 95% Confidence Interval for patients that were hospitalized without intensive care (Non-ICU), patients admitted to the intensive care unit and discharged (ICU-survivor) and patients who died (ICU-death), including: BDNF **(A–C)**, BDNF/adiponectin ratio **(D–F)**, and BDNF/leptin ratio **(G–I)** related to body index mass (BMI), sex and age, respectively. Dashed box presents linear regression curve of adiponectin **(J)**, leptin **(L)**, and adiponectin/leptin ratio **(M)** as dependent variable (Y axis) with outcome as independent variable (X axis). Significance: $^{*}p < 0.05$; $^{**}p < 0.01$.

the authors found that recovery from COVID-19 was associated with the augment of circulating BDNF (27). In the present study, 145 patients were examined, and we report a conspicuous association between BDNF levels and the severity of the disease, corroborating previous evidence that SARS-CoV-2 infection leads to down-regulation of the ACE2 receptors and this might be an aggravating factor for patients with medical conditions (28) and the suggestion that recovery from SARS-CoV-2 infection is associated with serum BDNF restauration (27).

BDNF plays a critical role in neuronal survival, growth, plasticity, and is essential for learning and memory (29). Wang and coworkers have demonstrated that ACE2 knockout mice exhibit a decrease in BDNF in the hippocampus region, and significant impairments of cognitive function compared with WT mice (30). In the same way, Angiotensin II type 1 receptor (AT1) blockade prevented memory impairment *via* up-regulation of BDNF (31). The infection of the SARS-CoV-2 in the brain increases the local levels of Angiotensin II by ACE2 down-regulation. It was suggested that the interaction of Angiotensin II with AT1 receptor increases kynurenine metabolites, producing pro-oxidative and pro-inflammatory effects, resulting in decreased levels of central BDNF (32). All these elements play a critical role in the impairment of cognitive function and a highly orchestrated immune-inflammatory response that ultimately could result in the development of depression (32). It is possible, therefore, that SARS-CoV-2 dampens BDNF synthesis and release and elicits neurologic symptoms (33). We show a clear association between COVID-19 prognosis and circulating BDNF, as patients with lower values consistently showed worsened outcome.

The involvement of BDNF in inflammatory conditions is complex (34). BDNF plays a role in the maturation and survival of T lymphocytes, especially under stress (35). Thus, in inflammatory conditions such as obesity and type 2 diabetes, immune cells (via increased IL-6) are stimulated to produce neurotrophins, like BDNF, to minimize the neuronal damage associated with obesity (36, 37). Consequently, it was suggested that a higher concentration of subunit pro-BDNF stimulates the infiltration of immune cells, culminating in an increase in the expression of proinflammatory cytokines (38). Thus, it is possible that in presence of viral infection and metabolic disturbance, as in COVID-19, the relationship between BDNF and inflammation is modified or even, impaired (seen by high BDNF levels, ∼100 ng/ml in obese patients with COVID-19 when they were admitted to hospital). Different studies have shown either that circulating BDNF levels are higher in obese subjects than in controls (39, 40) or that there are no differences between the two groups (41). An upregulation of pro-BDNF expression in PDGFRα^{+} adipocyte progenitors was indicated as a feature of adipose tissue aging, suggesting that inhibition of BDNF expression in adipocyte progenitors could be potentially beneficial to prevent age-related adipose tissue dysfunction (42). However, in our study, we evaluated serum mature BDNF levels that have opposite effects of pro-BDNF (43). Interestingly, serum BDNF levels didn't differ across severity groups in patients >60yrs, while a reduction of BDNF in patients <60 yrs was observed with the progression of COVID-19 severity. This data reinforces the idea that increased mature BDNF isoform is related to the improvement of metabolic function, while the pro-BDNF isoform is related to the adipose tissue disfunction as observed by Song et al. (42). In addition, higher cortisol levels found in obese subjects and a tendency ($p = 0.06$) for higher levels of the same hormone in patients who died (ICU-death) suggest central hyperstimulation on the hypothalamus-adrenal-pituitary axis during SARS-CoV-2 infection. This scenario might favor a disconnection between central and peripheral communication.

BDNF is an important pleiotropic protein directly related to neuron and brain health, commonly inversely associated with obesity (34). In addition, the sympathetic activity in the adipose tissue can regulate lipolysis *via* BDNF (23). Emerging evidence links BNDF with SARS-CoV-2 infection dampens BDNF synthesis and release, which favors COVID-19 associated neurologic symptoms (33), however the metabolic role of BDNF in COVID-19 patients has been largely overlooked. Recently, an interplay between BDNF and adiponectin in the regulation of fat mass was proposed (44). Furthermore, it was suggested that adiponectin, selectively produced by the white adipose tissue, strongly correlates to the inflammatory process triggered by Sars-CoV-2 infection (21). Adiponectin concentration is inversely associated with the detection of cardiometabolic risk markers, and this hormone reflects adipose tissue physiological status (45). Our results show that adiponectin levels increased linearly with aging, and adiponectin serum content was also higher in non-obese patients who died and in older patients who required IC, which could reflect an attempt by the adipose tissue to counteract inflammation in COVID-19 (21). The BDNF/adiponectin ratio seems to be a reliable marker of the outcome.

Our data show that both leptin and adiponectin alone are not predicting factors for IC requirement or outcome in obese individuals. Conversely, the adiponectin/leptin ratio exhibited differences related with BMI ($r = -0.274$, $p = 0.001$), and thus this ratio may be employed as a tool for the assessment of obesity-associated cardiometabolic risk (22). Likewise, this ratio may be also informative of COVID-19 prognostic, as the obese patients with lower values are also the ones with the more severe form of the disease. A recent study from Italy showed that Adip/Lep ratio was associated with systemic inflammation in COVID-19 patients, where patients with moderate severity showed the highest Adip/Lep ratio values (46). In addition, the aforementioned study found that mortality tended to decrease with increasing Adip/Lep tertiles, suggesting an inadequate anti-inflammatory response in these patients (46). Conversely, we didn't find association between the Adip/Lep ratio and Covid-19 outcome (life or death). But, our study showed that Adip/Lep ratio response is dependent of BMI and age, suggesting that this age and sex-specific changes should be considered when employing this potential marker for prognosis assessment of COVID-19. We also suggest that the described hormonal disruptions may impact lipoprotein profile. Two cohort studies (47, 48) demonstrated dysregulation of lipoprotein profile in COVID-19 patients, in particular, LDL-c and total cholesterol levels were reduced in patients with severe disease. These studies suggest a failure in liver metabolism control, due to a possible effect of the covid-related cytokine storm (47, 48).

However, more studies are needed for better understand the involved mechanism.

Many factors may potentially lead to dysregulation of adipose tissue- endocrine function. We speculate that SARS-CoV-2 infection can affect the white adipose tissue *via* ACE2 receptors, impairing its endocrine function. Understanding the relationship between the adipose tissue and its hormones, and their relationship with BDNF, may facilitate the development of new therapeutic and immunometabolic strategies for COVID-19 in obese patients. The expanded WAT depots in obese subjects may also act as a storage site for the virus, favoring the rapid progression of SARS-CoV-2 infection, associated with increased virus shedding, immune activation, and cytokine production (49).

Shortcomings of the study include the fact that patients were admitted to the hospital already with a variety of metabolic disorders, and within different infection time spans. Therefore, it is important to establish whether COVID-19 induces these metabolic changes or aggravates previously existing ones. Another limitation is that the source of circulating BDNF was not investigated.

In summary, according to this prospective study, BDNF and BDNF/adiponectin ratio are possible markers of adverse clinical outcomes for COVID-19. BDNF levels were clearly influenced by BMI and age. In detail, as BMI increased, BDNF concentration decreased, a finding more significantly in individuals >60 years old. BDNF content was also lower in obese patients that required intensive care and in older patients who died. We propose the measurement of BDNF and adiponectin at hospital admission and during the progression of disease as to optimize treatment choices.

DATA AVAILABILITY STATEMENT

The raw data supporting the conclusions of this article will be made available by the authors, without undue reservation.

ETHICS STATEMENT

The studies involving human participants were reviewed and approved by Human Research Ethics Committee of Pontificia Universidade Católica do Paraná (Number 31558020.8.0000.0103). The patients/participants provided their written informed consent to participate in this study.

AUTHOR CONTRIBUTIONS

LM, RP, and FL conceived the present idea. LM, EC, MD, FV, LM, and AG performed the experimental procedures. CB, AA, RP, and FL were responsible for the research funding and laboratory support. LM, MS, BS, and FL wrote the paper with input from all authors. TP and KK did a critical revision of the article. All authors read and approved the final manuscript.

FUNDING

We thank the National Council of Technological and Scientific Development (CNPq)/Brazil, Coordination for the Improvement of Higher Education Personnel (CAPES)/Brazil, the São Paulo Research Foundation (FAPESP)/Brazil (Process Number, 2019/25626-26, Pontifícia Universidade Católica do Paraná (PUCPR)/Brazil and Banco Regional de Desenvolvimento do Extremo Sul (BRDE)/Brazil, Brazil for providing the financial support to conduct the research activities in the laboratory.

SUPPLEMENTARY MATERIAL

The Supplementary Material for this article can be found online at: https://www.frontiersin.org/articles/10.3389/fnut.2021.784429/full#supplementary-material

REFERENCES

1. Yang J, Hu J, Zhu C. Obesity aggravates COVID-19: a systematic review and meta-analysis. *J Med Virol.* (2021) 93:257–61. doi: 10.1002/jmv.26237
2. Sanchis-Gomar F, Lavie CJ, Mehra MR, Henry BM, Lippi G. Obesity and outcomes in COVID-19: when an epidemic and pandemic collide. *Mayo Clin Proc.* (2020) 95:1445–53. doi: 10.1016/j.mayocp.2020.05.006
3. Rodrigues B, Lira FS, Consolim-Colombo FM, Rocha JA, Caperuto EC, De Angelis K, et al. Role of exercise training on autonomic changes and inflammatory profile induced by myocardial infarction. *Mediators Inflamm.* (2014) 2014:702473. doi: 10.1155/2014/702473
4. Teixeira AA de S, Lira FS, Pimentel GD, Oliveira de Souza C, Batatinha H, Biondo LA, et al. Aerobic exercise modulates the free fatty acids and inflammatory response during obesity and cancer cachexia. *Crit Rev Eukaryot Gene Expr.* (2016) 26:187–98. doi: 10.1615/CritRevEukaryotGeneExpr.2016016490
5. Lira FS, Antunes B de MM, Seelaender M, Rosa Neto JC. The therapeutic potential of exercise to treat cachexia. *Curr Opin Support Palliat Care.* (2015) 9:317–24. doi: 10.1097/SPC.0000000000000170
6. Pasquarelli-do-Nascimento G, Braz-de-Melo HA, Faria SS, Santos I de O, Kobinger GP, Magalhães KG. Hypercoagulopathy and adipose tissue exacerbated inflammation may explain higher mortality in Covid-19 patients with obesity. *Front Endocrinol.* (2020) 11:530. doi: 10.3389/fendo.2020.00530
7. Favre G, Legueult K, Pradier C, Raffaelli C, Ichai C, Iannelli A, et al. Visceral fat is associated to the severity of COVID-19. *Metabolism.* (2021) 115:154440. doi: 10.1016/j.metabol.2020.154440
8. Silverio R, Gonçalves DC, Andrade MF, Seelaender M. Coronavirus disease 2019 (COVID-19) and nutritional status: the missing link? *Adv Nutr.* (2020) 12:682–692. doi: 10.1093/advances/nmaa125
9. Dugail I, Amri EZ, Vitale N. High prevalence for obesity in severe COVID-19: Possible links and perspectives towards patient stratification. *Biochimie.* (2020) 179:257–65. doi: 10.1016/j.biochi.2020.07.001
10. Kruglikov IL, Scherer PE. The Role of Adipocytes and Adipocyte-Like Cells in the Severity of COVID-19 Infections. *Obesity.* (2020) 28:1187–90. doi: 10.1002/oby.22856
11. Alves C, Casqueiro J, Casqueiro J. Infections in patients with diabetes mellitus: a review of pathogenesis. *Indian J Endocrinol Metab.* (2012) 16:S27–36. doi: 10.4103/2230-8210.94253

12. Kornum JB, Thomsen RW, Riis A, Lervang HH, Schønheyder HC, Sørensen HT. Type 2 diabetes and pneumonia outcomes: a population-based cohort study. *Diabetes Care.* (2007) 30:2251–7. doi: 10.2337/dc06-2417
13. Peleg AY, Weerarathna T, McCarthy JS, Davis TME. Common infections in diabetes: pathogenesis, management and relationship to glycaemic control. *Diabetes Metab Res Rev.* (2007) 23:3–13. doi: 10.1002/dmrr.682
14. Yang JK, Feng Y, Yuan MY, Yuan SY, Fu HJ, Wu BY, et al. Plasma glucose levels and diabetes are independent predictors for mortality and morbidity in patients with SARS. *Diabet Med.* (2006) 23:623–8. doi: 10.1111/j.1464-5491.2006.01861.x
15. Schoen K, Horvat N, Guerreiro NFC, De Castro I, De Giassi KS. Spectrum of clinical and radiographic findings in patients with diagnosis of H1N1 and correlation with clinical severity. *BMC Infect Dis.* (2019) 19:964. doi: 10.1186/s12879-019-4592-0
16. De Heredia FP, Gómez-Martínez S, Marcos A. Chronic and degenerative diseases: obesity, inflammation and the immune system. *Proc Nutr Soc.* (2012) 71:332–8. doi: 10.1017/S0029665112000092
17. Bradley D, Shantaram D, Smith A, Hsueh WA. Adipose tissue t regulatory cells: implications for health and disease. *Adv Exp Med Biol.* (2021) 1278:125–139. doi: 10.1007/978-981-15-6407-9_8
18. De Bandt J-P, Monin C. Obesity, nutrients and the immune system in the era of COVID-19. *Nutrients.* (2021) 13:610. doi: 10.3390/nu13020610
19. Alwarawrah Y, Kiernan K, MacIver NJ. Changes in nutritional status impact immune cell metabolism and function. *Front Immunol.* (2018) 9:1055. doi: 10.3389/fimmu.2018.01055
20. Radigan KA, Morales-Nebreda L, Soberanes S, Nicholson T, Nigdelioglu R, Cho T, et al., Perlman H, et al. Impaired clearance of influenza a virus in obese, leptin receptor deficient mice is independent of leptin signaling in the lung epithelium and macrophages. *PLoS ONE.* (2014) 9:1055. doi: 10.1371/journal.pone.0108138
21. Caterino M, Gelzo M, Sol S, Fedele R, Annunziata A, Calabrese C, et al. Dysregulation of lipid metabolism and pathological inflammation in patients with COVID-19. *Sci Rep.* (2021) 11:2941. doi: 10.1038/s41598-021-82426-7
22. Frühbeck G, Catalán V, Rodríguez A, Gómez-Ambrosi J. Adiponectin-leptin ratio: A Promising index to estimate adipose tissue dysfunction. *Relation with obesity-associated cardiometabolic risk. Adipocyte.* (2018) 7:57–62. doi: 10.1080/21623945.2017.1402151
23. Wang P, Loh KH, Wu M, Morgan DA, Schneeberger M, Yu X, et al. A leptin–BDNF pathway regulating sympathetic innervation of adipose tissue. *Nature.* (2020) 583:839–844. doi: 10.1038/s41586-020-2527-y
24. Colitti M, Loor JJ, Stefanon B. Expression of NGF, BDNF and their receptors in subcutaneous adipose tissue of lactating cows. *Res Vet Sci.* (2015) 102:196–9. doi: 10.1016/j.rvsc.2015.08.016
25. Matthews D R, Hosker J P, Rudenski A S, Naylor B A, Treacher D F, Turner R C. Homeostasis model assessment: insulin resistance and beta-cell function from fasting plasma glucose and insulin concentrations in man. *Diabetologia.* (1985) 28:412–9. doi: 10.1007/BF00280883
26. Motaghinejad M, Gholami M. possible neurological and mental outcomes of COVID-19 infection: a hypothetical role of ace-2/mas/bdnf signaling pathway. *Int J Prev Med.* (2020) 11:84.
27. Azoulay D, Shehadeh M, Chepa S, Shaoul E, Baroum M, Horowitz NA, et al. Recovery from SARS-CoV-2 infection is associated with serum BDNF restoration. *J Clean Prod.* (2020) 81:e79–81. doi: 10.1016/j.jinf.2020.06.038
28. Verdecchia P, Cavallini C, Spanevello A, Angeli F. The pivotal link between ACE2 deficiency and SARS-CoV-2 infection. *Eur J Intern Med.* (2020) 76:14–20. doi: 10.1016/j.ejim.2020.04.037
29. Bathina S, Das UN. Brain-derived neurotrophic factor and its clinical Implications. *Arch Med Sci.* (2015) 11:1164–78. doi: 10.5114/aoms.2015.56342
30. Wang XL, Iwanami J, Min LJ, Tsukuda K, Nakaoka H, Bai HY, et al. Deficiency of angiotensin-converting enzyme 2 causes deterioration of cognitive function. *npj Aging Mech Dis.* (2016) 2:16024. doi: 10.1038/npjamd.2016.24
31. Wincewicz D, Juchniewicz A, Waszkiewicz N, Braszko JJ. Angiotensin II type 1 receptor blockade by telmisartan prevents stress-induced impairment of memory *via* HPA axis deactivation and up-regulation of brain-derived neurotrophic factor gene expression. *Pharmacol Biochem Behav.* (2016) 148:108–18. doi: 10.1016/j.pbb.2016.06.010
32. Bouças AP, Rheinheimer J, Lagopoulos J. Why severe Covid-19 patients are at greater risk of developing depression: a molecular perspective. *Neuroscientist.* (2020) 2:1073858420967892. doi: 10.1177/1073858420967892
33. De Paulis M, Oliveira DBL, Vieira RP, Pinto IC, MacHado RRG, Cavalcanti MP, et al. Multisystem inflammatory syndrome associated with covid-19 with neurologic manifestations in a child: a brief report. *Pediatr Infect Dis J.* (2020) 39:e321–e324. doi: 10.1097/INF.0000000000002834
34. Inoue DS, Antunes BM, Maideen MFBB, Lira FS. pathophysiological features of obesity and its impact on cognition: exercise training as a non-pharmacological approach. *Curr Pharm Des.* (2020) 26:916–31. doi: 10.2174/1381612826666200114102524
35. Papathanassoglou EDE, Miltiadous P, Karanikola MN. May BDNF be implicated in the exercise-mediated regulation of inflammation? critical review and synthesis of evidence. *Biol Res Nurs.* (2015) 17:521–39. doi: 10.1177/1099800414555411
36. Huang CJ, Mari DC, Whitehurst M, Slusher A, Wilson A, Shibata Y. Brain-derived neurotrophic factor expression ex vivo in obesity. *Physiol Behav.* (2014) 123:76–9. doi: 10.1016/j.physbeh.2013.10.004
37. Pedersen BK, Pedersen M, Krabbe KS, Bruunsgaard H, Matthews VB, Febbraio M. Role of exercise-induced brain-derived neurotrophic factor production in the regulation of energy homeostasis in mammals. *Exp Physiol. (*2009) 94:1153–1160. doi: 10.1113/expphysiol.2009.048561
38. Luo C, Zhong X-L, Zhou FH, Li J, Zhou P, Xu J-M, et al. Peripheral brain derived neurotrophic factor precursor regulates pain as an inflammatory mediator. *Sci Rep.* (2016) 6:27171. doi: 10.1038/srep27171
39. Golden E, Emiliano A, Maudsley S, Windham BG, Carlson OD, Egan JM, et al. Circulating brain-derived neurotrophic factor and indices of metabolic and cardiovascular health: data from the Baltimore Longitudinal Study of Aging. *PLoS One.* (2010) 5:e10099. doi: 10.1371/journal.pone.0010099
40. Slusher AL, Whitehurst M, Zoeller RF, Mock JT, Maharaj A, Huang CJ. Brain-derived neurotrophic factor and substrate utilization following acute aerobic exercise in obese individuals. *J Neuroendocrinol.* (2015) 27:370–6. doi: 10.1111/jne.12275
41. Hinderberger P, Rullmann M, Drabe M, Luthardt J, Becker GA, Blüher M, et al. The effect of serum BDNF levels on central serotonin transporter availability in obese vs. non-obese adults: a [11C]DASB positron emission tomography study. *Neuropharmacology.* (2016) 110:530–36. doi: 10.1016/j.neuropharm.2016.04.030
42. Song HD, Kim SN, Saha A, Ahn SY, Akindehin S, Son Y, et al. Aging-induced brain-derived neurotrophic factor in adipocyte progenitors contributes to adipose tissue dysfunction. *Aging Dis.* (2020) 11:575–87. doi: 10.14336/AD.2019.0810
43. Miranda M, Morici JF, Zanoni MB, Bekinschtein P. Brain-derived neurotrophic factor: a key molecule for memory in the healthy and the pathological brain. *Front Cell Neurosci.* (2019) 13:363. doi: 10.3389/fncel.2019.00363
44. Jo D, Son Y, Yoon G, Song J, Kim OY. Role of adiponectin and brain derived neurotrophic factor in metabolic regulation involved in adiposity and body fat browning. *J Clin Med.* (2020) 10:56. doi: 10.3390/jcm10010056
45. Vega GL, Grundy SM. Metabolic risk susceptibility in men is partially related to adiponectin/leptin ratio. *J Obes.* (2013) 2013:409679. doi: 10.1155/2013/409679
46. Di Filippo L, De Lorenzo R, Sciorati C, Capobianco A, Lorè NI, Giustina A, et al. Adiponectin to leptin ratio reflects inflammatory burden and survival in COVID-19: adiponectin and leptin in COVID-19. *Diabetes Metab.* (2021) 47:101268. doi: 10.1016/j.diabet.2021.101268

47. Wei X, Zeng W, Su J, Wan H, Yu X, Cao X, et al. Hypolipidemia is associated with the severity of COVID-19. *J Clin Lipidol.* (2020) 14:297–04. doi: 10.1016/j.jacl.2020.04.008
48. Fan J, Wang H, Ye G, Cao X, Xu X, Tan W, et al. Letter to the editor: low-density lipoprotein is a potential predictor of poor prognosis in patients with coronavirus disease 2019. *Metabolism.* (2020) 107:154243. doi: 10.1016/j.metabol.2020.154243
49. Ryan PMD, Caplice NM. Is adipose tissue a reservoir for viral spread, immune activation, and cytokine amplification in coronavirus disease 2019? *Obesity.* (2020) 28:1191–1194. doi: 10.1002/oby.22843

Conflict of Interest: The authors declare that the research was conducted in the absence of any commercial or financial relationships that could be construed as a potential conflict of interest.

Publisher's Note: All claims expressed in this article are solely those of the authors and do not necessarily represent those of their affiliated organizations, or those of the publisher, the editors and the reviewers. Any product that may be evaluated in this article, or claim that may be made by its manufacturer, is not guaranteed or endorsed by the publisher.

frontiers in Nutrition

ORIGINAL RESEARCH
published: 18 March 2022
doi: 10.3389/fnut.2022.870680

Aberrant Cholesterol Metabolic Genes Regulation in a Negative Feedback Loop Induced by an Alphacoronavirus

Hao-Yu Liu[1†], Haotian Gu[1†], Huan Qu[1], Wenbin Bao[1], Yanhua Li[2] and Demin Cai[1*]*

[1] College of Animal Science and Technology, Yangzhou University, Yangzhou, China, [2] College of Veterinary Medicine, Yangzhou University, Yangzhou, China

Porcine epidemic diarrhea virus (PEDV) is an alphacoronavirus that causes acute inflammation and severe diarrhea in newborn piglets with a high mortality rate. Given that cholesterol is required for coronavirus infection *in vitro*, the role of endogenous cholesterol metabolism in regulating coronavirus infection and the mechanism behind it ought to be elucidated. In this study, we found that the levels of cholesterol and bile acids were both elevated in the livers of PEDV-infected piglets compared to those of the control group. Consistently, in the livers of PEDV-infected piglets, the expression of key genes involved in cholesterol metabolism was significantly increased. Transcriptomic analysis indicated that the cholesterol homeostasis pathway was among the most enriched pathways in the livers of PEDV-infected piglets. Unexpectedly, the expression of key genes in the cholesterol metabolic pathway was downregulated at the messenger RNA (mRNA) level, but upregulated at the protein level. While the primary transcriptional factors (TFs) of cholesterol metabolism, including SREBP2 and FXR, were upregulated at both mRNA and protein levels in response to PEDV infection. Further Chromatin Immunoprecipitation Quantitative Real-time PCR (ChIP-qPCR) analysis demonstrated that the binding of these TFs to the locus of key genes in the cholesterol metabolic pathway was remarkably inhibited by PEDV infection. It was also observed that the occupancies of histone H3K27ac and H3K4me1, at the locus of the cholesterol metabolic genes *HMGCR* and *HMGCS1,* in the livers of PEDV-infected piglets, were suppressed. Together, the PEDV triggers an aberrant regulation of cholesterol metabolic genes *via* epigenetic inhibition of SREBP2/FXR-mediated transcription, which provides a novel antiviral target against PEDV and other coronaviruses.

Keywords: cholesterol, SREBP2, FXR, epigenetic, PEDV, coronaviruses

OPEN ACCESS

Edited by:
Lei Zhou,
Guangxi University, China

Reviewed by:
Abdelkareem Ahmed,
Nyala University, Sudan
Longfei Jia,
Cornell University, United States

***Correspondence:**
Yanhua Li
007206@yzu.edu.cn
Demin Cai
demincai@yzu.edu.cn

[†]These authors have contributed equally to this work

Specialty section:
This article was submitted to Nutrition and Metabolism, a section of the journal Frontiers in Nutrition

Received: *07 February 2022*
Accepted: *18 February 2022*
Published: *18 March 2022*

Citation:
Liu H-Y, Gu H, Qu H, Bao W, Li Y and Cai D (2022) Aberrant Cholesterol Metabolic Genes Regulation in a Negative Feedback Loop Induced by an Alphacoronavirus. Front. Nutr. 9:870680. doi: 10.3389/fnut.2022.870680

INTRODUCTION

Coronaviruses (CoVs) primarily infect birds and mammals; some of them lead to zoonotic diseases in humans, which has been a public health concern. During the past two decades, several emerging coronaviruses have caused severe diseases to humans and animals, such as Severe Acute Respiratory Syndrome Coronavirus (SARS-CoV) in 2002 (1), Middle East Respiratory Syndrome Coronavirus (MERS-CoV) in 2012 (2), the highly pathogenic PEDV variants in 2013 (3), and SARS-CoV-2 in 2019 (4). To date, the coronavirus disease 2019 (COVID-19) pandemic of SARS-CoV-2 infection

has caused an unprecedented crisis in global healthcare systems (5). Notably, on rare occasions, some CoVs from animals could cross the animal-human species barrier and establish zoonotic diseases in humans. Porcine epidemic diarrhea virus (PEDV) can infect pigs at all ages and cause grievously contagious enteric diseases with a mortality rate of newborn piglets up to 100% (3). The PEDV is a single-stranded positive-sense RNA virus and an alphacoronavirus in the family *Coronaviridae*, order *Nidovirales* (6). This virus contains four major structural proteins: the spike (S) protein, envelope (E) protein, matrix (M) protein, and nucleocapsid (N) proteins (7, 8). The PEDV is usually transmitted by the fecal-oral route, or through the air from the nasal cavity to the intestinal mucosa (9, 10).

As the unique liquid-ordered microenvironments in the plasma membrane, lipid rafts play a critical role in cellular physiological homeostasis during the virus life cycle (11). Lipid rafts are accumulated with cholesterol, which facilitates the maintenance of the tight sphingolipids packaging. Cholesterol depletion by MβCD could cause structural disorder and disorganization of the lipid raft (12). Plasma membrane cholesterol is required for the infection processes of non-enveloped and enveloped viruses. Since CoVs have a lipid envelope, cholesterol biosynthesis (CB) exerts functions in the steps of viral attachment, replication, and assembly (11). Moreover, it is documented that cellular cholesterol is important for PEDV infection *in vitro* (12). Therefore, cholesterol metabolism is a critical pathway for antiviral therapeutics to CoVs. Indeed, cholesterol-lowering drugs like statins and fibrates have been reported to inhibit SARS-CoV-2 infection (13, 14). Cholesterol 25-hydroxylase which is an enzyme to catalyze the oxidized form of cholesterol to 25-hydroxycholesterol is proved to be a natural host restriction factor against PEDV infection (15). On the contrary, a recent study reveals that lower blood concentrations of total cholesterol are correlated with more severe disease and increased mortality in patients with COVID-19 (16). Thus, further investigations are required to fully understand the relationship between cholesterol metabolism and coronavirus infection.

The liver, as the central metabolic organ, is the main site of CB (17, 18). The CB is primarily modulated by the TFs' sterol regulatory element-binding protein 2 (SREBP2) and farnesoid X receptor (FXR) (19–21). When low cholesterol levels are detected in the endoplasmic reticulum, SREBP2 is cleaved, translocated into the cell nucleus, and bound to sterol response elements to activate the expression of enzymes associated with cholesterol biosyntheses, such as 3-hydroxy-3-methylglutaryl-CoA reductase (HMGCR), 3-hydroxy-3-methylglutaryl-CoA synthase (HMGCS), and 24-dehydrocholesterol reductase (DHCR24) (22–24). On the contrary, SREBP2 is inactivated when cholesterol level increases at the cell membrane. Furthermore, cholesterol transformation is critical for maintaining hepatic cholesterol homeostasis. Cholesterol-7a-hydroxylase (CYP7a1) and cholesterol-27a-hydroxylase (CYP27a1) are the main enzymes catalyzing this biotransformation (20). It is modulated by nuclear transcription factor FXR in a negative-feedback loop, similar to that of SREBP2 (21). In recent years, the development of epigenetics provides new insights to solve the mechanism of coronavirus infection (25). Given that CB is valuable for epigenetic modulation of gene transcription involving histones modification (24, 26, 27), it is important to understand whether and, if so, how epigenetic mechanisms control CB in PEDV infection and the genetic networks behind. In this study, we aimed to uncover the mechanism of cholesterol metabolism regulated by PEDV infection in piglets. We found that the binding of SREBP2 and FXR to the locus of key genes in the pathways of cholesterol biosynthesis and cholesterol transformation was suppressed by PEDV infection, which results in failing to activate the expression of those genes at the messenger RNA (mRNA) level. Furthermore, we explored the epigenetic mechanisms involved in the abnormal programming of cholesterol metabolic genes during this alphacoronavirus infection.

RESULTS

Cholesterol Metabolism Is Modulated in Piglet Livers by PEDV Infection

A quantitative reverse transcription PCR (qRT-PCR) assay targeting the PEDV N gene was conducted to detect viral RNA in the jejunum and liver samples collected from both healthy and PEDV-infected piglets. As expected, viral RNA was detected in the jejunum and liver samples of PEDV-infected piglets, but not in those of control piglets (**Figure 1A**). To identify the effect of PEDV infection on the core transcription programs, RNA-seq analysis was performed using the liver tissues of PEDV-infected piglets and control piglets, respectively. The differentially expressed genes in the hepatic transcriptome between the two groups were visualized by a volcano plot. We found that the number of downregulated genes was significantly larger than that of the upregulated genes in the livers of PEDV-infected piglets (**Figure 1B**). the Gene Ontology (GO) analysis of the most downregulated 1,500 transcripts in the livers of PEDV-infected piglets showed that the cholesterol biosynthesis pathway was among the most enriched pathways (**Figure 1C**). The gene-set enrichment analysis (GSEA) also indicated that the hallmarks of the cholesterol-homeostasis pathway were strongly altered by PEDV infection (**Figure 1D**).

The Expression of Genes in the Cholesterol Biosynthesis Pathway vs. the Cholesterol Content in the PEDV-Infected Piglets

It is well-known that at least 21 enzymes are involved in the cholesterol-biosynthesis program to generate cholesterol (**Figure 2A**). Among them, the HMGCR and Squalene Epoxidase (SQLE) are the rate-limiting enzymes to determine the cholesterol synthesis rate and cholesterol level in circulation. The pathway-focused data analysis exhibited that a vast majority of the cholesterol-synthesis genes were strongly downregulated in the PEDV-infected piglets (**Figure 2B**). The transcriptional inhibition of key genes *3-Hydroxy-3-Methylglutaryl-CoA Synthase 1 (HMGCS1), HMGCR, Mevalonate Kinase (MVK), Lanosterol Synthase (LSS), Farnesyl-Diphosphate Farnesyltransferase 1 (FDFT1), SQLE,* and *DHCR24*

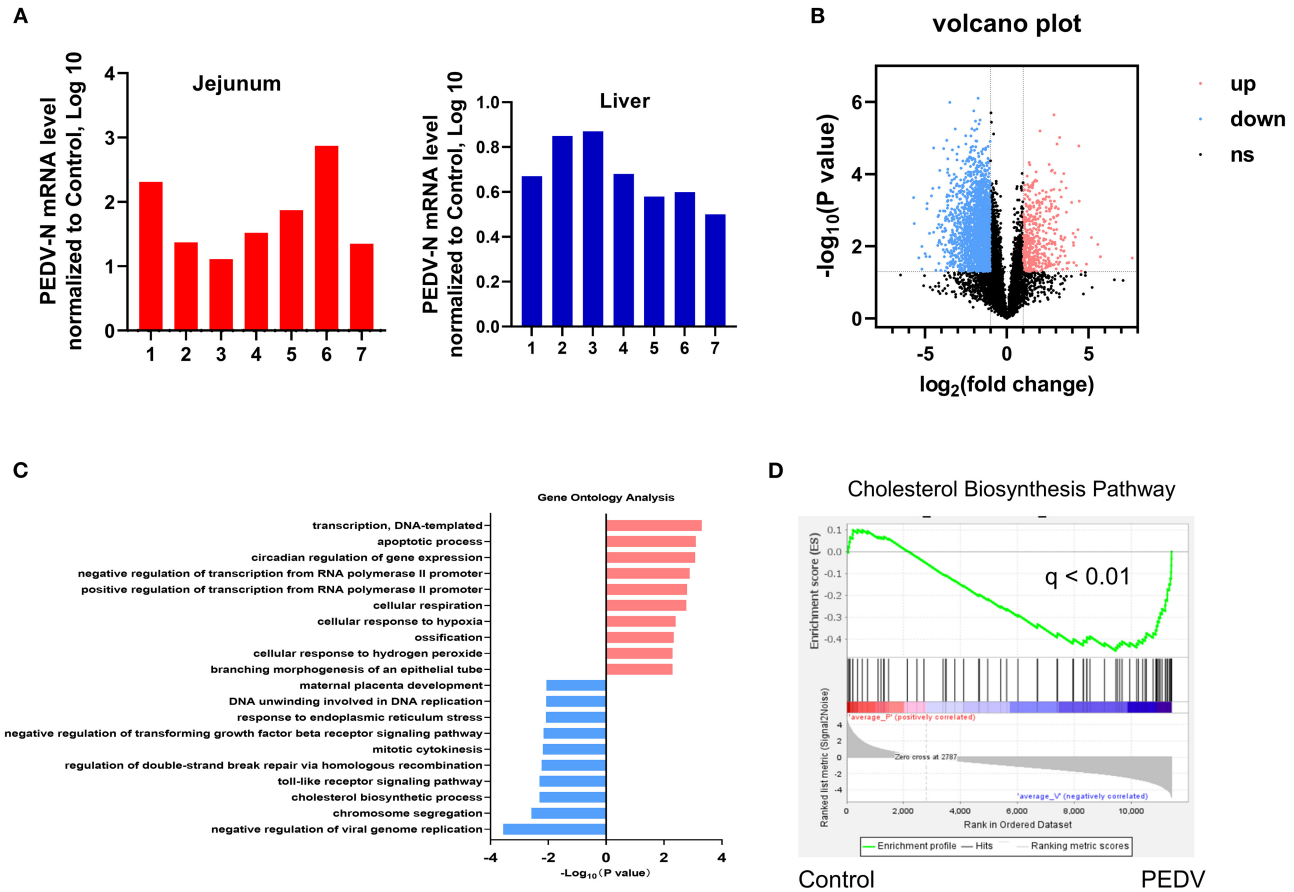

FIGURE 1 | Cholesterol metabolism was modulated by Porcine epidemic diarrhea virus (PEDV) infection indicated by transcriptional profiling of piglet livers. **(A)** PEDV RNA expression was determined by Quantitative Real-Time PCR (qRT-PCR) analysis in the jejunum and liver tissues of PEDV-infected and control piglets. **(B)** Volcano plot visualization of the hepatic transcriptome measured by RNA-seq analysis. **(C)** Genes involved in the cholesterol biosynthesis pathway were among the most enriched pathways based on gene ontology (GO) analysis. **(D)** The gene-set enrichment analysis (GSEA) plot of the differentially expressed genes in the cholesterol biosynthesis pathway of livers from PEDV-infected piglets compared to the controls. False-discovery rate (FDR).

was further validated by the qRT-PCR analysis (**Figure 2C**). Intriguingly, in contrast to the reduced expression of genes in the cholesterol biosynthesis pathway, we found that PEDV infection significantly increased the cholesterol content in the livers (**Figure 2D**). To figure out the incoordination between cholesterol content and the mRNA expression of cholesterol biosynthesis genes, we determined the expression of core enzymes in the CB pathway at the protein level. In agreement with the elevated cholesterol content, the PEDV infection strongly upregulated the expression of the core enzymes at the protein level, including HMGCS1, MVK, Mevalonate Diphosphate Decarboxylase (MVD), FDFT1, SQLE, and DHCR24 (**Figures 3A,B**).

PEDV Infection Modulates the Pathway of Cholesterol Transformation to Bile Acids

Bile acids are the end products of cholesterol catabolism. Herein, we examined the total bile acid (BA) content in the livers of piglets. Consistent with the increased total cholesterol content, the total BA content in the liver was raised in the piglets infected with PEDV (**Figure 4A**). We further determined the expression of the rate-limiting enzymes CYP7A1 and CYP27A1 at the protein level, which represent the classical and alternative pathways of bile acid biosynthesis respectively. In line with liver BA contents, we observed that the alternative pathway was remarkably activated because of the highly CYP27A1 expression at the translational level (**Figures 4B,C**). However, the CYP7A1 protein content was not changed in response to PEDV infection. Similar to genes in the cholesterol biosynthesis pathway, the genes involved in the BAs-biosynthesis pathway was among the most enriched program and was downregulated in the PEDV-infected piglets using GO and GSEA analysis (**Figure 5A**). The pathway-focused results revealed that the key genes functional in cholesterol transformation were strongly downregulated in the PEDV-infected piglets (**Figure 5B**). The transcriptional inhibition of these genes was also validated by the qRT-PCR analysis (**Figure 5C**).

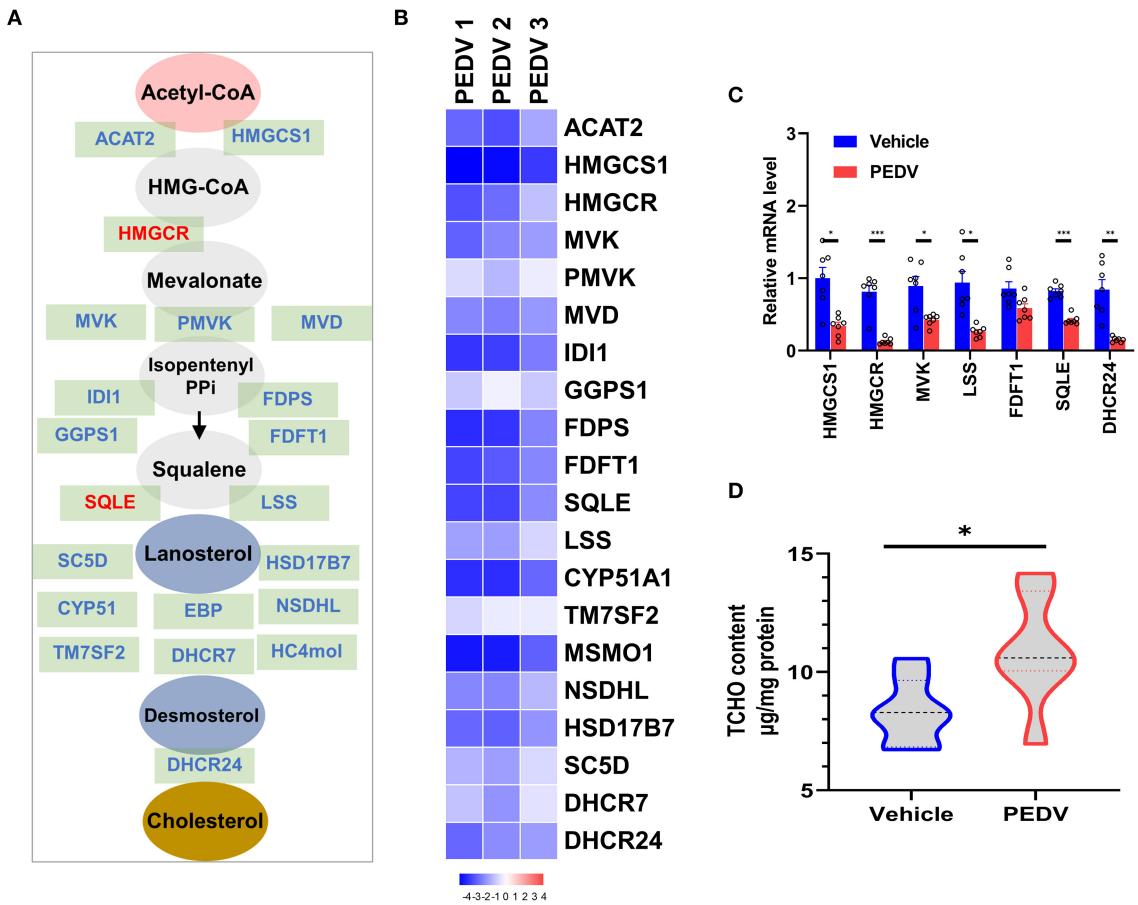

FIGURE 2 | The expression of genes in the cholesterol biosynthesis pathway and cholesterol content in piglet livers. **(A)** The graphic scheme of the cholesterol biosynthesis pathway from acetyl-CoA. The core genes involved in cholesterol biosynthesis were highlighted in blue, while two rate-limiting enzymes 3-hydroxy-3-methylglutaryl-CoA reductase (HMGCR) and SQLE were highlighted in red. **(B)** Heatmap of messenger RNA (mRNA) expression (RNA-seq) changes of the cholesterol biosynthesis genes in the livers of PEDV-infected piglets (log2 transformed, normalized to Control). **(C)** The qRT-PCR analysis confirmed changes of the cholesterol biosynthesis genes in the livers of PEDV-infected piglets. **(D)** Total cellular cholesterol contents in the livers of the control and PEDV-infected piglets were analyzed and normalized to total protein concentrations. The data are shown as the means ± SEM, $^{*}P < 0.05$, $^{**}P < 0.01$, $^{***}P < 0.001$, using the two-tailed Student *t*-test.

PEDV Infection Epigenetically Inhibits SREBP2 and FXR Transcriptional Activation

To maintain cholesterol homeostasis, both cholesterol and bile acids modulate the biosynthesis pathway in a negative-feedback manner by SREBP2 and FXR, respectively. In this regard, we hypothesize that the higher concentrations of cholesterol and bile acids would inhibit the nuclear translocation of these two factors. However, the results of western blot analysis showed that their expression was dramatically elevated in the cell nucleus of the PEDV-infected piglets (**Figures 6A,B**). Therefore, the markedly downregulated gene transcripts would be attributed to the loss of TFs' binding occupancies. Interestingly, the mRNA level of SREBP2 was decreased, while that of FXR was not changed in the PEDV-infected piglets (**Figure 6C**). The potential interactions among SREBP2, FXR, and the key enzymes involved in cholesterol metabolism during transcriptional regulation were predicted by Search Tool for the Retrieval of Interacting Genes (STRING) analysis from the European life-sciences Infrastructure for biological Information (ELIXIR) database (**Figure 7A**). To uncover the mechanism underlying the function of SREBP2 and FXR, we performed a ChIP-qPCR analysis of these two TFs in the livers of the two groups. Indeed, a strong reduction of SREBP2 and FXR binding was observed at promoters of their major targets, including *HMGCS1, HMGCR, MVK, DHCR24,* and *CYP7A1* (**Figures 7B,C**). In concomitant with the loss of TFs' enrichments, the transcriptional activation-linked histone mark Histone H3Ą(acetyl K27) (H3K27ac) and Histone H3 (mono methyl K4) (H3K4me1) were also diminished (**Figures 7D,E**). Collectively, these results implied that in the PEDV-infected piglets, histones modification exerts a pivotal role in inhibiting the expression of genes involved in cholesterol-biosynthesis and transformation *via* blunting the

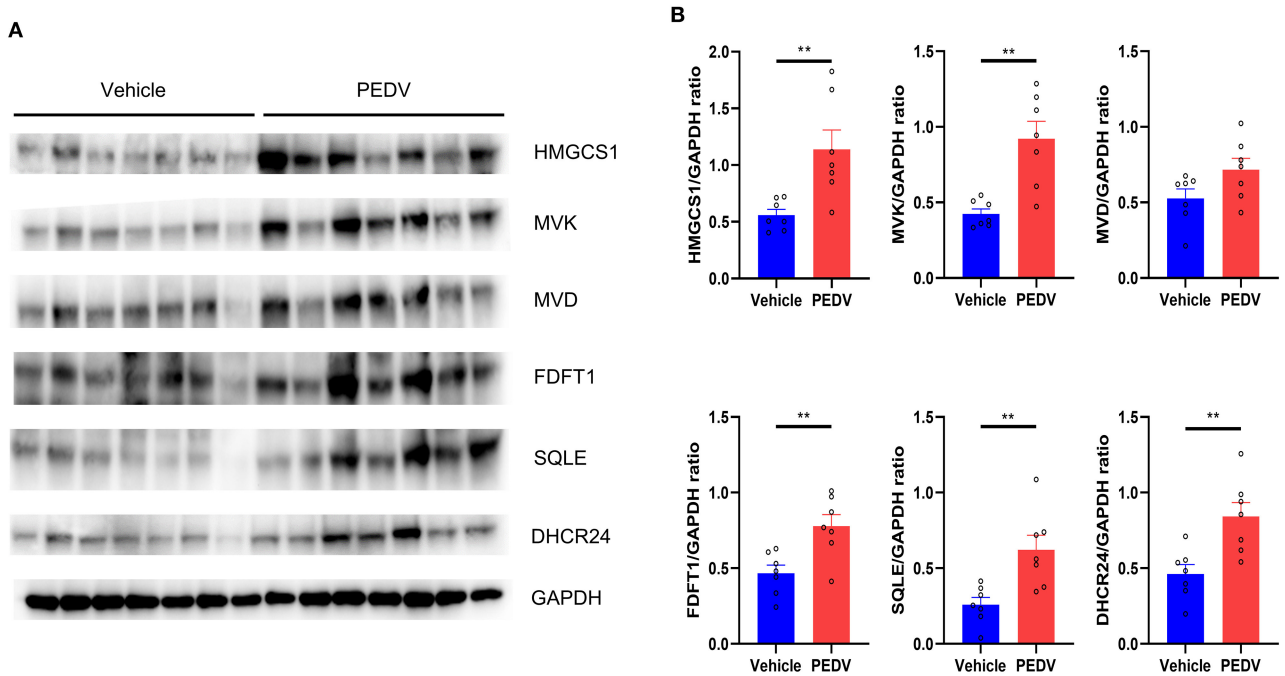

FIGURE 3 | The expression of core genes in the cholesterol biosynthesis pathway was upregulated at the protein level. **(A)** Western blotting analysis was conducted to evaluate the expression of HMGCS, MVK, MVD, FDFT1, SQLE, and 24-dehydrocholesterol reductase (DHCR24). **(B)** The relative expression levels of these genes were normalized to the housekeeping gene GAPDH. The data are shown as the means ± SEM, $n = 7$, $^{**}P < 0.01$, using the two-tailed Student *t*-test.

specific chromatin-DNA binding by two key TFs' SREBP2 and FXR.

DISCUSSION

To date, the coronaviruses have brought numerous illnesses, including enteritis in livestock, upper respiratory diseases in birds, and potentially lethal respiratory infections in humans (28), the epidemiology of PEDV is still extremely significant, with morbidity and mortality rates of piglets up to 100% (29). Despite the classic clinical symptoms of PEDV infection, such as watery diarrhea and vomiting, increasing research now pays more attention to the host physiology and homeostasis, like growth performance alteration, tissue accretion, and organ damages caused by virus infection (30, 31). In this regard, studies on porcine alphacoronaviruses are necessary not only for exploring strategies to control their infection in pig populations but also for understanding the underlying molecular mechanisms. Here, we found that cholesterol and its transformed products were both increased in the livers of the PEDV-infected piglets. This should be attributed to the elevated key enzymes involved in cholesterol metabolism, including HMGCS1, MVK, MVD, FDFT1, SQLE, DHCR24, and CYP27A1. Two main transcription factors, the SREBP2 and FXR, were highly upregulated at the translation level in the cell nucleus. Given the importance of the cholesterol balance, the overt cholesterol contents negatively inhibit the transcripts of the CB and cholesterol transformation pathways reflected by the transcriptomic results. However, this negative-feedback loop did not regulate through the well-known inhibition of the nuclear translocation of SREBP2 and FXR, but *via* the loss of DNA-binding at the transcription stage. We also demonstrated that histone repressive modifications *via* diminishing H3K27ac and H3K4me1 facilitate the trans-inactivation of SREBP2 and FXR.

It is well-known that cholesterol is an essential lipid component of cell membranes, thus, cholesterol depletion blocks the virus entry possibly due to lipid rafts (12). Lipid rafts are sub-domains of the plasma membrane enriched with cholesterol and glycosphingolipids. Often, lipid rafts play a couple of roles during coronavirus infection; for instance, providing the platforms for specific interaction between coronavirus S protein and Angiotensin Converting Enzyme 2 (ACE2) receptor, and facilitating viral endocytosis (12, 32, 33). It is worth noting that the potential functions of cholesterol in the viral entry have been documented for numerous coronaviruses, including SARS-CoV (32), infectious bronchitis (34), murine coronavirus (35), and porcine delta coronavirus (12). Similar to the alphacoronavirus we observed, it is reported that cholesterol accumulation results in virus replication by promoting viral entry. Therefore, it is suggested that high cholesterol content is a critical indicator of coronaviruses infection (11). Alternatively, it is noted that cholesterol exerts a role in virus entry into the host cell when it binds and alters the oligomeric pattern of the N-terminal fusion peptide of the coronavirus S protein (36, 37). The viral mRNA levels were strongly reduced by cholesterol depletion

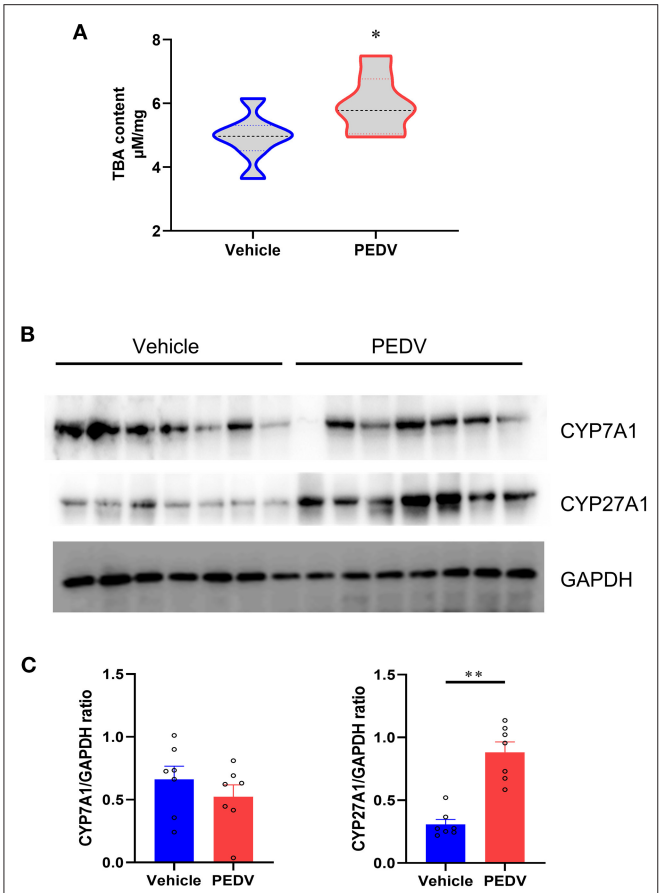

FIGURE 4 | Total bile acids (TBA) content and the expression of genes involved in cholesterol transformation were elevated in livers of PEDV-infected piglets. **(A)** TBA contents in the livers of piglets were analyzed and normalized to total protein concentrations. **(B,C)** Western blotting analysis was performed to evaluate the expression of Cholesterol-7a-hydroxylase (CYP7A1) and cholesterol-27a-hydroxylase (CYP27A1) at the protein level. Based on the intensity of protein bands, the relative expression levels of CYP7A1 and CYP27A1 were determined by normalization to GAPDH. The data are shown as the means ± SEM, $n = 7$, $^{*}P < 0.05$, $^{**}P < 0.01$, using the two-tailed Student *t*-test.

on coronavirus infection (37). Interestingly, ion channels on viral particles are suggested to be involved in cholesterol-driven coronavirus infection because that cholesterol level is crucial for the lipid environment which benefits the charge in cellular membranes (38). Further investigations need to address the interactions between cholesterol and iron metabolism in PEDV infection.

As the central site for cholesterol metabolism, the liver is vital for the equilibrium of cholesterol among organs (26, 39). Although the intestine tissues are the primary sites where PEDV initiates infection, we also detected the mRNA in the liver of PEDV-infected piglets previously (40). Indeed, Wu et al. have revealed that the porcine liver is susceptible to PEDV, and liver damages were reflected by the significantly increased aspartate aminotransferase (AST), alanine aminotransferase (ALT), and AST/ALT ratio (30). Moreover, the PEDV induced the elevated expression of the key proteins involved in liver diseases (41). Cholesterol biosynthesis and transformation are the critical biochemical reactions to maintain metabolic circulation between the liver and the gut (42, 43). We observed that the key enzymes involved in these two pathways are upregulated in the PEDV-infected piglets, while enough cholesterol benefits the entry of PEDV into the hepatic cells. Given the fact that gluconeogenesis is augmented to produce more energy and nutrients to protect the liver and jejunum from virus infection (31), we reasonably thought that the activated CB is attributed to the increasing number of fuels in response to coronavirus invasion. In addition, in agreement with previous findings of coronavirus-triggered hyper-expression (44, 45), the upregulation of SREBP2 and FXR could initiate the activation of the CB pathway in PEDV-infected piglets. Another interesting finding of this study should be the incongruity between the mRNA and protein levels for CYP7A1 and CYP27A1 genes. The CYP7A1was downregulated at the mRNA level but increased at the protein level, while CYP27A1 was increased at the protein level but remained unchanged at the mRNA level. The dissociation of mRNA abundance and protein content implies the possible involvement of post-transcriptional mechanisms. Indeed, our and other previous studies have revealed that CYP7A1 and CYP27A1 are vulnerable to microRNAs-mediated post-transcriptional regulation (20, 46). However, it is still a question whether the dis-association we observed here is attributed to post-transcriptional modification during virus entry, which remains to be clarified in the future.

Despite that cholesterol lowering is a novel potential coronavirus therapeutic strategy, small-molecule inhibitors have previously been studied in the treatment of a variety of respiratory viral infections (47, 48). There is almost no evidence of a direct connection between statins and coronavirus infection. Moreover, several studies have shown that a downtrend in total cholesterol is likely a negative acute phase reactant response (16, 49). We must address that the doses of statin used for the treatment of hypercholesterolemia are generally safe, as we and others claim that cholesterol and bile acids are the special ligands to modulate CB homeostasis. The dramatic inhibition of the cholesterol and cholic biosynthesis genes is a clear manifestation of a strong blockade of the SREBP2/FXR-mediated negative feedback (21). The disconnection between cholesterol metabolic genes expression and SREBP2 has previously been observed in the COVID-19-infected model (44). In the present study, we did not see that PEDV inhibited the translation of SREBP2 protein into the nucleus. However, we mechanistically pointed out that the histone modifications may be the dominant event to suppress the generation of the transcriptional complex, which further reduced the transactivation of genes associated with cholesterol metabolic homeostasis.

In conclusion, the PEDV triggers aberrant regulation of cholesterol metabolic genes *via* epigenetic inhibition of SREBP2/FXR-mediated transcription, which provides a novel antiviral target against PEDV and other coronaviruses.

MATERIALS AND METHODS

Animal Study Design

All experiments involving animals were reviewed and approved by the Institutional Animal Care and Use Committee of Jiangsu Province. Seven Large White piglets, naturally infected with

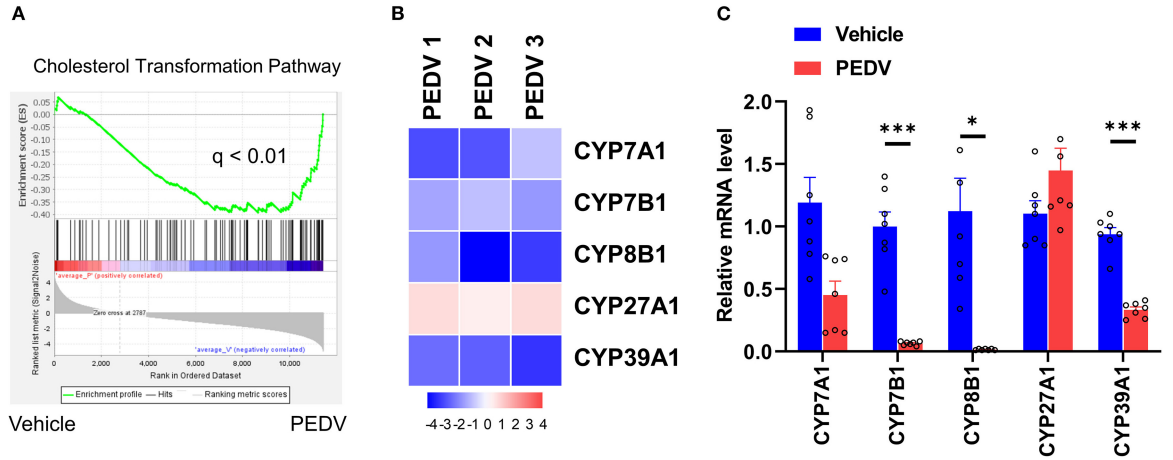

FIGURE 5 | The expression pattern of genes involved in the cholesterol transformation pathway. **(A)** GSEA plots depicting the enrichment of genes in the cholesterol transformation pathway of livers from PEDV-infected piglets compared to the controls. FDR, false-discovery rate. **(B)** Heatmap of mRNA expression (RNA-seq) changes of the genes involved in cholesterol transformation to bile acids in the livers of PEDV-infected piglets (log2 transformed, normalized to Control). **(C)** The qRT-PCR analysis confirmed expression changes of genes in the cholesterol transformation pathway in the livers of PEDV-infected piglets. The data are shown as the means ± SEM, $^{*}P < 0.05$, $^{***}P < 0.001$, using the two-tailed Student *t*-test.

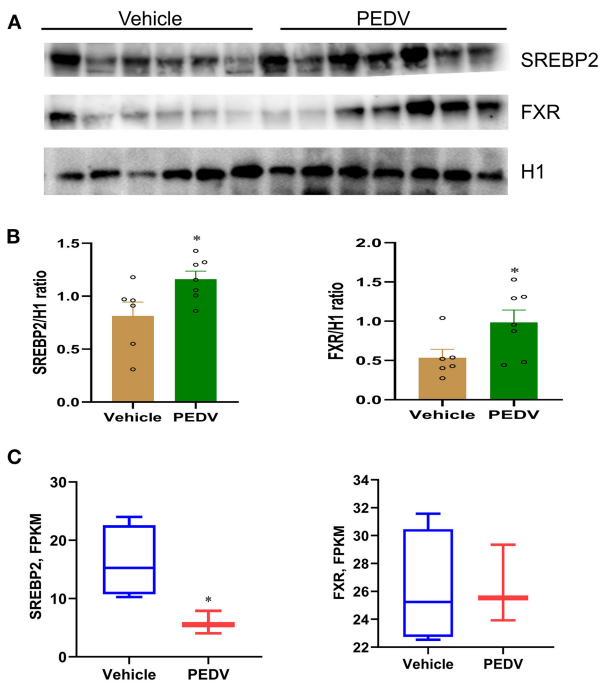

FIGURE 6 | The nuclear expression of SREBP2 and FXR was upregulated in the livers of PEDV-infected piglets. **(A,B)** Western blotting analysis was performed to evaluate the expression of nuclear SREBP2 and FXR at the protein level. Based on the intensity of protein bands, the expression of SREBP2 and FXR were normalized to that of histone H1, $n = 6$–7. **(C)** Graphic summary of mRNA expression of sterol regulatory element-binding protein 2 (SREBP2) and farnesoid X receptor (FXR) by RNA-seq analysis, $n = 3$–4. The data are shown as the means ± SEM, $^{*}P < 0.05$, using the two-tailed Student *t*-test.

PEDV featured with watery diarrhea and acute vomiting, together with seven control piglets as a negative control, were selected. All animals were raised under the same conditions and humanely euthanized for tissue collection. Liver tissues and jejunum tissues were sampled, snap-frozen in liquid nitrogen, and thereafter stored at −80°C until analysis.

Measurement of Total Cholesterol (TCHO) and Total Bile Acids (TBA)

Liver tissues were washed three times with cold phosphate-buffered saline (PBS) and subjected to extraction with organic solvents (7:11:0.1, chloroform/isopropanol/Triton X-100). The TCHO and TBA were measured using the Tissue Total Cholesterol Assay Kit (E1015, Applygen, Beijing, China) and the total Bile Acid Assay Kit (STA-631, Cell Biolabs, Inc., CA, USA), and normalized to total protein concentrations.

RNA-Seq Analysis

The RNA-seq libraries were generated as previously described (17), with modifications. The liver tissues of PEDV-infected piglets ($n = 3$) and control ($n = 4$) piglets were randomly selected and washed with cold PBS and subjected to total cellular RNA extraction. Total RNA (2 μg) was prepared using the Illumina Tru-Seq RNA Sample Prep Kit according to the manufacturer's instructions. The quality of libraries was checked with an Agilent Bioanalyzer (Agilent Technologies, Palo Alto, CA, USA). The high through sequencing was performed on an Illumina HiSeq 2000 sequencer at BGI Tech (Wuhan, China). The sequence data in FASTQ format was analyzed using standard BWA–Bowtie–Cufflinks workflow as described previously (24).

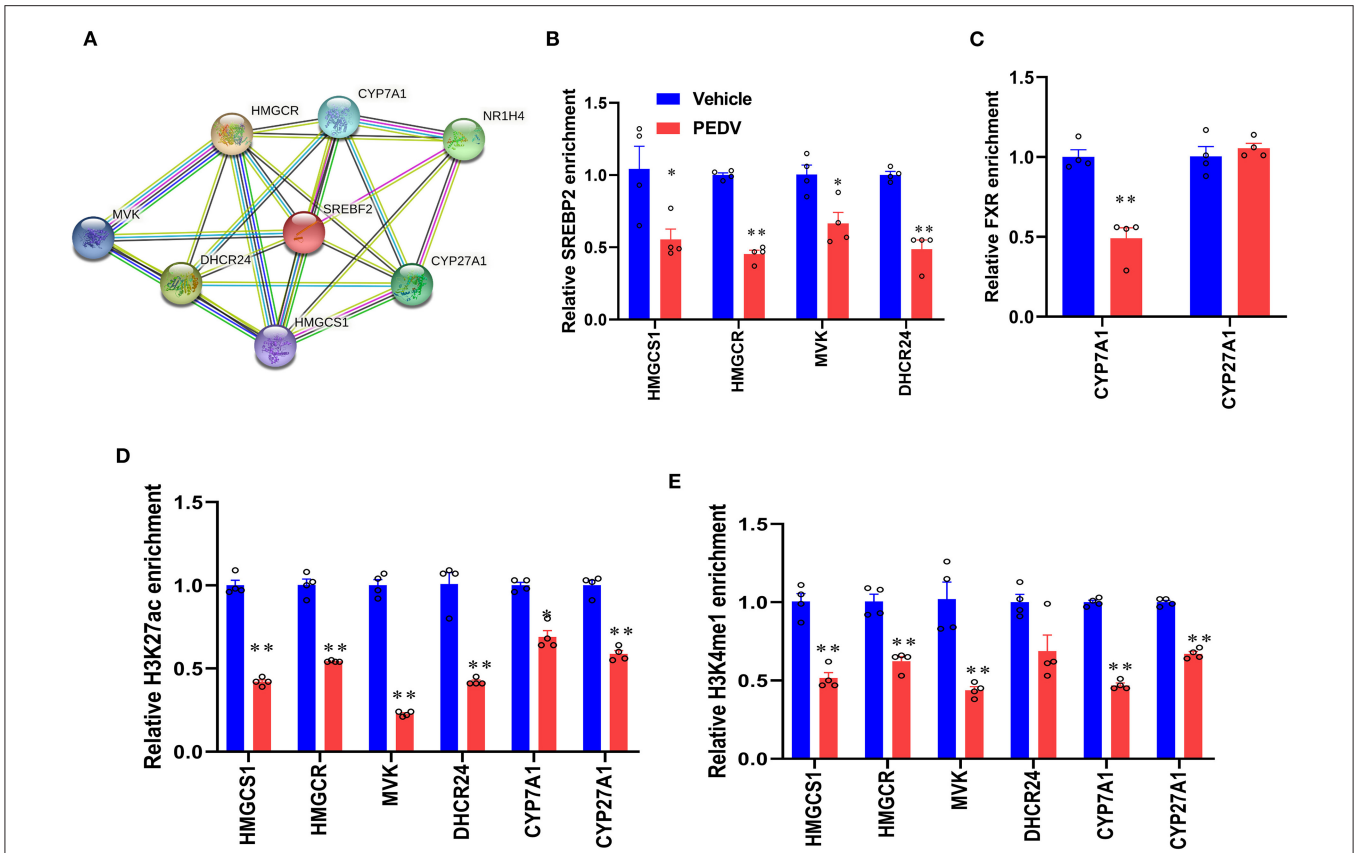

FIGURE 7 | PEDV infection epigenetically inhibited the transcriptional activation of gene expression by SREBP2 and FXR. **(A)** The interactions among SREBP2, FXR, and core proteins involved in cholesterol metabolism during transcriptional regulation were predicted by Search Tool for the Retrieval of Interacting Genes (STRING). **(B,C)** The relative enrichment of SREBP2 and FXR at the locus of indicated genes in livers was analyzed by ChIP-qPCR. **(D,E)** The relative enrichment of histone H3K27ac and H3K4me1 occupancy was analyzed by ChIP-qPCR. The data are shown as the means ± SEM, $^{*}P < 0.05$, $^{**}P < 0.01$ using the two-tailed Student *t*-test.

Briefly, sequence reads were mapped to susScr3 assembly with BWA and Bowtie software. The Cufflinks package was used for transcripts assembly, quantification of normalized gene and isoform expression, and analysis of differentially expressed genes. The Gene Set Enrichment Analysis (GSEA v.3.0) was applied to rank genes based on the shrunken limma log2 fold changes. The GSEA tool was used in the "pre-ranked" model with default parameters. A gene ontology analysis was performed using DAVID Bioinformatics Resources 6.8.

qRT-PCR Analysis

The total RNA extracted from liver tissues of control and PEDV-infected piglets using the TRIzol Reagent (Invitrogen, MA, USA) was reverse-transcribed to single-stranded DNA (cDNA) using the HiScript II Q RT SuperMix (Vazyme biotech, Nanjing, China) according to the manufacturer's instructions. The purity and concentration of total RNA were evaluated by electrophoresis in 1% agarose gel and NanoReady Spectrophotometer (Suizhen, Hangzhou, China). The qRT-PCR analysis was carried out on an ABI QuantStudio 3 Real-Time PCR Instrument (Applied Biosystems) using the SYBR Green Master Mix (Vazyme Biotech, Nanjing, China). The 10 μl reaction mixture contains 5 μl of AceQ qPCR SYBR Green Master Mix (2×),0.2 μl of ROX Reference Dye II (50×), 1 μl of cDNA template,0.2 μl of forward primer (10 μmol/L), and reverse primer (10 μmol/L), and 3.4 μl of ddH_2O. The Glyceraldehyde-3-Phosphate Dehydrogenase (GAPDH) mRNA was detected as an internal reference to normalize the expression level of each transcript. The relative expression levels of indicated genes were calculated using the ΔΔCt method.

Western Blotting Analysis

Liver tissues of PEDV-infected and control piglets were lysed with 500 μl cell lysis buffer for western blotting (Biosharp, Hefei, China) supplemented with phosphatase and protease inhibitor (Beyotime, Nanjing, China) according to the manufacturer's instructions. The tissue debris was removed by centrifugation at 12,000 rpm for 10 min at 4°C, cellular proteins in the supernatant were collected and separated in 10% sodium dodecyl sulfate polyacrylamide gel electropheresis (SDS-PAGE) gel. Next, the separated proteins were transferred to Polyvinylidene Fluoride (PVDF) membranes (Millipore, CA, USA). After being blocked with 5% skimming milk, the membranes were incubated with primary antibodies overnight at 4°C, respectively.

The membranes were further incubated with an Horseradish Peroxidase (HRP)-conjugated secondary antibody. Finally, the membranes were developed with a Chemiluminescent Western Blot Detection kit (Vazyme Biotech, Nanjing, China) using Tanon 5200 Multi imaging system.

The nuclear protein was extracted from a 200 mg frozen liver sample as described previously, with modifications [54]. Briefly, the tissues were washed three times and then lysed with lysis buffer (10 mM N-2-hydroxyethylpiperazine-N-ethanesulphonicacid (HEPES), pH 7.9, 10 mM KCl, 0.1 mM Horseradish Peroxidase (EDTA), 0.4% NP-40, and protease inhibitor cocktail) for 30 min at 4°C. The homogenates were centrifuged for 30 s at 15,000 × g at 4°C. The supernatant was removed. The pellets were lysed in extraction buffer (20 mM HEPES, pH 7.9, 0.4 M NaCl, 1 mM EDTA, and protease inhibitor cocktail) for 15 min for nuclear extract collection.

ChIP-QPCR

The ChIP-qPCR was performed as previously described (26, 27), with modifications. Briefly, the liver tissues of PEDV-infected piglets and control piglets were ground into powders with a mortar, then, resuspended in fixing buffer (50 mmol/L HEPES-KOH (Potassium Hydroxide), 100 mmol/L NaCl, 1 mmol/L EDTA, and 0.5 mol/L Ethylene Glycol Tetraacetic Acid (EGTA)) before being subjected to cross-linking with 1% formaldehyde for 5 min, followed by quenching with glycine on ice for 6 min. The precipitation was collected by centrifugation and resuspended in lysis buffer (50 mmol/L HEPES pH 8, 140 mmol/L NaCl, 1 mmol/L EDTA, 10% glycerol 0.5% NP40, 0.25% Triton X-100). The precipitation was then resuspended in washing buffer (10 mmol/L Tris pH 8, 1 mmol/L EDTA, 0.5 mmol/L EGTA, and 200 mmol/ L NaCl), washed, and resuspended in shearing buffer (0.1% SDS, 1 mmol/L EDTA, pH 8, 10 mmol/L Tris HCl, and pH 8) before sonication using Covaris M220 following the manufacturer's instructions. After being precipitated using gene-specific antibodies and protein G-conjugated beads, the chromatin fragments were treated with RNase A and proteinase K. Then, a purified ChIP DNA was used for qPCR analysis.

Statistical Analysis

Statistical analyses were performed with the GraphPad Prism software 8.0. The data are presented as mean values ± SEM from at least three independent experiments. Statistical analysis was performed using two-tailed Student's *t*-tests or ANOVA with Tukey's *post hoc* test to compare the means. The value of $P < 0.05$ was considered significant.

DATA AVAILABILITY STATEMENT

The datasets presented in this study can be found in online repositories. The names of the repository/repositories and accession number(s) can be found in the article/supplementary material.

ETHICS STATEMENT

The animal study was reviewed and approved by the Animal Care and Use Committee of Yangzhou University (YZUDWSY 2017-09-06).

AUTHOR CONTRIBUTIONS

DC and YL conceptualized the study. H-YL, HG, and HQ contributed to methodology and investigation. H-YL and DC wrote the original draft. H-YL, YL, WB, and DC reviewed and edited the manuscript. DC contributed to funding acquisition and supervision. H-YL, HG, and DC contributed to resources. All authors contributed to the article and approved the submitted version.

FUNDING

This work was supported by the National Natural Science Foundation of China (32002243), Natural Science Foundation of Jiangsu Province (BK20200932), Natural Science Foundation of the Higher Education Institutions of Jiangsu Province (20KJB230001), the Jiangsu Agricultural Science And Technology Innovation Fund [CX(21)2014 and CX(21)3125], and the Priority Academic Program Development of Jiangsu Higher Education Institutions (PAPD).

REFERENCES

1. Peiris JS, Lai ST, Poon LL, Guan Y, Yam LY, Lim W, et al. Coronavirus as a possible cause of the severe acute respiratory syndrome. *Lancet.* (2003) 361:1319–25. doi: 10.1016/S0140-6736(03)13077-2
2. Bermingham A, Chand MA, Brown CS, Aarons E, Tong C, Langrish C, et al. Severe respiratory illness caused by a novel coronavirus, in a patient transferred to the United Kingdom from the Middle East, September 2012. *Euro Surveill.* (2012) 17:20290. doi: 10.2807/ese.17.40.20290-en
3. Huang YW, Dickerman AW, Pineyro P, Li L, Fang L, Kiehne R, et al. evolution, and genotyping of emergent porcine epidemic diarrhea virus strains in the United States. *MBio.* (2013) 4:e00737–13. doi: 10.1128/mBio.00737-13
4. Hui DS, Azhar EI, Madani TA, Ntoumi F, Kock R, Dar O, et al. The continuing 2019-nCoV epidemic threat of novel coronaviruses to global health - The latest 2019 novel coronavirus outbreak in Wuhan, China. *Int J Infect Dis.* (2020) 91:264–6. doi: 10.1016/j.ijid.2020.01.009
5. Aleem A, Samad ABA, Slenker AK. *Emerging Variants of SARS-CoV-2 And Novel Therapeutics Against Coronavirus (COVID-19).* Treasure Island (FL): StatPearls. (2022).
6. Liu C, Ma Y, Yang Y, Zheng Y, Shang J, Zhou Y, et al. Cell entry of porcine epidemic diarrhea coronavirus is activated by lysosomal proteases. *J Biol Chem.* (2016) 291:24779–86. doi: 10.1074/jbc.M116.740746
7. Song D, Park B. Porcine epidemic diarrhoea virus: a comprehensive review of molecular epidemiology, diagnosis, and vaccines. *Virus Genes.* (2012) 44:167–75. doi: 10.1007/s11262-012-0713-1

8. Jung K, Saif LJ. Porcine epidemic diarrhea virus infection: etiology, epidemiology, pathogenesis and immunoprophylaxis. *Vet J.* (2015) 204:134–43. doi: 10.1016/j.tvjl.2015.02.017
9. Suzuki T, Shibahara T, Yamaguchi R, Nakade K, Yamamoto T, Miyazaki A, et al. Pig epidemic diarrhoea virus S gene variant with a large deletion non-lethal to colostrum-deprived newborn piglets. *J Gen Virol.* (2016) 97:1823–8. doi: 10.1099/jgv.0.000513
10. Li Y, Wu Q, Huang L, Yuan C, Wang J, Yang Q. An alternative pathway of enteric PEDV dissemination from nasal cavity to intestinal mucosa in swine. *Nat Commun.* (2018) 9:3811. doi: 10.1038/s41467-018-06056-w
11. Baglivo M, Baronio M, Natalini G, Beccari T, Chiurazzi P, Fulcheri E, et al. Natural small molecules as inhibitors of coronavirus lipid-dependent attachment to host cells: a possible strategy for reducing SARS-COV-2 infectivity? *Acta Biomed.* (2020) 91:161–4.
12. Jeon JH, Lee C. Cellular cholesterol is required for porcine nidovirus infection. *Arch Virol.* (2017) 162:3753–67. doi: 10.1007/s00705-017-3545-4
13. K. Buschard. Fenofibrate increases the amount of sulfatide which seems beneficial against Covid-19. *Med Hypotheses.* (2020) 143:110127. doi: 10.1016/j.mehy.2020.110127
14. Orlowski S, Mourad JJ, Gallo A, Bruckert E. Coronaviruses, cholesterol and statins: Involvement and application for Covid-19. *Biochimie.* (2021) 189:51–64. doi: 10.1016/j.biochi.2021.06.005
15. Zhang Y, Song Z, Wang M, Lan M, Zhang K, Jiang P, et al. Cholesterol 25-hydroxylase negatively regulates porcine intestinal coronavirus replication by the production of 25-hydroxycholesterol. *Vet Microbiol.* (2019) 231:129–38. doi: 10.1016/j.vetmic.2019.03.004
16. Zinellu A, Paliogiannis P, Fois AG, Solidoro P, Carru C, Mangoni AA. Cholesterol triglyceride concentrations. COVID-19 severity, and mortality: a systematic review and meta-analysis with meta-regression. *Front Public Health.* (2021) 9:705916. doi: 10.3389/fpubh.2021.705916
17. Liu HY, Gu H, Li Y, Hu P, Yang Y, Li K, et al. Dietary conjugated linoleic acid modulates the hepatic circadian clock program via pparalpha/rev-erbalpha-mediated chromatin modification in mice. *Front Nutr.* (2021) 8:711398. doi: 10.3389/fnut.2021.711398
18. Cai D, Li Y, Zhang K, Zhou B, Guo F, Holm L, et al. Co-option of PPARalpha in the regulation of lipogenesis and fatty acid oxidation in CLA-induced hepatic steatosis. *J Cell Physiol.* (2021) 236:4387–402. doi: 10.1002/jcp.30157
19. Miyata M, Tanaka T, Takahashi K, Funaki A, Sugiura Y. Cholesterol-lowering effects of taurine through the reduction of ileal FXR signaling due to the alteration of ileal bile acid composition. *Amino Acids.* (2021) 53:1523–32. doi: 10.1007/s00726-021-03068-7
20. Cai D, Jia Y, Lu J, Yuan M, Sui S, Song H, et al. Maternal dietary betaine supplementation modifies hepatic expression of cholesterol metabolic genes via epigenetic mechanisms in newborn piglets. *Br J Nutr.* (2014) 112:1459–68. doi: 10.1017/S0007114514002402
21. Xu Y, Li F, Zalzala M, Xu J, Gonzalez FJ, Adorini L, et al. Farnesoid X receptor activation increases reverse cholesterol transport by modulating bile acid composition and cholesterol absorption in mice. *Hepatology.* (2016) 64:1072–85. doi: 10.1002/hep.28712
22. R. Sato. Sterol metabolism and SREBP activation. *Arch Biochem Biophys.* (2010) 501:177–81. doi: 10.1016/j.abb.2010.06.004
23. Vallett SM, Sanchez HB, Rosenfeld JM, Osborne TF. A direct role for sterol regulatory element binding protein in activation of 3-hydroxy-3-methylglutaryl coenzyme A reductase gene. *J Biol Chem.* (1996) 271:12247–53. doi: 10.1074/jbc.271.21.12247
24. Cai D, Wang J, Gao B, Li J, Wu F, Zou JX, et al. RORγ is a targetable master regulator of cholesterol biosynthesis in a cancer subtype. *Nat Commun.* (2019) 10:4621. doi: 10.1038/s41467-019-12529-3
25. Chlamydas S, Papavassiliou AG, Piperi C. Epigenetic mechanisms regulating COVID-19 infection. *Epigenetics.* (2021) 16:263–70. doi: 10.1080/15592294.2020.1796896
26. Li K, Li H, Zhang K, Zhang J, Hu P, Li Y, et al. Orphan nuclear receptor rorgamma modulates the genome-wide binding of the cholesterol metabolic genes during mycotoxin-induced liver injury. *Nutrients.* (2021) 13. doi: 10.3390/nu13082539
27. Zhang K, Li H, Xin Z, Li Y, Wang X, Hu Y, et al. Time-restricted feeding downregulates cholesterol biosynthesis program via RORgamma-mediated chromatin modification in porcine liver organoids. *J Anim Sci Biotechnol.* (2020) 11:106. doi: 10.1186/s40104-020-00511-9
28. Fehr AR, Perlman S. Coronaviruses: an overview of their replication and pathogenesis. *Methods Mol Biol.* (2015) 1282:1–23. doi: 10.1007/978-1-4939-2438-7_1
29. Pan Y, Tian X, Li W, Zhou Q, Wang D, Bi Y, et al. Isolation and characterization of a variant porcine epidemic diarrhea virus in China. *Virol J.* (2012) 9:195. doi: 10.1186/1743-422X-9-195
30. Wu M, Yi D, Zhang Q, Wu T, Yu K, Peng M, et al. Puerarin enhances intestinal function in piglets infected with porcine epidemic diarrhea virus. *Sci Rep.* (2021) 11:6552. doi: 10.1038/s41598-021-85880-5
31. Curry SM, Burrough ER, Schwartz KJ, Yoon KJ, Lonergan SM, Gabler NK. Porcine epidemic diarrhea virus reduces feed efficiency in nursery pigs. *J Anim Sci.* (2018) 96:85–97. doi: 10.1093/jas/skx005
32. Lu Y, Liu DX, Tam JP. Lipid rafts are involved in SARS-CoV entry into Vero E6 cells. *Biochem Biophys Res Commun.* (2008) 369:344–9. doi: 10.1016/j.bbrc.2008.02.023
33. Li GM, Li YG, Yamate M, Li SM, Ikuta K. Lipid rafts play an important role in the early stage of severe acute respiratory syndrome-coronavirus life cycle. *Microbes Infect.* (2007) 9:96–102. doi: 10.1016/j.micinf.2006.10.015
34. Guo H, Huang M, Yuan Q, Wei Y, Gao Y, Mao L, et al. The important role of lipid raft-mediated attachment in the infection of cultured cells by coronavirus infectious bronchitis virus beaudette strain. *PLoS ONE.* (2017) 12:e0170123. doi: 10.1371/journal.pone.0170123
35. Choi KS, Aizaki H, Lai MM. Murine coronavirus requires lipid rafts for virus entry and cell-cell fusion but not for virus release. *J Virol.* (2005) 79:9862–71. doi: 10.1128/JVI.79.15.9862-9871.2005
36. Katsiki N, Banach M, Mikhailidis DP. Lipid-lowering therapy and renin-angiotensin-aldosterone system inhibitors in the era of the COVID-19 pandemic. *Arch Med Sci.* (2020) 16:485–9. doi: 10.5114/aoms.2020.94503
37. Meher G, Bhattacharjya S, Chakraborty H. Membrane cholesterol modulates oligomeric status and peptide-membrane interaction of severe acute respiratory syndrome coronavirus fusion peptide. *J Phys Chem B.* (2019) 123:10654–62. doi: 10.1021/acs.jpcb.9b08455
38. Chang HM, Reitstetter R, Gruener R. Lipid-ion channel interactions: increasing phospholipid headgroup size but not ordering acyl chains alters reconstituted channel behavior. *J Membr Biol.* (1995) 145:13–9. doi: 10.1007/BF00233303
39. Cai D, Yuan M, Liu H, Pan S, Ma W, Hong J, et al. Maternal betaine supplementation throughout gestation and lactation modifies hepatic cholesterol metabolic genes in weaning piglets via AMPK/LXR-mediated pathway and histone modification. *Nutrients.* (2016) 8. doi: 10.3390/nu8100646
40. Park JE, Shin HJ. Porcine epidemic diarrhea virus infects and replicates in porcine alveolar macrophages. *Virus Res.* (2014) 191:143–52. doi: 10.1016/j.virusres.2014.07.038
41. Ye Y, Zhu J, Ai Q, Wang C, Liao M, Fan H. Quantitative proteomics reveals changes in vero cells in response to porcine epidemic diarrhea virus. *J Proteome Res.* (2019) 18:1623–33. doi: 10.1021/acs.jproteome.8b00897
42. Xu J, Li X, Yao X, Xie S, Chi S, Zhang S, et al. Protective effects of bile acids against hepatic lipid accumulation in hybrid grouper fed a high-lipid diet. *Front Nutr.* (2022) 9:813249. doi: 10.3389/fnut.2022.813249
43. Joyce SA, Kamil A, Fleige L, Gahan CGM. The cholesterol-lowering effect of oats and oat beta glucan: modes of action and potential role of bile acids and the microbiome. *Front Nutr.* (2019) 6:171. doi: 10.3389/fnut.2019.00171
44. Lee W, Ahn JH, Park HH, Kim HN, Kim H, Yoo Y, et al. COVID-19-activated SREBP2 disturbs cholesterol biosynthesis and leads to cytokine storm. *Signal Transduct Target Ther.* (2020) 5:186. doi: 10.1038/s41392-020-00292-7
45. Brevini T, Maes M, Webb G, Gelson WTH, Forrest S, Mlcochova P, et al. Fxr as a New Therapeutic Target for Covid-19. *Hepatology.* (2021) 74:318a—318a.
46. Charvet CD, Laird J, Xu Y, Salomon RG, Pikuleva IA. Posttranslational modification by an isolevuglandin diminishes activity of the mitochondrial cytochrome P450 27A1. *J Lipid Res.* (2013) 54:1421–9. doi: 10.1194/jlr.M035790

47. D.S. Fedson. Pandemic influenza: a potential role for statins in treatment and prophylaxis. *Clin Infect Dis.* (2006) 43:199–205. doi: 10.1086/505116
48. Henry C, Zaizafoun M, Stock E, Ghamande S, Arroliga AC, White HD. Impact of angiotensin-converting enzyme inhibitors and statins on viral pneumonia. *Proc (Bayl Univ Med Cent).* (2018) 31:419–23. doi: 10.1080/08998280.2018.1499293
49. Wei X, Zeng W, Su J, Wan H, Yu X, Cao X, et al. Hypolipidemia is associated with the severity of COVID-19. *J Clin Lipidol.* (2020) 14:297–304. doi: 10.1016/j.jacl.2020.04.008

Conflict of Interest: The authors declare that the research was conducted in the absence of any commercial or financial relationships that could be construed as a potential conflict of interest.

Publisher's Note: All claims expressed in this article are solely those of the authors and do not necessarily represent those of their affiliated organizations, or those of the publisher, the editors and the reviewers. Any product that may be evaluated in this article, or claim that may be made by its manufacturer, is not guaranteed or endorsed by the publisher.

frontiers in Nutrition

BRIEF RESEARCH REPORT
published: 28 March 2022
doi: 10.3389/fnut.2022.831879

Hepatic PPARα Is Destabilized by SIRT1 Deacetylase in Undernourished Male Mice

Ji Ho Suh[1], Kang Ho Kim[2], Margaret E. Conner[3], David D. Moore[4] and Geoffrey A. Preidis[1]**

[1] Division of Gastroenterology, Hepatology and Nutrition, Department of Pediatrics, Baylor College of Medicine and Texas Children's Hospital, Houston, TX, United States, [2] Department of Anesthesiology, McGovern Medical School, The University of Texas Health Science Center at Houston, Houston, TX, United States, [3] Department of Molecular Virology and Microbiology, Department of Education, Innovation and Technology, Baylor College of Medicine, Houston, TX, United States, [4] Department of Nutritional Sciences and Toxicology, University of California, Berkeley, Berkeley, CA, United States*

The nutrient sensing nuclear receptor peroxisome proliferator-activated receptor-α (PPARα) regulates the host response to short-term fasting by inducing hepatic transcriptional programming of ketogenesis, fatty acid oxidation and transport, and autophagy. This adaptation is ineffective in chronically undernourished individuals, among whom dyslipidemia and hepatic steatosis are common. We recently reported that hepatic PPARα protein is profoundly depleted in male mice undernourished by a low-protein, low-fat diet. Here, we identify PPARα as a deacetylation target of the NAD-dependent deacetylase sirtuin-1 (SIRT1) and link this to the decrease in PPARα protein levels in undernourished liver. Livers from undernourished male mice expressed high levels of SIRT1, with decreased PPARα acetylation and strongly decreased hepatic PPARα protein. In cultured hepatocytes, PPARα protein levels were decreased by transiently transfecting constitutively active SIRT1 or by treating cells with the potent SIRT1 activator resveratrol, while silencing SIRT1 increased PPARα protein levels. SIRT1 expression is correlated with increased PPARα ubiquitination, suggesting that protein loss is due to proteasomal degradation. In accord with these findings, the dramatic loss of hepatic PPARα in undernourished male mice was completely restored by treating mice with the proteasome inhibitor bortezomib. Similarly, treating undernourished mice with the SIRT1 inhibitor selisistat/EX-527 completely restored hepatic PPARα protein. These data suggest that induction of SIRT1 in undernutrition results in hepatic PPARα deacetylation, ubiquitination, and degradation, highlighting a new mechanism that mediates the liver's failed adaptive metabolic responses in chronic undernutrition.

Keywords: undernutrition, PPARα (peroxisome proliferator-activated receptor alpha), sirtuin-1 (SIRT1), post-translational modification of proteins, mouse models, sex differences

OPEN ACCESS

Edited by:
Demin Cai,
Yangzhou University, China

Reviewed by:
Wei Zhong,
University of North Carolina at Greensboro, United States
Hyunbae Kim,
Wayne State University, United States

****Correspondence:***
David D. Moore
daviddmoore@berkeley.edu
Geoffrey A. Preidis
geoffrey.preidis@bcm.edu

Specialty section:
This article was submitted to Nutrition and Metabolism, a section of the journal Frontiers in Nutrition

Received: *09 December 2021*
Accepted: *10 February 2022*
Published: *28 March 2022*

Citation:
Suh JH, Kim KH, Conner ME, Moore DD and Preidis GA (2022) Hepatic PPARα Is Destabilized by SIRT1 Deacetylase in Undernourished Male Mice. Front. Nutr. 9:831879. doi: 10.3389/fnut.2022.831879

INTRODUCTION

The peroxisome proliferator-activated receptor (PPAR) family of lipid sensing transcription factors regulates whole-body metabolism and energy balance. The dominant PPAR isoform in human and mouse liver is PPARα, which promotes the adaptive response to short-term fasting by regulating the expression of genes that facilitate ketogenesis, fatty acid oxidation and transport, and nutrient reclamation *via* autophagy (1, 2). However, in chronic undernutrition this adaptation is ineffective, and metabolic abnormalities including dyslipidemia

and hepatic steatosis occur (3, 4). Steatosis, decreased hepatic peroxisome abundance, and impaired fatty acid oxidation are observed in rats chronically undernourished by a low-protein diet; these abnormalities are partially ameliorated by a PPARα agonist, suggesting a lack of PPARα signaling in chronic undernutrition (5). We recently confirmed that hepatic PPARα protein levels are dramatically reduced in chronically undernourished mice fed a low-protein, low-fat diet (LPLFD) (6). Mechanisms by which chronic undernutrition decreases hepatic PPARα protein levels have not been defined.

PPARα expression is thought to be regulated primarily at the mRNA level. Consistent with impaired hepatic fatty acid oxidation in non-alcoholic steatohepatitis (NASH), mRNA expression of *PPARA* is decreased in liver biopsies obtained from patients with NASH and inversely correlates with the severity of steatosis (7). Similarly, livers from patients infected with hepatitis C virus reveal profoundly decreased expression of PPARα at the transcriptional and protein levels (8–11). Mechanisms of transcriptional repression of PPARα by interleukin-6 (12), interleukin-1β (13), and tumor necrosis factor-α (14), as well as silencing by numerous micro-RNAs (15–18) have been described. In contrast, post-translational regulation of PPARα protein stability is poorly understood.

This study aimed to identify mechanisms underlying the dramatic loss of hepatic PPARα protein in undernutrition. Our data reveal that undernutrition induces the expression of sirtuin-1 (SIRT1), a NAD-dependent deacetylase that is known to decrease levels of other nuclear receptors including PPARγ by proteasome-mediated degradation. We identify PPARα as a novel target for SIRT1-mediated deacetylation, ubiquitination, and proteasomal degradation, and demonstrate that hepatic PPARα protein levels can be rescued in undernourished mice by inhibiting SIRT1. These results suggest SIRT1 inhibition as a potential therapy for undernutrition-induced liver and metabolic dysfunction.

MATERIALS AND METHODS

Animal Studies

Wild-type C57BL/6J mice (Charles River Laboratories, Wilmington, MA) were housed in the Baylor College of Medicine Center for Comparative Medicine in a temperature-controlled 14:10-h light–dark room. Dams with 8-day-old pups were randomized to receive a purified LPLFD (5% fat, 7% protein, and 88% carbohydrate) or an isocaloric control diet (15% fat, 20% protein, and 65% carbohydrate; #D09081701B and #D09051102, Research Diets, New Brunswick, NJ) *ad libitum* to model undernutrition (19). On day-of-life 21, pups were weaned to their respective dams' diets and continued on the LPLFD or control diet *ad libitum* for the remainder of the experiment.

Hepatic PPARα was manipulated in 8 week old male mice maintained on either diet by giving intraperitoneal injections of the SIRT1 inhibitor selisistat/EX-527 (#E7034, Sigma-Aldrich, St. Louis, MO), 10 mg/kg/day for 3 consecutive days. Alternatively, mice received a single intraperitoneal injection of 1 mg/kg of the proteasome inhibitor bortezomib (#2204, Cell Signaling Technology, Danvers, MA). Control groups for both experiments received equivalent volumes of sterile PBS. After 24 h, mice were euthanized by CO_2 inhalation. Liver lobes were harvested and stored at −80°C prior to analysis. All animal experiments were conducted in accordance with the Baylor College of Medicine Institutional Animal Care and Use Committee guidelines.

Cell Culture and Transient Transfection

HepG2 cells (American Type Culture Collection, Manassas, VA) were maintained in Dulbecco's modified Eagle's medium supplemented with 10% fetal bovine serum (Thermo Fisher Scientific, Waltham, MA) in 12- or 24-well-plates. Cells were transfected with expression vectors for wild type or H363Y mutant (dominant negative) human SIRT1 (#1791 and 1792, Addgene, Waltham, MA) (20) or an equivalent amount of empty expression vector, using FuGENE HD Transfection Reagent (Promega, Madison, WI) according to the manufacturer's protocol. Alternatively, cells were transfected with 100 nM SIRT1 siRNA or control siRNA (#12241S and 6568S, Cell Signaling Technology, Danvers, MA) using Lipofectamine RNAiMAX Transfection Reagent (Invitrogen, Waltham, MA) according to the manufacturer's instructions. Cells were harvested 24–36 h following transfection. Alternatively, 100 μM resveratrol (#1418, Tocris, Bristol, UK) or an equivalent volume of sterile water was added to cultures, and cells were harvested 24 h later.

Western Blot

Liver tissue was homogenized in RIPA buffer. Lysate (20–50 μg) was loaded onto NuPAGE 4–12% Bis-Tris precast gels and transferred onto PVDF Transfer Membranes (Thermo Fisher Scientific, Waltham, MA). Primary antibodies to PPARα (#PA5-85125, Thermo Fisher Scientific, Waltham, MA), SIRT1 (#2028, Cell Signaling Technology, Danvers, MA), PPARγ (#16643-1-AP, Thermo Fisher Scientific, Waltham, MA), or the proteasome marker PSMB5 (# PA1-977, Thermo Fisher Scientific, Thermo Fisher Scientific, Waltham, MA) were applied. For HepG2 cell experiments, primary antibodies to PPARα (#MA1-822, Thermo Fisher Scientific, Waltham, MA) and SIRT1 #9475 (Cell Signaling Technology, Danvers, MA) were used. GAPDH (#14C10, Cell Signaling Technology, Danvers, MA) served as a housekeeping protein for all western blots. Horseradish peroxidase-conjugated secondary antibodies were applied and protein was visualized with Chemiluminescent Substrate (Thermo Fisher Scientific, Waltham, MA) on the Amersham Imager 600 (GE Healthcare Life Sciences, Marlborough, MA).

Acetylation and Ubiquitination Assays

Immunoprecipitation was performed by incubating 400 μg liver or cell lysate with 2 μg anti-PPARα antibody (#MA1-822, Thermo Fisher Scientific, Waltham, MA) or anti-PPARγ antibody (#MA5-14889, Thermo Fisher Scientific, Waltham, MA) and Protein A/G beads (Santa Cruz Biotechnology, Santa Cruz, CA) for 12 h at 4°C. Antibody-conjugated beads were washed three times with RIPA buffer at 4°C, then PPAR protein was eluted in protein loading buffer and analyzed by SDS-PAGE. Western blot analysis was performed using antibodies to acetylated lysine (#9441, Cell Signaling Technology, Danvers, MA) or ubiquitin (#58395, Cell Signaling Technology, Danvers, MA).

Real-Time Quantitative Polymerase Chain Reaction

Total RNA was isolated from 30 to 50 mg liver or cultured hepatocytes using TRIzol Reagent (Invitrogen, Carlsbad, CA) and quantified with a NanoDrop 2000c spectrophotometer (Thermo Fisher Scientific, Waltham, MA). Complementary DNA was synthesized from 1 μg RNA using amfiRivert cDNA Synthesis Platinum Master Mix (GenDEPOT, Inc., Katy, TX). SYBR Green PCR Master Mix (Thermo Fisher Scientific, Waltham, MA) was used on the StepOnePlus Real-Time PCR System (Applied Biosystems, Foster City, CA). Relative expression level to GAPDH was calculated by the comparative cycle threshold (ΔΔCt) method. The following primer sequences were used:

Mouse SIRT1 F-5′-CGGCTACCGAGGTCCATATAC-3′ R-5′-CAGCTCAGGTGGAGGAATTGT-3′

Mouse PPARα F-5′-ACAAGGCCTCAGGGTACCA-3′ R-5′-GCCGAAAGAAGCCCTTACAG-3′

Human SIRT1 F-5′-TGGCAAAGGAGCAGATTAGTAGG-3′ R-5′-CTGCCACAAGAACTAGAGGATAAGA-3′

Human PPARα F-5′-CTATCATTTGCTGTGGAGATCG-3′ R-5′-AAGATATCGTCCGGGTGGTT-3′

Statistics

All data were normally distributed, thus results are presented as mean ± SD. For experiments consisting of two groups, the 2-tailed student *t*-test was used. For experiments involving more than 2 treatment groups, 1-way analysis of variance (ANOVA) was performed, and when the global test was significant ($P < 0.05$), *post-hoc* Sidak's multiple comparisons test was used to determine between-group differences. Calculations were made using Prism 9.2.0 (GraphPad Software, San Diego, CA).

RESULTS

Undernourished Male Mice Have Reduced Hepatic PPARα Protein Levels Despite Increased PPARα Transcript

We recently reported that undernutrition dramatically decreases hepatic concentrations of the nuclear receptor PPARα in male mice (6). This effect is not observed in female mice, which have low hepatic PPARα protein expression at baseline (**Figure 1**). In this study, we sought to identify mechanisms to account for this ∼85% decrease in hepatic PPARα protein ($P < 0.0001$; **Figure 2A**) in undernourished males. In contrast to expectations that PPARα levels are regulated primarily at the transcriptional level (21), qPCR showed a 1.5-fold compensatory increase in *Ppara* transcript in undernourished livers ($P = 0.006$; **Figure 2A**), leading us to consider post-transcriptional mechanisms of PPARα protein loss.

Induction of SIRT1 Corresponds With PPARα Deacetylation in Undernourished Livers

SIRT1 binds to and deacetylates multiple members of the nuclear receptor family of transcription factors. Deacetylation of PPARγ (22), farnesoid-X-receptor (23), liver X receptor-α (24), or thyroid receptor-β1 (25) in response to SIRT1 overexpression results in reduced levels of deacetylated nuclear receptors *via* ubiquitin-mediated proteasomal degradation. Although SIRT1 is known to interact directly with PPARα (26), whether this interaction results in PPARα deacetylation and degradation, and also whether SIRT1 is overexpressed in chronic undernutrition, was unknown. We used western blot and qPCR to determine expression levels of SIRT1 in liver from control and undernourished male mice. Livers from undernourished mice showed 2.4-fold increased expression of SIRT1 protein ($P = 0.007$) and 2.8-fold increased expression of *Sirt1* transcript ($P = 0.004$; **Figure 2B**). Next, we used co-immunoprecipitation to confirm that PPARα and SIRT1 directly interact in undernourished mouse livers (**Figure 2C**). These findings led us to explore whether increased hepatic expression of SIRT1 in undernutrition is a potential cause of PPARα protein degradation.

To determine whether PPARα deacetylation mechanistically links increased SIRT1 expression with decreased PPARα protein in the chronically undernourished liver, we purified PPARα by immunoprecipitation, then quantified the relative amount of acetylation using comparable amounts of total immunoprecipitated PPARα from control and undernourished livers by western blot. In parallel, we examined acetylation of PPARγ, which is a widely known SIRT1 deacetylation target (22). In accord with their increased expression of SIRT1, undernourished livers contained markedly decreased acetylation of the immunoprecipitated PPARα and PPARγ relative to control livers (**Figure 2D**). Taken together, these data suggest that PPARα may be a direct target for deacetylation by SIRT1.

SIRT1 Negatively Regulates PPARα Protein Levels

Next, we sought to determine whether altering SIRT1 expression influences PPARα protein levels. First, we overexpressed constitutively active or dominant negative forms of SIRT1 in HepG2 human hepatoma cells. Indeed, overexpression of constitutively active SIRT1, but not of a dominant negative SIRT1, decreased PPARα protein and acetylation (**Figure 3A**). Second, we treated HepG2 cells with the natural SIRT1 activator resveratrol (27), and confirmed decreased PPARα protein in conjunction with increased *PPARA* transcript (**Figure 3B**), in accord with our mouse model of undernutrition. Third, we transfected HepG2 cells with SIRT1 siRNA or non-silencing siRNA control and found that loss of SIRT1 results in increased PPARα protein and acetylation (**Figure 3C**). These data indicate that SIRT1 negatively regulates PPARα protein levels through deacetylation.

SIRT1 deacetylation causes ubiquitination and subsequent proteasome mediated degradation of multiple nuclear receptors (22–25). To determine whether SIRT1 deacetylation also results in ubiquitination and degradation of PPARα, we assessed ubiquitination of PPARα immunoprecipitated from HepG2 cells after treatment with the siRNAs in the above experiment. As expected, silencing SIRT1 decreased ubiquitination of PPARα

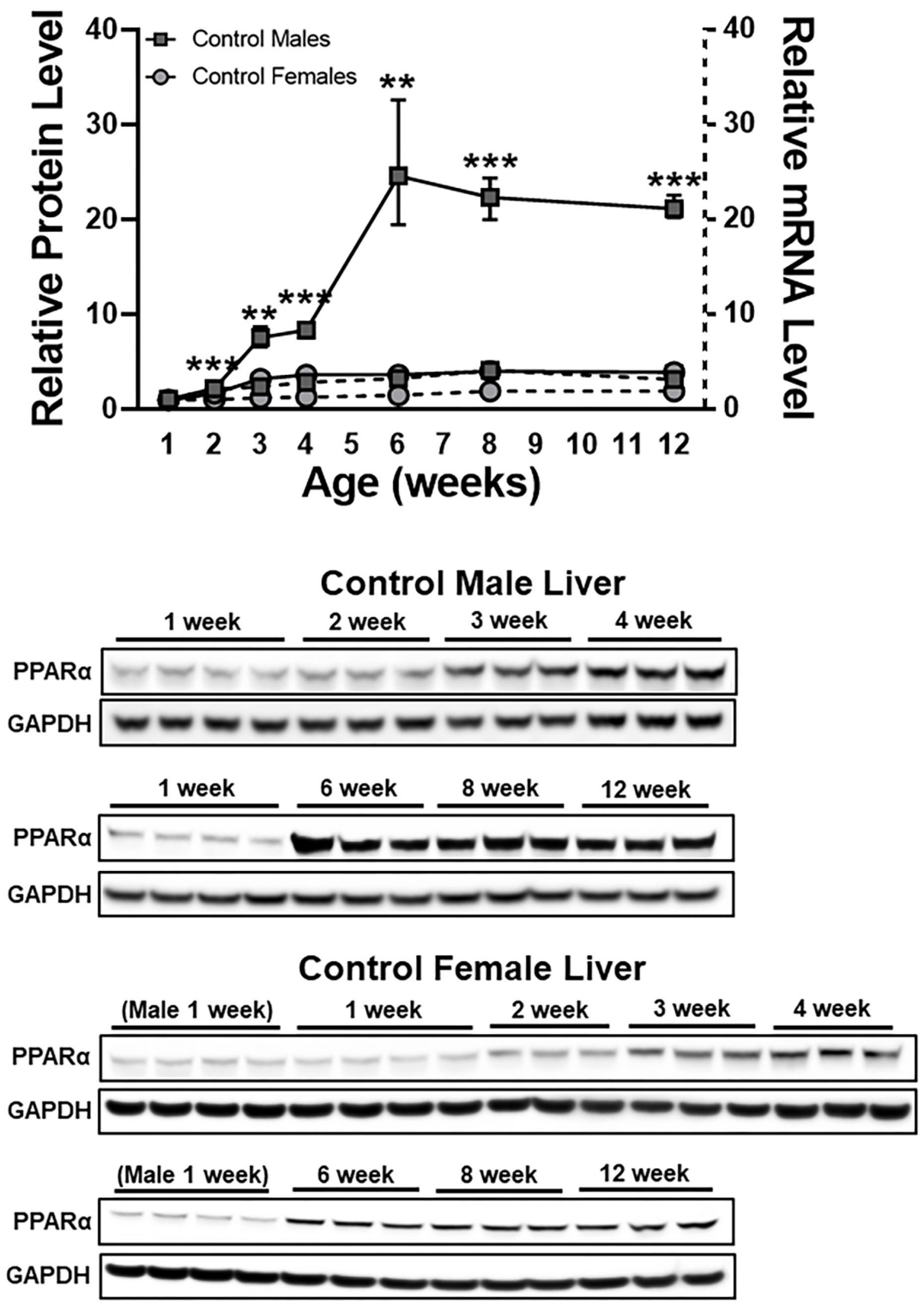

FIGURE 1 | Early life sex differences in hepatic PPARα expression at the protein (solid lines) and mRNA (dashed lines) levels. Although sex differences were most striking with respect to protein expression, mRNA expression also was greater in males compared to females ($P < 0.05$) at every time point after 1 week. $N = 3$–4 mice per time point per group; bars denote range. All data were normalized to 1 week old males. Mean + range; $N = 3$–4; $^{***}P < 0.001$; $^{**}P < 0.01$ between sexes at a given time point for protein expression. GAPDH, glyceraldehyde 3-phosphate dehydrogenase; PPARα, peroxisome proliferator-activated receptor-α.

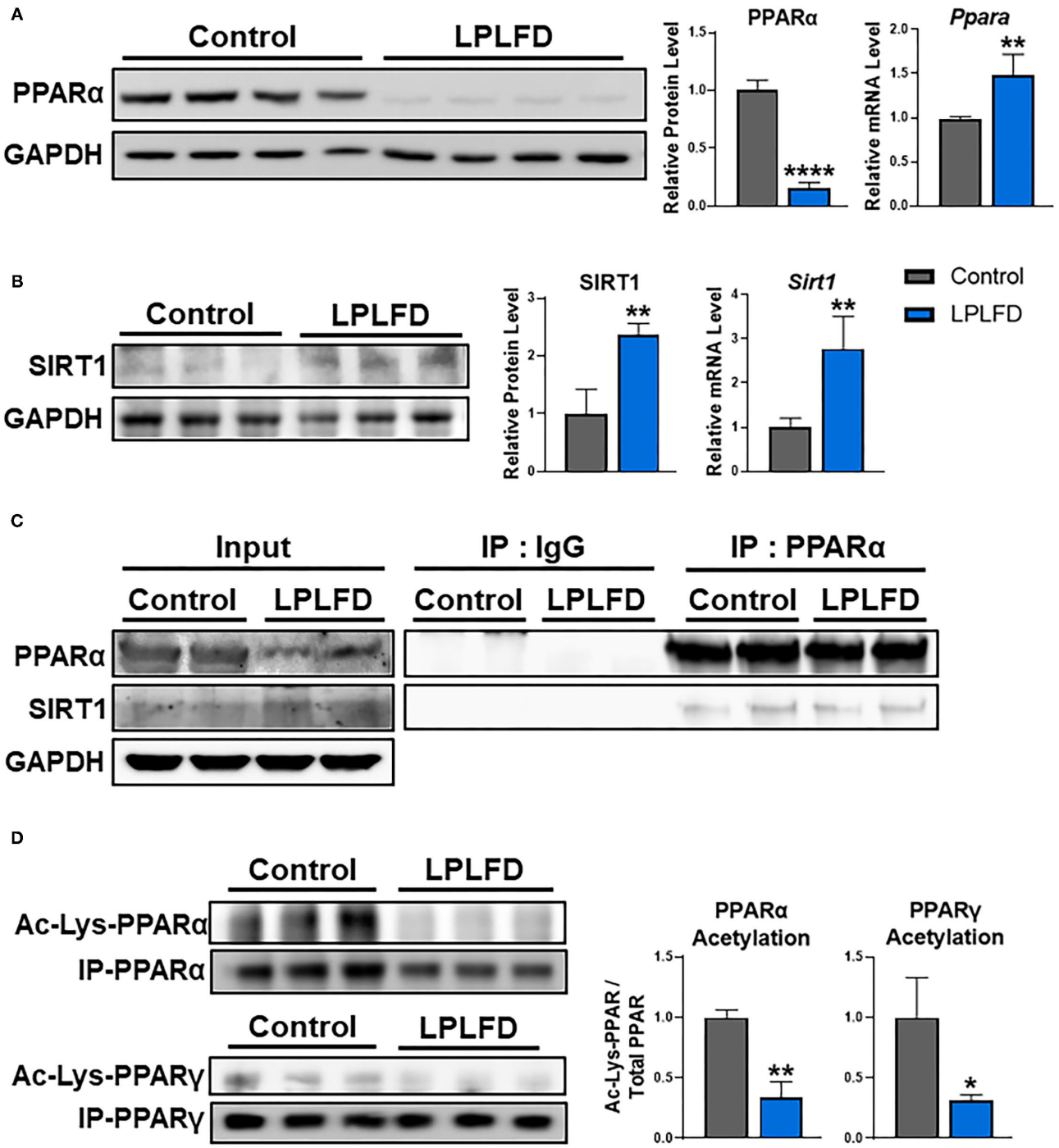

FIGURE 2 | Effects of undernutrition on hepatic PPARα expression and acetylation in male mice. **(A)** Whole livers from undernourished mice contained decreased PPARα protein and increased PPARα transcript relative to livers from control male mice. **(B)** Expression of SIRT1 was increased in undernourished livers at both the protein and the transcriptional level. **(C)** SIRT1 protein was detected bound to PPARα purified from whole liver by immunoprecipitation, suggesting a direct interaction in control and undernourished mouse livers. **(D)** PPAR protein was immunoprecipitated from liver, then comparable amounts were analyzed by western blot to illustrate decreased acetylation of both PPARα, which is not known to be an acetylation target of SIRT1, and PPARγ, which is a well-known acetylation target of SIRT1. Mean + SD; $n = 2$–4; $^{****}P < 0.0001$; $^{**}P < 0.01$; $^{*}P < 0.05$. Ac-Lys, acetylated lycine; GAPDH, glyceraldehyde 3-phosphate dehydrogenase; IgG, immunoglobulin G; IP, immunoprecipitation; LPLFD, low-protein, low-fat diet; PPAR, peroxisome proliferator-activated receptor; SIRT1, NAD-dependent deacetylase sirtuin-1.

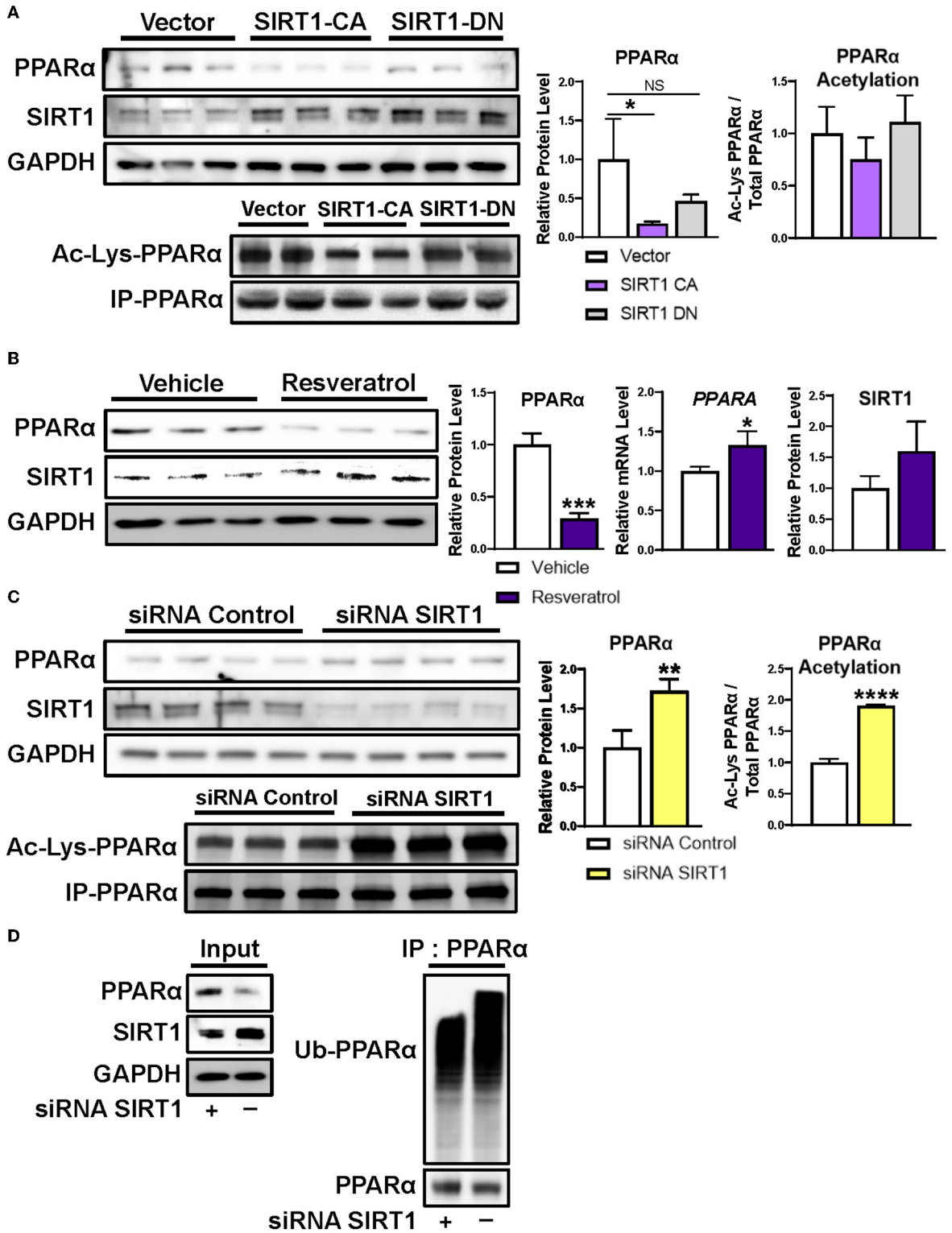

FIGURE 3 | Regulation of PPARα protein level by SIRT1. **(A)** Transient transfection of human-derived HepG2 hepatocellular carcinoma cells with constitutively active SIRT1 decreased PPARα protein levels and acetylation, whereas transfection with dominant negative SIRT1 did not. **(B)** Incubating HepG2 cells with 100 μM of the natural SIRT1 activator resveratrol decreased PPARα protein and increased PPARα mRNA, similar to our mouse model of undernutrition. **(C)** Silencing SIRT1 in HepG2 cells increased PPARα protein and acetylation and **(D)** decreased ubiquitination of PPARα. Mean + SD; $n = 3$–4; $^{****}P < 0.0001$; $^{***}P < 0.001$; $^{**}P < 0.01$; *adjusted $P < 0.05$. CA, constitutively active; DN, dominant negative; GAPDH, glyceraldehyde 3-phosphate dehydrogenase; IP, immunoprecipitation; NS, not significant; PPARα, peroxisome proliferator-activated receptor-α; siRNA, small interfering RNA; SIRT1, NAD-dependent deacetylase sirtuin-1; Ub-PPARα, ubiquitinated PPARα.

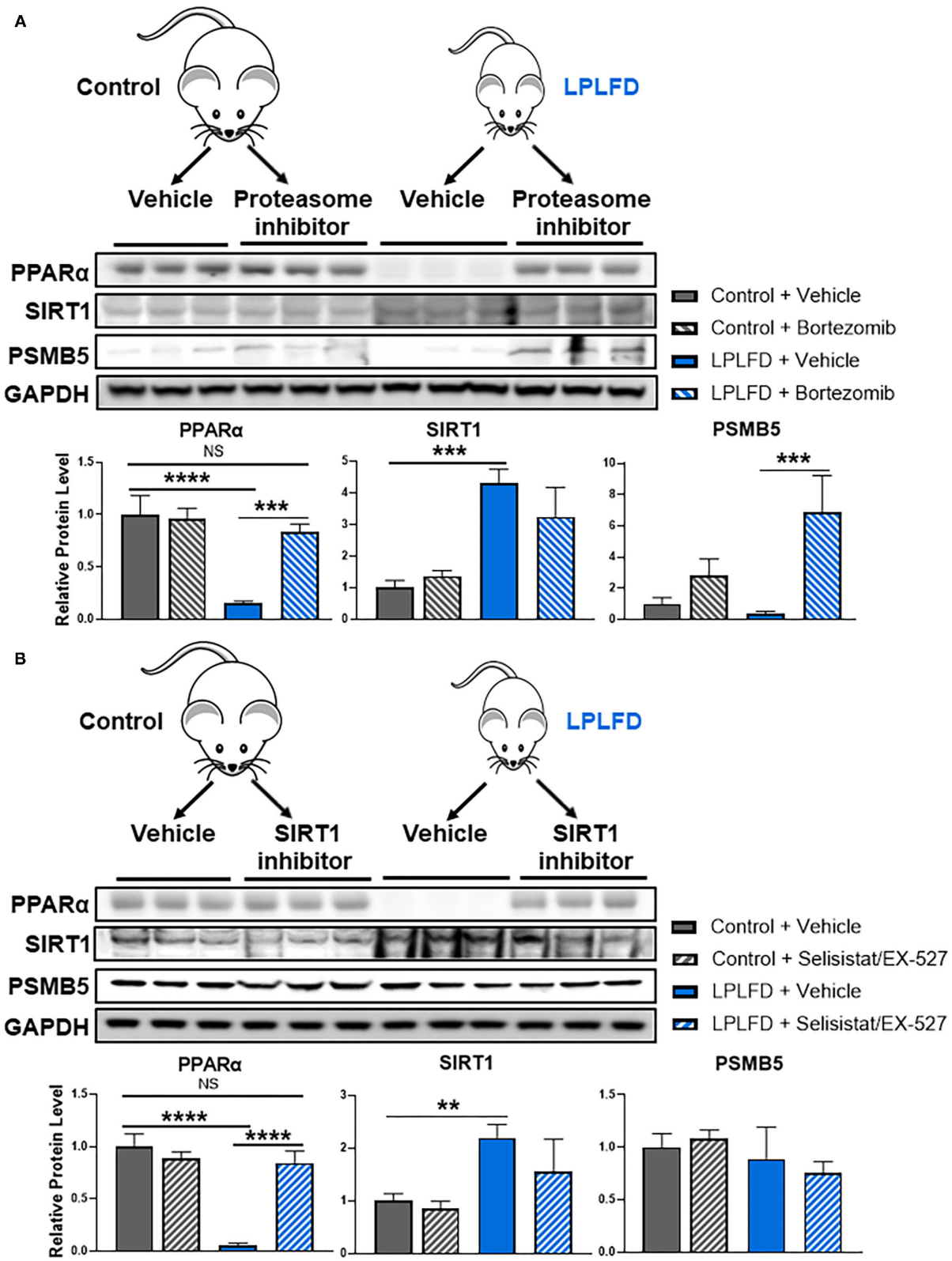

FIGURE 4 | Rescue of hepatic PPARα by blocking SIRT1-mediated proteasomal degradation in undernourished mice. **(A)** Eight-week-old control and undernourished male mice were treated with a single intraperitoneal injection of 1 mg/kg of the proteasome inhibitor bortezomib, or an equivalent volume of sterile PBS, and after 24

(Continued)

FIGURE 4 | hours whole livers were harvested for western blot. Hepatic PPARα levels were rescued completely in undernourished mice treated with proteasome inhibitor. **(B)** Alternatively, control and undernourished mice were treated with three daily intraperitoneal injections of 10 mg/kg/day of the SIRT1 inhibitor selisistat/EX-527, or an equivalent volume of sterile PBS, and 24 h after the third dose, whole livers were harvested for western blot. Hepatic PPARα levels were rescued completely in undernourished mice treated with SIRT1 inhibitor. Mean + SD, $N = 3$, ****adjusted $P < 0.0001$, ***adjusted $P < 0.001$, **adjusted $P < 0.01$. GAPDH, glyceraldehyde 3-phosphate dehydrogenase; LPLFD, low-protein, low-fat diet; NS, not significant; PPARα, peroxisome proliferator-activated receptor-α; PSMB5, proteasome subunit β type 5; SIRT1, NAD-dependent deacetylase sirtuin-1.

and increased its protein level (**Figure 3D**). All together, these data suggest that hepatic PPARα is reduced in undernourished males due in part to SIRT1 mediated deacetylation followed by ubiquitination and proteasome degradation.

Hepatic PPARα Is Rescued in Undernourished Mice by Inhibiting SIRT1-Directed Proteasomal Degradation

Finally, we sought to test the hypothesis that inhibiting SIRT1-directed proteasome degradation would prevent loss of hepatic PPARα in undernutrition. We first administered a single intraperitoneal injection of the proteasome inhibitor bortezomib, or vehicle, to healthy and undernourished male mice, then harvested livers 24 h later for western blot. PPARα was profoundly reduced in livers from vehicle-treated undernourished mice, confirming our previous findings (6). Strikingly, hepatic PPARα levels in undernourished mice were rescued completely by bortezomib (**Figure 4A**), confirming that proteasome mediated degradation is responsible for loss of hepatic PPARα in undernutrition. In a separate experiment, we administered the potent and specific SIRT1 inhibitor selisistat/EX-527 *via* intraperitoneal injection for 3 consecutive days. Once again, hepatic PPARα levels in undernourished mice were rescued completely by SIRT1 inhibition (**Figure 4B**). All together, these studies suggest that undernutrition induces expression of SIRT1, which deacetylates PPARα, resulting in subsequent ubiquitination and proteasomal degradation.

DISCUSSION

The purpose of this study was to identify mechanisms contributing to the loss of hepatic PPARα protein in undernutrition. We employed a mouse model that reproduces key features of chronic undernutrition in humans, including decreased peroxisome abundance and impaired synthesis of bile acids and coagulation factors (6). After ruling out the possibility of transcriptional repression of PPARα, we found that SIRT1 expression was markedly increased in livers from undernourished mice, and we revealed in cultured hepatocytes that SIRT1 negatively regulates PPARα protein levels *via* deacetylation and subsequent ubiquitination and proteasomal degradation. To confirm that this mechanism contributes to hepatic PPARα protein loss in undernutrition, we treated undernourished mice with a proteasome inhibitor or with a SIRT1 inhibitor and found that either drug fully restored hepatic PPARα protein levels.

SIRT1 negatively regulates levels of multiple proteins within the nuclear receptor family *via* deacetylation and subsequent ubiquitin-proteasomal degradation. Previous co-immunoprecipitation studies revealed that SIRT1 physically interacts with PPARα within nuclear protein complexes, but whether this interaction influences PPARα acetylation and protein levels was not known (26). This study confirmed direct interaction between PPARα and SIRT1 in undernourished mouse livers, and is the first study to our knowledge to identify PPARα as a SIRT1 deacetylation and degradation target. Ongoing work in sirtuin-targeted drug discovery (28) may ultimately lead to the consideration of SIRT1 inhibitors as therapeutic alternatives to or amplifiers of PPARα agonists (e.g., fibrates) for metabolic disorders.

For some nuclear receptors SIRT1 serves as a coactivator, increasing the expression of positive transcriptional targets of the receptor prior to its degradation (22–25). It has been proposed that deacetylation might facilitate the release of corepressors or the recruitment of coactivators, or enhance clearing from the promoter for subsequent rounds of transcription (24). Congruent with this working model, transcriptional analysis of our undernourished mouse livers revealed marked upregulation in PPAR signaling, including induction of the positive PPARα target genes *Fgf21*, *Acot1*, and *Cyp4a14* (6). PPARα is strongly activated in the fasted state (2), and it remains to be determined whether similarly strong PPARα activation is detected during the initial phases of acute undernutrition.

Acetylation sites have been described on PPARγ, including the lysine (K) residues K184/185, K268, and K293, which are confirmed to be SIRT1 deacetylation targets (22, 29, 30). We are not aware of any analogous acetylation sites that have been identified for PPARα. To begin to address this knowledge gap, we probed the PPARα gene sequence of seven mammalian species with a K-acetyltransferase predictive algorithm (31). We identified K232 as a highly conserved residue that is most likely to be responsible for PPARα acetylation (**Supplementary Table 1**). Further analyses to validate the functional implications of this putative PPARα acetylation site are needed.

SIRT1 induction by calorie restriction is an ancient evolutionary biological stress response that slows aging by increasing the long-term function and survival of cells (32). During periods of fasting that last 12–24 h, SIRT1 deacetylates and activates the PPARγ coactivator PGC-1α to increase fatty acid oxidation and decrease lipogenesis and fat storage (26, 33, 34). SIRT1 similarly deacetylates sterol regulatory element binding protein, farnesoid-X-receptor, and liver-X-receptor to increase bile acid biosynthesis and reduce cholesterol (24, 35). In addition, deacetylated PGC-1α increases the expression of CYP7A1 and CYP8B1 to increase bile acid synthesis from cholesterol (36–38). These pathways serve to

protect the host from dyslipidemia, but presumably they require levels of PPARα protein that exceed what is present during chronic undernutrition. We propose that the metabolic benefits of short-term coactivation by SIRT1 of transcriptional targets of PPARα gradually are lost as acute undernutrition progresses to chronic undernutrition, as new PPARα protein synthesis cannot keep up with continuous deacetylation, ubiquitination, and proteasome degradation. In this model, loss of PPARα in response to chronically increased SIRT1 expression undermines the beneficial impact of decreased acetylation of PGC-1α and potentially other SIRT1 targets.

We explored this mechanism of post-translational PPARα protein degradation exclusively in male mice because undernutrition does not decrease hepatic PPARα protein in female mice (6). Indeed, sex differences in PPARα protein levels in mice first appear between the second and third weeks of life, and by 6 weeks of life livers from male mice contain ∼13-fold as much PPARα protein as livers from female mice (**Figure 1**). In our model, undernutrition was initiated during the second week of life; it remains to be determined whether increased SIRT1 expression would cause PPARα deacetylation and degradation if malnourishment was initiated after mice reached adulthood. Sex differences in PPARα expression recently were reported in human monocytes (39). In addition to the known interactions between estrogen and PPARα transcriptional activity (40), sexual dimorphism of PPARα protein levels could have important implications for sex differences in the frequency of metabolic disorders and their treatment (41). Finally, because SIRT1 deacetylates histone proteins as well as non-histone proteins, hepatic SIRT1 induction in undernutrition has the potential to induce epigenetic effects much broader than those uncovered here. Histone deacetylation may be especially important early in development, given the clear link between early-life undernutrition and long-term risk for obesity and metabolic disorders; this link is presumed to have an epigenetic basis (42). Whether acute and long-term metabolic effects of early-life undernutrition could be mitigated by therapeutic strategies that preserve PPARα protein warrants further investigation.

DATA AVAILABILITY STATEMENT

The raw data supporting the conclusions of this article will be made available by the authors, without undue reservation.

ETHICS STATEMENT

The animal study was reviewed and approved by Baylor College of Medicine Institutional Animal Care and Use Committee.

AUTHOR CONTRIBUTIONS

JS, KK, MC, DM, and GP were responsible for the design of the study. JS performed the experiments. JS and GP performed data, statistical analyses, and prepared the manuscript. KK, MC, DM, and GP provided assistance and knowledge that was vital to the completion of the manuscript. All authors contributed to the review of the manuscript.

FUNDING

GP received funding from National Institute of Diabetes and Digestive and Kidney Diseases (Grants K08 DK-113114, R03 DK-129495, and P30 DK-056338), which funds the Texas Medical Center Digestive Diseases Center. Publication costs were generously supported by the Texas Children's Hospital Young Investigators Endowed Fund.

SUPPLEMENTARY MATERIAL

The Supplementary Material for this article can be found online at: https://www.frontiersin.org/articles/10.3389/fnut.2022.831879/full#supplementary-material

REFERENCES

1. Montaigne D, Butruille L, Staels B. PPAR control of metabolism and cardiovascular functions. *Nat Rev Cardiol.* (2021) 18:809–23. doi: 10.1038/s41569-021-00569-6
2. Lee JM, Wagner M, Xiao R, Kim KH, Feng D, Lazar MA, et al. Nutrient-sensing nuclear receptors coordinate autophagy. *Nature.* (2014) 516:112–5. doi: 10.1038/nature13961
3. Preidis GA, Kim KH, Moore DD. Nutrient-sensing nuclear receptors PPARalpha and FXR control liver energy balance. *J Clin Invest.* (2017) 127:1193–201. doi: 10.1172/JCI88893
4. Thaxton GE, Melby PC, Manary MJ, Preidis GA. New insights into the pathogenesis and treatment of malnutrition. *Gastroenterol Clin North Am.* (2018) 47:813–27. doi: 10.1016/j.gtc.2018.07.007
5. van Zutphen T, Ciapaite J, Bloks VW, Ackereley C, Gerding A, Jurdzinski A, et al. Malnutrition-associated liver steatosis and ATP depletion is caused by peroxisomal and mitochondrial dysfunction. *J Hepatol.* (2016) 65:1198–208. doi: 10.1016/j.jhep.2016.05.046
6. Preidis GA, Soni KG, Suh JH, Halder T, Kim KH, Choi JM, et al. Coagulopathy in malnourished mice is sexually dimorphic and regulated by nutrient-sensing nuclear receptors. *Hepatol Commun.* (2020) 4:1835–50. doi: 10.1002/hep4.1622
7. Francque S, Verrijken A, Caron S, Prawitt J, Paumelle R, Derudas B, et al. PPARα gene expression correlates with severity and histological treatment response in patients with non-alcoholic steatohepatitis. *J Hepatol.* (2015) 63:164–73. doi: 10.1016/j.jhep.2015.02.019
8. Dharancy S, Malapel M, Perlemuter G, Roskams T, Cheng Y, Dubuquoy L, et al. Impaired expression of the peroxisome proliferator-activated receptor alpha during hepatitis C virus infection. *Gastroenterology.* (2005) 128:334–42. doi: 10.1053/j.gastro.2004.11.016
9. Cheng Y, Dharancy S, Malapel M, Desreumaux P. Hepatitis C virus infection down-regulates the expression of peroxisome proliferator-activated receptor alpha and carnitine palmitoyl acyl-CoA transferase 1A. *World J Gastroenterol.* (2005) 11:7591–6. doi: 10.3748/wjg.v11.48.7591
10. Wu C, Gilroy R, Taylor R, Olyaee M, Abdulkarim B, Forster J, et al. Alteration of hepatic nuclear receptor-mediated signaling pathways in hepatitis C virus patients with and without a history of alcohol drinking. *Hepatology.* (2011) 54:1966–74. doi: 10.1002/hep.24645
11. Shores NJ, Mendes-Correa MC, Maida I, Turner J, High KP, Babudieri S, et al. Hepatic peroxisome proliferator-activated receptor gamma and alpha-mRNA expression in HCV-infected adults is decreased by HIV co-infection and is also affected by ethnicity. *Clinics (São Paulo).* (2015) 70:790–6. doi: 10.6061/clinics/2015(12)05

12. Chew CH, Chew GS, Najimudin N, Tengku-Muhammad TS. Interleukin-6 inhibits human peroxisome proliferator activated receptor alpha gene expression *via* CCAAT/enhancer-binding proteins in hepatocytes. *Int J Biochem Cell Biol.* (2007) 39:1975–86. doi: 10.1016/j.biocel.2007.05.015
13. Stienstra R, Saudale F, Duval C, Keshtkar S, Groener JE, van Rooijen N, et al. Kupffer cells promote hepatic steatosis *via* interleukin-1β-dependent suppression of peroxisome proliferator-activated receptor alpha activity. *Hepatology.* (2010) 51:511–22. doi: 10.1002/hep.23337
14. Lim WS, Ng DL, Kor SB, Wong HK, Tengku-Muhammad TS, Choo QC, et al. Tumour necrosis factor alpha down-regulates the expression of peroxisome proliferator activated receptor alpha (PPARα) in human hepatocarcinoma HepG2 cells by activation of NF-κB pathway. *Cytokine.* (2013) 61:266–74. doi: 10.1016/j.cyto.2012.10.007
15. Kida K, Nakajima M, Mohri T, Oda Y, Takagi S, Fukami T, et al. PPARα is regulated by miR-21 and miR-27b in human liver. *Pharm Res.* (2011) 28:2467–76. doi: 10.1007/s11095-011-0473-y
16. Hu W, Wang X, Ding X, Li Y, Zhang X, Xie P, et al. MicroRNA-141 represses HBV replication by targeting PPARA. *PLoS One.* (2012) 7:e34165. doi: 10.1371/journal.pone.0034165
17. Li B, Zhang Z, Zhang H, Quan K, Lu Y, Cai D, et al. Aberrant miR199a-5p/caveolin1/PPARα axis in hepatic steatosis. *J Mol Endocrinol.* (2014) 53:393–403. doi: 10.1530/JME-14-0127
18. Drakaki A, Hatziapostolou M, Polytarchou C, Vorvis C, Poultsides GA, Souglakos J, et al. Functional microRNA high throughput screening reveals miR-9 as a central regulator of liver oncogenesis by affecting the PPARA-CDH1 pathway. *BMC Cancer.* (2015) 15:542. doi: 10.1186/s12885-015-1562-9
19. Teodosio NR, Lago ES, Romani SA, Guedes RC. A regional basic diet from northeast Brazil as a dietary model of experimental malnutrition. *Arch Latinoam Nutr.* (1990) 40:533–47.
20. Brunet A, Sweeney LB, Sturgill JF, Chua KF, Greer PL, Lin Y, et al. Stress-dependent regulation of FOXO transcription factors by the SIRT1 deacetylase. *Science.* (2004) 303:2011–5. doi: 10.1126/science.1094637
21. Lemberger T, Saladin R, Vazquez M, Assimacopoulos F, Staels B, Desvergne B, et al. Expression of the peroxisome proliferator-activated receptor alpha gene is stimulated by stress and follows a diurnal rhythm. *J Biol Chem.* (1996) 271:1764–9. doi: 10.1074/jbc.271.3.1764
22. Qiang L, Wang L, Kon N, Zhao W, Lee S, Zhang Y, et al. Brown remodeling of white adipose tissue by SirT1-dependent deacetylation of Ppargamma. *Cell.* (2012) 150:620–32. doi: 10.1016/j.cell.2012.06.027
23. Kemper JK, Xiao Z, Ponugoti B, Miao J, Fang S, Kanamaluru D, et al. FXR acetylation is normally dynamically regulated by p300 and SIRT1 but constitutively elevated in metabolic disease states. *Cell Metab.* (2009) 10:392–404. doi: 10.1016/j.cmet.2009.09.009
24. Li X, Zhang S, Blander G, Tse JG, Krieger M, Guarente L. SIRT1 deacetylates and positively regulates the nuclear receptor LXR. *Mol Cell.* (2007) 28:91–106. doi: 10.1016/j.molcel.2007.07.032
25. Suh JH, Sieglaff DH, Zhang A, Xia X, Cvoro A, Winnier GE, et al. SIRT1 is a direct coactivator of thyroid hormone receptor beta1 with gene-specific actions. *PLoS One.* (2013) 8:e70097. doi: 10.1371/journal.pone.0070097
26. Purushotham A, Schug TT, Xu Q, Surapureddi S, Guo X, Li X. Hepatocyte-specific deletion of SIRT1 alters fatty acid metabolism and results in hepatic steatosis and inflammation. *Cell Metab.* (2009) 9:327–38. doi: 10.1016/j.cmet.2009.02.006
27. Borra MT, Smith BC, Denu JM. Mechanism of human SIRT1 activation by resveratrol. *J Biol Chem.* (2005) 280:17187–95. doi: 10.1074/jbc.M501250200
28. Dai H, Sinclair DA, Ellis JL, Steegborn C. Sirtuin activators and inhibitors: promises, achievements, and challenges. *Pharmacol Ther.* (2018) 188:140–54. doi: 10.1016/j.pharmthera.2018.03.004
29. Han L, Zhou R, Niu J, McNutt MA, Wang P, Tong T. SIRT1 is regulated by a PPAR{gamma}-SIRT1 negative feedback loop associated with senescence. *Nucleic Acids Res.* (2010) 38:7458–71. doi: 10.1093/nar/gkq609
30. Tian L, Wang C, Hagen FK, Gormley M, Addya S, Soccio R, et al. Acetylation-defective mutant of Ppargamma is associated with decreased lipid synthesis in breast cancer cells. *Oncotarget.* (2014) 5:7303–15. doi: 10.18632/oncotarget.2371
31. Wang L, Du Y, Lu M, Li T. ASEB: a web server for KAT-specific acetylation site prediction. *Nucleic Acids Res.* (2012) 40(Web Server issue):W376–W9. doi: 10.1093/nar/gks437
32. Cohen HY, Miller C, Bitterman KJ, Wall NR, Hekking B, Kessler B, et al. Calorie restriction promotes mammalian cell survival by inducing the SIRT1 deacetylase. *Science.* (2004) 305:390–2. doi: 10.1126/science.1099196
33. Rodgers JT, Lerin C, Haas W, Gygi SP, Spiegelman BM, Puigserver P. Nutrient control of glucose homeostasis through a complex of PGC-1α and SIRT1. *Nature.* (2005) 434:113–8. doi: 10.1038/nature03354
34. Nemoto S, Fergusson MM, Finkel T. SIRT1 functionally interacts with the metabolic regulator and transcriptional coactivator PGC-1{alpha}. *J Biol Chem.* (2005) 280:16456–60. doi: 10.1074/jbc.M501485200
35. Elibol B, Kilic U. High Levels of SIRT1 expression as a protective mechanism against disease-related conditions. *Front Endocrinol (Lausanne).* (2018) 9:614. doi: 10.3389/fendo.2018.00614
36. Shin DJ, Campos JA, Gil G, Osborne TF. PGC-1α activates CYP7A1 and bile acid biosynthesis. *J Biol Chem.* (2003) 278:50047–52. doi: 10.1074/jbc.M309736200
37. Bhalla S, Ozalp C, Fang S, Xiang L, Kemper JK. Ligand-activated pregnane X receptor interferes with HNF-4 signaling by targeting a common coactivator PGC-1alpha. Functional implications in hepatic cholesterol and glucose metabolism. *J Biol Chem.* (2004) 279:45139–47. doi: 10.1074/jbc.M405423200
38. Miao J, Fang S, Bae Y, Kemper JK. Functional inhibitory cross-talk between constitutive androstane receptor and hepatic nuclear factor-4 in hepatic lipid/glucose metabolism is mediated by competition for binding to the DR1 motif and to the common coactivators, GRIP-1 and PGC-1α. *J Biol Chem.* (2006) 281:14537–46. doi: 10.1074/jbc.M510713200
39. Wege N, Schutkowski A, Boenn M, Bialek J, Schlitt A, Noack F, et al. Men and women differ in their diurnal expression of monocyte peroxisome proliferator-activated receptor-alpha in the fed but not in the fasted state. *FASEB J.* (2015) 29:2905–11. doi: 10.1096/fj.14-267575
40. Kitson AP, Stroud CK, Stark KD. Elevated production of docosahexaenoic acid in females: potential molecular mechanisms. *Lipids.* (2010) 45:209–24. doi: 10.1007/s11745-010-3391-6
41. Gerdts E, Regitz-Zagrosek V. Sex differences in cardiometabolic disorders. *Nat Med.* (2019) 25:1657–66. doi: 10.1038/s41591-019-0643-8
42. Smith CJ, Ryckman KK. Epigenetic and developmental influences on the risk of obesity, diabetes, and metabolic syndrome. *Diabetes Metab Syndr Obes.* (2015) 8:295–302. doi: 10.2147/DMSO.S61296

Conflict of Interest: The authors declare that the research was conducted in the absence of any commercial or financial relationships that could be construed as a potential conflict of interest.

Publisher's Note: All claims expressed in this article are solely those of the authors and do not necessarily represent those of their affiliated organizations, or those of the publisher, the editors and the reviewers. Any product that may be evaluated in this article, or claim that may be made by its manufacturer, is not guaranteed or endorsed by the publisher.

frontiers in Nutrition

METHODS
published: 30 March 2022
doi: 10.3389/fnut.2022.858603

Identification and Spatial Visualization of Dysregulated Bile Acid Metabolism in High-Fat Diet-Fed Mice by Mass Spectral Imaging

Qi Zhang[1,2†], Zhen-Hua Wu[1,2,3†], Shan-Shan Zhao[1,2,3], Jing Yang[1,2,3], Lei Chen[1,2,3], Xiao-Yu Wang[1,2,3], Zhan-You Wang[1] and Hui-Xin Liu[1,2,3*]*

[1] Health Sciences Institute, China Medical University, Shenyang, China, [2] Institute of Life Sciences, China Medical University, Shenyang, China, [3] Liaoning Key Laboratory of Obesity and Glucose/Lipid Associated Metabolic Diseases, China Medical University, Shenyang, China

OPEN ACCESS

Edited by:
Lei Zhou,
Guangxi University, China

Reviewed by:
Feng Li,
Baylor College of Medicine, United States
Berta Cillero-Pastor,
Maastricht University, Netherlands

****Correspondence:***
Zhan-You Wang
wangzy@cmu.edu.cn
Hui-Xin Liu
liuhx@cmu.edu.cn

† These authors have contributed equally to this work and share first authorship

Specialty section:
This article was submitted to Nutrition and Metabolism, a section of the journal Frontiers in Nutrition

Received: *20 January 2022*
Accepted: *15 February 2022*
Published: *30 March 2022*

Citation:
Zhang Q, Wu Z-H, Zhao S-S, Yang J, Chen L, Wang X-Y, Wang Z-Y and Liu H-X (2022) Identification and Spatial Visualization of Dysregulated Bile Acid Metabolism in High-Fat Diet-Fed Mice by Mass Spectral Imaging. Front. Nutr. 9:858603. doi: 10.3389/fnut.2022.858603

Changes in overall bile acid (BA) levels and specific BA metabolites are involved in metabolic diseases, gastrointestinal, and liver cancer. BAs have become established as important signaling molecules that enable fine-tuned inter-tissue communication within the enterohepatic circulation. The liver, BAs site of production, displayed physiological and functional zonal differences in the periportal zone versus the centrilobular zone. In addition, BA metabolism shows regional differences in the intestinal tract. However, there is no available method to detect the spatial distribution and molecular profiling of BAs within the enterohepatic circulation. Herein, we demonstrated the application in mass spectrometry imaging (MSI) with a high spatial resolution (3 μm) plus mass accuracy matrix-assisted laser desorption ionization (MALDI) to imaging BAs and *N*-1-naphthylphthalamic acid (NPA). Our results could clearly determine the zonation patterns and regional difference characteristics of BAs on mouse liver, ileum, and colon tissue sections, and the relative content of BAs based on NPA could also be ascertained. In conclusion, our method promoted the accessibility of spatial localization and quantitative study of BAs on gastrointestinal tissue sections and demonstrated that MALDI-MSI was a valuable tool to investigate and locate several BA molecules in different tissue types leading to a better understanding of the role of BAs behind the gastrointestinal diseases.

Keywords: mass spectrometry imaging (MSI), MALDI, bile acid, zonation pattern, enterohepatic circulation, metabolic disease

INTRODUCTION

The liver and gut share an intimate relationship whose communication relies heavily on metabolites, among which bile acids (BAs) play a key role (1). Previous work from our lab and others demonstrated that BAs play a regulatory role in host metabolism and immune responses (1–5). Changes to the composition and distribution of the BAs have been implicated in the etiopathogenesis of multiple diseases ranging from the liver to the intestine (6). Liver diseases differentially affect BA concentration and distribution and composition, so as in the intestine (7).

Strong imbalance or disruption in BA synthesis and secretion processes are associated with various liver and gastrointestinal diseases, such as BA synthesis disorder (inborn) and primary biliary cholangitis (8). Recent studies demonstrated that microbial BA metabolism and its alterations by diet and host signaling are implicated in obesity associated metabolic diseases (9). However, the information of the abundance and spatial distribution of BAs and link them to the pathology of the corresponding diseases are still elusive.

Bile acids, whose functional role in the global mammalian system is multifaceted, are an important class of metabolites that undergo extensive enterohepatic recycling and gut microbial modification (10). To understand complex BA processes and disorders and develop effective treatments, it is important to have reliable information on the abundance and spatial distribution of BAs and their interplay with their receptors and link them to the pathology of the corresponding diseases. Because of the great diversity of BAs and the complexity of their signaling mechanisms, it is very useful to image several BAs in a single analysis in a way that enables simultaneous measurement and characterization of numerous BAs. However, simultaneous spatial mapping and quantitation of changes of BAs in enterohepatic circulation represent a significant challenge. Over the last few decades, mass spectrometry (MS)-based techniques for the detection of BAs are mostly indirect assays for detecting the content of BAs in tissue homogenate or the spatial distribution of BAs in tissues without quantification (11–14). In addition, benchmark methods for BA analysis, such as liquid chromatography (LC) and electrospray ionization (ESI)-MS, require extensive processing of liver or intestine tissue samples before analysis, which causes losses of anatomical information (11, 15, 16). Thus, there is a need for innovative imaging techniques that can simultaneously map and quantitate the BAs in tissue samples. However, mass spectrometry imaging (MSI) of BAs in the organs is challenging because of their poor ionization properties and the highly ion-suppressing tissue microenvironment. Despite the difficulties of imaging BAs and their metabolites in the colon and other organs, efforts have been made using commercially available or in-house constructed ion sources. Matrix assisted laser desorption ionization (MALDI)'s high tolerance to contaminants and simplicity of preparation make it ideal for the analysis of BAs from biological media. Recently, a novel imaging mass microscope (iMScope) shows promise in simultaneously assessing the spatial distribution and molecular profiling in a non-targeted manner (17, 18).

Thus, in our study, the iMScope was adapted to investigate the spatial distribution and molecular profiling of BAs in the liver and intestine slices of a mouse under high-fat diet (HFD) to indicate the effects of metabolism of BAs on the health and diseases of the body.

METHODS

Chemicals

Mass spectrometry grade chemicals and reagents were used in the present study. Matrix moieties inclusive of 9-aminoacridine (9AA, no. 92817), 2, 5-dihydroxybenzoic acid (DHB, no. 149357), α-cyano-4-hydroxycinnamic acid (CHCA, no. C2020) were obtained from Sigma-Aldrich (St Louis, MO, United States). The

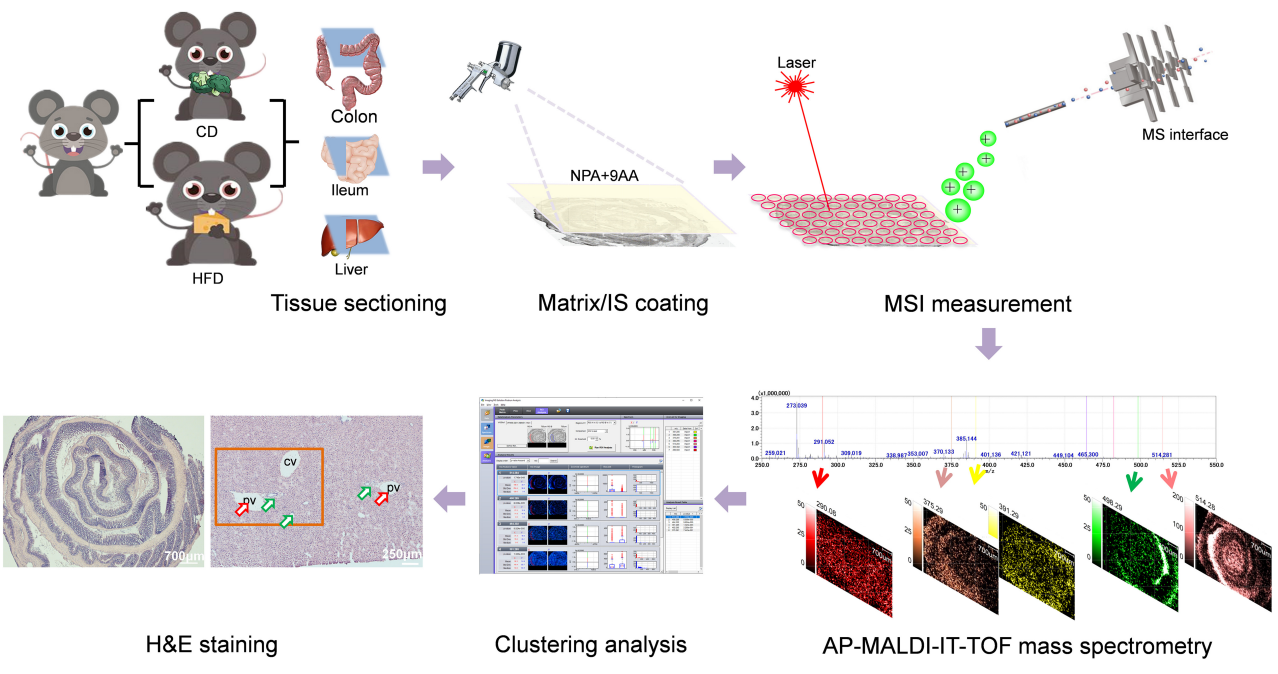

GRAPHICAL ABSTRACT | Schematic illustrations showing the mass spectrometry imaging based identification and spatial visualization of dysregulated bile acid metabolism in high-fat diet-fed mice.

internal standard (IS), *N*-1-naphthylphthalamic acid (NPA), was purchased from Chem Service (West Chester, PA, United States, no. N875498). Ultra-pure grade (18 MU) water was prepared by a Milli-Q system (Millipore Corporation, Billerica, MA, United States). Other reagents include formic acid (FA; Aladdin, no. F112034); Trifluoroacetic Acid (TFA; TEDIA, no. TS4295-013C); Methanol (MeOH; Honeywell, no. AH230-4HC); Ethanol (EtOH; Sigma-Aldrich, no. E7023); Ethanol (Tianjin Fuyu Fine Chemical Co., Ltd.); Acetonitrile (ACN; Honeywell, No. AH015-4HC); Xylene (Tianjin Fuyu Fine Chemical Co., Ltd.); Eosin (Beijing Solarbio Technology Co., Ltd., cat. no. G1100); Neutral gum (Beijing Solarbio Technology Co., Ltd., cat. no. G8590-100 ml), and indium tin oxide (ITO)-coated glass slides (Sigma-Aldrich, no. 578274).

Eleven BAs were selected for analysis: deoxycholic acid (DCA), chenodeoxycholic acid (CDCA), ursodeoxycholic acid (UDCA), taurodeoxycholic acid (TDCA), taurochenodeoxycholic acid (TCDCA), tauroursodeoxycholic acid (TUDCA), lithocholic acid (LCA), taurolithocholic acid (TLCA), taurocholic acid (TCA), tauromuricholic acid (TMCA), and glycocholic acid (GCA).

Animal Study

All animal procedures were approved by the Institutional Animal Care and Use Committee (IACUC) at the China Medical University. Six to eight weeks old male C57BL/6 mice were purchased from Beijing Huafukang Biotechnology Co., Ltd. The mice were fed with normal circadian circulation for 12 h and had enough food and water. Mice were fed an HFD (TP23520, Tropic diet, China) or a control diet (CD, TP23524, Tropic diet, China) for 4 weeks. There were 6–10 mice in both the CD group and the HFD group. After 4 weeks of feeding, animals were sacrificed for analysis.

Sample Preparation

After euthanasia, the tissues were quickly removed and all samples should be frozen immediately and stored at −80°C until further analysis. Set the cryomicrotome (Leica CM1950, Nussloch, Germany) to −25°C and cut the samples at a thickness of 10 μm. The slices were pasted on ITO-coated glass slide for analysis by MALDI-MSI. Three to five serial sections (each 10 μm thick) of sampled liver, ileum, and colon tissue were used to evaluate the reproducibility of the iMScope technique. A small droplet of optimal cutting temperature (OCT) compound is applied for mounting the tissue sample on the specimen holder. Because polyvinyl alcohol/polyethylene glycol-based media, such as OCT compound, cause ion suppression during MSI analysis, it is essential to avoid contamination of tissue sections, cryostat tables, or blades by OCT compounds (19). Subsequently, a "two-step matrix application," which combined with sublimation and airbrushing, was used to coat matrix for tissue sections (18, 20). (1) Sublimation: the electrically conductive glass slide bearing specimen (slice spiked with 10 ng ml^{-1} of NPA) was installed in a sample holder, which was then embedded in a vacuum deposition system (SVC-700TMSG iMLayer, Sanyu Electron, Tokyo, Japan). A matrix holder was filled with approximately 300 mg of matrix powder (9AA) and the sample holder and matrix bracket were positioned with 8 cm distance. The matrix power was then heated to the boiling point of the matrix crystals (220°C for 9AA) and the vapor covered the specimen surface for 8 min. The vacuum pressure of the chamber was maintained at 10^{-4} Pa in the process of sublimation. (2) Airbrushing: Matrix solution (10 mg ml^{-1} of 9AA) was prepared by dissolving matrix power in acetonitrile and distilled water (all containing 0.1% FA) at a ratio of 1:1. The matrix solution (1 ml) was added to the capacity of an artist's airbrush (MR. Linear Compressor L7/PS270 Airbrush, GSI Creos, Tokyo, Japan). The distance between the tip of the airbrush and the tissue surface was about 8 cm. For the first 3 cycles, the matrix was airbrushed for 2 s at 60 s intervals and, in the following 20 cycles, the matrix was continuously sprayed for 1.0 s at 30 s intervals. The glass slide was then placed in a vacuum dryer to vaporize the solvent for 5 min. After that, the glass slide was vacuum-dried, and then the BA distribution was observed with iMScope.

Matrix-Assisted Laser Desorption-Ionization Time-of-Flight-Mass Spectrometry

The parameters of IT-TOF (time-of-flight) MS were set as follows: ion polarity, negative; mass range, 350–550; sample voltage, 3.0 kV; and detector voltage, 1.90 kV. The imaging MS Solution Version 1.12.26 software (Shimadzu, Tokyo, Japan) was used to control the instrument, and the data acquisition, visualization, and quantification were also performed by the same software. The *m/z* values were externally calibrated using the DHB matrix. The identification of BAs was confirmed by MALDI-TOF-MS/MS with reference to product ion spectra of authentic BA standards.

Visualization of Bile Acids Distribution in Mice Tissue by Novel Imaging Mass Microscope

The iMScope TRIO (Shimadzu, Japan) instrument, a hybrid IT-TOF MS combining an optical microscope and atmospheric pressure MALDI/ionization system, was used to acquire the imaging MS data. One of the most critical processes in MSI is the creation of the region of interest (ROI). The optical microscope embedded in the iMScope permitted us to precisely choose the relevant tissue region prior to performing data acquisition. An ultraviolet laser, tightly focused with a triplet lens, was used to ensure high spatial resolution. Based on the advanced configuration above, a tissue ROI was freely selected *via* a charge-coupled device (CCD) camera (magnification, ×1.25/×2.5, Olympus Corporation, Tokyo, Japan) and the imaging area was then defined according to the maximum imaging point under a scan pitch of 40 μm. The illumination in the iMScope was operated under the following parameters: light type, *trans*-illumination; light intensity, 12%. Foci and observation points were controlled with a joystick and the XYZ stage (Kohzu Precision, Kanagawa, Japan) on which the electrically conductive glass slide was fixed. The XYZ coordinates, with position-feedback scales, immediately displayed the ROIs to make position reproducibility possible on a sub-micrometer order. The tissue

slices were then irradiated by a focused laser beam in synchrony with stage scanning. The laser in the iMScope system was a diode-pumped 355 nm Nd, YAG laser (Shimadzu Corporation, Kyoto, Japan), and operated under the following parameters: frequency, 1,000 Hz; laser intensity, 55.0; and laser diameter, 3 μm. All the experiments in this work were conducted with the minimum irradiation diameter and irradiated the tissue surface with 100 shots (repetition rate; 1,000 Hz) for each pixel.

Selection of Internal Standard and Semi-Quantitative of Bile Acids

Quantitative analysis with MALDI-TOF MS has been demonstrated for compounds of biological interest. For quantification, ISs are necessary to compensate for the poor shot-to-shot reproducibility inherent in the use of MALDI analysis. An ideal IS should be the stable isotope-labeled intact BAs during the qualitative and quantitative analyses of BAs (21). However, it was impractical in the present case due to synthesis challenges and time vs. cost concerns. Therefore, we want to search for some compounds that are chemically similar to BAs, have a quality close to BAs, and are chemically stable during the analysis process as ISs. Unfortunately, we did not find it either. While the NPA chosen for this analysis is chemically different from BAs, it still proved to be effective. NPA has been used to quantify BAs directly from plasma and urine by MALDI-TOF-MS (22, 23). The structure and MS spectrum of NPA are shown in **Supplementary Figure 1**. We used the average intensity ratio of each BA to NPA to quantitatively describe the relative exposure level of BAs in tissue sections. The average peak intensity ratio was calculated as follows: average peak intensity ratio = BAs average peak intensity/NPA average peak intensity.

Tissue Preparation for Histology

After MSI, the tissue sections were stained with hematoxylin and eosin (H&E) for examination based on a protocol (11). In brief, the tissue sections were stained with H&E as follows: the glass slides were gently washed with 70% ethanol to remove the matrix, followed by dipped in 100% ethanol at −20°C for 5 min, and then glass slides were put in distilled water for 2 min. The slides were then immersed in hematoxylin for 5 min, washed with tap water for 5 min, followed by differentiated with 1% hydrochloric acid alcohol for 5 s, and blued in running tap water for 10 min. Staining by eosin for 5 s was followed by a wash with tap water for 5 min. Slides were then dipped in 90% ethanol for 6 min, and 100% ethanol for 2 × 5 min, followed by placing them in three different xylene baths for 5 min each. Finally, The H&E slides were sealed with neutral gum and scanned using an iMScope TRIO (Shimadzu, Japan) instrument.

Statistical Analysis

Data in bar graphs are expressed as mean ± SEM. The Shapiro-Wilcoxon test was used to test the Gaussian distribution of biological parameters. The Student t test was used for comparison between two groups. The Mann-Whitney test was used for variables that were not normally distributed. Correlations were assessed with the Pearson correlation coefficient or as indicated in the graphs. All statistical analysis was performed using SPSS (version 25), considering value of $p < 0.05$ as statistically significant. ROI analysis by using Imaging MS Solution software (version 1.30). The p of comparison for ROI analyses was assessed *via* average peak intensities or signals acquired from MS spectra of areas indicated by ROI. Low values of p ($p < 0.05$) denote significant differences between average peak intensities or signals of targets within the stipulated ROIs.

RESULTS AND DISCUSSION

Determination of spatial distribution and quantification of BAs in animal models are challenging due to shortage of suitable methods. Here, we adopted a novel iMScope coupled with MALDI-TOF-MS for simultaneously mapping and semi-quantitating the BAs in tissues of mice. There is no precedent to analyze the spatial distribution and quantitative study of BAs within the enterohepatic circulation. Moreover, our work makes it possible to detect the relative content and spatial distribution of BAs in liver, ileum, and colon tissue sections from short-term HFD feeding mice, which provides a new perspective for the study of gastrointestinal diseases.

The Optimal Laser Intensity for Each Set "Laser Diameter" Value and the Diameter of the Laser in That Case

Supplementary Figure 2 shows approximate values of the optimal laser intensity for each set "Laser Diameter" value and the diameter of the laser in that case. Use this as a guide for the laser intensity and measurement pitch to be set when changing the laser diameter. The example in **Supplementary Figure 2** is for the optimal laser intensity when depositing DHB in mouse liver homogenate and measuring lipids in positive ion mode.

N-1-Naphthylphthalamic Acid Was Selected as an Internal Standard to Semi-Quantify Bile Acids in Tissues

As shown in **Supplementary Figure 1**, the IS (NPA) is seen at *m/z* 290.082, although NPA is chemically different from BAs, there are an adequate signal and no interference peaks in the mass spectrum of NPA. Therefore, it is a feasible method to quantitatively describe the relative exposure level of BAs in tissue sections by the average intensity ratio of each BA to NPA. Two of the major impediments to the application of MALDI to quantitative experiments are signal suppression and signal interference, especially, of less concentrated components (24). However, this effect can be compensated for the use of an IS and optimization of the experimental parameters (24). NPA, chemically different from BAs, has been proved to be effective in quantifying BAs directly from plasma and urine by MALDI-TOF-MS (22, 23). In our study, we compared the BA content of different groups, we sprayed 10 mg ml^{-1} NPA evenly on the tissue sections, and it could be clearly seen through iMScope that NPA exhibits good uniformity and stability. We divided the average peak intensity of BAs by the average peak intensity of

NPA to obtain the average peak intensity ratio of each BA. We compared the average peak intensity ratio of each BA in different groups to obtain the final results, which eliminated the influence of signal suppression and signal interference of different groups on the comparison results to a certain extent.

The Structures of Bile Acids

In our study, eleven BAs conjugates were selected for analysis: DCA, CDCA, UDCA, TDCA, TCDCA, TUDCA, LCA, TLCA, TCA, TMCA, and GCA. The structures for these compounds are shown in **Supplementary Figure 3**. It should be noted that the putative identification using MSI technology is only based on the measured accurate *m/z* value, so it is impossible to distinguish the isomers of the target compound with the same molecular formula (e.g., *m/z* 498.2895, putative identification as TCDCA/TUDCA/TDCA). BAs show a high degree of isomerism and similar binding (11, 25), as a result, many BAs share the same molecular formula, so it is impossible to determine the contribution of several isomers (e.g., TCDCA, TUDCA, and TDCA) in the net *m/z* signal peak intensity (*m/z* 498.2895 here) and the corresponding *m/z* image. Based on previous quantitative studies of BAs in rat liver, we assumed that all isomers contributed to the ion abundance (25, 26). In order to distinguish the contribution of each isomer to ion abundance, MS^n of commercially available standards of the different isomers should be considered.

9-Aminoacridine Was Selected as Matrix for the Analysis of Bile Acids Based on Novel Imaging Mass Microscope

The MALDI matrixes, aromatic compounds of low molecular mass, which are crucial for optimal signal-to-noise levels and the quality of data, are used to enhance the ionization efficiency and prevent the analytes from degrading. Owing to the specific ionization property of the individual matrix, the selection of a suitable matrix is understandably critical to MALDI-MS. MALDI matrices are chosen based on their ability to provide sufficient ionization efficiency for a given analytes class (e.g. low molecular weight metabolites, lipids, proteins, polymers, or inorganic compounds) or sub-class (27). Differences in observed analyte sensitivities can be attributed to the physical properties of a matrix such as molecular structure, pH, proton affinity, and peak wavelength absorbance (28). Thus, we investigated three conventional matrices, namely DHB, CHCA and 9AA, to screen the optimum matrix via studying their abilities to form co-crystals onto tissue sections. DHB is the most widely employed and studied MALDI matrix offering sufficient sensitives for many analyte classes in MS analysis (29). 9AA is often used for the analysis of low molecular weight compounds in negative ion mode MS analysis and CHCA ionizes many drugs with high sensitivity in both polarities (30). As shown in **Supplementary Figure 4**, the ion signal of BAs generated by iMScope is evenly scattered over the tissue sections. The average ion signal intensity of the BA images in **Supplementary Figures 4B,C** (using CHCA and DHB as the matrix) is much lower than that in **Supplementary Figure 4A** (using 9AA as the matrix). According to the findings above, 9AA was confirmed to be the most suitable matrix for the analysis of BAs based on iMScope. In conclusion, by using 9AA as the matrix and NPA as IS, we have developed a method for semi-quantitative BAs using MALDI-IMS.

Mass Spectrometry Imaging-Based Visual Mapping Profiles of Bile Acids Distributed Within Regions of Liver in High-Fat Diet-Fed Mice

Bile acid synthesis occurs in the liver. Before the synthetic BA enters the duodenum, the liver BAs bind to glycine or taurine. The conjugated BA is stored in the gallbladder until it is released to the duodenum after eating (31). BAs in the human body are mainly conjugated to glycine and less to taurine, while BAs in mice and rats are almost completely conjugated to taurine (6). Here, we detected non-conjugated BAs CDCA/UDCA/DCA and conjugated BAs TCDCA/TUDCA/TDCA and TCA/TMCA in the liver. We found that when compared with the control group MS ion image, the ion intensity of CDCA/UDCA/DCA, TCDCA/TUDCA/TDCA and TCA/TMCA in liver tissue sections of mice fed with HFD for 4 weeks was decreased significantly, especially, TCDCA/TUDCA/TDCA, TCA/TMCA (**Figure 1**). **Supplementary Figures 5A,C,E**, respectively, shows the mass spectra of CDCA/UDCA/DCA, TCDCA/TUDCA/TDCA, TCA/TMCA and NPA. NPA-based mean peak intensity ratios also showed that CDCA/UDCA/DCA, TCDCA/TUDCA/TDCA and TCA/TMCA in liver tissue sections of mice fed with HFD for 4 weeks were lower than those in the control group (**Supplementary Figures 5B,D,F**). BAs have become established as important signaling molecules that enable fine-tuned inter-tissue communication within the enterohepatic circulation. Mounting pieces of evidence indicate that changes in overall BA levels and specific BA metabolites are involved in metabolic diseases, gastrointestinal, and liver cancer (32).

Here, we clearly showed that 1 month of HFD-feeding resulted in visible multiple BAs zonation patterns and might have disturbed the inherent BAs gradients or functional zonal differences in enterohepatic circulation. Taking the spatial information into account is crucial to investigate the underlying mechanisms of injury induced by site-specific BA alterations. Combined with the transport network of BAs in the liver, we analyzed the distribution of TCDCA/TUDCA/TDCA and TCA/TMCA in mouse liver tissue sections at high spatial resolution. As expected, BAs were not evenly distributed in the liver and showed a certain regional aggregation pattern, which had been clearly shown from the MS ion image (**Figure 2**). It should be pointed out that **Figure 2** is derived from the HFD group in **Figure 1A**. The green arrows indicated bile ducts, whereas the red arrows showed blood vessels. **Figure 2** shows MS ion images of the spatial distribution of taurine-conjugated BAs identified in the same tissue section at high spatial resolution. The results showed that there were higher ion signal intensities at *m/z* 498.2895 $\pm$ 0.05 (TCDCA/TUDCA/TDCA) and *m/z* 514.2844 $\pm$ 0.05 (TCA/TMCA) at the bile ducts indicated by the green arrows. The bile duct, portal venule, and portal arteriole form the portal trial, in which the bile duct receives bile from

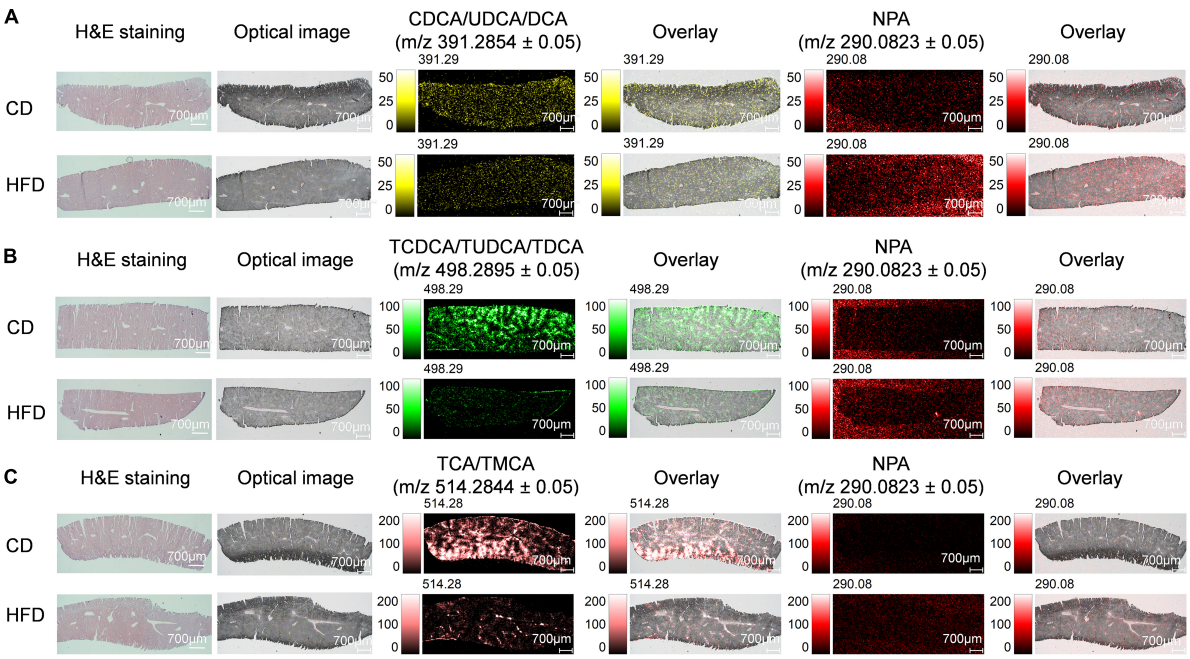

FIGURE 1 | MS imaging-based visual mapping profiles of BAs distributed within regions of liver. MS ion images representing spatial distributions of NPA (*m/z* 290.0823 ± 0.05) and the identified BAs at CDCA/UDCA/DCA *m/z* 391.2854 ± 0.05 **(A)**, TCDCA/TUDCA/TDCA *m/z* 498.2895 ± 0.05 **(B)** and TCA/TMCA *m/z* 514.2844 ± 0.05 **(C)** for the whole section of mouse liver (Scale bars: 1,000 μm). Overlay: Overlay of each MS ion image and optical image. All ion images were normalized to the 9AA matrix signal. Abbreviation: CD, control diet group; HFD, high-fat diet group.

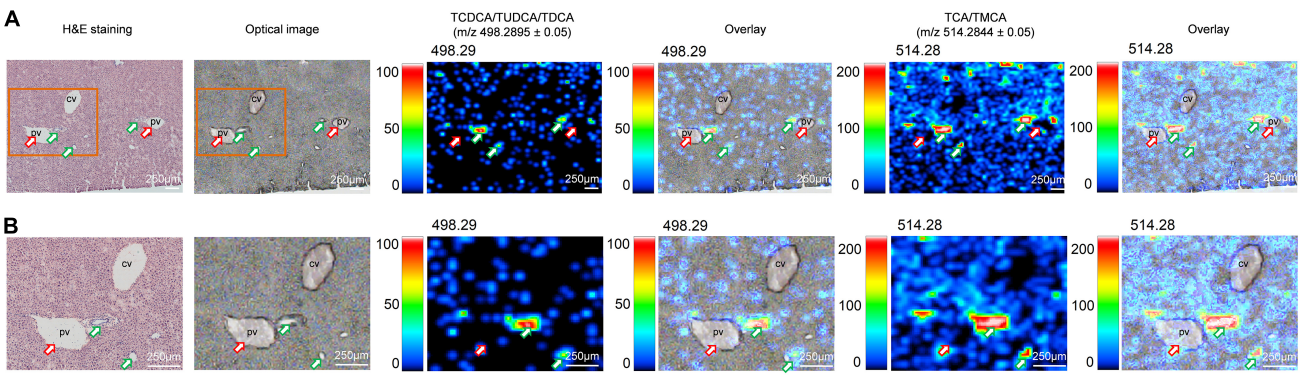

FIGURE 2 | Imaging MS visualize the zonation patterns of BA metabolism in liver of HFD-fed mice. MS ion images representing spatial distributions of the identified taurine-conjugated BAs at *m/z* 498.2895 ± 0.05 (TCDCA/TUDCA/TDCA) and *m/z* 514.2844 ± 0.05 (TCA/TMCA) for the mouse liver in same tissue section at high spatial resolution. Overlay: Overlay of each MS ion image and optical image. All ion images were normalized to the 9AA matrix signal. The green arrows indicated bile ducts, whereas the red arrows showed blood vessels. Scale bars: 250 μm.

bile canaliculi. Our results have shown that MS ion images in the same liver tissue section at high spatial resolution show that there are zonation patterns and regional differences characteristics of BAs in tissues. Thus, the liver, BAs site of production, displayed physiological and functional zonal differences in the periportal zone versus the centrilobular zone. Therefore, our method can not only explore the spatial distribution characteristics and content variety of BAs in the liver but also intuitively see the distribution characteristics of BAs around blood vessels and bile ducts in liver tissue.

Mass Spectrometry Imaging-Based Visual Mapping Profiles of Bile Acids Distributed Within Regions of Ileum and Colon in High-Fat Diet-Fed Mice

The intestinal tract, modified by the gut microbiota, showed regional differences in BA metabolism (33). After exerting physiological functions, such as dissolving and digesting fat-soluble nutrients, most of BAs are then absorbed by passive diffusion and active transport from the terminal

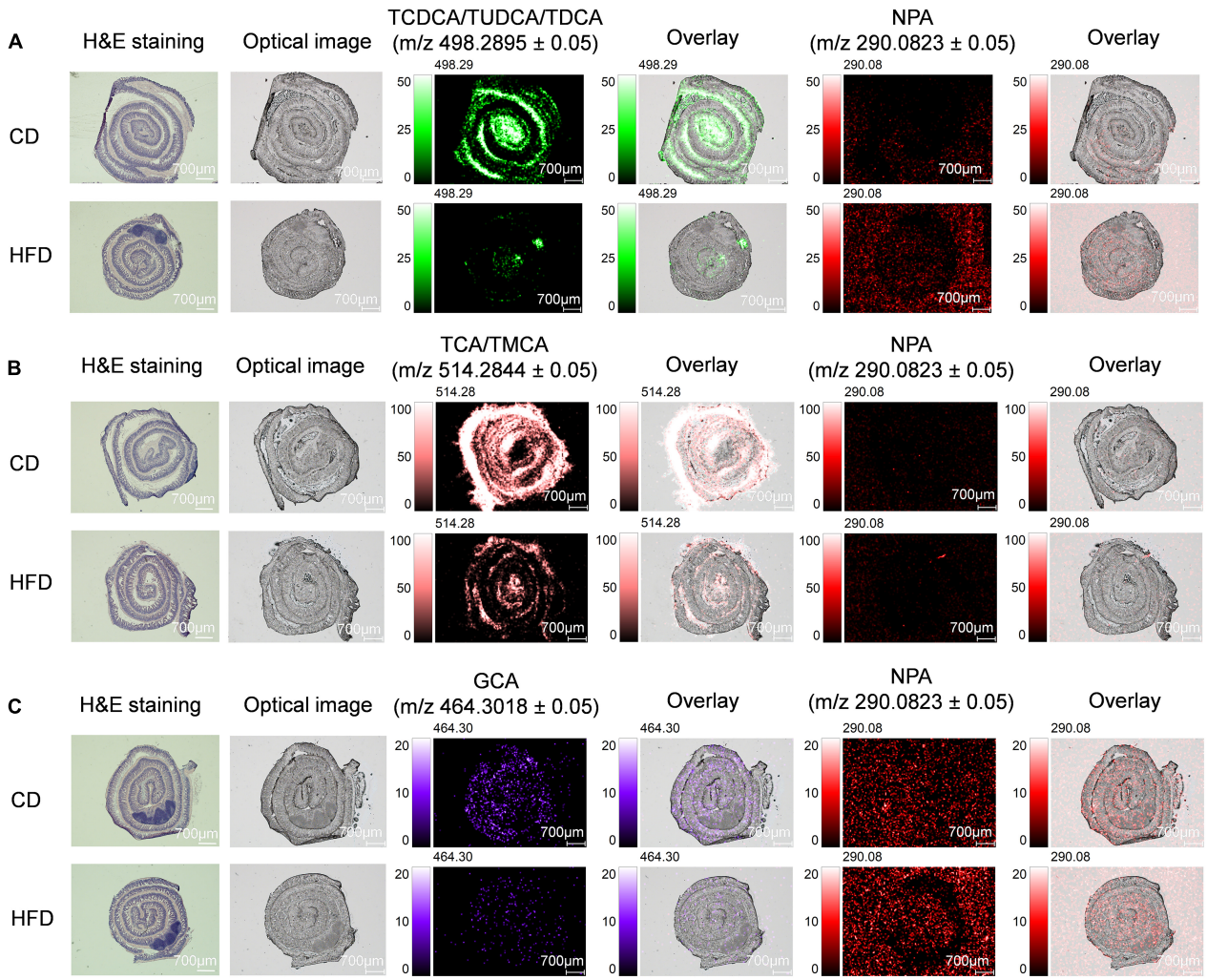

FIGURE 3 | MS imaging-based visual mapping profiles of BAs distributed within regions of ileum. MS ion images representing spatial distributions of NPA (*m/z* 290.0823 ± 0.05) and the identified BAs at TCDCA/TUDCA/TDCA *m/z* 498.2895 ± 0.05 **(A)**, TCA/TMCA *m/z* 514.2844 ± 0.05 **(B)** and GCA *m/z* 464.3018 ± 0.05 **(C)** for the whole section of mouse ileum (Scale bars: 700 μm). Overlay: Overlay of each MS ion image and optical image. All ion images were normalized to the 9AA matrix signal. Abbreviation: CD, control diet group; HFD, high-fat diet group.

ileum and transported back to the liver *via* the portal vein, and the rest is excreted with feces. Therefore, the terminal ileum is also the main site of BAs accumulation, especially, conjugated BAs. We took a 3-cm long mouse terminal ileum and rolled it up in a "Swiss roll" (34). Here, we focused on the level of BAs in the ileum. The spatial distribution of TCDCA/TUDCA/TDCA, TCA/TMCA, GCA, and NPA in ileum sections is shown in **Figure 3**. We found that when compared with the control group MS ion image, the ion intensity of TCDCA/TUDCA/TDCA, TCA/TMCA, and GCA in ileum tissue sections of mice fed with HFD for 4 weeks was decreased significantly, especially TCDCA/TUDCA/TDCA and TCA/TMCA decreased more significantly, which were also proved by the average peak intensity ratio based on NPA (**Supplementary Figures 6B,D,F**). TCA/TMCA signal strength was the highest. **Supplementary Figures 6A,C,E** shows the mass spectra of TCDCA/TUDCA/TDCA, TCA/TMCA, GCA, and NPA.

In the colon, bacterial enzymes catalyze the deconjugation and dehydroxylation of primary BAs to produce secondary BAs. Here, we focused on the level of BAs in the colon, eleven BA signals are found in the tissue, as shown in **Figure 4**. All ion images were created based on the signals from the deprotonated molecules: NPA at *m/z* 290.0823 ± 0.05, CDCA/UDCA/DCA at *m/z* 391.2854 ± 0.05, TCDCA/TUDCA/TDCA at *m/z* 498.2895 ± 0.05, LCA at *m/z* 375.2905 ± 0.05, TLCA at *m/z* 482.2946 ± 0.05, TCA/TMCA at *m/z* 514.2844 ± 0.05, and GCA at *m/z* 464.3018 ± 0.05. The grating width of the whole tissue section was 700 μm (**Figure 4**). The spatial distribution of CDCA/UDCA/DCA and NPA in colon sections is shown in **Figure 4A**. **Supplementary Figure 7A** shows the mass spectra of CDCA/UDCA/DCA and NPA. We found that

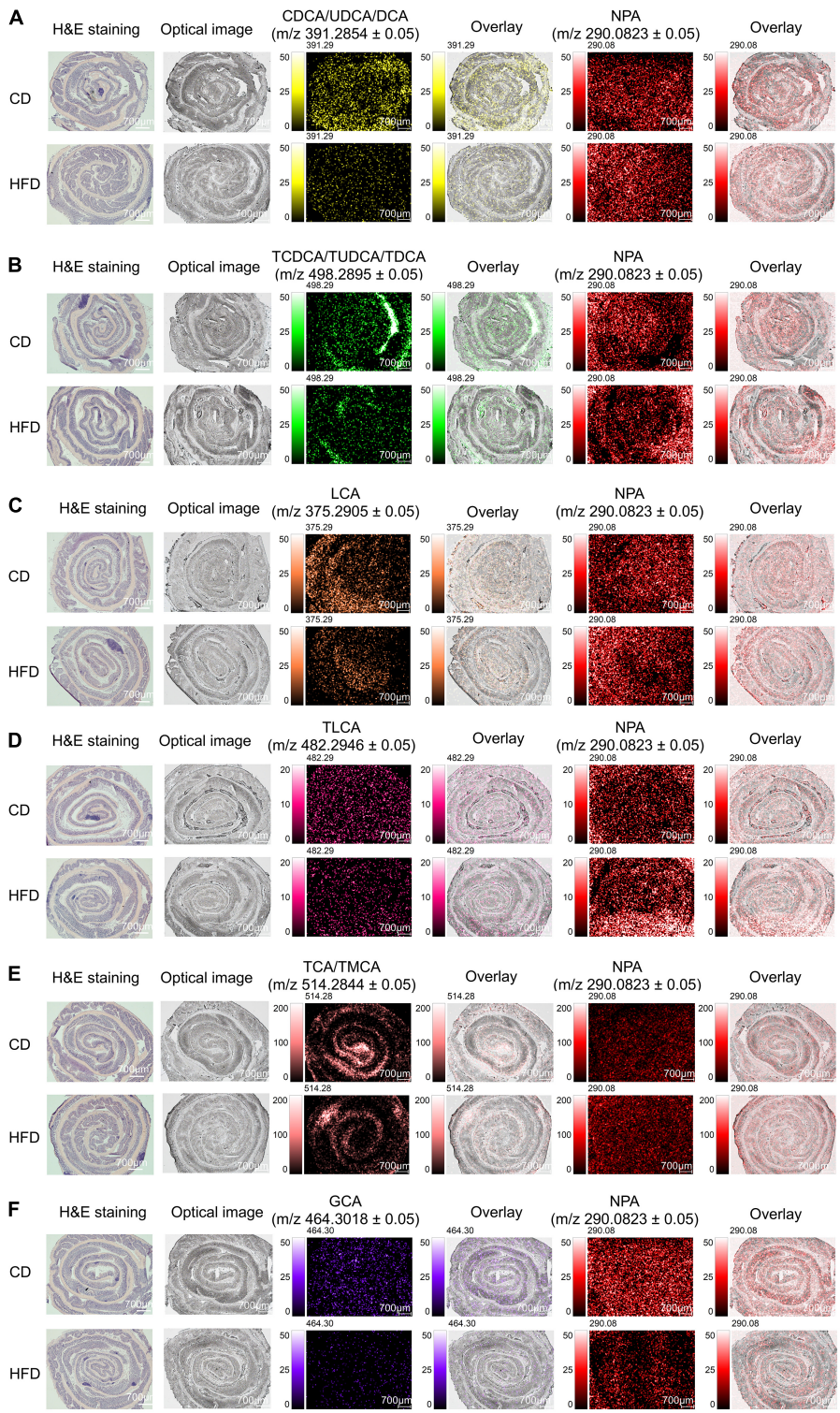

FIGURE 4 | MS imaging-based visual mapping profiles of BAs distributed within regions of colon. MS ion images representing spatial distributions of NPA (*m/z* 290.0823 ± 0.05) and the identified BAs at CDCA/UDCA/DCA *m/z* 391.2854 ± 0.05 **(A)**, TCDCA/TUDCA/TDCA *m/z* 498.2895 ± 0.05 **(B)**, LCA *m/z* 375.2905 ± 0.05 **(C)**, TLCA *m/z* 482.2946 ± 0.05 **(D)**, TCA/TMCA *m/z* 514.2844 ± 0.05 **(E)** and GCA *m/z* 464.3018 ± 0.05 **(F)** for the whole section of mouse colon (Scale bars: 700 μm). Overlay: Overlay of each MS ion image and optical image. All ion images were normalized to the 9AA matrix signal. Abbreviation: CD,control diet group; HFD, high-fat diet group.

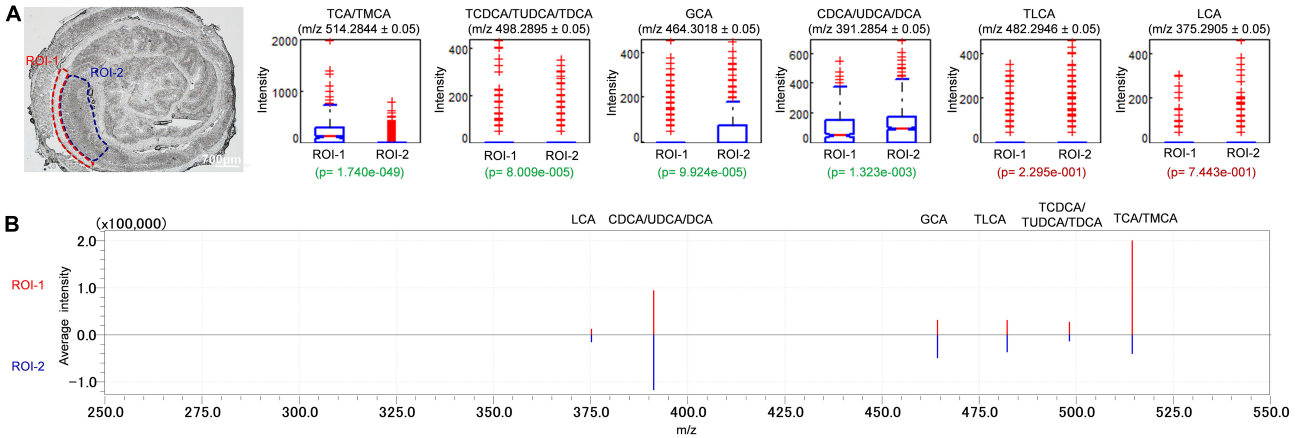

FIGURE 5 | Distribution profiles of BAs in colon were studied through comparison of relative intensities of BAs by the values of p between ROI-1 and ROI-2. Signal intensities of targeted BAs in ROI of two different regions of colon were depicted and signal normalization was performed by pixel. ROI-1: submucosa, muscular layer and adventitia; ROI-2: mucosa layer. The letter '*p*' denotes the statistical *p*-value of the comparison, significant differences were highlighted in green font while insignificant differences were highlighted in red font **(A)**. The spectrum of each ROI which set in **(A)**. The spectra were vertically inverted, with that of ROI-1 above in red and that of ROI-2 below in blue **(B)**.

when compared with the control group MS ion image, the ion intensity of CDCA/UDCA/DCA in colonic tissue sections of mice fed with HFD for 4 weeks was decreased significantly, which was also proved by the average peak intensity ratio of CDCA/UDCA/DCA based on NPA (**Supplementary Figure 7B**). The MS ion images of the other eight observed BAs showed the same tendency as CDCA/UDCA/DCA. After feeding with HFD for 4 weeks, the ion intensities of TCDCA/TUDCA/TDCA, LCA, TLCA, TCA/TMCA, and GCA were decreased significantly (**Figures 4B–F**). The average peak intensity ratio of each BA based on NPA was also significantly different (**Supplementary Figures 7D,F,H,J,L**), and the trend was consistent with their MS ion images. **Supplementary Figures 7C,E,G,I,K** shows the mass spectra of TCDCA/TUDCA/TDCA, LCA, TLCA, TCA/TMCA, GCA, and NPA. By overlaying the acquired MS ion images with their respective optical images (**Figure 4**), it was discovered that the intensities of BAs were diffusely distributed in colonic tissue. Our results indicate that HFD feeding reduced BAs signal in colon sections by impairing the active and passive reabsorption of BAs in the intestine, which resulted in a significant increase in fecal excretion of BAs. In addition, it is worth noting that BAs play a crucial role in limiting bacterial overgrowth through intestinal FXR, so as to protect the intestine from bacterial damage, and the chronic low-grade inflammation of the intestine caused by HFD may be related to the decrease of BAs content in the intestinal tissue sections observed in this study (1–5).

To evaluate the relative abundance and distribution of detectable BAs in the sampled colon tissues, we further analyzed the mass spectra data through multiple ROI analyses of detectable BAs (**Figure 5**). Several serial sections (each measuring 10 μm) of sampled colon tissues were used to evaluate the reproducibility of iMScope technique. The relative abundance of BAs by their values of *p* were compared between randomly selected ROIs in submucosa, muscular layer, and adventitia (ROI-1) and mucosa layer (ROI-2) of the sectioned colon tissues. The *p* in this context is defined as the statistical analyses of average intensities/signals acquired from areas specified by ROI. A small p ($p < 0.05$) denotes a low likelihood that average intensity values are equal between ROIs. For colonic tissue sections, the relative abundances of TCA/TMCA, TCDCA/TUDCA/TDCA, GCA, and CDCA/UDCA/DCA in the ROI-1 were significantly different from ROI-2 (**Figure 5A**). The box plot displays the intensity distribution of each measurement point for the applicable *m/z* value. ROI-1 is displayed on the left and ROI-2 on the right. The upper and lower blue lines are displayed at the position of 25% (25th if there are 100 measurement points) and 75%, respectively. The red line in the center of the "box" is the median. The notches of the "box" represent the difference of the median. The notches indicate the 95% confidence interval (CI) of the median (the median range of the population estimated from the median of samples with a probability of 95%). If the 95% CI of median (notch length) does not overlap between two groups (ROI-1 and ROI-2), the two groups are considered different in the median with a probability of 95% ($p < 0.05$). However, overlapping does not always indicate that there is no significant difference between the two groups. In other words, if the notches of ROI-1 and ROI-2 are not at the same height, this means that the intensity of ROI-1 and that of ROI-2 have medians that differ by a significance level of 5%. The "whiskers" extending upward and downward from the "box" indicate the range of 1.5× the length of the box. Intensity values beyond the length of the "whiskers" are displayed with a red+ as outliers with significant deviance from the median. If the median is not in the center of the "box," this means that the intensity distribution is skewed. When checking the test results, the statistical values of the samples (spectrum peak intensity at measurement points) visualized with box plots can be referred to values of *p*. **Figure 5B** is the spectrum of each ROI which is set in **Figure 5A**.

The spectra are vertically inverted, with that of ROI-1 above in red and that of ROI-2 below in blue. The abundances of TCA/TMCA and TCDCA/TUDCA/TDCA were higher in the ROI-1, while the relative abundances of GCA and CDCA/UDCA/DCA in the ROI-2 were higher than ROI-1. In addition, there were no significant differences in the distribution of TLCA and LCA in ROI-1 and ROI-2. A significant advantage of the iMScope we used was that we further analyzed the mass spectra data through multiple ROI analyses of detectable BAs. We have identified that the relative abundances of TCA/TMCA, TCDCA/TUDCA/TDCA, GCA, and CDCA/UDCA/DCA in the ROI of the colonic mucosal layer were significantly different from submucosa, muscular layer, and adventitia. Overall, one important future direction of ROI analyses and high spatial resolution is to connect the spatial distribution and signal intensity of BAs with tissue damage in a disease state, so as to provide guidance for us to study the pathogenesis and treatment of gastrointestinal diseases.

Our previous work, and the work of others, showed that only relevant BA changes but not spatial information were obtained since the whole tissue is extracted in one homogenate when traditional MS spectrometry techniques [such as high-performance liquid chromatography (HPLC)-MS/MS] were adopted (2–4, 35–38). However, huge increasing demand on the spatial distribution and content of BAs has become an essential part of metabolic-associated diseases and cancer research (6–10, 32, 33, 39). MALDI-MS can not only analyze and visualize selected molecules but also maintain their spatial distribution and the integrity of the sample, which is an advantage that other MS technologies do not have (40, 41). Genangeli et al. investigated the effect of soyasaponin on the distribution of BAs in duodenum and colon by MALDI-MSI (41). In other study, Kampa et al. (25) investigated the spatial abundances of Amitriptyline, lipids, and BAs in Amitriptyline-treated male rat liver tissue by using MALDI-MSI, and they found two BA signals *m/z* 498.289 (TCDCA/TDCA) and *m/z* 514.284 (TCA/TMCA) showed slight downregulation due to Amitriptyline treatment without comment upon the role of BAs homeostasis in the observed toxicological response. Specifically, the fold change of Bas is based on the average peak intensity of the particular monoisotopic peak within the analyzed region (25). Furthermore, MSI, which combines detailed molecular characterization with spatial distribution measurements, has been applied for determining spatial distribution of BAs in mouse liver biliary networks and also has a certain application in the spatial distribution of BAs in the intestine (11, 25, 41). Although there are important discoveries revealed by these studies, there are also limitations. First, less high-resolution spatial location information; second, without quantitative research combined with spatial location information. Thus, further exploration of BAs on quantitative and interaction with histopathological damage should be examined. iMScope is a powerful tool for MSI, which combines detailed molecular characterization with spatial distribution measurement. Especially the combination of optical microscope and mass spectrometer. The microscope area can be enlarged from 1.25 to 40 times with a CCD camera. In the mass spectrum, the combination of the ion trap and TOF enables it to have both the MS capability of the ion trap and the high-precision mass measurement capability based on TOF, which can achieve excellent sensitivity, good repeatability, and stable mass accuracy (42). Therefore, iMScope is ideal to accurately determine the ROI of the liver and intestines. In addition, the MALDI-MSI technique does not require *a priori* information about the chemical substances present in the tissue section, thus allowing the distribution of many different substances to be mapped in a single experiment (43). Our method, in which 9AA is used as matrix and NPA as IS, can simultaneously measure eleven different BAs by the MALDI-MSI technique. Meanwhile, iMScope can also provide information about the morphology and tissue heterogeneity of specific regions (44, 45). It can increase the applicability of the experimental method.

In summary, in addition to MS ion images that can identify the spatial distribution of BAs with low spatial resolution, the iMScope can also display high spatial resolution MS ion images of the same tissue section. Using a short-term HFD feeding mice model, we fully verified the feasibility and sensitivity of our current method for analyzing the spatial distribution and content of BAs in tissues. Our study further demonstrates even greater potency for a more clear understanding of the mechanism and treatment of gastrointestinal diseases by given spatial distribution and content information of BAs within the enterohepatic circulation.

CONCLUSION

Our method can not only detect the relative content of BAs in tissues, but also intuitively display and compare the changes and spatial distribution of BAs content or intensity in different parts of the same tissue. This method has wide application value. Taking the spatial information of BAs into account is crucial to investigate the underlying mechanisms of tissues injury induced by site-specific metabolic alterations, one important future direction of analysis of BAs is fully deciphering the complete molecular signatures of BAs in different biological samples and link them to the pathology of the corresponding diseases. Our method has laid a solid foundation for this development direction.

DATA AVAILABILITY STATEMENT

The original contributions presented in the study are included in the article/**Supplementary Material**, further inquiries can be directed to the corresponding authors.

ETHICS STATEMENT

The animal study was reviewed and approved by China Medical University.

AUTHOR CONTRIBUTIONS

H-XL and Z-YW conceived of the study and participated in its design and coordination. QZ and Z-HW carried out the experimental work and were responsible for analyzing the data. Z-HW, S-SZ, JY, LC, and X-YW were responsible for animal experiments. All authors have given approval to the final version of the manuscript.

FUNDING

This research received financial support from the General Project of Liaoning Provincial Department of Education under grant no. LJKZ0758.

SUPPLEMENTARY MATERIAL

The Supplementary Material for this article can be found online at: https://www.frontiersin.org/articles/10.3389/fnut.2022.858603/full#supplementary-material

Supplementary Figure 1 | The structures and mass spectrum of NPA.

Supplementary Figure 2 | Approximate values of the optimal laser intensity for each set "laser diameter" value and the diameter of the laser in that case.

Supplementary Figure 3 | The structures of BAs.

Supplementary Figure 4 | Imaging MS analysis of the BAs in mouse liver generated by iMScope (The scale bar is 700 μm). Imaging MS analysis of TDCA/TCDCA/TUDCA at *m/z* 498.2895 ± 0.05; TCA/TMCA at *m/z* 514.2844 ± 0.05 with 9AA as the matrix **(A)**. Imaging MS analysis of TDCA/TCDCA/TUDCA at *m/z* 498.2895 ± 0.05; TCA/TMCA at *m/z* 514.2844 ± 0.05 with CHCA as the matrix **(B)**. Imaging MS analysis of TDCA/TCDCA/TUDCA at *m/z* 498.2895 ± 0.05; TCA/TMCA at *m/z* 514.2844 ± 0.05 with DHB as the matrix **(C)**. The structures of 9AA, DHB and CHCA **(D)**.

Supplementary Figure 5 | MALDI-MSI single pixel mass spectra from liver tissue and average peak intensity ratio of BAs. $^{**}p < 0.01$, $^{***}p < 0.001$ versus CD group (*n ge* 6).

Supplementary Figure 6 | MALDI-MSI single pixel mass spectra from ileum tissue and average peak intensity ratio of BAs. $^{**}p < 0.01$, $^{***}p < 0.001$ versus CD group (*n ge* 6).

Supplementary Figure 7 | MALDI-MSI single pixel mass spectra from colon tissue and average peak intensity ratio of BAs. $^{*}p < 0.05$, $^{**}p < 0.01$, $^{***}p < 0.001$ versus CD group (*n ge* 6).

REFERENCES

1. Liu HX, Keane R, Sheng L, Wan YJ. Implications of microbiota and bile acid in liver injury and regeneration. *J Hepatol.* (2015) 63:1502–10. doi: 10.1016/j.jhep.2015.08.001
2. Liu HX, Rocha CS, Dandekar S, Wan YJ. Functional analysis of the relationship between intestinal microbiota and the expression of hepatic genes and pathways during the course of liver regeneration. *J Hepatol.* (2016) 64:641–50. doi: 10.1016/j.jhep.2015.09.022
3. Hu Y, Liu HX, Jena PK, Sheng L, Ali MR, Wan YY. miR-22 inhibition reduces hepatic steatosis via FGF21 and FGFR1 induction. *JHEP Rep.* (2020) 2:100093. doi: 10.1016/j.jhepr.2020.100093
4. Sheng L, Jena PK, Liu HX, Hu Y, Nagar N, Bronner DN, et al. Obesity treatment by epigallocatechin-3-gallate-regulated bile acid signaling and its enriched *Akkermansia muciniphila*. *FASEB J.* (2018) 32:fj201800370R. doi: 10.1096/fj.201800370R
5. Sheng L, Jena PK, Hu Y, Liu HX, Nagar N, Kalanetra KM, et al. Hepatic inflammation caused by dysregulated bile acid synthesis is reversible by butyrate supplementation. *J Pathol.* (2017) 243:431–41. doi: 10.1002/path.4983
6. Jia W, Xie G, Jia W. Bile acid-microbiota crosstalk in gastrointestinal inflammation and carcinogenesis. *Nat Rev Gastroenterol Hepatol.* (2018) 15:111–28. doi: 10.1038/nrgastro.2017.119
7. Li T, Chiang JY. Bile acid signaling in metabolic disease and drug therapy. *Pharmacol Rev.* (2014) 66:948–83. doi: 10.1124/pr.113.008201
8. Yang J, Palmiotti A, Kuipers F. Emerging roles of bile acids in control of intestinal functions. *Curr Opin Clin Nutr Metab Care.* (2021) 24:127–33. doi: 10.1097/MCO.0000000000000709
9. Li R, Andreu-Sánchez S, Kuipers F, Fu J. Gut microbiome and bile acids in obesity-related diseases. *Best Pract Res Clin Endocrinol Metab.* (2021) 35:101493. doi: 10.1016/j.beem.2021.101493
10. Swann JR, Want EJ, Geier FM, Spagou K, Wilson ID, Sidaway JE, et al. Systemic gut microbial modulation of bile acid metabolism in host tissue compartments. *Proc Natl Acad Sci USA.* (2011) 108(Suppl. 1):4523–30. doi: 10.1073/pnas.1006734107
11. Rzagalinski I, Hainz N, Meier C, Tschernig T, Volmer DA. MALDI mass spectral imaging of bile acids observed as deprotonated molecules and proton-bound dimers from mouse liver sections. *J Am Soc Mass Spectrom.* (2018) 29:711–22. doi: 10.1007/s13361-017-1886-6
12. Griffiths WJ, Sjovall J. Bile acids: analysis in biological fluids and tissues. *J Lipid Res.* (2010) 51:23–41. doi: 10.1194/jlr.R001941-JLR200
13. Bobeldijk I, Hekman M, de Vries-van der Weij J, Coulier L, Ramaker R, Kleemann R, et al. Quantitative profiling of bile acids in biofluids and tissues based on accurate mass high resolution LC-FT-MS: compound class targeting in a metabolomics workflow. *J Chromatogr B Analyt Technol Biomed Life Sci.* (2008) 871:306–13. doi: 10.1016/j.jchromb.2008.05.008
14. Alnouti Y, Csanaky IL, Klaassen CD. Quantitative-profiling of bile acids and their conjugates in mouse liver, bile, plasma, and urine using LC-MS/MS. *J Chromatogr B Analyt Technol Biomed Life Sci.* (2008) 873:209–17. doi: 10.1016/j.jchromb.2008.08.018
15. Tian Y, Cai J, Allman EL, Smith PB, Patterson AD. Quantitative analysis of bile acid with UHPLC-MS/MS. *Methods Mol Biol.* (2021) 2194:291–300. doi: 10.1007/978-1-0716-0849-4_15
16. Lajczak-McGinley NK, Porru E, Fallon CM, Smyth J, Curley C, McCarron PA, et al. The secondary bile acids, ursodeoxycholic acid and lithocholic acid, protect against intestinal inflammation by inhibition of epithelial apoptosis. *Physiol Rep.* (2020) 8:e14456. doi: 10.14814/phy2.14456
17. Kurabe N, Igarashi H, Ohnishi I, Tajima S, Inoue Y, Takahashi Y, et al. Visualization of sphingolipids and phospholipids in the fundic gland mucosa of human stomach using imaging mass spectrometry. *World J Gastrointest Pathophysiol.* (2016) 7:235–41. doi: 10.4291/wjgp.v7.i2.235
18. Shimma S, Kumada HO, Taniguchi H, Konno A, Yao I, Furuta K, et al. Microscopic visualization of testosterone in mouse testis by use of imaging mass spectrometry. *Anal Bioanal Chem.* (2016) 408:7607–15. doi: 10.1007/s00216-016-9594-9
19. Nelson KA, Daniels GJ, Fournie JW, Hemmer MJ. Optimization of whole-body zebrafish sectioning methods for mass spectrometry imaging. *J Biomol Tech.* (2013) 24:119–27. doi: 10.7171/jbt.13-2403-002
20. Shimma S, Takashima Y, Hashimoto J, Yonemori K, Tamura K, Hamada A. Alternative two-step matrix application method for imaging mass spectrometry to avoid tissue shrinkage and improve ionization efficiency. *J Mass Spectrom.* (2013) 48:1285–90. doi: 10.1002/jms.3288
21. Wegner K, Just S, Gau L, Mueller H, Gérard P, Lepage P, et al. Rapid analysis of bile acids in different biological matrices using LC-ESI-MS/MS for the investigation of bile acid transformation by mammalian gut bacteria. *Anal Bioanal Chem.* (2017) 409:1231–45. doi: 10.1007/s00216-016-0048-1
22. Mims D, Hercules D. Quantification of bile acids directly from urine by MALDI-TOF-MS. *Anal Bioanal Chem.* (2003) 375:609–16. doi: 10.1007/s00216-003-1771-y
23. Mims D, Hercules D. Quantification of bile acids directly from plasma by MALDI-TOF-MS. *Anal Bioanal Chem.* (2004) 378:1322–6. doi: 10.1007/s00216-003-2475-z

24. Prentice BM, Chumbley CW, Hachey BC, Norris JL, Caprioli RM. Multiple time-of-flight/time-of-flight events in a single laser shot for improved matrix-assisted laser desorption/Ionization tandem mass spectrometry quantification. *Anal Chem.* (2016) 88:9780–8. doi: 10.1021/acs.analchem.6b02821
25. Kampa JM, Sahin M, Slopianka M, Giampà M, Bednarz H, Ernst R, et al. Mass spectrometry imaging reveals lipid upregulation and bile acid changes indicating amitriptyline induced steatosis in a rat model. *Toxicol Lett.* (2020) 325:43–50. doi: 10.1016/j.toxlet.2020.02.007
26. Suzuki Y, Kaneko R, Nomura M, Naito H, Kitamori K, Nakajima T, et al. Simple and rapid quantitation of 21 bile acids in rat serum and liver by UPLC-MS-MS: effect of high fat diet on glycine conjugates of rat bile acids. *Nagoya J Med Sci.* (2013) 75:57–71.
27. Zhou Q, Fulop A, Hopf C. Recent developments of novel matrices and on-tissue chemical derivatization reagents for MALDI-MSI. *Anal Bioanal Chem.* (2021) 413:2599–617. doi: 10.1007/s00216-020-03023-7
28. Perry WJ, Patterson NH, Prentice BM, Neumann EK, Caprioli RM, Spraggins JM. Uncovering matrix effects on lipid analyses in MALDI imaging mass spectrometry experiments. *J Mass Spectrom.* (2020) 55:e4491. doi: 10.1002/jms.4491
29. Schroter J, Fülöp A, Hopf C, Schiller J. The combination of 2,5-dihydroxybenzoic acid and 2,5-dihydroxyacetophenone matrices for unequivocal assignment of phosphatidylethanolamine species in complex mixtures. *Anal Bioanal Chem.* (2018) 410:2437–47. doi: 10.1007/s00216-018-0926-9
30. Kubo A, Kajimura M, Suematsu M. Matrix-assisted laser desorption/ionization (MALDI) imaging mass spectrometry (IMS): a challenge for reliable quantitative analyses. *Mass Spectrom (Tokyo).* (2012) 1:A0004. doi: 10.5702/massspectrometry.A0004
31. Thomas C, Pellicciari R, Pruzanski M, Auwerx J, Schoonjans K. Targeting bile-acid signalling for metabolic diseases. *Nat Rev Drug Discov.* (2008) 7:678–93. doi: 10.1038/nrd2619
32. Sun L, Cai J, Gonzalez FJ. The role of farnesoid X receptor in metabolic diseases, and gastrointestinal and liver cancer. *Nat Rev Gastroenterol Hepatol.* (2021) 18:335–47. doi: 10.1038/s41575-020-00404-2
33. Wahlström A, Sayin SI, Marschall HU, Bäckhed F. Intestinal crosstalk between bile acids and microbiota and its impact on host metabolism. *Cell Metab.* (2016) 24:41–50. doi: 10.1016/j.cmet.2016.05.005
34. Park CM, Reid PE, Walker DC, MacPherson BR. A simple, practical 'swiss roll' method of preparing tissues for paraffin or methacrylate embedding. *J Microsc.* (1987) 145(Pt 1):115–20. doi: 10.1111/j.1365-2818.1987.tb01321.x
35. Yang F, He Y, Liu HX, Tsuei J, Jiang X, Yang L, et al. All-trans retinoic acid regulates hepatic bile acid homeostasis. *Biochem Pharmacol.* (2014) 91:483–9. doi: 10.1016/j.bcp.2014.08.018
36. Sheng L, Jena PK, Liu HX, Kalanetra KM, Gonzalez FJ, French SW, et al. Gender differences in bile acids and microbiota in relationship with gender dissimilarity in steatosis induced by diet and FXR inactivation. *Sci Rep.* (2017) 7:1748. doi: 10.1038/s41598-017-01576-9
37. Jena PK, Sheng L, Liu HX, Kalanetra KM, Mirsoian A, Murphy WJ, et al. Western diet-induced Dysbiosis in Farnesoid X receptor knockout mice causes persistent hepatic inflammation after antibiotic treatment. *Am J Pathol.* (2017) 187:1800–13. doi: 10.1016/j.ajpath.2017.04.019
38. Jantti SE, Kivilompolo M, Ohrnberg L, Pietiläinen KH, Nygren H, Orešiè M, et al. Quantitative profiling of bile acids in blood, adipose tissue, intestine, and gall bladder samples using ultra high performance liquid chromatography-tandem mass spectrometry. *Anal Bioanal Chem.* (2014) 406:7799–815. doi: 10.1007/s00216-014-8230-9
39. Dermadi D, Valo S, Ollila S, Soliymani R, Sipari N, Pussila M, et al. Western diet deregulates bile acid homeostasis, cell proliferation, and tumorigenesis in Colon. *Cancer Res.* (2017) 77:3352–63. doi: 10.1158/0008-5472.CAN-16-2860
40. Vaysse PM, Heeren RMA, Porta T, Balluff B. Mass spectrometry imaging for clinical research - latest developments, applications, and current limitations. *Analyst.* (2017) 142:2690–712. doi: 10.1039/c7an00565b
41. Genangeli M, Heijens AMM, Rustichelli A, Schuit ND, Micioni Di Bonaventura MV, Cifani C, et al. MALDI-mass spectrometry imaging to investigate lipid and bile acid modifications caused by lentil extract used as a potential hypocholesterolemic treatment. *J Am Soc Mass Spectrom.* (2019) 30:2041–50. doi: 10.1007/s13361-019-02265-9
42. Fraga M, Vilariño N, Louzao MC, Fernández DA, Poli M, Botana L. Detection of palytoxin-like compounds by a flow cytometry-based immunoassay supported by functional and analytical methods. *Anal Chim Acta.* (2016) 903:1–12. doi: 10.1016/j.aca.2015.09.040
43. Norris JL, Caprioli RM. Analysis of tissue specimens by matrix-assisted laser desorption/ionization imaging mass spectrometry in biological and clinical research. *Chem Rev.* (2013) 113:2309–42. doi: 10.1021/cr3004295
44. Shariatgorji M, Svenningsson P, Andren PE. Mass spectrometry imaging, an emerging technology in neuropsychopharmacology. *Neuropsychopharmacology.* (2014) 39:34–49. doi: 10.1038/npp.2013.215
45. Tareke E, Bowyer JF, Doerge DR. Quantification of rat brain neurotransmitters and metabolites using liquid chromatography/electrospray tandem mass spectrometry and comparison with liquid chromatography/electrochemical detection. *Rapid Commun Mass Spectrom.* (2007) 21:3898–904. doi: 10.1002/rcm.3295

Conflict of Interest: The authors declare that the research was conducted in the absence of any commercial or financial relationships that could be construed as a potential conflict of interest.

Publisher's Note: All claims expressed in this article are solely those of the authors and do not necessarily represent those of their affiliated organizations, or those of the publisher, the editors and the reviewers. Any product that may be evaluated in this article, or claim that may be made by its manufacturer, is not guaranteed or endorsed by the publisher.

frontiers | Frontiers in Nutrition

ORIGINAL RESEARCH
published: 14 April 2022
doi: 10.3389/fnut.2022.849684

Maternal High-Fat Diet Impairs Placental Fatty Acid β-Oxidation and Metabolic Homeostasis in the Offspring

Ling Zhang, Ziwei Wang, Honghua Wu, Ying Gao, Jia Zheng and Junqing Zhang**

Department of Endocrinology, Peking University First Hospital, Beijing, China

Maternal overnutrition can affect fetal growth and development, thus increasing susceptibility to obesity and diabetes in later life of the offspring. Placenta is the central organ connecting the developing fetus with the maternal environment. It is indicated placental fatty acid metabolism plays an essential role in affecting the outcome of the pregnancy and fetus. However, the role of placental fatty acid β-oxidation (FAO) in maternal overnutrition affecting glucose metabolism in the offspring remains unclear. In this study, C57BL/6J female mice were fed with normal chow or high-fat diet before and during pregnancy and lactation. The placenta and fetal liver were collected at gestation day 18.5, and the offspring's liver was collected at weaning. FAO-related genes and AMP-activated protein kinase (AMPK) signaling pathway were examined both in the placenta and in the human JEG-3 trophoblast cells. FAO-related genes were further examined in the liver of the fetuses and in the offspring at weaning. We found that dams fed with high-fat diet showed higher fasting blood glucose, impaired glucose tolerance at gestation day 14.5 and higher serum total cholesterol (T-CHO) at gestation day 18.5. The placental weight and lipid deposition were significantly increased in maternal high-fat diet group. At weaning, the offspring mice of high-fat diet group exhibited higher body weight, impaired glucose tolerance, insulin resistance and increased serum T-CHO, compared with control group. We further found that maternal high-fat diet downregulated mRNA and protein expressions of carnitine palmitoyltransferase 2 (CPT2), a key enzyme in FAO, by suppressing the AMPK/Sirt1/PGC1α signaling pathway in the placenta. In JEG-3 cells, protein expressions of CPT2 and CPT1b were both downregulated by suppressing the AMPK/Sirt1/PGC1α signaling pathway under glucolipotoxic condition, but were later restored by the AMPK agonist 5-aminoimidazole-4-carboxyamide ribonucleoside (AICAR). However, there was no difference in CPT2 and CPT1 gene expression in the liver of fetuses and offspring at weaning age. In conclusion, maternal high-fat diet can impair gene expression involved in FAO in the placenta by downregulating the AMPK signaling pathway, and can cause glucose and lipid dysfunction of offspring at weaning, indicating that placental FAO may play a crucial role in regulating maternal overnutrition and metabolic health in the offspring.

Keywords: maternal high-fat diet, placenta, fatty acid β-oxidation, AMPK, offspring

OPEN ACCESS

Edited by:
Demin Cai,
Yangzhou University, China

Reviewed by:
Kate J. Claycombe,
United States Department of Agriculture (USDA), United States
Amanda Brandon,
The University of Sydney, Australia

****Correspondence:***
Jia Zheng
zhengjia@bjmu.edu.cn
Junqing Zhang
junqing.zhang@pkufh.com

Specialty section:
This article was submitted to Nutrition and Metabolism, a section of the journal Frontiers in Nutrition

Received: *06 January 2022*
Accepted: *22 March 2022*
Published: *14 April 2022*

Citation:
Zhang L, Wang Z, Wu H, Gao Y, Zheng J and Zhang J (2022) Maternal High-Fat Diet Impairs Placental Fatty Acid β-Oxidation and Metabolic Homeostasis in the Offspring. Front. Nutr. 9:849684. doi: 10.3389/fnut.2022.849684

INTRODUCTION

Diabetes and obesity are worsening problems worldwide, and the onset of metabolic diseases could be associated with an abnormal development environment in early life (1–3). In recent years, unhealthy diets, maternal diabetes, obesity, and excess gestation weight gain have been identified as the common and preventable risk factors that determine susceptibility to obesity and diabetes in the offspring (2, 3). Maternal nutrition during pregnancy and lactation is correlated with fetal and neonatal growth (4–7). Our previous study found that maternal overnutrition was associated with glucose intolerance, insulin intolerance, hyperglycemia and hyperlipidemia in the offspring (6–9). Increasing studies also indicate that this transgenerational effect even can be transmitted to the next generation (10–12). However, the underlying mechanisms remain largely unknown.

Placenta is a transient support organ that controls the crosstalk between mother and offspring (13, 14). Changes in placental function can alter the supply of key nutrients hormones, reactive oxygen species and inflammatory cytokines to the fetus (13, 15–17). It is indicated placental fatty acid metabolism plays an essential role in affecting the outcome of the pregnancy and fetus. Studies have presented that decreased fatty acid β-oxidation (FAO) in the placenta can lead to intracellular lipid accumulation, affecting fetal fatty acid delivery and altering fetal growth and development (18, 19). The process of FAO consists of two steps (20–22). At the first step, fatty acids are activated into acyl-coenzyme A (acyl-CoA) esters in the cytoplasm and then transported to the mitochondrial matrix. This step is determined by the carnitine palmitoyltransferase (CPT) system. The expression and activity of CPT1 and CPT2 are key factors that can regulate FAO. CPT1 is an enzyme located in the outer membrane of mitochondria which transfers the acyl group from acyl-CoA to carnitine (21). CPT2 is an enzyme located in the inner membrane of mitochondria which recovers acylcarnitine into acyl-CoA esters (21). At the second step, acyl-CoA is hydrolyzed into acetyl-CoA controlled by a series of enzymes, such as long chain acyl-CoA dehydrogenase (LCAD) and long-chain 3-hydroxyacyl-coa dehydrogenase (LCHAD). Then, acetyl-CoA enters the tricarboxylic acid (TCA) cycle to be completely oxidized to yield adenosine triphosphate (ATP). Several factors can influence the development of FAO in different tissues (23), of which AMP-activated protein kinase (AMPK) plays an essential role in regulating FAO (20). AMPK can enhance sirtuin 1 (Sirt1) activity, resulting in the deacetylation and modulation of the activity of peroxisome proliferator-activated receptor gamma coactivator 1-alpha (PGC1α) (24). Then, PGC1α can modulate the expression of CPT1 and CPT2 by recruiting peroxisome proliferator-activated receptors (PPARs) (24–27), such as peroxisome proliferator-activated receptor γ (PPAR γ) (27).

It is reported that FAO capacity is decreased in the placenta from women with obese and gestational diabetes mellitus (28–31). However, the effects and underlying mechanisms of maternal overnutrition on placental FAO and metabolic health in the offspring have not been fully elucidated. And little is known whether maternal overnutrition affects the FAO capacity of the offspring at fetal and weaning stage. Thus, our purpose is to investigate the impact of maternal overnutrition on placental gene expression involved in FAO and the role of the AMPK/Sirt1/PGC1α signaling pathway in regulating gene expression involved in FAO, and to further explore whether maternal overnutrition can affect hepatic FAO gene expression at the fetal and weaning stage in the offspring.

MATERIALS AND METHODS

Ethics Statement

All experimental procedures were carried out in compliance with the Ethics Committee for Animal Experimentation of the Faculty of Peking University First Hospital (NO. J201827).

Animals and Diets

Five-week-old female C57BL/6J mice were raised under specific pathogen free (SPF) conditions (12 h light-dark cycle; 22 ± 2°C). All animals had unlimited access to water and food. After 1 week of acclimation, all female mice were randomly assigned either to a normal chow (NC) diet group or to a high-fat (HF) diet group. The NC diet contained (kcal %): fat, 13%; protein, 24%; carbohydrate, 63%. and delivered 3.44 kcal/g of energy (Keao Xieli Feed Co. Ltd., Beijing, China, **Supplementary Table 1**). The HF diet contained (kcal %): fat, 60%; protein, 20%; carbohydrate, 20%. and delivered 5.24 kcal/g of energy (Keao Xieli Feed Co. Ltd, Beijing, China, **Supplementary Table 1**). After 4 weeks of feeding, mating was performed by housing female mice with male mice for 4 days with a NC diet (female: male = 2:1), in order to eliminating the confounding effects of sires' diets. Vaginal plugs were checked every morning, and the presence of vaginal plugs was considered as day 0.5 of pregnancy. The pregnant mice (F0) were raised individually and remained their respective diets throughout gestation. There were two cohorts of dams in this study. In the first cohort, dams were anesthetized with pentobarbital and euthanized after 10 h of fasting on day 18.5 of pregnancy. Dams' blood samples were collected from the intraorbital retrobulbar plexus for further serum biochemical analysis. The placenta and fetuses were quickly dissected and weighed. Placenta and livers of fetuses were stored at −80°C. In the second cohort, the pregnant females remained their respective diets throughout gestation and lactation. The number of pups in each litter is 6–10. To avoid nutritional bias between litters, all litters were culled to six pups on day 1 after birth. On day 21, all pups were weaned. Body weight and fasting blood glucose (FBG) of offspring were examined weekly from birth to weaning. To prevent confounding causes associated the estrus cycle and hormone profile of female offspring, we paid close attention to male offspring in the present study. On day 21, one male offspring from every litter was selected for further analysis. After 10 h of fasting, the offspring were anesthetized with pentobarbital and euthanized. Blood samples were collected from the intraorbital retrobulbar plexus in anesthetized mice. Livers were collected and stored at −80°C for future analysis.

Glucose Tolerance Tests in Dams and Offspring Mice

Oral glucose tolerances tests (OGTTs) were carried out in dams after 6 h of fasting, in order to reduce stress for dams. Intraperitoneal glucose tolerance tests (IPGTTs) were performed in male offspring after 10 h of fasting at weaning age. Before giving a glucose administration, blood glucose levels were monitored in the tail vein using a glucometer and glucose test strips (Contour TS, Bayer, Beijing, China) as the baseline level (time 0). Then blood glucose levels were monitored at 15, 30, 60, 120 min after given a glucose administration (2 g/kg body weight). The area under the curve (AUC) of OGTTs and IPGTTs was calculated as previously described (6).

Serum Biochemical Parameters Measurement

Blood samples taken from dams and male offspring were centrifuged at 4,000 g for 15 min and stored at −80°C. Serum samples were subjected to detect insulin concentrations using the Mouse Ultrasensitive Insulin ELISA kit (80-INSMSU-E01, ALPCO Diagnostics, Salem, NH, USA). Serum total cholesterol (T-CHO), triacylglycerol (TG), free fatty acids (FFA) were detected using commercial kits (A111-1, A110-1, A402-2-1, Jiancheng Bioengineering Institute, Nanjing, China). Each sample was detected in duplicate.

Oil Red O Staining

The frozen placenta was embedded in Tissue-Tek O.C.T.Compound. Samples were cut at a thickness of 10 μm from each sample. Slides were washed in distilled water for 2 min and 60% isopropanol for 2 min. Afterward, slides were stained for 10 min in 60% working Oil Red O (G1015, ServiceBio, Beijing, China). Then slides were washed shortly with distilled water and 60% isopropanol, stained for 1 min with Hematoxylin (C0107, Beyotime, Shanghai, China), washed in running water for 10 min, mounted using glycerol jelly mounting medium (C0187, Beyotime, Shanghai, China). Images were captured using an Olympus DP71 microscope. Five random fields of view per tissue section were used to quantify the integrated optical density (IOD) using ImageJ software.

Histological Analysis

Placental tissues embedded in wax were sliced at a thickness of 5 μm. For the hematoxylin and eosin (H&E) assay, the slides were stained with hematoxylin for 5 min and eosin Y for 30 s (C0105S, Beyotime, Beijing, China). Images were captured using an Olympus DP71 microscope. For immunohistochemistry assay, antigen retrieval was carried out in citrate buffer pH 6.0 (P0083, Beyotime, Shanghai, China) using a pressure cooker for 3 min, followed by blocking endogenous peroxidases using 0.3% H_2O_2 for 15 min. After blocking 20 min by blocking buffer (P0260, Beyotime, Shanghai, China), the slides were incubated overnight at 4°C with an anti-CPT2 antibody (1:150, ab181114, Abcam, Cambridge, UK), anti-CPT1b antibody (1:150, 22170-1-AP, Proteintech, Wuhan, China). On the next day, the slides were washed and then incubated with a secondary antibody (PV9001, Zhongshan Gold Bridge Biotechnology Co, Beijing, China) for 20 min at room temperature. The slides were incubated with DAB (ZLI9018, Zhongshan Gold Bridge Biotechnology Co, Beijing, China) to detect side-specific antigen-antibody binding, followed by staining with hematoxylin. Then, the slides were dehydrated and sealed with neutral gum. Images were captured using an Olympus DP71 microscope. Five random views per tissue section were used to quantify the mean IOD (IOD/area) using Image-Pro Plus 6.0.

RNA Preparation and RT-PCR Analysis

Total RNA from placenta tissues and liver tissues was extracted using TRIzol reagent (15596026, Invitrogen, Waltham, MA, USA) and 1.5 μg of RNA was reversed to cDNA using the High-Capacity cDNA Reverse Transcription Kits (4375222, ThermoFisher Scientific Hudson, NH, USA). Real-time PCR was carried out using 15 ng of cDNA to detect the gene expression of CPT2, CPT1a, CPT1b, LCAD, LCHAD, AMPKα, Sirt1, PGC1α, PPARγ and mitochondrial transcription factor A (TFAM). β-actin was selected as the reference gene. Primers were presented in **Table 1**. The $2^{-\Delta\Delta Ct}$ method was used to calculate gene relative expression.

Protein Isolation and Western Blot Analysis

Total protein from placenta tissues was ground and lysed in RIPA lysis buffer (P0013, Beyotime, Shanghai, China) and recovered by centrifuging at 12,000 g for 15 min at 4°C. After quantifying the protein concentration using bicinchoninic acid (BCA) protein quantification kit (23225, Thermo Fisher Scientific, Hudson, NH, USA), 20 μg protein was run on a 10% acrylamide SDS-PAGE gel. Then the protein was transferred onto a PVDF or nitrocellulose membrane. After blocking with 5% milk, the membranes were incubated overnight at 4°C with anti-p-AMPKα (1:1000; #2535, Cell Signaling Technology, Danvers, MA, USA), anti-AMPKα (1:1000; #5831s, Cell Signaling Technology, Danvers,

TABLE 1 | Primer sequences of study genes.

Genes	Forward	Reverse
AMPKα	GTCAAAGCCGACCCAATGATA	CGTACACGCAAATAATAGGGGTT
Sirt1	ATGACGCTGTGGCAGATTGTT	CCGCAAGGCGAGCATAGAT
PGC1α	TATGGAGTGACATAGAGTGTGCT	CCACTTCAATCCACCCAGAAAG
PPARγ	TCGCTGATGCACTGCCTATG	GAGAGGTCCACAGAGCTGATT
CPT1a	CTCCGCCTGAGCCATGAAG	CACCAGTGATGATGCCATTCT
CPT1b	GCACACCAGGCAGTAGCTTT	CAGGAGTTGATTCCAGACAGGTA
CPT2	CAGCACAGCATCGTACCCA	TCCCAATGCCGTTCTCAAAAT
LCHAD	TGCATTTGCCGCAGCTTTAC	GTTGGCCCAGATTTCGTTCA
LCAD	TCTTTTCCTCGGAGCATGACA	GACCTCTCTACTCACTTCTCCAG
TFAM	ATTCCGAAGTGTTTTTCCAGCA	TCTGAAAGTTTTGCATCTGGGT
β-actin	TATTGGCAACGAGCGGTTCC	GGCATAGAGGTCTTTACGGATGTC

AMPKα, AMP-activated protein kinase α; Sirt1, sirtuin 1; PGC1α, peroxisome proliferator-activated receptor gamma coactivator 1-alpha; PPARγ, Peroxisome proliferator-activated receptor γ; CPT1a, carnitine palmitoyltransferase 1a; CPT1b, carnitine palmitoyltransferase 1b; CPT2, carnitine palmitoyltransferase 2; LCAHD, long-chain 3-hydroxyacyl-coa dehydrogenase; LCAD, long chain acyl-CoA dehydrogenase; TFAM, mitochondrial transcription factor A.

MA, USA), anti-Sirt1 (1:1000; #3931, Cell Signaling Technology, Danvers, MA, USA), anti-PGC1α (1:1000; #2178, Cell Signaling Technology, Danvers, MA, USA), anti-CPT2 (1:1000; ab181114, Abcam, Cambridge, UK), anti-CPT1b (1:1000; 22170-1-AP, Proteintech, Wuhan, China), and anti-PPARγ (1:1000; #2435, Cell Signaling Technology, Danvers, MA, USA). On the next day, membranes were incubated with a secondary antibody (1:5000; Zhongshan Golden Bridge Biotechnology Co, Beijing, China) for 1 h at room temperature. The images of bands were visualized and taken using an enhanced chemiluminescent (ECL) detection kit. β-actin (1:10,000, AC026, ABclonal, China) was used as the control for total protein. Densitometry analysis was performed using Image J software.

Cell Culture and Glucolipotoxic Treatment

Human JEG-3 trophoblast cells were obtained from the Chinese National Infrastructure of Cell Line Resource and maintained in Eagle's minimum essential medium (EMEM) (No.30-3003, ATCC, Manassas, VA, USA). The medium was supplemented with 10% fetal bovine serum (FBS, Gibco, Life Science, Pittsburgh, PA, USA) and 1% penicillin-streptomycin (Sigma, Steinheim, Germany) at 37°C under 5% CO2.

Glucolipotoxicity treatment was a combination of 33.3 mM glucose, 400 μM oleic acid (OA, O7501, Sigma, Steinheim, Germany) and 400 μM linoleic acid (LA, L8134, Sigma, Steinheim, Germany) in the medium. Cells were seeded into 6-well plates at a density of 3×10^5 cells/well. After attachment, cells were incubated for 24 h in either BSA or glucose/FFA or glucose/FFA/AMPK agonist 5-aminoimidazole-4-carboxamide ribonucleotide (AICAR) (0.5 mM, S1802, Selleckchem, USA) in the medium. The concentration and incubation period used in the experiment is based on previous studies (32–34). After treatment, cells were harvested in RIPA buffer and recovered by centrifuging at 12,000 g for 15 min. The protein sample was collected and quantified by a BCA protein quantification kit. Protein expression was detected using western blot as aforementioned.

Statistical Analysis

GraphPad Prism 9.0 software was applied to calculate the data. Quantitative data were presented as the mean ± standard errors (SEM) for normally distributed variables. The difference between the two groups was performed with two-tailed Student's *t*-test. The difference among the three groups was performed with a one-way analysis of variance (ANOVA). OGTTs and IPGTTs were performed with a two-way ANOVA followed by Bonferroni's *post-hoc* test. A *P*-value <0.05 was considered statistically significant.

RESULTS

Maternal HF Feeding Impaired Glucose and Lipid Metabolism in Dams

Body weight and FBG before mating were not affected by maternal HF diet ($P > 0.05$, **Figures 1A,B**). At gestation day 14.5 (P14.5), no difference in body weight was observed between the two groups ($P > 0.05$, **Figure 1C**). However, HF-fed dams had higher FBG ($P < 0.01$, **Figure 1D**) and impaired glucose tolerance at P14.5. After oral glucose administration, HF-fed dams showed significantly higher glucose levels at 15 min ($P < 0.01$), 30 min ($P < 0.001$), and 60 min ($P < 0.001$) (**Figure 1E**). The overall glucose AUC was higher in HF dams compared with control group ($P < 0.01$, **Figure 1F**).

At gestation day 18.5 (P18.5), no significant difference in serum insulin levels of dams was observed between the two groups ($P > 0.05$, **Figure 1G**). Dams fed with HF diet had significantly increased serum T-CHO concentration ($P < 0.01$, **Figure 1H**). However, serum TG and FFA levels were similar between the two groups ($P > 0.05$, **Figures 1I,J**). These results indicated that maternal HF feeding before and during pregnancy could impair both glucose and lipid metabolism in dams.

Maternal HF Feeding Altered the Development of Placenta and Fetus, and Induced Lipid Deposition in the Placenta

Analysis of placental H&E staining revealed interstitial edema, enlarged blood sinusoid and architectural distortion in the labyrinth of the placenta in the HF feeding dams (**Figure 2A**). The average weight of each litter was used for the calculation of placental and fetal weight. The placental weight was significantly higher due to maternal HF diet ($P < 0.05$, **Figure 2B**). Fetal weight was not affected by maternal HF diet ($P > 0.05$, **Figure 2C**). However, there is a trend of decreased fetal/placental weight ratio in the HF diet group at P18.5 ($P = 0.067$, **Figure 2D**). For Oil Red O staining, HF dams presented a massive accumulation of large lipid droplets in the placenta, compared with the NC diet group ($P < 0.001$, **Figure 2E**).

Maternal HF Feeding Impairs FAO by Suppressing AMPK Signaling Pathway in the Placenta

To evaluate the effects of HF feeding on placental FAO, we measured mRNA expressions of related genes involved in FAO in the placenta. A maternal HF diet downregulated the gene expression of CPT2 ($P < 0.05$, **Figure 3A**), and had a trend of decreased CPT1b mRNA expression in the placenta ($P = 0.085$, **Figure 3C**). However, mRNA expression of CPT1a, LCAD, and LCHAD were similar in the placenta between the two groups ($P > 0.05$, **Figures 3B,D,E**). Then we measured related gene expression in the AMPK signaling pathway and found that there was no difference in placental AMPKα gene expression between the two groups ($P > 0.05$, **Figure 3F**). The mRNA expressions of Sirt1 ($P < 0.01$), PGC1α ($P < 0.05$), and PPARγ ($P < 0.01$) in the placenta were significantly decreased in the HF group (**Figures 3G–I**). Since FAO occurs in the mitochondria (21), we evaluated placental mitochondrial biogenesis by measuring the gene expression of TFAM. TFAM is a DNA-binding protein that plays a central role in transcriptional activation, mitochondrial DNA (mtDNA) organization and FAO capacity (35). The result showed that the mRNA expression of TFAM was reduced by HF die ($P < 0.05$, **Figure 3J**).

Then we applied immunohistology to determine the expression of CPT2 and CPT1b in the placenta. It was shown

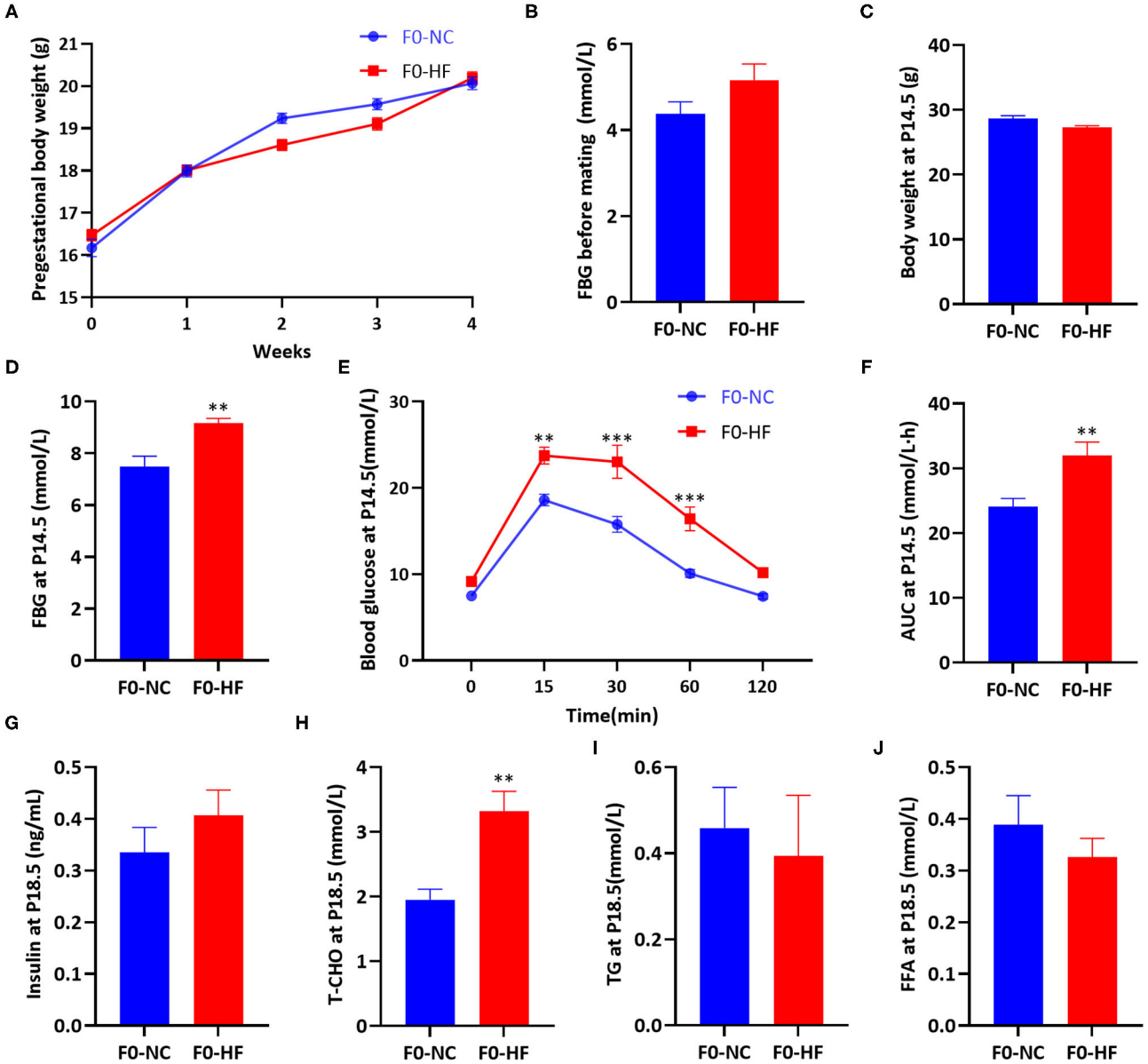

FIGURE 1 | Maternal HF feeding impaired glucose and lipid metabolism in dams. **(A)** Body weight of dams during 4 weeks before mating; **(B)** FBG of dams before mating; **(C)** Body weight of dams at P14.5; **(D)** FBG of dams at P14.5; **(E)** OGTT of dams at P14.5; **(F)** AUC of dams at P14.5; **(G)** Serum insulin of dams at P18.5; **(H)** Serum T-CHO of dams at P18.5; **(I)** Serum TG of dams at P18.5; **(J)** Serum FFA of dams at P18.5. Data represented as the mean ± SEM. (F0-NC, $n = 5$–6; F0-HF, $n = 6$–7). $^{*}p < 0.05$, $^{**}p < 0.01$, $^{***}p < 0.001$ vs. F0-NC. NC, normal chow diet; HF, high-fat diet; FBG, fasting blood glucose; OGTT, oral glucose tolerances tests; AUC, the area under the glucose curve; T-CHO, total cholesterol; TG, triglyceride; FFA, free fatty acid.

that maternal HF diet downregulated placental CPT2 expression ($P < 0.05$, **Figure 3K**). There was no significant difference in placental CPT1b expression between the HF diet and NC diet groups ($P > 0.05$, **Figure 3K**).

Then we measured the protein levels of the above genes (**Figure 4**). Maternal HF diet downregulated placental CPT2 protein expression ($P < 0.05$, **Figure 4B**) and did not affect CPT1b protein level ($P > 0.05$, **Figure 4C**). Then we measured the protein expression of the AMPK signaling pathway. A maternal HF diet did not alter placental total AMPKα (t-AMPKα) protein level but downregulated placental phosphorylated AMPKα (p-AMPKα) level. The p-AMPKα/t-AMPKα ratio was significantly decreased in the placenta of maternal HF diet ($P < 0.01$, **Figure 4D**). Maternal HF diet downregulated placental Sirt1 ($P < 0.05$, **Figure 4E**), and PGC1α ($P < 0.05$, **Figure 4F**) protein expression. However, there was no difference in placental PPARγ protein level between the NC and HF groups ($P > 0.05$, **Figure 4G**). Meanwhile, the protein expression of TFAM in the placenta was decreased by HF diet ($P < 0.05$, **Figure 4H**).

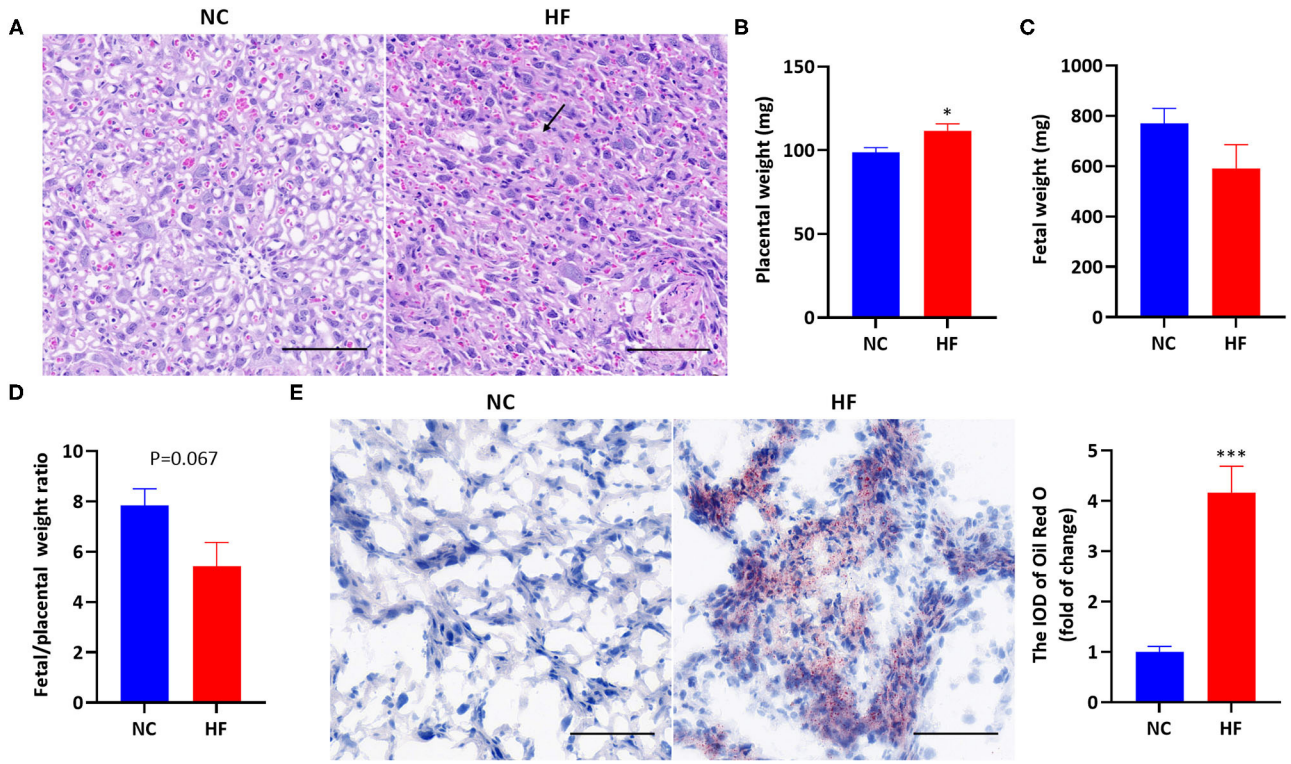

FIGURE 2 | Maternal HF feeding altered the development of the placenta and fetal, and induced lipid deposition in the placenta. **(A)** Representative images of H&E staining in the placenta. The black arrow indicates interstitial edema, magnification 400x. The scale bar indicates 100 μm; **(B)** Placental weight; **(C)** Fetal weight; **(D)** Fetal/ placental weight ratio; **(E)** Representative images and quantitative assessment of Oil Red O staining in the placenta, magnification 400x. The scale bar indicates 100 μm. Data represented as the mean ± SEM. (NC, $n = 6$; HF, $n = 6$–7). *$p < 0.05$, ***$p < 0.001$ vs. NC. NC, normal chow diet; HF, high-fat diet; H&E, hematoxylin and eosin; IOD, integrated optical density.

Glucolipotoxicity Reduced FAO by Suppressing AMPK Signaling Pathway and Restored by AICAR

As maternal HF feeding impaires glucose and lipid metabolism in mice, and hyperglycemia can enhance the toxicity of fatty acid termed glucolipotoxicity (36). We investigated the effect of glucolipotoxicity on FAO in trophoblasts. We treated JEG-3 cells with a combination of glucose and FFA mixture to induce glucolipotoxicity. During the 24 h incubation with glucolipotoxicity, glucolipotoxicity-treated cells responded with significantly downregulated CPT2 and CPT1b protein expression ($P < 0.05$, **Figures 5A,B**). Glucolipotoxicity did not alter t-AMPKα protein level. However, p-AMPKα levels were reduced by glucolipotoxicity in JEG-3 cells. The p-AMPKα/t-AMPKα ratio was decreased ($P < 0.05$, **Figure 5C**), which indicated that AMPK activity was suppressed by glucolipotoxicity. Then we evaluated the downstream of the AMPK signaling pathway, and found that glucolipotoxicity reduced the protein expressions of Sirt1 ($P < 0.05$, **Figure 5D**) and PGC1α ($P < 0.05$, **Figure 5E**) in JEG-3 cells.

To explore whether the effect of glucolipotoxicity on FAO is mediated by AMPK, we treated JEG-3 cells with AMPK activator, AICAR. The protein expressions of CPT2 ($P < 0.05$) and CPT1b ($P < 0.05$) were increased upon AICAR treatment (**Figures 5F,G**). Meanwhile, the suppressive effect in the protein expression of Sirt1 ($P < 0.05$) and PGC1α ($P < 0.05$) induced by glucolipotoxicity was also blocked by AICAR treatment (**Figures 5H,I**). These results suggested that glucolipotoxicity reduced FAO by suppressing the AMPK signaling pathway and restored by AICAR in JEG-3 cells.

Maternal HF Feeding Impaired Glucose and Lipid Metabolism of Offspring at Weaning

After birth, we measured the offspring's body weight every week. No significant differences in body weight at birth, the first and the second week were observed between the male offspring of two groups. However, at weaning, male offspring presented increased body weight due to maternal HF diet ($P < 0.05$, **Figure 6A**). There was no substantial difference in FBG between the offspring of the two groups at weaning ($P > 0.05$, **Figure 6B**). Compared with the offspring of dams fed a NC diet, offspring of HF feeding dams had impaired glucose tolerance at weaning, which presented higher blood glucose levels at 60 min ($P < 0.05$, **Figure 6C**). The overall

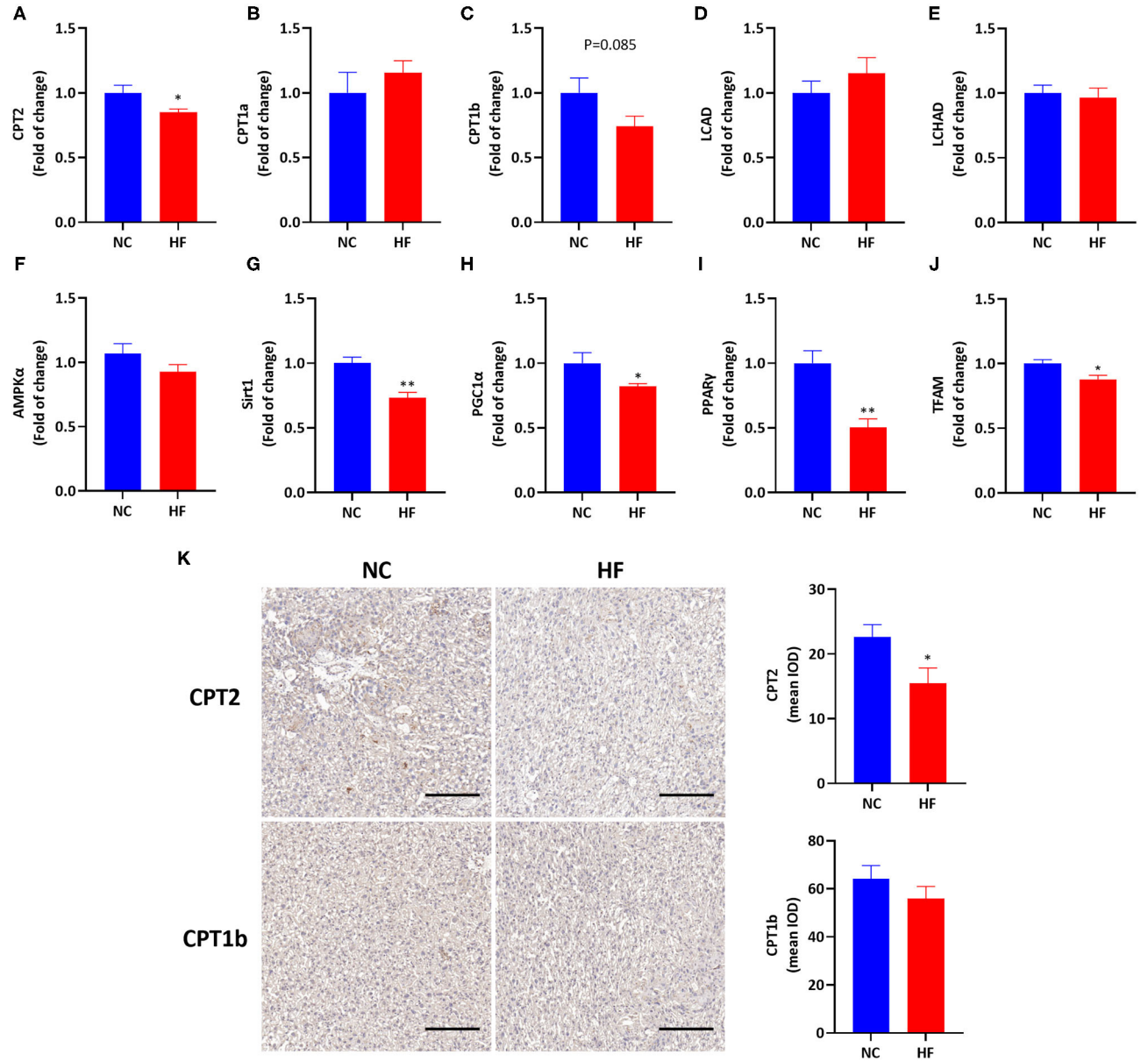

FIGURE 3 | HF feeding reduced placental FAO gene expression by suppressing the AMPK signaling pathway. **(A–J)** Placental mRNA expression of genes. **(A)** CPT2; **(B)** CPT1a; **(C)** CPT1b; **(D)** LCAD; **(E)** LCHAD; **(F)** AMPKα; **(G)** Sirt1; **(H)** PGC1α; **(I)** PPARγ; **(J)** TFAM; **(K)** Immunohistological analysis of CPT2 and CPT1b in the placenta, magnification 200x. The scale bar indicates 200 μm. Data represented as the mean ± SEM. (NC, $n = 5$–6; HF, $n = 7$). *$p < 0.05$, **$p < 0.01$, vs. NC. NC, normal chow diet; HF, high-fat diet; CPT2, carnitine palmitoyltransferase 2; CPT1a, carnitine palmitoyltransferase 1a; CPT1b, carnitine palmitoyltransferase 1b; LCAHD, long-chain 3-hydroxyacyl-coa dehydrogenase; LCAD, long chain acyl-CoA dehydrogenase; AMPKα, AMP-activated protein kinase α; Sirt1, sirtuin 1; PGC1α, peroxisome proliferator-activated receptor gamma coactivator 1-alpha; PPARγ, peroxisome proliferator-activated receptor γ; TFAM, mitochondrial transcription factor A; IOD, integrated optical density.

glucose AUC was higher in male offspring of HF feeding dams ($P < 0.05$, **Figure 6D**). Serum insulin concentration ($P < 0.01$, **Figure 6E**) and T-CHO concentration ($P < 0.01$, **Figure 6F**) were significantly higher in the offspring of dams fed a HF diet at weaning. However, serum TG and FFA levels were similar between the offspring of the two groups ($P > 0.05$, **Figures 6G,H**).

Maternal HF Feeding Did Not Affect FAO Gene Expression in Offspring at Fetal and Weaning Age

Apart from CPT1 and CPT2, carnitine is an important cofactor in transferring acyl-CoA from the cytoplasm to mitochondrial membranes in carnitine cycle system (21), which can stimulate the rate of transcription CPT1 and CPT2 (37), as well as the

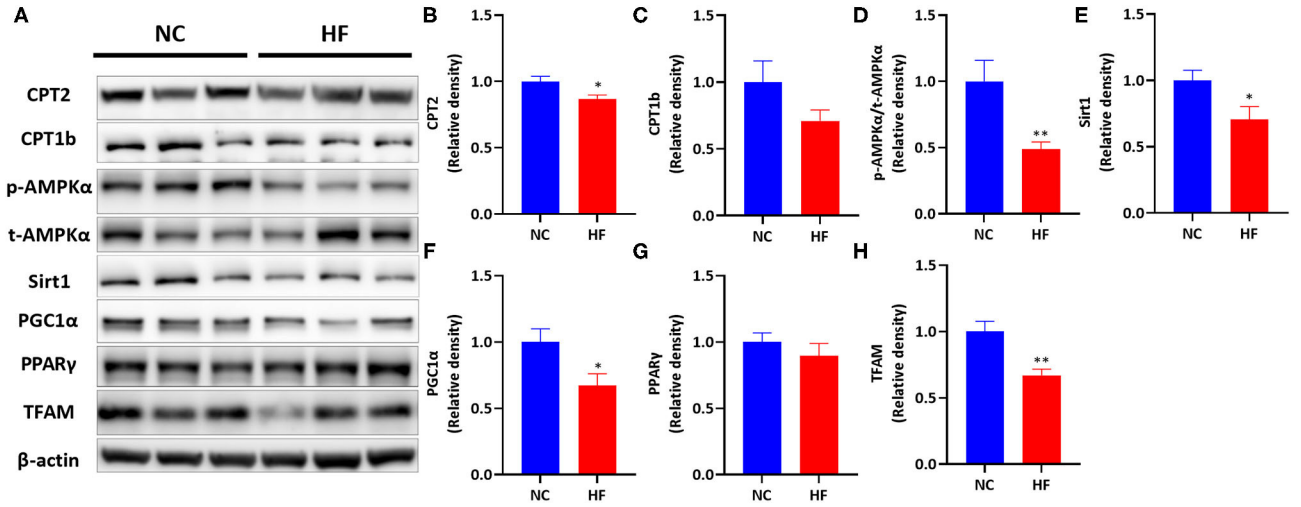

FIGURE 4 | HF feeding reduced protein expression of placental FAO by suppressing the AMPK signaling pathway. **(A)** Bands' representative images of **(B–G)**. **(B)** CPT2; **(C)** CPT1b; **(D)** p-AMPKα/t-AMPKα; **(E)** Sirt1; **(F)** PGC1α; **(G)** PPARγ; **(H)** TFAM. Data represented as the mean ± SEM. (NC, $n = 5$–6; HF, $n = 6$–7). $^{*}p < 0.05$, $^{**}p < 0.01$, vs. NC. NC, normal chow diet; HF, high-fat diet; AMPKα, AMP-activated protein kinase α; Sirt1, sirtuin 1; PGC1α, peroxisome proliferator-activated receptor gamma coactivator 1-alpha; PPARγ, Peroxisome proliferator-activated receptor γ; CPT1a, carnitine palmitoyltransferase 1a; CPT1b, carnitine palmitoyltransferase 1b; CPT2, carnitine palmitoyltransferase 2; TFAM, mitochondrial transcription factor A.

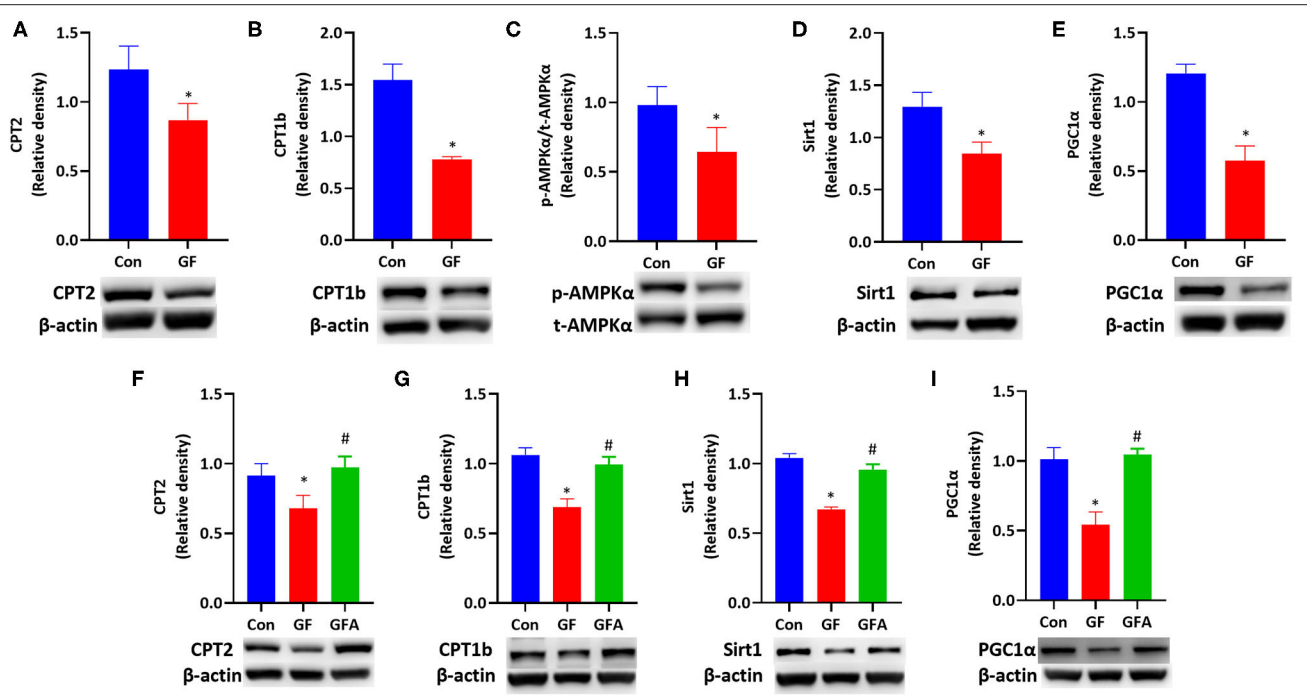

FIGURE 5 | Glucolipotoxicity reduced FAO-related protein expression by suppressing the AMPK signaling pathway and reversed by AICAR. **(A–E)** JEG-3 cells were treated with BSA (Con) or glucose/FFA (GF), which were treated for 10 min for AMPKα and treated for 24h for other proteins. **(A)** CPT2; **(B)** CPT1b; **(C)** p-AMPKα/t-AMPKα protein ratio; **(D)** Sirt1; **(E)** PGC1α. **(F–I)** JEG-3 cells were treated with BSA (Con) or glucose/FFA (GF) or glucose/FFA/AICAR (GFA) for 24 h. **(F)** CPT2; **(G)** CPT1b; **(H)** Sirt1; **(I)** PGC1α. The experiment was repeated three-five times. Data represented as the mean ± SEM. $^{*}p < 0.05$, vs. Con. $^{\#}p < 0.05$, vs. GF. GF, glucose/FFA; GFA, glucolipotoxicity plus AICAR; AICAR, 5-aminoimidazole-4-carboxamide ribonucleotide; AMPKα, AMP-activated protein kinase α; Sirt1, sirtuin 1; PGC1α, peroxisome proliferator-activated receptor gamma coactivator 1-alpha; CPT1b, carnitine palmitoyltransferase 1b; CPT2, carnitine palmitoyltransferase 2.

enzyme activity of CPT1 in the liver (37–39). Since the fetus and sucking infant have a very limited ability to synthesize carnitine, it is largely dependent on the transfer of carnitine from the placenta in the uterus (23) and breast milk after birth (40, 41). Previous

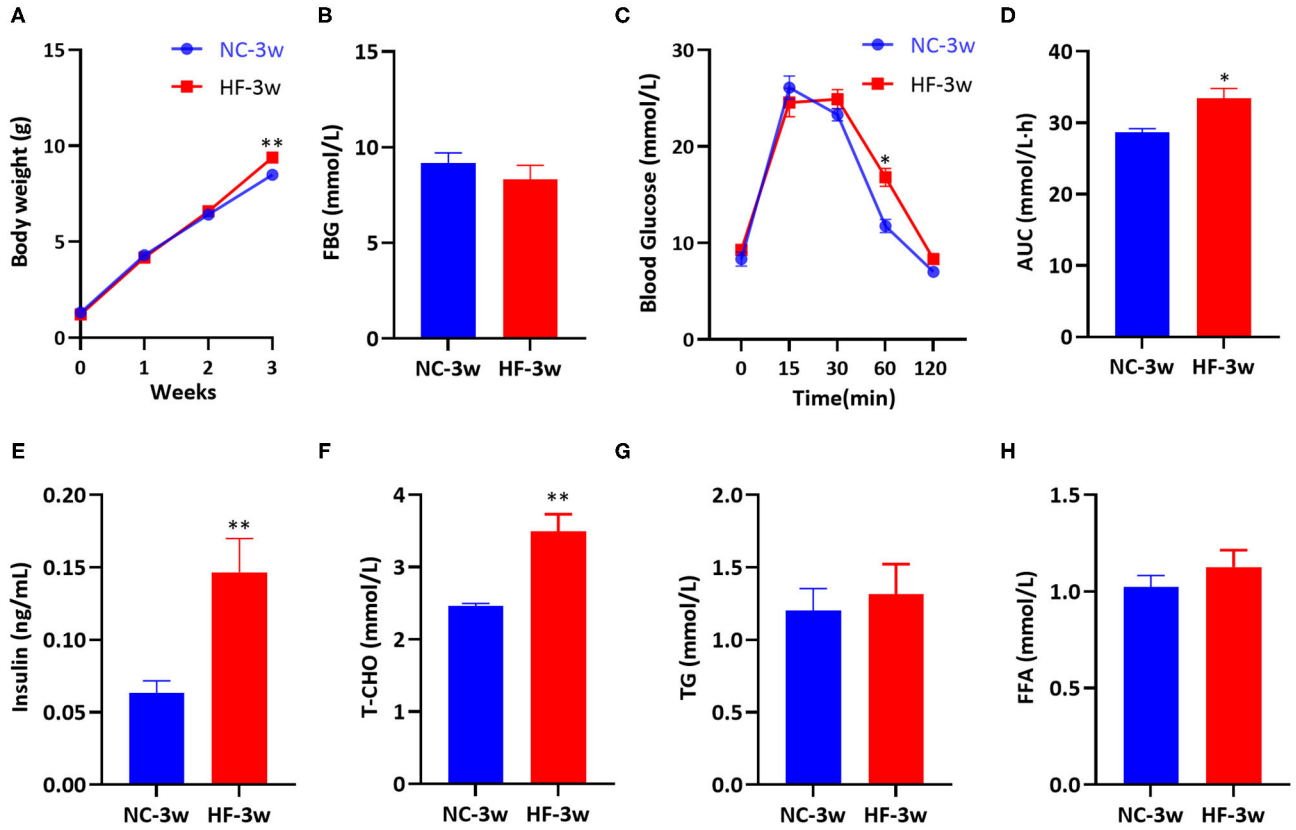

FIGURE 6 | Maternal HF feeding impaired glucose and lipid metabolism of offspring at weaning. **(A)** Body weight of male offspring from birth to weaning; **(B)** FBG of male offspring at weaning; **(C)** IPGTT and **(D)** AUC of male offspring at weaning; **(E)** Serum insulin; **(F)** Serum T-CHO; **(G)** Serum TG; **(H)** Serum FFA of male offspring at weaning. Data represented as the mean ± SEM. (NC-3w, $n = 8$; HF-3w, $n = 6$–8). $^{*}p < 0.05$, $^{**}p < 0.01$ vs. NC-3w. NC, normal chow diet; HF, high-fat diet; 3w, the third week; FBG, fasting blood glucose; IPGTT, intraperitoneal glucose tolerance test; AUC, the area under the glucose curve; T-CHO, total cholesterol; TG, triglyceride; FFA, free fatty acid.

studies showed that obese women exhibited lower placental total carnitine content (free carnitine and acylcarnitines) accompanied by defects of FAO, and reduced umbilical venous plasma total carnitine content (29). And it was reported that maternal HF feeding reduced the level of free-carnitine, short-chain and medium-chain acylcarnitines in the placenta (42), and decreased the level of L-carinitine in the liver of offspring (43). Oral L-carnitine administration can increase AMPK protein expression (44, 45). Thus, we supposed that maternal HF feeding may affect the FAO in the offspring through imbalanced carnitine. To test this XX, we measured the expression of hepatic genes related to FAO in the fetus and offspring at weaning. However, mRNA expression of CPT2, CPT1a, CPT1b, and LCAD in the liver were similar between the two groups' offspring at fetal and weaning age ($P > 0.05$, **Figure 7**). Then, we tested the AMPK signaling pathway in the liver to evaluate whether AMPK signaling pathway was activated. Correspondingly, there was no difference in hepatic AMPK, Sirt1 and PGC1α mRNA expression between the NC and HF groups (**Supplementary Figure 1**). These results indicated that AMPK/Sirt1/PGC1α pathway was not activated, so that FAO related gene expression was not altered.

DISCUSSION

Maternal overnutrition is common in developed countries and developing nations (46), which increases the risk of gestational diabetes mellitus and determines susceptibility to obesity and diabetes in the offspring (3). FAO defects can cause energy deficiency, accumulated substrates and oxidative stress (47). However, the effect and mechanism of maternal overnutrition on FAO in the placenta has not been fully depicted, and studied about whether FAO is altered in the liver of the offspring are limited, especially during fetal age and weaning age. The present study showed that maternal HF feeding could induce glucose and lipid metabolism disorders in dams. Compared with the NC diet group, a maternal HF diet caused heavier placenta and a decreased trend of fetal/placental weight ratio. In addition, a maternal HF diet decreased the gene expression involved in FAO by inhibiting the AMPK/Sirt1/PGC1α signaling pathway in the placenta. In addition, a maternal HF diet caused a higher body weight, glucose intolerance, hyperinsulinemia and hypercholesteremia of offspring at weaning age. However, FAO-related genes expression in the liver of fetal and offspring at weaning age had not been altered.

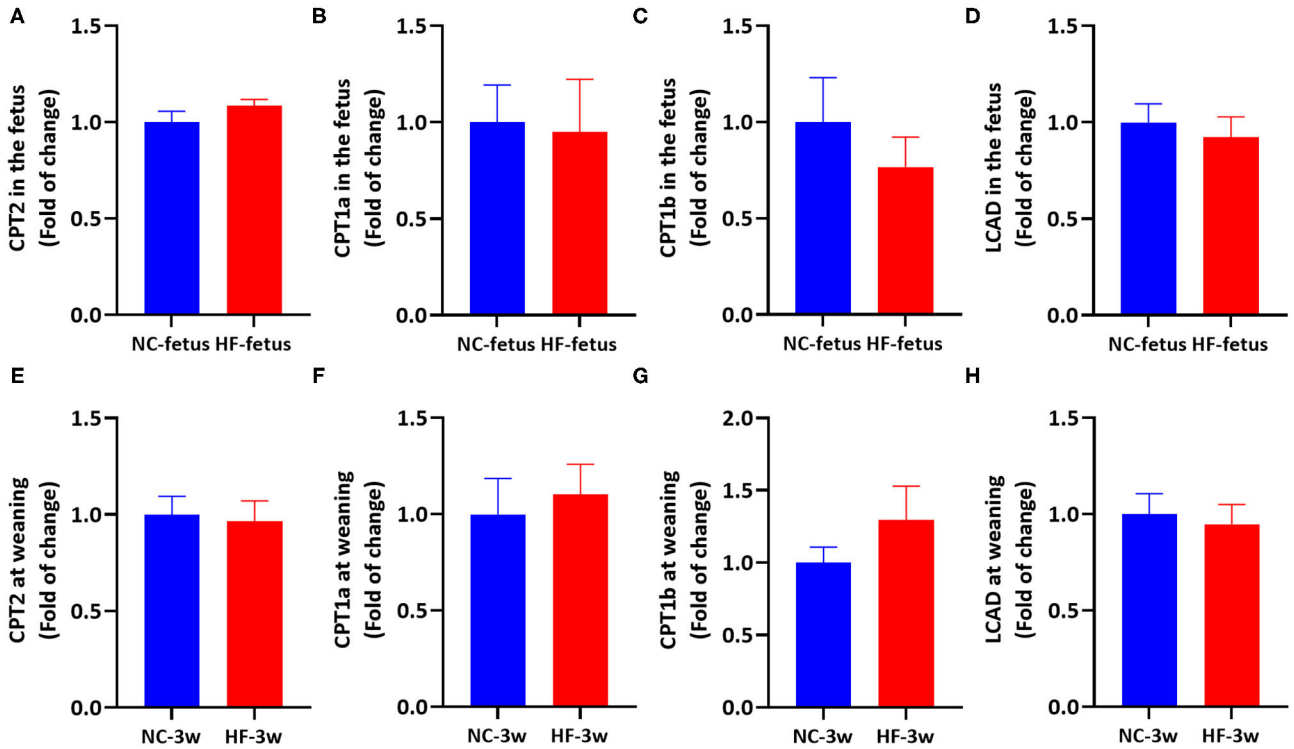

FIGURE 7 | Maternal HF feeding did not affect FAO-related gene mRNA expression in offspring at fetal and weaning age. **(A–D)** hepatic mRNA expression in the fetus. **(A)** CPT2; **(B)** CPT1a; **(C)** CPT1b; **(D)** LCAD; **(E–H)** hepatic mRNA expression in the offspring at weaning. **(E)** CPT2, **(F)** CPT1a, **(G)** CPT1b, **(H)** LCAD. Data represented as the mean ± SEM. (NC-fetus, $n = 6$; HF-fetus, $n = 7$; NC-3w, $n = 8$; HF-3w, $n = 8$). NC, normal chow diet; HF, high-fat diet; 3w, the third week. CPT2, carnitine palmitoyltransferase 2; CPT1a, carnitine palmitoyltransferase 1a; CPT1b, carnitine palmitoyltransferase 1b; LCAD, long chain acyl-CoA dehydrogenase.

The placenta plays a central role in linking mother and fetus (13, 14). Development and metabolic requirement of the placenta and fetus can be changed to meet the pregnant mother's metabolism and nutrient availability (15, 48). Fetal growth is influenced by the process of placental nutrient transfer. Fetal/placental weight ratio can be an indicator of placental efficiency (49). The present study showed that the maternal HF diet group had a heavier placenta and a decreased trend of fetal/placental weight ratio, which indicated impaired placental efficiency in transport nutrition. In line with our study, several studies have reported that a pregestational and/or gestational exposure to the maternal HF diet resulted in increased placental weight and decreased fetal weight, which is characterized by growth restriction (6, 50, 51). Low birth weight is correlated with a higher risk of diabetes, obesity and other metabolic diseases in later life (7, 9, 52). Though birth weight was not affected by maternal HF feeding, the offspring did exhibit higher body weight, impaired glucose tolerance, hyperinsulinemia and hypercholesteremia at weaning age in the present study. These results suggest that maternal HF feeding has profound consequences for the offspring later in life.

Fatty acids act as metabolic fuel and an energy source in the placenta (53). A deficiency of mitochondrial FAO can result in the accumulation of upstream metabolites, impaired ATP production, increased reactive oxygen species levels and inflammatory cytokines, which might be transferred to the fetus (54, 55). Furthermore, a computational experiment explored the rate-determining processes of fatty acid transfer across the placenta in isolated perfused human placenta (19). They found that the rate of fatty acid delivery to the fetal compartment was modulated by the incorporation of fatty acids into placental lipid pools (19). FAO reduction can shift the flux of fatty acids away from oxidation toward lipid pools (30), which suggests that FAO capacity can affect fatty acid delivery to the fetus (29, 56). There are studies showed that FAO capacity was reduced in trophoblast cells isolated from obese women (29), and acylcarnitine concentration and CPT1 and/or CPT2 expression were lower in the placenta (28). Placenta explants from women with gestational diabetes mellitus exhibited a reduction in FAO capacity (30, 57). Placental explants exposed to high glucose levels showed impaired FAO capacity by phosphorylation acetyl-CoA carboxylase and increased triglyceride accumulation from normal pregnancy women (30). Corresponding with these results, our study demonstrated that the maternal HF diet group showed downregulated CPT2 expression and a decreased trend of CPT1b, which indicated impaired gene expression involved in FAO.

AMPK, which plays an essential role in energy metabolism, is a metabolic master regulator of FAO (58). High AMPK activity can enhance Sirt1 activity, resulting in the deacetylation

and modulation of the activity of PGC1α (24). PGC1α is a transcriptional coactivator and can modulate the expression of many genes related to FAO, such as CPT1 and CPT2 (24–26, 59). We found a lower placental phosphorylated AMPKα ratio (p-AMPKα/ t-AMPKα) due to a maternal HF diet, which suppressed the expression of Sirt1 and PGC1α. To further investigate the molecular mechanism of whether gene expression involved in FAO was regulated by the AMPK signaling pathway, we used a glucose/FFA-induced glucolipotoxicity cell model. In the present study, we chose the JEG-3 cell line to study placental function. Extravillous trophoblasts, which connect maternal with fetal interfaces, are frequently used to investigate placental function (60). The results suggested that exposure to glucolipotoxicity downregulated protein expression of CPT1b and CPT2 through reduced AMPK activity and protein expression of Sirt1 and PGC1α. And the decreases in protein expression of Sirt1, PGC1α, CPT1b and CPT2 induced by glucolipotoxicity were significantly elevated by AICAR, indicating that impaired protein expression involved in FAO was restored by AICAR treatment.

Previous studies showed that hepatic FAO-related genes of offspring were reduced by maternal HF diet at the fetal (61) and weaning age (62). However, in our experiment, gene expression involved in FAO was not altered by maternal HF diet both in the fetus and the offspring at the weaning age. It is proposed that the duration of HF exposure, the ingredient of diets and maternal metabolic stage program the offspring differently (50, 63). These conflict results may be due to diet composition, duration of HF exposure and/or maternal metabolic state.

In conclusion, to the best of our knowledge, our study for the first time demonstrated that maternal high-fat diet can impair gene expression involved in FAO in the placenta by downregulating the AMPK signaling pathway and can cause glucose and lipid dysfunction of offspring at weaning. It is indicated that placental FAO may play a essential/crucial/central role in regulating maternal overnutrition and metabolic health in the offspring. These findings can advance our thinking about placental FAO capacity between maternal overnutrition and metabolic homeostasis in the offspring.

DATA AVAILABILITY STATEMENT

The datasets presented in this study can be found in online repositories. The names of the repository/repositories and accession number(s) can be found in the article/**Supplementary Material**.

ETHICS STATEMENT

All experimental procedures were carried out in compliance with the Ethics Committee for Animal Experimentation of the Faculty of Peking University First Hospital (NO. J201827).

AUTHOR CONTRIBUTIONS

JZha and JZhe conceived and designed the experiments. JZhe, LZ, and ZW carried out the experiments. HW and YG analyzed the data. All authors were involved in writing the paper and had final approval of the submitted and published versions.

FUNDING

This study was sponsored by National Natural Science Foundation of China (Nos. 81800703 and 81970701), Beijing Nova Program (No. Z201100006820117), Beijing Municipal Natural Science Foundation (No. 7184252 and No. 7214258), Peking University Medicine Seed Fund for Interdisciplinary Research, the Fundamental Research Funds for the Central Universities, China Diabetes Young Scientific Talent Research Project and Bethune-Merck Diabetes Research Fund of Bethune Charitable Foundation. The funders had no role in study design, data collection and analysis, or preparation of the manuscript.

SUPPLEMENTARY MATERIAL

The Supplementary Material for this article can be found online at: https://www.frontiersin.org/articles/10.3389/fnut.2022.849684/full#supplementary-material

REFERENCES

1. Burlina S, Dalfra MG, Lapolla A. Short- and long-term consequences for offspring exposed to maternal diabetes: a review. *J Matern Fetal Neonatal Med.* (2019) 32:687–94. doi: 10.1080/14767058.2017.1387893
2. Ravelli GP, Stein ZA, Susser MW. Obesity in young men after famine exposure in utero and early infancy. *N Engl J Med.* (1976) 295:349–53. doi: 10.1056/NEJM197608122950701
3. Perng W, Oken E, Dabelea D. Developmental overnutrition and obesity and type 2 diabetes in offspring. *Diabetologia.* (2019) 62:1779–88. doi: 10.1007/s00125-019-4914-1
4. Wong WW, Hachey DL, Insull W, Opekun AR, Klein PD. Effect of dietary cholesterol on cholesterol synthesis in breast-fed and formula-fed infants. *J Lipid Res.* (1993) 34:1403–11. doi: 10.1016/S0022-2275(20)36969-8
5. Calabuig-Navarro V, Puchowicz M, Glazebrook P, Haghiac M, Minium J, Catalano P, et al. Effect of omega-3 supplementation on placental lipid metabolism in overweight and obese women. *Am J Clin Nutr.* (2016) 103:1064–72. doi: 10.3945/ajcn.115.124651
6. Zheng J, Xiao X, Zhang Q, Yu M, Xu J, Wang Z. Maternal high-fat diet modulates hepatic glucose, lipid homeostasis and gene expression in the PPAR pathway in the early life of offspring. *Int J Mol Sci.* (2014) 15:14967–83. doi: 10.3390/ijms150914967
7. Zheng J, Zhang L, Wang Z, Zhang J. Maternal high-fat diet regulates glucose metabolism and pancreatic beta cell phenotype in mouse offspring at weaning. *PeerJ.* (2020) 8:e9407. doi: 10.7717/peerj.9407
8. Zheng J, Zhang Q, Mul JD, Yu M, Xu J, Qi C, et al. Maternal high-calorie diet is associated with altered hepatic microRNA expression and impaired metabolic health in offspring at weaning age. *Endocrine.* (2016) 54:70–80. doi: 10.1007/s12020-016-0959-9
9. Zheng J, Xiao X, Zhang Q, Yu M, Xu J, Qi C, et al. The effects of maternal and post-weaning diet interaction on glucose metabolism and gut microbiota in male mice offspring. *Biosci Rep.* (2016) 36:e00341. doi: 10.1042/BSR20160103
10. Dunn GA, Bale TL. Maternal high-fat diet promotes body length increases and insulin insensitivity in second-generation mice. *Endocrinology.* (2009) 150:4999–5009. doi: 10.1210/en.2009-0500
11. Huang YH, Ye TT, Liu CX, Wang L, Chen YW, Dong Y. Maternal high-fat diet impairs glucose metabolism, beta-cell function and

proliferation in the second generation of offspring rats. *Nutr Metab.* (2017) 14:67. doi: 10.1186/s12986-017-0222-2
12. Barbosa CM, Figueiredo VP, Barbosa MA, Cardoso LM, Alzamora AC. Maternal high-fat diet triggers metabolic syndrome disorders that are transferred to first and second offspring generations. *Br J Nutr.* (2020) 123:59–71. doi: 10.1017/S0007114519002708
13. Carter AM. Evolution of placental function in mammals: the molecular basis of gas and nutrient transfer, hormone secretion, and immune responses. *Physiol Rev.* (2012) 92:1543–76. doi: 10.1152/physrev.00040.2011
14. Hemberger M, Hanna CW, Dean W. Mechanisms of early placental development in mouse and humans. *Nat Rev Genet.* (2020) 21:27–43. doi: 10.1038/s41576-019-0169-4
15. Song L, Sun B, Boersma GJ, Cordner ZA, Yan J, Moran TH, et al. Prenatal high-fat diet alters placental morphology, nutrient transporter expression, and mtorc1 signaling in rat. *Obesity.* (2017) 25:909–19. doi: 10.1002/oby.21821
16. Huang W, Zhou J, Zhang G, Zhang Y, Wang H. Decreased H3K9 acetylation level of LXRalpha mediated dexamethasone-induced placental cholesterol transport dysfunction. *Biochim Biophys Acta Mol Cell Biol Lipids.* (2019) 1864:158524. doi: 10.1016/j.bbalip.2019.158524
17. Sun Y, Kopp S, Strutz J, Gali CC, Zandl-Lang M, Fanaee-Danesh E, et al. Gestational diabetes mellitus modulates cholesterol homeostasis in human fetoplacental endothelium. *Biochim Biophys Acta Mol Cell Biol Lipids.* (2018) 1863:968–79. doi: 10.1016/j.bbalip.2018.05.005
18. Pathmaperuma AN, Mana P, Cheung SN, Kugathas K, Josiah A, Koina ME, et al. Fatty acids alter glycerolipid metabolism and induce lipid droplet formation, syncytialisation and cytokine production in human trophoblasts with minimal glucose effect or interaction. *Placenta.* (2010) 31:230–9. doi: 10.1016/j.placenta.2009.12.013
19. Perazzolo S, Hirschmugl B, Wadsack C, Desoye G, Lewis RM, Sengers BG. The influence of placental metabolism on fatty acid transfer to the fetus. *J Lipid Res.* (2017) 58:443–54. doi: 10.1194/jlr.P072355
20. Serra D, Mera P, Malandrino MI, Mir JF, Herrero L. Mitochondrial fatty acid oxidation in obesity. *Antioxid Redox Signal.* (2013) 19:269–84. doi: 10.1089/ars.2012.4875
21. Houten SM, Violante S, Ventura FV, Wanders RJ. The biochemistry and physiology of mitochondrial fatty acid beta-oxidation and its genetic disorders. *Annu Rev Physiol.* (2016) 78:23–44. doi: 10.1146/annurev-physiol-021115-105045
22. Bartlett K, Eaton S. Mitochondrial beta-oxidation. *Eur J Biochem.* (2004) 271:462–9. doi: 10.1046/j.1432-1033.2003.03947.x
23. Girard J, Duee PH, Ferre P, Pegorier JP, Escriva F, Decaux JF. Fatty acid oxidation and ketogenesis during development. *Reprod Nutr Dev.* (1985) 25:303–19. doi: 10.1051/rnd:19850221
24. Canto C, Gerhart-Hines Z, Feige JN, Lagouge M, Noriega L, Milne JC, et al. AMPK regulates energy expenditure by modulating NAD+ metabolism and SIRT1 activity. *Nature.* (2009) 458:1056–60. doi: 10.1038/nature07813
25. Boufroura FZ, Le Bachelier C, Tomkiewicz-Raulet C, Schlemmer D, Benoist JF, Grondin P, et al. A new AMPK activator, GSK773, corrects fatty acid oxidation and differentiation defect in CPT2-deficient myotubes. *Hum Mol Genet.* (2018) 27:3417–33. doi: 10.1093/hmg/ddy254
26. Gerhart-Hines Z, Rodgers JT, Bare O, Lerin C, Kim SH, Mostoslavsky R, et al. Metabolic control of muscle mitochondrial function and fatty acid oxidation through SIRT1/PGC-1alpha. *EMBO J.* (2007) 26:1913–23. doi: 10.1038/sj.emboj.7601633
27. Shen S, Jiang H, Bei Y, Zhang J, Zhang H, Zhu H, et al. Qiliqiangxin attenuates adverse cardiac remodeling after myocardial infarction in ovariectomized mice via activation of PPARgamma. *Cell Physiol Biochem.* (2017) 42:876–88. doi: 10.1159/000478641
28. Bucher M, Montaniel KRC, Myatt L, Weintraub S, Tavori H, Maloyan A. Dyslipidemia, insulin resistance, and impairment of placental metabolism in the offspring of obese mothers. *J Dev Orig Health Dis.* (2021) 12:738–47. doi: 10.1017/S2040174420001026
29. Calabuig-Navarro V, Haghiac M, Minium J, Glazebrook P, Ranasinghe GC, Hoppel C, et al. Effect of maternal obesity on placental lipid metabolism. *Endocrinology.* (2017) 158:2543–55. doi: 10.1210/en.2017-00152
30. Visiedo F, Bugatto F, Sanchez V, Cozar-Castellano I, Bartha JL, Perdomo G. High glucose levels reduce fatty acid oxidation and increase triglyceride accumulation in human placenta. *Am J Physiol Endocrinol Metab.* (2013) 305:E205–12. doi: 10.1152/ajpendo.00032.2013
31. Balachandiran M, Bobby Z, Dorairajan G, Jacob SE, Gladwin V, Vinayagam V, et al. Placental accumulation of triacylglycerols in gestational diabetes mellitus and its association with altered fetal growth are related to the differential expressions of proteins of lipid metabolism. *Exp Clin Endocrinol Diabetes.* (2021) 129:803–12. doi: 10.1055/a-1017-3182
32. Jiang S, Teague AM, Tryggestad JB, Jensen ME, Chernausek SD. Role of metformin in epigenetic regulation of placental mitochondrial biogenesis in maternal diabetes. *Sci Rep.* (2020) 10:8314. doi: 10.1038/s41598-020-65415-0
33. Strakovsky RS, Pan YX. A decrease in DKK1, a WNT inhibitor, contributes to placental lipid accumulation in an obesity-prone rat model. *Biol Reprod.* (2012) 86:81. doi: 10.1095/biolreprod.111.094482
34. Wu L, Liu C, Chang DY, Zhan R, Zhao M, Man Lam S, et al. The attenuation of diabetic nephropathy by annexin A1 via regulation of lipid metabolism through the AMPK/PPARalpha/CPT1b pathway. *Diabetes.* (2021) 70:2192–203. doi: 10.2337/db21-0050
35. Ngo HB, Lovely GA, Phillips R, Chan DC. Distinct structural features of TFAM drive mitochondrial DNA packaging versus transcriptional activation. *Nat Commun.* (2014) 5:3077. doi: 10.1038/ncomms4077
36. Lytrivi M, Castell AL, Poitout V, Cnop M. Recent insights into mechanisms of beta-cell lipo- and glucolipotoxicity in type 2 diabetes. *J Mol Biol.* (2020) 432:1514–34. doi: 10.1016/j.jmb.2019.09.016
37. Karlic H, Lohninger S, Koeck T, Lohninger A. Dietary l-carnitine stimulates carnitine acyltransferases in the liver of aged rats. *J Histochem Cytochem.* (2002) 50:205–12. doi: 10.1177/002215540205000208
38. Heo K, Lin X, Odle J, Han IK. Kinetics of carnitine palmitoyltransferase-I are altered by dietary variables and suggest a metabolic need for supplemental carnitine in young pigs. *J Nutr.* (2000) 130:2467–70. doi: 10.1093/jn/130.10.2467
39. Li P, Xia Z, Kong W, Wang Q, Zhao Z, Arnold A, et al. Exogenous L-carnitine ameliorates burn-induced cellular and mitochondrial injury of hepatocytes by restoring CPT1 activity. *Nutr Metab.* (2021) 18:65. doi: 10.1186/s12986-021-00592-x
40. Lamhonwah AM, Mai L, Chung C, Lamhonwah D, Ackerley C, Tein I. Upregulation of mammary gland OCTNs maintains carnitine homeostasis in suckling infants. *Biochem Biophys Res Commun.* (2011) 404:1010–5. doi: 10.1016/j.bbrc.2010.12.100
41. Sandor A, Pecsuvac K, Kerner J, Alkonyi I. On carnitine content of the human breast milk. *Pediatr Res.* (1982) 16:89–91. doi: 10.1203/00006450-198202000-00001
42. Gohir W, Kennedy KM, Wallace JG, Saoi M, Bellissimo CJ, Britz-McKibbin P, et al. High-fat diet intake modulates maternal intestinal adaptations to pregnancy and results in placental hypoxia, as well as altered fetal gut barrier proteins and immune markers. *J Physiol.* (2019) 597:3029–51. doi: 10.1113/JP277353
43. Peng H, Xu H, Wu J, Li J, Zhou Y, Ding Z, et al. Maternal high-fat diet disrupted one-carbon metabolism in offspring, contributing to nonalcoholic fatty liver disease. *Liver Int.* (2021) 41:1305–19. doi: 10.1111/liv.14811
44. Salama A, Elgohary R. L-carnitine and Co Q10 ameliorate potassium dichromate -induced acute brain injury in rats targeting AMPK/AKT/NF-kappabeta. *Int Immunopharmacol.* (2021) 101 (Pt B):107867. doi: 10.1016/j.intimp.2021.107867
45. Shahouzehi B, Barkhordari K, Aminizadeh S, Masoumi-Ardakan? Y. Effect of L-carnitine administration on serum insulin and adiponectin levels, and AMPK, APPL1 and PPAR? Gene expression in STZ-induced diabetic rat liver. *Ukrainian Biochem J.* (2017) 89:48–55. doi: 10.15407/ubj89.06.048
46. Hruby A, Hu FB. The epidemiology of obesity: a big picture. *Pharmacoeconomics.* (2015) 33:673–89. doi: 10.1007/s40273-014-0243-x
47. Olsen RK, Cornelius N, Gregersen N. Genetic and cellular modifiers of oxidative stress: what can we learn from fatty acid oxidation defects? *Mol Genet Metab.* (2013) 110(Suppl.):S31–9. doi: 10.1016/j.ymgme.2013.10.007
48. Delhaes F, Giza SA, Koreman T, Eastabrook G, McKenzie CA, Bedell S, et al. Altered maternal and placental lipid metabolism and fetal fat development in obesity: current knowledge and advances in non-invasive assessment. *Placenta.* (2018) 69:118–24. doi: 10.1016/j.placenta.2018.05.011

49. Hayward CE, Lean S, Sibley CP, Jones RL, Wareing M, Greenwood SL, et al. Placental adaptation: what can we learn from birthweight:placental weight ratio? *Front Physiol.* (2016) 7:28. doi: 10.3389/fphys.2016.00028
50. Sasson IE, Vitins AP, Mainigi MA, Moley KH, Simmons RA. Pre-gestational vs gestational exposure to maternal obesity differentially programs the offspring in mice. *Diabetologia.* (2015) 58:615–24. doi: 10.1007/s00125-014-3466-7
51. Mark PJ, Sisala C, Connor K, Patel R, Lewis JL, Vickers MH, et al. A maternal high-fat diet in rat pregnancy reduces growth of the fetus and the placental junctional zone, but not placental labyrinth zone growth. *J Dev Orig Health Dis.* (2011) 2:63–70. doi: 10.1017/s2040174410000681
52. Fall CHD, Kumaran K. Metabolic programming in early life in humans. *Philos Trans R Soc Lond B Biol Sci.* (2019) 374:20180123. doi: 10.1098/rstb.2018.0123
53. Shekhawat P, Bennett MJ, Sadovsky Y, Nelson DM, Rakheja D, Strauss AW. Human placenta metabolizes fatty acids: implications for fetal fatty acid oxidation disorders and maternal liver diseases. *Am J Physiol Endocrinol Metab.* (2003) 284:E1098–105. doi: 10.1152/ajpendo.00481.2002
54. Ding X, Yang Z, Han Y, Yu H. Correlation of long-chain fatty acid oxidation with oxidative stress and inflammation in pre-eclampsia-like mouse models. *Placenta.* (2015) 36:1442–9. doi: 10.1016/j.placenta.2015.10.014
55. Elshenawy S, Pinney SE, Stuart T, Doulias PT, Zura G, Parry S, et al. The metabolomic signature of the placenta in spontaneous preterm birth. *Int J Mol Sci.* (2020) 21:1043. doi: 10.3390/ijms21031043
56. Bowman CE, Arany Z, Wolfgang MJ. Regulation of maternal-fetal metabolic communication. *Cell Mol Life Sci.* (2021) 78:1455–86. doi: 10.1007/s00018-020-03674-w
57. Visiedo F, Bugatto F, Quintero-Prado R, Cozar-Castellano I, Bartha JL, Perdomo G. Glucose and fatty acid metabolism in placental explants from pregnancies complicated with gestational diabetes mellitus. *Reprod Sci.* (2015) 22:798–801. doi: 10.1177/1933719114561558
58. Hardie DG. AMP-activated/SNF1 protein kinases: conserved guardians of cellular energy. *Nat Rev Mol Cell Biol.* (2007) 8:774–85. doi: 10.1038/nrm2249
59. Rius-Perez S, Torres-Cuevas I, Millan I, Ortega AL, Perez S. PGC-1alpha, inflammation, and oxidative stress: an integrative view in metabolism. *Oxid Med Cell Longev.* (2020) 2020:1452696. doi: 10.1155/2020/1452696
60. Ikeda K, Utoguchi N, Tsutsui H, Yamaue S, Homemoto M, Nakao E, et al. In vitro approaches to evaluate placental drug transport by using differentiating JEG-3 human choriocarcinoma cells. *Basic Clin Pharmacol Toxicol.* (2011) 108:138–45. doi: 10.1111/j.1742-7843.2010.00634.x
61. Kusuyama J, Alves-Wagner AB, Conlin RH, Makarewicz NS, Albertson BG, Prince NB, et al. Placental superoxide dismutase 3 mediates benefits of maternal exercise on offspring health. *Cell Metab.* (2021) 33:939–56 e8. doi: 10.1016/j.cmet.2021.03.004
62. Benatti RO, Melo AM, Borges FO, Ignacio-Souza LM, Simino LA, Milanski M, et al. Maternal high-fat diet consumption modulates hepatic lipid metabolism and microRNA-122 (miR-122) and microRNA-370 (miR-370) expression in offspring. *Br J Nutr.* (2014) 111:2112–22. doi: 10.1017/S0007114514000579
63. Rebholz SL, Burke KT, Yang Q, Tso P, Woollett LA. Dietary fat impacts fetal growth and metabolism: uptake of chylomicron remnant core lipids by the placenta. *Am J Physiol Endocrinol Metab.* (2011) 301:E416–25. doi: 10.1152/ajpendo.00619.2010

Conflict of Interest: The authors declare that the research was conducted in the absence of any commercial or financial relationships that could be construed as a potential conflict of interest.

frontiers | Frontiers in Nutrition

ORIGINAL RESEARCH
published: 26 April 2022
doi: 10.3389/fnut.2022.861750

Different Interactive Effects of Metformin and Acarbose With Dietary Macronutrient Intakes on Patients With Type 2 Diabetes Mellitus: Novel Findings From the MARCH Randomized Trial in China

Yu An†, Yinhui Li†, Nannan Bian, Xiaoyu Ding, Xiaona Chang, Jia Liu and Guang Wang**

Department of Endocrinology, Beijing Chao-Yang Hospital, Capital Medical University, Beijing, China

OPEN ACCESS

Edited by:
Hui-Xin Liu,
China Medical University, China

Reviewed by:
Xingen Lei,
Cornell University, United States
Yang Xia,
Sheng Jing Hospital of China Medical University, China

***Correspondence:**
Jia Liu
liujia0116@126.com
Guang Wang
wangguang@bjcyh.com

†These authors have contributed equally to this work

Specialty section:
This article was submitted to Nutrition and Metabolism, a section of the journal Frontiers in Nutrition

Received: *25 January 2022*
Accepted: *29 March 2022*
Published: *26 April 2022*

Citation:
An Y, Li Y, Bian N, Ding X, Chang X, Liu J and Wang G (2022) Different Interactive Effects of Metformin and Acarbose With Dietary Macronutrient Intakes on Patients With Type 2 Diabetes Mellitus: Novel Findings From the MARCH Randomized Trial in China. Front. Nutr. 9:861750. doi: 10.3389/fnut.2022.861750

Antidiabetic oral agents and nutrition management are frequently used together as first-line therapies for type 2 diabetes mellitus (T2DM). However, less is known about their interaction. The interactive effect of two classic antidiabetic medications, namely, acarbose and metformin, with dietary intakes of macronutrients on glycemic control and cardiometabolic risk factors was investigated in the metformin and acarbose in Chinese as the initial hypoglycemic treatment (MARCH) randomized clinical trial. The patients with newly diagnosed T2DM from China were included in the trial. Participants were randomized to receive either metformin or acarbose monotherapy as the initial treatment, followed by a 24-week treatment phase, during which add-on therapy was used if necessary. Dietary intakes of carbohydrate, protein, fat, and total energy were calculated by a 24-h food diary recall method. Linear mixed-effect models combined with a subgroup analysis were used to investigate independent and interactive effects of drugs and diet on clinical outcomes. A data analysis was performed on 551 of the 788 patients randomly assigned to treatment groups. Metformin therapy was independently associated with higher triglycerides (TGs, $\beta = 0.471$, $P = 0.003$), 2 h postprandial plasma glucose (2hPPG, $\beta = 0.381$, $P = 0.046$) but lower low-density lipoprotein cholesterol (LDL-C, $\beta = -0.149$, $P = 0.013$) compared with acarbose therapy. Higher carbohydrates and lower fat intakes were independently associated with poorer glycemic control, less weight loss, and greater insulin secretion. Higher total energy intake was also independently associated with higher fasting ($\beta = 0.0002$, $P = 0.001$) and postprandial blood glucose ($\beta = 0.0004$, $P = 0.001$). Interaction and subgroup analyses demonstrated that glucagon-like peptide-1 (GLP-1) was positively related to total energy ($\beta = 0.268$, $P = 0.033$), carbohydrates intake, and insulin secretion ($\beta = 2{,}045.2$, $P = 0.003$) only in the acarbose group, while systolic blood pressure (SBP) was negatively related to protein intake in the metformin group ($\beta = 23.21$, $P = 0.014$). The results

of this study showed that metformin and acarbose mainly exerted different interactive effects with dietary energy, carbohydrate, and protein intakes on GLP-1 secretion, insulin release, and SBP. The interaction between drug therapy and nutrition intervention in glycemia highlights the complexity of combination therapy.

Keywords: type 2 diabetes mellitus, macronutrients, drug-diet interaction, MARCH trial, acarbose and metformin

INTRODUCTION

The number of patients with type 2 diabetes mellitus (T2DM) is increasing annually, which poses a global health threat and causes high health care costs, especially in the Asian region (1). It has been reported that the prevalence of diabetes in Asian countries, ranging from 3 to 47%, continues to surge despite therapeutic advances, with more than 60% of patients with diabetes worldwide living in Asia (2). T2DM is also reaching epidemic proportions in China, a country with the largest number of patients with diabetes (3), and thus there is an urgent need for more effective or targeted treatment strategies for it.

Nowadays, the treatment for T2DM is based on lifestyle changes, especially diet and antidiabetic oral agents, according to the needs of the patients. The treatment aims to achieve and maintain the optimal glycemic control, prevent acute diabetic complications, and reduce the risk of chronic complications, which require a combination of diabetic diet and conventional medications (4). Although numerous clinical trials are helpful in comparing different treatment strategies or medication regimens, the results of these trials should be considered in combination with patients' specific conditions, the availability and cost of drugs, and physicians' judgment in decision-making.

Metformin has been recommended as a first-line drug for monotherapy or combination therapy by Western authoritative clinical practice guidelines when lifestyle interventions can no longer achieve glycemic control (5). In China, acarbose has been taken as one of the first-line drugs in treatment for diabetes because acarbose can slow down the digestion and absorption of dietary carbohydrates in small intestines by inhibiting brush-border α-glucosidase, and Chinese diet is characterized by a higher percentage of carbohydrates (6). Zhu et al. have confirmed that the hypoglycemic effect of acarbose in patients with T2DM consuming an Eastern diet is superior to that in those consuming a Western diet by a systematic meta-analysis of studies (7). Because of the specific mechanism of glycemic control and weight loss, dietary components may alter the hypoglycemic effect of acarbose.

In fact, in addition to pharmacological interventions, dietary interventions are another cornerstone therapy for diabetes prevention and management (8, 9). The essential therapeutic approach to reducing the incidence and severity of T2DM focuses on the nature and quality of nutrients, especially consumed energy and macronutrients (10). The macronutrients in the diet are utilized by the body as sources of energy, including carbohydrate, protein, and fat. Restriction on any one of these macronutrients will have to be compensated by increase in the proportion of energy derived from the other two (11). Diets have evolved with changes in time, cultural traditions, as well as geographic and economic factors, all of which interact in a complex manner to shape different dietary consumption patterns among countries and regions (12). It has been reported that most Asians follow an Eastern diet pattern, characterized by higher intakes of whole grains, legumes, vegetables, fruits, and fish, thus making dietary carbohydrates the major source of energy (13). Evidence has suggested that the macronutrient composition of the diet also plays a key role in the postprandial and diurnal glucose excursions in patients with T2DM, and its changes may contribute to reducing postprandial glycemia, HbA1c, and diabetic complications (14).

However, there is a lack of information on Chinese dietary patterns and the efficacy of acarbose. The metformin and acarbose in Chinese as the initial hypoglycemic treatment (MARCH) trial was thus conducted to compare the effects of acarbose and metformin as the initial therapy for Chinese patients newly diagnosed with T2DM. It became the first and unique trial to investigate the effect of dietary macronutrients on glycemic control in the context of intensive drug therapy (ClinicalTrial.gov, number ChiCTR-TRC-08000231) (15–17). The trial showed that acarbose has a similar efficacy to metformin, making it a viable option for Chinese patients. Nevertheless, no previous studies of drug–diet interaction were conducted by systematic analysis of the diet and clinical data from MARCH. In this study, data from the MARCH trial were used to examine whether the effects of two classic antidiabetic medications, namely, acarbose and metformin, on glycemic control and cardiometabolic risk factors are related to dietary macronutrient intakes in patients with T2DM.

MATERIALS AND METHODS

Study Design

The study design, preliminary results, and the full study protocol of the MARCH trial were previously published (15). The MARCH trial was a multicenter (11 clinical sites in China), randomized controlled clinical trial in patients newly diagnosed T2DM. In the trial, the changes in the dietary intakes of energy and macronutrients, HbA1c, and fasting plasma glucose (FPG), postprandial 2-h glycemic profile, body mass index (BMI), insulin, glucagon, GLP-1, and insulin sensitivity or β-cell function by homoeostatic model assessment (HOMA) index in patients were evaluated. These patients received sustained-released metformin hydrochloride up to 1,500 mg, one time per day (500 mg per tablet, Beijing Double Crane Pharma, Beijing, China), or up to 100 mg of acarbose, three times per day (50 mg per tablet, Bayer Healthcare, <city>Beijing</city>, China), and there will be a 24-week monotherapy and a 24-week insulin

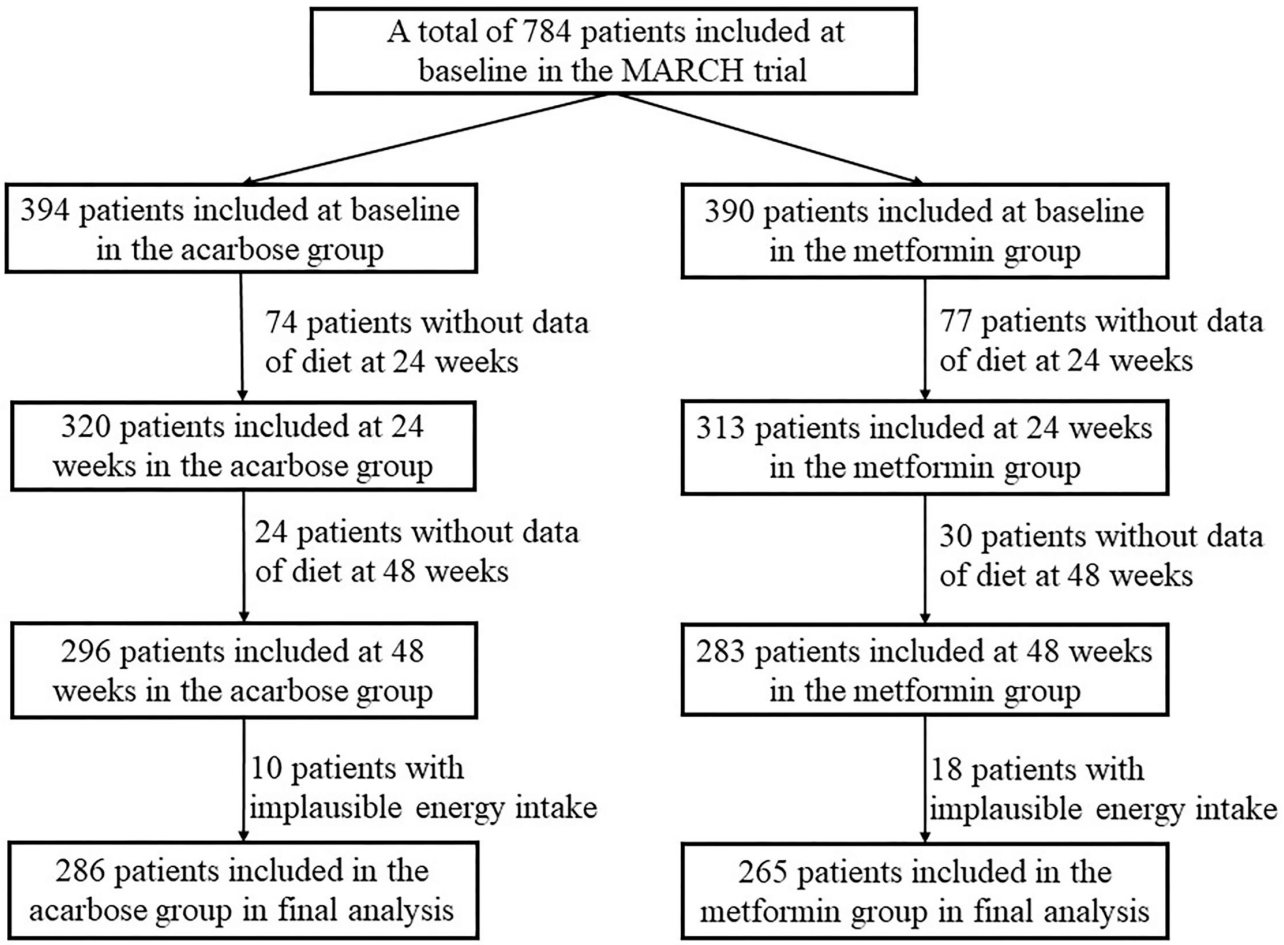

FIGURE 1 | Flowchart for the selection process of the current study population in the metformin and acarbose in Chinese as the initial hypoglycemic treatment (MARCH) trial.

secretagogue add-on therapy if necessary. At Chinese diabetic clinics, outpatients who met the inclusion criteria were provided with written notification and oral explanations on this trial. This study began after the acquisition of written informed consent and confirmation of willingness to participate from all the participating patients. The protocol was approved by the ethics committee from each clinical site and implemented in accordance with the provisions of the Declaration of Helsinki and Good Clinical Practice guidelines.

Participants

Patients would be eligible for this study if they fulfilled the following criteria: (1) diagnosed with T2DM within the past 12 months according to 1999 WHO criteria, (2) without oral antidiabetic agents or short-term (i.e., 1 month) treatment discontinued 3 months before enrollment, and (3) suboptimum glucose control (HbA1c between 7.0% and 10.0%, FPG $\leq$ 11·1 mmol/L, and BMI 19–30 kg/m^2). The full details of exclusion criteria were previously described. During the recruitment phase, 788 eligible individuals were invited to participate. Four participants withdrew consent before drug intervention and were excluded. Subsequently, 98 participants were excluded from the acarbose group and 107 from the metformin group due to insufficient dietary data. In addition, 10 participants in the acarbose group and 18 in the metformin group with implausible energy intake (<800 kcal/day or >6,000 kcal/day for men; <600 kcal/day or >4,000 kcal/day for women) were further excluded (18). Finally, a total of 551 participants (286 in the acarbose group and 265 in the metformin group) were included in this study. A flowchart of the selection process of the study population is shown in **Figure 1**.

Dietary Assessment

Dietary macronutrient intake and energy intake were assessed at baseline, 24 and 48 weeks by the 24-h dietary recall method, and an author's semiquantitative diet history questionnaire, in which questions concern the quantity and the frequency of product consumption in each group. The questionnaire has been reviewed by clinical nutritionists and dietitians (19). A well-trained dietitian conducted face-to-face interviews with the

TABLE 1 | Baseline characteristics of patients treated with acarbose or metformin.

Variables	Acarbose	Metformin	*P* value
	(*n* = 286)	(*n* = 265)	
Sex			0.748
Male, *n*%	171 (59.79%)	162 (61.13%)	
Female, *n*%	115 (40.21%)	103 (38.87%)	
Age, years	51 (44, 57)	51 (43, 57)	0.672
Duration of diabetes	0.13 (0.09, 0.26)	0.16 (0.09, 0.30)	0.039*
BMI, kg/m^2	25.26 (23.39, 27.12)	25.26 (23.65, 27.38)	0.853
SBP, mmHg	121 (118, 130)	120 (120, 130)	0.853
DBP, mmHg	80 (70.5, 82)	80 (73, 82)	0.917
TC, mmol/L	5.12 (4.46, 5.84)	5.10 (4.32, 5.93)	0.755
TG, mmol/L	1.80 (1.23, 2.71)	1.96 (1.38, 2.76)	0.166
HDL-C, mmol/L	1.18 (1.02, 1.39)	1.18 (1.00, 1.37)	0.712
LDL-C, mmol/L	3.07 (2.53, 3.59)	3.02 (2.43, 3.63)	0.359
FBG, mmol/L	8.2 (7.5, 9.1)	8.3 (7.6, 9.5)	0.197
HbA1c, %	7.2 (6.6, 8.1)	7.5 (6.7, 8.4)	0.108
2hPPG$, mmol/L	12.44 (10.55, 14.40)	12.58 (10.23, 14.80)	0.796
FINS, uIU/mL	11.06 (7.24, 16.58)	11.71 (7.24, 16.83)	0.733
EISI$	2.54 (1.08, 4.48)	2.59 (1.13, 4.49)	0.902
AUC for plasma GLP-1$, pmol/mL × min	2,797.35 (1,753.20, 4,427.85)	2,829.68 (1,716.30, 4,884.60)	0.628
AUC for glucagon$, pg/mL × min	12,256.35 (9,936.15, 15,887.93)	12,353.10 (9,730.20, 15,813.34)	0.922
AUC for serum insulin$, uIU/mL × min	4,528.50 (3,198.00, 6,236.70)	4,435.05 (3,017.48, 6,160.95)	0.437
HOMA-IR	3.87 (2.44, 6.30)	4.09 (2.56, 6.60)	0.606
HOMA-β	48.58 (29.13, 77.62)	51.43 (28.25, 73.06)	0.985
WBISI$	3.83 (2.64, 5.85)	3.85 (2.63, 5.88)	0.947

Data shown as median (interquartile range) were compared between 2 groups using Mann-Whitney U-test.
Data shown as n (%) were compared between 2 groups using the chi-square test.
BMI, body mass index; SBP, systolic blood pressure; DBP, diastolic blood pressure; TGs, triglycerides; TC, total cholesterol; LDL-C, low-density lipoprotein cholesterol; HDL-C, high-density lipoprotein cholesterol; FBG, fasting blood glucose; 2hPPG, 2-h postprandial plasma glucose; FINS, fasting insulin; HOMA-IR, homeostasis model assessment of insulin resistance; HOMA-β, homeostasis model assessment of β-cell function; EISI, early insulin secretion index; WBISI, whole body insulin sensitivity index; AUC, area under the curve; GLP-1, plasma glucagon-like peptide-1. $ After a standard meal test.
*$P < 0.05$.

patients and asked them to report an average portion size of commonly consumed food. Food models, pictures, and other visual presentations were used to designate portion sizes of food and thus guide participants in estimating the portion size of consumed food. Additionally, a pilot study was performed on several patients and modified accordingly. The food data in the questionnaires were matched with nutrient information from China Food Composition Database for the analysis of macronutrient content. All data of food intake frequencies were converted to times per day, and then the portion size of each food item per day as well as the daily energy and macronutrient intakes from it were calculated and derived. The percentage of total kilocalories from carbohydrate, protein, and fat intakes was then derived.

Outcomes and End Points

The primary end points were reduction in HbA1c at 24 and 48 weeks. Key secondary end points included changes in fasting blood glucose (FBG), 2-h postprandial glycemic profile, BMI, insulin, glucagon, glucagon-like peptide-1 (GLP-1), and insulin sensitivity or β-cell function (HOMA index), which were all measured at baseline, 24, and 48 weeks. The glucose metabolism variables included HbA1c, FBG, 2-h postprandial plasma glucose (2hPPG), HOMA of insulin resistance (HOMA-IR), and whole-body insulin sensitivity index (WBISI). Hormone secretion parameters included fasting insulin (FINS), HOMA of β-cell function (HOMA-β), early insulin secretion index (EISI, I_{30}/G_{30}), and the area under the curve (AUC) of insulin, glucagon, and GLP-1. The measurement of cardiometabolic risk factors related to obesity, dyslipidemia, and high blood pressure included height, weight, serum levels of total cholesterol (TC), low-density lipoprotein cholesterol (LDL-C), high-density lipoprotein cholesterol (HDL-C) and triglycerides (TGs), systolic blood pressure (SBP), and diastolic blood pressure (DBP). BMI was calculated from the measured height and weight (kg/m^2). The following formulas were used to calculate some of the indexes mentioned above: HOMA-IR = FINS (μIU/ml) × FBG (mmol/L)/22.5; HOMA-B = 20 × FINS (μIU/ml)/[FBG (mmol/L) −3.5] early insulin secretion index (EISI) = $\Delta I_{30}/\Delta G_{30}$ = ($insulin_{30min}$ − $insulin_{0min}$)/ΔG_{30} ($glucose_{30min}$ − $glucose_{0min}$); and WBISI = 10,000/square root of [(mean plasma insulin × mean plasma glucose during OGTT) × (FINS × FPG). The AUC was calculated with the following equations: AUC for serum insulin = ($insulin_{0min}$ + $insulin_{30min}$) × 30/2 + ($insulin_{30min}$ + $insulin_{120min}$) × 90/2 + ($insulin_{120min}$ + $insulin_{180min}$) × 60/2, AUC for glucagon= (glucagon $_{0min}$ + glucagon $_{30min}$) × 30/2 + (glucagon $_{30min}$ + glucagon $_{120min}$) × 90/2 + (glucagon $_{120min}$ + glucagon $_{180min}$) × 60/2 and AUC for plasma GLP-1 = ($GLP\text{-}1_{0min}$ + $GLP\text{-}1_{30min}$) × 30/2 + ($GLP\text{-}1_{30min}$ + $GLP\text{-}1_{120min}$) × 90/2 + ($GLP\text{-}1_{120min}$ + $GLP\text{-}1_{180min}$) × 60/2.

Statistical Analysis

Statistical analyses were performed by STATA version 13.0 (STATA, College Station, TX) and R 3.5.1. Prior to analysis, the normality of data distribution was checked. Continuous variables were expressed as medians (interquartile range, IQR) when nonnormally distributed, and they were the mean ± standard deviation (SD) when normally distributed. The Student's *t*-test or the Mann-Whitney *U*-test was used for continuous variables as appropriate at baseline. The differences in frequencies of the categorical variables were evaluated using the chi-square test. The Friedman's two-way analysis of variance by ranks test was adopted to determine changes in treatment outcomes and dietary intakes of energy and macronutrients in two treatment groups during three time periods (i.e., baseline, 24 weeks, and 48 weeks).

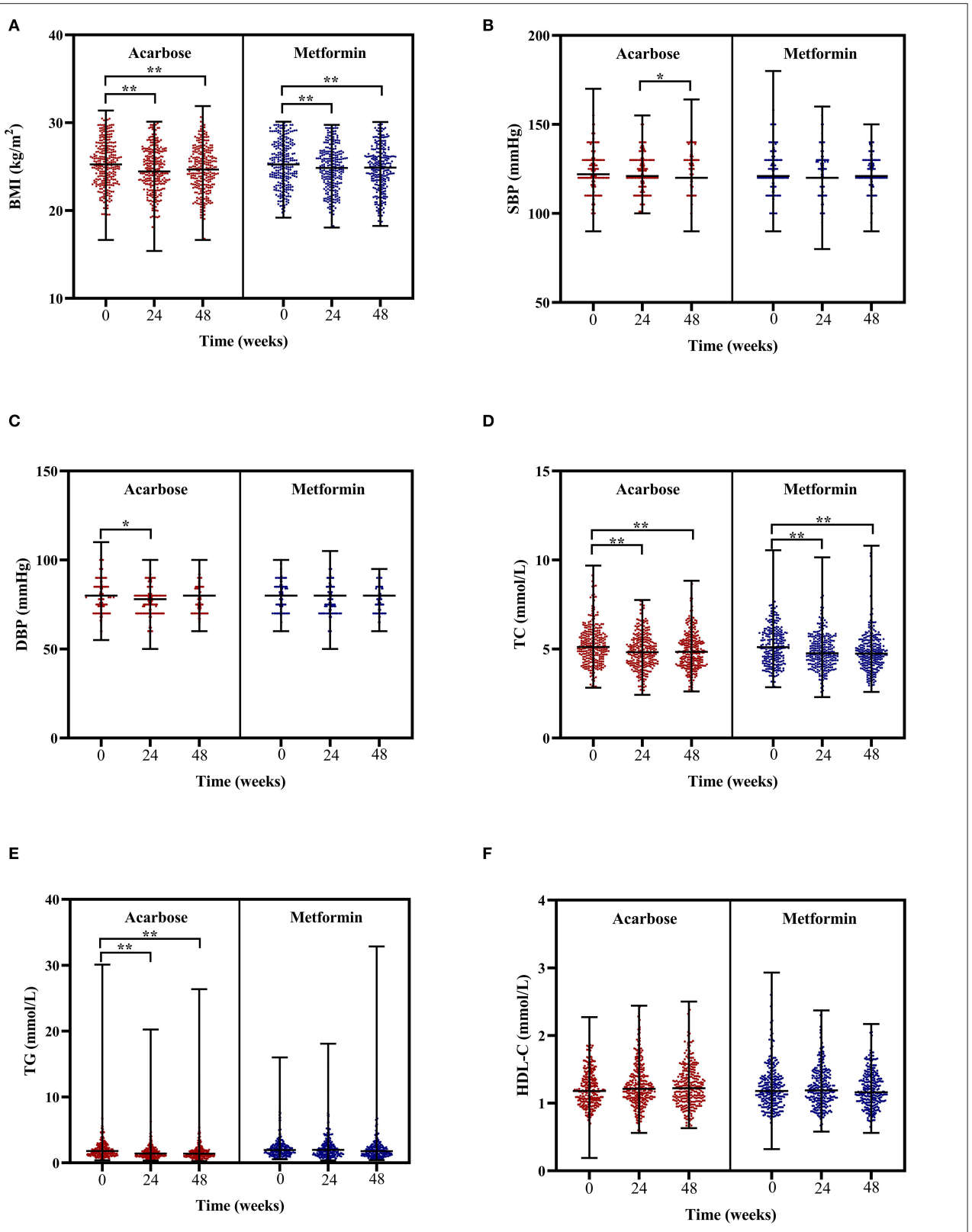

FIGURE 2 | Continued

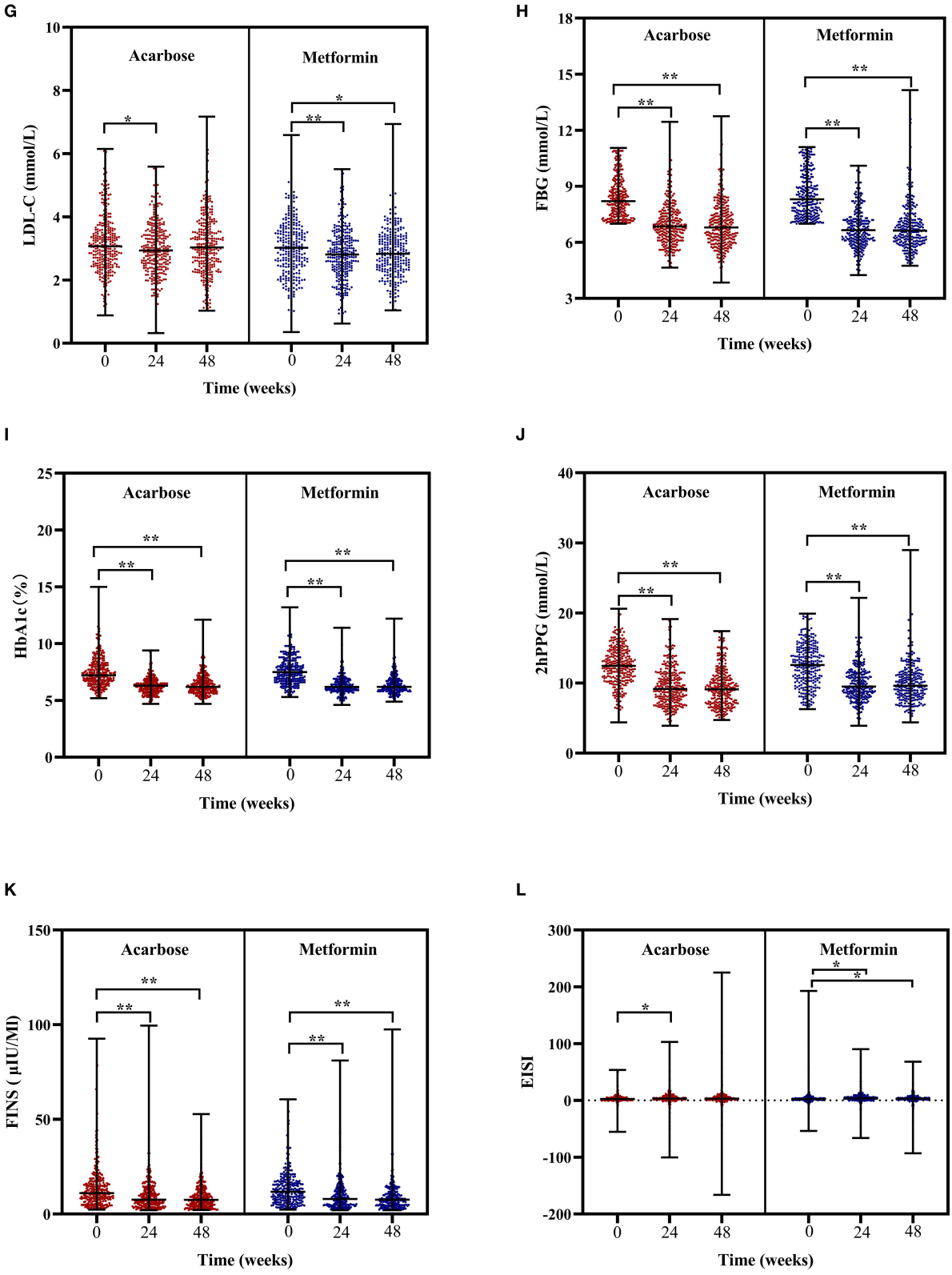

FIGURE 2 | Continued

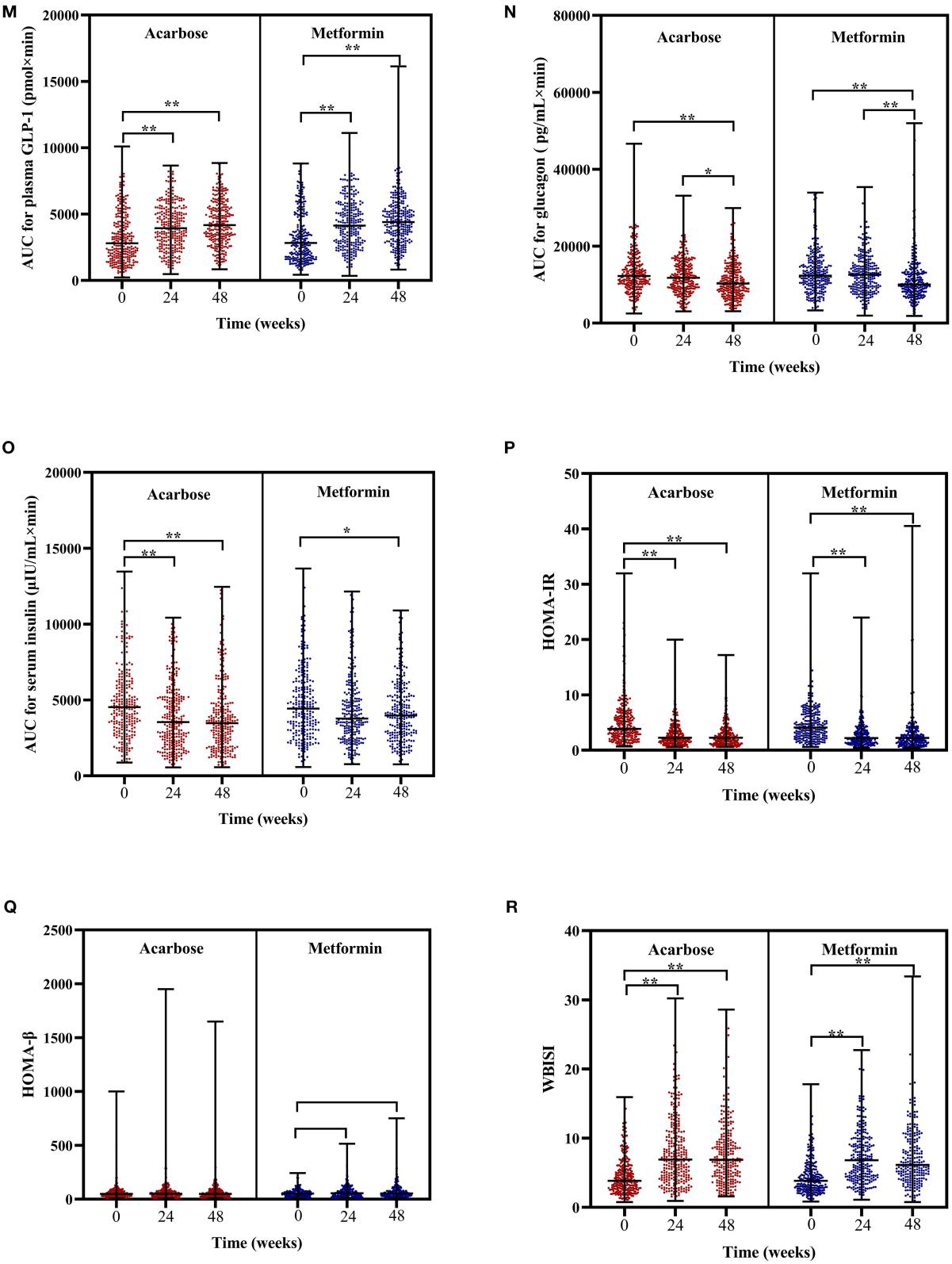

FIGURE 2 | Scatter plots of BMI **(A)**, SBP **(B)**, DBP **(C)**, TC **(D)**, TG **(E)**, HDL-C **(F)**, LDL-C **(G)**, FBG **(H)**, HbA1c **(I)**, 2hPPG **(J)**, FINS **(K)**, EISI **(L)**, AUC for plasma GLP-1 **(M)**, AUC for glucagon **(N)**, AUC for serum insulin **(O)**, HOMA-IR **(P)**, HOMA-β **(Q)**, and WBISI **(R)** in patients subjected to metformin or acarbose groups at

(Continued)

FIGURE 2 | baseline, 24 weeks, and 48 weeks. Data were tested by Friedman's two-way analysis of variance by ranks test during three time periods (i.e., baseline, 24 weeks, and 48 weeks) in two treatment groups. **post-hoc* pairwise comparison adjusted $P < 0.05$, *** post-hoc* pairwise comparison adjusted $P < 0.01$. BMI, body mass index; SBP, systolic blood pressure; DBP, diastolic blood pressure; TGs, triglycerides; TC, total cholesterol; LDL-C, low-density lipoprotein cholesterol; HDL-C, high-density lipoprotein cholesterol; FBG, fasting blood glucose; 2hPPG, 2-h postprandial plasma glucose; FINS, fasting insulin; HOMA-IR, homeostasis model assessment of insulin resistance; HOMA-β, homeostasis model assessment of β-cell function; EISI, early insulin secretion index; WBISI, whole body insulin sensitivity index; AUC, area under the curve; GLP-1, plasma glucagon-like peptide-1.

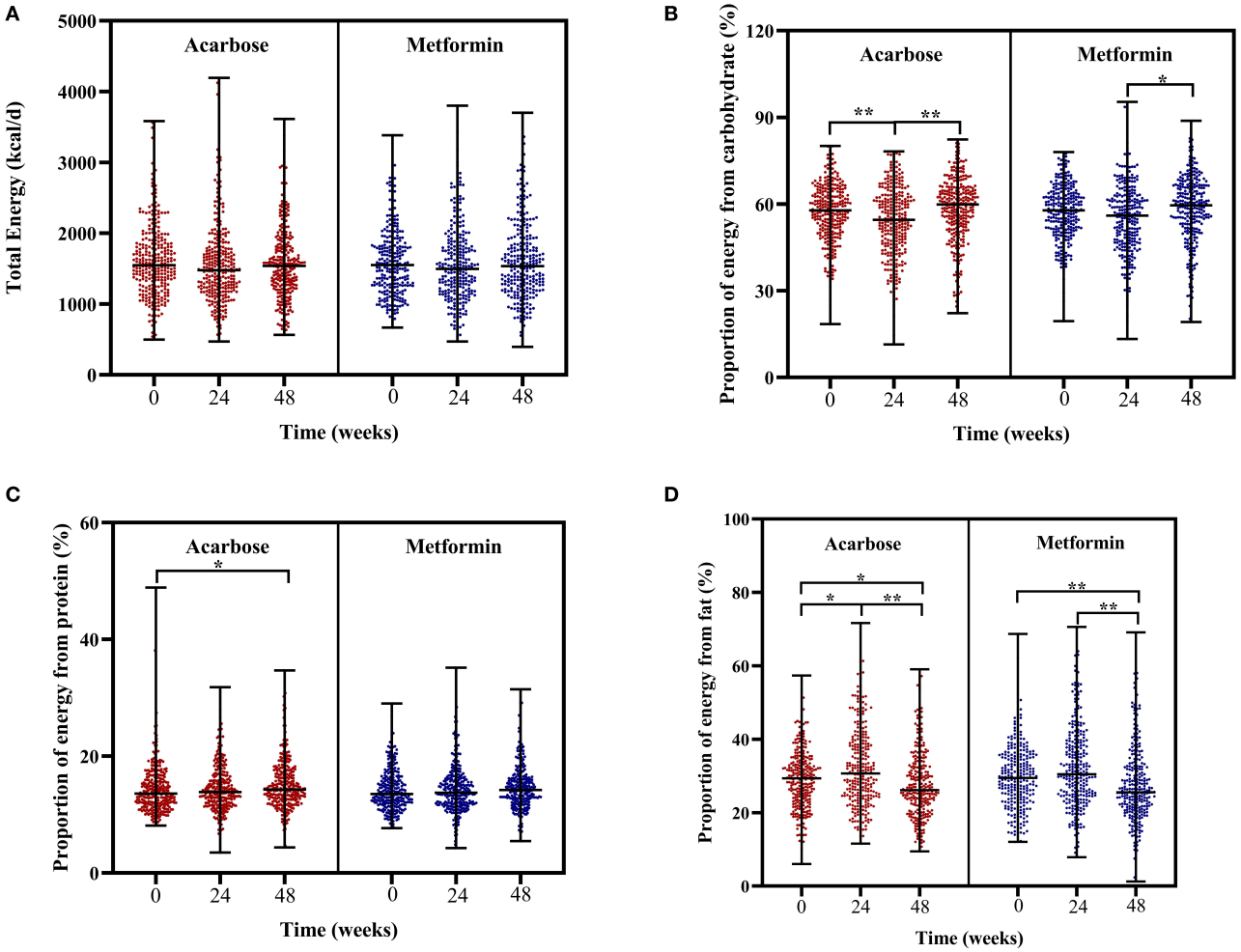

FIGURE 3 | Scatter plots of total energy intake **(A)**, proportion of energy from carbohydrate **(B)**, proportion of energy from protein **(C)**, and proportion of energy from fat **(D)** in patients subjected to metformin or acarbose groups at baseline, 24 weeks, and 48 weeks. Data were tested by Friedman's two-way analysis of variance by ranks test during three time periods (i.e., baseline, 24 weeks, and 48 weeks) in two treatment groups. **post-hoc* pairwise comparison adjusted $P < 0.05$, ***post-hoc* pairwise comparison adjusted $P < 0.01$.

This nonparametric test was used since the data did not meet the requirements for parametric analysis. When the difference was significant (Friedman's test, $P < 0.05$), *post-hoc* pairwise comparison tests with a Bonferroni correction were performed, and scatter plots were used to visually display changes over time. Multilevel mixed-effect linear regression models were adopted (maximum likelihood method, unstructured variance-covariance structure, and center and individual used as random effect components) to determine the independent associations between dietary energy and macronutrient intakes or between two antidiabetic oral drug classes and treatment outcomes over time. Furthermore, to analyze the effect of the drug–diet interaction between acarbose or metformin treatment and dietary energy and macronutrients intakes on treatment outcomes, interaction terms of drug class were added to each intake of nutrient in the adjusted linear mixed-effect regression models, respectively. In addition, subgroup analysis was performed on acarbose or metformin treatment groups to test the significant interactive associations of dietary energy and macronutrient intakes and treatment outcomes in each group. Coefficients (β) were adopted

to express the effect size of the associations. All effect size estimates were adjusted for covariates, including age, sex, time of intervention, and duration of diabetes. A two-sided $P < 0.05$ showed statistical significance.

RESULTS

Participant Characteristics

Demographic, anthropometric, and clinical characteristics of the patients with diabetes receiving different treatments are shown in **Table 1**. There were 286 patients in the acarbose group and 265 in the metformin group. The median age of the 551 participants was 51 (IQR: 43–57), of which 218 were women (39.6%). Among them, the patients only in the metformin group had significantly longer duration of diabetes ($P = 0.039$). There were no statistically significant differences in age, sex, glucose metabolism variables, hormone secretion parameters, and cardiometabolic risk factors between participants (all $P > 0.05$).

Changes in Clinical Outcomes and Dietary Intakes Over Time

The Friedman's two-way analysis of variance by ranks combined with *post-hoc* pairwise comparisons indicated that there was the significant effect of overall treatment time on most treatment outcomes. The scatter plots of *post-hoc* pairwise comparison revealed that the BMI, TC, FBG, HbA1c, 2hPPG, FINS, AUC for plasma GLP-1, HOMA-IR, and WBISI significantly decreased in both treatment groups at 24 and 48 weeks compared with those at baseline. SBP significantly increased at 48 weeks compared with that at 24 weeks, while DBP significantly decreased at 24 weeks compared with that at baseline only in acarbose group. TG significantly decreased at 24 and 48 weeks compared with that at baseline only in the acarbose group. LDL-C in the acarbose group significantly decreased at 24 weeks compared with that at baseline but significantly decreased both at 24 and 48 weeks compared with that at baseline in the metformin group. Meanwhile, the change trend of EISI in two groups was opposite to that of LDL-C. AUC for glucagon significantly decreased at 48 weeks compared with that at baseline and at 24 weeks in both treatment groups. AUC for serum insulin significantly decreased at 24 and 48 weeks compared with that at baseline in the acarbose group but significantly decreased at 48 weeks compared with that at baseline in the metformin group (adjusted $P < 0.05$, **Figures 2A–R**).

In regard to changes in dietary intakes of total energy and macronutrients, the Friedman's two-way analysis of variance by ranks indicated that there was a significant effect of overall treatment time on proportion of energy from carbohydrate, protein, and fat. *Post-hoc* pairwise comparisons showed the following results: the proportion of energy from carbohydrate significantly decreased at 24 weeks compared with that at baseline but significantly increased at 48 weeks compared with that at 24 weeks in the acarbose group and in the metformin group; the proportion of energy from carbohydrate only significantly increased at 48 weeks compared with that at 24 weeks; the proportion of energy from protein significantly increased at 48 weeks compared with that at baseline only in the acarbose group; the proportion of energy from fat significantly increased at 24 weeks compared with that at baseline only in the acarbose group but significantly decreased at 48 weeks compared with that at 24 weeks and at baseline in both groups (adjusted $P < 0.05$, **Figures 3A–D**).

TABLE 2 | Independent effects of drug treatment on clinical outcomes in linear mixed-effect models.

Outcomes	Acarbose	Metformin	
		β (95%CI)	*P* value
BMI, kg/m^2	Ref	0.149 (−0.267–0.565)	0.483
SBP, mmHg		−0.049 (−1.490–1.392)	0.947
DBP, mmHg		0.060 (−0.840–0.959)	0.897
TC, mmol/L		−0.021 (−0.169–0.128)	0.786
TG, mmol/L		0.471 (0.159–0.782)	0.003*
HDL-C, mmol/L		−0.198 (−0.059–0.020)	0.323
LDL-C, mmol/L		−0.149 (−0.266 −0.032)	0.013*
FBG, mmol/L		−0.086 (−0.229–0.056)	0.236
HbA1c, %		0.041 (−0.080–0.163)	0.506
2hPPG, mmol/L		0.381 (0.007–0.756)	0.046*
FINS, μIU/Ml		0.035 (−1.007–1.077)	0.947
EISI		0.357 (−1.135–1.849)	0.639
AUC for plasma GLP-1, pmol×min		134.3 (−48.2–316.8)	0.149
AUC for glucagon, pg/mL×min		182.0 (−483.2–847.2)	0.592
AUC for serum insulin, μIU/mL×min		170.1 (−136.8–477.1)	0.277
HOMA-IR		0.033 (−0.330–0.396)	0.857
HOMA-β		−3.021 (−12.492–6.451)	0.532
WBISI		−0.271 (−0.810–0.268)	0.324

Models adjusted for age, sex, time of intervention, and duration of diabetes.
BMI, body mass index; SBP, systolic blood pressure; DBP, diastolic blood pressure; TGs, triglycerides; TC, total cholesterol; LDL-C, low-density lipoprotein cholesterol; HDL-C, high-density lipoprotein cholesterol; FBG, fasting blood glucose; 2hPPG, 2-h postprandial plasma glucose; FINS, fasting insulin; HOMA-IR, homeostasis model assessment of insulin resistance; HOMA-β, homeostasis model assessment of β-cell function; EISI, early insulin secretion index; WBISI, whole body insulin sensitivity index; AUC, area under the curve; GLP-1, plasma glucagon-like peptide-1.
*$P < 0.05$.

Independent or Interactive Associations of Treatment Effects and Dietary Intakes With Clinical Outcomes

Linear mixed-effect models were used to assess the effects of acarbose or metformin treatment on changes in clinical parameters adjusted for age, sex, time of intervention, and disease duration. Results were expressed as estimated mean changes from baseline with 95% confidence intervals (CIs). In drug treatment effects, metformin therapy was independently associated with higher TG (0.471 mmol/L, 95% CI: 0.159–0.782 mmol/L), higher 2hPPG (0.381 mmol/L, 95% CI: 0.007–0.756 mmol/L), and lower LDL-C (0.149 mmol/L, 95% CI: −0.266 to −0.032 mmol/L) but had comparable effects on other outcomes compared with acarbose therapy (**Table 2**). Dietary intakes of energy, carbohydrate, and fat also demonstrated independent associations with certain clinical outcomes (**Table 3**). Each unit increase in total energy intake was significantly associated with higher FBG (0.002 mmol/L, 95% CI: 0.00008–0.0003 mmol/L)

and higher 2hPPG (0.004 mmol/L, 95% CI: 0.0002–0.0007 mmol/L). Each unit increase in proportion of energy from carbohydrate was significantly associated with higher BMI (0.607 kg/m^2, 95% CI: 0.167–1.047 kg/m^2), higher HbA1c (0.685%, 95% CI: 0.251–1.120%), higher 2hPPG (1.255 mmol/L, 95% CI: 0.103–2.407 mmol/L), and higher AUC for serum insulin (1,090.1 μIU/ml × min, 95% CI: 176.6–2,003.6 μIU/ml × min). In contrast, each unit increase in proportion of energy from fat was significantly associated with lower BMI (0.808 kg/m^2, 95% CI: −1.314 to −0.303 kg/m^2), lower FBG (0.770 mmol/L, 95% CI: −1.370 to −0.170 mmol/L), lower HbA1c (0.969%, 95% CI: −1.476% to −0.462%), lower 2hPPG (1.954 mmol/L, 95% CI: −1.476 to −0.462 mmol/L), lower AUC for serum insulin (1,135.1 μIU/ml×min, 95% CI: −2,193.8 to −76.4 μIU/ml×min) but higher WBISI (2.673, 95% CI: 0.059–4.758).

The results of two-way interaction analysis of the interactive effect of two drug classes with dietary intakes of total energy and macronutrients on clinical outcomes are shown in **Table 4**. The following was found: the interaction terms of total energy × drug therapy were associated with lower AUC for plasma GLP-1 ($\beta = -0.335$, 95% CI: −0.665 to −0.004, $P = 0.047$); the proportion of energy from carbohydrate × drug therapy was associated with lower AUC for serum insulin ($\beta = -1{,}885.8$, 95% CI: −3,709.7 to −62.0, $P = 0.043$); the proportion of energy from protein × drug therapy was associated with higher SBP ($\beta = 31.71$, 95% CI: 7.77–55.65, $P = 0.009$). Given the interactive effect of drug therapy with dietary intakes of total energy and macronutrients, subgroup analyses were performed on two drug classes to investigate the associations between dietary intakes and clinical outcomes (**Figures 4–6**). **Figure 4** shows that a higher total energy intake was significantly associated with higher AUC for plasma GLP-1 ($\beta = 0.268$, $P = 0.033$) among acarbose users but with lower AUC for plasma GLP-1 among metformin users ($\beta = -0.264$ acarbose, $P = 0.049$). Additionally, it was observed that there was a significant association between higher intake of carbohydrates and AUC for serum insulin ($\beta = 2{,}045.2$, $P = 0.003$) in the acarbose group, but the association was not statistically significant in the metformin group ($\beta = 194.7$, $P = 0.754$, **Figure 5**). However, among acarbose users, no significant association was detected between dietary intake of protein and SBP, but significantly positive association was detected among metformin users ($\beta = 23.21$, $P = 0.014$, **Figure 6**).

DISCUSSION

Recent studies have drawn attention to the potential interactive effects of chronic medication use with nutrient intakes on chronic noncommunicable diseases (20, 21). Drug-nutrient interactions are of great clinical and public health significance, especially in patients with T2DM. The treatment for T2DM involved dietary manipulation that can reduce both glucose and insulin aberrant levels, and cardiovascular complications. This study first showed two classic antidiabetic medications of acarbose and metformin and their interaction with macronutrient intakes in the context of MARCH clinical trial. Among the included Chinese patients being treated for T2DM, metformin and acarbose mainly exerted different interactive effects with dietary energy, carbohydrate, and protein intakes on GLP-1 secretion, insulin release, and SBP.

The results of this study have shown that the daily intake of total energy, carbohydrates, protein, and fat for included newly diagnosed patients with T2DM fell into the normal range before treatment, and total energy intake remained relatively stable in both two groups during treatment. Even so, independent and positive associations were still found between total energy and FBG, as well as 2hPPG during treatment, suggesting additional benefits of glycemic control from total energy restriction even under antidiabetic oral agent therapy, which was also observed among Korean patients (22). Meanwhile, different oral drugs may change the association between total energy intake and treatment outcomes due to different mechanisms of action related to the gastrointestinal tract. In the subgroup analysis, total energy intake and AUC for plasma GLP-1 showed inverse associations under metformin and acarbose treatment, indicating that total energy intake stimulates distinct patterns of GLP-1 release. The incretin hormone of GLP-1 plays a critical role in regulating glucose homeostasis and dietary intakes of nutrients are a primary stimulus to the release of intestinal GLP-1 (23). In generally, carbohydrate, lipid, and protein digestion, also known as sources of total energy, can induce postprandial glycemic and GLP-1 secretion through different pathways, to promote the absorption of glucose and maintain the level of blood glucose (24). Consequently, strategies to slow down the digestion of these macronutrients are needed to achieve a sustained release of GLP-1 for improvement of the glucose homeostasis. It has been confirmed that postprandial GLP-1 secretion under acarbose treatment is stimulated in patients with T2DM by induction of transfer of carbohydrates to the distal parts of the intestine (25). Therefore, under acarbose treatment, a sustained release of GLP-1 can still be achieved even following an increase in total energy intake by slowing down the digestion and absorption of dietary carbohydrates in small intestine, suggesting a positive association between total energy intake and AUC for plasma GLP-1. However, under metformin treatment, a higher total energy intake was associated with lower AUC for plasma GLP-1. It has also been showed that metformin increases plasma GLP-1 concentrations in healthy controls and patients with T2DM (26). Nevertheless, it has been reported that metformin does not directly stimulate GLP-1 secretion *in vitro*, suggesting that its effect observed *in vivo* are indirect (27). It may be speculated that the GLP-1 secretion induced by metformin can be disturbed by total energy intake, which deserves further investigation.

Contrary to relatively stable intake of total energy, carbohydrate intake significantly decreased at 24 weeks but increased at 48 weeks in the acarbose group and significantly increased at 48 weeks in the metformin group. Considering that the staple food is rich in carbohydrate in most Asian countries, the changes in quantity of dietary carbohydrates indicated a gradually loose restriction on carbohydrate and a relative imbalance between dietary desires and adherence to diet modification in disease management. Dietary carbohydrates are one of fundamental macronutrients in terms of their capacities to affect blood glucose and insulin levels (28). In linear mixed-effect models, higher intake of carbohydrates was

TABLE 3 | Independent effects of dietary intakes on clinical outcomes in linear mixed-effect models.

Outcomes	Total energy		Proportion of energy from carbohydrate		Proportion of energy from protein		Proportion of energy from fat	
	β (95%CI)	*P* value	β (95%CI)	*P* value	β (95%CI)	*P* value	β (95%CI)	*P* value
BMI, kg/m^2	0.00006 (−0.00004–0.0002)	0.227	0.607 (0.167–1.047)	0.007*	−0.177 (−1.389–1.034)	0.774	−0.808 (−1.314 −0.303))	0.002*
SBP, mmHg	−0.0002 (−0.001–0.0008)	0.754	1.023 (−3.312–5.357)	0.644	4.971 (−7.054–16.995)	0.418	−1.116 (−6.155–3.923)	0.664
DBP, mmHg	0.0002 (−0.0005–0.0009)	0.654	1.580 (−1.545–4.704)	0.322	−2.051 (−10.765–6.662)	0.644	−2.884 (−6.531–0.762)	0.121
TC, mmol/L	0.00002 (−0.00006–0.0001)	0.588	0.196 (−0.183–0.576)	0.311	0.348 (−0.703–1.400)	0.516	−0.244 (−0.683–0.194)	0.274
TG, mmol/L	0.00005 (−0.0001–0.0002)	0.588	−0.442 (−1.296–0.412)	0.31	0.041 (−2.351–2.432)	0.973	0.289 (−0.698–1.275)	0.566
HDL-C, mmol/L	−0.00001 (−0.00004–0.000009)	0.23	−0.085 (−0.191–0.021)	0.115	0.005 (−0.287–0.298)	0.972	0.101 (−0.021–0.224)	0.106
LDL-C, mmol/L	−0.00002 (−0.00009–0.00005)	0.568	0.209 (−0.108–0.526)	0.196	0.345 (−0.532–1.223)	0.44	−0.017 (−0.384–0.351)	0.93
FBG, mmol/L	0.0002 (0.00008–0.0003)	0.001*	0.322 (−0.192–0.836)	0.219	0.794 (−0.644–2.233)	0.279	−0.770 (−1.370 −0.170)	0.012*
HbA1c, %	0.00006 (−0.00004–0.0002)	0.239	0.685 (0.251–1.120)	0.002*	0.187 (−0.129–1.404)	0.763	−0.969 (−1.476–−0.462)	<0.001*
2hPPG, mmol/L	0.0004 (0.0002–0.0007)	0.001*	1.255 (0.103–2.407)	0.033*	−0.576 (−3.787–2.636)	0.725	−1.954 (−3.291 −0.617)	0.004*
FINS, μIU/Ml	0.0003 (−0.0006–0.001)	0.553	1.990 (−2.047–6.028)	0.334	3.253 (−9.051–13.756)	0.686	−2.031 (−6.739–2.677)	0.398
EISI	0.0004 (−0.0009–0.002)	0.551	−1.726 (−7.998–4.546)	0.59	10.430 (−7.798–28.657)	0.262	1.042 (−6.212–8.296)	0.778
AUC for plasma GLP-1, pmol×min	−0.007 (−0.189–0.175)	0.942	86.2 (−720.4–892.8)	0.834	−1,029.6 (−3,311.8–1,252.6)	0.377	249.8 (−702.2–1,201.9)	0.607
AUC for glucagon, pg/mL×min	−0.226 (−0.733–0.282)	0.384	−688.5 (−2,963.9–1,586.8)	0.553	−2,632.0 (−8,957.6–3,693.7)	0.415	2,371.9 (−272.3–5,016.2)	0.079
AUC for serum insulin, μIU/mL×min	0.083 (−0.118–0.285)	0.418	1,090.1 (176.6–2,003.6)	0.019*	200.1 (−2,370.5–2,770.8)	0.879	−1,135.1 (−2,193.8 −76.4))	0.036*
HOMA-IR	0.0001 (−0.0002–0.0005)	0.399	0.907 (−0.550–2.363)	0.222	0.960 (−3.149–5.069)	0.647	−0.887 (−2.598–0.815)	0.307
HOMA-β	0.0008 (−0.008–0.010)	0.864	15.773 (−23.861–55.408)	0.435	4.694 (−108.3–117.7)	0.935	−10.021 (−56.205–36.164)	0.671
WBISI	−0.0002 (−0.0006–0.0002)	0.227	−1.736 (−3.538–0.061)	0.058	1.819 (−3.230–6.869)	0.48	2.673 (0.059–4.758)	0.012*

Models adjusted for age, sex, time of intervention, and duration of diabetes. * *P* < 0.05.*

BMI, body mass index; SBP, systolic blood pressure; DBP, diastolic blood pressure; TGs, triglycerides; TC, total cholesterol; LDL-C, low- density lipoprotein cholesterol; HDL-C, high-density lipoprotein cholesterol; FBG, fasting blood glucose; 2hPPG, 2-h postprandial plasma glucose; FINS, fasting insulin; HOMA-IR, homeostasis model assessment of insulin resistance; HOMA-β, homeostasis model assessment of β-cell function; EISI, early insulin secretion index; WBISI, whole body insulin sensitivity index; AUC, area under the curve; GLP-1, plasma glucagon-like peptide-1.

TABLE 4 | Diet-drug interaction on clinical outcomes in linear mixed-effect models.

Outcomes	Total energy × Drug therapy		Proportion of energy from carbohydrate × Drug therapy		Proportion of energy from protein × Drug therapy		Proportion of energy from fat × Drug therapy	
	β (95%CI)	*P* value	β (95%CI)	*P* value	β (95%CI)	*P* value	β (95%CI)	*P* value
BMI, kg/m^2	0.00002 (−0.0002–0.0002)	0.858	0.149 (−0.729–1.027)	0.739	−1.012 (−3.644–1.621)	0.451	−0.095 (−1.177–0.987)	0.864
SBP, mmHg	0.0009 (−0.0010–0.0027)	0.348	−6.269 (−14.741–2.202)	0.147	31.71 (7.77–55.65)	0.009*	4.660 (−5.087–14.407)	0.349
DBP, mmHg	0.00016 (−0.0012–0.0015)	0.815	−1.288 (−7.346–7.770)	0.677	5.257 (−12.107–22.620)	0.533	1.758 (−5.256–8.773)	0.623
TC, mmol/L	0.00002 (−0.0001–0.0002)	0.789	0.420 (−0.328–1.168)	0.271	0.468 (−1.703–2.639)	0.673	0.018 (−0.866–0.901)	0.969
TG, mmol/L	0.00005 (−0.0003–0.0004)	0.810	1.165 (−0.541–2.871)	0.181	4.048 (−0.764–8.861)	0.099	−0.628 (−2.586–1.330)	0.529
HDL-C, mmol/L	−0.0000004 (−0.00005–0.00005)	0.985	−0.015 (−0.222–0.193)	0.888	−0.041 (−0.627–0.545)	0.890	−0.019 (−0.257–0.219)	0.875
LDL-C, mmol/L	−0.00004 (−0.0002–0.00009)	0.541	−0.105 (−0.729–0.519)	0.741	−0.888 (−2.652–0.876)	0.324	0.205 (−0.513–0.922)	0.576
FBG, mmol/L	0.0001 (−0.0001–0.0003)	0.364	−0.086 (−1.250–1.077)	0.885	−1.242 (−4.607–2.124)	0.470	−0.129 (−1.476–1.218)	0.852
HbA1c, %	−0.000001 (−0.0002–0.0002)	0.991	0.061 (−0.886–1.008)	0.900	−0.080 (−2.813–2.653)	0.954	−0.232 (−1.329–0.865)	0.679
2hPPG, mmol/L	−0.00007 (−0.0006–0.0004)	0.772	−0.905 (−3.450–1.640)	0.486	−2.333 (−9.578–4.913)	0.528	1.284 (−1.654–4.221)	0.392
FINS, μIU/Ml	0.0003 (−0.0013–0.0020)	0.747	−6.760 (−14.675–1.154)	0.094	4.027 (−18.854–26.908)	0.730	2.957 (−6.143–12.057)	0.524
EISI	0.0015 (−0.0011–0.0042)	0.253	4.768 (−7.760–17.297)	0.456	−10.995 (−47.379–25.388)	0.554	−2.613 (−17.023–11.797)	0.722
AUC for plasma GLP-1, pmol×min	−0.335 (−0.665 −0.004)	0.047*	−6.446 (−1,588.6–1,576.7)	0.994	−122.01 (−4,723.1–4,479.1)	0.959	143.5 (−1,690.9–1,977.9)	0.878
AUC for glucagon, pg/mL×min	0.186 (−0.772–1.144)	0.704	938.8 (−3,550.4–5,428.0)	0.682	−6,141.4 (−18,886.8–6,604.0)	0.345	−1,162.8 (−6,322.2–3,996.6)	0.659
AUC for serum insulin, μIU/mL×min	−0.345 (−0.732–0.042)	0.081	−1,885.8 (−3,709.7 −62.0)	0.043*	−2,000.8 (−7,225.9–3,224.4)	0.453	1,670.1 (−427.7–3,767.9)	0.119
HOMA-IR	0.0001 (−0.0005–0.0007)	0.723	−2.056 (−4.954–0.842)	0.164	1.090 (−7.301–9.482)	0.799	0.500 (−2.837–3.838)	0.769
HOMA-β	0.0039 (−0.0125–0.0203)	0.639	−70.508 (−147.4–6.368)	0.072	67.24 (−155.97–290.45)	0.555	50.00 (−38.53–138.54)	0.268
WBISI	0.00008 (−0.0007–0.0008)	0.839	2.297 (−1.493–6.087)	0.235	−2.756 (−13.635–8.123)	0.62	−1.317 (−5.667–3.033)	0.553

Models adjusted for age, sex, time of intervention, and duration of diabetes.

BMI, body mass index; SBP, systolic blood pressure; DBP, diastolic blood pressure; TGs, triglycerides; TC, total cholesterol; LDL-C, low-density lipoprotein cholesterol; HDL-C, high-density lipoprotein cholesterol; FBG, fasting blood glucose; 2hPPG, 2-h postprandial plasma glucose; FINS, fasting insulin; HOMA-IR, homeostasis model assessment of insulin resistance; HOMA-β, homeostasis model assessment of β-cell function; EISI, early insulin secretion index; WBISI, whole body insulin sensitivity index; AUC, area under the curve; GLP-1, plasma glucagon-like peptide-1.

*$P < 0.05$.

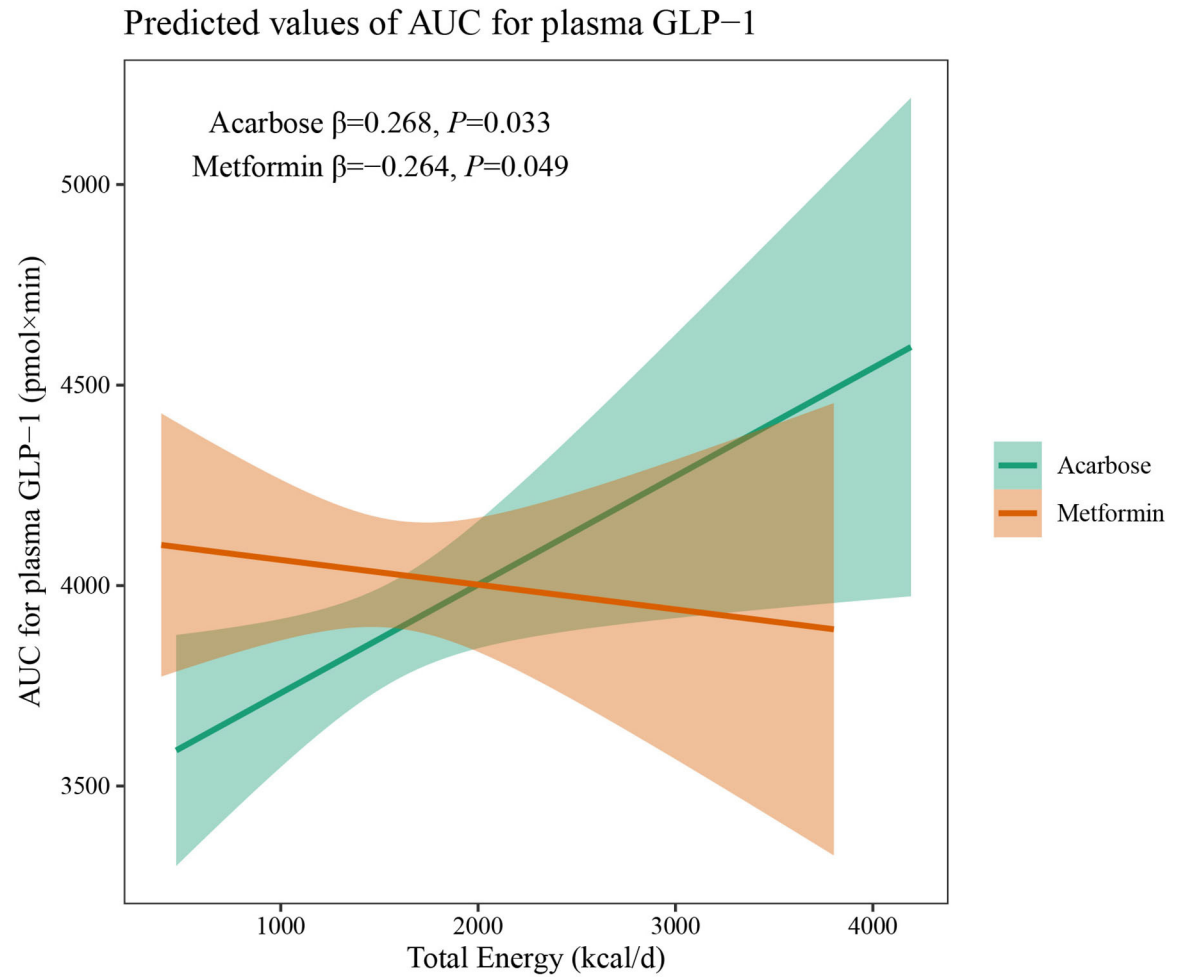

FIGURE 4 | Differential associations between total energy intake and AUC for plasma GLP-1 in metformin and acarbose groups. The β value adjusted for age, sex, time of intervention, and duration of diabetes.

independently associated with higher BMI, HbA1c, 2hPPG, and AUC for serum insulin, which was also observed in Saudi patients (29), suggesting that carbohydrate restriction is essential for the achievement of good glycemic control, weight loss, and reduced insulin secretion. In addition, under acarbose and metformin treatment, significant and comparable effects on reduction of BMI and HbA1c were still achieved, while under acarbose treatment, significantly lower postprandial blood glucose was achieved after 48 weeks, and AUC for serum insulin decreased to a greater extent than under metformin treatment, demonstrating that acarbose is superior to metformin in reducing postprandial hyperglycemia and hyperinsulinemia in patients with T2DM consuming an Asian diet. Meanwhile, the association between dietary carbohydrates and AUC for serum insulin was only significant under acarbose but not metformin treatment, which may contradict the insulin-sparing effect of acarbose (30). However, it also reflected, from another perspective, beneficial effects of acarbose on preserving β-cell function (31).

Finally, synergetic effects of protein intake and metformin treatment on lowering SBP were found. Some intervention studies have proved that a high protein intake can significantly decrease SBP and DBP in patients with T2DM (32). Furthermore, Garnett et al. (33) also observed that the SBP and DBP of metformin-treated prediabetic adolescents significantly decreased over time when receiving an increased-protein diet, all of which may suggest that consuming more proteins may help metformin users feel more at ease over time.

Since total energy and protein intake remained relatively stable in this study, the increase in the proportion of energy from carbohydrates was accompanied by the decrease in energy from fat. Not surprisingly, this led to the positive associations of higher dietary fat intake with better glycemic control, weight loss, the improvement of insulin secretion, and higher WBISI, an indicator of insulin sensitivity. In spite of contradicting the results reported in most studies that a reduction in dietary fat can promote weight loss benefiting blood lipid and glucose profiles (34–36), the result of association between a relatively

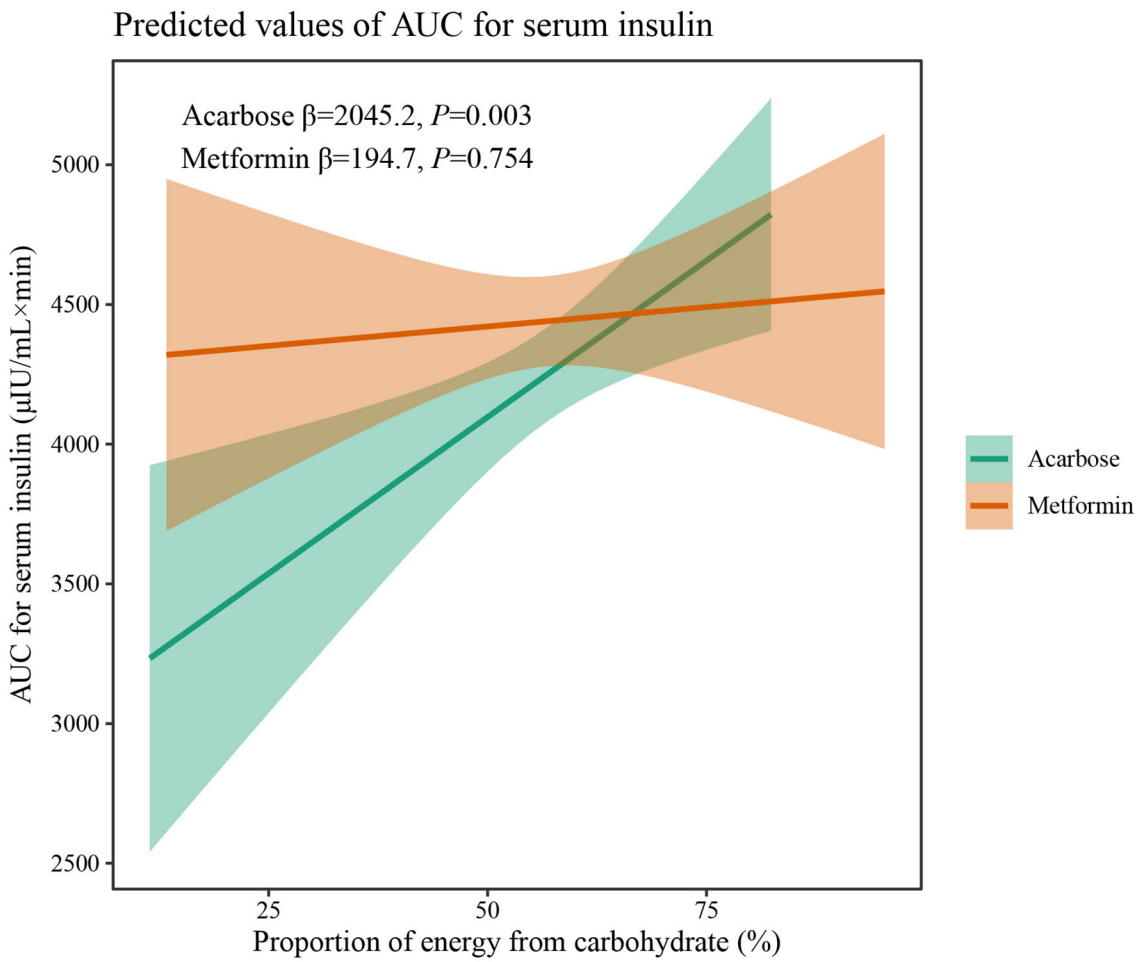

FIGURE 5 | Differential associations between proportion of energy from carbohydrate intake and AUC for serum insulin in metformin and acarbose groups. The β value adjusted for age, sex, time of intervention, and duration of diabetes.

higher fat intake and better treatment outcomes may reflect interactions between macronutrients, which make it difficult to interpret the individual contributions of each source to clinical outcomes. Moreover, aside from the quantity of dietary fat and carbohydrates, growing evidence suggests that the quality of dietary fat and carbohydrates (with a preference for foods with natural unsaturated fat, high fiber, low glycemic index, and whole grain instead of those with trans or saturated fat) are stronger determinants of the effects of diet on metabolic control than the quantity of each macronutrient in the diet (37), which may be further investigated in the following studies.

The MARCH trial provided evidence that both acarbose and metformin have a similar effect as initial therapy on HbA1c reduction in Chinese patients with T2DM. Shortly after, a meta-analysis systematically searched the Chinese and English literature for eligible randomized controlled trials to compare glucose-lowering effects of metformin and acarbose, which also implied that the effect of metformin is at least as good as that of acarbose (38). In this study, it was also found that acarbose treatment was not inferior to metformin treatment in view of most clinical outcomes. However, linear mixed-effect models showed metformin treatment was associated with higher TG and 2hPPG but lower LDL-C compared with acarbose treatment. Although none of these outcomes was affected by interaction of drug and dietary macronutrients, the superior effect of acarbose on postprandial plasma glucose still demonstrated a stronger response to dietary intakes compared with metformin. The research results only showed three significant interactions. Perhaps, due to a relatively shorter observation, there were limited changes in dietary macronutrients over time and relatively overwhelming effects of intensive drug therapy. Although there is little evidence of drug–diet interaction, the potential mechanism may be explainable or incidental in this study. Therefore, great importance should be attached to drug–diet interaction, and further investigation should be conducted in physiological studies and clinical solutions.

To the best of our knowledge, this study is the first of its kind to document the interaction of between pharmacotherapies and dietary intakes of macronutrients in patients with T2DM. However, there are several limitations to consider. First, all

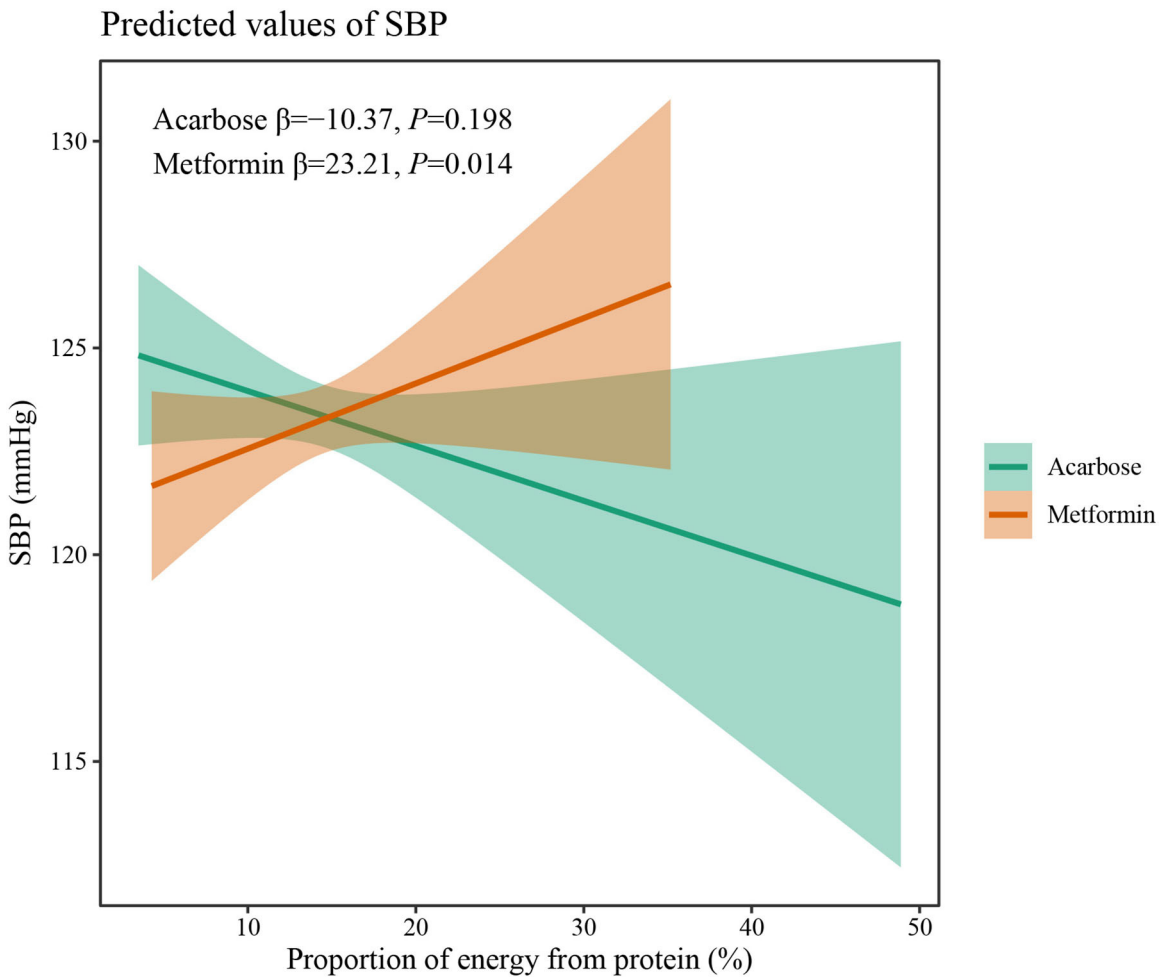

FIGURE 6 | Differential associations between proportion of energy from protein intake and SBP in metformin and acarbose groups. The β value adjusted for age, sex, time of intervention, and duration of diabetes.

participants were Chinese patients newly diagnosed with T2DM, which may limit the application to other patients to some extent, and the association may be largely different in patients with longer duration of diabetes or following Western dietary patterns. However, the results may be applicable to other Chinese populations with diabetes, with characteristics similar to the sample in this study. Second, only limited food and beverage items were evaluated by the 24-h dietary recall method, which may lead to an underestimation of energy and macronutrients intake. Third, measurement errors in self-reported dietary behaviors were inevitable. Finally, the fat type and quality of carbohydrates were not considered in this study.

CONCLUSION

The MARCH trail provided a unique opportunity to investigate the drug–diet interactive effect on treatment outcomes in patients with T2DM. Metformin and acarbose mainly exerted different interactive effects with dietary macronutrients on GLP-1 secretion, insulin release, and SBP, suggesting that the complexities of drug-diet therapies may confer distinct benefits of glycemic control.

DATA AVAILABILITY STATEMENT

The raw data supporting the conclusions of this article will be made available by the authors, without undue reservation.

ETHICS STATEMENT

The studies involving human participants were reviewed and the protocol was approved by an Ethics Committee from each clinical site. The patients/participants provided their written informed consent to participate in this study.

AUTHOR CONTRIBUTIONS

GW and JL conceptualized and designed the study, obtained, and supervised data collection. YA and YL conducted the data analysis and drafted the manuscript. NB, XD, and XC helped perform data processing and analysis. All authors contributed to the article and approved the submitted version.

ACKNOWLEDGMENTS

We thank Dr. Chen Wei from the Department of Clinical Nutrition, Peking Union Medical College Hospital, Beijing, China, for provision of data and methods for dietary surveys. We also thank Wenying Yang from the Department of Endocrinology, China-Japan Friendship Hospital, Beijing, China, for provision of data from MARCH trial.

REFERENCES

1. Ramachandran A, Ma RC, Snehalatha C. Diabetes in Asia. *Lancet.* (2010) 375:408–18. doi: 10.1016/S0140-6736(09)60937-5
2. Nanditha A, Ma RC, Ramachandran A, Snehalatha C, Chan JC, Chia KS, et al. Diabetes in Asia and the Pacific: Implications for the Global Epidemic. *Diabetes Care.* (2016) 39:472–85. doi: 10.2337/dc15-1536
3. Xu Y, Wang L, He J, Bi Y, Li M, Wang T, et al. Prevalence and control of diabetes in Chinese adults. *JAMA.* (2013) 310:948–59. doi: 10.1001/jama.2013.168118
4. Triggiani V, Resta F, Guastamacchia E, Sabba C, Licchelli B, Ghiyasaldin S, et al. Role of antioxidants, essential fatty acids, carnitine, vitamins, phytochemicals and trace elements in the treatment of diabetes mellitus and its chronic complications. *Endocr Metab Immune Disord Drug Targets.* (2006) 6:77–93. doi: 10.2174/187153006776056611
5. Standards of medical care in diabetes—2013. *Diabetes Care.* (2013) 36 (Suppl 1):S11-66. doi: 10.2337/dc13-S011
6. DiNicolantonio JJ, Bhutani J, O'Keefe HJ. Acarbose: safe and effective for lowering postprandial hyperglycaemia and improving cardiovascular outcomes. *Open Heart.* (2015) 2:e000327. doi: 10.1136/openhrt-2015-000327
7. Zhu Q, Tong Y, Wu T, Li J, Tong N. Comparison of the hypoglycemic effect of acarbose monotherapy in patients with type 2 diabetes mellitus consuming an Eastern or Western diet: a systematic meta-analysis. *Clin Ther.* (2013) 35:880–99. doi: 10.1016/j.clinthera.2013.03.020
8. Moller G, Andersen HK, Snorgaard O. A systematic review and meta-analysis of nutrition therapy compared with dietary advice in patients with type 2 diabetes. *Am J Clin Nutr.* (2017) 106:1394–400. doi: 10.3945/ajcn.116.139626
9. Barnard ND. Ignorance of Nutrition Is No Longer Defensible. *JAMA Intern Med.* (2019) 179:1021–2. doi: 10.1001/jamainternmed.2019.2273
10. Henry CJ, Kaur B, Quek R. Chrononutrition in the management of diabetes. *Nutr Diabetes.* (2020) 10:6. doi: 10.1038/s41387-020-0109-6
11. Mohan V, Unnikrishnan R, Shobana S, Malavika M, Anjana RM, Sudha V. Are excess carbohydrates the main link to diabetes & its complications in Asians? *Indian J Med Res.* (2018) 148:531–8. doi: 10.4103/ijmr.IJMR_1698_18
12. Hu FB. Dietary pattern analysis: a new direction in nutritional epidemiology. *Curr Opin Lipidol.* (2002) 13:3–9. doi: 10.1097/00041433-200202000-00002
13. Wei W, Jiang W, Han T, Tian M, Ding G, Li Y, et al. The future of prevention and treatment of diabetes with nutrition in China. *Cell Metab.* (2021) 33:1908–10. doi: 10.1016/j.cmet.2021.09.012
14. Samkani A, Skytte MJ, Kandel D, Kjaer S, Astrup A, Deacon CF, et al. A carbohydrate-reduced high-protein diet acutely decreases postprandial and diurnal glucose excursions in type 2 diabetes patients. *Br J Nutr.* (2018) 119:910–7. doi: 10.1017/S0007114518000521
15. Yang W, Liu J, Shan Z, Tian H, Zhou Z, Ji Q, et al. Acarbose compared with metformin as initial therapy in patients with newly diagnosed type 2 diabetes: an open-label, non-inferiority randomised trial. *Lancet Diabetes Endocrinol.* (2014) 2:46–55. doi: 10.1016/S2213-8587(13)70021-4
16. Li J, Li J, Shan Z, Yang W, Liu J, Tian H, et al. Gender-differential effects on blood glucose levels between acarbose and metformin in Chinese patients with newly diagnosed type 2 diabetes: a sub-analysis of the MARCH trial. *Endocr J.* (2021) 68:69–79. doi: 10.1507/endocrj.EJ20-0006
17. Fu J, Liu J, Xu Y, Yang N, Yang W, Wang G. Comparison of therapeutic effects of acarbose and metformin under different beta-cell function status in Chinese patients with type 2 diabetes. *Endocr J.* (2019) 66:443–50. doi: 10.1507/endocrj.EJ18-0466
18. Tan LJ, Kim SA, Shin S. Association between Three Low-Carbohydrate Diet Scores and Lipid Metabolism among Chinese Adults. *Nutrients.* (2020) 12:1307. doi: 10.3390/nu12051307
19. Palkowska-Gozdzik E, Piotrowicz K, Krzesinski P, Stanczyk A, Skrobowski A, Gielerak G. Crosstalk Between Dietary Pattern, Anthropometric Parameters, and Adiponectin Concentration Among Patients with Metabolic Syndrome. *Metab Syndr Relat Disord.* (2021) 19:137–43. doi: 10.1089/met.2020.0058
20. Daniels MS, Park BI, McKay LD. Adverse Effects of Medications on Micronutrient Status: From Evidence to Guidelines. *Annu Rev Nutr.* (2021) 41:411–31. doi: 10.1146/annurev-nutr-120420-023854
21. Luciano-Mateo F, Hernandez-Aguilera A, Cabre N, Camps J, Fernandez-Arroyo S, Lopez-Miranda J, et al. Nutrients in Energy and One-Carbon Metabolism: learning from Metformin Users. *Nutrients.* (2017) 9:121. doi: 10.3390/nu9020121
22. Kang HM, Kim JD. Total energy intake may be more associated with glycemic control compared to each proportion of macronutrients in the korean diabetic population. *Diabetes Metab J.* (2012) 36:300–6. doi: 10.4093/dmj.2012.36.4.300
23. Beloqui A, Alhouayek M, Carradori D, Vanvarenberg K, Muccioli GG, Cani PD, et al. A Mechanistic Study on Nanoparticle-Mediated Glucagon-Like Peptide-1 (GLP-1) Secretion from Enteroendocrine L Cells. *Mol Pharm.* (2016) 13:4222–30. doi: 10.1021/acs.molpharmaceut.6b00871
24. Caron J, Cudennec B, Domenger D, Belguesmia Y, Flahaut C, Kouach M, et al. Simulated GI digestion of dietary protein: Release of new bioactive peptides involved in gut hormone secretion. *Food Res Int.* (2016) 89(Pt 1):382–90. doi: 10.1016/j.foodres.2016.08.033
25. Dalsgaard NB, Gasbjerg LS, Hansen LS, Hansen NL, Stensen S, Hartmann B, et al. The role of GLP-1 in the postprandial effects of acarbose in type 2 diabetes. *Eur J Endocrinol.* (2021) 184:383–94. doi: 10.1530/EJE-20-1121
26. Mannucci E, Ognibene A, Cremasco F, Bardini G, Mencucci A, Pierazzuoli E, et al. Effect of metformin on glucagon-like peptide 1 (GLP-1) and leptin levels in obese nondiabetic subjects. *Diabetes Care.* (2001) 24:489–94. doi: 10.2337/diacare.24.3.489
27. Wu T, Thazhath SS, Bound MJ, Jones KL, Horowitz M, Rayner KC. Mechanism of increase in plasma intact GLP-1 by metformin in type 2 diabetes: stimulation of GLP-1 secretion or reduction in plasma DPP-4 activity? *Diabetes Res Clin Pract.* (2014) 106:e3–6. doi: 10.1016/j.diabres.2014.08.004
28. Grosskopf A, Simm A. Carbohydrates in nutrition: friend or foe? *Z Gerontol Geriatr.* (2020) 53:290–4. doi: 10.1007/s00391-020-01726-1
29. Al-Mssallem MQ, Al-Qarni AA, Al-Jamaan M. Dietary carbohydrate intake in patients with type 2 diabetes mellitus and diabetes control: a cross-sectional study. *Food Nutr Res.* (2020) 64:4751. doi: 10.29219/fnr.v64.4751
30. Kalra S. Alpha glucosidase inhibitors. *J Pak Med Assoc.* (2014) 64:474–6.
31. Joshi SR, Standl E, Tong N, Shah P, Kalra S, Rathod R. Therapeutic potential of alpha-glucosidase inhibitors in type 2 diabetes mellitus: an evidence-based review. *Expert Opin Pharmacother.* (2015) 16:1959–81. doi: 10.1517/14656566.2015.1070827
32. Sargrad KR, Homko C, Mozzoli M, Boden G. Effect of high protein vs high carbohydrate intake on insulin sensitivity, body weight, hemoglobin A1c, and blood pressure in patients with type 2 diabetes mellitus. *J Am Diet Assoc.* (2005) 105:573–80. doi: 10.1016/j.jada.2005.01.009
33. Garnett SP, Gow M, Ho M, Baur LA, Noakes M, Woodhead HJ, et al. Optimal macronutrient content of the diet for adolescents with prediabetes; RESIST a randomised control trial. *J Clin Endocrinol Metab.* (2013) 98:2116–25. doi: 10.1210/jc.2012-4251

34. Wycherley TP, Moran LJ, Clifton PM, Noakes M, Brinkworth DG. Effects of energy-restricted high-protein, low-fat compared with standard-protein, low-fat diets: a meta-analysis of randomized controlled trials. *Am J Clin Nutr.* (2012) 96:1281–98. doi: 10.3945/ajcn.112.044321
35. Astrup A, Astrup A, Buemann B, Flint A, Raben A. Low-fat diets and energy balance: how does the evidence stand in 2002? *Proc Nutr Soc.* (2002) 61:299–309. doi: 10.1079/PNS2002149
36. Watson NA, Dyer KA, Buckley JD, Brinkworth GD, Coates AM, Parfitt G, et al. Comparison of two low-fat diets, differing in protein and carbohydrate, on psychological wellbeing in adults with obesity and type 2 diabetes: a randomised clinical trial. *Nutr J.* (2018) 17:62. doi: 10.1186/s12937-018-0367-5
37. San-Cristobal R, Navas-Carretero S, Martinez-Gonzalez MA, Ordovas JM, Martinez AJ. Contribution of macronutrients to obesity: implications for precision nutrition. *Nat Rev Endocrinol.* (2020) 16:305–20. doi: 10.1038/s41574-020-0346-8
38. Gu S, Shi J, Tang Z, Sawhney M, Hu H, Shi L, et al. Comparison of glucose lowering effect of metformin and acarbose in type 2 diabetes mellitus: a meta-analysis. *PLoS ONE.* (2015) 10:e0126704. doi: 10.1371/journal.pone.0126704

Conflict of Interest: The authors declare that the research was conducted in the absence of any commercial or financial relationships that could be construed as a potential conflict of interest.

frontiers | Frontiers in Nutrition

PERSPECTIVE
published: 10 May 2022
doi: 10.3389/fnut.2022.862071

A New Way of Investigating the Relationship Between Fasting Blood Sugar Level and Drinking Glucose Solution

Muhammad Aslam[*†] *and Mohammed Albassam*[†]

Department of Statistics, Faculty of Science, King Abdulaziz University, Jeddah, Saudi Arabia

The existing *t*-test of a correlation coefficient works under a determinate environment. In uncertainty, the existing *t*-test of a correlation coefficient is unable to investigate the significance of correlation. The study presents a modification of the existing *t*-test of a correlation coefficient using neutrosophic statistics. The test statistic is designed to investigate the significance of correlation when imprecise observations or uncertainties in the level of significance are presented. The test is applied to data obtained from patients with diabetes. From the data analysis, the proposed *t*-test of a correlation coefficient is found to be more effective than existing tests.

Keywords: classical statistics, imprecise observations, medical data, neutrosophy, simulation

OPEN ACCESS

Edited by:
Demin Cai,
Yangzhou University, China

Reviewed by:
Said Broumi,
University of Hassan II Casablanca, Morocco
Vijander Singh,
Netaji Subhas University of Technology, India

***Correspondence:**
Muhammad Aslam
aslam_ravian@hotmail.com

***ORCID:**
Muhammad Aslam
orcid.org/0000-0003-0644-1950
Mohammed Albassam
orcid.org/0000-0002-5012-4832

Specialty section:
This article was submitted to Nutrition and Metabolism, a section of the journal Frontiers in Nutrition

Received: *25 January 2022*
Accepted: *18 March 2022*
Published: *10 May 2022*

Citation:
Aslam M and Albassam M (2022) A New Way of Investigating the Relationship Between Fasting Blood Sugar Level and Drinking Glucose Solution. Front. Nutr. 9:862071. doi: 10.3389/fnut.2022.862071

INTRODUCTION

Correlation analysis is conducted to see the degree of relationship between two variables. Correlation analysis helps in determining the positive or negative correlation between two variables. The value of a correlation coefficient lies between −1 and +1. The computed value of the correlation coefficient from data always lies in this interval. Statistical tests have been conducted in various fields for decision-making purposes. Among the statistical tests, the *t*-test for correlation is applied to investigate the significance of the correlation between two variables. In the *t*-test for correlation, the null hypothesis that there is no association between two variables is tested against the alternative hypothesis that two variables are associated. Values of the statistic of the *t*-test for correlation are calculated from given data and compared with tabulated values. The null hypothesis of no association between two variables is accepted if the calculated value is less than the tabulated value. Bartroff and Song (1) conducted a correlation analysis to investigate the relationship between impact factors and the ranking of electrical journals. Aleixandre-Benavent et al. (2) discussed the correlation between impact factors and published papers' research data. McGillivray and Astell (3) provided a correlation between usage and citations of open access journals. For more information, the reader may refer to Tang and Landes (4) and e Silva et al. (5).

Correlation analysis has been widely applied in medical research. It is conducted to investigate the association between variables causing a specific disease. Schober et al. (6) applied correlation analysis on anesthesia data. Najmi and Balakrishnan Sadasivam (7) provided guidelines for medical students related to statistical tests. Statistical analysis has also been conducted to investigate the relationship among various causes of diabetes.Khan et al. (8) discussed a statistical analysis for patients with diabetes. Liu et al. (9) applied various statistical methods for data on diabetes. Wani et al. (10) investigated the effect of weight and smoking on type-2 diabetes. Nedyalkova et al. (11)

presented a statistical analysis on type-2 diabetes. Adaobi et al. (12) presented an analysis using blood glucose data. More information can be seen in Mukasheva et al. (13), Eynizadeh et al. (14), Balamurugan et al. (15), Alsaqr (16), Janse et al. (17), and Sun et al. (18).

Neutrosophic logic was introduced by Smarandache (19), which is the generalization of fuzzy-logic. The former gives information about three measures (truth, false, and indeterminacy), while the latter gives information about two measures (truth and false). Smarandache (20) showed the efficiency of neutrosophic logic over fuzzy-logic and interval-based analysis. Neutrosophic logic has many applications in medical science. Ansari et al. (21) discussed an application of neutrosophic sets in artificial intelligence. Jafar et al. (22) used the neutrosophic logic in medical diagnosis. Basha et al. (23) applied neutrosophic logic in the classification of X-rays of the chest of patients with coronavirus disease 2019 (COVID-19). More information on applications of neutrosophic logic in medical science can be seen in Zhang et al. (24) and Zhang et al. (25). Neutrosophic statistics was developed by Smarandache (26) using the idea of neutrosophy in numbers. Chen et al. (27) and Chen et al. (28) discussed methods to analyze neutrosophic data. Aslam et al. (29) applied neutrosophic statistics on diabetics' data. Ling et al. (30) analyzed neutrosophic numbers in medical waste treatment. More applications can be seen in Das et al.'s studies (31) and Saeed et al.'s studies (32).

Aslam (33) proposed a neutrosophic Z-test for two samples to investigate the relationship between metrological variables. By exploring the literature and to the best of our knowledge, there is still a gap to work on t-test for correlation under neutrosophic statistics for a single sample. We will present the design of a t-test for correlation using neutrosophic statistics in this study. The neutrosophic statistic will be given and applied using data obtained from patients with diabetes. We expect that the proposed t-test for correlation will beat the existing t-tests for correlations in terms of information, adequacy, and flexibility.

METHOD

The existing t-test of a correlation coefficient using classical statistics works only when decision-makers are sure about the parameters involved in the implementation of the test. In practice, it may not be possible to the level of significance, sample size, and observations obtained from a measurement or a complex process are always certain; see, for example, Doll and Carney (34). Modification of the existing t-test of a correlation coefficient is needed to investigate the significance of the correlation between variables in an indeterminate environment. Now, we will develop a t-test of a correlation coefficient using neutrosophic statistics with the expectation that the proposed test will be efficient and a general form of the existing t-test of a correlation coefficient. The procedure of the proposed t-test of a correlation coefficient using neutrosophic statistics will be explained as: Let $X_N = X_L + X_U I_{X_N}; I_{X_N} \epsilon \left[I_{X_L}, I_{X_U}\right]$ and $Y_N = Y_L + Y_U I_{Y_N}; I_{Y_N} \epsilon \left[I_{Y_L}, I_{Y_U}\right]$ be neutrosophic random variables, where the first values denote the determinate parts, the second values denote the indeterminate parts, and $I_{X_N} \epsilon \left[I_{X_L}, I_{X_U}\right]$, *and* $I_{Y_N} \epsilon \left[I_{Y_L}, I_{Y_U}\right]$ are indeterminacy. Let $n_N = n_L + n_U I_{n_N}; I_{n_N} \epsilon \left[I_{n_L}, I_{n_U}\right]$ be a neutrosophic random sample of size $n_N \epsilon [n_L, n_U]$, and $\alpha_N = \alpha_L + \alpha_U I_{\alpha N}; I_{\alpha N} \epsilon [I_{\alpha L}, I_{\alpha U}]$ be a level of significance under uncertainty, where n_L and, α_L are determinate values, $n_U I_{n_N}$ *and* $\alpha_U, I_{\alpha N}$ are indeterminate values, and $I_{n_N} \epsilon \left[I_{n_L}, I_{n_U}\right]$ and $I_{\alpha N} \epsilon [I_{\alpha L}, I_{\alpha U}]$ are measures of uncertainty. Suppose that (X_{iN}, Y_{iN}) to be pair data and let $r_N = r_L + r_U I_{r_N}; I_{r_N} \epsilon \left[I_{r_L}, I_{r_U}\right]$ be a neutrosophic correlation, where r_L is a determinate part, the $r_U I_{r_N}$ is an indeterminate part, and $I_{r_N} \epsilon \left[I_{r_L}, I_{r_U}\right]$ is the measure of correlations. The neutrosophic correlation $r_N \epsilon [r_L, r_U]$, by following Aslam and Albassam (35), is defined as:

$$r_N = \frac{\sum_{i=1}^{n_L} \left(X_{iL} - \overline{X}_L\right)\left(Y_{iL} - \overline{Y}_L\right)}{\sqrt{\sum_{i=1}^{n_L} \left(X_{iL} - \overline{X}_L\right)^2 \sum_{i=1}^{n_L} \left(Y_{iL} - \overline{Y}_L\right)^2}} + \frac{\sum_{i=1}^{n_U} \left(X_{iU} - \overline{X}_U\right)\left(Y_{iU} - \overline{Y}_U\right)}{\sqrt{\sum_{i=1}^{n_U} \left(X_{iU} - \overline{X}_U\right)^2 \sum_{i=1}^{n_U} \left(Y_{iU} - \overline{Y}_U\right)^2}} I_{r_N}; \quad I_{r_N} \epsilon \left[I_{r_L}, I_{r_U}\right] \tag{1}$$

where $r_L = r_U$, and the neutrosophic correlation $r_{SN} \epsilon [r_L, r_U]$ can be written as:

$$r_{SN} = \left(1 + I_{r_{SN}}\right) \frac{\sum_{i=1}^{n_S} \left(X_{iS} - \overline{X}_S\right)\left(Y_{iS} - \overline{Y}_S\right)}{\sqrt{\sum_{i=1}^{n_S} \left(X_{iS} - \overline{X}_S\right)^2 \sum_{i=1}^{n_S} \left(Y_{iS} - \overline{Y}_S\right)^2}}; \quad I_{r_{SN}} \epsilon \left[I_{r_{SL}}, I_{r_{SU}}\right] \tag{2}$$

Note that the neutrosophic correlation $r_N \epsilon [r_L, r_U]$ is a generalization of the existing correlation under classical statistics. The neutrosophic correlation $r_N \epsilon [r_L, r_U]$ reduces to correlation using classical statistics when $I_{r_{SL}} = 0$. To test the null hypothesis H_{0N} that there is no correlation between the variables vs. the alternative hypothesis H_{1N} that both variables are associated, the neutrosophic test statistic $t_N \epsilon [t_L, t_U]$ is defined as:

$$t_N = t_L + t_U I_{t_N} \epsilon \left[I_{t_L}, I_{t_U}\right] \tag{3}$$

The alternative form of $t_N \epsilon [t_L, t_U]$ is defined as:

$$t_N = \frac{r_L}{\sqrt{1 - r_L^2}} \times \sqrt{n_L - 2} + \frac{r_U}{\sqrt{1 - r_U^2}} \times \sqrt{n_U - 2} I_{t_N}; I_{t_N} \epsilon \left[I_{t_L}, I_{t_U}\right] \tag{4}$$

where $t_L = t_U$ and the neutrosophic correlation $t_{SN} \epsilon [t_{SL}, t_{SU}]$ can be written as:

$$t_{SN} = \left(1 + I_{t_{SN}}\right) \frac{r_{SN}}{\sqrt{1 - r_{SN}^2}} \times \sqrt{n_S - 2}; I_{t_{SN}} \epsilon \left[I_{t_{SL}}, I_{t_{SU}}\right] \tag{5}$$

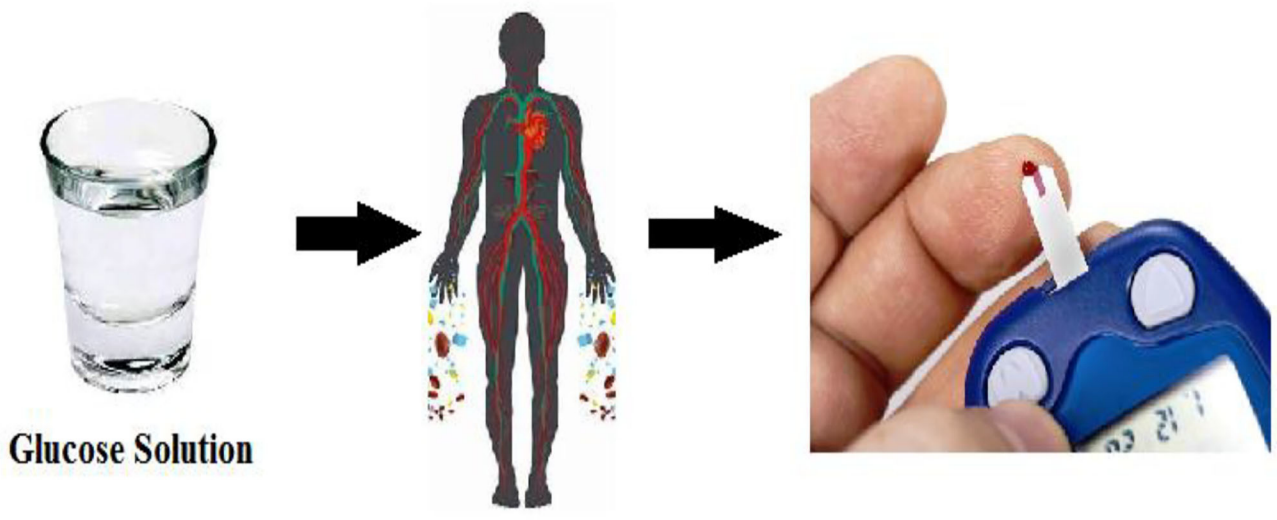

FIGURE 1 | Schematic diagram of the data measurement of sugar level in blood.

Note that $t_N \epsilon\ [t_L, t_U]$ follows the neutrosophic t-distribution with the degree of freedom $n_N - 2$.

Note that the neutrosophic statistics $t_N \epsilon\ [t_L, t_U]$ is a generalization of the existing statistics under classical statistics. The neutrosophic statistics $t_N \epsilon\ [t_L, t_U]$ reduces to statistic using classical statistics when $I_{r_{SL}} = 0$.

The proposed t-test of a correlation coefficient will be carried out through the following steps:

Step-1: state $H_{0N} : r_N \epsilon\ [r_L, r_U] = 0$ vs. $H_{1N} : r_N \epsilon\ [r_L, r_U] \neq 0$;.
Step 2: fix the level of significance $\alpha_N = \alpha_L + \alpha_U I_{\alpha N}$; $I_{\alpha N} \epsilon\ [I_{\alpha L}, I_{\alpha U}]$ and select the tabulated value t_C from (36);
Step 3: compute statistic $t_N \epsilon\ [t_L, t_U]$ and compare with t_C;.
Step 4: do not reject $H_{0N} : r_N \epsilon\ [r_L, r_U] = 0$ if $t_N \epsilon\ [t_L, t_U] < t_C$.

APPLICATION USING DATA ON DIABETES

To investigate the significance of the correlation between the sugar level and Drinking Glucose Solution about 237 ml contained 75 g of sugar, the data from 320 diabetics patients aged from 45 to 60 were collected from a hospital located in Hafizabad, Pakistan. A group of 20 patients at each age level is formed and the minimum and maximum blood sugar levels are recorded from 16 groups of patients. The schematic diagram to measure blood sugar level is depicted in **Figure 1**.

The data of blood sugar levels are reported in **Table 1**. The minimum and maximum levels of blood sugar (in mg/dl) after 8 h of fasting (G1) and 2 h after drinking, the glucose solution of about 237 ml and containing 75 g sugar (G2) are shown in **Table 1**. From **Table 1**, it can be seen that blood sugar level is expressed in intervals; therefore, investigation on the significance of correlation cannot be performed using the existing t-test for correlation. Decision-makers can apply the proposed t-test for correlation using neutrosophic statistics. To test the null hypothesis H_{0N} that there is no correlation between G1 and G2 vs. H_{1N} that G1 and G2 are associated, the neutrosophic correlation $r_N \epsilon\ [r_L, r_U]$ for G1 and G2 is calculated as follows: $r_N = 0.9900 - 0.9899 I_{r_N}$; $I_{r_N} \epsilon\ [0, 0.0001]$. The value of statistic $t_N \epsilon\ [t_L, t_U]$ for G1 and G2 is calculated as: $t_N = 26.29 - 26.22 I_{t_N} \epsilon\ [0, 0.0027]$.

To investigate the relationship between G1 and G2, the following steps will be carried out:

TABLE 1 | Data of sugar levels in the blood.

Age (years)	Data of "G1" (mg/dL)	Data of "G2" (mg/dL)
45	[159, 199]	[166, 206]
46	[150, 196]	[156, 202]
47	[139, 199]	[147, 207]
48	[142, 167]	[148, 173]
49	[152, 210]	[160, 218]
50	[143, 187]	[150, 194]
51	[151, 177]	[159, 185]
52	[140, 195]	[147, 207]
53	[154, 200]	[160, 206]
54	[142, 197]	[149, 204]
55	[150, 189]	[157, 196]
56	[160, 198]	[168, 206]
57	[162, 190]	[170, 198]
58	[146, 198]	[152, 204]
59	[149, 188]	[155, 194]
60	[177, 198]	[179, 205]

Step 1: state H_{0N} : no correlation between G1 and G2 vs. H_{1N} : G1 and G2 are associated;
Step 2: fix the level of significance $\alpha_N = 0.05$ and the tabulated value is $t_C = 1.76$ at the degree of freedom 14 from (36);
Step 3: compute statistic $t_N \epsilon [t_L, t_U] = [26.29, 26.22]$ and compare with $t_C = 1.76$;
Step 4: As $[26.29, 26.22 > 1.76]$, it is concluded that blood sugar levels between G1 and G2 are significant.

Based on the analysis, it can be concluded that there is a significant correlation between 8-h fasting sugar level and 2 h after drinking, the glucose solution of about 237 ml and containing75 g of sugar.

ADVANTAGES

The proposed *t*-test for correlation is a generalization of *t*-test for correlation using classical statistics, interval-based statistics, and fuzzy logic. Now, the efficiency of the proposed *t*-test for correlation will be discussed over these tests in terms of flexibility and information. For comparisons, we will consider the neutrosophic form of the statistic $t_N \epsilon [t_L, t_U]$ that is $t_N = 26.29 - 26.22 I_{t_N} \epsilon [0, 0.0027]$. This neutrosophic form has two parts of information: the first one is about the statistic of classical statistics, and the second one is about the indeterminate part of the proposed test. For example, when $t_L = 0$, the value 26.29 presents the value of test statistic using classical statistics. According to the proposed test, the value of $t_N \epsilon [t_L, t_U]$ will in the interval from 26.29 to 26.22 rather than the exact value. The proposed test also indicates the measure of indeterminacy associated with the interval that is 0.0027. From this comparison, it is clear that the *t*-test using neutrosophic statistics has an edge over the existing *t*-test for correlation. The *t*-test using interval statistics and fuzzy-based logic gives the values of the test statistic in intervals without giving any information about the measure of indeterminacy. For example, for testing the hypothesis H_{0N} : no correlation between G1 and G2, the probability of committing a type-1 error is 0.05 (false), the probability of accepting H_{0N} : no correlation between G1 and G2 is 0.95 (true), and the measure of indeterminacy is 0.0027. The *t*-test using fuzzy logic will give information only about the measures of falseness and truth. Based on the analysis, it is concluded that the proposed *t*-test for correlation is better than the existing tests.

DISCUSSIONS

As the data is collected from a group having 20 people at the fasting time and then after two hours of drinking glucose solution about 237 milliliters contained 75-gram. The neutrosophic form of the correlation between G1 and G2 is $r_N = 0.99 - 0.9899 I_{r_N}$; $I_{r_N} \epsilon [0, 0.0001]$. It is interesting to note that the correlation between the two groups, G1 and G2, varies from 0.99 to 0.9899, with the measure of indeterminacy $I_{r_N} = 0.001$. From this correlation analysis, it can be seen that there is a strong positive correlation between fasting of 8 h and after 2 h of drinking the glucose solution. It means that if an 8-h fasting blood sugar level is high, then the blood sugar level after 2 h of drinking the glucose solution is also high and vice versa. It is important to note that after the 8-h fasting, the minimum blood sugar level of those aged 45 is 159. The value 159 indicates that these patients should take some energy drink before 2 h before sleeping, so that blood sugar can be utilized properly by the body. In addition, with an increase in 8-h fasting sugar, patients aged 45 to 60 should avoid taking carbohydrate or glucose items.

CONCLUDING REMARKS

The *t*-test of a correlation coefficient under neutrosophic statistics was presented in the article. The proposed *t*-test of a correlation coefficient was a generalization of the existing *t*-test of a correlation coefficient under classical statistics. From the real example, the proposed *t*-test of a correlation coefficient was found to be effective for investigating the significance of correlation in an indeterminate environment. The simulation study showed that measures of indeterminacy affect the decision on the significance of correlation. The proposed test can be applied to investigate correlations in the fields of economics, business, medicine, and industry. The proposed *t*-test of a correlation coefficient using a double sampling scheme can be considered as future research. Further statistical properties can be studied in future research. The proposed study can be extended for blood sugar measurement under different conditions and validation methods as future research. In addition, some disturbances can also be considered for blood glucose measurement in future studies.

DATA AVAILABILITY STATEMENT

The original contributions presented in the study are included in the article/supplementary material, further inquiries can be directed to the corresponding author/s.

AUTHOR CONTRIBUTIONS

Both authors listed have made a substantial, direct, and intellectual contribution to the work and approved it for publication.

FUNDING

This work was funded by the Deanship of Scientific Research at King Abdulaziz Univesity.

ACKNOWLEDGMENTS

We are thankful to the editor, reviewers, and Usama Afzal from the University of the Education Lahore for their valuable suggestions to improve the quality and presentation of the article.

REFERENCES

1. Bartroff J, Song J. Sequential tests of multiple hypotheses controlling type I and II familywise error rates. *J Stat Plan Infer.* (2014) 153:100–14. doi: 10.1016/j.jspi.2014.05.010
2. Aleixandre-Benavent R, Moreno-Solano LM, Sapena AF, Pérez EAS. Correlation between impact factor and public availability of published research data in Information Science and Library Science journals. *Scientometrics.* (2016) 107:1–13. doi: 10.1007/s11192-016-1868-7
3. McGillivray B, Astell M. The relationship between usage and citations in an open access mega-journal. *Scientometrics.* (2019) 121:817–38. doi: 10.1007/s11192-019-03228-3
4. Tang J, Landes RD. Some t-tests for N-of-1 trials with serial correlation. *PLoS ONE.* (2020) 15:e0228077. doi: 10.1371/journal.pone.0228077
5. e Silva LO, Maldonado G, Brigham T, Mullan AF, Utengen A, Cabrera D. Evaluating scholars' impact and influence: cross-sectional study of the correlation between a novel social media–based score and an author-level citation metric. *J Med Internet Res.* (2021) 23:e28859. doi: 10.2196/28859
6. Schober P, Boer C, Schwarte LA. Correlation coefficients: appropriate use and interpretation. *Anesth Analg.* (2018) 126:1763–8. doi: 10.1213/ANE.0000000000002864
7. Najmi A, Balakrishnan Sadasivam AR. How to choose and interpret a statistical test? *An update for budding researchers. J Family Med Prim Care.* (2021) 10:2763. doi: 10.4103/jfmpc.jfmpc_433_21
8. Khan HM, Mende S, Rafiq A, Gabbidon K, Reddy PH. Methods needed to measure predictive accuracy: a study of diabetic patients. *Biochim Biophys Acta Molec Basis Dis.* (2017) 1863:1046–53. doi: 10.1016/j.bbadis.2017.01.007
9. Liu S, Gao Y, Shen Y, Zhang M, Li J, Sun P. Application of three statistical models for predicting the risk of diabetes. *BMC Endocr Disord.* (2019) 19:1–10. doi: 10.1186/s12902-019-0456-2
10. Wani HA, Majid S, Khan MS, Bhat AA, Wani RA, Bhat SA, et al. Scope of honey in diabetes and metabolic disorders. In: *Therapeutic Applications of Honey and its Phytochemicals*. Springer. (2020). p. 195–217. doi: 10.1007/978-981-15-7305-7_9
11. Nedyalkova M, Madurga S, Ballabio D, Robeva R, Romanova J, Kichev I, et al. Diabetes mellitus type 2: exploratory data analysis based on clinical reading. *Open Chem.* (2020) 18:1041–1053. doi: 10.1515/chem-2020-0086
12. Adaobi OO, Iwueze IS, Biu EO, Arimie CO. On the analysis of blood glucose levels of diabetic patients. *Fortune J Health Sci.* (2021) 4:257–83. doi: 10.26502/fjhs021
13. Mukasheva A, Saparkhojayev N, Akanov Z, Apon A, Kalra S. Forecasting the prevalence of diabetes mellitus using econometric models. *Diab Ther.* (2019) 10:2079–93. doi: 10.1007/s13300-019-00684-1
14. Eynizadeh Z, Ameli Z, Sahranavard M, Daneshparvar M, Dolagh MA, Roozkhosh M, et al. Biostatistical Investigation of Correlation Between COVID-19 and Diabetes Mellitus. *medRxiv.* (2020). doi: 10.1101/2020.11.21.20235853
15. Balamurugan SAA, Saranya K, Sasikala S, Chinthana G. Statistical and machine learning approaches for clinical decision on drug usage in diabetes with reference to competence and safeness. *Int J Comput Intell Syst.* (2021) 14:859–68. doi: 10.2991/ijcis.d.210212.002
16. Alsaqr AM. Remarks on the use of Pearson's and Spearman's correlation coefficients in assessing relationships in ophthalmic data. *African Vision Eye Health.* (2021) 80:10. doi: 10.4102/aveh.v80i1.612
17. Janse RJ, Hoekstra T, Jager KJ, Zoccali C, Tripepi G, Dekker FW, et al. Conducting correlation analysis: important limitations and pitfalls. *Clin Kidney J.* (2021) 14:2332–7. doi: 10.1093/ckj/sfab085
18. Sun Q, Tang L, Zeng Q, Gu M. Assessment for the correlation between diabetic retinopathy and metabolic syndrome: a cross-sectional study. *Diab Metabol Syndr Obesity.* (2021) 14:1773. doi: 10.2147/DMSO.S265214
19. Smarandache F. Neutrosophy neutrosophic probability, set, and logic, proquest information and learning. *Ann Arbor.* (1998) 105:118–23.
20. Smarandache F. *Introduction to Neutrosophic Measure, Neutrosophic Integral, and Neutrosophic Probability*. Infinite Study. (2013).
21. Ansari AQ, Biswas R, Aggarwal S. Proposal for applicability of neutrosophic set theory in medical AI. *Int J Comput Applic.* (2011) 27:5–11. doi: 10.5120/3299-4505
22. Jafar MN, Imran R, Riffat SH, Shuaib R. *Medical Diagnosis Using Neutrosophic Soft Matrices and Their Compliments.* Infinite Study. (2020).
23. Basha SH, Anter AM, Hassanien AE, Abdalla A. Hybrid intelligent model for classifying chest X-ray images of COVID-19 patients using genetic algorithm and neutrosophic logic. *Soft Comput.* (2021). doi: 10.1007/s00500-021-06103-7
24. Zhang C, Li D, Broumi S, Sangaiah AK. Medical diagnosis based on single-valued neutrosophic probabilistic rough multisets over two universes. *Symmetry.* (2018) 10:213. doi: 10.3390/sym10060213
25. Zhang D, Zhao M, Wei G, Chen X. Single-valued neutrosophic TODIM method based on cumulative prospect theory for multi-attribute group decision making and its application to medical emergency management evaluation. In: *Economic Research-Ekonomska Istraživanja.* (2021). p. 1–17. doi: 10.1080/1331677X.2021.2013914
26. Smarandache, F. (2014). *Introduction to Neutrosophic Statistics*. Infinite Study.
27. Chen J, Ye J, Du S. Scale effect and anisotropy analyzed for neutrosophic numbers of rock joint roughness coefficient based on neutrosophic statistics. *Symmetry.* (2017) 9:208. doi: 10.3390/sym9100208
28. Chen J, Ye J, Du S, Yong R. Expressions of rock joint roughness coefficient using neutrosophic interval statistical numbers. *Symmetry.* (2017) 9:123. doi: 10.3390/sym9070123
29. Aslam M, Arif OH, Sherwani RAK. New diagnosis test under the neutrosophic statistics: an application to diabetic patients. *BioMed Res Int.* (2020). doi: 10.1155/2020/2086185
30. Ling J, Lin M, Zhang L. Medical waste treatment scheme selection based on single-valued neutrosophic numbers. *AIMS Mathematics.* (2021) 6:10540–64. doi: 10.3934/math.2021612
31. Das R, Mukherjee A, Tripathy BC. Application of neutrosophic similarity measures in Covid-19. *Ann Data Sci.* (2022) 9:55–70. doi: 10.1007/s40745-021-00363-8
32. Saeed M, Ahsan M, Saeed MH, Mehmood A, Abdeljawad T. An application of neutrosophic hypersoft mapping to diagnose hepatitis and propose appropriate treatment. *IEEE Access.* (2021) 9:70455–71. doi: 10.1109/ACCESS.2021.3077867
33. Aslam M. Assessing the significance of relationship between metrology variables under indeterminacy. *J Meterol Soc India.* (2021) 37:119–24. doi: 10.1007/s12647-021-00503-8
34. Doll H, Carney S. Statistical approaches to uncertainty: p values and confidence intervals unpacked. *BMJ Evid-Based Med.* (2005) 10:133–134. doi: 10.1136/ebm.10.5.133
35. Aslam M, Albassam M. Application of neutrosophic logic to evaluate correlation between prostate cancer mortality and dietary fat assumption. *Symmetry.* (2019) 11:330. doi: 10.3390/sym11030330
36. Kanji GK. *100 Statistical Tests.* Sage. (2006). doi: 10.4135/9781849208499

Conflict of Interest: The authors declare that the research was conducted in the absence of any commercial or financial relationships that could be construed as a potential conflict of interest.

frontiers | Frontiers in Nutrition

ORIGINAL RESEARCH
published: 16 May 2022
doi: 10.3389/fnut.2022.888960

Protective Effect of Oyster Peptides Derived From *Crassostrea gigas* on Intestinal Oxidative Damage Induced by Cyclophosphamide in Mice Mediated Through Nrf2-Keap1 Signaling Pathway

Hui Chen[1,2,3], *Huizhen Zheng*[1,2], *Tiejun Li*[4], *Qihong Jiang*[1,2], *Shulai Liu*[1,2], *Xuxia Zhou*[1,2], *Yuting Ding*[1,2] *and Xingwei Xiang*[1,2]*

[1] College of Food Science and Technology, Zhejiang University of Technology, Hangzhou, China, [2] Key Laboratory of Marine Fishery Resources Exploitment and Utilization of Zhejiang Province, Zhejiang University of Technology, Hangzhou, China, [3] National Engineering Research Center of Seafood, Collaborative Innovation Center of Seafood Deep Processing, School of Food Science and Technology, Dalian Polytechnic University, Dalian, China, [4] Zhejiang Marine Fisheries Research Institute, Zhoushan, China

OPEN ACCESS

Edited by:
Demin Cai,
Yangzhou University, China

Reviewed by:
Zhenjun Zhu,
Jinan University, China
Bin Zheng,
Zhejiang Ocean University, China

***Correspondence:**
Xingwei Xiang
xxw11086@zjut.edu.cn

Specialty section:
This article was submitted to Nutrition and Metabolism, a section of the journal Frontiers in Nutrition

Received: *03 March 2022*
Accepted: *08 April 2022*
Published: *16 May 2022*

Citation:
Chen H, Zheng H, Li T, Jiang Q, Liu S, Zhou X, Ding Y and Xiang X (2022) Protective Effect of Oyster Peptides Derived From Crassostrea gigas on Intestinal Oxidative Damage Induced by Cyclophosphamide in Mice Mediated Through Nrf2-Keap1 Signaling Pathway. Front. Nutr. 9:888960. doi: 10.3389/fnut.2022.888960

Oyster peptide (OP) has exhibited useful biological activities and can be used in multi-functional foods. OP has been reported to play a significant role in intestinal protection, but its specific mechanism is still not completely understood. The aim of this study was to analyze the potential effect of OP on oxidative damage of mice intestine induced by cyclophosphamide (Cy). The experimental results revealed that intragastric administration of OP significantly increased average bodyweight, improved ileum tissue morphology and villus structure, as well as increased the activities of superoxide dismutase (SOD), catalase (CAT) and glutathione peroxidase (GSH-Px) in oxidized mice serum and liver. The content of malondialdehyde (MDA) in the mice serum and liver homogenate was found to be markedly decreased. Moreover, OP significantly increased the relative mRNA expression levels of superoxide dismutase (SOD), glutathione peroxidase (GSH-P_X), quinone oxidoreductase (NQO1) and heme oxidase-1 (HO-1) in ileum. Western-blot results indicated that prior administration of OP significantly up-regulated the Nrf2 production in ileum, and substantially decreased then Keap1 gene expression. In conclusion, intake of OP was found to markedly improve intestinal oxidative stress *in vivo*, and this effect was primarily mediated through the simulation of antioxidant Nrf2-Keap1 signaling pathway. This study is beneficial to the application of peptide nutrients in the prevention or mitigation of intestinal oxidative damage.

Keywords: oyster peptides, cyclophosphamide, oxidative stress, intestinal mucosa, Nrf2-Keap1 antioxidant pathway

INTRODUCTION

Oxidative stress related injury refers to the imbalance between oxidative and anti-oxidative reactions caused by excessive production of reactive oxygen species (ROS) in the body (1). The various ROS species are primarily generated and exhibit their functions in mitochondria. These include superoxide anion radical, hydrogen peroxide (H_2O_2), alkane peroxide radical, lipid peroxide radical, nitric oxide (NO·) and hydroxyl radical (HO·) (2). At low concentrations, ROS generally plays a beneficial regulatory role through inducing apoptosis of injured or senescent cells and acting as the different mediators of cell signaling pathway regulation (3). However, excessive production of ROS can be harmful to the body, leading to significant oxidative stress and can substantially weaken intestinal mucosal immune barrier function (4). The intestine is a vital organ of the human body and the major site of digestion and absorption. As a biological barrier (5), it is frequently exposed to oxidative stress and other stress conditions, resulting in increased infiltration of the toxins. Excessive accumulation of oxygen free radicals can effectively destroy the gut mucosal barrier and disrupt intestinal flora, thus affecting the body's homeostasis system (6). Furthermore, oxidative stress can function as an important factor in intestinal inflammation. Accumulating evidences suggest that the use of antioxidants could be useful for the treatment of inflammatory bowel disease, intestinal mucosal infections, ulcerative colitis and colon cancer (7–9).

Cyclophosphamide (Cy) is an alkylating compound, which is often used as an antitumor agent and chemotherapeutic agent (10, 11). It mainly acts through causing cross-linking in DNA, blocking DNA replication as well as synthesis, and thus preventing cell proliferation. The effects of Cy have been found to be non-specific and it can not only eliminate the malignant cells, but at the same time can also damage the various normal cells (such as lymphocytes, gastrointestinal mucosa cells, etc.) (12). It can also disrupt the normal structure of gastrointestinal mucosa and adversely affect intestinal mucosa thereby causing immune disorders and severe side-effects. Extensive use of Cy can cause nausea and vomiting, diarrhea, intestinal barrier destruction, increase intestinal permeability, gastrointestinal mucosal damage, enhance exposure to immune deficiency and secondary infection, oxidative stress, intestinal microflora structural disorders and other side effects (13). Thus, in this study, Cy was used as an inducer to establish a model of intestinal oxidative damage in mice.

Antioxidants present in the food can significantly improve the oxidative state of the body and help to maintain the oxidative/antioxidant balance in the gut (14, 15). The use of food proteins and their constituent peptides which exhibit relatively fewer side effects as antioxidants can serve as an effective approach. Oyster is one of the largest shellfish varieties found in the world. It is extremely rich in different nutrients, including the trace elements, proteins, fatty acids, glycogen, vitamins and taurine. Oyster, as the largest shellfish cultured in the world, is rich in various marine based active peptides, which has become a research hotspot at home and abroad (16, 17). The Marine oyster peptides (OP) possess specific amino acid compositions and sequences, which are quite different from those of the terrestrial proteins. There may be some peptides with specific biological activities. In recent years, a number of studies have reported that oyster active peptide can display multifarious biological activities, such as those related to anti-oxidation (18), lowering of blood pressure (19), inhibition of tumor cancer (20), improving learning and memory (21), and enhancing immunity (22). In addition, a few studies have found that the peptides obtained from the various substances can also exhibit potent antioxidant properties. For example, the antioxidant peptide (ATVY) obtained by Yang et al. from the hydrolyzed protein of black shark skin has displayed good free radical scavenging activity and can be used for the production of antioxidant food additives (23). In addition, the purified peptides obtained from the extract of *Marphysa sanguinea* have demonstrated significant antioxidant activity and reduced the contents of catalase (CAT), superoxide dismutase (SOD), glutathione peroxidase (GSH-PX) and malondialdehyde (MDA) (24). It also inhibited the abnormal secretion of proinflammatory cytokines such as nitric oxide (NO), inducible nitric oxide synthase (iNOS) and cyclooxygenase 2 (COX-2). In another study, Mirzapour-kouhdasht et al. prepared gelatin peptides from fish by-products which displayed potent free radical scavenging effects and pronounced antioxidant effects after gastrointestinal digestion *in vitro* (25). In addition, the small molecule peptides obtained from ALI have exhibited strong DPPH (26), hydroxyl radical and superoxide radical scavenging activities, iron reducing antioxidant and metal chelating properties, and inhibited enzymatic activities of ACE, α-amylase and glucosidase. However, there are only few studies which have examined the effect of OP on oxidative damage of intestinal mucosa induced by Cy.

Here, the potential protective effects of OP on intestinal mucosa were explored by establishing a oxidative injury mouse model of intestinal mucosa, and the underlying mechanism was elucidated. As the advance and the novelty, this study analyzed the relationship between antioxidative peptide and Nrf2-Keap1 pathway *in vivo*. The findings of this study might provide evidence for further understanding the protective mechanism of OP on intestinal mucosal injury, and thus provide a better natural alternative health food both for the prevention and treatment of oxidative stress injury.

MATERIALS AND METHODS

Experimental Animals

Male SPF BALB/C mice aged 5–7 weeks and weighing 15–18 g were used in the present study. The mice were purchased from Slack Laboratory Animal Co., LTD. (Shanghai, China), and the license number was: SCXK (Shanghai) 2017-0005. Before the formal beginning of the experiments, the mice were placed in the animal room for adaptive feeding for 7 days, during which they were free to ingest food and water. Environmental conditions were set as: temperature 25 ± 1°C, humidity 50 ± 3%, light and dark cycle for 12 h. This study was carried out by the guidelines of the Animal Welfare Act and the Guide for the Care and Use

TABLE 1 | Experimental grouping of mice.

Groups	Oral administration (days 1–21)	Intraperitoneal injection (days 18, 19, 20, 21)
C	Saline	Saline
Y	Saline	50 mg Cy /kg BW/day
LP	200 mg OP/kg BW/day	50 mg Cy /kg BW/day
HP	400 mg OP/kg BW/day	50 mg Cy /kg BW/day

of Laboratory Animals, which is approved by the Animal Ethics Committee of Zhejiang University of Technology (20210308038).

Chemicals and Reagents

Cyclophosphamide was obtained from Aladdin Chemical Co., LTD (Shanghai, China). Catalase (CAT), superoxide dismutase (SOD), glutathione peroxidase (GSH-PX), and malondialdehyde (MDA) detection kits were purchased from Nanjing Jianguo Institute of Biological Engineering (Nanjing, China). Antibodies against Nrf2 and Keap1 were obtained from Abcam (Cambridge, UK). In addition, monoclonal antibody against β-actin was purchased from Santa Cruz Biotechnology, Inc. (Santa Cruz, CA, USA). All other reagents obtained were commercially available and of analytical grade.

Management of Animals

The acclimated mice were randomly divided into four different groups according to body weight ($n = 8$): control group (C), Cy model group (Y), OP high-dose group (HP) and low-dose group (LP). Mice were intragastrically administered OP for 21 successive days, and intraperitoneal Cy was injected for 3 days (days 18–21). The dose of Cy was determined according to our previous research, as shown in **Table 1**. The body weight and the vital physical signs of the mice were examined and recorded daily. At the end of the experiment, all the mice were sacrificed by cervical dislocation. The cardiac blood samples were collected at 2,000 r/min and centrifuged for 10 min, −80 °C. The samples of thymus, spleen, liver, ileum, serum and feces were obtained and stored at −80°C for further experiment, respectively.

Determination of Average Daily Gain in Mice

On the 21st day of the experiment, the organ index of the mice after the death was determined by using the following formula:

$$\text{Organ Index} = \text{organ weight (mg)/body weight (g)} \times 10$$

Hematoxylin-Eosin Staining of Ileum of Mice

The fresh ileum of mice was rinsed several times with the normal saline and placed in a clean eppendorf tube. The ileum was fixed in 10 mL 4% paraformaldehyde at room temperature for 24 h. Thereafter, ethanol dehydration, xylene transparent and paraffin embedding were carried out, respectively. Finally, the paraffin blocks were continuously cut by a slicer to obtain intestinal sections with a thickness of approximately 6 μm. Three sections of each tissue block were randomly selected for hematoxylin-eosin (HE) staining (27), and the histopathological changes of the intestine were observed under the microscope (Olympus CX23, Japan).

Electron Microscopic Observation

The ileum was removed after mouse the dissection, washed with PBS solution, and dried with filter article. A section of the empty intestine was obtained and fixed in a centrifuge tube containing glutaraldehyde. Transmission electron microscope (TEM) samples were treated as follows: The ileum of mice was washed several times with PBS solution and fixed in 1% osmium solution for 1 h. After rinsing with the distilled water for three times, the ileum was dehydrated with gradient ethanol and pure acetone successively. The ileum tissue was placed overnight in Spurr resin and polymerized at the temperature of 70°C. Thereafter, the intestine was cut into slices and then stained with uranium acetate and lead citrate. The ileum tissue was observed by TEM and SEM photographed (28). The sample was dehydrated with the gradient ethanol and embedded in the sample section. The samples were dried with liquid carbon dioxide critical point. The ileum surface was coated with a layer of metal composite material with a thickness of about 30 nm by ion sputtering.

Detection of Antioxidant Enzyme Content in the Serum of Mice

The mice were anesthetized and sacrificed by neck amputation, followed by blood collection. The blood was subjected to the centrifugation at 4000 r/min and incubated at 4°C for 15 min. SOD, GSH-Px, CAT and MDA antioxidant kits were used to detect the contents of the various antioxidant factors in the serum of different groups of mice, according to the manufacturer's instructions.

Determination of Antioxidant Factors in Mouse Liver Tissue Homogenate

The mouse livers were weighed to about 100 mg and thoroughly ground in a tissue homogenizer. The supernatant was obtained after centrifugation at 3000 r/min for 10 min and stored at the temperature of 4°C. The contents of antioxidant enzymes SOD, GSH-Px, CAT and MDA were detected on the basis of the manufacturer's instructions of the commercial antioxidant kits.

Quantitative Real-Time Polymerase Chain Reaction

The relative mRNA expression levels of GSH-PX, SOD, CAT, NQO1 and HO-1 were detected through RT-PCR. The total RNA of the sample was extracted from the ileum by using 1 mL ice-cold TRIzol reagent (Ambion, Carlsbad, USA). The mass and concentrations of extracted RNA were determined via spectrophotometry at 260 and 280 nm, respectively. The first strand of cDNA was synthesized by using a Prime-Script 1st Strand cDNA Synthesis Kit (Takara, Dalian, Japan). The different primer sequences were designed by Primer 5 software and synthesized by Shanghai Shenggong Biotechnology Co., Ltd. (Shanghai, China), the details of which have been shown in

TABLE 2 | RT-PCR primer sequences.

Gene	Gene accession number	Primer sequence 5′-3′	Product size (bp)
SOD	NM_011434.1	F: ATGGCGATGAAAGCGGTGTG R: TTACTGCGCAATCCCAATCACTC	465
GPX	NM_ 008160.6	F: GCAATCAGTTCGGACACCAG R: CACCATTCACTTCGCACTTCTC	126
HO-1	NM_010442.2	F: GATAGAGCGCAACAAGCAGAA R: CAGTGAGGCCCATACCAGAAG	111
NQO1	NM_008706.5	F: GGACATGAACGTCATTCTCT R: TTCTTCTTCTGCTCCTCTTG	261
β-actin	NM_007393	F: AGTGTGACGTTGACATCCGT R: GCAGCTCAGTAACAGTCCGC	298

Table 2. The qRT-PCR was performed by using the Applied Biosystems ViiA^{TM}7 Real-Time PCR system. Thereafter, PCR reaction was carried out according to the standard operation process of SYBR Green qPCR test kit. The RT-PCR reaction was carried out based on the following procedure: pre-denaturation at the temperature of 95°C for 30 s, followed by 40 cycles of the conditions: 95°C for 5 s and 65°C for 34 s. The cyclic threshold (CT) values of each gene were normalized using β-actin. With β-actin as internal reference gene, the relative mRNA expression level of target gene was calculated according to the $2^{-\Delta\Delta Ct}$ method (29). The experiment was repeated in triplicate.

Western Blot Analysis

The ileum lysates were prepared using the Radio Immunoprecipitation Assay (RIPA) lysate buffer. The protein concentrations of the lysates were analyzed through bicinchoninic acid (BCA) protein determination kit (Beyotime, Shanghai, China). Approximately 30 μg of proteins were isolated using SDS-PAGE (10%) solution and then transferred to a 0.45 μm polyvinylidene fluoride (PVDF) membrane (Merck Millipore, MA, USA). The membrane was then blocked with 5% skim milk and incubated with the primary antibody (Abcam, Cambridge, UK) at the temperature of 4°C overnight. The membranes were washed three times with TBS for 5 min. Thereafter, the membrane was incubated within HRP-conjugated secondary antibody at the room temperature for about 2 h and rinsed three times for 15 min. The chemiluminescence imaging was carried out using the protein using enhanced chemiluminescence (ECL) reagent (Beyotime, Shanghai, China) (30). Finally, Image J software was used to test and analyze the band density, and each sample was analyzed three times.

Statistical Analysis

All experimental data was analyzed using SPSS17.0 software. The experimental data was expressed as mean ± standard error (SEM). One-way variance (ANOVA) and Tukey tests were adopted for the statistical significance analysis. $P < 0.05$ was considered to be statistically significant.

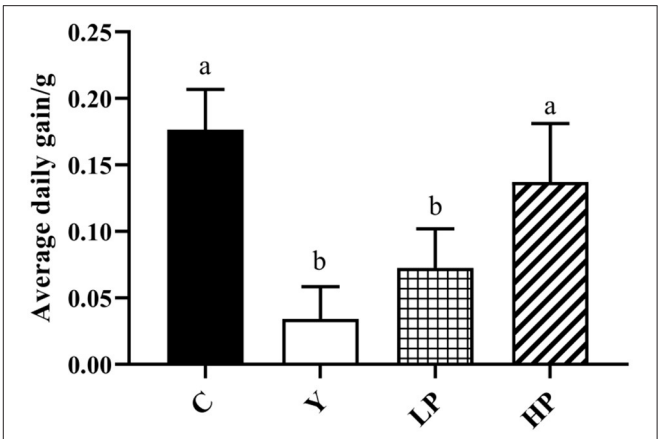

FIGURE 1 | Effects of OP on the average daily gain in oxidative injured mice. Different letters in the figure represent significant differences ($P < 0.05$). C: the normal group; Y: the Cy-induced group; LP: Cy+200 mg/kg OP; HP: Cy+400 mg/kg OP.

RESULTS AND DISCUSSION

Effect of OP on Average Daily Gain in Mice

The mice in Cy treated group showed significant stress reactions such as hair loss and luster, lethargy, slow movement and yellow feces on the second day after intraperitoneal injection of Cy, compared to the normal group (**Figure 1**). In addition, the average daily gain of mice after Cy injection was found to be decreased ($P < 0.05$). Compared with Cy group, early intragastric administration of high-dose OP significantly increased the average daily gain of mice ($P < 0.05$). However, the mice treated with low dose OP also significantly increased the average daily gain, but the effect was not found to be significant ($P > 0.05$).

Effects of OP on Ileum Morphology in Mice

The potential effects of OP on ileum tissue morphology of mice were also analyzed and the results have been shown in **Figure 2**. It was found that in the normal group of mice ileum, villi was arranged orderly, appeared slender and compact with complete structure as well as thick intestinal wall. In the Cy treated group, the villi of ileum were observed to be loose and short, and some of the villi were broken and detached. After the OP pre-treatment, the length of villi in the LP and HP group was restored, and the structure was observed to be more complete as well as orderly, and the damaged condition was substantially improved. These results suggested that intake of OP can effectively protect ileum tissue of immunosuppressed mice to a certain extent, and reduce intestinal villi damage caused by Cy.

Electron Microscopic Observation of Ileum in Mice

TEM results of ileum of all mice have been shown in **Figures 3A–C**. In the normal group, the microvilli were found to be arranged and distributed in a very orderly manner, with long villi and almost no gap, and the close connection was clearly visible in the figure. However, compared with the normal

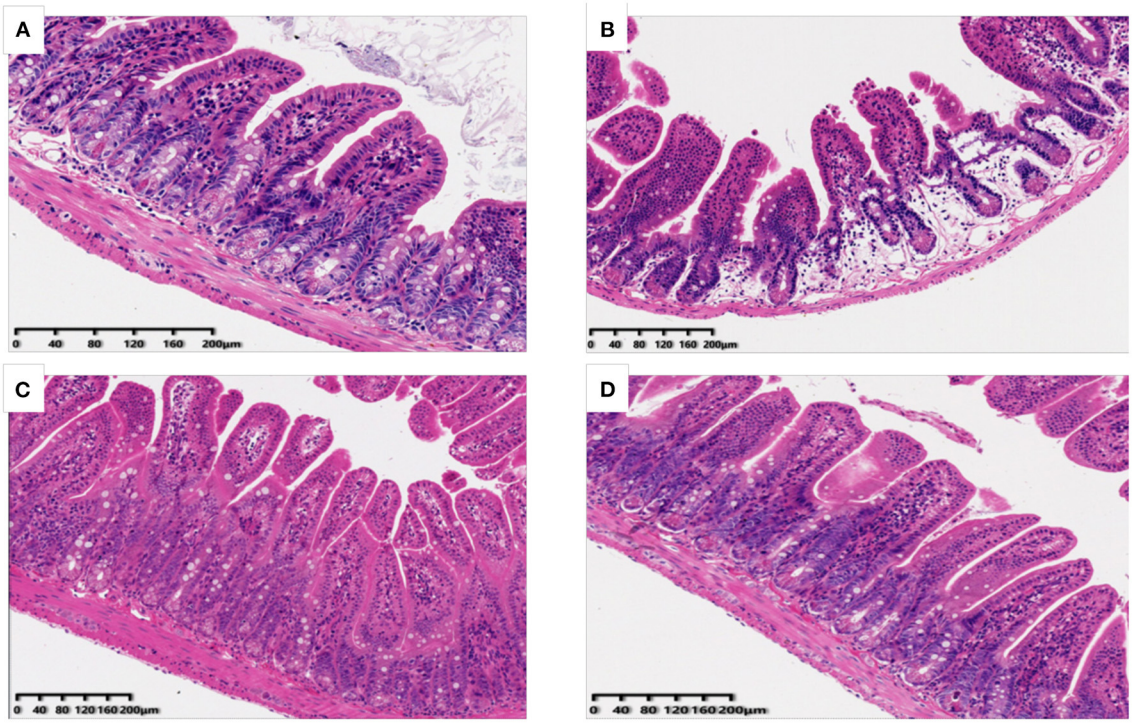

FIGURE 2 | Effects of OP on ileum histomorphology in oxidative injured mice [**(A)**: Normal group; **(B)**: Cy-induced group; **(C)**: LP: Cy+200 mg/kg OP; **(D)**: HP Cy+400 mg/kg OP; 200x].

group, Cy induced the intestinal microvilli of mice into rare and disordered state, with irregular tight connections, and the intestinal villi were observed to be severely damaged. After early intragastric administration of OP, the intestinal mucosa structure of the mice was noted to be significantly improved and the structure of microvilli was restored. The SEM results of ileum showed that the ileum structure of mice in the normal group was flat as well as smooth, and the microvilli were closely connected, in **Figures 3D–F**. The microvilli in the Cy model group were not consistent in height and were arranged irregularly, and some microvilli were found to be broken and fractured. The intestinal microvilli of mice treated with OP appeared to be relatively repaired, with small spaces between them as well as smooth surface, and almost returned to the normal state. These results indicated that intake of OP can markedly repair the damage of Cy induced ileum mucosa in mice.

Effect of OP on Serum Antioxidant Enzyme Level in Mice

We also investigated the dose dependent effects of OP on the content or activities of serum antioxidant enzyme in mice, as shown in **Figure 4**. The activities of SOD, CAT and GSH-Px in serum of Cy treated mice were distinctly decreased, and the activity of MDA was significantly increased ($P < 0.05$), compared with normal group. The intervention with high dose OP increased the contents of SOD, CAT and GSH-Px in serum of mice ($P < 0.05$), but significantly decreased the activity of MDA ($P < 0.05$), compared with the Cy group. Interestingly, low dose of OP intake also increased GSH-Px activity of serum in mice ($P < 0.05$), and decreased the content of MDA in the serum ($P < 0.05$), but did not display significant effect on the activities of SOD and CAT in the serum ($P > 0.05$). These findings suggested that the prior administration of OP boosted the antioxidant capacity *in vivo*, thereby modulating the oxidative stress response caused by Cy even in a dose-dependent manner.

Effect of OP on Antioxidant Enzyme Level in Mouse Liver

In addition, the dose dependent effects of OP on the activities of the various antioxidant factors in the mouse liver tissue was also analyzed (**Figure 5**). It was found that compared with Cy treated mice, the activities of CAT, GSH-Px and SOD in liver decreased significantly ($P < 0.05$), while the content of MDA was observed to be increased more than 3 times ($P < 0.05$), thereby suggesting that serious oxidative stress occurred in liver after Cy was injected into the mice. Moreover, Compared with Cy group, CAT, GSH-Px and SOD in the liver of mice increased substantially ($P < 0.05$), and MDA production was decreased approximately by 50% in LP mice and 70% in HP mice ($P < 0.05$) under OP prevention. The above findings indicated that OP also exhibited a specific recovery and regulation effect on oxidative damage caused in the mouse liver tissues, and can display a dose-dependent protective effect.

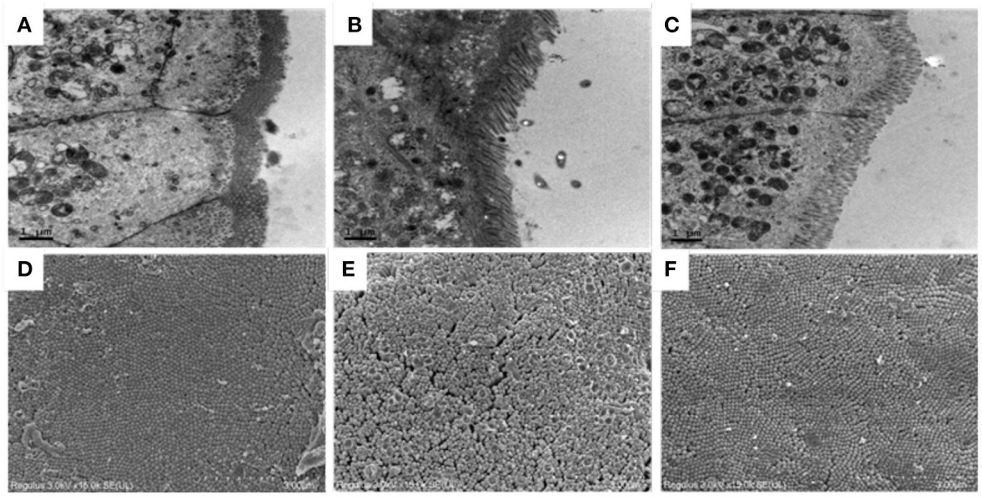

FIGURE 3 | Effects of OP on ileum villi morphology in immunosuppressed mice. **(A–C)** Transmission electron microscopy, 10K×, **(A)**: Normal group, **(B)**: Cy-induced group, **(C)**: Cy+400 mg/kg OP, **(D–F)**: Scanning electron microscopy, 15K×, **(D)**: Normal group, **(E)**: Cy-induced group, and **(F)**: Cy+400 mg/kg OP.

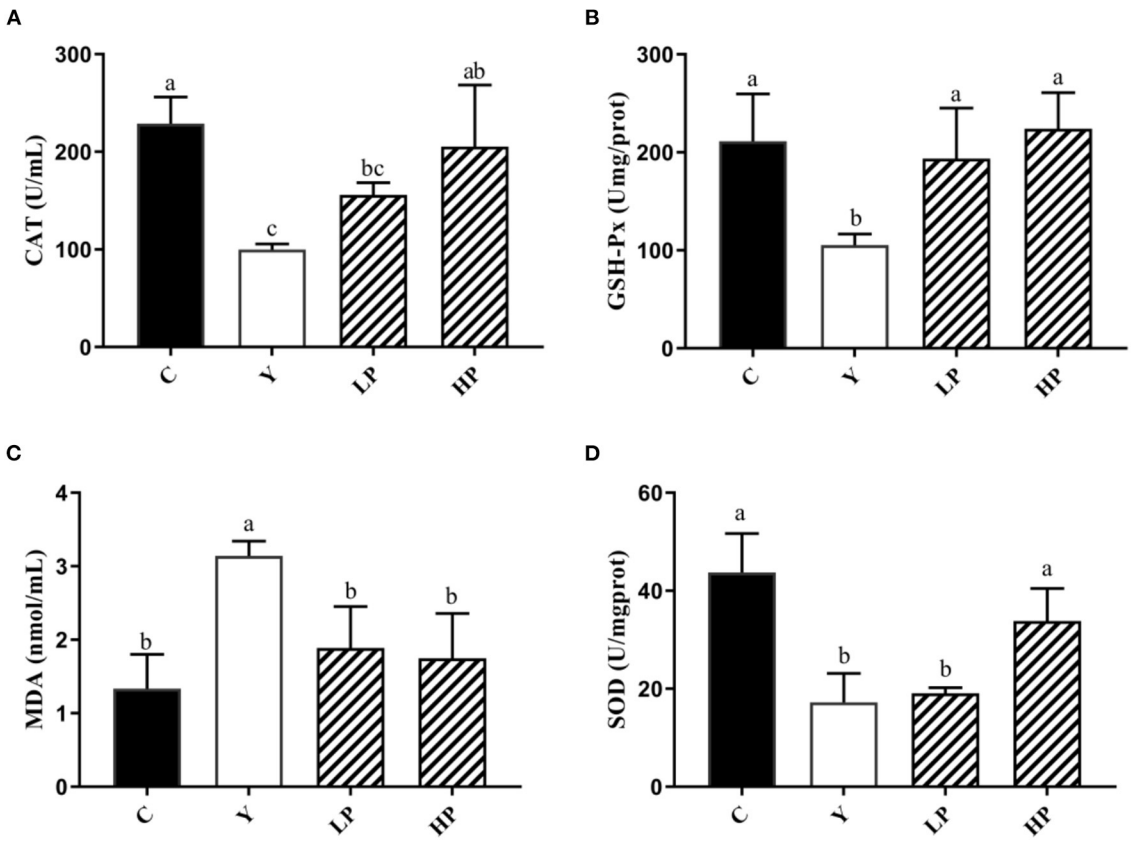

FIGURE 4 | Effects of OP on the contents of CAT **(A)**, GSH-Px **(B)**, MDA **(C)**, and SOD **(D)** in serum of oxidative injured mice. Different letters in the figure represent significant differences ($P < 0.05$). C: the normal group; Y: the Cy-induced group; LP: Cy+200 mg/kg OP; HP: Cy+400 mg/kg OP.

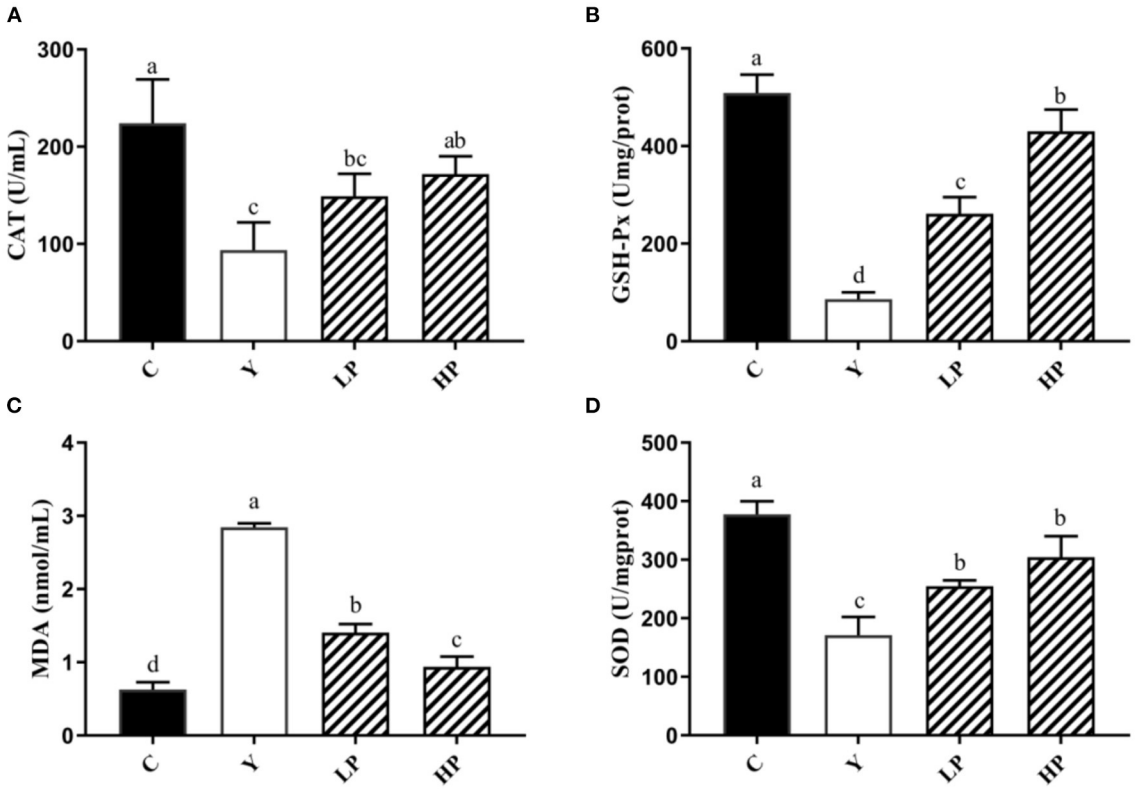

FIGURE 5 | Effects of OP on the contents of CAT **(A)**, GSH-Px **(B)**, MDA **(C)**, and SOD **(D)** in liver of oxidative injured mice. Different letters in the figure represent significant differences ($P < 0.05$). C: the normal group; Y: the Cy-induced group; LP: Cy+200 mg/kg OP; HP: Cy+400 mg/kg OP.

Effects of OP on the Relative Expression Levels of the Various Antioxidant Genes in Ileum of Mice

The effect of OP on the relative expression of antioxidant related genes in the ileum of Cy-induced mice was also examined. The experimental results have been shown as in **Figure 6**. It was noted that compared with the normal group, intraperitoneal injection of Cy significantly reduced the relative mRNA expression of SOD, GSH-Px, HO-1 and NQO1 ($P < 0.05$). Moreover, compared with the Cy treated group, the relative expression of SOD, GSH-Px, HO-1 and NQO1 genes were significantly increased upon prior intake of OP ($P < 0.05$) in a dose-dependent manner. These results suggested that OP can regulate the expression of various antioxidant genes and exert substantial protective effect on intestinal oxidation in immunosuppressed mice, which can partially recover the decreased antioxidant capacity caused by Cy.

Effects of OP on Nrf2-Keap1 Protein Expression in Ileum of Mice

Finally, we investigated the dose dependent effect of OP on the relative expression of major proteins of Nrf2-Keap1 pathway in the mice ileum. The result has been shown in **Figure 7**. The relative expression level of Nrf2 protein in ileum tissue of mice after Cy treatment was found to be significantly reduced ($P < 0.05$), but the relative expression level of Keap1 protein was significantly increased ($P < 0.05$) as compared with the normal group. Interestingly, prior intake of OP significantly upregulated Nrf2 protein expression level in ileum of the mice ($P < 0.05$), while it significantly decreased Keap1 protein expression in a dose-dependent manner ($P < 0.05$), as compared with the Cy group. These findings suggested that OP might play a protective role on intestinal oxidative stress in immunosuppressed mice through activating Nrf2-Keap1 pathway.

DISCUSSION

Cy is widely employed in the treatment of different cancers as well as autoimmune diseases (31), and can cause oxidative stress and intestinal mucosal damage while exerting anti-tumor effects (32). It has been established that administration of large doses of Cy can cause severe side effects such as intestinal barrier disruption, increased intestinal permeability, gastrointestinal mucosal destruction, immune deficiency as well as secondary infections, and the production of excessive free oxygen radicals. In recent years, several studies have found that diverse bioactive peptides isolated from the different sources can exhibit strong antioxidant activity (23), which can improve or restore the body's immunity. Solenocera Crassicornis head protein Hydrolysates-Fraction 1 (SCHPS-F1) is mainly composed of different low

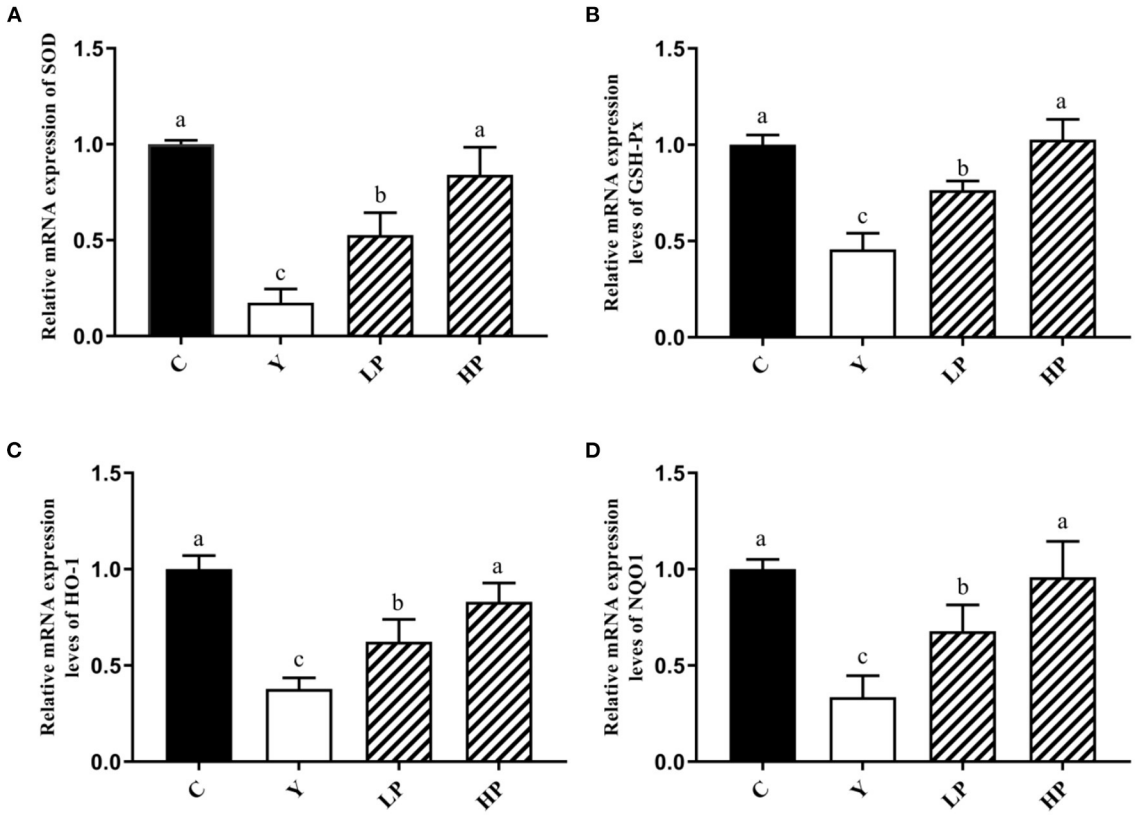

FIGURE 6 | Effects of OP on the relative mRNA expression levels of intestinal antioxidant factors SOD **(A)**, GSH-Px **(B)**, HO-1 **(C)**, and NQO1 **(D)** in oxidative injured mice. Different letters in the figure represent significant differences ($P < 0.05$). C: the normal group; Y: the Cy-induced group; LP: Cy+200 mg/kg OP; HP: Cy+400 mg/kg OP.

molecular weight peptides. It has been reported that Cy-induced nephrotoxicity could be alleviated by restoring antioxidant enzyme activity and Nrf2-Keap1 antioxidant pathway-related protein expression. In addition, Fontoura et al. isolated a novel antioxidant peptide from the protease hydrolysates of the feather keratin from corn germ which caused substantial hydroxyl radical scavenging and lipid peroxidation inhibition (33). Here, we investigated the potential protective effects of OP on intestinal mucosal loss and oxidative stress in immunosuppressed mice upon intraperitoneal injection of Cy and pre-gavage administration of OP.

The experimental results showed that most of the mice exhibited decrease in weight, loss of appetite and mental malaise after the treatment with Cy. However, when OP was administered, the appetite began to recover and weight loss in mice was significantly reduced. Intestinal tract not only plays a vital role in nutrient digestion and absorption, but also is the biggest immune organ. The results of HE staining and electron microscopy suggested that the intestinal villi of Cy treated mice was loose, some villi were broken and their structural integrity was destroyed. The villi of LP as well as HP groups were found to be compact, the intestinal injury was improved, and the villi length was close to the normal group. SOD), CAT) and GSH-Px are the key enzymes and regulatory factors involved in the body's antioxidant defense system. For instance, SOD can effectively catalyze superoxide anion and remove free radicals, thereby reducing the lipid peroxidation and maintaining the balance between oxidative and anti-oxidative states (34–36). Meanwhile, GSH-Px and CAT can functionally remove H_2O_2 and reduce ·OH level, thus reducing the damage caused by free radicals to the body (37, 38). MDA is the final by-product of endogenous lipid peroxidation, which can lead to DNA rearrangement and even apoptosis (39, 40). Both the ileum and liver are important immune organs of the body. When the intestinal environment is affected by inflammation, oxidative stress and disorder of bacterial community structure, the liver can also produce corresponding adverse reactions. Therefore, the relative expression level of anti-oxidant genes, and the content of antioxidant enzymes in the serum and liver were also measured in this study. The results indicated that the contents of SOD, CAT and GSH-Px in the serum and mice liver were decreased markedly, whereas the content of MDA was substantially increased after the treatment with Cy, thus suggesting that Cy caused oxidative stress in mice. Moreover,

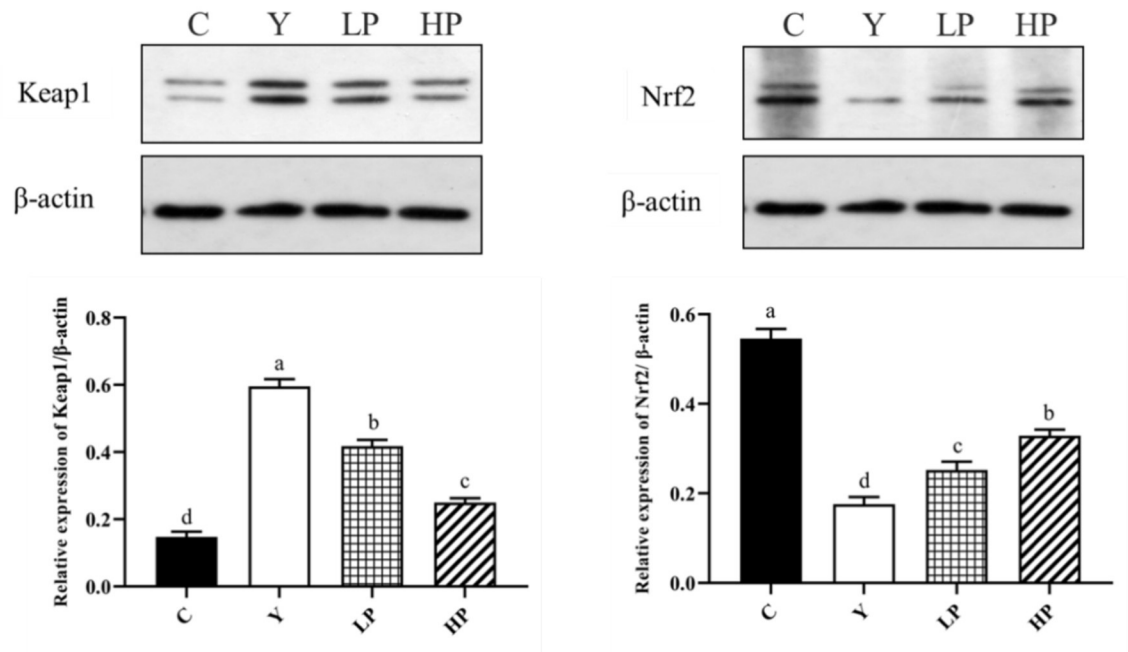

FIGURE 7 | Effects of OP on Keap1-Nrf2 signaling pathway in the ileum of oxidative injured mice. Different letters in the figure represent significant differences ($P < 0.05$). C: the normal group; Y: the Cy-induced group; LP: Cy+200 mg/kg OP; HP: Cy+400 mg/kg OP.

compared with Cy treated group, gavage of OP significantly increased the mRNA expression contents of SOD and GSH-Px in the mice ileum, decreased the MDA content and enhanced the secretion of the SOD, CAT, and GSH-Px in the mice serum and liver. These findings suggested that early intake of OP can significantly reduce the lipid peroxidation in the serum, ileum and liver tissues, and alleviate the oxidative lesions induced by Cy. The possible mechanisms contributing to these protective effects may be due to improvement in the contents of antioxidant enzymes by up-regulation of their relative mRNA expression. A number of previous studies have reported many similar results. For example, fucoidan has been shown to significantly reduce the contents of MDA, IL-6, IL-1β, and TNF-α in the liver and kidney tissues of mice induced by Cy (41), and it also increased the activities of SOD, GSH-Px and CAT. In addition, fucoidan can also activate Nrf2/HO-1 pathway, by increasing Nrf2, GCLM, HO-1 and NQO1 protein levels. Sulfate polysaccharide AL1-1 in sea cucumber can significantly increase intestinal total antioxidant capacity (T-AOC) and decrease intestinal MDA level (42). AL1-1 can also increase the levels of CAT and GSH-Px, and significantly enhance the immune response. These studies are consistent with the conclusion of our experiment results.

Nrf2 is a critical transcription factor which can effectively regulate oxidative stress in the body and restore oxidative damage by modulating the secretion of antioxidant enzymes (43, 44). Under regular physiological conditions, Nrf2 remains bound to Keap1 (Kelch-like ECH-associated protein 1), in the cytoplasm, which can also regulate degradation of Nrf2 by the ubiquitin–proteasome pathway. In response to oxidative stress, the continuous production and accumulation of ROS causes Nrf2 to dissociate from Keap1 and migrate into the nucleus to bind to antioxidant response elements (ARE) and regulate the secretion of various cytoprotective genes (HO-1, NQO1) downstream of Nrf2-Keap1 signaling pathway (45). The experimental results showed that intake of OP significantly increased the gene expression levels of major detoxifying enzymes, HO-1 and NQO1 in the Nrf2 signaling pathway of mice ileum. Interestingly, the Western-blot results also indicated that the expression of Keap1 protein in ileum mice induced by Cy was substantially reduced and the expression of Nrf2 protein was up-regulated by OP intake in a dose-dependent manner as compared with the Cy treatment group. Overall, the findings suggest that OP can regulate oxidative stress in Cy treated mice, and the mechanism may be relevant to the activation of pathway of Nrf2-Keap1 to combat the oxidative stress. OP also showed potent antioxidant activity *in vitro*. By regulating Nrf2-Keap1 pathway in CPP-treated mice, the expression of upstream factor Keap1 was decreased, whereas that of Nrf2 was increased, and then the expression of downstream factors (NQO1, HO-1, GSH-Px, SOD and CAT) was found to be enhanced. It prevented oxidative damage induced by Cy in mice. As an effective antioxidant, OP can significantly reduce reproductive oxidative stress damage associated with the Nrf2-Keap1/ARE pathway.

STUDY LIMITATION

This finding may be some potential limitations. First, Cy-induced long-term intestinal oxidative damage is not equivalent to

ordinary oxidative damage. The Cy modeling method has indeed increased the success rate and achieved excellent results *in vivo*, but at the same time, it is necessary to ignore the interference effects of other negative effects. In addition, peptides are hydrolyzed in the gastrointestinal tract into free amino acids, which also have the antioxidant capacity in the body. However, it is worth noting that it is also due to the characteristic products of different peptide sequences that cause the different results.

CONCLUSION

In this study, intragastric administration of OP was found to significantly increase the average daily gain of Cy-induced oxidative stress mice. OP treatment also improved SOD, CAT and GSHPx activity levels in the serum and liver, and significantly reduced MDA content. Moreover, OP increased the relative mRNA expression of SOD, GSH-Px, Nrf2, HO-1 and NQO1 in ileum significantly, up-regulated Nrf2 protein expression but down-regulated Keap1 protein expression. Overall, OP can regulate the intestinal oxidative damage induced by Cy in mice, and its mechanism may be primarily mediated by enhancing the expression of various antioxidant genes, antioxidant enzyme activities and activating Nrf2-Keap1 pathway. The results showed that OP might have useful potential in the treatment of intestinal oxidative damage and other similar related diseases.

DATA AVAILABILITY STATEMENT

The original contributions presented in the study are included in the article/supplementary materials, further inquiries can be directed to the corresponding author.

ETHICS STATEMENT

The animal study was reviewed and approved by the Animal Welfare Act and the Guide for the Care and Use of Laboratory Animals, which is approved by the Animal Ethics Committee of Zhejiang University of Technology (20210308038).

AUTHOR CONTRIBUTIONS

HC, XX, and SL provided the project administration and funding acquisition. HZ and XZ designed the research and wrote the manuscript. HZ, TL, and QJ executed the experiments and analyzed the data. HC, XX, and YD reviewed and edited this manuscript. All authors have read and agreed to the published version of the manuscript.

FUNDING

This work was supported by grants from the National Key Research and Development Program of China (2020YFD0900902) and the National Natural Science Foundation of China (32101947).

REFERENCES

1. Apel K, Hirt H. Reactive oxygen species: metabolism, oxidative stress, and signal transduction. *Annu Rev Plant Biol.* (2004) 55:373–99. doi: 10.1146/annurev.arplant.55.031903.141701
2. Scherz-Shouval R, Elazar Z. ROS mitochondria and the regulation of autophagy. *Trends Cell Biol.* (2007) 17:422–7. doi: 10.1016/j.tcb.2007.07.009
3. Sakai Y, Yamamori T, Yoshikawa Y, Bo T, Suzuki M, Yamamoto K, et al. Oxidase 4 mediates ROS production in radiation-induced senescent cells and promotes migration of inflammatory cells. *Free Radic Res.* (2018) 52:92–102. doi: 10.1080/10715762.2017.1416112
4. Li L, Feng L, Jiang WD, Jiang J, Wu P, Kuang SY, et al. Dietary pantothenic acid deficiency and excess depress the growth, intestinal mucosal immune and physical functions by regulating NF-κB, TOR, Nrf2 and MLCK signaling pathways in grass carp (*Ctenopharyngodon idella*). *Fish Shellfish Immunol.* (2015) 45:399–413. doi: 10.1016/j.fsi.2015.04.030
5. Ramachandran A, Prabhu R, Thomas S, Reddy JB, Pulimood A, Balasubramanian KA. Intestinal mucosal alterations in experimental cirrhosis in the rat: role of oxygen free radicals. *Hepatology.* (2002) 35:622–9. doi: 10.1053/jhep.2002.31656
6. Szelenyi I, Brune K. Possible role of oxygen free radicals in ethanol-induced gastric mucosal damage in rats. *Dig Dis Sci.* (1988) 33:865–71. doi: 10.1007/BF01550977
7. Chung CH, Jung W, Keum H, Kim TW, Jon S. Nanoparticles derived from the natural antioxidant rosmarinic acid ameliorate acute inflammatory bowel disease. *ACS Nano.* (2020) 14:6887–96. doi: 10.1021/acsnano.0c01018
8. Tian T, Wang Z, Zhang J. Pathomechanisms of oxidative stress in inflammatory bowel disease and potential antioxidant therapies. *Oxid Med Cell Longev.* (2017) 2017:1–18. doi: 10.1155/2017/4535194
9. Guan G, Lan S. Implications of antioxidant systems in inflammatory bowel disease. *Biomed Res Int.* (2018) 2018:1–7. doi: 10.1155/2018/1290179
10. Stallmach A, Wittig BM, Moser C, Fischinger J, Duchmann R, Zeitz M. Safety and efficacy of intravenous pulse cyclophosphamide in acute steroid refractory inflammatory bowel disease. *Gut.* (2003) 52:377–82. doi: 10.1136/gut.52.3.377
11. Martí JL, Mayordomo JI, Isla MD, Saenz A, Escudero P, Tres A, et al. Autotransplant for inflammatory bowel disease (IBD): a case of ulcerative colitis. *Bone Marrow Transplant.* (2001) 28:109–10. doi: 10.1038/sj.bmt.1703103
12. Miao M, Cheng B, Guo L, Shi J. Effects of fuzheng paidu tablet on peripheral blood T lymphocytes, intestinal mucosa T lymphocytes, and immune organs in cyclophosphamide-induced immunosuppressed mice. *Hum Vaccin Immunother.* (2015) 11:2659–63. doi: 10.1080/21645515.2015.1082694
13. Russo F, Linsalata M, Clemente C, D'Attoma B, Orlando A, Campanella G, et al. The effects of fluorouracil, epirubicin, and cyclophosphamide (FEC60) on the intestinal barrier function and gut peptides in breast cancer patients: an observational study. *BMC Cancer.* (2013) 13:56. doi: 10.1186/1471-2407-13-56
14. Yan S, Wang K, Wang X, Ou A, Wang F, Wu L, et al. Effect of fermented bee pollen on metabolic syndrome in high-fat diet-induced mice. *Food Sci Hum Wellness.* (2021) 10:345–55. doi: 10.1016/j.fshw.2021.02.026
15. Truong V-L, Jeong W-S. Antioxidant and anti-inflammatory roles of tea polyphenols in inflammatory bowel diseases. *Food Sci Hum Wellness.* (2022) 11:502–11. doi: 10.1016/j.fshw.2021.12.008
16. Hao L, Wang X, Cao Y, Xu J, Xue C. A comprehensive review of oyster peptides: preparation, characterisation and bioactivities. *Rev Aquac.* (2022) 14:120–38. doi: 10.1111/raq.12588
17. Jo C, Khan FF, Khan MI, Iqbal J. Marine bioactive peptides: types, structures, and physiological functions. *Food Rev Int.* (2017) 33:44–61. doi: 10.1080/87559129.2015.1137311
18. Miao J, Liao W, Kang M, Jia Y, Wang Q, Duan S, et al. Anti-fatigue and anti-oxidant activities of oyster (*Ostrea rivularis*) hydrolysate prepared by compound protease. *Food Funct.* (2018) 9:6577–85. doi: 10.1039/C8FO01879K

19. Shiozaki K, Shiozaki M, Masuda J, Yamauchi A, Ohwada S, Nakano T, et al. Identification of oyster-derived hypotensive peptide acting as angiotensin-I-converting enzyme inhibitor. *Fish Sci.* (2010) 76:865–72. doi: 10.1007/s12562-010-0264-0
20. Umayaparvathi S, Arumugam M, Meenakshi S, Dräger G, Kirschning A, Balasubramanian T. Purification and characterization of antioxidant peptides from oyster (*Saccostrea cucullata*) hydrolysate and the anticancer activity of hydrolysate on human colon cancer cell lines. *Int J Pept Res Ther.* (2014) 20:231–43. doi: 10.1007/s10989-013-9385-5
21. Wang X, Yu H, Xing R, Liu S, Chen X, Li P. Effect and mechanism of oyster hydrolytic peptides on spatial learning and memory in mice. *RSC Adv.* (2018) 8:6125–35. doi: 10.1039/C7RA13139A
22. Xiang XW, Zheng HZ, Wang R, Chen H, Xiao JX, Zheng B, et al. Ameliorative effects of peptides derived from oyster (*Crassostrea gigas*) on immunomodulatory function and gut microbiota structure in cyclophosphamide-treated mice. *Mar Drugs.* (2021) 19:456. doi: 10.3390/md19080456
23. Yang Q, Cai X, Yan A, Tian Y, Du M, Wang S, et al. Specific antioxidant peptide: its properties in controlling oxidation and possible action mechanism. *Food Chem.* (2020) 327:126984. doi: 10.1016/j.foodchem.2020.126984
24. Park YR, Park CI, Soh Y. Antioxidant and anti-inflammatory effects of NCW peptide from clam worm (*Marphysa sanguinea*). *J Microbiol Biotechnol.* (2020) 30:1387–94. doi: 10.4014/jmb.2003.03050
25. Mirzapour-Kouhdasht A, Moosavi-Nasab M, Kim YM, Eun JB. Antioxidant mechanism, antibacterial activity, and functional characterization of peptide fractions obtained from barred mackerel gelatin with a focus on application in carbonated beverages. *Food Chem.* (2021) 342:128339. doi: 10.1016/j.foodchem.2020.128339
26. Senisterra G, Wu H, Allali-Hassani A, Wasney GA, Barsyte-Lovejoy D, Dombrovski L, et al. Small-molecule inhibition of MLL activity by disruption of its interaction with WDR5. *Biochem J.* (2013) 449:151–9. doi: 10.1042/BJ20121280
27. D'Haens GR, Geboes K, Peeters M, Baert F, Penninckx F, Rutgeerts P. Early lesions of recurrent Crohn's disease caused by infusion of intestinal contents in excluded ileum. *Gastroenterology.* (1998) 114:262–7. doi: 10.1016/S0016-5085(98)70476-7
28. Sawczyn T, Zimmermann J, Stygar D, Kukla M, Nabrdalik K, Matysiak N, et al. Ileal transposition (IT) surgery changing the ultrastructure of the transposed segment as well as jejunum. Histomorphometric and electron microscopy analysis. *Obes Surg.* (2018) 28:1232–9. doi: 10.1007/s11695-017-2992-z
29. Mio K, Yamanaka C, Matsuoka T, Kobayashi T, Aoe S. Effects of β-glucan rich barley flour on glucose and lipid metabolism in the ileum, liver, and adipose tissues of high-fat diet induced-obesity model male mice analyzed by DNA microarray. *Nutrients.* (2020) 12:1–18. doi: 10.3390/nu12113546
30. Ying M, Yu Q, Zheng B, Wang H, Wang J, Chen S, et al. Cultured cordyceps sinensis polysaccharides modulate intestinal mucosal immunity and gut microbiota in cyclophosphamide-treated mice. *Carbohydr Polym.* (2020) 235:115957. doi: 10.1016/j.carbpol.2020.115957
31. Floudas CS, Brar G, Mabry-Hrones D, Duffy AG, Wood B, Levy E, et al. A pilot study of the PD-1 targeting agent AMP-224 used with low-dose cyclophosphamide and stereotactic body radiation therapy in patients with metastatic colorectal cancer. *Clin Colorectal Cancer.* (2019) 18:e349–60. doi: 10.1016/j.clcc.2019.06.004
32. Lorinczy D. Cyclophosphamide treatment evoked side effects on skeletal muscle monitored by DSC. *J Therm Anal Calorim.* (2020) 142:1897–901. doi: 10.1007/s10973-020-09388-2
33. Fontoura R, Daroit DJ, Corrêa APF, Moresco KS, Santi L, Beys-da-Silva WO, et al. Characterization of a novel antioxidant peptide from feather keratin hydrolysates. *N Biotechnol.* (2019) 49:71–6. doi: 10.1016/j.nbt.2018.09.003
34. Yim MB, Chock PB, Stadtman ER. Copper, zinc superoxide dismutase catalyzes hydroxyl radical production from hydrogen peroxide. *Proc Natl Acad Sci U S A.* (1990) 87:5006–10. doi: 10.1073/pnas.87.13.5006
35. Klug-Roth D, Rabani J, Fridovich I. Pulse radiolytic investigations of superoxide catalyzed disproportionation. Mechanism for bovine superoxide dismutase. *J Am Chem Soc.* (1973) 95:2786–90. doi: 10.1021/ja00790a007
36. Liochev SI, Fridovich I. Copper- and zinc-containing superoxide dismutase can act as a superoxide reductase and a superoxide oxidase. *J Biol Chem.* (2000) 275:38482–5. doi: 10.1074/jbc.M007891200
37. Wang W, Zhang F, Li Q, Chen H, Zhang W, Yu P, et al. Structure characterization of one polysaccharide from Lepidium meyenii Walp, and its antioxidant activity and protective effect against H_2O_2-induced injury RAW264.7 cells. *Int J Biol Macromol.* (2018) 118:816–33. doi: 10.1016/j.ijbiomac.2018.06.117
38. Hao W, Guo H, Zhang J, Hu G, Yao Y, Dong J. Hydrogen peroxide is involved in salicylic acid-elicited rosmarinic acid production in salvia miltiorrhiza cell cultures. *Sci World J.* (2014) 2014:843764. doi: 10.1155/2014/843764
39. Masiello MG, Cucina A, Proietti S, Palombo A, Coluccia P, D'Anselmi F, et al. Phenotypic switch induced by simulated microgravity on MDA-MB-231 breast cancer cells. *Biomed Res Int.* (2014) 2014:652434. doi: 10.1155/2014/652434
40. Catera R, Silverman GJ, Hatzi K, Seiler T, Didier S, Zhang L, et al. Chronic lymphocytic leukemia cells recognize conserved epitopes associated with apoptosis and oxidation. *Mol Med.* (2008) 14:665–74. doi: 10.2119/2008-00102.Catera
41. Tian S, Jiang X, Tang Y, Han T. Laminaria japonica fucoidan ameliorates cyclophosphamide-induced liver and kidney injury possibly by regulating Nrf2/HO-1 and TLR4/NF-κB signaling pathways. *J Sci Food Agric.* (2021) 102:2604-12. doi: 10.1002/jsfa.11602
42. Feng G, Laijin S, Chen S, Teng W, Dejian Z, Yin C, et al. *In vitro* and *in vivo* immunoregulatory activity of sulfated fucan from the sea cucumber A. *leucoprocta*. *Int J Biol Macromol.* (2021) 187:931–8. doi: 10.1016/j.ijbiomac.2021.08.008
43. Kang KW, Lee SJ, Kim SG. Molecular mechanism of Nrf2 activation by oxidative stress. *Antioxid Redox Signal.* (2005) 7:1664–73. doi: 10.1089/ars.2005.7.1664
44. Ma Q. Role of Nrf2 in oxidative stress and toxicity. *Annu Rev Pharmacol Toxicol.* (2013) 53:401–26. doi: 10.1146/annurev-pharmtox-011112-140320
45. Li W, Kong AN. Molecular mechanisms of Nrf2-mediated antioxidant response. *Mol Carcinog.* (2009) 48:91–104. doi: 10.1002/mc.20465

Conflict of Interest: The authors declare that the research was conducted in the absence of any commercial or financial relationships that could be construed as a potential conflict of interest.

frontiers | Frontiers in Nutrition

REVIEW
published: 18 May 2022
doi: 10.3389/fnut.2022.867150

Nutrition, Epigenetics, and Major Depressive Disorder: Understanding the Connection

Miguel A. Ortega[1,2,3*], *Óscar Fraile-Martínez*[1,2], *Cielo García-Montero*[1,2], *Miguel Angel Alvarez-Mon*[1,2,4], *Guillermo Lahera*[1,2,4,5], *Jorge Monserrat*[1,2], *Maria Llavero-Valero*[4], *Fernando Mora*[4,6], *Roberto Rodríguez-Jiménez*[6,7], *Sonia Fernandez-Rojo*[4,6], *Javier Quintero*[4,6] *and Melchor Alvarez De Mon*[1,2,8]

[1] *Department of Medicine and Medical Specialities, University of Alcala, Alcalá de Henares, Spain,* [2] *Ramón y Cajal Institute of Sanitary Research (IRYCIS), Madrid, Spain,* [3] *Cancer Registry and Pathology Department, Hospital Universitario Principe de Asturias, Alcalá de Henares, Spain,* [4] *Department of Psychiatry and Mental Health, Hospital Universitario Infanta Leonor, Madrid, Spain,* [5] *Psychiatry Service, Center for Biomedical Research in the Mental Health Network, University Hospital Príncipe de Asturias, Alcalá de Henares, Spain,* [6] *Department of Legal Medicine and Psychiatry, Complutense University, Madrid, Spain,* [7] *Institute for Health Research 12 de Octubre Hospital, (Imas 12)/CIBERSAM (Biomedical Research Networking Centre in Mental Health), Madrid, Spain,* [8] *Immune System Diseases-Rheumatology, Oncology Service an Internal Medicine, University Hospital Príncipe de Asturias, (CIBEREHD), Alcalá de Henares, Spain*

OPEN ACCESS

Edited by:
Haoyu Liu,
Uppsala University, Sweden

Reviewed by:
Frances Nkechi Adiukwu,
University of Port Harcourt Teaching Hospital, Nigeria
Ping Hu,
Yangzhou University, China

****Correspondence:***
Miguel A. Ortega
miguel.angel.ortega92@gmail.com

Specialty section:
This article was submitted to Nutrition and Metabolism, a section of the journal Frontiers in Nutrition

Received: *31 January 2022*
Accepted: *19 April 2022*
Published: *18 May 2022*

Citation:
Ortega MA, Fraile-Martínez Ó, García-Montero C, Alvarez-Mon MA, Lahera G, Monserrat J, Llavero-Valero M, Mora F, Rodríguez-Jiménez R, Fernandez-Rojo S, Quintero J and Alvarez De Mon M (2022) Nutrition, Epigenetics, and Major Depressive Disorder: Understanding the Connection. Front. Nutr. 9:867150. doi: 10.3389/fnut.2022.867150

Major depressive disorder (MDD) is a complex, multifactorial disorder of rising prevalence and incidence worldwide. Nearly, 280 million of people suffer from this leading cause of disability in the world. Moreover, patients with this condition are frequently co-affected by essential nutrient deficiency. The typical scene with stress and hustle in developed countries tends to be accompanied by eating disorders implying overnutrition from high-carbohydrates and high-fat diets with low micronutrients intake. In fact, currently, coronavirus disease 2019 (COVID-19) pandemic has drawn more attention to this underdiagnosed condition, besides the importance of the nutritional status in shaping immunomodulation, in which minerals, vitamins, or omega 3 polyunsaturated fatty acids (ω-3 PUFA) play an important role. The awareness of nutritional assessment is greater and greater in the patients with depression since antidepressant treatments have such a significant probability of failing. As diet is considered a crucial environmental factor, underlying epigenetic mechanisms that experience an adaptation or consequence on their signaling and expression mechanisms are reviewed. In this study, we included metabolic changes derived from an impairment in cellular processes due to lacking some essential nutrients in diet and therefore in the organism. Finally, aspects related to nutritional interventions and recommendations are also addressed.

Keywords: major depressive disorder, malnutrition, epigenetics, S-adenosylmethionine, micronutrients, omega 3 polyunsaturated fatty acids, pre/probiotics, mineral deficiency

INTRODUCTION

Major depressive disorder (MDD) is a complex and multifactorial neuropsychiatric disease occurring as a result of multiple changes in the brain and the entire organism (1). The World Health Organization (WHO) ranked MDD as the third cause of the burden of diseases globally in 2008, projecting that by 2030, it will become the leading one (2). The estimated global prevalence

of MDD was about 4.7% with an annual incidence of a 3% (3). However, the global burden of MDD has been increasing during the last years, specially due to the coronavirus disease 2019 (COVID-19) pandemic (4). Likewise, the risk for suffering from MDD is 2-fold higher in woman than in men, showing some particularities in the underpinning biological mechanisms (5), and although the prevalence may vary across ages, this condition may appear virtually at any stage of life (6). Furthermore, MDD entails devastating individual and socioeconomic consequences. For instance, the risk of suicide is notably higher in subjects with depression, especially for young men (7). In the same manner, being diagnosed with MDD is also related to an increased risk of suffering from cardiovascular death, functional impairment, disability, and decreased workplace productivity and absenteeism (8). Collectively, these events lead to huge economic losses, which may also be attributed to the cost of their derived medical treatments, that frequently are not enough to aid neither in the clinical management of depression nor in their complications (9, 10).

In general terms, psychiatric disorders are considered multifactorial conditions resulting from an interplay of genetic and environmental factors that drive to a set of molecular, cellular, circuitry, structural, and functional changes in the brain (11). In this sense, there are no single gene identified as a causative agent of any psychiatric disorder, including MDD, and there has been a recognition in the need of different environmental factors to explain the onset and progression of these conditions (12, 13). Epigenetics are the central link between genetics and environmental agents, as it modulates the expression of critical genes products under certain environmental conditions (14). Hence, growing efforts are being placed to influence in the epigenetic mechanisms involved in the development of different psychiatric disorders, including MDD (15, 16). Diet is a promising modulator of several epigenetic mechanisms in the entire organism, also in the brain, where it modulates the expression of several genes involved in the function of this organ (17–19). The patient with depression is frequently co-affected by malnutrition. It is not easy to assure if depressive status leads to bad dietary habits and hence micronutrient deficiencies or if those deficiencies are part of the onset of MDD. What it has been observed is that these patients are likely to lose weight involuntarily or suffer deficiencies of essential nutrients (20). Thus, the aim of this review is to collect the available evidence of the epigenetic origins of MDD, concretely evaluating the actions of diet in the onset and development of MDD. Furthermore, we will focus on the translational opportunities derived from this knowledge, and future directions to follow to unravel these complex interactions.

EPIGENETIC BASIS OF MDD

Is MDD an Epigenetic Malady?

To answer this question, starting with the definition of epigenetics is a need. This term refers to "the changes in gene function that cause their activation or deactivation without any alteration in the DNA sequence" [National Human Genome Research Institute (21)]. In this context, multifactorial diseases such as psychiatric disorders emphasize the importance of stress-related and environmental factors, which have pointed more prominence in the etiology than genetic factors. Discordances among identical twins studies have justified that frequent exposure to environmental stressors prompts stable changes (i.e., epigenetic marks) in the gene expression with a consequent impact on neuronal functions and, therefore, behavior (22).

The modifications that cause those events can be mediated by DNA methylation, histone modification, and also the expression of signaling non-coding RNAs, mainly represented by long-noncoding RNAs (lncRNAs) and microRNAs (miRNAs) (23–25). That epigenetic regulation can occur not only from nervous system development but also in the mature brain with long-lasting effects and the possibility to be heritable for multiple generations (26). These changes can lead to maladaptive neuronal plasticity, poorer resilience to stress, depressive mood, and different response to antidepressants (27). Recent work reviews have denoted the lack of information regarding the validation of depression-associated epigenetic modifications due to the short age of this field of study, the small sample size of patients, and the difficulties to study functioning changes in alive brains instead of postmortem (23), although there are some epigenetic markers that could be studied in serum and body fluids such as miRNAs (25). Besides, sometimes it is not possible to establish a clear causality of the epigenetic findings because of the difficulty of replicate the experimental results from animals to humans (28).

Systematic reviews have identified so far several alterations in the expression pathways of genes such as brain-derived neurotrophic factor (BDNF), oxytocin receptor (OXTR), nuclear receptor subfamily 3 group C member 1 (NRC31), sodium-dependent serotonin transporter (SLC6A4), FK506 binding protein 5 gene (FKBP5), spindle and kinetochore-associated complex subunit 2 (SKA2), leucine-rich repeat and Ig domain containing 3 (LINGO3), POU class 3 homeobox 1 (POU3F1), a transcriptional repressor of myelin-specific genes, and integrin beta-1 (ITGB1), effect on cell adhesion and several viruses receptor; in the signaling of glucocorticoids, serotonin, and neurotrophins (mainly, BDNF pathways) among others, all these are associated to traumatic events such as childhood maltreatment (29–31). This knowledge has provided a field to understand the long-term effects of adverse life events and aberrant gene expression related to MDD pathogenesis and psychiatric disorders in adulthood in general (32, 33).

Chronic stress has been reported to have pleiotropic effects altering selectively DNA methylome and chromatin compaction, involving mood and even pain perception (34). For these reasons, many authors have argued about an epigenetic basis for the onset of psychiatric disorders, so, it can be affirmed that depression is an epigenetic malady as queried.

Epigenetic Marks Described in Patients With MDD

Histone Modifications

Histones are pivotal structural elements of the chromatin in eukaryotic cells together with DNA and non-histone proteins. There are five major groups of histones, namely, H2A, H2B, H3,

H4 (considered core histones and implicated in the formation of nucleosomes with DNA), and H1/H5, involved in the link of multiple nucleosomes and further DNA packaging (35). Far beyond its structural relevance, histones closely impact chromatin function and dynamics, affecting the chromatin expression due to the presence of specific histone variants (i.e., H2A.X, H2A.Z, macroH2A, H3.3, and CENP-A) or through posttranslational modifications (36). In this context, cumulative evidence is supporting the role of the histone variant H3.3 in the pathogenesis of MDD. Specifically, H3.3 dynamics is activated in the depressed human nucleus accumbens (NA) and in response to chronic social defeat stress in mice, whereas the use of antidepressants prevents H3.3 dynamics, limiting its negative effects (37). More data are available regarding the role of posttranslational modifications of histones. Histones are basic proteins particularly rich in lysine and arginine, also presenting other critical amino acids such as serine and threonine, which are prone to suffer from different modifications. These modifications include acetylations/deacetylations (at lysine), methylations/demethylations (at lysine and arginine), phosphorylations/dephosporylations (at serine or threonine), or ubiquitylations/deubiquitylations (36). Of them, histone methylation and acetylation are the most important posttranslational modifications implicated in the pathophysiology of MDD. The upregulation or downregulation of genes depend on the brain region and histone modification involved. Sun et al. (38) summarized many prodepressive epigenetic changes of this type: in the NA, there is an increase of histone deacetylases (HDACs), HDAC2 expression, and decrease of HDAC5 and H3K9me2 (demethylation of lysine 9 of histone 3); in the hippocampus, there is a decrease in H3/H4 acetylation and H3K9me3 and increase in the HDAC activity and HDAC5 expression; and in peripheral blood also aberrant epigenetic marks are found, such as increasing levels of HDAC2, 4, 5, and SIRTs (1,2,6) (sirtuins, a group of enzymes closely related to HDACs) (30). Histone lysine methylation affects neurons of the central nervous system (CNS), being considered a critical regulator of complex processes such as long-term memory formation and behavior (39). HDACs also alter Rac1 transcription (RAS superfamily of small GTP-binding proteins) in NA, leading to an impairment in the synapsis interfering in social defeat stress, social avoidance, and anhedonia (40).

There has been arising promising therapeutic approaches targeting HDACs and other hallmarks in pharmaco-epigenomics of MDD, which may offer broader effectiveness. For instance, HDAC inhibitors can upregulate neurotrophic factors, allowing an enhanced neural plasticity and exerting antidepressant-like behavior (41). In the same manner, HDAC inhibitors can attenuate the neuroinflammation being now considered as an anti-inflammatory treatment (42). Antidepressants have shown to reduce levels of HDAC4 recruitment along with an increased transcriptional activity of glial cell-derived neurotrophic factor (GDNF) in mice (43). Many preclinical models of HDAC inhibitors such as sodium butyrate, alone or in combination with antidepressants, have shown better antidepressant responses (44). These benefits can also be due to the modulation of this drug of DNA methylation, upregulating the enzyme ten-eleven translocation methylcytosine dioxygenase 1 (TET1), resulting in BDNF overexpression in the prefrontal cortex (45).

DNA Methylation

Many studies have been focusing on DNA methylation in CNS or peripheral tissue. Despite the small sample sizes and low replicative results, omics data and candidate-gene approaches (many about SLC6A4, BDNF, and NR3C1) are on the way to answer more etiological questions (46). Interestingly, maternal stress during pregnancy is key for the fetal epigenetic programming. Part of the maternal cortisol can pass to fetus and consequently, increase the expression of DNA methyltransferase 3a (DNMT3a) and then increase DNA methylation at the promoter region of converting active-to-inactive cortisol enzyme 11β-hydroxysteroid dehydrogenase type 2 (HSD11B2), leading to a lower expression of this enzyme at the fetal cortex and increasing the susceptibility to stress in later life (47). Not only emotional stress but also other stressors such as nutritional restriction can alter highly GC-rich zones in promoter core and downregulate HSD11B2 expression in placenta (48). All in all, the glucocorticoid exposure in the intrauterine environment is key for the DNA methylation of stress response genes, including HSD11B2 and also NR3C1. Some researchers have conducted studies to observe the joint contribution of these genes' expression in newborns neurobehavior, describing different phenotypes, including babies with low NR3C1 methylation but high HSD11B2 methylation had lower excitability scores; babies with high NR3C1 methylation but low HSD11B2 methylation had more asymmetrical reflexes; and lastly, those with high DNA methylation in both genes had higher habituation scores (49). These statements are in agreement with what several scientists have hypothesized as "the fetal origin of diseases" from the epigenetic reprogramming, in this case, "the fetal origin of psychopathology" (50). Although there is still little support from observational studies, there is much consideration about fetal origins of mental health in later life. Maternal depression in pregnancy is considered a serious public health concern, being estimated to increase the depression risk to a 4-fold in the offspring (28). Some evidence has also suggested that several infections and their inflammation during pregnancy may cause injuries in neurodevelopment and then increase the risk for autism spectrum disorder and depression (51).

Furthermore, early childhood stressful experiences have been also linked to changes in gene expression of hypothalamic-pituitary-adrenal axis (HPA), glucocorticoid signaling pathway (i.e., NR3C1 and FKBP5), neurotrophic factors (i.e., BDNF), serotonergic neurotransmission (i.e., SLC6A4), estrogen receptors, and arginine vasopressin, among others. In this line, it has been questioned if these early adverse events establish the features of our personality (52). The link between early-life social stress and different methylation patterns has been studied in animal models. High methylation by DNMT3 in CpG islands from promoter regions entails the downregulation of serotonin and its transporter (i.e., SERT) together with the upregulation of monoamine oxidase A (MAO-A) and tryptophan hydroxylase 2 (TPH2). All these genes are part of the process of brain development, stress response, and emotional control (53).

Moreover, maltreated children have shown hypermethylation in the promoter region of GR gene NR3C1 compared with non-maltreated children, entailing transcriptional silencing. These results corresponded with emotional negativity, ego under control, and more externalizing behavior with depressive symptoms (54, 55).

Long-lasting affection of the HPA axis function has implications for health and well-being in later life. Those environment challenges make changes in brain plasticity, neuronal function, and behavioral adaptation to neuropsychological stress in MDD (56). The dysregulation at this axis is generally accepted to be a consequence from the chronic and exacerbated exposure to glucocorticoids, disturbing already mentioned signaling/levels (57). HPA-dysregulated functioning also entails NRC1 and SLC6A4 hypermethylation, explaining the worse reactivity to stress and disrupted serotonin transport in MDD (58). Either early or later, events that happen throughout our lives may have a long-lasting impact on behavior, bringing a maladaptation that results in changes at limbic regions such as the hippocampus and amygdala. *Reul*'s research group studied these processes and found a link in ERK-MAPK signaling pathway with c-Fos induction, histone H3 acetylation, and DNA methylation at promoter locations. In addition, they concluded that gamma-aminobutyric acid (GABA) could control the different response to such psychological stress and shape those epigenetic changes *via* "local GABAergic interneurons and limbic afferent inputs" (59). The synaptic activity *via* neurotransmitter receptors regulate these epigenetic markers that underlie learning and memory (60), whose impairments are serious incapacitating symptoms in MDD (61).

Whether inherited or acquired, discoveries in non-Mendelian biology demonstrate that epigenetic markers offer new insights in the deeper understanding of complex multifactorial psychiatric disorder of MDD. It is one more variable for MDD multiparametric equation, without forgetting other cumulative effects such as accompanying DNA sequence polymorphisms (62).

Noncoding RNAs

Other novelty epigenetic malleable regulators include non-coding RNAs. First, miRNAs are small molecules carried in vesicles, which are implicated in cell-cell communication, being crucial for neuronal morphogenesis, activity, and plasticity, besides having prominent systemic effects. During the last decade, numerous miRNAs with pleiotropic effects have been identified to be involved in several processes that concern MDD pathogenesis, including neuroinflammation, endotoxemia, microglial apoptosis, altered neurotransmission, worse stress response and sensitivity, altered cell signaling, and circadian disruption. Most of these effects are reviewed and summarized by Ortega et al. (25). In light of the evidence, it is undeniable that miRNAs are key elements implicated in MDD pathogenesis, representing promising therapeutical targets (63). In the similar manner, *lncRNAs* are similar to non-coding RNAs with important signaling and epigenetic actions. In fact, it is now known that they play a synergistic effect with miRNAs. Apparently, these lncRNAs are highly expressed in the brain, and their dysregulation shapes negatively neural stem cell maintenance, neurogenesis and gliogenesis, HPA axis, neurotransmission, neuroinflammation, neurotrophic factors expression, stress responses, and neural plasticity, being currently considered new biomarker candidates of MDD (24, 64, 65). Compiling written evidence about miRNAs and other epigenetic mechanisms in MDD is summarized in **Figure 1**.

NUTRITION, EPIGENETICS, AND MDD: IS THERE A LINK?

The question that comes next is if those epigenetic marks lead to a worse nutritional status, if bad dietary habits lead to acquire different gene expressions, or both may be actually occurring. First, it would be helpful to describe a general picture from the nutritional status in a patient with depression and, afterward, focus on the effect of specific deficits and metabolic impairments in the context of malnutrition-related MDD.

Malnutrition in the Patient With Depression

Currently, it is broadly accepted that there is a link between MDD and malnutrition. Actually, the allowed evidence is not based on standardized methods of the nutritional assessment in the patient with depression, what complicates the drawing of conclusions beyond known micronutrient deficiencies. Although clinical practice nowadays includes the recommendation of supplementation intake to supply certain common deficiencies, mainly vitamin D and omega 3 polyunsaturated fatty acid (ω-3 PUFA), it is also unusual to find observational studies of patients with MDD who have undergone a nutritional assessment. Considering the nutritional status in the management of a patient with depression is relatively new, and, over the last 10 years, surveys, anthropometric, and biochemical measures have started to be used for studying depression in the elderly population both at developed and in developing countries.

Nutritional Assessment in MDD

First, *Mini Nutritional Assessment* (MNA) questionnaire and the *Geriatric Depression Scale* (GDS) have been strongly associated. Malnourished geriatric patients or patients at risk of malnutrition have higher risk of suffering from MDD. These studies have been useful for determining the prevalence and severity of MDD and its relationship with malnutrition (66); moreover, a worsening of the nutritional status is also observed in old subjects with depression (67). An evaluation of nutritional status and GDS in community-dwelling elderly people have also been valuable for an early identification of non-diagnosed depression in individuals with nutritional disorders (68). MNA is considered a useful tool for monitoring patients of any age, at risk of undernutrition, which is more common in MDD than overnutrition (69). Thus, there has been a growing awareness of the importance of this fact, and every time, more hospitals are contemplating the role of nutritionists to reduce health costs. In poor infrastructure areas, it has been a cost-effective measure to warn about the struggles in the quality of life of their population, always finding an association between MDD and malnourishment (70–72).

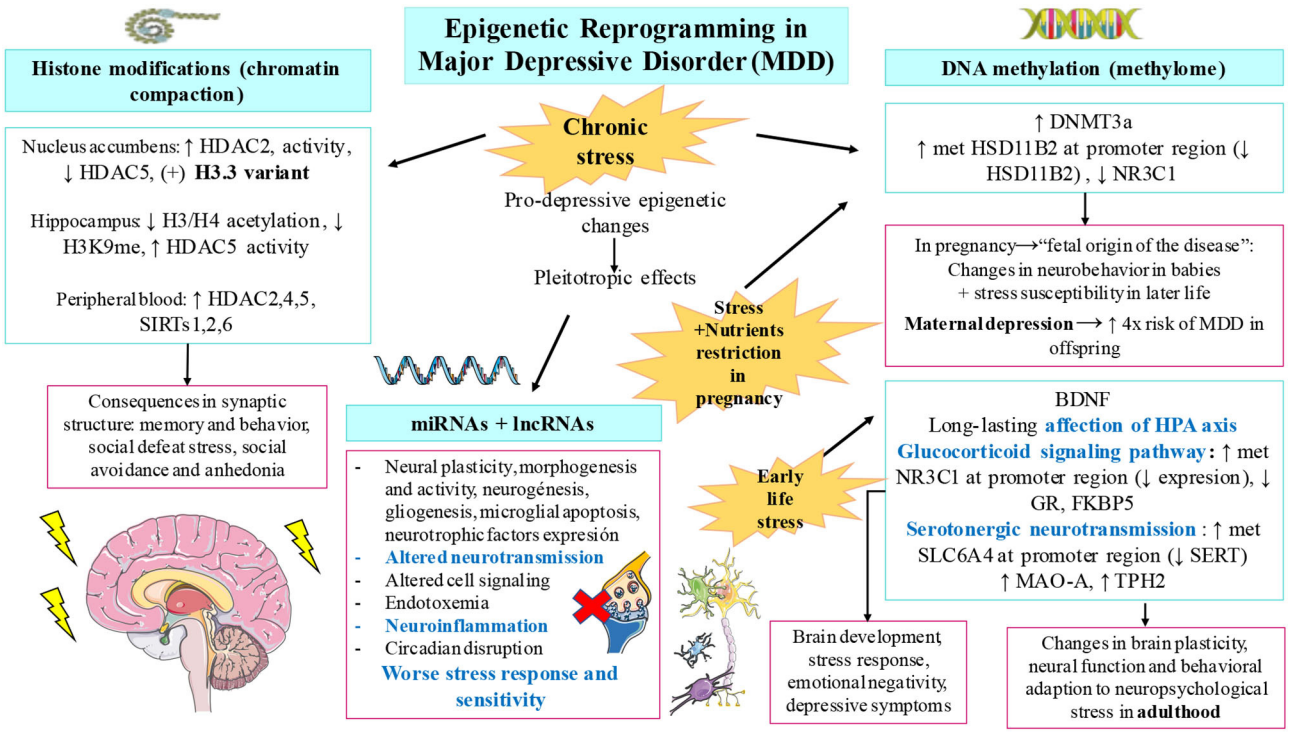

FIGURE 1 | Compiled evidence related to epigenetic changes involved in major depressive disorder (MDD). As shown, chronic stress, early-life stress, and prenatal stress accompanied with nutrient restriction are pivotal drivers of the epigenetic modifications observed in patients with MDD. These changes include histone modifications, altered DNA methylation patterns, and the dysregulation of non-coding RNAs including microRNAs (miRNAs) and long non-coding RNA (lnRNA). Some of the most relevant findings collected in this manuscript for each modification are summarized. These variations lead to important alterations in the brain synapsis, anhedonia, social defeat stress, neurodevelopment, brain plasticity and function, and many other depressive symptoms.

Furthermore, some studies have introduced anthropometric parameters where the tendency showed abdominal obesity or higher amount of abdominal fat in patients with depression (73). Systematic reviews have found solid data in the association between depression, anthropometric parameters, and body image in all included studies, notwithstanding the different statistical methods employed. It is frequent to find among individuals with depressive symptoms: women perceiving their body bigger than reality and men perceiving themselves as underweight idealizing larger bodies (74). Recent studies have identified anthropometric parameters as risk markers (e.g., waist-to-hip ratio) for suicide ideation and severity of illness in women with postnatal depression (75).

Furthermore, to assess concretely nutritional deficiencies, questionnaires about food intake and biochemical markers measurements are the norm. Metabolic parameters include low hematocrit, low high-density lipoprotein cholesterol (HDL-C), and high triglyceride levels in patients with depression (76). More precisely and above mentioned, concrete groups of essential micronutrients are often much lower in these patients. Patients with MDD lack vitamin B consumption, especially cobalamin (B12) and folate (B9) (73, 77), as well as pyridoxin (B6) (78). Low vitamin D serum levels are positively associated with depression (79), although insufficient dietary intake is not the only cause, being little outdoor exposure to sunshine is more relevant (80). Moreover, low circulating ω-3 PUFA has been linked not only to MDD but also to preterm birth and prenatal depression associates with preterm birth (81). Low intake of marine ω-3 PUFA, especially docosahexaenoic acid (DHA), increases the risk of many mental issues, besides MDD, suicidal ideation, bipolar disorder, autism, and attention deficit hyperactivity disorder (82). Eventually, there is an insufficient intake in minerals, commonly calcium, iron, magnesium, and zinc (83). The list is even longer in the case of women, but not men, with depressive symptoms according to recent studies, including also potassium, phosphorus, and copper (84). All these nutrients are vital for monoamines synthesis, neuroinflammation control, neuroprotection, and the synthesis of growth factors (85).

To address these deficiencies, it is of note to be aware about changing patients' nutritional behavior and the diet composition prior to the onset of MDD and during the course. Food patterns heading depression are kept in the course of the disorder: poor appetite, skipping meals, and sometimes, a dominant preference for high-sugar foods (emotional eating) (86). There is recent research establishing relationship between macronutrients and depression through surveys in big samples of patients. The results showed a significant low proportion of protein intake associated with the prevalence of MDD (87). Food frequency questionnaires have shown the important issue of quality and quantity of protein intake, being low consumption of protein-rich foods such as milk,

and legumes significantly associated with higher mean scores of depression and anxiety symptoms (88, 89). Diet is also known to be the greatest shaper of gut microbiota, and this complex "organ" is even involved in the synthesis of vitamin B and may affect host vitamin B usage (90, 91). In fact, B12 intake or status is associated with microbial diversity, relative abundance of bacteria, and short chain fatty acids (SCFAs) production (92). Then, the underlying characteristic gut dysbiosis of MDD might not supply those vitamins apart from dietary sources.

Comorbidities and Eating Disorders in MDD

Furthermore, several comorbidities associated to dietary habits and intestinal problems frequently co-occur with high prevalence in patients diagnosed with MDD and vice versa. In this context, there is a high co-occurrence of inflammatory bowel disease (IBD) with MDD and/or anxiety, and observational prospective studies denote a high incidence of MDD in patients with diagnosed IBD (93). There is bidirectionality: on one hand, this is observed to be due to poor self-management, which leads to disease chronicity (94), but in contrast, there is evidence that the course of IBD is worse in patients with depression, being the corticosteroid treatment able to induce the psychiatric symptom onset (95). Systematic reviews explain that patients with IBD had 20% prevalence rate of anxiety and 15% prevalence rate of depression until 2016 (96), but the rising prevalence of both kind of maladies has changed numbers until 2021, being 33 and 25% currently, respectively (97). Some empirical studies demonstrated that the symptoms of anxiety/depression are related to more aggressive forms of IBD, emphasizing that psychiatric treatment is also vitally important to ameliorate the prognosis of IBD (98, 99). Fortunately, some statistical data have been reunited identifying the selectively protective role of certain antidepressants for Crohn's disease and ulcerative colitis, including monoamine oxidase inhibitors, serotonin norepinephrine reuptake inhibitors, selective serotonin reuptake inhibitors, serotonin modulators; and tricyclic antidepressants (100).

Metabolic disturbances can also occur after the onset of MDD or before, including obesity, type 2 diabetes mellitus, or metabolic syndrome. Some evidence alleges that metabolic signaling of leptin and ghrelin might play a great part in the dysregulation of mood (101). In this line, metabolic dysregulation seems to go hand in hand with chronic stress and mental disorders. High leptin levels and binge eating and emotional eating are positively associated. This hormone is involved in reward circuits whose maladjustment leads to pathological eating behaviors (102). High daily cortisol is sometimes related to hyperleptinemia, making individuals more vulnerable to stress-induced eating (103). Moreover, emotional eating is not the norm; especially in late-life depression, there is a high tendency to appetite loss and involuntary weight loss (104). In scientific literature, we may find two subgroups of MDD according to appetite changes; these are the terms, "depression-related increases in appetite" and "depression-related appetite loss." The first one is associated with a hyperactivation of mesocorticolimbic dopamine reward circuits, whereas the latter is associated with a hypoactivation of mid-insular cortex implicated in interoceptive and homeostatic signaling (105).

All in all, overconsumption does not guarantee vitamins, minerals, and other essential nutrients herein discussed and definitely neither does undernutrition. A consequent maladaptation from inadequate dietary habits entails metabolic changes, which are associated to severity of symptoms and other comorbidities. The turning point that comes next is to find the link between those deficiencies and subjacent epigenetic molecular mechanisms, which take part in the basis of MDD pathophysiology.

Epigenetic Roles of Diet and Nutritional Status in MDD

Diet is being considered an environmental epigenetic factor, with nutritional epigenetics being the science that intends to explain the effects of nutrients on gene expression and metabolism (106). This field aims to explain the association of suboptimal nutritional environment as a driver of potential adult-onset chronic illnesses due to shifts in genome functions (107). *Landecker* reviewed and argued that some genomes immersed in food molecules might be more susceptible to epigenetic lability than others predisposing them to a determined susceptibility to disease (108). On the one hand, some bioactive food compounds are able to exert protective properties, and in contrast, recently, it has been studied that some components from western-type diets, ultraprocessed food, and their lack of essential nutrients also modulates negatively epigenetics machinery (109, 110).

Diet as Lifestyle Habit

An adequate nutrition is essential during development, in prenatal and postnatal periods of life, what in fact, it is called "window of opportunity," the first 1,000 days from pregnancy to 2nd birthday (111, 112). Epidemiological studies assure that maternal nutrition in development provides a wide variety of epigenetic changes being key for susceptibility to disease phenotypes in later life (113). A great part of modifications occurs during early embryonic and primordial cell development, although what we have not completely understood is their potential echo in this "later life" (114).

The underlying biological mechanisms have been deeply watched in animal models. What evidence says is that inadequate maternal nutrition patterns, either undernutrition or overnutrition, exert alterations in DNA methylation mechanisms in the hypothalamus, concretely in pathways involved in energy homeostasis, with an echo in adulthood. A maintained protein restriction in postnatal development was related to an immature hypothalamus as well (115–117). Other findings related to high-fat diet consumption during pregnancy were the upregulation of dopamine reuptake transporter (DAT) in the ventral tegmental area, NA, and prefrontal cortex and a downregulation of DAT in the hypothalamus. These data result from changes in DNA hypomethylation at promoter regions of DAT, and the association observed was long-term alterations in the expression of dopamine and opioid-related genes, as well as changes in food behavior (preference for more palatability) (118). Conversely, undernutrition is associated with hypomethylation

of hypothalamic GR without changes in the hippocampus, contributing to altered energy balance regulation in the offspring (119). Nevertheless, even in adult life, maladaptive embryonic and perinatal epigenetic changes can potentially be reversed or attenuated; it is known that epigenetic marks are really plastic (120). Although the epigenome is shaped by nutritional states, even those more stable are malleable by implementing a different diet (121). This can be possible with nutrient-rich bioactive foods or with food-based bioactive components (e.g., polyphenols, ω-3 PUFA, resveratrol, curcumin, and green-tea compounds, among many others), opening the gate to prevention and treatment of multifactorial non-communicable diseases and mental disorders, including MDD (122) as it will be addressed later. Many dietary components have the power to influence pathways that change DNA methylation patterns, and the evidence has demonstrated the biochemical routes between the diet quality and mental health (123). Maintaining an environmental stressor such as western-type diets, full of ultraprocessed foods, denotes imbalance of macronutrients and deficiencies in micronutrient levels, as above reported in malnutrition associated with the patients with depression. These have been correlated with alterations in behavior, but the consequent maladaptation of the epigenome has not been elucidated yet in the context of MDD pathophysiology.

Nutrients are needed to accomplish biological functions. One of the epigenome-diet hallmarks involves methionine and folate from the diet, whose metabolism gives rise to S-adenosylmethionine (SAMe), considered as the universal methyl donor for DNA and histone methylation reactions. Nutrient availability will provide SAMe, and this will heavily control gene expression (124). Affecting SAMe metabolism and deficiencies in B6, B9, B12, and zinc (which act many times as cofactors for enzymes and methyl donors) are correlated to high homocysteine levels, a risk factor traditionally associated with multifactorial inflammatory diseases and now also with MDD, psychosis, suicide ideation, or alexithymia (125–127).

Psychiatric involvement of B12 deficiencies with high homocysteine and methylmalonic acid denotes memory impairment, depression, and other manifestations (i.e., mania, psychotic symptoms, and obsessive compulsive disorder) (128–131). For these reasons, B12 levels were proposed to be assessed in neuropsychiatric disorders and neurodegenerative diseases and advised to be evaluated with treatment resistant disorders and certain risk factors that link malnutrition with MDD, including alcoholism, advancing age with neurological symptoms, anemia, intestinal problems, and malabsorption or strict vegetarian diets (132, 133). These causes would also explain the associated dysbiosis that, due to cobalamin deficiency, destabilizes microbial communities, who would also not be able to produce microbial B12 (134, 135).

Low levels of B6, B9, and B12 are shown to affect methylation levels of redox-related genes. This has been observed in NUDT15 (Nudix hydrolase 15, a hydrolase of nucleoside diphosphates) and TXNRD1 (thioredoxin reductase 1) hypermethylation (31, 136). Thus, the role of oxidative stress of these vitamins is crucial for brain protection (137, 138). In addition, lacking these essential vitamins for neuronal function affects monoamine oxidase production and the repair of phospholipids (139). This could be extrapolated to the reported neurotransmission impairments first due to imbalanced neurotransmission synthesis and second due to damage at axonal and soma membranes (128, 140). These symptoms are in concordance with co-deficiencies of ω-3 PUFA, especially DHA, which is important for neuronal membrane fluidity and neurotransmitter release (82).

Moreover, low protein intake entails scarcity of essential amino acids such as valine, leucine, isoleucine, lysine, phenylalanine, tyrosine, arginine, histidine, and tryptophan, which are necessary precursors for neurotransmitter and neuromodulator synthesis (141–143). For instance, phenylalanine and tyrosine are two essential precursors for the biosynthesis of dopamine, norepinephrine, and epinephrine (144). For its part, vitamin D deficiency is one of the most repeated manifestations in MDD (145), and the reasons are not only subjacent an insufficient dietary intake but also an insufficient outdoor exposure to sunshine (80). The clinical relevance of these observations is known, thanks to preclinical models that have identified their immunomodulator and neuromodulator roles, with protective effects for oxidative stress as well (146). It is known that vitamin D is key for the proper development of dopaminergic neurons and the expression of GDNF (147), and now many vitamin D receptors (VDRs) are found in the substantia nigra, where the enzyme 1α-hydroxylase (CYP27B1) converts it to its active form (148, 149). VDR and CYP27B1 genes can become hypermethylated at promoter regions becoming silenced, and also VDR protein when meeting its ligands can establish contact with histone demethylases, reconfiguring chromatin modeling (150). Vitamin D also has the ability to exert potent antioxidant effects that ease DNA repair, defense against infections, and protection from oxidative stress-related protein oxidation (151).

Notably, many nutrient-related links that may alter MDD pathophysiology have overlapping etiology aspects with neurodegenerative diseases such as Alzheimer's and Parkinson's diseases (152). A deep understanding of these diet-related epigenetic shifts becomes necessary, highlighting complementary branches such as nutritional neuroscience and nutritional psychology for the integrative study of MDD aiming to improve prognosis or prevent the onset of MDD and neurological impairments.

Diet in Microbiota Neuromodulation

Regarding food consumption, much research has focused on the effects of diet and lifestyle on epigenetic reprogramming. Although some dietary components may exert some direct epigenetic effects, prior studies have noticed a critical interplay between diet and gut microbiota in the epigenetic profile of the host (153). As we know, the microbiota-gut-brain axis is a bidirectional system, and considering diet as the greatest shaper of gut microbiome, microbial metabolite production is undeniably diet-dependent. For example, it is known that tryptophan levels allow microbial serotonin synthesis (154), or dietary fiber allows GABA, norepinephrine, tryptamine, and dopamine microbial synthesis (155). Thus, we emphasized that diet potentially modulates microbial contributions to the neurotransmission system in the human gut.

Moreover, mainly, dietary fiber drives to the production of SCFAs using the gut microbiota, acting as HDAC inhibitors, and regulating DNA methylation, histone modifications, and chromatin restructuring to alter gene expression (156). One proven effect of the epigenetic and antidepressant action of SCFAs was described in a mice model. In this study, the inhibition of HDAC by SCFAs led to the hyperacetylation of histones H3/H4 resulting in an increased BDNF expression (157). SCFAs production is even lessened due to the co-deficiencies of certain vitamins, which exert important roles in intestinal homeostasis too. *Pham et al.* reviewed and summarized the positive effects of adequate levels of vitamins on gut microbiota health: vitamins A, B2, D, E, and beta-carotene increase relative abundance of commensals; vitamins A, B2, B3, C, and K increase diversity; vitamin D boosts diversity; and vitamin C, B2, and E enhance SCFAs production (158).

Diet and miRNAs

In this study, it faced an emerging and challenging research area. Some disease-specific miRNAs profiles have been associated to MDD, and the expression of these molecules can be affected by dietary factors (25). Posttranscriptional regulation through miRNAs depends on sensory functions from carbohydrates, proteins, fat, vitamins, minerals, and fiber (159). Deficiency or excess of certain nutrients at any age, from embryonic development to senescence, has been correlated to disease onset. The mechanisms exerted from nutrient absorption are the expression of different profiles of miRNAs, which will target other components from epigenetic machinery, affecting DNA methylation and histone modification and then the gene expression at different levels: immunophenotypes and inflammation/immunoregulation balance, cardiovascular health, insulin sensitivity/resistance, and muscle health (160). For instance, the research says that over intake of fat combined with low vitamin D intake leads to dyslipidemia by impairments in miRNAs expression, which is also related to macrophages polarization in associated digestive comorbidities mentioned such as IBD (160, 161).

More recently, in the past decade, it was discovered that some food-derived miRNAs (xenomiRs) from plant and animal sources affect individual's gene expression, suggesting a cross-kingdom communication (162, 163). However, several studies have found difficulties to distinguish most dietary from endogenous miRNAs and disparity of results in this new field of food science. In this sense, there are already hypothesis to prove, for instance, for checking how miRNAs-deficient diet may influence health and disease (164). Nonetheless, milk exosomes and their miRNA cargos have been found in different mammalian organs (e.g., liver, spleen, brain, and intestinal mucosa) (165), and exogenous plant miRNAs have been found in mammalian tissues targeting low-density lipoprotein receptor adapter protein 1 (LDLRAP1), decreasing low-density lipoproteins (LDLs) in plasma (166). Some authors have also suggested that gut microbiota status may ease or not xenomiRs bioavailability through exosome like nanoparticles at the same time that xenomiRs may modulate microbiome functions (163). There are interesting studies about it, for example, ginger exosomes are mainly absorbed by *Lactobacillus rhamnosus* and promote IL-22 production improving intestinal barrier (167).

A proposal of further research would be interesting for the link between miRNAs profiles that have been already identified in MDD and if certain dietary behaviors contribute to their different expression having an impact on the pathophysiology.

TRANSLATIONAL APPROACHES: TARGETING THE EPIGENOME THROUGH DIET FOR THE PATIENT WITH MDD

In the last section, the nutritional status of subjects with depression and the epigenetic consequences were reviewed. In this study, we will discuss the most relevant studies regarding the benefits from receiving nutritional support and how this may modulate the epigenetics of brain and the body of individuals with MDD.

First, it should be mentioned here the main strategies currently used in the clinical management for MDD. As mentioned above, MDD is presented by the diagnosis of at least one of the two main criteria, namely, loss of interest (i.e., anhedonia) or depressed mood and $\geq$4 somatic and non-somatic items (such as loss of appetite, insomnia, and low energy), minimum presented in a period of 2 weeks (168). These makes MDD a very heterogeneous disorder, with many therapeutic difficulties. For instance, notwithstanding the use of antidepressants is widely accepted for the therapy of MDD, cumulative evidence supports that the use of antidepressants and current clinical guidelines may not be sufficient for an important part of subjects with depression, especially for those with severe symptoms, that exert worse clinical outcomes despite receiving greater intensity of treatment (169). Besides, $\sim$30% of people with MDD are resistant to conventional treatment (170), and there is still a big debate about if the main benefits of antidepressants are due to their action or if conversely, it may be attributed to the placebo effect (171, 172). This could be due to the fact that many antidepressants target serotoninergic and monoamine neurotransmission, which traditionally has been claimed as the major pathophysiological mechanism of MDD (173, 174). However, as previously described, currently, it is widely accepted that MDD is associated with a plethora of additional pathophysiological mechanisms. Because of that, it is necessary to accept the huge difficulties in the clinical management of patients with MDD; there is an urgent need for improving the clinical guidelines and for reviewing multidisciplinary approaches that may bring the maximum benefits to these patients.

In this great context, nutritional interventions can be excellent supportive strategies in MDD. A meta-analysis conducted by Firth et al. (175) including 45,826 participants show that dietary interventions may be of great aid for the prevention and amelioration of depressive symptoms. However, most subjects were not diagnosed with clinical depression, so their conclusions might not be extrapolated to MDD. Recently, an umbrella meta-analysis conducted by Xu et al. (176) has obtained some important results establishing an inverse relationship between different nutritional approaches, group of foods, and nutrients

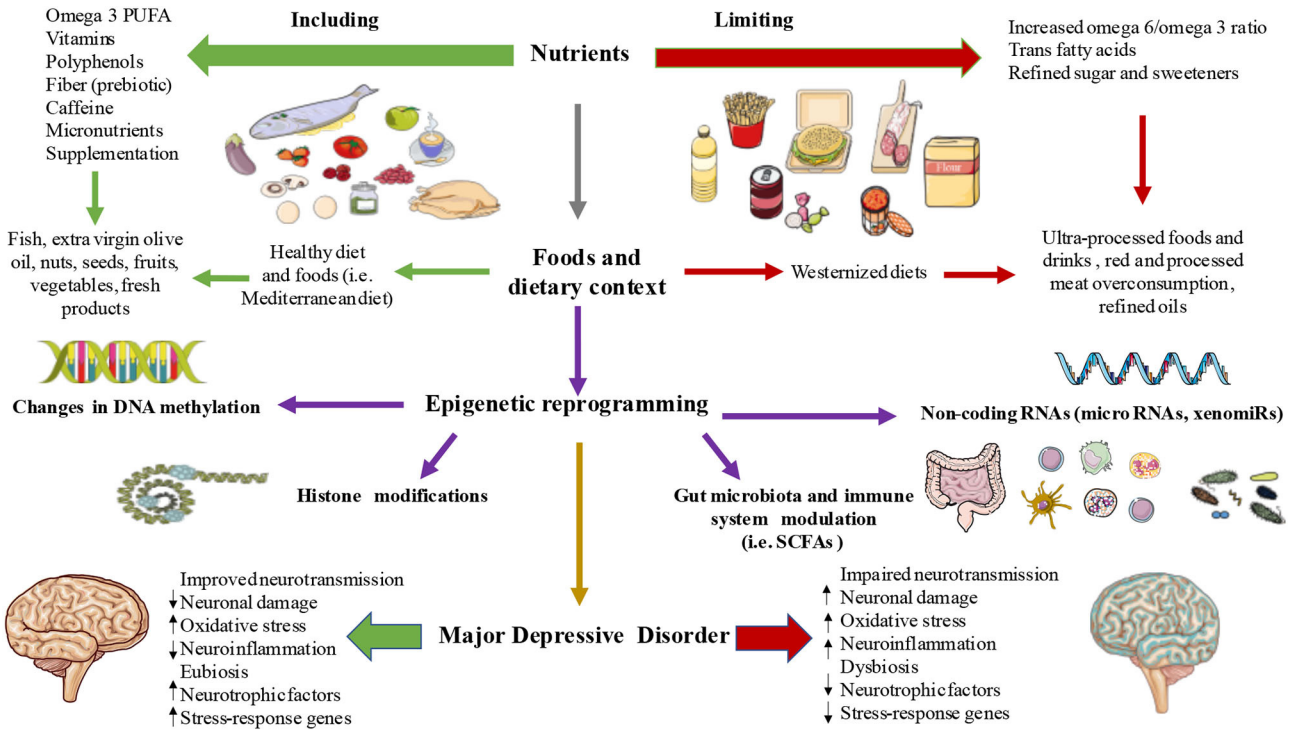

FIGURE 2 | The link between diet, epigenetics, and MDDs. As summarized, a set of nutrients, foods, and dietary strategies are able to influence different epigenetic mechanisms like DNA methylation, histone modifications, non-coding RNAs, and gut microbiota-immune system composition and their products thereby influencing in the pathophysiology of MDD.

in the prevention and treatment of depression. However, the methodological quality of most of the selected meta-analysis was low or very low, which may also bring some caution with their results. In fact, some studies have argued that most narrative reviews come to strong benefits from dietary interventions in patients with MDD, despite the level of evidence is still inconsistent (177). Then, they conclude that more systematic reviews and objective data are needed before stablishing some conclusions, and we encourage for further research and studies in this field.

Previously, we defined the epigenetic consequences of malnutrition in patients with MDD. As detailed, subjects with depression often exhibited different concerns in their intake of macro- and micronutrients. Then, by modulating the levels of these nutrients, it is possible to address the multiple issues related to their nutritional deficits and overconsumption. Thus, patients with MDD will benefit from two different ways of the nutritional intervention, namely, (1) By limiting their consumption of unhealthy products and nutrients and (2) by addressing the nutritional deficiencies. In this sense, diet has the potential to aid in the clinical management of MDD. It is worthy to mention that there are neither a single nor best option for the general population with depression; conversely, the most important part of a healthy diet is to provide an adequate intake of macronutrients, micronutrients, and hydration to meet the physiological needs of the body (178). Thus, a healthy diet contains a wide variety of foods of nutritional interest, which are crucial for health preservation. Besides, to those foods or part of them with promising actions either in the prevention or as a therapeutic adjuvant of different NCDs are defined as "Nutraceuticals" (179). What evidence seems to support is that there are specific group of foods and nutrients with promising antidepressant effects, most of them included in a healthy dietary pattern such as Mediterranean diet (180–183).

Overall, because of the growing awareness of the critical role of diet in the management and prevention of MDD, we encourage for the development of further studies in this area regarding different dietary approaches and group of foods and nutrients/bioactive compounds with promising benefits for the treatment of MDD, focusing on their epigenetic role as a promising point to consider explaining their positive effects.

CONCLUSION

The link between nutritional epigenetics and MDD composes a new field of research. A deep understanding of these diet-related epigenetic shifts becomes necessary highlighting complementary branches such as nutritional neuroscience and nutritional psychology for the integrative study of MDD. This review intended to unify different areas of research to serve as a link between malnutrition-related epigenetic changes that seem to be involved in MDD pathophysiology as summarized in **Figure 2**. Perhaps, not many studies have demonstrated the

clear association to determine causality from observational studies, and it is undeniable that more empirical data are needed. However, as we herein followed, the epigenetic role of diet demonstrates that it can alter several neuronal pathways (e.g., DAT, GR, HPA axis, neuronal membrane fluidity, neurotransmission, microbial neurotransmitters synthesis, neuronal damage, oxidative stress, and a long etcetera), that have been studied in the context of MDD pathophysiology, and new advances in clinical trials are demonstrating promising results in the reversion or attenuation of those epigenetic marks. There are misunderstandings yet in the pathophysiology of MDD in general and in the still developing field of associated epigenetic drivers, even more, especially in the knowledge of the relationship between malnutrition-consequent epigenetic markers involved in MDD pathophysiology. Fortunately, we are on the era in which precision medicine, integrative therapies, and the premise "we are what we eat" are gaining stronger echo.

AUTHOR CONTRIBUTIONS

All authors listed have made a substantial, direct, and intellectual contribution to the work and approved it for publication.

FUNDING

This study was partially supported by grants from the Fondo de Investigación de la Seguridad Social, Instituto de Salud Carlos III (PI18/01726 and PI19/00766), Spain, Programa de Actividades de I+D de la Comunidad de Madrid en Biomedicina (B2017/BMD3804 and B2020/MITICAD-CM), and HALEKULANI S.L.

ACKNOWLEDGMENTS

ÓF-M had a predoctoral fellowship from the University of Alcalá during the course of this work.

REFERENCES

1. Otte C, Gold SM, Penninx BW, Pariante CM, Etkin A, Fava M, et al. Major depressive disorder. *Nat Rev Dis Prim.* (2016) 2:16065. doi: 10.1038/nrdp.2016.65
2. Malhi GS, Mann JJ. Depression. *Lancet.* (2018) 392:2299–312. doi: 10.1016/S0140-6736(18)31948-2
3. Ferrari AJ, Somerville AJ, Baxter AJ, Norman R, Patten SB, Vos T, et al. Global variation in the prevalence and incidence of major depressive disorder: a systematic review of the epidemiological literature. *Psychol Med.* (2013) 43:471–81. doi: 10.1017/S0033291712001511
4. Santomauro DF, Mantilla Herrera AM, Shadid J, Zheng P, Ashbaugh C, Pigott DM, et al. Global prevalence and burden of depressive and anxiety disorders in 204 countries and territories in 2020 due to the COVID-19 pandemic. *Lancet.* (2021) 398:1700–12. doi: 10.1016/S0140-6736(21)02143-7
5. García-Montero C, Ortega MA, Alvarez-Mon MA, Fraile-Martinez O, Romero-Bazán A, Lahera G, et al. The problem of malnutrition associated with major depressive disorder from a sex-gender perspective. *Nutrients.* (2022) 14:1107. doi: 10.3390/nu14051107
6. Arias de la Torre J, Vilagut G, Ronaldson A, Dregan A, Ricci-Cabello I, Hatch SL, et al. Prevalence and age patterns of depression in the United Kingdom a population-based study. *J Affect Disord.* (2021) 279:164–72. doi: 10.1016/j.jad.2020.09.129
7. Orsolini L, Latini R, Pompili M, Serafini G, Volpe U, Vellante F, et al. Understanding the complex of suicide in depression: from research to clinics. *Psychiatry Investig.* (2020) 17:207. doi: 10.30773/pi.2019.0171
8. Lépine JP, Briley M. The increasing burden of depression. *Neuropsychiatr Dis Treat.* (2011) 7:3–7. doi: 10.2147/NDT.S19617
9. Greenberg PE, Fournier AA, Sisitsky T, Simes M, Berman R, Koenigsberg SH, et al. The economic burden of adults with major depressive disorder in the United States (2010 and 2018). *Pharmacoeconomics.* (2021) 39:653–65. doi: 10.1007/s40273-021-01019-4
10. Culpepper L. Understanding the burden of depression. *J Clin Psychiatry.* (2011) 72:e19. doi: 10.4088/JCP.10126tx1c
11. Namkung H, Lee BJ, Sawa A. Causal inference on pathophysiological mediators in psychiatry. *Cold Spring Harb Symp Quant Biol.* (2018) 83:17–23. doi: 10.1101/sqb.2018.83.037655
12. Driver MN, Kuo SIC, Dick DM. Genetic feedback for psychiatric conditions: where are we now and where are we going. *Am J Med Genet B Neuropsychiatr Genet.* (2020) 183:423. doi: 10.1002/ajmg.b.32815
13. Assary E, Vincent JP, Keers R, Pluess M. Gene-environment interaction and psychiatric disorders: review and future directions. *Semin Cell Dev Biol.* (2018) 77:133–43. doi: 10.1016/j.semcdb.2017.10.016
14. Hamilton JP. Epigenetics: principles and practice. *Dig Dis.* (2011) 29:130–5. doi: 10.1159/000323874
15. Ptak C, Petronis A. Epigenetic approaches to psychiatric disorders. *Dialogues Clin Neurosci.* (2010) 12:25. doi: 10.31887/DCNS.2010.12.1/cptak
16. Keverne J, Binder EB. A review of epigenetics in psychiatry: focus on environmental risk factors. *Medizinische Genet.* (2020) 32:57–64. doi: 10.1515/medgen-2020-2004
17. McGowan PO, Meaney MJ, Szyf M. Diet and the epigenetic (re)programming of phenotypic differences in behavior. *Brain Res.* (2008) 1237:12–24. doi: 10.1016/j.brainres.2008.07.074
18. Pizzorusso T, Tognini P. Interplay between metabolism, nutrition and epigenetics in shaping brain DNA methylation, neural function and behavior. *Genes.* (2020) 11:1–18. doi: 10.3390/genes11070742
19. Allison J, Kaliszewska A, Uceda S, Reiriz M, Arias N. Targeting DNA methylation in the adult brain through diet. *Nutrients.* (2021) 13:3979. doi: 10.3390/nu13113979
20. Gezahegn E, Edris M, Dachew BA. Prevalence and factors associated with undernutrition among adults with major depressive disorder in northwest Ethiopia. *Psychiatry J.* (2016) 2016:1–7. doi: 10.1155/2016/7034582
21. National Human Genome Research Institute (NIH). *Epigenetics.* Available online at: https://www.genome.gov/genetics-glossary/Epigenetics (accessed January 12, 2022).
22. Nestler EJ, Peña CJ, Kundakovic M, Mitchell A, Akbarian S. Epigenetic basis of mental illness. *Neuroscientist.* (2016) 22:447–63. doi: 10.1177/1073858415608147
23. Penner-Goeke S, Binder EB. Epigenetics and depression. *Dial Clin Neurosci.* (2019) 21:397–405. doi: 10.31887/DCNS.2019.21.4/ebinder
24. Huang X, Luo YL, Mao YS, Ji JL. The link between long noncoding RNAs and depression. *Prog Neuropsychopharmacol Biol Psychiatry.* (2017) 73:73–8. doi: 10.1016/j.pnpbp.2016.06.004
25. Ortega MA, Alvarez-Mon MA, García-Montero C, Fraile-Martinez O, Lahera G, Monserrat J, et al. MicroRNAs as critical biomarkers of major depressive disorder: a comprehensive perspective. *Biomedicines.* (2021) 9:1659. doi: 10.3390/biomedicines9111659
26. Nestler EJ. Epigenetic mechanisms of depression. *JAMA Psychiatry.* (2014) 71:454. doi: 10.1001/jamapsychiatry.2013.4291
27. Uchida S, Yamagata H, Seki T, Watanabe Y. Epigenetic mechanisms of major depression: targeting neuronal plasticity. *Psychiatry Clin Neurosci.* (2018) 72:212–27. doi: 10.1111/pcn.12621

28. Lester BM, Conradt E, Marsit CJ. Epigenetic basis for the development of depression in children. *Clin Obstet Gynecol.* (2013) 56:556. doi: 10.1097/GRF.0b013e318299d2a8
29. Park C, Rosenblat JD, Brietzke E, Pan Z, Lee Y, Cao B, et al. Stress, epigenetics and depression: a systematic review. *Neurosci Biobehav Rev.* (2019) 102:139–52. doi: 10.1016/j.neubiorev.2019.04.010
30. UniProt. Available online at: https://www.uniprot.org/ (accessed January 15, 2022).
31. *GeneCards - Human Genes | Gene Database | Gene Search.* Available online at: https://www.genecards.org/ (accessed January 15, 2022).
32. Dalton VS, Kolshus E, McLoughlin DM. Epigenetics and depression: return of the repressed. *J Affect Disord.* (2014) 155:1–12. doi: 10.1016/j.jad.2013.10.028
33. Bagot RC, Labonté B, Peña CJ, Nestler EJ. Epigenetic signaling in psychiatric disorders: stress and depression. *Dialogues Clin Neurosci.* (2014) 16:281–95. doi: 10.31887/DCNS.2014.16.3/rbagot
34. Wiley JW, Higgins GA, Athey BD. Stress and glucocorticoid receptor transcriptional programming in time and space: implications for the brain–gut axis. *Neurogastroenterol Motil.* (2016) 28:12. doi: 10.1111/nmo.12706
35. Bhasin M, Reinherz EL, Reche PA. Recognition and classification of histones using support vector machine. *J Comput Biol.* (2006) 13:102–12. doi: 10.1089/cmb.2006.13.102
36. Peterson CL, Laniel MA. Histones and histone modifications. *Curr Biol.* (2004) 14:R546–51. doi: 10.1016/j.cub.2004.07.007
37. Peña CJ, Nestler EJ. Progress in epigenetics of depression. *Prog Mol Biol Transl Sci.* (2018) 157:41–66. doi: 10.1016/bs.pmbts.2017.12.011
38. Sun H, Kennedy PJ, Nestler EJ. Epigenetics of the depressed brain: role of histone acetylation and methylation. *Neuropsychopharmacology.* (2013) 38:124–37. doi: 10.1038/npp.2012.73
39. Jarome TJ, Lubin FD. Histone lysine methylation: critical regulator of memory and behavior. *Rev Neurosci.* (2013) 24:375–87. doi: 10.1515/revneuro-2013-0008
40. Golden SA, Christoffel DJ, Heshmati M, Hodes GE, Magida J, Davis K, et al. Epigenetic regulation of synaptic remodeling in stress disorders. *Nat Med.* (2013) 19:337. doi: 10.1038/nm.3090
41. Park HS, Kim J, Ahn SH, Ryu HY. Epigenetic targeting of histone deacetylases in diagnostics and treatment of depression. *Int J Mol Sci.* (2021) 22:5398. doi: 10.3390/ijms22105398
42. Dai Y, Wei T, Shen Z, Bei Y, Lin H, Dai H. Classical HDACs in the regulation of neuroinflammation. *Neurochem Int.* (2021) 150:105182. doi: 10.1016/j.neuint.2021.105182
43. Otsuki K, Uchida S, Hobara T, Yamagata H, Watanabe Y. Epigenetic regulation in depression. *Japanese J Neuropsychopharmacol.* (2012) 32:181–6.
44. Valvassori S, Varela R, Arent C, Dal-Pont G, Bobsin T, Budni J, et al. Sodium butyrate functions as an antidepressant and improves cognition with enhanced neurotrophic expression in models of maternal deprivation and chronic mild stress. *Curr Neurovasc Res.* (2014) 11:359–66. doi: 10.2174/1567202611666140829162158
45. Wei Y. Bin; Melas PA, Wegener G, Mathe AA, Lavebratt C. Antidepressant-like effect of sodium butyrate is associated with an increase in TET1 and in 5-hydroxymethylation levels in the Bdnf gene. *Int J Neuropsychopharmacol.* (2015) 18:pyu032. doi: 10.1093/ijnp/pyu032
46. Januar V, Saffery R, Ryan J. Epigenetics and depressive disorders: a review of current progress and future directions. *Int J Epidemiol.* (2015) 44:1364–87. doi: 10.1093/ije/dyu273
47. Peña CJ, Monk C, Champagne FA. Epigenetic effects of prenatal stress on 11β-hydroxysteroid dehydrogenase-2 in the placenta and fetal brain. *PLoS ONE.* (2012) 7:e39791. doi: 10.1371/journal.pone.0039791
48. Zhu P, Wang W, Zuo R, Sun K. Mechanisms for establishment of the placental glucocorticoid barrier, a guard for life. *Cell Mol Life Sci.* (2019) 76:13–26. doi: 10.1007/s00018-018-2918-5
49. Appleton AA, Lester BM, Armstrong DA, Lesseur C, Marsit CJ. Examining the joint contribution of placental NR3C1 and HSD11B2 methylation for infant neurobehavior. *Psychoneuroendocrinology.* (2015) 52:32–42. doi: 10.1016/j.psyneuen.2014.11.004
50. O'Donnell KJ, Meaney MJ. Fetal origins of mental health: the developmental origins of health and disease hypothesis. *Am J Psychiatry.* (2017) 174:319–28. doi: 10.1176/appi.ajp.2016.16020138
51. Al-Haddad BJS, Oler E, Armistead B, Elsayed NA, Weinberger DR, Bernier R, et al. The fetal origins of mental illness. *Am J Obstet Gynecol.* (2019) 221:549–62. doi: 10.1016/j.ajog.2019.06.013
52. Talarowska M. Epigenetic mechanisms in the neurodevelopmental theory of depression. *Depress Res Treat.* (2020) 2020:6357873. doi: 10.1155/2020/6357873
53. Soga T, Teo CH, Parhar I. Genetic and epigenetic consequence of early-life social stress on depression: role of serotonin-associated genes. *Front Genet.* (2021) 11:1757. doi: 10.3389/fgene.2020.601868
54. Cicchetti D, Handley ED. Methylation of the glucocorticoid receptor gene (NR3C1) in maltreated and nonmaltreated children: associations with behavioral undercontrol, emotional lability/negativity, and externalizing and internalizing symptoms. *Dev Psychopathol.* (2017) 29:1795. doi: 10.1017/S0954579417001407
55. Watkeys OJ, Kremerskothen K, Quidé Y, Fullerton JM, Green MJ. Glucocorticoid receptor gene (NR3C1) DNA methylation in association with trauma, psychopathology, transcript expression, or genotypic variation: a systematic review. *Neurosci Biobehav Rev.* (2018) 95:85–122. doi: 10.1016/j.neubiorev.2018.08.017
56. Dirven BCJ, Homberg JR, Kozicz T, Henckens MJAG. Epigenetic programming of the neuroendocrine stress response by adult life stress. *J Mol Endocrinol.* (2017) 59:R11–31. doi: 10.1530/JME-17-0019
57. Farrell C, O'Keane V. Epigenetics and the glucocorticoid receptor: a review of the implications in depression. *Psychiatry Res.* (2016) 242:349–56. doi: 10.1016/j.psychres.2016.06.022
58. Bakusic J, Vrieze E, Ghosh M, Bekaert B, Claes S, Godderis L. Increased methylation of NR3C1 and SLC6A4 is associated with blunted cortisol reactivity to stress in major depression. *Neurobiol Stress.* (2020) 13:100272. doi: 10.1016/j.ynstr.2020.100272
59. Reul JMHM. Making memories of stressful events: a journey along epigenetic, gene transcription, and signaling pathways. *Front Psychiatry.* (2014) 5:5. doi: 10.3389/fpsyt.2014.00005
60. Cortés-Mendoza J, Díaz de. León-Guerrero S, Pedraza-Alva G, Pérez-Martínez L. Shaping synaptic plasticity: the role of activity-mediated epigenetic regulation on gene transcription. *Int J Dev Neurosci.* (2013) 31:359–69. doi: 10.1016/j.ijdevneu.2013.04.003
61. Darcet F, Mendez-David I, Tritschler L, Gardier AM, Guilloux JP, David DJ. Learning and memory impairments in a neuroendocrine mouse model of anxiety/depression. *Front Behav Neurosci.* (2014) 8:136. doi: 10.3389/fnbeh.2014.00136
62. Kostic M, Canu E, Agosta F, Munjiza A, Novakovic I, Dobricic V, et al. The cumulative effect of genetic polymorphisms on depression and brain structural integrity. *Hum Brain Mapp.* (2016) 37:2173–84. doi: 10.1002/hbm.23165
63. Zhou L, Zhu Y, Chen W, Tang Y. Emerging role of microRNAs in major depressive disorder and its implication on diagnosis and therapeutic response. *J Affect Disord.* (2021) 286:80–6. doi: 10.1016/j.jad.2021.02.063
64. . Seki T, Yamagata H, Uchida S, Chen C, Kobayashi A, Kobayashi M, et al. Altered expression of long noncoding RNAs in patients with major depressive disorder. *J Psychiatr Res.* (2019) 117:92–9. doi: 10.1016/j.jpsychires.2019.07.004
65. Liu N, Wang ZZ, Zhao M, Zhang Y, Chen NH. Role of non-coding RNA in the pathogenesis of depression. *Gene.* (2020) 735:144276. doi: 10.1016/j.gene.2019.144276
66. Alam MR, Karmokar S, Reza S, Kabir MR, Ghosh S, Mamun MA. Al geriatric malnutrition and depression: evidence from elderly home care population in Bangladesh. *Prev Med Rep.* (2021) 23:101478. doi: 10.1016/j.pmedr.2021.101478
67. Ahmadi SM, Mohammadi MR, Mostafavi SA, Keshavarzi S, Kooshesh SMA, Joulaei H, et al. Dependence of the geriatric depression on nutritional status and anthropometric indices in elderly population Iran. *J Psychiatry.* (2013) 8:92–6.
68. Cabrera, M.A.S.; Mesas AE, Garcia, A.R.L.; de Andrade SM. Malnutrition and depression among community-dwelling elderly people. *J Am Med Dir Assoc.* (2007) 8:582–4. doi: 10.1016/j.jamda.2007.07.008
69. Tsai AC, Chou YT, Chang TL. Usefulness of the Mini Nutritional Assessment (MNA) in predicting the nutritional status of

people with mental disorders in Taiwan. *J Clin Nurs.* (2011) 20:341–50. doi: 10.1111/j.1365-2702.2010.03467.x
70. Payahoo L, Khaje-Bishak Y, Gargari BP, Kabir-Alavi MB, AsghariJafarabadi M. Assessment of nutritional and depression status in free-living elderly in Tabriz, Northwest Iran. *Heal Promot Perspect.* (2013) 3:288–93. doi: 10.5681/hpp.2013.033
71. Naidoo I, Charlton KE, Esterhuizen TM, Cassim B. High risk of malnutrition associated with depressive symptoms in older South Africans living in KwaZulu-Natal, South Africa: a cross-sectional survey. *J Heal Popul Nutr.* (2015) 33:1–8. doi: 10.1186/s41043-015-0030-0
72. Akodu BA, Akinwunmi SO, Onajole A. 79 Relationship between depression and nutritional status among the elderly attending selected primary healthcare centers in Lagos. *Age Ageing.* (2021) 50:i12–42. doi: 10.1093/ageing/afab030.40
73. Kaner G, Soylu M, Yüksel N, Inanç N, Ongan D, Başmisirli E. Evaluation of nutritional status of patients with depression. *Biomed Res Int.* (2015) 2015:521481. doi: 10.1155/2015/521481
74. Silva D, Ferriani L, Viana MC. Depression, anthropometric parameters, and body image in adults: a systematic review. *Rev Assoc Med Bras.* (2019) 65:731–38. doi: 10.1590/1806-9282.65.5.731
75. AS, Nachane HB. Maternal anthropometric determinants as risk markers of suicidality and severity of illness in women with postnatal depression. *J Postgrad Med.* (2020) 66:11. doi: 10.4103/jpgm.JPGM_541_18
76. Lee BJ. Association of depressive disorder with biochemical and anthropometric indices in adult men and women. *Sci Rep.* (2021) 11:13596. doi: 10.1038/s41598-021-93103-0
77. Gargari BP, Saboktakin M, Mahboob S, Pourafkari N. Nutritional status in patients with major depressive disorders: a pilot study in Tabriz, Iran. *Heal Promot Perspect.* (2012) 2:145–52. doi: 10.5681/hpp.2012.017
78. Gougeon L, Payette H, Morais JA, Gaudreau P, Shatenstein B, Gray-Donald K. Intakes of folate, vitamin B6 and B12 and risk of depression in community-dwelling older adults: the Quebec Longitudinal Study on Nutrition and Aging. *Eur J Clin Nutr.* (2016) 70:380–85. doi: 10.1038/ejcn.2015.202
79. Anglin, R.E.S.; Samaan Z, Walter SD, Sarah DM. Vitamin D deficiency and depression in adults: systematic review and meta-analysis. *Br J Psychiatry.* (2013) 202:100–107. doi: 10.1192/bjp.bp.111.106666
80. Penckofer S, Kouba J, Byrn M, Estwing Ferrans C. Vitamin D and depression: where is all the sunshine? *Issues Ment Health Nurs.* (2010) 31:385. doi: 10.3109/01612840903437657
81. Ciesielski TH, Williams SM. Low Omega-3 intake is associated with high rates of depression and preterm birth on the country level. *Sci Rep*. (2020) 10:19749. doi: 10.1038/s41598-020-76552-x
82. Dinicolantonio JJ, O'keefe JH. The importance of marine omega-3s for brain development and the prevention and treatment of behavior, mood, and other brain disorders. *Nutrients.* (2020) 12:1–15. doi: 10.3390/nu12082333
83. Miki T, Kochi T, Eguchi M, Kuwahara K, Tsuruoka H, Kurotani K, et al. Dietary intake of minerals in relation to depressive symptoms in Japanese employees: the Furukawa Nutrition and Health Study. *Nutrition.* (2015) 31:686–90. doi: 10.1016/j.nut.2014.11.002
84. Nguyen, T.T.T.; Miyagi S, Tsujiguchi H, Kambayashi Y, Hara A, Nakamura H, et al. Association between lower intake of minerals and depressive symptoms among elderly Japanese women but not men: findings from Shika study. *Nutrients.* (2019) 11:389. doi: 10.3390/nu11020389
85. Aly J, Engmann O. The way to a human's brain goes through their stomach: dietary factors in major depressive disorder. *Front Neurosci.* (2020) 14:582853. doi: 10.3389/fnins.2020.582853
86. Rao TSS, Asha MR, Ramesh BN, Rao KSJ. Understanding nutrition, depression and mental illnesses. *Indian J Psychiatry.* (2008) 50:77. doi: 10.4103/0019-5545.42391
87. Oh J, Yun K, Chae JH, Kim TS. Association between macronutrients intake and depression in the United States and South Korea. *Front Psychiatry.* (2020) 11:207. doi: 10.3389/fpsyt.2020.00207
88. Khanna P, Aeri BT. Association of quantity and quality of protein intake with depression and anxiety symptoms among adolescent boys and girls (13-15 years) studying in public schools of Delhi. *J Nutr Sci Vitaminol.* (2020) 66:S141–8. doi: 10.3177/jnsv.66.S141
89. Li Y, Zhang C, Li S, Zhang D. Association between dietary protein intake and the risk of depressive symptoms in adults. *Br J Nutr.* (2020) 123:1290–301. doi: 10.1017/S0007114520000562
90. Yoshii K, Hosomi K, Sawane K, Kunisawa J. Metabolism of dietary and microbial vitamin b family in the regulation of host immunity. *Front Nutr.* (2019) 6:48. doi: 10.3389/fnut.2019.00048
91. LeBlanc JG, Milani C, de Giori GS, Sesma F, van Sinderen D, Ventura M. Bacteria as vitamin suppliers to their host: a gut microbiota perspective. *Curr Opin Biotechnol.* (2013) 24:160–8. doi: 10.1016/j.copbio.2012.08.005
92. Guetterman HM, Huey SL, Knight R, Fox AM, Mehta S, Finkelstein JL. Vitamin B-12 and the gastrointestinal microbiome: a systematic review. *Adv. Nutr.* (2021) 13:530–58. doi: 10.1093/advances/nmab123
93. Byrne G, Rosenfeld G, Leung Y, Qian H, Raudzus J, Nunez C, et al. Prevalence of anxiety and depression in patients with inflammatory bowel disease. *Can J Gastroenterol Hepatol.* (2017) 2017:6496727. doi: 10.1155/2017/6496727
94. Keefer L, Kane SV. Considering the bidirectional pathways between depression IBD: recommendations for comprehensive IBD care. *Gastroenterol Hepatol.* (2017) 13:164–9.
95. Graff LA, Walker JR, Bernstein CN. Depression and anxiety in inflammatory bowel disease: a review of comorbidity and management. *Inflamm Bowel Dis.* (2009) 15:1105–18. doi: 10.1002/ibd.20873
96. Neuendorf R, Harding A, Stello N, Hanes D, Wahbeh H. Depression and anxiety in patients with Inflammatory Bowel Disease: a systematic review. *J Psychosom Res.* (2016) 87:70–80. doi: 10.1016/j.jpsychores.2016.06.001
97. Barberio B, Zamani M, Black CJ, Savarino EV, Ford AC. Prevalence of symptoms of anxiety and depression in patients with inflammatory bowel disease: a systematic review and meta-analysis. *Lancet Gastroenterol Hepatol.* (2021) 6:359–70. doi: 10.1016/S2468-1253(21)00014-5
98. Gao X, Tang Y, Lei N, Luo Y, Chen P, Liang C, et al. Symptoms of anxiety/depression is associated with more aggressive inflammatory bowel disease. *Sci Rep.* (2021) 111:1440. doi: 10.1038/s41598-021-81213-8
99. Hu S, Chen Y, Chen Y, Wang C. Depression and anxiety disorders in patients with inflammatory bowel disease. *Front Psychiatry.* (2021) 12:1643. doi: 10.3389/fpsyt.2021.714057
100. Frolkis AD, Vallerand IA, Shaheen AA, Lowerison MW, Swain MG, Barnabe C, et al. Depression increases the risk of inflammatory bowel disease, which may be mitigated by the use of antidepressants in the treatment of depression. *Gut.* (2019) 68:1606–12. doi: 10.1136/gutjnl-2018-317182
101. Lutter M, Elmquist J. Depression and metabolism: linking changes in leptin and ghrelin to mood. *F1000 Biol Rep.* (2009) 1:63. doi: 10.3410/B1-63
102. Cassioli E, Rossi E, Squecco R, Baccari MC, Maggi M, Vignozzi L, et al. Reward and psychopathological correlates of eating disorders: the explanatory role of leptin. *Psychiatry Res.* (2020) 290:113071. doi: 10.1016/j.psychres.2020.113071
103. Michels N, Sioen I, Ruige J, De Henauw S. Children's psychosocial stress and emotional eating: a role for leptin? *Int J Eat Disord.* (2017) 50:471–80. doi: 10.1002/eat.22593
104. Potter GG, McQuoid DR, Steffens DC. Appetite loss and neurocognitive deficits in late-life depression. *Int J Geriatr Psychiatry.* (2015) 30:647. doi: 10.1002/gps.4196
105. Simmons WK, Burrows K, Avery JA, Kerr KL, Bodurka J, Savage CR, et al. Depression-related increases and decreases in appetite reveal dissociable patterns of aberrant activity in reward and interoceptive neurocircuitry. *Am J Psychiatry.* (2016) 173:418. doi: 10.1176/appi.ajp.2015.15020162
106. Niculescu MD. Nutritional epigenetics. *ILAR J.* (2012) 53:270–8. doi: 10.1093/ilar.53.3-4.270
107. De Luca A, Hankard R, Borys JM, Sinnett D, Marcil V, Levy E. Nutriepigenomics and malnutrition. *Epigenomics.* (2017) 9:893–917. doi: 10.2217/epi-2016-0168
108. Landecker H. Food as exposure: nutritional epigenetics and the new metabolism. *Biosocieties.* (2011) 6:167. doi: 10.1057/biosoc.2011.1
109. Edalati S, Bagherzadeh F, Asghari Jafarabadi M, Ebrahimi-Mamaghani M. Higher ultra-processed food intake is associated with higher DNA damage in healthy adolescents. *Br J Nutr.* (2021) 125:568–76. doi: 10.1017/S0007114520001981
110. Zhang Y, Kutateladze TG. Diet and the epigenome. *Nat Commun.* (2018) 9:3375. doi: 10.1038/s41467-018-05778-1

111. Shapira N. Prenatal nutrition: a critical window of opportunity for mother and child. *Womens Health.* (2008) 4:639–59. doi: 10.2217/17455057.4.6.639
112. Barker DJP, Bergmann RL, Ogra PL. Concluding remarks the window of opportunity: pre-pregnancy to 24 months of age. *Nestle Nutr Workshop Ser Pediatr Prog.* (2008) 61:255–60. doi: 10.1159/000113499
113. Jang H, Serra C. Nutrition, epigenetics, and diseases. *Clin Nutr Res.* (2014) 3:1. doi: 10.7762/cnr.2014.3.1.1
114. Bishop KS, Ferguson LR. The interaction between epigenetics, nutrition and the development of cancer. *Nutrients.* (2015) 7:922. doi: 10.3390/nu7020922
115. Coupé B, Amarger V, Grit I, Benani A, Parnet P. Nutritional programming affects hypothalamic organization and early response to leptin. *Endocrinology.* (2010) 151:702–13. doi: 10.1210/en.2009-0893
116. Shin BC Dai Y, Thamotharan M, Gibson LC, Devaskar SU. Pre- and postnatal calorie restriction perturbs early hypothalamic neuropeptide and energy balance. *J Neurosci Res.* (2012) 90:1169–82. doi: 10.1002/jnr.23013
117. Li G, Kohorst JJ, Zhang W, Laritsky E, Kunde-Ramamoorthy G, Baker MS, et al. Early postnatal nutrition determines adult physical activity and energy expenditure in female mice. *Diabetes.* (2013) 62:2773–83. doi: 10.2337/db12-1306
118. Vucetic Z, Kimmel J, Totoki K, Hollenbeck E, Reyes TM. Maternal high-fat diet alters methylation and gene expression of dopamine and opioid-related genes. *Endocrinology.* (2010) 151:4756–64. doi: 10.1210/en.2010-0505
119. Begum G, Stevens A, Smith EB, Connor K, Challis JRG, Bloomfield F, et al. Epigenetic changes in fetal hypothalamic energy regulating pathways are associated with maternal undernutrition and twinning. *FASEB J.* (2012) 26:1694–703. doi: 10.1096/fj.11-198762
120. Jiménez-Chillarón JC, Díaz R, Martínez D, Pentinat T, Ramón-Krauel M, Ribó S, et al. The role of nutrition on epigenetic modifications and their implications on health. *Biochimie.* (2012) 94:2242–63. doi: 10.1016/j.biochi.2012.06.012
121. Remely M, Stefanska B, Lovrecic L, Magnet U, Haslberger AG. Nutriepigenomics: the role of nutrition in epigenetic control of human diseases. *Curr Opin Clin Nutr Metab Care.* (2015) 18:328–33. doi: 10.1097/MCO.0000000000000180
122. Mazzio EA, Soliman KFA. Epigenetics and nutritional environmental signals. *Integr Comp Biol.* (2014) 54:21. doi: 10.1093/icb/icu049
123. Stevens AJ, Rucklidge JJ, Kennedy MA. Epigenetics, nutrition and mental health. Is there a relationship? *Nutr Neurosci.* (2018) 21:602–13. doi: 10.1080/1028415X.2017.1331524
124. Mentch SJ, Locasale JW. One-carbon metabolism and epigenetics: understanding the specificity. *Ann N Y Acad Sci.* (2016) 1363:91–8. doi: 10.1111/nyas.12956
125. Chung KH, Chiou HY, Chen YH. Associations between serum homocysteine levels and anxiety and depression among children and adolescents in Taiwan. *Sci Rep.* (2017) 7:8330. doi: 10.1038/s41598-017-08568-9
126. De Berardis D, Olivieri L, Rapini G, Di Natale S, Serroni N, Fornaro M, et al. Alexithymia, suicide ideation and homocysteine levels in drug naïve patients with major depression: a study in the "real world" clinical practice. *Clin Psychopharmacol Neurosci.* (2019) 17:318. doi: 10.9758/cpn.2019.17.2.318
127. Narayan SK, Verman A, Kattimani S, Ananthanarayanan PH, Adithan C. Plasma homocysteine levels in depression and schizophrenia in South Indian Tamilian population. *Indian J Psychiatry.* (2014) 56:46. doi: 10.4103/0019-5545.124746
128. Jatoi S, Hafeez DA, Riaz SU, Ali A, Ghauri MI, Zehra M. Low vitamin B12 levels: an underestimated cause of minimal cognitive impairment and dementia. *Cureus.* (2020) 12:e6976. doi: 10.7759/cureus.6976
129. Esnafoglu E, Ozturan DD. The relationship of severity of depression with homocysteine, folate, vitamin B12, and vitamin D levels in children and adolescents. *Child Adolesc Ment Health.* (2020) 25:249–55. doi: 10.1111/camh.12387
130. Moore EM, Watters DK, Ames D, Mander AG. Vitamin B12 and cognitive impairment. *Diet Nutr Dement Cogn Decline.* (2015) 2015:637–48. doi: 10.1016/B978-0-12-407824-6.00059-8
131. Black MM. Effects of vitamin B12 and folate deficiency on brain development in children. *Food Nutr Bull.* (2008) 29:S126. doi: 10.1177/15648265080292S117
132. Durand C, Mary S, Brazo P, Dollfus S. [Psychiatric manifestations of vitamin B12 deficiency: a case report]. *Encephale.* (2003) 29:560–5.
133. Hanna S, Lachover L, Rajarethinam RP. Vitamin B12 Deficiency and depression in the elderly: review and case report. Prim Care Companion. *J Clin Psychiatry.* (2009) 11:269. doi: 10.4088/PCC.08l00707
134. Degnan PH, Taga ME, Goodman AL. Vitamin B12 as a modulator of gut microbial ecology. *Cell Metab.* (2014) 20:769. doi: 10.1016/j.cmet.2014.10.002
135. Lurz E, Horne RG, Määttänen P, Wu RY, Botts SR, Li B, et al. Vitamin B12 deficiency alters the gut microbiota in a murine model of colitis. *Front Nutr.* (2020) 7:83. doi: 10.3389/fnut.2020.00083
136. An Y, Feng L, Zhang X, Wang Y, Wang Y, Tao L, et al. Dietary intakes and biomarker patterns of folate, vitamin B 6, and vitamin B 12 can be associated with cognitive impairment by hypermethylation of redox-related genes NUDT15 and TXNRD1. *Clin Epigenet.* (2019) 11:139. doi: 10.1186/s13148-019-0741-y
137. Zhong J, Karlsson O, Wang G, Li J, Guo Y, Lin X, et al. B vitamins attenuate the epigenetic effects of ambient fine particles in a pilot human intervention trial. *Proc Natl Acad Sci USA.* (2017) 114:3503–8. doi: 10.1073/pnas.1618545114
138. Bito T, Misaki T, Yabuta Y, Ishikawa T, Kawano T, Watanabe F. Vitamin B12 deficiency results in severe oxidative stress, leading to memory retention impairment in *Caenorhabditis elegans*. *Redox Biol.* (2017) 11:21–9. doi: 10.1016/j.redox.2016.10.013
139. Mikkelsen K, Stojanovska L, Apostolopoulos V. The effects of vitamin B in depression. *Curr Med Chem.* (2016) 23:4317–37. doi: 10.2174/0929867323666160920110810
140. Tangney CC, Aggarwal NT Li H, Wilson RS, DeCarli C, Evans DA, et al. Vitamin B12, cognition, and brain MRI measures: a cross-sectional examination. *Neurology.* (2011) 77:1276–82. doi: 10.1212/WNL.0b013e3182315a33
141. Sato H, Tsukamoto-Yasui M, Takado Y, Kawasaki N, Matsunaga K, Ueno S, et al. Protein deficiency-induced behavioral abnormalities and neurotransmitter loss in aged mice are ameliorated by essential amino acids. *Front Nutr.* (2020) 7:23. doi: 10.3389/fnut.2020.00023
142. Patri M. Synaptic transmission and amino acid neurotransmitters. *Neurochem Basis Brain Funct Dysfunct.* (2019) doi: 10.5772/intechopen.82121
143. Dalangin R, Kim A, Campbell RE. The role of amino acids in neurotransmission and fluorescent tools for their detection. *Int J Mol Sci.* (2020) 21:1–36. doi: 10.3390/ijms21176197
144. Fernstrom JD, Fernstrom MH. Tyrosine, phenylalanine, and catecholamine synthesis and function in the brain. *J Nutr.* (2007) 137:1539–47S. doi: 10.1093/jn/137.6.1539S
145. Parker GB, Brotchie H, Graham RK. Vitamin D and depression. *J Affect Disord.* (2017) 208:56–61. doi: 10.1016/j.jad.2016.08.082
146. Snegarova V, Naydenova D. Vitamin D: a review of its effects on epigenetics and gene regulation. *Folia Med.* (2020) 62:662–7. doi: 10.3897/folmed.62.e50204
147. Pertile RAN, Cui X, Hammond L, Eyles DW. Vitamin D regulation of GDNF/Ret signaling in dopaminergic neurons. *FASEB J.* (2018) 32:819–28. doi: 10.1096/fj.201700713R
148. Fullard ME, Duda JE, A. Review of the relationship between vitamin D and Parkinson disease symptoms. *Front Neurol.* (2020) 11:454. doi: 10.3389/fneur.2020.00454
149. Cui X, Pelekanos M, Liu PY, Burne THJ, McGrath JJ, Eyles DW. The vitamin D receptor in dopamine neurons; its presence in human *Substantia nigra* and its ontogenesis in rat midbrain. *Neuroscience.* (2013) 236:77–87. doi: 10.1016/j.neuroscience.2013.01.035
150. Fetahu IS, Höbaus J, Kállay E. Vitamin D and the epigenome. *Front. Physiol.* (2014) 5:164. doi: 10.3389/fphys.2014.00164
151. Wimalawansa SJ. Vitamin D deficiency: effects on oxidative stress, epigenetics, gene regulation, and aging. *Biology.* (2019) 8:30. doi: 10.3390/biology8020030
152. Hussain M, Kumar P, Khan S, Gordon DK, Khan S. Similarities between depression and neurodegenerative diseases: pathophysiology, challenges in diagnosis and treatment options. *Cureus.* (2020) 12:e11613. doi: 10.7759/cureus.11613
153. Krautkramer KA, Kreznar JH, Romano KA, Vivas EI, Barrett-Wilt GA, Rabaglia ME, et al. Diet-microbiota interactions mediate global

epigenetic programming in multiple host tissues. *Mol Cell.* (2016) 64:982–92. doi: 10.1016/j.molcel.2016.10.025
154. Jenkins TA, Nguyen JCD, Polglaze KE, Bertrand PP. Influence of tryptophan and serotonin on mood and cognition with a possible role of the gut-brain axis. *Nutrients.* (2016) 8:56. doi: 10.3390/nu8010056
155. Otaru N, Ye K, Mujezinovic D, Berchtold L, Constancias F, Cornejo FA, et al. GABA production by human intestinal *Bacteroides* spp: prevalence, regulation, and role in acid stress tolerance. *Front Microbiol.* (2021) 12:860. doi: 10.3389/fmicb.2021.656895
156. Ortega MA, Alvarez-Mon MA, García-Montero C, Fraile-Martinez O, Guijarro LG, Lahera G, et al. Gut microbiota metabolites in major depressive disorder—deep insights into their pathophysiological role and potential translational applications. *Metabolites.* (2022) 12:50. doi: 10.3390/metabo12010050
157. Zalar B, Haslberger A, Peterlin B. The role of microbiota in depression - a brief review. *Psychiatr Danub.* (2018) 30:136–41. doi: 10.24869/psyd.2018.136
158. Pham VT, Dold S, Rehman A, Bird JK, Steinert RE. Vitamins, the gut microbiome and gastrointestinal health in humans. *Nutr Res.* (2021) 95:35–53. doi: 10.1016/j.nutres.2021.09.001
159. Beckett EL, Yates Z, Veysey M, Duesing K, Lucock M. The role of vitamins and minerals in modulating the expression of microRNA. *Nutr Res Rev.* (2014) 27:94–106. doi: 10.1017/S0954422414000043
160. Yu Y, Zhang J, Wang J, Sun B. MicroRNAs: the novel mediators for nutrient-modulating biological functions. *Trends Food Sci Technol.* (2021) 114:167–75. doi: 10.1016/j.tifs.2021.05.028
161. Zhu X, Zhu Y, Li C, Yu J, Ren DD, Qiu S, et al. 1,25-Dihydroxyvitamin D regulates macrophage polarization and ameliorates experimental inflammatory bowel disease by suppressing miR-125b. *Int Immunopharmacol.* (2019) 67:106–18. doi: 10.1016/j.intimp.2018.12.015
162. Wagner AE, Piegholdt S, Ferraro M, Pallauf K, Rimbach G. Food derived microRNAs. *Food Funct.* (2015) 6:714–18. doi: 10.1039/C4FO01119H
163. Díez-Sainz E, Lorente-Cebrián S, Aranaz P, Riezu-Boj JI, Martínez JA, Milagro FI. Potential mechanisms linking food-derived MicroRNAs, gut microbiota and intestinal barrier functions in the context of nutrition and human health. *Front Nutr.* (2021) 8:85. doi: 10.3389/fnut.2021.586564
164. Zhang L, Chen T, Yin Y, Zhang CY, Zhang YL. Dietary microRNA—a novel functional component of food. *Adv Nutr.* (2019) 10:711–21. doi: 10.1093/advances/nmy127
165. Manca S, Upadhyaya B, Mutai E, Desaulniers AT, Cederberg RA, White BR, et al. Milk exosomes are bioavailable and distinct microRNA cargos have unique tissue distribution patterns. *Sci Rep.* (2018) 8:11321. doi: 10.1038/s41598-018-29780-1
166. Zhang L, Hou D, Chen X, Li D, Zhu L, Zhang Y, et al. Exogenous plant MIR168a specifically targets mammalian LDLRAP1: evidence of cross-kingdom regulation by microRNA. *Cell Res.* (2012) 22:107–26. doi: 10.1038/cr.2011.158
167. Teng Y, Ren Y, Sayed M, Hu X, Lei C, Kumar A, et al. Plant-derived exosomal MicroRNAs shape the gut microbiota. *Cell Host Microbe.* (2018) 24:637–52.e8. doi: 10.1016/j.chom.2018.10.001
168. Black DW, Grant JE. *DSM-5 R Guidebook: The Essential Companion to the Diagnostic and Statistical Manual of Mental Disorders*. 5th ed. Arlington TX: American Psychiatric Publishing (2014).
169. Katon W, Unützer J, Russo J. Major depression: the importance of clinical characteristics and treatment response to prognosis. *Depress Anxiety.* (2010) 27:19–26. doi: 10.1002/da.20613
170. Voineskos D, Daskalakis ZJ, Blumberger DM. Management of treatment-resistant depression: challenges and strategies. *Neuropsychiatr Dis Treat.* (2020) 16:221. doi: 10.2147/NDT.S198774
171. . Kirsch I. Antidepressants and the placebo effect. *Z Psychol.* (2014) 222:128–34. doi: 10.1027/2151-2604/a000176
172. Khan A, Brown WA. Antidepressants versus placebo in major depression: an overview. *World Psychiatry.* (2015) 14:294–300. doi: 10.1002/wps.20241
173. Owens MJ. Selectivity of antidepressants: from the monoamine hypothesis of depression to the SSRI revolution and beyond. *J Clin Psychiatry.* (2004) 65:19194.
174. Heninger GR, Delgado PL, Charney DS. The revised monoamine theory of depression: a modulatory role for monoamines, based on new findings from monoamine depletion experiments in humans. *Pharmacopsychiatry.* (1996) 29:2–11. doi: 10.1055/s-2007-979535
175. Firth J, Marx W, Dash S, Carney R, Teasdale SB, Solmi M, et al. The effects of dietary improvement on symptoms of depression and anxiety: a meta-analysis of randomized controlled trials. *Psychosom Med.* (2019) 81:265. doi: 10.1097/PSY.0000000000000673
176. Xu Y, Zeng L, Zou K, Shan S, Wang X, Xiong J, et al. Role of dietary factors in the prevention and treatment for depression: an umbrella review of meta-analyses of prospective studies. *Transl Psychiatry.* (2021) 111:478. doi: 10.1038/s41398-021-01590-6
177. Thomas-Odenthal F, Molero P, van der Does W, Molendijk M. Impact of review method on the conclusions of clinical reviews: a systematic review on dietary interventions in depression as a case in point. *PLoS ONE.* (2020) 15:e0238131. doi: 10.1371/journal.pone.0238131
178. Cena H, Calder PC. Defining a healthy diet: evidence for the role of contemporary dietary patterns in health and disease. *Nutrients.* (2020) 12:334. doi: 10.3390/nu12020334
179. Das L, Bhaumik E, Raychaudhuri U, Chakraborty R. Role of nutraceuticals in human health. *J Food Sci Technol.* (2012) 49:173–83. doi: 10.1007/s13197-011-0269-4
180. Li Y, Lv MR, Wei YJ, Sun L, Zhang JX, Zhang HG, et al. Dietary patterns and depression risk: a meta-analysis. *Psychiatry Res.* (2017) 253:373–82. doi: 10.1016/j.psychres.2017.04.020
181. García-Montero C, Fraile-Martínez O, Gómez-Lahoz AM, Pekarek L, Castellanos AJ, Noguerales-Fraguas F, et al. Nutritional components in western diet versus mediterranean diet at the gut microbiota-immune system interplay. Implications for Health and Disease. *Nutrients.* (2021) 13:1–53. doi: 10.3390/nu13020699
182. Arpón A, Milagro FI, Razquin C, Corella D, Estruch R, Fitó M, et al. Impact of consuming extra-virgin olive oil or nuts within a mediterranean diet on DNA methylation in peripheral white blood cells within the PREDIMED-Navarra randomized controlled trial: a role for dietary lipids. *Nutrients.* (2017) 10:15. doi: 10.3390/nu10010015
183. Sánchez-Villegas A, Álvarez-Pérez J, Toledo E, Salas-Salvadó J, Ortega-Azorín C, Zomeño MD, et al. Seafood consumption, omega-3 fatty acids intake, and life-time prevalence of depression in the PREDIMED-plus trial. *Nutrients.* (2018) 10:2000. doi: 10.3390/nu10122000

Conflict of Interest: The authors declare that the research was conducted in the absence of any commercial or financial relationships that could be construed as a potential conflict of interest.

Publisher's Note: All claims expressed in this article are solely those of the authors and do not necessarily represent those of their affiliated organizations, or those of the publisher, the editors and the reviewers. Any product that may be evaluated in this article, or claim that may be made by its manufacturer, is not guaranteed or endorsed by the publisher.

frontiers | Frontiers in Nutrition

ORIGINAL RESEARCH
published: 07 June 2022
doi: 10.3389/fnut.2022.899829

Short-Term High-Fat Diet Fuels Colitis Progression in Mice Associated With Changes in Blood Metabolome and Intestinal Gene Expression

Zhen-Hua Wu[1,2,3†], Jing Yang[4†], Lei Chen[1,2,3], Chuang Du[1,2,3], Qi Zhang[1], Shan-Shan Zhao[1,2,3], Xiao-Yu Wang[1,2,3], Jing Yang[1,2,3], Yang Liu[1,3], Demin Cai[5], Jian Du[4] and Hui-Xin Liu[1,2,3]**

[1] Health Sciences Institute, China Medical University, Shenyang, China, [2] Institute of Life Sciences, China Medical University, Shenyang, China, [3] Liaoning Key Laboratory of Obesity and Glucose/Lipid Associated Metabolic Diseases, China Medical University, Shenyang, China, [4] Department of Endocrinology, The Fourth Affiliated Hospital, China Medical University, Shenyang, China, [5] Laboratory of Animal Physiology and Molecular Nutrition, College of Animal Science and Technology, Yangzhou University, Yangzhou, China

OPEN ACCESS

Edited by:
Clare Marie Reynolds,
University College Dublin, Ireland

Reviewed by:
Xihong Zhou,
Institute of Subtropical Agriculture (CAS), China
Tien Sy Dong,
UCLA Health System, United States

***Correspondence:**
Jian Du
dujian035@sina.com
Hui-Xin Liu
liuhx@cmu.edu.cn

† These authors have contributed equally to this work and share first authorship

Specialty section:
This article was submitted to Nutrition and Metabolism, a section of the journal Frontiers in Nutrition

Received: 19 March 2022
Accepted: 29 April 2022
Published: 07 June 2022

Citation:
Wu Z-H, Yang J, Chen L, Du C, Zhang Q, Zhao S-S, Wang X-Y, Yang J, Liu Y, Cai D, Du J and Liu H-X (2022) Short-Term High-Fat Diet Fuels Colitis Progression in Mice Associated With Changes in Blood Metabolome and Intestinal Gene Expression. Front. Nutr. 9:899829. doi: 10.3389/fnut.2022.899829

Clinical cases and animal experiments show that high-fat (HF) diet is involved in inflammatory bowel disease (IBD), but the specific mechanism is not fully clear. A close association between long-term HF-induced obesity and IBD has been well-documented. However, there has been limited evaluation of the impact of short-term HF feeding on the risk of intestinal inflammation, particularly on the risk of disrupted metabolic homeostasis. In this study, we analyzed the metabolic profile and tested the vulnerability of 2,4,6-trinitrobenzenesulfonic acid (TNBS)-induced colitis after short-term HF feeding in mice. The results showed that compared with the control diet (CD), the fatty acid (FA), amino acid (AA), and bile acid (BA) metabolisms of mice in the HF group were significantly changed. HF-fed mice showed an increase in the content of saturated and unsaturated FAs and a decrease in the content of tryptophan (Trp). Furthermore, the disturbed spatial distribution of taurocholic acid (TCA) in the ileum and colon was identified in the HF group using matrix-assisted laser desorption/ionization-mass spectrometry imaging (MALDI-MSI). After HF priming, mice on TNBS induction were subjected to more severe colonic ulceration and histological damage compared with their CD counterparts. In addition, TNBS enema induced higher gene expressions of mucosal pro-inflammatory cytokines under HF priming conditions. Overall, our results show that HF may promote colitis by disturbing lipid, AA, and BA metabolic homeostasis and inflammatory gene expressions.

Keywords: nutrition, metabolism, homeostasis, imaging mass microscope, inflammatory bowel disease

Abbreviations: BA, bile acid; BAs, bile acids; TNBS, 2,4,6-trinitrobenzenesulfonic acid; CD, control diet; CT, control diet and TNBS administration; HF, high-fat diet; HT, high-fat diet and TNBS administration; MSI, mass spectrometry imaging; NPA, N-1-naphthylphthalic acid; 9AA, 9-aminoacridine; DCA, deoxycholic acid; CDCA, chenodeoxycholic acid; UDCA, ursodeoxycholic acid; TDCA, taurodeoxycholic acid; TCDCA, taurochenodeoxycholic acid; TUDCA, tauroursodeoxycholic acid; LCA, lithocholic acid; TLCA, taurolithocholic acid; TCA, taurocholic acid; TMCA, tauromuricholic acid; GCA, glycocholic acid; H&E, hematoxylin and eosin; AAs, amino acids; FAs, fatty acids; IBD, inflammatory bowel disease; MALDI, matrix-assisted laser desorption/ionization; EPA, eicosapentaenoic acid; EAAs, essential amino acids.

INTRODUCTION

It is well established that the diet and the microbiome can contribute to the occurrence of metabolic diseases in part by causing intestinal inflammation and increased permeability (1). Our previous studies and others show that a long-term high-fat (HF) diet causes nutritional imbalance, resulting in obesity, insulin resistance, and other diseases (2–4). HF intake can cause the disorder of lipid metabolism and induce systemic chronic low-grade inflammation, and the colon may be the first organ affected by inflammation caused by HF (5, 6). The intestinal mucosa is the largest interface between the body itself and the external environment, which has barrier functions such as selective infiltration and absorption of nutrients and defense against the invasion of microorganisms and inflammatory factors in the intestine (7). The altered intestinal environment could influence metabolic homeostasis, especially the metabolism of amino acids (AAs), fatty acids (FAs), and bile acids (BAs) (8–10).

Although the exact etiology of inflammatory bowel disease (IBD) is not fully understood, nutrition and dietary factors, in particular HF, have been recognized to play an important role in the pathogenesis of IBD (11). IBD comprises Crohn's disease and ulcerative colitis, which are characterized by chronic and relapsing inflammation of the gastrointestinal tract (12). IBD has become a global disease with accelerating incidence in newly industrialized countries whose societies have become more westernized, and this increase has paralleled a "westernization" of lifestyle (13). Many studies have described the relationship between fat intake and IBD pathogeny. Several studies have investigated the development of colitis in long-term HF-fed animals (14, 15). Studies have shown that long-term HF consumption will destroy the intestinal immune homeostasis and induce inflammation in animal models, and epidemiological studies have also shown that excessive HF intake is closely related to the occurrence and relapse of IBD (16, 17). A high intake of unsaturated fats may be associated with an increased risk of ulcerative colitis (18). However, most of the previous studies have ignored the effect of HF on the serum metabolites and intestines before disease induction. Furthermore, the effects of short-term HF feeding in colitis and the underlying molecular mechanisms at the levels of metabolism profile need to be further explored. In this context, a better understanding of the pathogenesis of short-term HF-driven metabolic disorders may help to reduce the IBD burden worldwide.

In this study, we proposed a 4-week HF priming to evaluate the effects of short-term fat intake on the risk of inflammatory diseases. Metabolomic and gene expression investigation results indicate that BA, FA, and AA metabolisms are significantly reprogrammed in the HF-fed group. In addition, mass spectrometry microscopy discovered that HF-feeding disturbs the spatial distribution of BAs and causes the decrease of taurocholic acid (TCA) in the intestinal wall, which may weaken the ability of the intestinal mucosal barrier to resist the invasion of bacteria, toxins, and antigens under inflammatory state. Moreover, under short-term HF priming conditions, 2,4,6-trinitrobenzenesulfonic acid (TNBS) administration aggravates the severity of colitis companied with dysregulated metabolism.

MATERIALS AND METHODS

Animals and Experimental Treatment

All animal procedures were approved by the Institutional Animal Care and Use Committee (IACUC) at the China Medical University. Notably, 6–8 weeks old male C57BL/6 mice (n = 10 per group) were purchased from Beijing HFK Biotechnology Co., Ltd. All experimental mice were housed in specific pathogen-free environments under a controlled condition of normal circadian circulation for 12 h at 20–22°C and 45 ± 5% humidity, with free access to food and water. Mice were fed an HF diet (TP23520, Trophic Diet, China) or a control diet (CD, TP23524, Trophic Diet, China) for 4 weeks. HF contained 60% available energy as fat, 20% available energy as carbohydrate, and 20% available energy as protein. CD contained 10% available energy as fat, 70% available energy as carbohydrate, and 20% available energy as protein. After 4 weeks of feeding, colitis was induced using the reported TNBS (P2297-10 ml, sigma)-colitis model with some modifications (19). In brief, mice were fed with HF or CD for 3 weeks and then pre-sensitized with 150 μl of 1% (wt/vol) TNBS solution applied to the back skin for 8 days. Next, the animals were fasted overnight and treated under anesthesia with a 100 mg/kg mixture of 5% TNBS and 100% alcohol (1:1) *via* intrarectal injection, and the control mice received 50% alcohol treatment. Then, the mice were placed upside down for 5 min after TNBS injection. Body weight, stool consistence, and rectal bleeding were monitored daily. Animals were sacrificed on the third day after TNBS treatment. During the experimental period, the food intake of mice was recorded two times a week, and the body weights were documented per week.

Sample Collection

Animals were sacrificed, and the blood was collected with anticoagulant and then centrifuged at 1,000 × g for 10 min at 22–25°C for serum collection. Then, the liver, ileum, colon, and colon content were carefully dissected and kept in liquid nitrogen before storage at −80°C. Besides, parts of the colons and livers were harvested for histological analysis.

Biochemical Analysis

The analysis of triglyceride (TG), total cholesterol (TC), low-density lipoprotein cholesterol (LDL-c), high-density lipoprotein cholesterol (HDL-c), aspartate aminotransferase (AST), alanine aminotransferase (ALT), and total bile acid (TBA) were quantified using commercial kits (Nanjing Jiancheng Bioengineering Institute, Nanjing, China) in accordance with manufacturer's instructions.

Colon Histology Assay

After the mice were euthanized, the colons were quickly removed and rolled up using the "swiss roll" method (20). Then, the colons were fixed in 4% neutral formalin for 24 h and embedded in paraffin. The embedded tissue blocks were cut into 4 μm sections and stained with hematoxylin and eosin (H&E). The histological injury was evaluated according to the existing standard (16, 21).

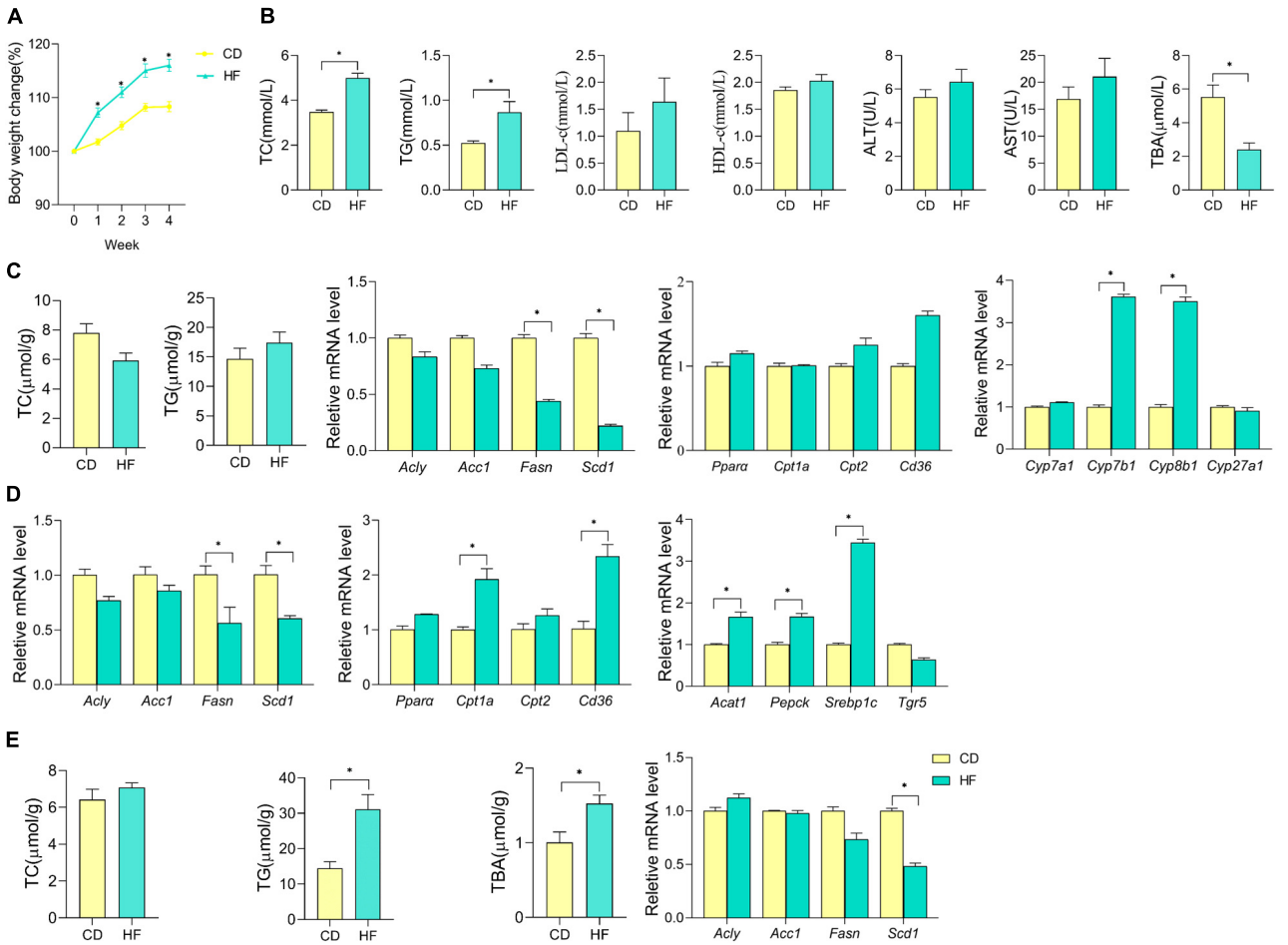

FIGURE 1 | Effect of HF on the blood, liver, ileum, and colon lipid metabolism in mice. **(A)** Body weight changes in mice on CD or HF for 4 weeks. **(B)** Cholesterol (TC), triglyceride (TG), low-density lipoprotein cholesterol (LDL-c), high-density lipoprotein cholesterol (HDL-c), alanine aminotransferase (ALT), and aspartate aminotransferase (AST) contents in the serum of each group of mice. **(C)** Cholesterol (TC) and triglyceride (TG) contents in the liver of each group of mice; hepatic mRNA expression of genes involved in lipid metabolism and BA synthesis, and data were from seven pooled samples of each group. **(D)** Ileum mRNA expression of genes involved in lipid and carbohydrate metabolism in each group of mice (data were from seven pooled samples of each group). **(E)** Cholesterol (TC), triglyceride (TG), and total bile acid (TBA) contents in the colon; colonic mRNA expression of genes involved in lipid metabolism in each group of mice (data were from seven pooled samples of each group). $n \geq 6$. The data were shown as mean ± SEM. $^*p < 0.05$. CD, control diet group; HF, high-fat diet group.

RNA Extraction and qPCR

Total RNAs were extracted using TRIzol reagent (Invitrogen), and then the extracted total RNAs were reverse-transcribed into cDNA using the PrimeScript RT reagent kit (TaKaRa, Mountain View, CA, United States) according to the manufacturer's instructions. The relative expression levels of genes were calculated using the $2^{-\Delta\Delta CT}$ formula (22), and GAPDH was chosen as an internal control. The primers are listed in **Supplementary Table 1**.

Metabolomics

Bile acids, FAs, and AAs were quantified as previously described methods (23, 24). In brief, AAs and FAs were quantified by HPLC coupled to tandem mass spectrometry (MS/MS) based on deuterated purified standards. Serum AA and FA concentrations were expressed in μmol/L and mmol/L, respectively.

Sample Preparation for Imaging Mass Microscope

Frozen 10 μm of mouse intestinal sections were sliced at −20°C with a cryomicrotome (Leica CM1950, Nussloch, Germany) and then thaw-mounted onto electrically conductive glass slides. Subsequently, a "two-step matrix application," which combined with sublimation and airbrushing, was used to coat the matrix (9AA) for tissue sections.

Imaging Mass Spectrum Analysis Based on Imaging Mass Microscope

iMScope was performed using a 1,000 Hz solid laser. A 40-μm pitch of special resolution was used, and the data were acquired in negative ionization. The *m/z* values were internally calibrated with DHB. All the spectra were acquired using atmospheric pressure matrix-assisted laser desorption/ionization (MALDI)

(Shimadzu Corporation). The laser in the iMScope system was a diode-pumped 355 nm Nd: YAG laser (Shimadzu Corporation, Kyoto, Japan) and operated under the following parameters: frequency, 1,000 Hz; laser intensity, 55.0; laser diameter, 3 μm. The parameters of IT-TOF MS were set as follows: ion polarity, negative; mass range, 250–550; sample voltage, 3.0 kV; detector voltage, 1.90 kV. The imaging MS Solution Version 1.30 software (Shimadzu, Tokyo, Japan) was used to control the instrument, and the data acquisition, visualization, and quantification were also performed using the same software.

Tissue Preparation for Histology After Mass Spectrometry Imaging

The tissue sections were stained with H&E for examination following the previous protocol (25). In brief, the matrix (9AA) covered on the glass slides was removed with 70% ethanol, and then the tissues were fixed with 100% ethanol. The tissues were then stained with H&E. Finally, the H&E slides were sealed with neutral gum and scanned using an iMScope TRIO (Shimadzu, Japan) instrument.

Statistical Analysis

Data in bar graphs are expressed as mean ± SEM. The unpaired two-tailed Student's *t*-test and the two-tailed Wilcox test were used to compare two groups of independent samples. The Kruskal–Wallis ANOVA test was utilized to determine significance in multiple groups. The SPSS Statistics version 25.0 software and the GraphPad Prism 8 software were used for statistical analyses. All statistical tests with a *p*-value of <0.05 were considered statistically significant.

RESULTS

Lipid Metabolism-Related Parameters in Serum, Liver, Ileum, and Colon of Mice Fed With High-Fat Diet

We have noticed that the impact of HF on the weight of mice was detectable within the first week of dietary intake. Compared with the CD, the HF statistically increased the body weight of mice at the end of this dietary treatment ($p < 0.05$) (**Figure 1A**). Abnormal levels of lipid metabolism-related parameters in the serum, liver, ileum, and colon were observed among mice fed with HF. As shown in **Figure 1B**, HF-fed mice had an increase in serum TC and TG levels and a decrease in serum TBA levels than CD-fed mice ($p < 0.05$), and no significant differences were observed in the serum levels of LDL-c, HDL-c, ALT, and AST between CD and HF groups. Meanwhile, there was no significant difference in the TC and TG levels between CD and HF group livers (**Figure 1C**). To understand the effect of HF on metabolism at the genetic level, we examined the changes in several related genes in CD and HF groups by qPCR. The expression levels of genes associated with hepatic FA synthesis (*Fasn*, *Scd1*) were downregulated in the HF group compared with those in the CD group ($p < 0.05$) (**Figure 1C**), but the expression of key genes involved in BA synthesis (*Cyp7b1*, *Cyp8b1*) was upregulated in HF fed livers ($p < 0.05$). Moreover, 4 weeks of HF feeding might disturb carbohydrate and lipid metabolism in the mouse ileum, which was indicated by the changes of key genes involved in the above-mentioned pathways at mRNA levels (**Figure 1D**). Interestingly, HF feeding prominently increased the contents of TG in colonic mucosa and the content of TBA in colonic feces compared with CD feeding ($p < 0.05$) (**Figure 1E**). In the colon, the expression levels of *Scd1* were downregulated in the HF group compared with those in the CD group ($p < 0.05$) (**Figure 1E**). Taken together, these results highly suggested that HF feeding rendered the disturbance of metabolic homeostasis.

Dysbiosis of Serum Metabolic Patterns in High-Fat Diet Feeding Mice

As shown in **Figures 2A–C**, regarding the effect of HF feeding on serum FA and AA levels analyzed at week 4, the levels of nine FA species were higher ($p < 0.05$), namely, C16, C18, C20, C22, C18:2, C18:3, C20:2, C22:4, and C22:5, while the levels of three FAs and one AA species were lower ($p < 0.05$), namely, C16:1, eicosapentaenoic acid (EPA, namely, C20:5), C24:1, and tryptophan (Trp), in HF as compared with CD mice. In addition, the serum *Scd1* desaturation index (C16:1/C16) was decreased significantly in the HF-fed mice ($p < 0.05$), and we further noticed that the percentage of C20:5/C20 also decreased in HF feeding mice ($p < 0.05$). Through Spearman correlation between changed metabolites and biochemical indexes, as shown in **Figures 2D–H**, overall serum LDL-c, TC, TG levels, colon TG level, feces TBA level, and body weight were positively correlated with nine FA species, namely, C18:2, C18:3, C22, C18, C16, C20, C20:2, C22:4, and C22:5, besides they were negatively correlated with TCA, C20:5, C20:5/C20, C16:1, C16:1/C16, Trp, and C24:1. Moreover, for serum TBA level, positive correlation with TCA, C20:5, C20:5/C20, C16:1, and C16:1/C16 and a negative correlation with C18:2, C18:3, C22, C18, C16, C20, C20:2, C22:4, and C22:5 were observed.

High-Fat Diet Decreases the Spatial Distribution of Taurocholic Acid in the Ileum and Colon of Mice

Recently, we developed a method for identification and spatial visualization of dysregulated BA metabolism in HF-fed mice by mass spectrometry imaging (MSI) (26). The spatially resolved profiling of the altered BA metabolism was detected in the HF group with the most significant changes in TCA. In this study, we focused on the detection of TCA due to its biological activity on anti-inflammation (26, 27). As the MSI technique putative identification is only based on the measured exact *m*/*z* value, we used secondary mass spectrometry to distinguish isomers of target compounds with the same molecular formula by MSI (e.g., *m*/*z* 514.2844 ± 0.05, putative identification as TCA/TMCA). The mass spectra of the TCA standard are shown in **Supplementary Figure 1A**, with a negative ion scan at *m*/*z* 514.284 as a $[M\text{-}H]^-$ peak. Secondary mass spectrometry analysis of the *m*/*z* 514.284 ion yielded *m*/*z* 353.247 and *m*/*z* 496.272 fragment ions. These two fragment ion peaks can be regarded as the characteristic ion peaks of TCA. We performed secondary mass

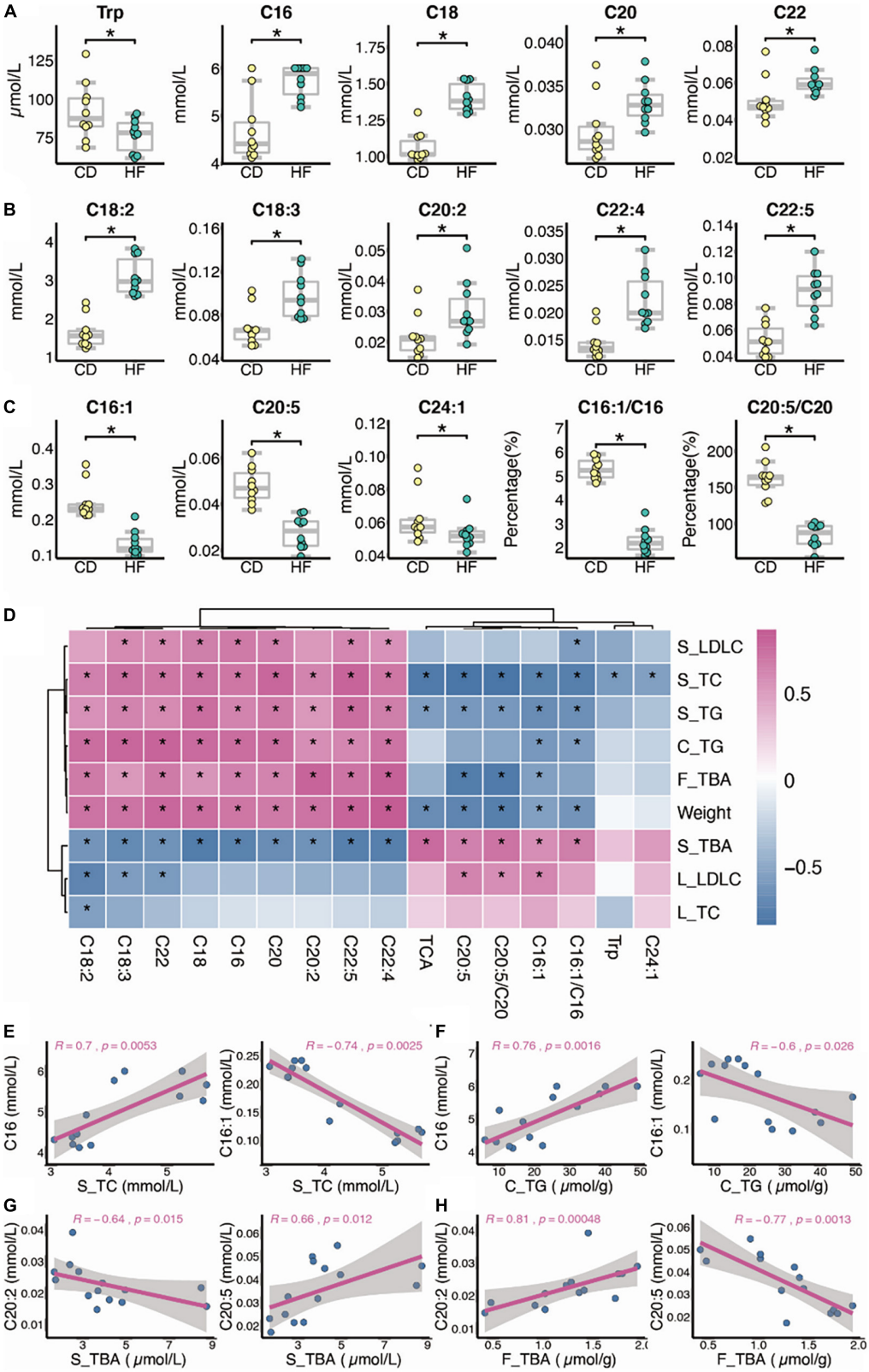

FIGURE 2 | Dysbiosis of serum metabolic patterns in HF feeding mice. **(A–C)** Differential metabolites between CD and HF groups (n = 10). **(D–H)** Spearman correlation between changed metabolites and biochemical indexes (n = 7; S, serum; L, liver; C, colon; F, feces). The two-tailed Wilcox test was used to determine the significant difference in CD and HF groups. *p < 0.05. CD, control diet group; HF, high-fat diet group.

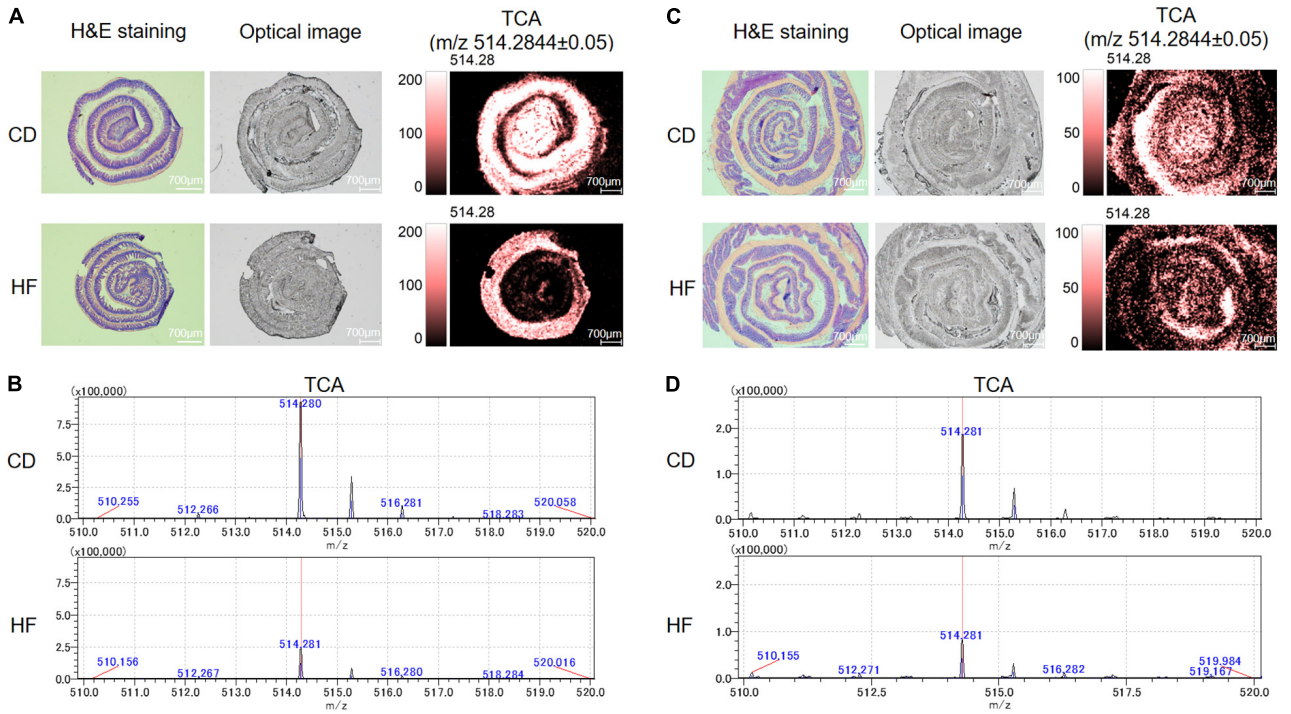

FIGURE 3 | Detection of TCA distributed within the regions of the ileum and colon by MALDI-MSI. **(A)** MS ion images of the spatial distribution of TCA from ileum tissue. Experimental *m/z* values were presented in parentheses. TCA (*m/z* 514.2844 ± 0.05). All ion images were normalized to the 9-AA matrix signal. **(B)** MALDI-MSI single-pixel mass spectra of TCA from ileum tissue. **(C)** MS ion images of the spatial distribution of TCA from colon tissue. Experimental *m/z* values were presented in parentheses. TCA (*m/z* 514.2844 ± 0.05). All ion images were normalized to the 9-AA matrix signal. **(D)** MALDI-MSI single-pixel mass spectra of TCA from colon tissue. CD, control diet group; HF, high-fat diet group.

spectrometry analysis on ileum and colon tissue sections (shown in **Supplementary Figures 1B,C**) and also found characteristic fragment ion peaks at *m/z* 353.247 and *m/z* 496.272. Therefore, we confirmed that the material on the ileum and colon was TCA. BAs were ionized in negative mode, and all ion images were normalized to the 9AA matrix signal. Thus, we cut down a 3-cm long terminal ileum and whole colon and rolled them up in a "swiss roll" (20). The spatial distribution of TCA in ileum and colon sections is shown in **Figures 3A,C**. The ion intensity of TCA in ileum and colon tissue sections of HF-treated mice dramatically decreased when compared with the CD group's MS ion image. **Figures 3B,D** show the mass spectra of TCA in the ileum and colon, respectively. These data indicated that HF-treated mice suffered a more severe decrease of TCA in colonic tissue, and we speculated that this is associated with HF exacerbating colitis.

Changes of Metabolic Patterns in Control Diet and High-Fat Diet Feeding Mice After 2,4,6-Trinitrobenzenesulfonic Acid Installation

Following TNBS installation, we found that the levels of alanine (Ala), asparagine (Asn), glycine (Gly), isoleucine (Ile), leucine (Leu), lysine (Lys), methionine (Met), serine (Ser), threonine (Thr), tryptophan (Trp), valine (Val), tyrosine (Tyr), glutamine (Gln), and proline (Pro) in serum were significantly lower in the two TNBS groups than their counterparts (data not shown). Notably, the distribution of significantly differential serum metabolites in the respective comparisons of CT and CD (the CT group represents CD-fed mice, which are treated with TNBS) and HT and HF (the HT group represents HF-fed mice, which are treated with TNBS) is shown in **Figure 4A**. The metabolites represented by the red triangle in the upper left corner are specific to the comparison between HT and HF, including Leu, histidine (His), C18, C18:2, C18:3, C22:4, C22:5, C24:1, and TUDCA, and these metabolites were significantly changed in the HF group instead of the CD group after TNBS enema (**Figure 4A**). Additionally, the metabolites represented by the orange triangle in the upper right corner were both changed when compared with CT and CD and HT and HF, which were not identified in detail (**Figure 4A**). Furthermore, the unique change of metabolites between the HT and HF groups rather than the CD and CT groups is shown in **Figures 4B,C**. The data showed that C24:1 was upregulated in the HF group after TNBS treatment ($p < 0.05$), but the other metabolites were downregulated ($p < 0.05$) (**Figures 4B,C**). As for the commonly changed metabolites when we compared CT and CD and HT and HF, we have especially noticed that glutamic acid (Glu) and C20:5 showed a greater degree of change in HT and HF than in CT and CD, but the Asn and C16:1 showed a greater degree of change in CT and CD than HT and HF (**Figure 4D**). In addition, Glu, Asn,

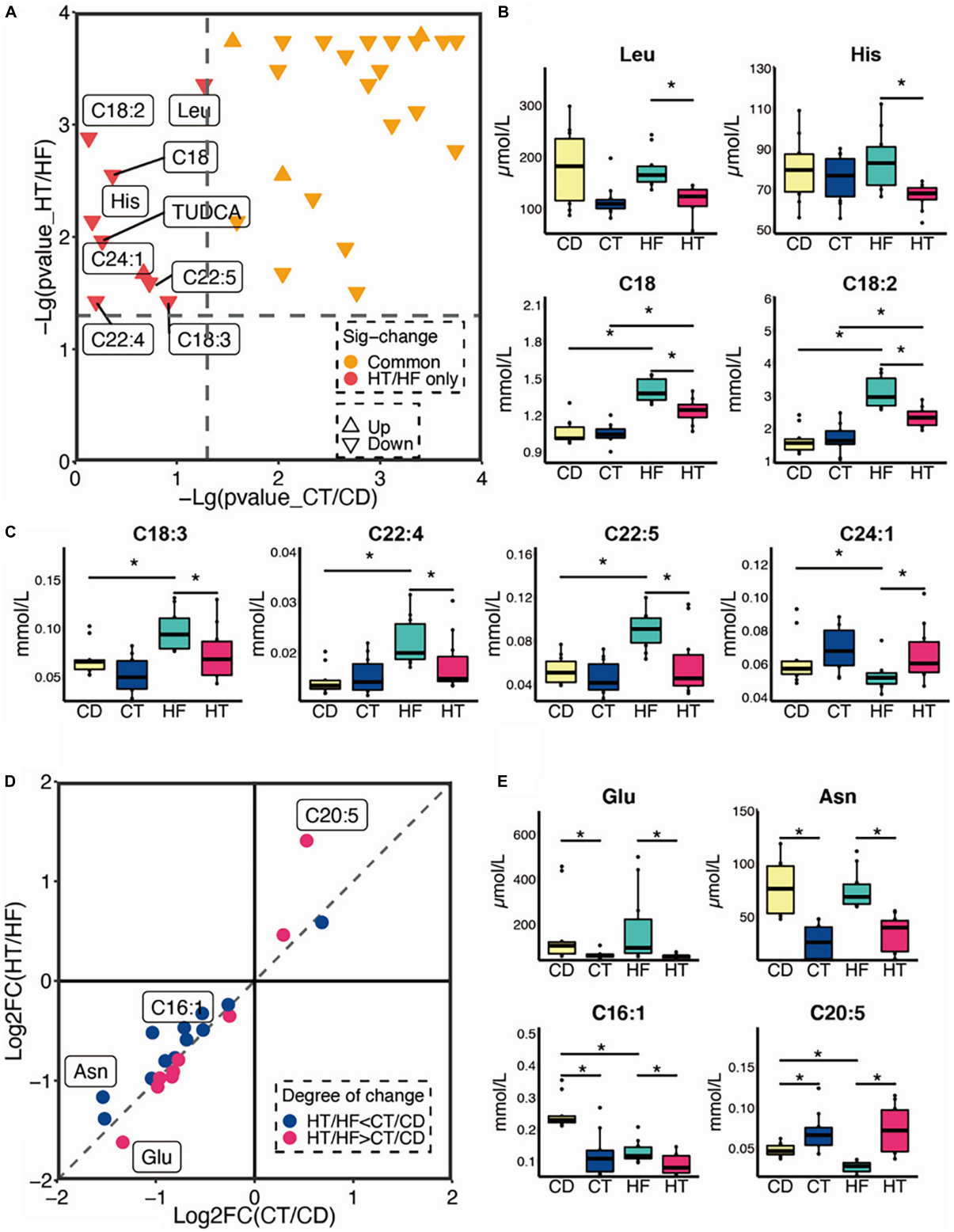

FIGURE 4 | Changes in metabolic patterns in CD and HF feeding mice after being treated with TNBS. **(A)** Distribution of significantly differential serum metabolites in comparisons of CT and CD and HT and HF (n = 10). **(B,C)** The unique change of metabolites between the HT and HF groups rather than in the CT and CD groups. **(D,E)** The degree of change in common metabolites when compared with CT and CD and HT and HF. The Kruskal–Wallis ANOVA test was utilized to determine the significant difference in multiple groups. *$p < 0.05$. CD, control diet group; HF, high-fat diet group; CT, control diet and TNBS group; HT, high-fat diet and TNBS group.

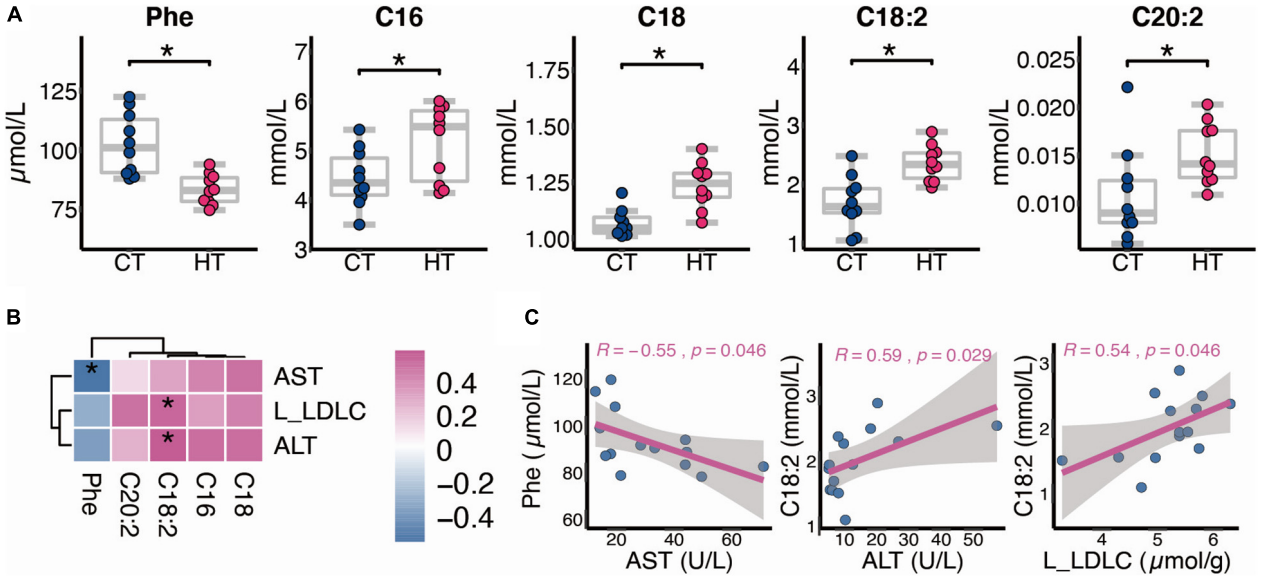

FIGURE 5 | Alternation of serum metabolism between the CT and HT groups. **(A)** Differential metabolites between the CT and HT groups (n = 10). **(B,C)** Spearman correlation between changed metabolites and biochemical indexes (n = 7, L, liver). The two-tailed Wilcox test was used to determine the significant difference in CT and HT groups. *$p < 0.05$. CT, control diet and TNBS group; HT, high-fat diet and TNBS group.

and C16:1 were decreased following TNBS installation, and C20:5 was increased (**Figure 4E**).

Alternation of Serum Metabolism Between CT and HT Groups

Data from our targeted metabolomics suggested that HF affects the AAs and FAs after TNBS treatment. As shown in **Figure 5A**, compared with the CT group, phenylalanine (Phe) decreased in the HT group ($p < 0.05$), whereas C16, C18, C18:2, and C20:2 increased in the HT group ($p < 0.05$). Besides, liver LDL-c level and serum ALT activity were positively correlated with C18:2, and serum AST activity was negatively correlated with Phe (**Figures 5B,C**).

High-Fat Diet Aggravated the Disease Severity in 2,4,6-Trinitrobenzenesulfonic Acid-Induced Colitis

As shown in **Supplementary Figure 2A**, male C57BL/6 mice were primed with an HF, and CD primed mice were used as normal control. Three weeks later, mice of the model group were pre-sensitized with 1% (wt/vol) TNBS solution, and 8 days later, mice were treated with 2.5% (wt/vol) TNBS solution *via* intrarectal injection for 3 days to induce colitis. Several studies have shown that mice fed an HF diet showed increased levels of inflammatory cytokines (*Tnfα* and *Il6*) in the ileum, colon, and surrounding mesenteric fat, even before the development of obesity (28, 29). In this study, we found that *Cxcl10* was elevated in the colonic tissue of mice fed an HF for 4 weeks ($p < 0.05$), and *Tnfα*, *Socs1*, and *Socs3* were not changed (**Supplementary Figure 2D**). It is common knowledge that *Cxcl10* mainly induces the chemotaxis of monocytes and macrophages, participates in regulating the migration, activation, and differentiation of a variety of immune cells, and affects acquired immunity and inflammation response (30). Therefore, the colon tissue in the HF group may have low-grade inflammation, which may be a reason for the more serious colitis after TNBS treatment compared with the CD group. Following TNBS installation, HF-primed mice caused much more severe colitis than mice of CD, as evidenced by a significant decrease in the body weight and shortening of colon length ($p < 0.05$) and significantly higher colonic ulceration and histological damage (**Figures 6A,D**). Then, we measured AST and ALT activities in serum. As shown in **Figure 6B**, we have noticed that the HT group had higher AST and ALT activities than the CT group ($p < 0.05$); moreover, no obvious histological alterations in H&E staining were observed in the liver of the HT group when compared with the CT group (data not shown). It is known that ALT and AST can sensitively reflect whether hepatocytes are damaged or not and the degree of injury. Importantly, as shown in **Figure 6C**, HF-treated mice expressed much higher levels of pro-inflammatory cytokines and chemokines (including *Tnfα* and *Cxcl10*) in the colonic mucosa compared with CD-treated mice following TNBS induction ($p < 0.05$). Cytokines, such as *Tnfα*, are known to play key roles in the induction of gut inflammation and tumorigenesis (31). In addition, we further studied the effect of HF on TNBS-induced colitis within 7 days. As shown in **Figure 6D**, CD-primed mice developed weight loss following TNBS treatment, and the loss reached the maximum on days 2–3 followed by a gradual recovery, but it decreased again on days 5 until day 7. In contrast, the weight loss of HF-primed mice was more severe and was almost not recovered within 7 days ($p < 0.05$) (**Figure 6D**), approximately 50% of HF-primed mice died within 7 days after TNBS treatment (**Figure 6D**), and during this period, the

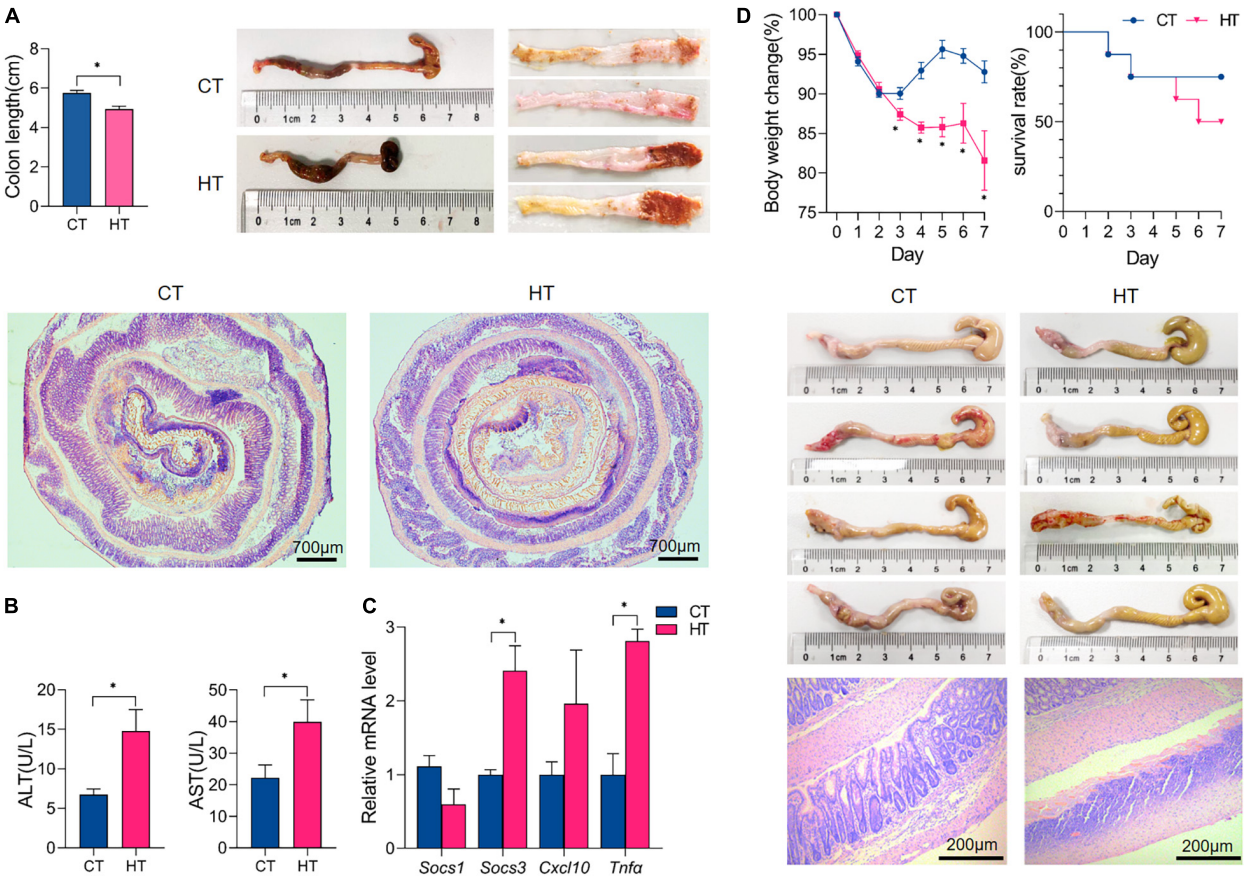

FIGURE 6 | High-fat exacerbated the disease severity of TNBS-induced colitis. **(A)** All mice were sacrificed on day 3, and the colons were collected to estimate mucosal damage by detecting colon lengths; gross morphology of the colons on day 3 after TNBS treatment; the representative histological sections were observed under microscopy (magnification: 2.5×). **(B)** The alanine aminotransferase (ALT) and aspartate aminotransferase (AST) activity in the serum of each group of mice. **(C)** qPCR quantitation of pro-inflammatory cytokines and chemokines in colonic mucosa on day 3 after TNBS treatment. **(D)** Body weight changes for each group of mice within 7 days after TNBS installation and survival curve within 7 days; gross morphology of the colons on day 7 after TNBS treatment; and colon histology by hematoxylin and eosin staining on day 7 (magnification: 100×). $n \geq 3$. The data were shown as mean ± SEM. $^*p < 0.05$. CT, control diet and TNBS group; HT, high-fat diet and TNBS group.

mortality of CD-primed mice was only 25% after TNBS treatment (**Figure 6D**). Following TNBS installation, the colons from the surviving HF-primed mice remained short by day 7 compared with CD-primed mice after TNBS treatment (**Figure 6D**), and the colons were swollen with no visible fecal pellet formation in both groups. Moreover, histological examination revealed severe ulceration in the colon of the HT group (**Figure 6D**). These data indicated that HF-primed mice suffered more severe colonic inflammation than CD-primed mice. Taken together, HF-primed mice showed dysregulated metabolic homeostasis, which might promote the disease severity in TNBS-induced colitis.

DISCUSSION

The incidence of metabolic-related diseases has gradually increased throughout the world, such as diabetes, hypertension, and IBD, especially in emerging market countries with gradually westernized eating habits, which is thought closely related to the increase in HF intake (6, 32). Previous studies show that due to the imbalance between energy intake and expenditure, long-term HF could cause severe disorders of metabolism, which highly increased susceptibility to the development of metabolic diseases (33, 34). Meanwhile, accumulating evidence shows that the involvement of HF increases in intestinal levels of secondary BAs, characterized by the substantial increase of DCA in the feces, might be highly relevant to the pathogenesis of IBD (35, 36). HF consumption promotes and exacerbates experimental colitis in dietary and genetic mouse models of IBD (37). Taken together, dietary fats play an important role in intestinal disease pathogenesis. However, most of these studies examined the relationship between westernized diets and the pathogenesis of metabolic-related diseases and focused on secondary effects of HF, such as effects on gut microbes or BAs (38, 39). The current study focuses on the specific effects of short-term HF feeding on the levels of free FAs, AAs, and BAs in serum and the resulting effects on colitis development. In this study, we

discovered that 1 month of HF feeding disturbed FA and AA metabolisms in serum and caused the reduction of the spatial distribution of TCA in the ileum and colon wall of mice, which may result in increasing the lipid peroxidation and the weakening of the resistance of colon wall to pathogens such as bacteria, thus aggravating epithelial barrier dysfunction and colonic mucosal inflammation. Consistently, we found that short-term HF-priming deteriorated TNBS-induced colitis, proved by more violent mucosal inflammation and broader colonic damage compared with CD-primed mice after TNBS treatment. These data indicated that short-term HF priming distributed metabolism, which led to increased susceptibility and severity of IBD.

For only 4 weeks of HF-feeding in mice, not only the blood lipid (TC and TG) increased but also TG accumulated in the colon, which may lead to mitochondrial dysfunction, oxidative stress, and other damage. In addition, the content of total BAs in mice colonic feces increased significantly, which is similar to previous reports that HF increased the production of secondary BAs (40). Compared with other internal organs, the liver is considered to be prone to fat accumulation (41), but our results showed that short-term (4 weeks) HF feeding did not cause significant fat accumulation in the liver. An interesting feature of gene expression was the suppression of enzymes involved in lipid synthesis, and these included *Fasn* and *Scd1*. It is worth noting that similar phenomena were observed in the ileum and colon. *Scd1* is considered one of the key enzymes in lipid homeostasis and body weight regulation (42). Our studies have shown that HF feeding decreased mRNA level and desaturation index of *Scd1*. The decrease of *Scd1* may cause lipid acylation disorder and change the lipid composition of the cell membrane, resulting in serious lipid toxicity (43).

Metabolomic investigations show that Trp was significantly lower in the serum of mice on HF than in the control group. Trp is one of the important essential AAs (EAAs). Research shows that disorders in Trp metabolism results in lower levels of bacterial-derived and beneficial metabolites, and some Trp metabolites can provide protection against gastroenteric effects and IBD (1, 44). For instance, Trp exerts a beneficial regulatory function in mucosal growth or maintenance and alleviation of intestinal inflammation by the 5-hydroxytryptophan (5-HT) signaling pathway (45). Other studies also suggest that Trp plays a role in the recovery of colitis and in the function of intestinal homeostasis by caspase recruitment domain family member 9 (Card9), calcium-sensing receptor (CaSR), and aryl hydrocarbon receptor (AHR) ligands in the intestine (46–48). Therefore, the significant decrease of serum Try in mice fed an HF for 1 month may be a risk factor for TNBS-induced colitis. Furthermore, saturated FAs are non-essential FAs, and excessive intake will increase the content of blood lipids in the body. Our results show that the increase of C16, C18, C20, and C22 in serum is closely related to dyslipidemia caused by HF. It should be noted that compared with the CD group, essential FAs C18:2, C18:3, C20:2, C22:4, and C22:5 were significantly increased in the HF group. Although we have known that polyunsaturated FAs positively affect insulin sensitivity, cardiovascular, mental health, and development and reduce hypertension and inflammation (49), the increase of serum-free FAs will lead to systemic low-grade inflammation, and the increase of HF-derived free FAs in the intestinal cavity will lead to the increased production of pro-inflammatory cytokines in the intestinal tract (50). These results indicated that HF intake had a regulating effect on FA metabolisms. Thus, we speculated that polyunsaturated FAs are a double-edged sword, and their advantages and disadvantages depend on the specific physiological conditions and reasonable physiological concentration of the body. Further study on their particular physiological significance is needed in the short-term HF feeding model. Notably, palmitoleic acid (C16:1) and EPA decreased in the HF group. Lipogenesis is mediated by *Scd1*, the rate-limiting enzyme catalyzing the synthesis of monounsaturated FAs, and the predominant substrates for *Scd1* are palmitic (C16) and stearic acids (C18) which generate C16:1 and oleic acid (C18:1), respectively (49). The reduction of C16:1 and increase of C16 and C18 are consistent with the decreased expression of *Scd1* in the liver in our results. C16:1 is a monounsaturated FA and has therapeutic effects on some chronic diseases such as metabolic syndrome, diabetes, and inflammation (49). EPA is an important polyunsaturated FA, also known as arachidonic acid and deep-sea fish oil, which belongs to the ω-3 series of polyunsaturated FAs. It is an important and indispensable nutrient that cannot be synthesized by the human body itself. EPA is known to have a variety of health benefits including well-established hypotriglyceridemic, antioxidant, and anti-inflammatory effects (49). It could be of interest to human health and the prevention of cardiovascular disease (51). Therefore, the decrease of C16:1 and EPA in the HF group may be conducive to the production of metabolic diseases.

Following TNBS installation, the distribution of significantly differential serum metabolites also changed. We did not find any metabolites changed significantly which only occurred in the CD and its colitis model. Importantly, the serum levels of Leu, His, C18, C18:2, C18:3, C22:4, and C22:5 are decreased significantly when we compared HT with HF instead of CT and CD, which may be the result of the joint action of HF and TNBS. Studies have shown that branched-chain AAs (e.g., Leu, Val, and Ile) supplementation with protein-restricted diet improved intestinal immune defense function by protecting villous morphology and by increasing levels of intestinal immunoglobulins in weaned piglets (52). His is a conditionally EAA and an important anti-inflammatory factor in the intestinal epithelial cells, and His supplement alleviates colitis of murine (53). Moreover, the decrease of His increases relapsing risk in the emission of ulcerative colitis patients, and it may be a non-invasive predictive marker in intestinal inflammation (54). It must be noted that the levels of Leu and His were significantly lower in the HT group than in the HF group, which might indicate that the intestinal immune defense function in the HT group is lower than that in the CT group. Furthermore, compared with CD, Glu decreased significantly in CT, but its change degree was less than that of HF and HT. Collectively, these results highlight the significant changes of some metabolites, and these changes may exist only in the HF and its colitis model. In addition, changes

in serum metabolism between the CT group and the HT group were also observed. EAAs have significant effects on intestinal inflammation (10). It has been reported that Phe manifests beneficial effects in the treatment of IBD by inhibiting *Tnf*α productions and enhancing immune responses (55). In addition, the antioxidant and anti-inflammatory properties of Phe give Phe with chromium a protective effect on indomethacin-induced IBD in rats (56). Phe, as one of the EAAs for humans and animals, was decreased significantly in the HT group compared with the CT group in our study. This change may be caused by colitis in an HF state, which suggests that HF might induce severer colitis compared with CD following TNBS enema.

There exists a highly efficient BA preservation and recycling system within the body, which is termed the enterohepatic circulation (57). BAs, which are biosynthesized by the catabolism of cholesterol in the liver, are involved in maintaining lipid, glucose, and energy metabolism in the liver, intestine, and adipose tissue (58). HF feeding did not disturb BA synthesis regulators, such as FXR-SHP or FXR-FGF15 (data not shown), but one of the key BA synthesis enzymes (*Cyp8b1*) was increased in the liver of HF mice, suggesting that HF may change the ratio of CA and CDCA synthesized by the liver, which leads to disturbed BA metabolism. Through the microscopic MSI analysis of the terminal ileum, we found that HF significantly reduced the distribution of TCA in the ileum tissue section. Interestingly, in the microscopic MSI of colon tissue, we also noticed that HF reduced the distribution of TCA in colon tissue. In view of previous studies have confirmed that TCA has strong anti-inflammatory effects in the gut that control gut bacteria overgrowth and protect intestinal barrier function (26, 27), we speculated that the molecular basis of HF aggravating TNBS-induced colitis is partly to reduce TCA distribution in colonic tissue, so as to reduce the anti-inflammatory ability of colonic mucosal that leads to gut bacteria overgrowth and intestinal barrier dysfunction. The main limitation is that the current study cannot determine which specific changes induced by HF feeding lead to worse IBD in a TNBS model. All the above-mentioned changes in BA, metabolites, or gene expression are to some distance associated with colitis susceptibility. As shown in **Figure 5, Phe** and **C18**:2 are strongly associated with AST and ALT, respectively, which indicated the potential role as indicators of colitis formation. Further study will be determined to distinguish the contribution of metabolic changes caused by change of diet to colitis susceptibility.

CONCLUSION

In summary, our results clearly indicate the possibility of the adverse effects of short-term HF on the metabolism of mice, including metabolic changes in FAs, AAs, and BAs, which might continue to have negative effects on health and promote the occurrence and development of IBD. Therefore, dietary fat intake is a factor that must be carefully considered, especially in the IBD population. Our results also suggest that HF-primed mice might be more likely to develop abnormal liver function or even hepatitis after TNBS-induced colitis, which needs to be further studied.

DATA AVAILABILITY STATEMENT

The original contributions presented in the study are included in the article/**Supplementary Material**, further inquiries can be directed to the corresponding authors.

ETHICS STATEMENT

The animal study was reviewed and approved by the Institutional Animal Care and Use Committee (IACUC) at the China Medical University.

AUTHOR CONTRIBUTIONS

H-XL and JD conceived of the study and participated in its design and coordination. Z-HW, JY, LC, and QZ carried out the experimental work and were responsible for analyzing the data. Z-HW, QZ, S-SZ, JY, LC, and X-YW were responsible for animal experiments. Z-HW, YL, and DC involved in manuscript revision. All authors have given approval to the final version of the manuscript.

FUNDING

This research received financial support from the General Project of Liaoning Provincial Department of Education under Grant No. LJKZ0758.

SUPPLEMENTARY MATERIAL

The Supplementary Material for this article can be found online at: https://www.frontiersin.org/articles/10.3389/fnut.2022.899829/full#supplementary-material

Supplementary Figure 1 | (A) The mass spectrum and secondary mass spectrometry of TCA standard. **(B)** Secondary mass spectrometry of ileum (precursor ion *m/z* 514.284). **(C)** Secondary mass spectrometry of colon (precursor ion *m/z* 514.284). Matrix: 9AA.

Supplementary Figure 2 | Phenotypes of mice fed a CD and HF for 4 weeks. **(A)** Schematic diagram for colitis model in CD and HF feeding mice. Male C57BL/6 mice were fed with a HF for 4 weeks, and control diet feeding mice were used as normal control. Three weeks later, mice of model group were presensitized with 1% (wt/vol) TNBS solution. Eight days after that, mice were treated under anesthesia with 2.5% (wt/vol) TNBS solution via intrarectal injection for 3 days to induce colitis. pre, before treatment. i.r., intrarectal delivery. The control group fed with CD or HF was not treated with TNBS. **(B)** All mice were sacrificed on day 3, and colons were collected to estimate mucosal damage by detecting colon lengths; gross morphology of the colons on day 3. **(C)** The representative histological sections were observed under microscopy (magnification: 2.5×). **(D)** qPCR quantitation of pro-inflammatory cytokines and chemokines in colonic mucosa on day 3. **(E)** The average daily food intake per mouse during the period of CD or HF feeding. The food intake of mice was recorded twice a week. $n \geq 3$. The data were shown as mean ± SEM. $^*p < 0.05$. CD, control diet group; HF, high-fat diet group.

REFERENCES

1. Galligan JJ. Beneficial actions of microbiota-derived tryptophan metabolites. *Neurogastroenterol Motil.* (2018) 30:e13283. doi: 10.1111/nmo.13283
2. Denver P, Gault VA, McClean PL. Sustained high-fat diet modulates inflammation, insulin signalling and cognition in mice and a modified xenin peptide ameliorates neuropathology in a chronic high-fat model. *Diabetes Obes Metab.* (2018) 20:1166–75. doi: 10.1111/dom.13210
3. Jena PK, Sheng L, Liu HX, Kalanetra KM, Mirsoian A, Murphy WJ, et al. Western diet-induced dysbiosis in farnesoid x receptor knockout mice causes persistent hepatic inflammation after antibiotic treatment. *Am J Pathol.* (2017) 187:1800–13. doi: 10.1016/j.ajpath.2017.04.019
4. Sheng L, Jena PK, Liu HX, Kalanetra KM, Gonzalez FJ, French SW, et al. Gender differences in bile acids and microbiota in relationship with gender dissimilarity in steatosis induced by diet and FXR inactivation. *Sci Rep.* (2017) 7:1748. doi: 10.1038/s41598-017-01576-9
5. Wang L, Gong Z, Zhang X, Zhu F, Liu Y, Jin C, et al. Gut microbial bile acid metabolite skews macrophage polarization and contributes to high-fat diet-induced colonic inflammation. *Gut Microbes.* (2020) 12:1–20. doi: 10.1080/19490976.2020.1819155
6. Duan Y, Zeng L, Zheng C, Song B, Li F, Kong X, et al. Inflammatory links between high fat diets and diseases. *Front Immunol.* (2018) 9:2649. doi: 10.3389/fimmu.2018.02649
7. Turpin W, Lee SH, Raygoza Garay JA, Madsen KL, Meddings JB, Bedrani L, et al. Increased intestinal permeability is associated with later development of Crohn's disease. *Gastroenterology.* (2020) 159:2092–2100.e5. doi: 10.1053/j.gastro.2020.08.005
8. de Aguiar Vallim TQ, Tarling EJ, Edwards PA. Pleiotropic roles of bile acids in metabolism. *Cell Metab.* (2013) 17:657–69. doi: 10.1016/j.cmet.2013.03.013
9. Perry RJ, Peng L, Barry NA, Cline GW, Zhang D, Cardone RL, et al. Acetate mediates a microbiome-brain-beta-cell axis to promote metabolic syndrome. *Nature.* (2016) 534:213–7. doi: 10.1038/nature18309
10. He F, Wu C, Li P, Li N, Zhang D, Zhu Q, et al. Functions and signaling pathways of amino acids in intestinal inflammation. *Biomed Res Int.* (2018) 2018:9171905. doi: 10.1155/2018/9171905
11. Guan Q. A comprehensive review and update on the pathogenesis of inflammatory bowel disease. *J Immunol Res.* (2019) 2019:7247238. doi: 10.1155/2019/7247238
12. Liu TC, Stappenbeck TS. Genetics and pathogenesis of inflammatory bowel disease. *Annu Rev Pathol.* (2016) 11:127–48.
13. Ng SC, Shi HY, Hamidi N, Underwood FE, Tang W, Benchimol EI, et al. Worldwide incidence and prevalence of inflammatory bowel disease in the 21st century: a systematic review of population-based studies. *Lancet.* (2017) 390:2769–78. doi: 10.1016/S0140-6736(17)32448-0
14. Wei M, Gao X, Liu L, Li Z, Wan Z, Dong Y, et al. Visceral adipose tissue derived exosomes exacerbate colitis severity via pro-inflammatory MiRNAs in high fat diet fed mice. *ACS Nano.* (2020) 14:5099–110. doi: 10.1021/acsnano.0c01860
15. Cheng L, Jin H, Qiang Y, Wu S, Yan C, Han M, et al. High fat diet exacerbates dextran sulfate sodium induced colitis through disturbing mucosal dendritic cell homeostasis. *Int Immunopharmacol.* (2016) 40:1–10. doi: 10.1016/j.intimp.2016.08.018
16. Hou JK, Abraham B, El-Serag H. Dietary intake and risk of developing inflammatory bowel disease: a systematic review of the literature. *Am J Gastroenterol.* (2011) 106:563–73. doi: 10.1038/ajg.2011.44
17. Richman E, Rhodes JM. Review article: evidence-based dietary advice for patients with inflammatory bowel disease. *Aliment Pharmacol Ther.* (2013) 38:1156–71. doi: 10.1111/apt.12500
18. Ananthakrishnan AN, Khalili H, Konijeti GG, Higuchi LM, de Silva P, Fuchs CS, et al. Long-term intake of dietary fat and risk of ulcerative colitis and Crohn's disease. *Gut.* (2014) 63:776–84. doi: 10.1136/gutjnl-2013-305304
19. Wirtz S, Popp V, Kindermann M, Gerlach K, Weigmann B, Fichtner-Feigl S, et al. Chemically induced mouse models of acute and chronic intestinal inflammation. *Nat Protoc.* (2017) 12:1295–309. doi: 10.1038/nprot.2017.044
20. Park CM, Reid PE, Walker DC, MacPherson BR. A simple, practical 'swiss roll' method of preparing tissues for paraffin or methacrylate embedding. *J Microsc.* (1987) 145:115–20. doi: 10.1111/j.1365-2818.1987.tb01321.x
21. Molodecky NA, Soon IS, Rabi DM, Ghali WA, Ferris M, Chernoff G, et al. Increasing incidence and prevalence of the inflammatory bowel diseases with time, based on systematic review. *Gastroenterology.* (2012) 142:46–54e42;quize30. doi: 10.1053/j.gastro.2011.10.001
22. Degirolamo C, Modica S, Palasciano G, Moschetta A. Bile acids and colon cancer: solving the puzzle with nuclear receptors. *Trends Mol Med.* (2011) 17:564–72. doi: 10.1016/j.molmed.2011.05.010
23. Deng P, Hoffman JB, Petriello MC, Wang CY, Li XS, Kraemer MP, et al. Dietary inulin decreases circulating ceramides by suppressing neutral sphingomyelinase expression and activity in mice. *J Lipid Res.* (2020) 61:45–53. doi: 10.1194/jlr.RA119000346
24. Ericksen RE, Lim SL, McDonnell E, Shuen WH, Vadiveloo M, White PJ, et al. ., Loss of BCAA catabolism during carcinogenesis enhances mTORC1 activity and promotes tumor development and progression. *Cell Metab.* (2019) 29:1151–1165.e6. doi: 10.1016/j.cmet.2018.12.020
25. Rzagalinski I, Hainz N, Meier C, Tschernig T, Volmer DA. MALDI Mass spectral imaging of bile acids observed as deprotonated molecules and proton-bound dimers from mouse liver sections. *J Am Soc Mass Spectrom.* (2018) 29:711–22. doi: 10.1007/s13361-017-1886-6
26. Wang C, Li L, Guan H, Tong S, Liu M, Liu C, et al. Effects of taurocholic acid on immunoregulation in mice. *Int Immunopharmacol.* (2013) 15:217–22. doi: 10.1016/j.intimp.2012.12.006
27. Yang Y, He J, Suo Y, Lv L, Wang J, Huo C, et al. Anti-inflammatory effect of taurocholate on TNBS-induced ulcerative colitis in mice. *Biomed Pharmacother.* (2016) 81:424–30. doi: 10.1016/j.biopha.2016.04.037
28. Lam YY, Ha CW, Campbell CR, Mitchell AJ, Dinudom A, Oscarsson J, et al. Increased gut permeability and microbiota change associate with mesenteric fat inflammation and metabolic dysfunction in diet-induced obese mice. *PLoS One.* (2012) 7:e34233. doi: 10.1371/journal.pone.0034233
29. Ding S, Chi MM, Scull BP, Rigby R, Schwerbrock NM, Magness S, et al. High-fat diet: bacteria interactions promote intestinal inflammation which precedes and correlates with obesity and insulin resistance in mouse. *PLoS One.* (2010) 5:e12191. doi: 10.1371/journal.pone.0012191
30. Metzemaekers M, Vanheule V, Janssens R, Struyf S, Proost P. Overview of the mechanisms that may contribute to the non-redundant activities of interferon-inducible CXC chemokine receptor 3 ligands. *Front Immunol.* (2017) 8:1970. doi: 10.3389/fimmu.2017.01970
31. Cho YW, Kwon YH. Regulation of gene expression in the development of colitis-associated colon cancer in mice fed a high-fat diet. *Biochem Biophys Res Commun.* (2022) 592:81–6. doi: 10.1016/j.bbrc.2022.01.016
32. Lasker S, Rahman MM, Parvez F, Zamila M, Miah P, Nahar K, et al. High-fat diet-induced metabolic syndrome and oxidative stress in obese rats are ameliorated by yogurt supplementation. *Sci Rep.* (2019) 9:20026. doi: 10.1038/s41598-019-56538-0
33. Koska J, Ozias MK, Deer J, Kurtz J, Salbe AD, Harman SM, et al. A human model of dietary saturated fatty acid induced insulin resistance. *Metabolism.* (2016) 65:1621–8. doi: 10.1016/j.metabol.2016.07.015
34. Li J, Wu H, Liu Y, Yang L. High fat diet induced obesity model using four strainsof mice: kunming, C57BL/6, BALB/c and ICR. *Exp Anim.* (2020) 69:326–35. doi: 10.1538/expanim.19-0148
35. Liu L, Dong W, Wang S, Zhang Y, Liu T, Xie R, et al. Deoxycholic acid disrupts the intestinal mucosal barrier and promotes intestinal tumorigenesis. *Food Funct.* (2018) 9:5588–97. doi: 10.1039/c8fo01143e
36. Stenman LK, Holma R, Korpela R. High-fat-induced intestinal permeability dysfunction associated with altered fecal bile acids. *World J Gastroenterol.* (2012) 18:923–9. doi: 10.3748/wjg.v18.i9.923
37. Rohr MW, Narasimhulu CA, Rudeski-Rohr TA, Parthasarathy S. Negative effects of a high-fat diet on intestinal permeability: a review. *Adv Nutr.* (2020) 11:77–91. doi: 10.1093/advances/nmz061
38. Xu M, Cen M, Shen Y, Zhu Y, Cheng F, Tang L, et al. Deoxycholic acid-induced gut dysbiosis disrupts bile acid enterohepatic circulation and promotes intestinal inflammation. *Dig Dis Sci.* (2021) 66:568–76. doi: 10.1007/s10620-020-06208-3
39. Dermadi D, Valo S, Ollila S, Soliymani R, Sipari N, Pussila M, et al. Western diet deregulates bile acid homeostasis, cell proliferation, and tumorigenesis in colon. *Cancer Res.* (2017) 77:3352–63. doi: 10.1158/0008-5472.CAN-16-2860
40. Stenman LK, Holma R, Eggert A, Korpela R. A novel mechanism for gut barrier dysfunction by dietary fat: epithelial disruption by hydrophobic bile acids. *Am J Physiol Gastrointest Liver Physiol.* (2013) 304:G227–34. doi: 10.1152/ajpgi.00267.2012

41. Pheiffer C, Jacobs C, Patel O, Ghoor S, Muller C, Louw J. Expression of UCP2 in Wistar rats varies according to age and the severity of obesity. *J Physiol Biochem.* (2016) 72:25–32. doi: 10.1007/s13105-015-0454-4
42. Dobrzyn P, Dobrzyn A, Miyazaki M, Cohen P, Asilmaz E, Hardie DG, et al. Stearoyl-CoA desaturase 1 deficiency increases fatty acid oxidation by activating AMP-activated protein kinase in liver. *Proc Natl Acad Sci USA.* (2004) 101:6409–14. doi: 10.1073/pnas.0401627101
43. Am AL, Syed DN, Ntambi JM. Insights into stearoyl-CoA desaturase-1 regulation of systemic metabolism. *Trends Endocrinol Metab.* (2017) 28:831–42. doi: 10.1016/j.tem.2017.10.003
44. Yu FY, Huang SG, Zhang HY, Ye H, Chi HG, Zou Y, et al. Comparison of 5-hydroxytryptophan signaling pathway characteristics in diarrhea-predominant irritable bowel syndrome and ulcerative colitis. *World J Gastroenterol.* (2016) 22:3451–9. doi: 10.3748/wjg.v22.i12.3451
45. Mawe GM, Hoffman JM. Serotonin signalling in the gut–functions, dysfunctions and therapeutic targets. *Nat Rev Gastroenterol Hepatol.* (2013) 10:473–86. doi: 10.1038/nrgastro.2013.105
46. Lamas B, Richard ML, Leducq V, Pham HP, Michel ML, Da Costa G, et al. CARD9 impacts colitis by altering gut microbiota metabolism of tryptophan into aryl hydrocarbon receptor ligands. *Nat Med.* (2016) 22:598–605. doi: 10.1038/nm.4102
47. Guseva D, Holst K, Kaune B, Meier M, Keubler L, Glage S, et al. Serotonin 5-HT7 receptor is critically involved in acute and chronic inflammation of the gastrointestinal tract. *Inflamm Bowel Dis.* (2014) 20:1516–29. doi: 10.1097/MIB.0000000000000150
48. Liu H, Tan B, Huang B, Li J, Wang J, Liao P, et al. Involvement of calcium-sensing receptor activation in the alleviation of intestinal inflammation in a piglet model by dietary aromatic amino acid supplementation. *Br J Nutr.* (2018) 120:1321–31. doi: 10.1017/S0007114518002891
49. Siriwardhana N, Kalupahana NS, Moustaid-Moussa N. Health benefits of n-3 polyunsaturated fatty acids: eicosapentaenoic acid and docosahexaenoic acid. *Adv Food Nutr Res.* (2012) 65:211–22. doi: 10.1016/B978-0-12-416003-3.00013-5
50. Bleau C, Karelis AD, St-Pierre DH, Lamontagne L. Crosstalk between intestinal microbiota, adipose tissue and skeletal muscle as an early event in systemic low-grade inflammation and the development of obesity and diabetes. *Diabetes Metab Res Rev.* (2015) 31:545–61. doi: 10.1002/dmrr.2617
51. Rioux V, Catheline D, Bouriel M, Legrand P. Dietary myristic acid at physiologically relevant levels increases the tissue content of C20:5 n-3 and C20:3 n-6 in the rat. *Reprod Nutr Dev.* (2005) 45:599–612. doi: 10.1051/rnd:2005048
52. Ren M, Zhang SH, Zeng XF, Liu H, Qiao SY. Branched-chain amino acids are beneficial to maintain growth performance and intestinal immune-related function in weaned piglets fed protein restricted diet. *Asian Australas J Anim Sci.* (2015) 28:1742–50. doi: 10.5713/ajas.14.0131
53. Andou A, Hisamatsu T, Okamoto S, Chinen H, Kamada N, Kobayashi T, et al. Dietary histidine ameliorates murine colitis by inhibition of proinflammatory cytokine production from macrophages. *Gastroenterology.* (2009) 136:564–74.e2. doi: 10.1053/j.gastro.2008.09.062
54. Hisamatsu T, Ono N, Imaizumi A, Mori M, Suzuki H, Uo M, et al. Decreased plasma histidine level predicts risk of relapse in patients with ulcerative colitis in remission. *PLoS One.* (2015) 10:e0140716. doi: 10.1371/journal.pone.0140716
55. Li P, Yin YL, Li D, Kim SW, Wu G. Amino acids and immune function. *Br J Nutr.* (2007) 98:237–52.
56. Nagarjun S, Dhadde SB, Veerapur VP, Thippeswamy BS, Chandakavathe BN. Ameliorative effect of chromium-d-phenylalanine complex on indomethacin-induced inflammatory bowel disease in rats. *Biomed Pharmacother.* (2017) 89:1061–6. doi: 10.1016/j.biopha.2017.02.042
57. Cai H, Wen Z, Meng K, Yang P. Metabolomic signatures for liver tissue and cecum contents in high-fat diet-induced obese mice based on UHPLC-Q-TOF/MS. *Nutr Metab (Lond).* (2021) 18:69. doi: 10.1186/s12986-021-00595-8
58. Chiang JYL, Ferrell JM. Bile acid metabolism in liver pathobiology. *Gene Expr.* (2018) 18:71–87. doi: 10.3727/105221618X15156018385515

Conflict of Interest: The authors declare that the research was conducted in the absence of any commercial or financial relationships that could be construed as a potential conflict of interest.

Publisher's Note: All claims expressed in this article are solely those of the authors and do not necessarily represent those of their affiliated organizations, or those of the publisher, the editors and the reviewers. Any product that may be evaluated in this article, or claim that may be made by its manufacturer, is not guaranteed or endorsed by the publisher.

frontiers | Frontiers in Nutrition

ORIGINAL RESEARCH
published: 27 June 2022
doi: 10.3389/fnut.2022.893344

The Protective Effect of Sulforaphane on Dextran Sulfate Sodium-Induced Colitis Depends on Gut Microbial and Nrf2-Related Mechanism

Canxia He[1,2], *Mingfei Gao*[2], *Xiaohong Zhang*[2], *Peng Lei*[3], *Haitao Yang*[4], *Yanping Qing*[1*] *and Lina Zhang*[2*]

[1] *The Affiliated Hospital of Medical School, Ningbo University, Ningbo, China,* [2] *Institute of Preventative Medicine, School of Medicine, Ningbo University, Ningbo, China,* [3] *Center for Engineering in Medicine and Surgery, Department of Surgery, Massachusetts General Hospital, Boston, MA, United States,* [4] *Department of Pathology, Mingzhou Hospital of Zhejiang University, Ningbo, China*

Sulforaphane (SFN), an isothiocyanate present in cruciferous vegetables such as broccoli and brussels sprouts, has a variety of biological functions. This study was undertaken to assess the potential efficacy of SFN in ameliorating dextran sulfate sodium (DSS)-induced ulcerative colitis (UC) in mice and to elucidate the underlying mechanisms. UC was induced in mice with administration of 2% DSS in drinking water for 7 days. Male C57BL/6 mice were treated with Mesalazine (50 and 100 mg/kg body weight) and various doses of SFN (2.5, 5, 10, and 20 mg/kg body weight). In DSS colitis mice, the hallmarks of disease observed as shortened colon lengths, increased disease activity index (DAI) scores and pathological damage, higher proinflammatory cytokines and decreased expression of tight junction proteins, were alleviated by SFN treatment. SFN also partially restored the perturbed gut microbiota composition and increased production of volatile fatty acids (especially caproic acid) induced by DSS administration. The heatmap correlation analysis indicated that *Lactobacillus johnsonii*, *Bacteroides acidifaciens*, unclassified *Rikenellaceae RC9*, and unclassified *Bacteroides* were significantly correlated with disease severity. Nuclear factor (erythroid-derived 2)-like 2 (Nrf2), Signal Transducer and Activator of Transcription 3 (STAT3), and Phase II enzyme UDP-glucuronosyltransferase (UGT) were involved in the protective effect of SFN against DSS-induced colitis. This study's findings suggest that SFN may serve as a therapeutic agent protecting against UC.

Keywords: sulforaphane, ulcerative colitis, gut microbiota, Nrf2, inflammation, intestinal barrier, inflammatory bowel disease

OPEN ACCESS

Edited by:
Hui-Xin Liu,
China Medical University, China

Reviewed by:
Matthew Philip Greig Barnett,
AgResearch Ltd, New Zealand
Peijun Tian,
Jiangnan University, China

***Correspondence:**
Lina Zhang
zhanglina@nbu.edu.cn
Yanping Qing
willfly0703@163.com

Specialty section:
This article was submitted to Nutrition and Metabolism, a section of the journal Frontiers in Nutrition

Received: *10 March 2022*
Accepted: *12 May 2022*
Published: *27 June 2022*

Citation:
He C, Gao M, Zhang X, Lei P, Yang H, Qing Y and Zhang L (2022) The Protective Effect of Sulforaphane on Dextran Sulfate Sodium-Induced Colitis Depends on Gut Microbial and Nrf2-Related Mechanism. Front. Nutr. 9:893344. doi: 10.3389/fnut.2022.893344

INTRODUCTION

Inflammatory bowel disease (IBD), including Crohn's disease and ulcerative colitis (UC), is a chronic inflammatory disease of the gastrointestinal tract. Over 1 million residents in the United States and 2.5 million across Europe are estimated to have IBD with substantial costs for health care (1). Even in China, owing to the industrialization of society, incidence and prevalence of IBD has strikingly increased (2). Diet, frequent antibiotics use, and smoking are potential risk factors in IBD (3). The complex and precise underlying mechanisms are yet to be completely understood, however, the intestinal barrier function, immune system, and cross-talk

between host and gut microbiota, are various processes known to be involved in the pathogenesis of IBD (4).

The disruption of intestinal barrier function is a hallmark of IBD. This leads to increased intestinal permeability and a significant impact on the gut microbial composition and diversity. Emerging evidence highlights the pivotal role played by gut microbiota in maintaining normal physiological functions of colon along with regulation of local immune system. An altered intestinal barrier and immune signaling dysregulation lead to mucosal inflammation, associated with an increased secretion of pro-inflamatory cytokines (5). Pro-inflammatory cytokines like interleukin-6 (IL-6) and tumor necrosis factor TNF-α), have been demonstrated as substantially upregulated, and strongly correlate with the severity of active IBD. Moreover, elevated levels of these cytokines, such as TNF-α, are known to damage intestinal tight junctions and permeability (6). Subsequently, an ongoing cycle ensues between the intestinal immune system, gut microbiota, and barrier function, responsible for the various clinical presentations of IBD. Given the multi-factorial etiology and complex pathophysiology of IBD, existing therapies have fallen short in terms of limited efficacy, multiple side effects and recurrence of attacks (7). Thereby, the need to identify alternative treatment modalities for IBD remains.

Sulforaphane (SFN), an isothiocyanate present in cruciferous vegetables such as broccoli and brussels sprouts, has attracted a lot of attention due to its unique ability to activate Kelch-like ECH-associated protein 1 (Keap1)–nuclear factor erythroid-2-related factor 2 (Nrf2)–antioxidant response elements (ARE) pathway (8). A variety of beneficial functions, such as anti-oxidant owned by SFN, rely on the induction of Nrf2-driven proteins. Most recently, there has been an increased focus on the anti-inflammatory and mucosa protective effects of SFN. Our previous results have confirmed that SFN significantly increased tight junction proteins expression both *in vitro* and *in vivo* models (9). In addition, SFN also exhibits a protective role against inflammation by notably decreasing the expression of various pro-inflammatory cytokines (9, 10). Furthermore, SFN has been shown to reverse the gut microbiota dysbiosis in mice, and also increased levels of intestinal short-chain fatty acids (9). Therefore, we hypothesized that SFN would be effective in ameliorating intestinal damage and dysfunction seen in IBD. The results from a previous study by Wagner et al. found that pretreatment with SFN at a dose of 25 mg/kg for 7 days significantly improved symptoms and reduced the inflammatory biomarker's expression in dextran sulfate sodium (DSS)-induced UC mice (11). Another study by Zhang et al. (12) reported that SFN reversed the gut dysbiosis and also reduced the damage in DSS-induced colitis mice. Thereby, in this study, we utilized a DSS-induced colitis model in mice to thoroughly investigate the protective effects and uncover the associated mechanism of SFN in treatment of IBD.

MATERIALS AND METHODS

Materials and Chemicals

SFN was purchased from Toronto Research Chemicals (Toronto, Canada). DSS (36,000–50,000 Da molecular weight) was obtained from MP Biomedicals, Inc. (Solon, USA). Mesalazine was obtained from Ipsen Pharmaceutical Co. (France). NP40 lysis buffer, BCA protein assay kit, dimethylsulfoxide, and normal saline were purchased from the Beyotime Institute of Biotechnology (Nantong, China). Primary antibodies against ZO-1, Occludin, Claudin-1, Nrf2, UDP-glucuronosyltransferase (UGT), Signal Transducer, and Activator of Transcription-3 (STAT3), Cyclooxygenase-2 (COX-2), β-actin, and horseradish peroxidase (HRP)-conjugated secondary antibodies were obtained from Proteintech Group, Inc. (Wuhan, China). Mouse IL-6, interferon (IFN)-γ, TNF-α, and IL-1β enzyme-linked immunosorbent (ELISA) kits were obtained from Elabscience Biotechnology Co., Ltd (Wuhan, China). A Western blot enhanced chemiluminescence kit was purchased from Advansta, Inc. (San Jose, USA).

Animal Experiment and Dosage Regimen

Seventy 8-week-old male C57BL/6 mice were purchased from Shanghai Slac Laboratory Animal Co. Ltd (Shanghai, China) and housed in the facilities of Laboratory Animal Services at Ningbo University (temperature 22 ± 2°C and humidity 55 ± 5% with a 12-h/12-h light/dark cycle). Mice were allowed to acclimate for 2 weeks prior to the experiment. The mice (nearly 25 g) were randomly assigned to eight groups (10 mice for the groups B–F; six mice for the group A; and seven mice for the groups G and H). DSS was dissolved in drinking water at a concentration of 2% DSS (w/v) to induce colitis. In the DSS treatment groups, mice received distilled water for 7 days, then 2% DSS for 7 days, followed by 5 days of distilled water. SFN was dissolved in a small volume of DMSO and diluted to the appropriate concentration with normal saline. The final concentration of DMSO did not exceed 1%. In the SFN-treated groups, mice were gavaged with SFN (2.5, 5, 10, and 20 mg/kg/day for the groups C–F, separately) during the whole experimental procedure. In the groups G and H, mice were orally administrated with Mesalazine (50 and 100 mg/kg/day) during DSS treatment time that served as a positive medical treatment group. All mice in each group had identical total gavage volume and identical contents of solvent.

All mice were maintained in solid-bottom cages and were allowed free access to food and water during the entire experimental procedure. Body weight and consumption of food and water for all mice were monitored every day throughout the whole experimental procedure. Mouse survival was closely monitored throughout the experimental period. The whole experimental period lasted for 19 days. The experimental scheme is shown in **Figure 1A**. The study was approved by the Ethics Committee of Ningbo University (Registration Number: NBU20210028) and performed according to the Guidelines for Animal Care.

Sample Collection and Disease Activity Index

DAIs of mice, including body weight loss (%), stool consistency, and blood in feces, were measured and recorded according to the DAI scoring system in **Supplementary Table 1**. DAI score, which is defined as the average of body weight loss score, fecal character score, and blood stool fraction, was used to evaluate

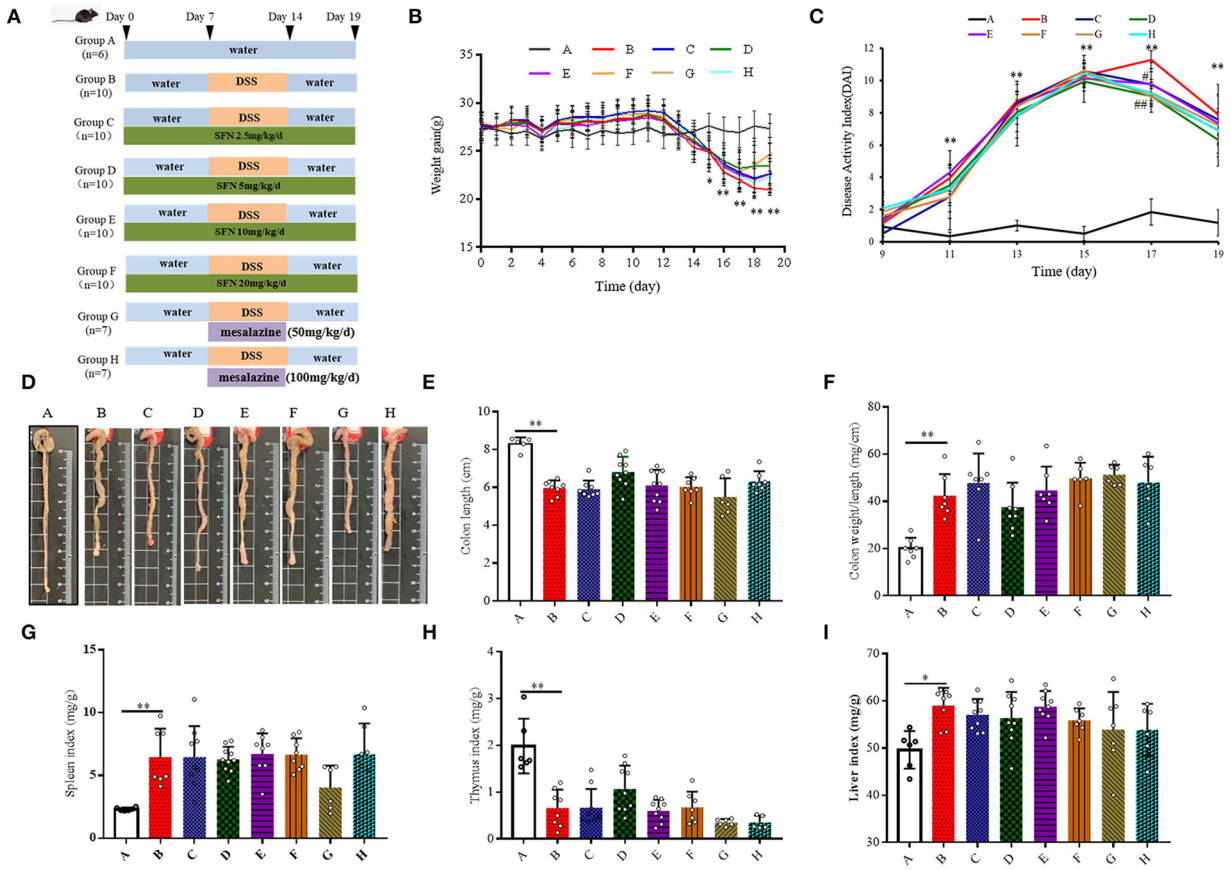

FIGURE 1 | Effect of SFN on colitis symptoms in mice. **(A)** Scheme of the animal experimental design. Group A: Negative control; Group B: Colitis model (2% DSS in drinking water); Group C: SFN (2.5 mg/kg/d) + colitis model (2% DSS in drinking water); Group D: SFN (5 mg/kg/day) + colitis model (2% DSS in drinking water); Group E: SFN (10 mg/kg/day) + colitis model (2% DSS in drinking water); Group F: SFN (20 mg/kg/day) + colitis model (2% DSS in drinking water); Group G: Mesalazine (50 mg/kg/day) + colitis model (2% DSS in drinking water); Group H: Mesalazine (100 mg/kg/day) + colitis model (2% DSS in drinking water). **(B)** Mean body weight over time. **(C)** DAI score. **(D)** Representative macroscopic pictures of colons in each group. **(E)** Colon length. **(F)** Colon weight/ length ratio. **(G)** Spleen index. **(H)** Thymus index. **(I)** Liver index. All data are presented as the mean ± SD. *P* value < 0.05 was considered to indicate statistical significance (**P* < 0.05 and ***P* < 0.01 compared with Group A, #*P* < 0.05 and ##*P* < 0.01 compared with Group B).

the severity of colitis. At the end of the experiment, all of the mice were sacrificed and tissues (colon, spleen, thymus, and liver) were collected. Colon segments between the ileocecal junction and the anus were removed. Colons were weighed and washed with ice-cold PBS, and colonic contents were collected and stored at −80°C. Distal colon parts were fixed in 4% paraformaldehyde, embedded in paraffin, and stained with hematoxylin & eosin (H&E) to observe the tissue morphological changes with an optical microscope and conduct histological evaluation, while the other parts were stored at −80°C for further studies.

Histological Assessment

Colon specimens were embedded in paraffin and cut into 4 μm sections for H&E staining. The slides were examined with an Olympus BX40 microscope (200× and 400× magnification). All the slides were grossly inspected in a blinded fashion by two pathological experts. The inflammatory scores are presented as the sum of the four parameters as shown in **Supplementary Table 2**.

Determination of Cytokines Concentration in Serum

Blood samples from mice were collected by retro-orbital sinus puncture under isoflurane anesthesia *via* the medial canthus of the eye using clean heparinized microhematocrit tubes. Blood was collected and centrifuged at 3,000 rpm for 15 min, and then the serum was obtained. Aliquots of each serum sample were stored at −80°C. The concentrations of IL-6, IFN-γ, TNF-α, and IL-1β were determined using ELISA kits (Elabscience Biotechnology Co., Ltd, China) according to the manufacturer's instructions. The concentrations were spectrophotometrically quantified by measuring the absorbance at 450 nm. The data were measured in pg mL^{-1}.

DNA Extraction and 16S rRNA Gene Sequencing Analysis

Total genomic DNA was extracted from fecal samples using the E.Z.N.A.® DNA Kit (Omega Bio-Tek, Norcross, GA, USA). DNA concentration was assessed using a Nanodrop (Thermo Scientific). DNA integrity and size

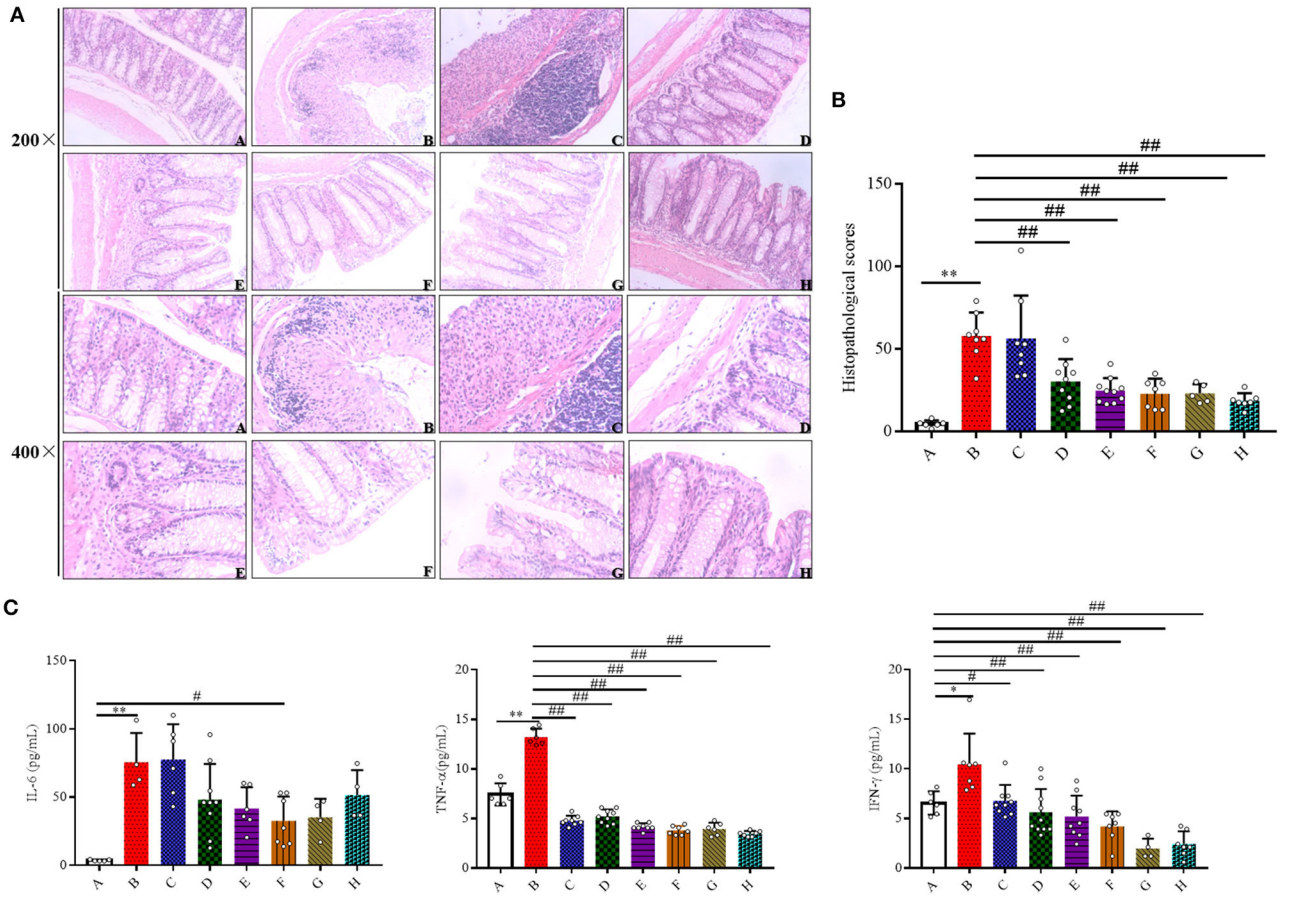

FIGURE 2 | Effects of SFN on histopathological characteristics and inflammatory in colitis mice. **(A)** Representative H&E staining of colon tissues (magnification ×200, and ×400). **(B)** Colonic histological score. **(C)** Effects of SFN on the concentrations of IL-6, TNF-α, and IFN-γ in plasma were determined by ELISA at a concentration of pg/ml. All data are presented as the mean ± SD. *P*-value < 0.05 was considered to indicate statistical significance (**P* < 0.05 and ***P* < 0.01 compared with Group A, #*P* < 0.05 and ##*P* < 0.01 compared with Group B).

were assessed using agarose gel electrophoresis, and all the samples that were showing adequate concentration and integrity were kept for further sequencing analysis. The V3–V4 variable regions of the 16S rRNA gene extracted from each fecal sample were amplified using primers 338F (5′-ACTCCTACGGGAGGCAGCA-3′) and 806R (5′-GGACTACHVGGGTWTCTAAT-3′) on a GeneAmp 9700 thermal cycler PCR system (Applied Biosystems, USA). PCR amplicons were purified using the AxyPrep DNA Gel Extraction Kit (Axygen, USA) and quantified using a QuantiFluor™-ST fluorometer (Promega, USA). After the individual quantification step, amplicons were pooled in equal amounts, and pair-end 2×300-base pair (bp) sequencing was performed using the Illumina MiSeq platform. Raw fastq files were demultiplexed and quality-filtered by the Quantitative Insights into Microbial Ecology (QIIME) platform and R packages (v3.2.0). Operational taxonomic units (OTUs) were picked using a criterion of 97% nucleotide identity. α-Diversity was measured by species richness and evenness from the rarefied OTU and indicated as the Shannon and Simpson indices. Sequencing data were analyzed using the free online Majorbio Cloud Platform (https://cloud.majorbio.com/).

Gas Chromatography Analysis of Volatile Fatty Acids in the Samples of Colonic Contents

The whole procedure was performed as mentioned in the previous study (9). Briefly, the samples of colonic contents (1 g) from all the groups of mice were homogenized in 5 ml of deionized water for 10 min and then centrifuged at 13,200 × *g* for 20 min at 4°C. The supernatant was immediately filtered through a 0.45 μm microfiber filter. Then, 1 ml of supernatant was placed in a 1.5 ml GC vial, to which 100 μL of formic acid was added. Standard curves for seven fatty acids (99%, analytical standard, Sigma) were made to analyze the concentrations of volatile fatty acids from the colonic contents of the mice. Volatile fatty acids were quantified by GC (Agilent 7,890; Agilent Technologies, USA) equipped with a flame ionization detector (FID). The concentrations of total fatty acids were calculated as the sum of those of volatile fatty acids (acetic acid, propionic acid,

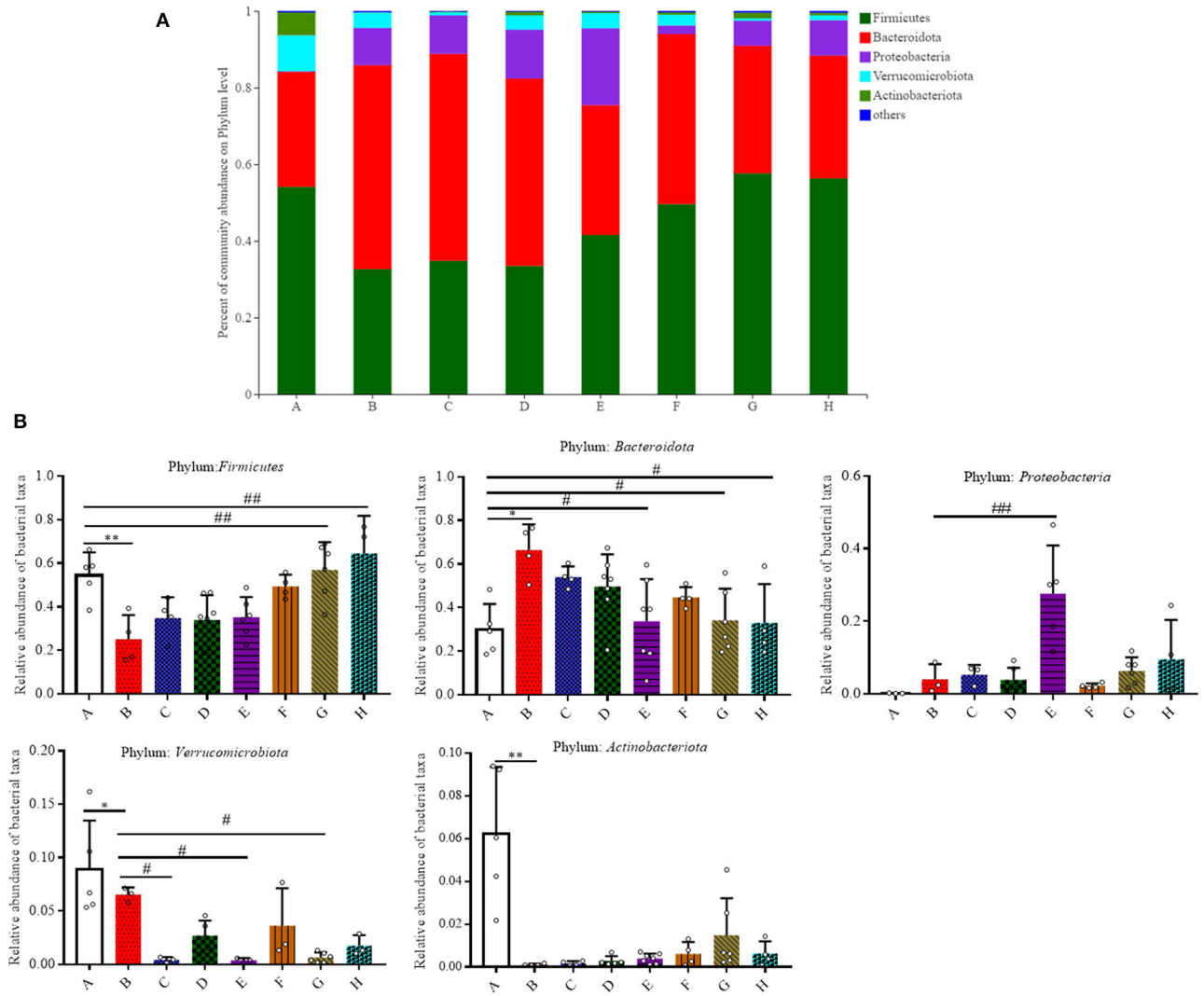

FIGURE 3 | Effect of SFN on gut microbiota compositions at the phylum level in colitis mice. **(A)** Gut microbiota compositions at the phylum level in each group. **(B)** Relative abundance of predominant bacterial community members at the phylum level. All data are presented as the mean ± SD. *P*-value <0.05 was considered to indicate statistical significance (*$P < 0.05$ and **$P < 0.01$ compared with Group A, $^{\#}P < 0.05$ and $^{\#\#}P < 0.01$ compared with Group B).

butyric acid, iso-butyric acid, valeric acid, iso-valeric acid, and caproic acid).

Protein Extraction and Western Blotting Analysis

Frozen colon samples were ground into powder in liquid nitrogen and lysed in ice-cold NP-40 lysis buffer containing 1 mM of protease inhibitor PMSF for 30 min. Colon tissue homogenate was centrifuged at 16,000×*g* for 20 min at 4°C, the supernatants were collected for Western blot analysis. Equal amounts of proteins (60 μg) were subsequently separated with SDS–polyacrylamide gel electrophoresis and transferred to PVDF membranes. After blocking with 5% skimmed milk at room temperature for 1 h, the membranes were incubated with primary antibodies at 4°C overnight, washed with TBST, and incubated with HRP-conjugated secondary antibodies at room temperature for 1.5 h. The membranes were visualized with an enhanced chemiluminescence reagent. The relative densities of the individual bands were analyzed densitometrically using the ChemiImager 4,000 instrument (Alpha Innotech, USA).

Statistical Analyses

All data were reported as the mean ± standard deviation (SD). Statistical analysis was carried out using SPSS 19.0 software (SPSS Inc., Chicago, IL, USA) and Graphpad prism 6. For data sets confirmed with normal distribution (Shapiro-Wilk test), an unpaired Student's *t*-test was performed between Group A and Group B, and one-way ANOVA was performed to compare the effects of SFN and Mesalazine treatment in the DSS-treated group, followed by Dunnett's multiple comparison test against

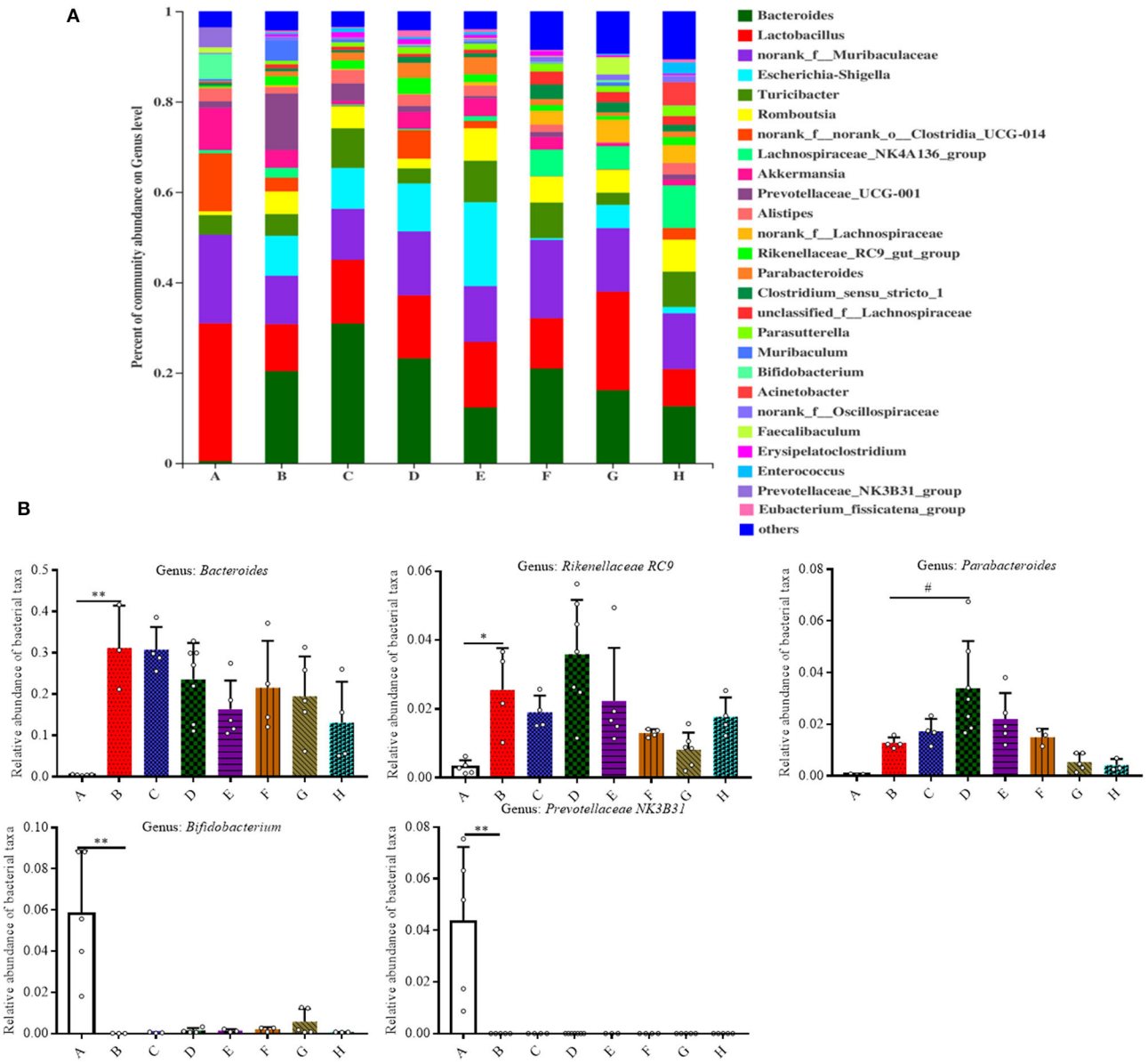

FIGURE 4 | Effect of SFN on gut microbiota compositions at the genus level in colitis mice. **(A)** Gut microbiota compositions at the genus level in each group. **(B)** Relative abundance of predominant bacterial community members at the genus level. All data are presented as the mean ± SD. *P*-value <0.05 was considered to indicate statistical significance (*$P < 0.05$ and **$P < 0.01$ compared with Group A, $^{\#}P < 0.05$ and $^{\#\#}P < 0.01$ compared with Group B).

Group B. For the data sets that are not normally distributed, the Mann–Whitney test was performed between Group A and Group B, and the Kruskal-Wallis tests were performed for Groups B–H with Dunn's *post-hoc* test against Group B. The *P*-value generated from the multiple comparisons has already been adjusted by family-wise significance and confidence levels of 0.05.

RESULTS

SFN-Alleviated DSS-Induced Colitis in Mice

Body weight was recorded at the same time point every day. As shown in **Figure 1B** and **Supplementary Table 3**, the body weight of all DSS treatment groups (i.e., the Groups B–F) decreased significantly on the 15th-19th day. On the 19th day, 20 mg/kg/day of SFN (Group F) improved the body weight loss in contrast to Group B ($P < 0.05$). DAI scores were used to evaluate the severity of colitis (**Figure 1C**). On the 11th, 13th, 15th, and 19th day, the DAI scores were increased significantly in Group B than that in Group A. On the 17th day, the DAI scores in the SFN- and Mesalazine-treatment groups (groups D, F–H) were decreased significantly than that in Group B ($P < 0.05$). The detailed DAI scores at six different time points are shown in **Supplementary Table 4**.

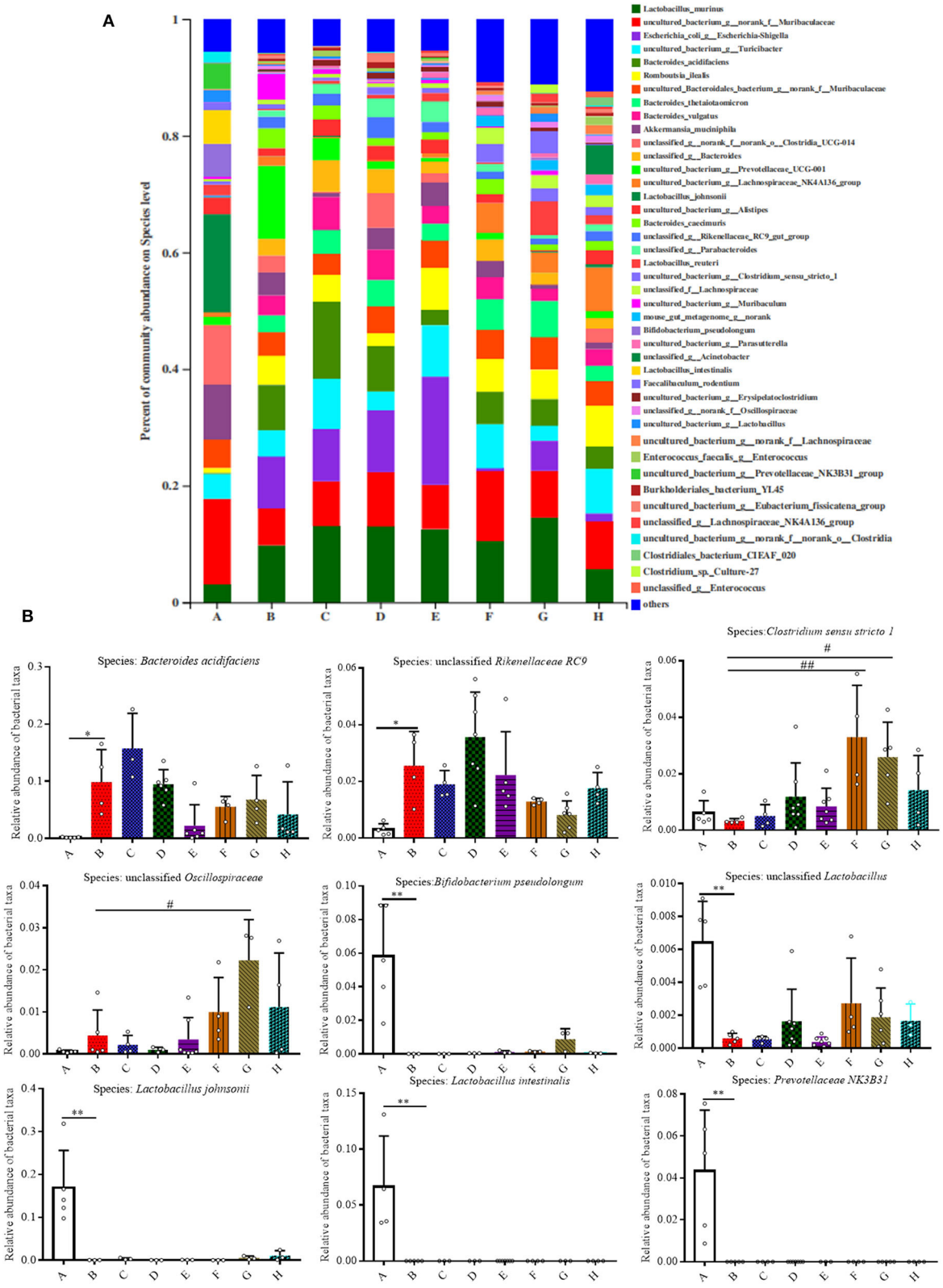

FIGURE 5 | Effect of SFN on gut microbiota compositions at the species level in colitis mice. **(A)** Gut microbiota compositions at the species level in each group. **(B)** Relative abundance of predominant bacterial community members at the species level. All data are presented as the mean ± SD. *P*-value <0.05 was considered to indicate statistical significance (*$P < 0.05$ and **$P < 0.01$ compared with Group A, $^{\#}P < 0.05$ and $^{\#\#}P < 0.01$ compared with Group B).

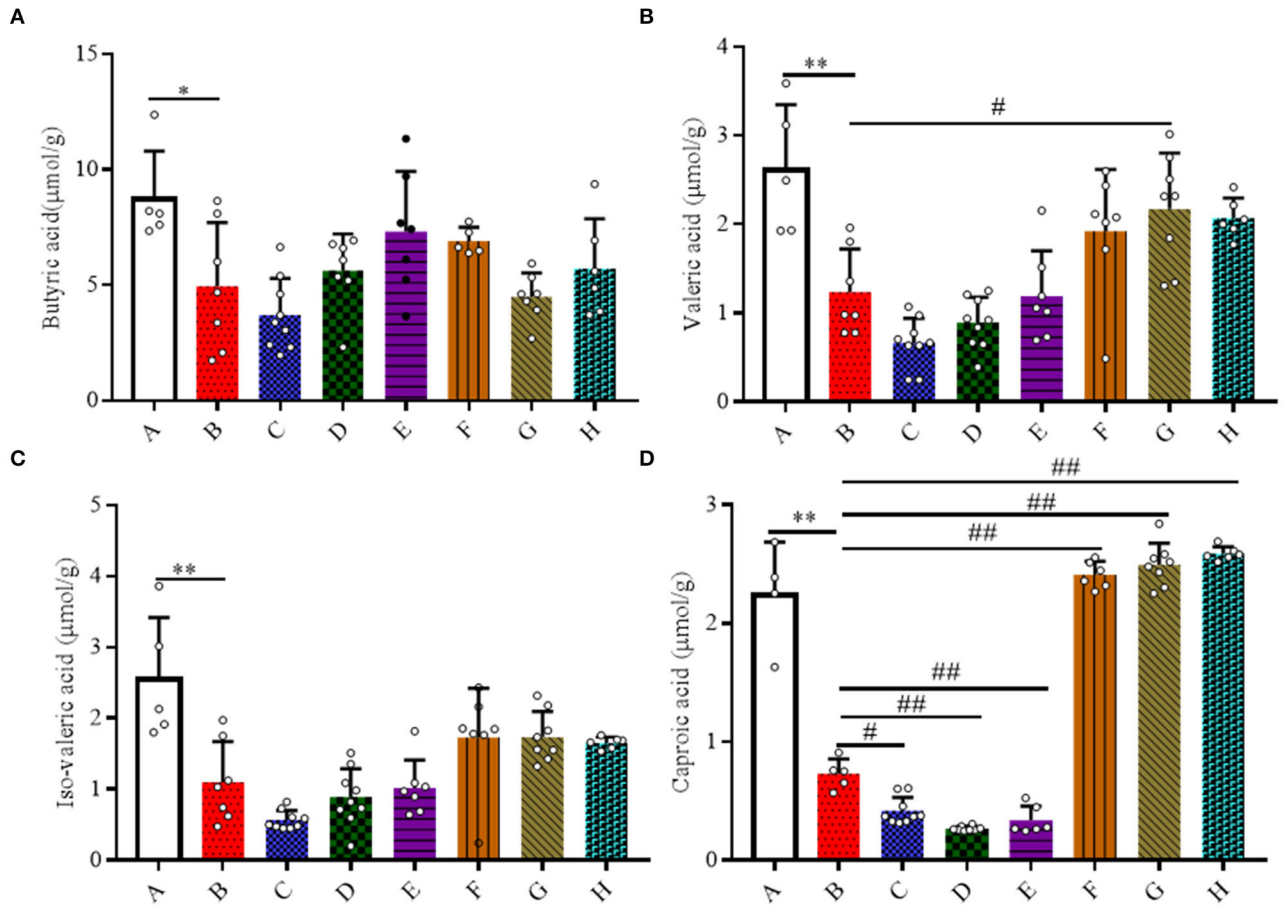

FIGURE 6 | Effect of SFN on volatile fatty acids concentrations in colitis mice. The samples were collected from colonic contents of all groups of mice. **(A)** Butyric acid; **(B)** Valeric acid; **(C)** Iso-valeric acid; **(D)** Caproic acid. All data are presented as the mean ± SD. *P*-value <0.05 was considered to indicate statistical significance (*$P < 0.05$ and **$P < 0.01$ compared with Group A, #$P < 0.05$ and ##$P < 0.01$ compared with Group B).

As shown in **Figure 1D**, in Group B, characteristic macroscopic manifestations of DSS colitis-colon length shortening, hyperemia, and edema were observed. The colon length and weight/length ratio of mice in Group B shortened significantly in comparison to that in Group A (**Figures 1E,F**).

The spleen, thymus, and liver of mice from all groups were also measured at the end of the experiment (**Figures 1G–I**). Compared with Group A, the indices of the spleen and liver both increased, whereas the thymus index decreased significantly in Group B ($P < 0.05$). The survival rate and the consumption of food and water are shown in **Supplementary Figures 1A–C**.

SFN Ameliorated Colonic Tissue Damage in Colitis Mice

The protective effects of SFN on histological damages in the colons were examined. Compared with Group A, the colonic specimens obtained from Group B were characterized by significant loss of normal crypts, alteration of epithelial structure, increase of neutrophil and lymphocyte infiltration into the mucosal and submucosal layers, extensive loss of glands, and severe lesions in the colon mucosa, which collectively resulted in a significant higher histological score (**Figures 2A,B**). As observed in Group B, 5, 10, and 20 mg/kg/day of SFN and Mesalazine treatment (50 and 100 mg/kg) remarkably mitigated the morphological alterations and protected the colonic tissue integrity, which ultimately lead to a significant decrease in the total histological score. However, 2.5 mg/kg/day of SFN treatment showed more severe morphological damages in colonic specimens, resulting in a higher histological score.

SFN Inhibited Inflammatory Cytokines Production in Colitis Mice

To evaluate if the SFN treatment could ameliorate colitis by modulating the inflammatory response, inflammatory cytokines were measured. As shown in **Figure 2C**, the concentrations of IL-6 were increased in the DSS-treated groups when compared with the negative control group. A 20 mg/kg/day of SFN treatment decreased IL-6 concentration in Group B (30.04 ± 18.07 vs. 75.49 ± 21.60 pg/ml, $P < 0.05$). TNF-α production was increased significantly in Group B in contrast with Group A (7.44 ± 1.12

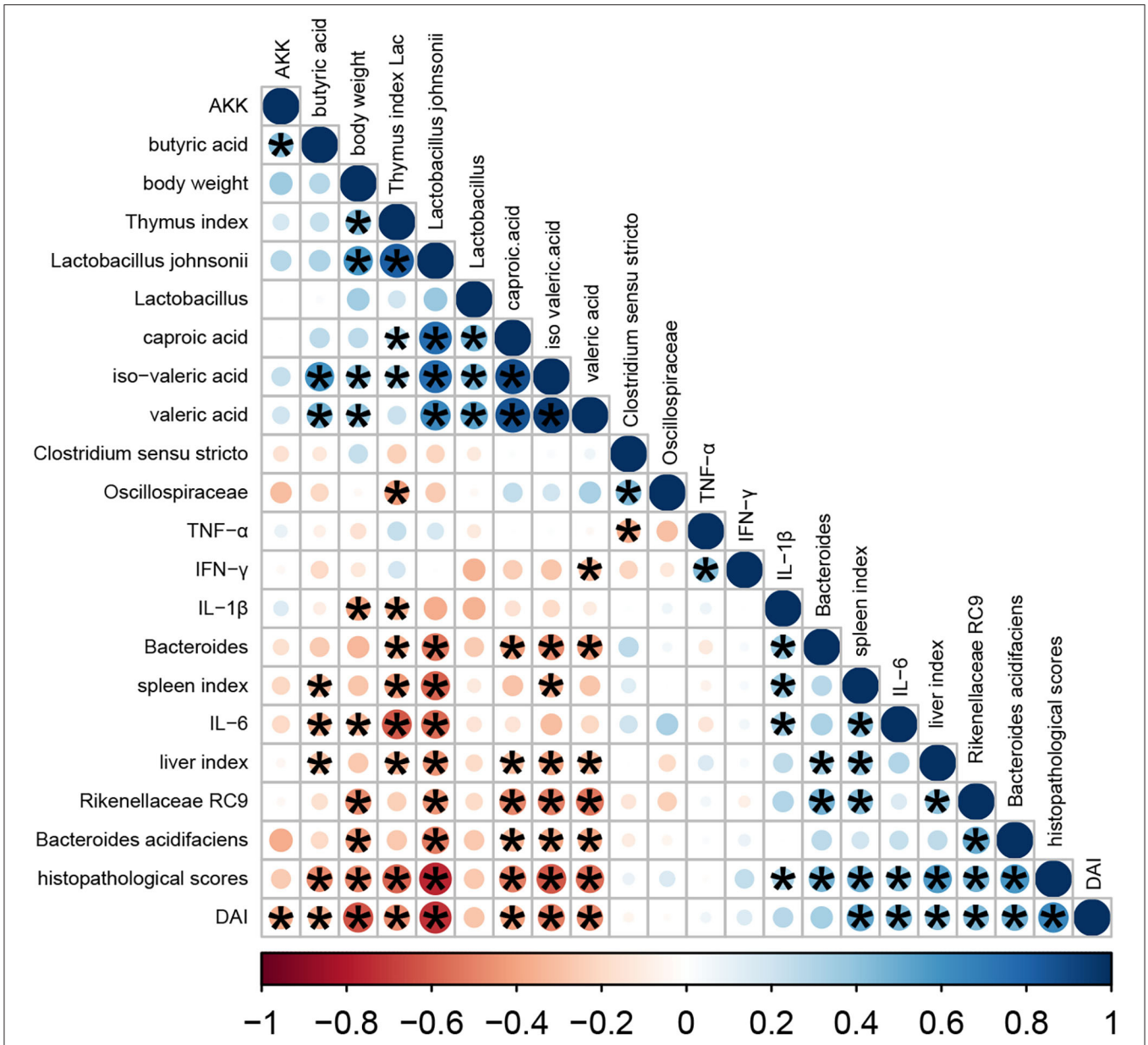

FIGURE 7 | Heatmap of Pearson correlation analysis. The color scale bar ranged from −1.0 (red) to 1.0 (blue). The size and color of the circles indicate the magnitude of the correlation between parameters. Red and blue, respectively, denote negative and positive correlations. These were done in R.

vs. 13.24 ± 0.83 pg/mL, $P < 0.05$). TNF-α concentrations were decreased significantly in the SFN- and Mesalazine-treatment groups when contrasted with Group B ($P < 0.01$). IFN-γ concentration was increased significantly in Group B than that in the control group (6.57 ± 1.18 vs. 10.48 ± 3.78 pg/ml, $P < 0.05$). In the SFN- (2.5, 5, 10, and 20 mg/kg/day) and Mesalazine-treatment groups, the concentrations of IFN-γ were decreased significantly when compared with Group B ($P < 0.05$). IL-1β concentrations were slightly increased in Group B although no significant difference has been observed (data not shown).

SFN-Modulated Gut Microbiota Composition

Given the critical role of gut microbiota in the pathogenesis of colitis, the effect of SFN on the state of gut microbiota composition in DSS-treated mice was investigated. The influences of SFN on the richness and evenness of gut microbiota were assessed. OTU numbers, Shannon diversity, Simpson, ACE, and Chao 1 indices were measured as they are common measures of α diversity that indicate the depth of sequence coverage and community diversity. As shown

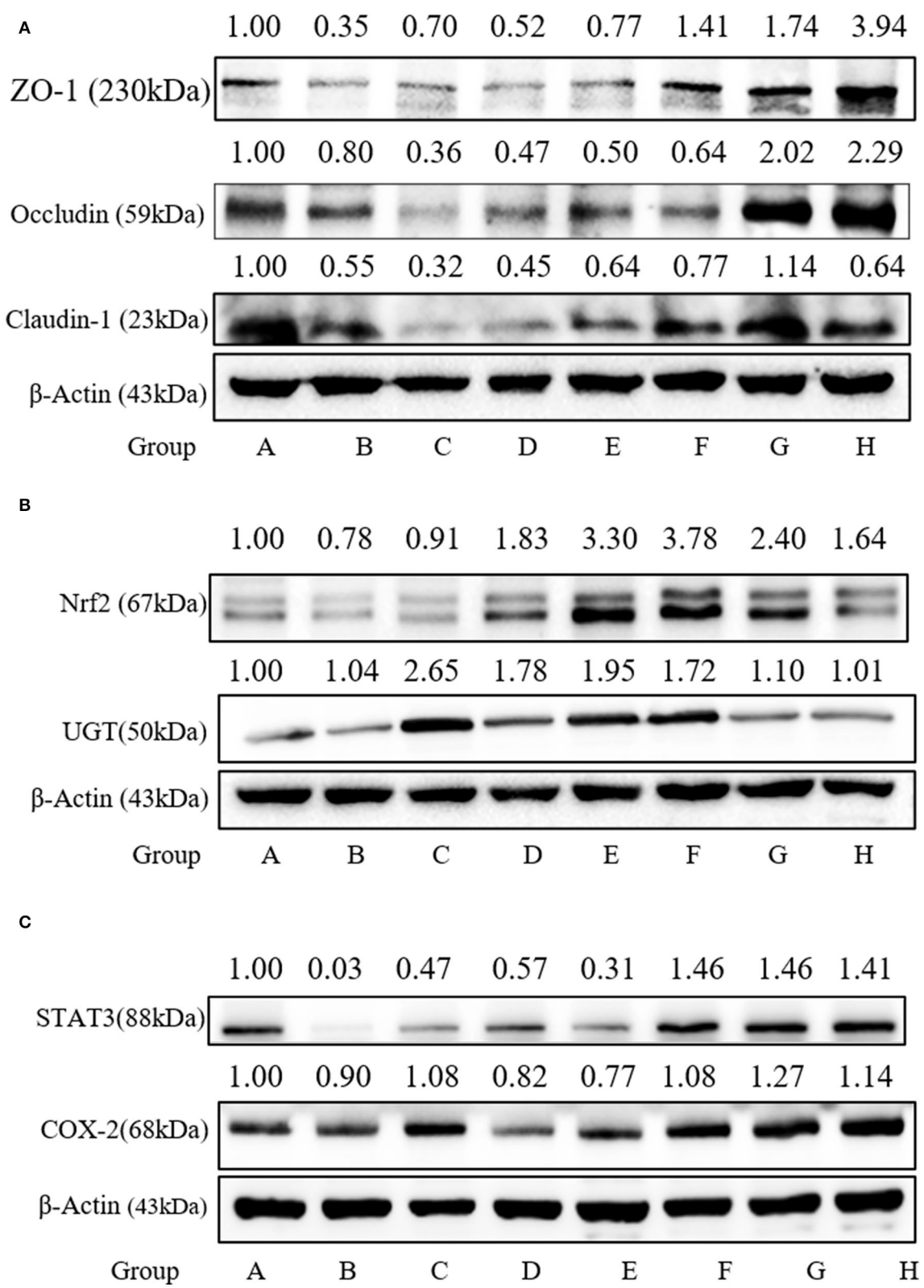

FIGURE 8 | Effect of SFN on tight junction and Nrf2-related protein expression in colitis mice. **(A)** Relative expression of ZO-1, Occludin, and Claudin-1 in colon tissues as measured by Western blotting. **(B)** Relative expression of Nrf2 and UGT in colon tissues as measured by Western blotting. **(C)** Relative expression of STAT3 and COX-2 in colon tissues as measured by Western blotting. All data are presented as the mean ± SD.

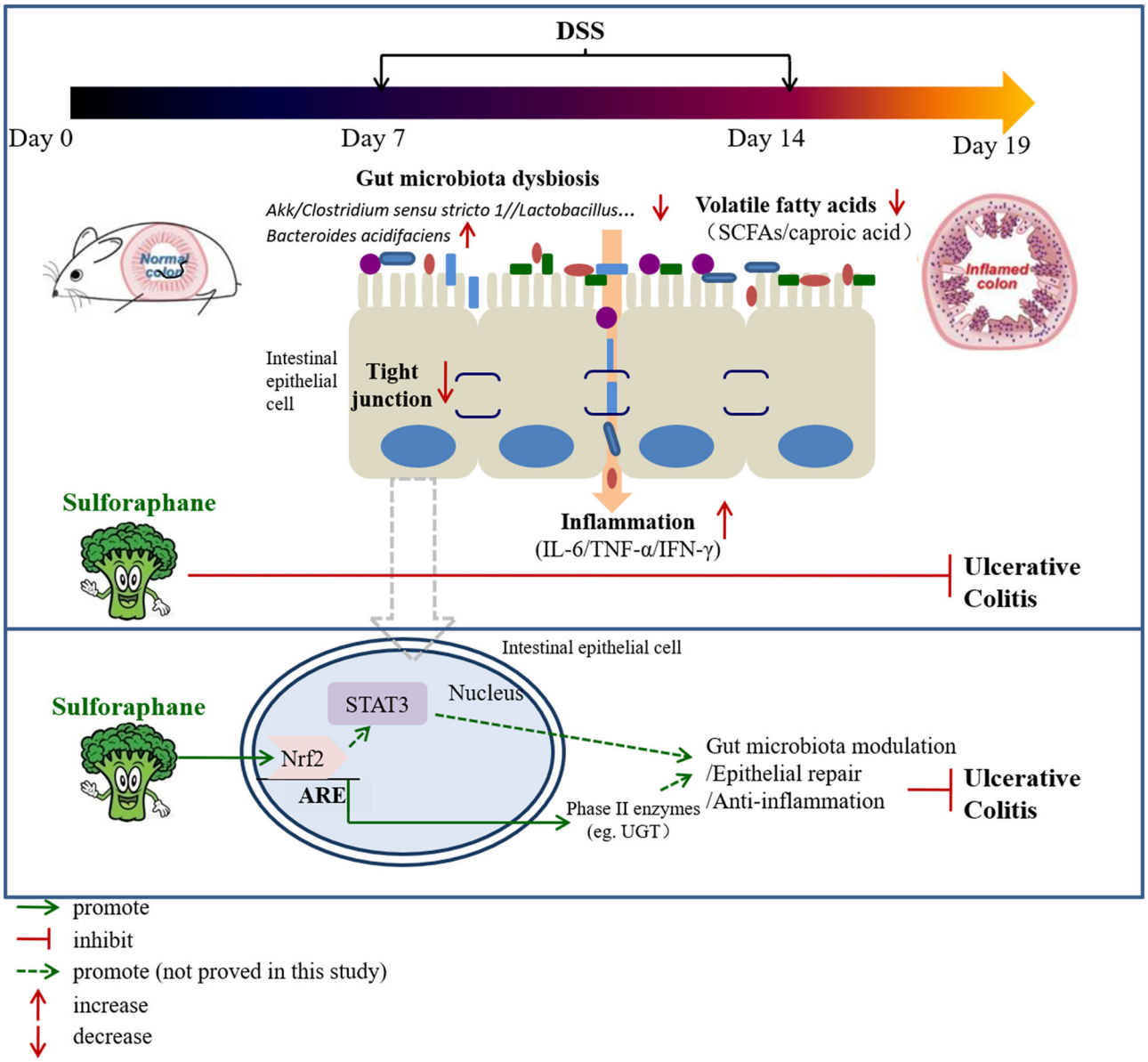

FIGURE 9 | A proposed mechanism by which SFN protects against colitis.

in **Supplementary Figures 1D,E**, there were no significant differences among all the groups at α-diversity.

The relative abundance of the predominant taxa among groups was evaluated (**Figures 3A,B**). *Firmicutes*, *Bacteroidota*, *Proteobacteria*, *Verrucomicrobiota,* and *Actinobacteriota* were five major phyla that account for more than 95.0% of the whole gut microbial composition in all the mice. As shown in **Figure 3B**, at the phylum level, the relative abundance of *Firmicutes* was significantly decreased in Group B when compared to Group A (0.54 ± 0.10 vs. 0.25 ± 0.11, $P < 0.05$). In comparison to Group A, *Bacteroidota* were elevated in Group B (0.30 ± 0.12 vs. 0.66 ± 0.12, $P < 0.05$). SFN (10 mg/kg/day) and Mesalazine treatment was shown to significantly lower the relative abundance of *Bacteroidota* in contrast with the counterparts in Group B ($P < 0.05$). DSS-treated mice with 10 mg/kg/day SFN had a relative higher abundance of *Proteobacteria* when compared to Group B ($P < 0.01$). In comparison to Group A, the relative abundance of *Verrucomicrobiota* was decreased in Group B ($P < 0.05$). While the results in the SFN—(2.5 and 10 mg/kg/day) and Mesalazine-treatment (50 mg/kg/day) groups had a relative lower abundance of *Verrucomicrobiota* in contrast with Group B ($P < 0.05$). The abundance of *Actinobacteriota* in Group B was significantly decreased than that in Group A ($P < 0.05$).

We then analyzed the relative abundance of bacteria at the genus level (**Figures 4A,B**). Among all the treatment groups,

Bacteroides, *Rikenellaceae RC9*, *Parabacteroides*, *Bifidobacterium,* and *Prevotellaceae NK3B31* were the most affected genera. In comparison to Group A, the relative abundance of *Bacteroides* and *Rikenellaceae RC9* was significantly increased in the DSS group ($P < 0.05$). The relative abundance of *Parabacteroides* was significantly increased in Group D in contrast with Group B ($P < 0.05$). In contrast with Group A, the relative abundance of *Bifidobacterium* and *Prevotellaceae NK3B31* was significantly decreased in Group B ($P < 0.01$).

As shown in **Figures 5A,B**, the relative abundances of bacteria at the species level were also analyzed for all the groups, and it was found that 42 species accounted for more than 90% of the fecal pellet. Of these detected species there were nine species that showed significant changes. In comparison to Group A, the relative abundances of *Bacteroides acidifaciens* and *Rikenellaceae* RC9 both increased in Group B ($P < 0.05$). Meanwhile, the relative abundances of *Bifidobacterium pseudolongum*, *unclassified Lactobacillus*, *Lactobacillus johnsonii*, *Lactobacillus intestinalis,* and *uncultured Prevotellaceae NK3B31* in Group B were all significantly lower than that in Group A ($P < 0.01$). The relative abundance of *Akkermansia mucinphila* was lower in Group B than that in Group A, although no significant difference is shown (**Supplementary Figure 2**).

SFN Promoted the Production of Volatile Fatty Acids

Here, the quantities of SCFAs (acetic acid, propionic acid, butyric acid, iso-butyric acid, valeric acid, and iso-valeric acid) and caproic acid in the colonic contents of mice were measured (**Figure 6**). A 20 mg/kg/day dose of SFN significantly increased the concentration of caproic acid in contrast with Group B ($P < 0.01$). For the levels of acetic acid, propionic acid, iso-butyric acid, and total fatty acids, there were no obvious differences among all the groups (**Supplementary Figure 3**).

Correlation Analysis

In this study, we performed a correlation analysis to evaluate the statistical relationship among microbial species at the genus level, volatile fatty acids, and phenotype indicators (namely, organ indexes, DAI, body weight, and histopathological score) (**Figure 7**). Heatmap analyses revealed that the histopathological score had a negative correlation with body weight, thymus index, and volatile fatty acids (mainly, butyric acid, valeric acid, iso-valeric acid, and caproic acid) and *Lactobacillus johnsonii* ($P < 0.05$). Meanwhile, histopathological score had a positive correlation with DAI, spleen index, liver index, proinflammatory cytokines, *Bacteroides acidifaciens*, unclassified *Rikenellaceae RC9*, and unclassified g *Bacteroides* ($P < 0.05$).

SFN Upgraded Tight Junction Protein Expression

To confirm the protective effect of SFN against the gut barrier disruption in colitis mice, tight junction proteins, including ZO-1, Claudin-1, and Occludin, serving as the basis of structure for the paracellular permeability barrier, were measured. As shown in **Figure 8A**, the expressions of tight junction proteins were all decreased in Group B. The expression of ZO-1 in Group F was increased significantly when compared to Group A ($P < 0.05$).

SFN-Regulated Nrf2-Related Protein Expression

SFN exerts multi-functional effects *via* the activation of Nrf2 antioxidants responsive element pathways. Nrf2 can regulate the expression of more than 200 genes, such as phase 2 enzymes and STAT3. Here, the expressions of Nrf2 and UGT in the colonic species were measured. As shown in **Figure 8B**, the Nrf2 expression was increased significantly by 5, 10, and 20 mg/kg/day of SFN treatment. As shown in **Figure 8C**, STAT3 expression is decreased by 0.03-fold in the colitis group. SFN- and Mesalazine treatment increased the STAT3 expression significantly when compared to Group B. COX-2, an important enzyme in the synthesis of prostaglandin from arachidonic acid, is inducible in response to cytokines. In the present study, there were no significant changes among all the groups for COX-2 expression (**Figure 8C**).

DISCUSSION

In this study, the utilization of 2% DSS successfully established a mice colitis model, in mice according to Stefan's protocol, as evidenced by decreased body weight, reduced food intake, shortened colon length, and increased DAI scores (13). In comparison to Group B, mice treated with SFN presented with weight gain, decreased DAI score, and colon length growth. Moreover, histological results clearly showed that SFN ameliorated pathological damage in the colitis mice. These present findings strongly indicate that treatment with SFN is highly effective against DSS-induced colitis. The potential mechanisms were also explored, including the suppression of inflammation, improvement of intestinal mucosa barrier defects, and modulation of microbiota dysbiosis.

Cytokines have been directly implicated in the pathogenesis of IBD in recent studies, and they have been established as playing a pivotal role in aggravating and controlling intestinal inflammation and the associated clinical symptoms of IBD (14). The results from H&E staining analysis clearly showed obvious infiltration of inflammatory cells, multiple erosions, and ulcers in the colon tissue of DSS treated mice. Three critical pro-inflammatory cytokines - IL-6, TNF-α and IFN-γ are known to be predominantly involved in IBD. IL-6 production by lamina propria macrophages and $CD4^+$ cells is increased in the experimental colitis and in IBD patients (15). Additionally, Robust IFN-γ production has been observed in colitis in mice and IBD patients (16). A study using *IFN-*$\gamma^{-/-}$ mice showed significantly decreased inflammation in DSS colitis, indicating an indispensable role of IFN-γ in colitis initiation (17). Furthermore, anti-TNF antibodies are now successfully used in the therapy of IBD, suggesting its pivotal role in the initiation and progression of IBD (18). In this present study, 5, 10, and 20 mg/kg/day of SFN treatment significantly ameliorated the inflammatory damage in mice colon tissue when compared to

the colitis group, which is similar to the effect in the Mesalazine-treatment group. Accordingly, the increased concentrations of pro-inflammatory cytokines in the colitis mice, such as IL-6, IFN-γ, and TNF-α, were all significantly decreased by SFN treatment. Therefore, SFN treatment can alleviate IBD by decreasing the secretion of inflammatory cytokines.

We further analyzed inflammation-related molecules that are implicated in the etiology of UC. STAT3, a pleiotropic transcription factor, is an essential mediator of epithelial repair and inflammatory processes in colitis and colitis-associated colon cancer. In animal models, loss of STAT3 leads to more severe chronic inflammation following acute injury (19, 20). STAT3 activation in intestinal epithelial cells is essential for mucosal wound healing through its ability to regenerate epithelium, thereby playing an integral role in recovery from colitis (21). In this present study, the expression of STAT3 in the DSS-induced colitis mice was markedly decreased and significantly elevated when treated with SFN.

Gut microbiota dysbiosis closely relates to the pathogenesis of IBD. Our previous results have shown that SFN has the ability to modulate the gut microbiota (9). Typically, gut microbiota in IBD patients is characterized with a decrease in the commensal and beneficial fecal bacteria such as *Firmicutes*, but an increase in the inflammatory strains such as *Proteobacteria,* which is consistent with our findings in colitis mice (22, 23). As shown in **Figures 3A,B**, the DSS administration significantly decreased the relative abundance of *Firmicutes*, and this trend was reversed by treatment with SFN and Mesalazine. *Clostridium sensu stricto*, *Oscillospiraceae*, and *Prevotellaceae*, belonging to *Firmicutes* phylum, are known to produce butyrate from their fermentable carbon sources (24, 25). As shown in **Figure 5**, SFN treatment significantly increased the abundance of *Clostridium sensu stricto* 1 and *unclassified Oscillospiraceae*.

It has been reported that the patients with IBD have shown an increased number of *Bacteroidota* compared to that of the controls (26). In this present study, the relative abundance of *Bacteroidota* was increased significantly in the colitis mice, whereas it was decreased significantly by SFN and Mesalazine treatment. According to the results at the genus and species level, the increased abundance of *Bacteroidota* should be attributed to *Bacteroides acidifaciens* and unclassified *Bacteroides*. *Bacteroides acidifaciens* leads to the progression and development of colitis (27). *Bacteroides acidifaciens* has several features, for example, degrading mucin, which is a protective layer in the colon produced by epithelial layers. Moreover, *Bacteroides acidifaciens* is also known to increase acetic and succinic acid production, both of which can contribute to colitis-associated inflammation (27). Notably, SFN treatment decreased this abundance of *Bacteroides acidifaciens* in DSS mice. *Rikenellaceae RC9* belongs to the *Rikenellaceae* family, *Bacteroidota* phylum. It is reported that *Rikenellaceae RC9* is significantly positively correlated with systemic inflammatory cytokines, such as IL-6,IL-1β,and TNF-α (28).

We noticed decreased relative abundances of both *Verrucomicrobiota* and *Actinobacteriota* in the colitis mice. The abundance of *Akkermansia muciniphila,* the only cultivated intestinal representative of the *Verrucomicrobiota,* was decreased in the DSS-induced mice. However, this decreased trend for *Akkermansia muciniphila* was reversed by SFN treatment. *Akkermansia muciniphila,* a Gram-negative and strictly anaerobic bacterium, is an important mucus-degrading intestinal bacterium that encodes mucin-degrading enzymes by increasing the thickness of the gut mucus. The abundance of *Akkermansia muciniphila* is known to be markedly reduced in IBD patients as compared with the abundance in healthy individuals (29). *Akkermansia muciniphila* administration improved DSS-induced colitis *via* its protective effect on the gut barrier and its ability to reduce inflammatory cytokines (30). *Actinobacteriota* are Gram positive, non-motile, non-spore-forming, anaerobic bacteria with multiple branching rods. *Bifidobacterium*, one of the most present *Actinobacteriota* in the human gut, have beneficial effects on the maintenance of the gut barrier because of its ability to produce SCFAs, especially butyric acid (31). As shown in **Figure 5**, the genus of *Bifidobacterium pseudolongum*, belonging to *Bifidobacterium* species, was significantly decreased in DSS-induced colitis mice.

Lactobacilli are important members of the commensal flora within intestinal tract. They are generally considered non-pathogenic and recognized as probiotics with ability to modulate host immune responses with function of strengthening the epithelial junction complexes, decreasing the pro-inflammatory cytokines, and increasing the anti-inflammatory cytokine production (32). A clinical trial of *Lactobacillus* found it to be moderately effective in ameliorating colitis symptoms (33). Here, the relative abundances of unclassified *Lactobacillus*, *Lactobacillus johnsonii*, and *Lactobacillus intestinalis* were all significantly decreased in colitis mice than controls. Heatmap analysis demonstrated the close connection of this disrupted microbial flora with disease severity, especially *Lactobacillus johnsonii*, *Bacteroides acidifaciens*, *Rikenellaceae RC9*, and unclassified *Bacteroides.* Further studies are needed to confirm these relationships and mechanistic role of these bacteria in IBD.

Bacteria in the gut are known to produce short-chain fatty acids along with medium- and long-chain fatty acids as end products of metabolism. The contents of butyric acid, iso-butyric acid, valeric acid, and iso-valeric acid were all decreased in DSS-induced colitis mice and in 2.5 mg/kg/day of the SFN treatment group, whereas this decreased tendency was reversed by 10 and 20 mg/kg/day of SFN. Recent studies regarding SCFAs, have highlighted their protective effects on various systems *in vivo* and *in vitro*. SCFAs, especially butyric acid, are quickly absorbed and utilized as a major energy source by intestinal epithelial cells with multiple beneficial effects on the host, from improving barrier function to attenuating inflammatory response to immune-regulatory effect (34). Butyrate administration can markedly ameliorate the inflammatory response and maintain the epithelium barrier integrity in mice with colitis. Our previous results have shown that SFN possesses the ability of increasing the quantities of butyric acid and iso-butyric acid in mice (9). Valeric acid ameliorates pro-inflammatory cytokine production and improves gastrointestinal tract function and intestinal epithelial integrity (9, 35). It is reported that the contents of propionic acid, butyric acid, iso-butyric acid, and valeric acid evidently decreased in the colonic contents in DSS-induced colitis mice, which is

quite consistent with our results (36). Caproic acid shows anti-inflammatory effect for its reduction in NF-κB transactivation and decrease in inflammatory cytokine production (37, 38). More importantly, fecal levels of caproic acid have been shown to inversely correlate with Crohn's disease activity (39). Here, our results show that the colonic contents of caproic acid were significantly decreased in DSS-induced colitis mice and in 2.5 mg/kg/day of the SFN treatment group. The concentrations of caproic acid were markedly increased by 20 mg/kg/day of SFN treatment.

Disrupted intestinal epithelial barrier is an important characteristic of IBD. The paracelluar permeability of the epithelial barrier and their function in the colon are primarily governed by tight junction proteins, such as ZO-1, Occludin, and Claudin-1 (40). As shown in **Figure 8A**, DSS administration decreased expression of ZO-1, and SFN and Mesalazine treatment reversed this tendency. Our previous results from both *in vitro* and *in vivo* models also suggest that SFN upregulated the tight junction protein expression (9).

Numerous studies suggested that a variety of beneficial functions owned by SFN relied on the induction of Nrf2 and Nrf2-driven proteins. Our results here clearly show that SFN significantly increase the expression of Nrf2 and the representative Phase II enzyme UGT. It has been shown that Nrf2-deficient mice were more susceptible to DSS-induced colitis (41). Many agents involved with Nrf2 activation, have been found to improve DSS-induced colitis, establishing evidence for a Nrf2-dependent mechanism as a promising strategy for treating UC (42, 43).

CONCLUSION

Our data establishes evidence that SFN ameliorates UC through modulation of gut microbiota composition, increasing the contents of fecal volatile fatty acids (especially caproic acid), increasing expression of tight junction proteins, and reduction of pro-inflammatory cytokines (**Figure 9**). Nrf2 activation followed by STAT3 signaling pathway play a pivotal role in the protective effect of SFN on colitis. Therefore, SFN can be considered a potential candidate in the treatment of IBD.

DATA AVAILABILITY STATEMENT

The datasets presented in this study can be found in online repositories. The names of the repository/repositories and accession number(s) can be found below: NCBI [Accession: PRJNA815035].

ETHICS STATEMENT

The animal study was reviewed and approved by Ethics Committee of Ningbo University (registration number: NBU20210028) and performed according to the Guidelines for Animal Care.

AUTHOR CONTRIBUTIONS

CH performed experiments, wrote and edited the manuscript, and contributed to funding acquisition. MG and HY performed experiments. XZ and PL analyzed the data. YQ and LZ partly funded the acquisition. All authors contributed to the article and approved the submitted version.

FUNDING

This work was financially supported by the projection form the National Natural Science Foundation of China (No. 82103819), Natural Science Foundation of Zhejiang Province (Nos. LQ20H260007 and LY21H260001), and Natural Science Foundation of Ningbo City (Nos. 2021J125 and 202003N4202).

ACKNOWLEDGMENTS

The authors are grateful to Dr. Prabh Roohan Pannu (Massachusetts General Hospital, Boston, USA) for critical comments and correction of the language.

SUPPLEMENTARY MATERIAL

The Supplementary Material for this article can be found online at: https://www.frontiersin.org/articles/10.3389/fnut.2022.893344/full#supplementary-material

REFERENCES

1. Kaplan GG. The global burden of IBD: from 2015 to 2025. *Nat Rev Gastroenterol Hepatol.* (2015) 12:720–7. doi: 10.1038/nrgastro.2015.150
2. Kaplan GG, Ng SC. Globalisation of inflammatory bowel disease: perspectives from the evolution of inflammatory bowel disease in the UK and China. *Lancet Gastroenterol Hepatol.* (2016) 1:307–16. doi: 10.1016/S2468-1253(16)30077-2
3. Cui G, Yuan A. A systematic review of epidemiology and risk factors associated with Chinese inflammatory bowel disease. *Front Med.* (2018) 5:183. doi: 10.3389/fmed.2018.00183
4. Xavier RJ, Podolsky DK. Unravelling the pathogenesis of inflammatory bowel disease. *Nature.* (2007) 448:427–34. doi: 10.1038/nature06005
5. Schoultz I, Keita AV. Cellular and molecular therapeutic targets in inflammatory bowel disease-focusing on intestinal barrier function. *Cells.* (2019) 8:193. doi: 10.3390/cells8020193
6. Bauer C, Duewell P, Mayer C, Lehr HA, Fitzgerald KA, Dauer M, et al. Colitis induced in mice with dextran sulfate sodium (DSS) is mediated by the NLRP3 inflammasome. *Gut.* (2010) 59:1192–9. doi: 10.1136/gut.2009.197822
7. Thompson KD, Connor SJ, Walls DM, Gollins J, Stewart SK, Bewtra M, et al. Patients with ulcerative colitis are more concerned about complications of their disease than side effects of medications. *Inflamm Bowel Dis.* (2016) 22:940–7. doi: 10.1097/MIB.0000000000000740
8. Thimmulappa RK, Mai KH, Srisuma S, Kensler TW, Yamamoto M, Biswal S. Identification of Nrf2-regulated genes induced by the chemopreventive agent sulforaphane by oligonucleotide microarray. *Cancer Res.* (2002) 62:5196–203. doi: 10.1002/cncr.10878
9. He C, Huang L, Lei P, Liu X, Li B, Shan Y. Sulforaphane normalizes intestinal flora and enhances gut barrier in mice with bbn-induced bladder cancer. *Mol Nutr Food Res.* (2018) 62:e1800427. doi: 10.1002/mnfr.201800427
10. Shan Y, Zhao R, Geng W, Lin N, Wang X, Du X, et al. Protective effect of sulforaphane on human vascular endothelial cells against

lipopolysaccharide-induced inflammatory damage. *Cardiovasc Toxicol.* (2010) 10:139–45. doi: 10.1007/s12012-010-9072-0
11. Wagner AE, Will O, Sturm C, Lipinski S, Rosenstiel P, Rimbach G. DSS-induced acute colitis in C57BL/6 mice is mitigated by sulforaphane pre-treatment. *J Nutr Biochem.* (2013) 24:2085–91. doi: 10.1016/j.jnutbio.2013.07.009
12. Zhang Y, Tan L, Li C, Wu H, Ran D, Zhang Z. Sulforaphane alter the microbiota and mitigate colitis severity on mice ulcerative colitis induced by DSS. *AMB Express.* (2020) 10:119. doi: 10.1186/s13568-020-01053-z
13. Wirtz S, Neufert C, Weigmann B, Neurath MF. Chemically induced mouse models of intestinal inflammation. *Nat Protoc.* (2007) 2:541–6. doi: 10.1038/nprot.2007.41
14. Neurath MF. Cytokines in inflammatory bowel disease. *Nat Rev Immunol.* (2014) 14:329–42. doi: 10.1038/nri3661
15. Podolsky DK. Inflammatory bowel disease. *N Engl J Med.* (2002) 347:417–29. doi: 10.1056/NEJMra020831
16. Singh UP, Singh NP, Murphy EA, Price RL, Fayad R, Nagarkatti M, et al. Chemokine and cytokine levels in inflammatory bowel disease patients. *Cytokine.* (2016) 77:44–9. doi: 10.1016/j.cyto.2015.10.008
17. Nava P, Koch S, Laukoetter MG, Lee WY, Kolegraff K, Capaldo CT, et al. Interferon-gamma regulates intestinal epithelial homeostasis through converging beta-catenin signaling pathways. *Immunity.* (2010) 32:392–402. doi: 10.1016/j.immuni.2010.03.001
18. Farrell RJ. Biologics beyond anti-TNF agents for ulcerative colitis—efficacy, safety, and cost? *N Engl J Med.* (2019) 381:1279–81. doi: 10.1056/NEJMe1910742
19. Willson TA, Jurickova I, Collins M, Denson LA. Deletion of intestinal epithelial cell STAT3 promotes T-lymphocyte STAT3 activation and chronic colitis following acute dextran sodium sulfate injury in mice. *Inflamm Bowel Dis.* (2013) 19:512–25. doi: 10.1097/MIB.0b013e31828028ad
20. Grivennikov S, Karin E, Terzic J, Mucida D, Yu GY, Vallabhapurapu S, et al. IL-6 and Stat3 are required for survival of intestinal epithelial cells and development of colitis-associated cancer. *Cancer Cell.* (2009) 15:103–13. doi: 10.1016/j.ccr.2009.01.001
21. Pickert G, Neufert C, Leppkes M, Zheng Y, Wittkopf N, Warntjen M, et al. STAT3 links IL-22 signaling in intestinal epithelial cells to mucosal wound healing. *J Exp Med.* (2009) 206:1465–72. doi: 10.1084/jem.20082683
22. Frank DN, St Amand AL, Feldman RA, Boedeker EC, Harpaz N, Pace NR. Molecular-phylogenetic characterization of microbial community imbalances in human inflammatory bowel diseases. *Proc Natl Acad Sci U.S.A.* (2007) 104:13780–5. doi: 10.1073/pnas.0706625104
23. Eom T, Kim YS, Choi CH, Sadowsky MJ, Unno T. Current understanding of microbiota- and dietary-therapies for treating inflammatory bowel disease. *J Microbiol.* (2018) 56:189–98. doi: 10.1007/s12275-018-8049-8
24. Vital M, Karch A, Pieper DH. Colonic butyrate-producing communities in humans: an overview using omics data. *mSystems.* (2017) 2:e00130–17. doi: 10.1128/mSystems.00130-17
25. Le Roy T, Van der Smissen P, Paquot A, Delzenne N, Muccioli GG, Collet JF, et al. Dysosmobacter welbionis gen. nov., sp. nov., isolated from human faeces and emended description of the genus oscillibacter. *Int J Syst Evol Microbiol.* (2020) 70:4851–8. doi: 10.1099/ijsem.0.003547
26. Rehman A, Lepage P, Nolte A, Hellmig S, Schreiber S, Ott SJ. Transcriptional activity of the dominant gut mucosal microbiota in chronic inflammatory bowel disease patients. *J Med Microbiol.* (2010) 59:1114–22. doi: 10.1099/jmm.0.021170-0
27. Alrafas HR, Busbee PB, Nagarkatti M, Nagarkatti PS. Resveratrol modulates the gut microbiota to prevent murine colitis development through induction of tregs and suppression of Th17 cells. *J Leukoc Biol.* (2019) 106:467–80. doi: 10.1002/JLB.3A1218-476RR
28. Cai B, Pan J, Chen H, Chen X, Ye Z, Yuan H, et al. Oyster polysaccharides ameliorate intestinal mucositis and improve metabolism in 5-fluorouracil-treated S180 tumour-bearing mice. *Carbohydr Polym.* (2021) 256:117545. doi: 10.1016/j.carbpol.2020.117545
29. Png CW, Linden SK, Gilshenan KS, Zoetendal EG, McSweeney CS, Sly LI, et al. Mucolytic bacteria with increased prevalence in IBD mucosa augment *in vitro* utilization of mucin by other bacteria. *Am J Gastroenterol.* (2010) 105:2420–8. doi: 10.1038/ajg.2010.281
30. Bian X, Wu W, Yang L, Lv L, Wang Q, Li Y, et al. Administration of akkermansia muciniphila ameliorates dextran sulfate sodium-induced ulcerative colitis in mice. *Front Microbiol.* (2019) 10:2259. doi: 10.3389/fmicb.2019.02259
31. Binda C, Lopetuso LR, Rizzatti G, Gibiino G, Cennamo V, Gasbarrini A. Actinobacteria: a relevant minority for the maintenance of gut homeostasis. *Dig Liver Dis.* (2018) 50:421–8. doi: 10.1016/j.dld.2018.02.012
32. Singh AK, Hertzberger RY, Knaus UG. Hydrogen peroxide production by lactobacilli promotes epithelial restitution during colitis. *Redox Biol.* (2018) 16:11–20. doi: 10.1016/j.redox.2018.02.003
33. Saez-Lara MJ, Gomez-Llorente C, Plaza-Diaz J, Gil A. The role of probiotic lactic acid bacteria and bifidobacteria in the prevention and treatment of inflammatory bowel disease and other related diseases: a systematic review of randomized human clinical trials. *Biomed Res Int.* (2015) 2015:505878. doi: 10.1155/2015/505878
34. Chen X, Su W, Wan T, Yu J, Zhu W, Tang F, et al. Sodium butyrate regulates Th17/Treg cell balance to ameliorate uveitis *via* the Nrf2/HO-1 pathway. *Biochem Pharmacol.* (2017) 142:111–9. doi: 10.1016/j.bcp.2017.06.136
35. Li Y, Dong J, Xiao H, Zhang S, Wang B, Cui M, et al. Gut commensal derived-valeric acid protects against radiation injuries. *Gut Microbes.* (2020) 11:789–806. doi: 10.1080/19490976.2019.1709387
36. Su L, Mao C, Wang X, Li L, Tong H, Mao J, et al. The anti-colitis effect of schisandra chinensis polysaccharide is associated with the regulation of the composition and metabolism of gut microbiota. *Front Cell Infect Microbiol.* (2020) 10:519479. doi: 10.3389/fcimb.2020.519479
37. Tayyeb JZ, Popeijus HE, Mensink RP, Konings M, Mokhtar FBA, Plat J. Short-chain fatty acids (except hexanoic acid) lower nf-kb transactivation, which rescues inflammation-induced decreased apolipoprotein A-I transcription in HepG2 cells. *Int J Mol Sci.* (2020) 21:5088. doi: 10.3390/ijms21145088
38. El-Far M, Durand M, Turcotte I, Larouche-Anctil E, Sylla M, Zaidan S, et al. Upregulated IL-32 expression and reduced gut short chain fatty acid caproic acid in people living with HIV with subclinical atherosclerosis. *Front Immunol.* (2021) 12:664371. doi: 10.3389/fimmu.2021.664371
39. De Preter V, Machiels K, Joossens M, Arijs I, Matthys C, Vermeire S, et al. Faecal metabolite profiling identifies medium-chain fatty acids as discriminating compounds in IBD. *Gut.* (2015) 64:447–58. doi: 10.1136/gutjnl-2013-306423
40. Fanning AS, Mitic LL, Anderson JM. Transmembrane proteins in the tight junction barrier. *J Am Soc Nephrol.* (1999) 10:1337–45. doi: 10.1681/ASN.V1061337
41. Khor TO, Huang MT, Kwon KH, Chan JY, Reddy BS, Kong AN. Nrf2-deficient mice have an increased susceptibility to dextran sulfate sodium-induced colitis. *Cancer Res.* (2006) 66:11580–4. doi: 10.1158/0008-5472.CAN-06-3562
42. Zhang Y, Yan T, Sun D, Xie C, Wang T, Liu X, et al. Rutaecarpine inhibits KEAP1-NRF2 interaction to activate NRF2 and ameliorate dextran sulfate sodium-induced colitis. *Free Radic Biol Med.* (2020) 148:33–41. doi: 10.1016/j.freeradbiomed.2019.12.012
43. Deng Z, Cui C, Wang Y, Ni J, Zheng L, Wei HK, et al. FSGHF3 and peptides, prepared from fish skin gelatin, exert a protective effect on DSS-induced colitis *via* the Nrf2 pathway. *Food Funct.* (2020) 11:414–23. doi: 10.1039/C9FO02165E

Conflict of Interest: The authors declare that the research was conducted in the absence of any commercial or financial relationships that could be construed as a potential conflict of interest.

Publisher's Note: All claims expressed in this article are solely those of the authors and do not necessarily represent those of their affiliated organizations, or those of the publisher, the editors and the reviewers. Any product that may be evaluated in this article, or claim that may be made by its manufacturer, is not guaranteed or endorsed by the publisher.

frontiers | Frontiers in Nutrition

MINI REVIEW
published: 05 July 2022
doi: 10.3389/fnut.2022.933130

Applications of Machine Learning Models to Predict and Prevent Obesity: A Mini-Review

Xiaobei Zhou[1,2], *Lei Chen*[1,2,3] *and Hui-Xin Liu*[1,2,3]*

[1] *Health Sciences Institute, China Medical University, Shenyang, China,* [2] *Liaoning Key Laboratory of Obesity and Glucose/Lipid Associated Metabolic Diseases, China Medical University, Shenyang, China,* [3] *Institute of Life Sciences, China Medical University, Shenyang, China*

Research on obesity and related diseases has received attention from government policymakers; interventions targeting nutrient intake, dietary patterns, and physical activity are deployed globally. An urgent issue now is how can we improve the efficiency of obesity research or obesity interventions. Currently, machine learning (ML) methods have been widely applied in obesity-related studies to detect obesity disease biomarkers or discover intervention strategies to optimize weight loss results. In addition, an open source of these algorithms is necessary to check the reproducibility of the research results. Furthermore, appropriate applications of these algorithms could greatly improve the efficiency of similar studies by other researchers. Here, we proposed a mini-review of several open-source ML algorithms, platforms, or related databases that are of particular interest or can be applied in the field of obesity research. We focus our topic on nutrition, environment and social factor, genetics or genomics, and microbiome-adopting ML algorithms.

Keywords: nutrition, obesity, machine learning, algorithm, genetics, environment

OPEN ACCESS

Edited by:
Lei Zhou,
Guangxi University, China

Reviewed by:
Haitham Nobanee,
Abu Dhabi University,
United Arab Emirates
He Ma,
Northeastern University, China

***Correspondence:**
Hui-Xin Liu
liuhx@cmu.edu.cn

Specialty section:
This article was submitted to Nutrition and Metabolism, a section of the journal Frontiers in Nutrition

Received: *30 April 2022*
Accepted: *19 May 2022*
Published: *05 July 2022*

Citation:
Zhou X, Chen L and Liu H-X (2022) Applications of Machine Learning Models to Predict and Prevent Obesity: A Mini-Review. Front. Nutr. 9:933130. doi: 10.3389/fnut.2022.933130

INTRODUCTION

Obesity is considered to be a chronic progressive disease caused by a combination of multiple determinants, including biological, genetic, social, environmental, and behavioral factors (1, 2). Research on obesity and related diseases has received attention from government policymakers; interventions targeting nutrient intake, dietary patterns, and physical activity are deployed globally. Considerable current effort has been made by the computer community and industry to apply artificial intelligence (AI) technology in the field of biology and biomedicine (3, 4); a possible solution is to use modified machine learning (ML) algorithms to detect obesity disease biomarkers or discover intervention strategies to optimize the weight loss results. ML is seen as part of AI, allowing software applications to predict outcomes without being interpretable (5). ML models can be summarized as two categories: (I) supervised learning models relying on labeled data to train a function that can finish the prediction tasks, and (II) unsupervised learning models focusing on summarizing the characteristics of data, such as dimensionality reduction analysis.

Machine learning models have been successfully used in many studies on obesity to predict obesity rates and identify the risk factors in samples of interest (6–9). In the field of ML research, it is important and necessary to share the code used in research to check the reproducibility of a related work. In addition, open-source tools could greatly improve the efficiency of similar studies by other researchers. However, these studies ignored one significant thing: They did not share

their ML methodologies and frameworks with the public for use by other researchers. At this stage, obesity-related research is considered a public health field and is mostly published in certain professional or medical journals, and these journals do not have strict requirements on the openness of the algorithms or frameworks used in the manuscripts, which are far less than the requirements for data sharing. After matching the keyword "github" (which is the world's most popular public code repository) in 491 abstract texts of obesity-ML-related research [using the PubMed search strategy "Obesity and Machine Learning and" ("1990/01/ 01" [PDAT]: "2022/04/01" [PDAT])], only one related paper was found. Open-source tools are tools for which the original source code is freely available and can be redistributed and modified (10). As a new and booming branch of computer science, ML inherits the tradition of open sharing in the computer community; relevant top journals or conferences have requirements for code sharing of published papers, and most researchers are also willing to upload their codes to the software source code repository.

Several existing reviews focused on the detailed illustration of the status (including the fundamentals, strength, limitation, and evaluation metric) of ML methods in obesity, while ignoring the discussion on the openness of algorithms (7, 11–13). To address this point, we proposed a mini-review for collecting open-source ML algorithms or platforms particularly focusing on the field of obesity research or that could be used in related problems in this article. Since the etiology and pathogenesis of obesity are extremely complex, we set the starting point of our study on the prior knowledge of the current authoritative study of obesity epidemiology (14). The traditional approach to epidemiological obesity research is to study numerous risk citations for obesity through specialized cohorts or epidemiological surveys (14). These customized ML tools for these specialized studies did not take our interest because of their low generality. We focused on ML algorithms related to obesity into several segments, including diet and nutrition, physical activity, geographic environment, genetics or genomics, and microbiome, in which the required data of ML models are available from the database (e.g., GEO database) or public platform (Google Map) without special input (**Figure 1**). In addition, we collected detailed information of 25 open-source ML algorithms or models applied in obesity or that could be used in related filed, including the project name, the relative website, applicable data types, and the simplified description of usage (**Table 1**).

METHODS

We designed a custom semi-automated data collection method incorporating data mining techniques for this mini-review. The PubMed and Google Scholar databases were searched from the inception until March 2022. The search terms used were: "obesity AND machine learning"; "nutrigenetics AND machine learning"; "food recommendation AND machine learning"; "obesity AND geographic information system"; "mhealth" AND ("smartphones" OR "mobile app" OR "mobile applications") AND ("platform" OR "framework")"; "(Genetics OR Genomics) AND machine learning"; "microbiome AND machine learning." The inclusion criteria were as follows: (1) the abstract text contains the keyword "github" (text mining (TM) technology); (2) studies applying at least one ML algorithm focusing on predicting obesity and obesity-related diseases, preventing the obesity prevalence, or conducting the relationship between obesity and obesity risk factors [manually screening (MS)]; (3) the algorithms or frameworks in the studies must be suitable for a common data format, such as fasta or fastq format (MS). Articles excluded were the following: (1) the main text of studies was not available in the English language (TM technology); (2) review papers and papers not considered original studies (TM technology). The PRISMA flowchart of assessment of the literature is illustrated in **Figure 2**.

RESULTS

In summary, we included 25 open-source ML algorithms or models applied in obesity in this mini-review. In the following sections, we discuss each algorithm and describe its applications.

Personalized Food Recommender

A recommendation system can be considered a specified ML model predicting the "rating" or "preference" when given certain information about the user. Deep learning approaches based on the embedding models are now popularly used in modern recommendation systems (15). The core utility of the food recommendation system is to provide recipe retrieval (16). PFoodReq is a novel question-answering food recommendation system based on a large-scale food knowledge base/graph (17). In general, PFoodReq will follow the user's question, such as "What's good with bread for breakfast?", and then output all recipes from the model. The ingredients in these recipes are then rated for suitability and the top-rated recipes are recommended. FlavorGraph is a knowledge graph (KG) system by relations extracted from food recipes and information on flavor molecules from food databases (18). The two main usages of FlavorGraph are predicting compound food relationships and selecting or optimizing food pairings. Yum-me is a nutrition-based meal recommender that integrates state-of-the-art food image analysis models (19). Its input variables rely on two parts: (I) a survey of user dietary restrictions and nutritional expectations and (II) a visual interface that represents the user's food preferences. DeepFood, based on a deep learning approach, can recognize multi-item (food) images by detecting candidate regions or using a deep convolutional neural network (CNN) for food classification tasks (20). Market2Dish focused on the extension utility of user health profiling and health-aware food recommendation (21).

Nutrigenetic Model

Nutrigenetics is the science of studying the interaction between nutrition and gene information. LC-N2G is a novel statistical method inheriting genetic algorithm for ranking and identifying combinations of nutrients with gene expression (22). NutriGenomeDB is a nutrigenomics data platform based on the GSEA algorithm, which collects signature gene information of

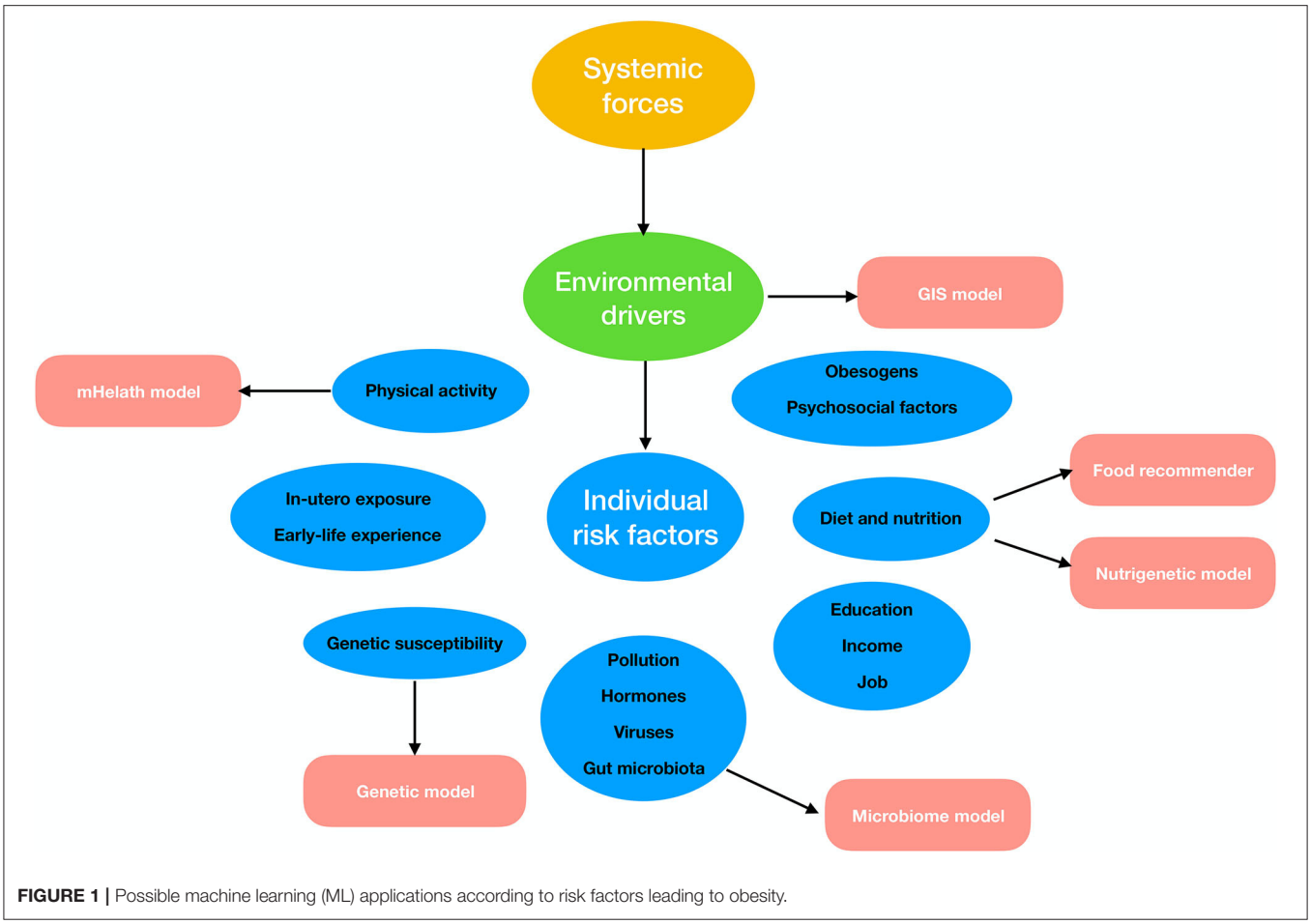

FIGURE 1 | Possible machine learning (ML) applications according to risk factors leading to obesity.

nutrigenomics experimental expression data obtained from the gene expression omnibus (GEO) (23).

Geographic Information System (GIS) Model

Studying obesity-related issues through GIS data and methods is one of the hotspots in current public health research. A US team pioneered the use of deep learning techniques to assess obesity levels by identifying key patterns in the built environment from satellite imagery (24). The key idea is to extract thousands of hidden features from satellite images and identify the potential relationship between the hidden features and the body mass index (BMI). Unfortunately, the framework is not open to the public. MapMetadataEnrichment, a deep learning–based approach that can automatically generate labeled training map images using GIS data, is highly recommended as an alternative framework (25). Without a deep learning approach, spatial models could not be directly used to analyze GIS data to study obesity (26). In this article, we recommend the GWmodel, which is a widely used R-based package that implements geographically weighted models for exploring spatial heterogeneity (27). A classic use case of the application of the GWmodel can be found in a recent study in which a geographically weighted regression (GWR) model (based on the GWmodel package) was adopted to analyze the relationship between socioeconomic factors, obesity, and air temperature and unhealthy behaviors in the USA (28).

mHealth Platform

Recently, digital technologies that can monitor and manage our physical and mental health in our daily lives have rapidly developed and are being used to solve obesity-related problems (29, 30). Mobile health applications denoted mHealth apps have become increasingly popular with researchers and clinicians as effective tools for improving health behaviors. Several open-source mHealth platforms are available, including schema (31), mHealthDroid (32), and MobileCoach (33). These platforms are mentioned here since they can cooperate with ML models in the situation where the model uses the data provided by the platform. The mHealthDroid platform is designed to facilitate the fast and easy development of mHealth and biomedical applications; the schema platform is a lightweight cross-platform mobile application focused on mobile health monitoring and intervention research; the MobileCoach platform provides a one-stop solution for fully automated digital interventions.

TABLE 1 | Detailed information on these ML algorithms.

Name	Usage	Core algorithm	Input data	URL
PFoodReq	Food recommendation system	Knowledge graph (KG) & question answering (QA) & recipe retrieval	Text	https://github.com/hugochan/PFoodReq
FlavorGraph	Food recommendation system	KG & recipe retrieval & compound food relationship	Vector	https://github.com/lamypark/FlavorGraph
DeepFood	Food recommendation system	Deep learning (DL)& image recognition & recipe retrieval	Image	https://github.com/deercoder/DeepFood
Market2Dish	Food recommendation system	DL& image recognition & recipe retrieval	Image	https://github.com/WenjieWWJ/FoodRec
LC-N2G	Nutrigenetics analysis method	Statistical methods	Gene expression data (GSE85998)	https://sydneybiox.github.io/LCN2G/
NutriGenomeDB	Nutrigenetics platform	None	None	https://github.com/rmartin84/NutriGenomeDB (locally deployment)
MapMetadataEnrichment	GIS satellite image analysis tool	DL	Satellite image	https://github.com/geoai-lab/MapMetadataEnrichment
GWmodel	An R package for exploring spatial heterogeneity	Spatial regression models	POI data	https://cran.r-project.org/web/packages/GWmodel/index.html
Schema	Digital intervention	None	None	https://github.com/schema-app/schema
mHealthDroid	mHealth platform	None	None	https://github.com/mHealthTechnologies/mHealthDroid
MobileCoach	Digital intervention	None	None	https://github.com/schlegel11/MobileCoach
PGS Catalog	Polygenic score (PRS) database	None	None	https://www.pgscatalog.org/
Impute.me	Platform for direct-to-consumer genetic testing	none	23AndMe	https://github.com/lassefolkersen/impute-me
DeepVariant	Deep learning-based variant caller	DL	BAM or CRAM	https://github.com/google/deepvariant
NeuralCVD	Cardiovascular risk predictor	Survival machine algorithm	UK Biobank data	https://github.com/thbuerg/NeuralCVD
DeepCOMBI	AI tool for analysis of GWAS data	DL	GWAS data	https://github.com/AlexandreRozier/DeepCombi
DeepMicro	Taxonomic classifier	DL	Microbe data (csv)	https://github.com/minoh0201/DeepMicro
DeepMicrobes	Taxonomic classifier	DL	Microbe data (fasta)	https://github.com/MicrobeLab/DeepMicrobes
SortMeRNA	Taxonomic classifier	ML	Microbe data (fasta)	https://github.com/biocore/sortmerna
q2-feature-classifier	Taxonomic classifier	ML	Microbe data (fasta)	https://github.com/qiime2/q2-feature-classifier
Swarm	Taxonomic classifier	ML	Microbe data (fasta)	https://github.com/torognes/swarm
GEDFN	Microbial biomarker' identification	DL	OTU & IBD	https://github.com/MicroAVA/GEDFN
MDeep	Microbe-disease predictor	DL	OTU	https://github.com/lichen-lab/mdeep
TaxoNN	Microbe-disease predictor	DL	OTU	https://github.com/divya031090/taxonn_otu.
MetaPheno	Microbe-disease predictor	DL	Microbe data (fasta)	https://github.com/nlapier2/metapheno

Genetic Model

Genetics studies genes and the way certain traits or conditionsare passed from one generation to the next. The polygenic score (PGS) database collects published PGS information that provides the community with an open platform for PGS research. (34). PRS estimates an individual's genetic risk for complex diseases based on many genetic variants across the genome. In fact, a polygenic risk score (PRS) could be considered a specified regression model; there are many obesity PRS models available in the PGS database, such as PGP000017 and PGP000211. Impute.me is the first non-commercial platform for using data from direct-to-consumer genetic testing to calculate and interpret polygenic risk scores (35). DeepVariant was launched by Google, which uses deep neural networks to fast and accurately

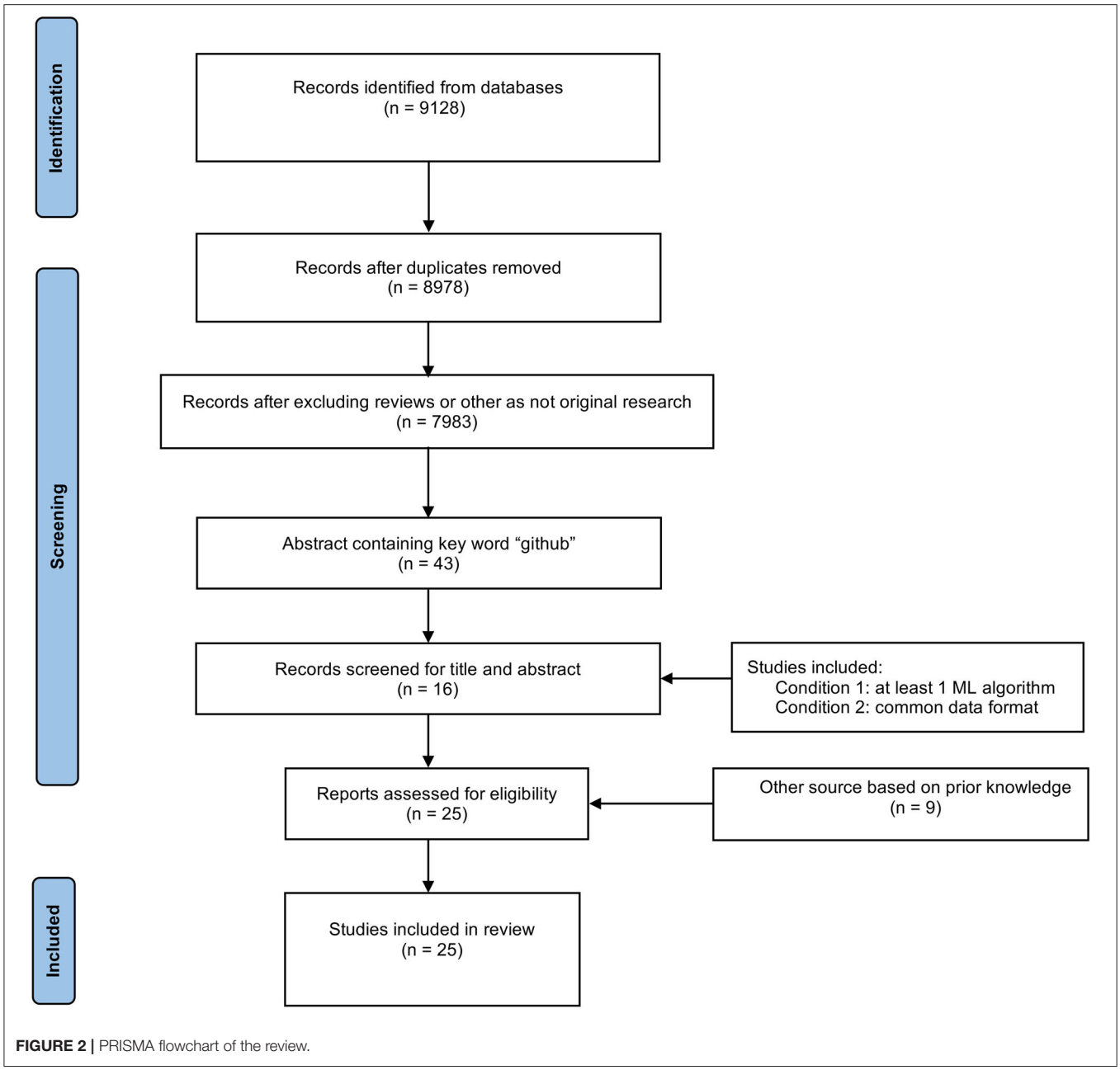

FIGURE 2 | PRISMA flowchart of the review.

identify variation sites from DNA sequencing data (36). The NeuralCVD-based deep survival machine algorithm can estimate the cardiovascular risk for coronary heart disease prevention (37). DeepCOMBI uses AI for analysis and discovery in genome-wide association studies (38).

Microbiome Model

The gut microbiome is closely related to overall health. More and more studies suggest that obesity is associated with specific changes in the composition and function of the human gut microbiome (39, 40). Any study of the gut microbiome associated with obesity cannot skip the step of taxonomic classification to infer the relative abundance of different taxa. Typical ML taxonomic classifiers are DeepMicro (41), DeepMicrobes (42), SortMeRNA (43), q2-feature-classifier (44), swarm (45), etc. We mentioned that q2 feature classifier has been implemented in QIIME 2 which is the most popular microbiome analysis platform (46). ML models [GEDFN (47), MDeep (48), TaxoNN (49), and MetaPheno (50)] can also be used to predict patient phenotype or obesity from their microbiome sequence data. MIPMLP provides a reproducible preprocessing ML pipeline for a microbiome analysis (51).

LIMITATIONS

Obesity, with its complex etiologies, is difficult to describe with a single theoretical model. The current trend in obesity research is to integrate health and medical big data and use high-throughput sequencing technology for multi-omics joint research. In general,

the current ML models and algorithms for obesity research are separated from a single field, and no model can span multiple fields or integrate multiple types of data across platforms for a joint analysis of homologous and heterogeneous data. For the nutrigenetic model, the development of open-source models is far behind the industry. Several startups have launched genetics-based food recipes and recommendation systems, while their models are "black box." A major limitation of genetic models of obesity is weak evidence from small sample sizes due to small variants of genetic mutations. For the mHealth platforms, we could not find open-source ML models in obesity, although we believe that ML models in obesity must be existing in commercial mobile APPs. For the open-source mHealth platform, we were unable to find an open-source ML model related to obesity, although we believe that such ML models already exist in commercial mobile apps.

PERSPECTIVE

Machine learning algorithms are a powerful analytic tool that enables us to conceptualize and study metabolic disorders within a fundamentally novel framework. In contrast to conventional statistical methods assessing single modality predictors, ML methods are capable of integrating multiple data types and sources to inform predictive models. Nonetheless, ML algorithms are limited by the type of data captured, the quality of available data, the conceptual frameworks algorithms are applied to, and the underlying assumptions. The use of ML algorithms in obesity will dramatically increase in the future, and a large number of ML algorithms will be implemented on a few specific platforms such as QIMME 2 to facilitate rapid application and collaborative work between multiple algorithms. Presently, most of the ML algorithms used in obesity-related research are isolated in a single field or the factor that causes obesity; in the future, the algorithms will work together across platforms or data types. Future research vistas are to optimize and prospectively test predictive models using external datasets.

AUTHOR CONTRIBUTIONS

All authors listed have made a substantial, direct, and intellectual contribution to the work and approved it for publication.

FUNDING

This research received financial support from the General Project of the Liaoning Provincial Department of Education under Grant No. LJKZ0758 and the Liaoning Provincial Natural Science Foundation (2021-MS-194).

REFERENCES

1. Apovian CM. Obesity: definition, comorbidities, causes, and burden. *Am J Manag Care*. (2016) 22(7 Suppl.):s176–85.
2. Kyle TK, Dhurandhar EJ, Allison DB. Regarding obesity as a disease: evolving policies and their implications. *Endocrinol Metab Clin North Am*. (2016) 45:511–20. doi: 10.1016/j.ecl.2016.04.004
3. Ching T, Himmelstein DS, Beaulieu-Jones BK, Kalinin AA, Do BT, Way GP, et al. Opportunities and obstacles for deep learning in biology and medicine. *J R Soc Interface*. (2018) 15:20170387. doi: 10.1098/rsif.2017.0387
4. Zhao Z, Woloszynek S, Agbavor F, Mell JC, Sokhansanj BA, Rosen GL. Learning, visualizing and exploring 16S rRNA structure using an attention-based deep neural network. *PLoS Comput Biol*. (2021) 17:e1009345. doi: 10.1371/journal.pcbi.1009345
5. Mitchell TM. *Machine Learning*. 1st ed. McGraw-Hill, Inc. (1997).
6. Chatterjee A, Gerdes MW, Martinez SG. Identification of risk factors associated with obesity and overweight-a machine learning overview. *Sensors*. (2020) 20:2734. doi: 10.3390/s20092734
7. Colmenarejo G. Machine learning models to predict childhood and adolescent obesity: a review. *Nutrients*. (2020) 12:2466. doi: 10.3390/nu12082466
8. Duran I, Martakis K, Rehberg M, Semler O, Schoenau E. Diagnostic performance of an artificial neural network to predict excess body fat in children. *Pediatr Obes*. (2019) 14:e12494. doi: 10.1111/ijpo.12494
9. Safaei M, Sundararajan EA, Driss M, Boulila W, Shapi'i A. A systematic literature review on obesity: Understanding the causes & consequences of obesity and reviewing various machine learning approaches used to predict obesity. *Comput Biol Med*. (2021) 136:104754. doi: 10.1016/j.compbiomed.2021.104754
10. Corbly JE. The free software alternative: freeware, open-source software, and libraries. *Inform Technol Librar*. (2014) 33:65–75. doi: 10.6017/ital.v33i3.5105
11. Chimunhu P, Topal E, Ajak AD, Asad W. A review of machine learning applications for underground mine planning and scheduling. *Resour Policy*. (2022) 77:102693. doi: 10.1016/j.resourpol.2022.102693
12. DeGregory KW, Kuiper P, DeSilvio T, Pleuss JD, Miller R, Roginski JW, et al. A review of machine learning in obesity. *Obes Rev*. (2018) 19:668–85. doi: 10.1111/obr.12667
13. Triantafyllidis A, Polychronidou E, Alexiadis A, Rocha CL, Oliveira DN, da Silva AS, et al., Computerized decision support and machine learning applications for the prevention and treatment of childhood obesity: A systematic review of the literature. *Artif Intell Med*. (2020) 104:101844. doi: 10.1016/j.artmed.2020.101844
14. Pan XF, Wang L, Pan A. Epidemiology and determinants of obesity in China. *Lancet Diabetes Endocrinol*. (2021) 9:373–92. doi: 10.1016/S2213-8587(21)00045-0
15. Zhang S, Yao L, Sun A, Tay Y. Deep learning based recommender system: a survey and new perspectives. *ACM Comput Surv*. (2017) 52:1–35. doi: 10.1145/3285029
16. De Croon R, Van Houdt L, Htun NN, Štiglic G, Vanden Abeele V, Verbert K. Health recommender systems: systematic review. *J Med Internet Res*. (2021) 23:e18035. doi: 10.2196/18035
17. Chen Y, Subburathinam A, Chen CH, Zaki MJ. Personalized food recommendation as constrained question answering over a large-scale food knowledge graph. In: *WSDM '21: The Fourteenth ACM International Conference on Web Search and Data Mining*. New York, NY: Association for Computing Machinery. (2021). doi: 10.1145/3437963.3441816
18. Park D, Kim K, Kim S, Spranger M, Kang J. FlavorGraph: a large-scale food-chemical graph for generating food representations and recommending food pairings. *Sci Rep*. (2021) 11:931. doi: 10.1038/s41598-020-79422-8
19. Yang L, Hsieh C-K, Yang H, Pollak JP, Dell N, Belongie S, et al. Yum-Me: a personalized nutrient-based meal recommender system. *ACM Trans Inf Syst*. (2017) 36:7. doi: 10.1145/3072614
20. Jiang L, Qiu B, Liu X, Huang C, Lin K. DeepFood: food image analysis and dietary assessment via deep model. *IEEE Access*. (2020) 1–1. doi: 10.1109/ACCESS.2020.2973625
21. Wang W, Duan LY, Jiang H, Jing P, Song X, Nie L. Market2Dish: health-aware food recommendation. *ACM Trans Multimedia Comput Commun Applic*. (2021) 17:1–19. doi: 10.1145/3418211

22. Xu X, Solon-Biet SM, Senior A, Simpson SJ, Fontana L, Mueller S, et al. LC-N2G: a local consistency approach for nutrigenomics data analysis. *BMC Bioinformatics*. (2020) 21:530. doi: 10.1186/s12859-020-03861-3
23. Martín-Hernández R, Reglero G, Ordovás JM, Dávalos A. NutriGenomeDB: a nutrigenomics exploratory and analytical platform. *Database*. (2019) 2019:baz097. doi: 10.1093/database/baz097
24. Maharana A, Nsoesie EO. Use of deep learning to examine the association of the built environment with prevalence of neighborhood adult obesity. *JAMA Netw Open*. (2018) 1:e181535. doi: 10.1001/jamanetworkopen.2018.1535
25. Hu Y, Gui Z, Wang J, Li M. Enriching the metadata of map images: a deep learning approach with GIS-based data augmentation. *Int J Geogr Inform Sci*. (2021) 36:1–23. doi: 10.1080/13658816.2021.1968407
26. Kamel Boulos MN, Peng G, VoPham T. An overview of GeoAI applications in health and healthcare. *Int J Health Geogr*. (2019) 18:7. doi: 10.1186/s12942-019-0171-2
27. Cao S, Zheng H. A POI-based machine learning method for predicting residents' health status. In: *The International Conference on Computational Design and Robotic Fabrication*. Singapore: Springer. (2021). doi: 10.1007/978-981-16-5983-6_13
28. Lotfata A. Using geographically weighted models to explore obesity prevalence association with air temperature, socioeconomic factors, and unhealthy behavior in the USA. *J Geovisualiz Spatial Anal*. (2022) 6:1–12. doi: 10.1007/s41651-022-00108-y
29. Goldstein SP, Thomas JG, Foster GD, Turner-McGrievy G, Butryn ML, Herbert JD, et al. Refining an algorithm-powered just-in-time adaptive weight control intervention: a randomized controlled trial evaluating model performance and behavioral outcomes. *Health Informatics J*. (2020) 26:2315–31. doi: 10.1177/1460458220902330
30. Stein N, Brooks K. A fully automated conversational artificial intelligence for weight loss: longitudinal observational study among overweight and obese adults. *JMIR Diabetes*. (2017) 2:e28. doi: 10.2196/diabetes.8590
31. Shatte ABR, Teague SJ. Schema: an open-source, distributed mobile platform for deploying mhealth research tools and interventions. *BMC Med Res Methodol*. (2020) 20:91. doi: 10.1186/s12874-020-00973-5
32. Banos O, Garcia R, Holgado-Terriza JA, Damas M, Pomares H, Rojas I, et al. *mHealthDroid: A Novel Framework for Agile Development of Mobile Health Applications*. Cham: Springer International Publishing (2014). doi: 10.1007/978-3-319-13105-4_14
33. Kowatsch T, Volland D, Shih I, Rüegger D, Künzler F, Barata F, et al. Design and evaluation of a mobile Chat App for the open source behavioral health intervention platform MobileCoach. In: *International Conference on Design Science Research in Information System and Technology*. Cham: Springer. (2017). doi: 10.1007/978-3-319-59144-5_36
34. Lambert SA, Gill L, Jupp S, Ritchie SC, Xu Y, Buniello A, et al. The Polygenic Score Catalog as an open database for reproducibility and systematic evaluation. *Nat Genet*. (2021) 53:420–5. doi: 10.1038/s41588-021-00783-5
35. Folkersen L, Pain O, Ingason A, Werge T, Lewis CM, Austin J. Impute.me: an open-source, non-profit tool for using data from direct-to-consumer genetic testing to calculate and interpret polygenic risk scores. *Front Genet*. (2020) 11:578. doi: 10.3389/fgene.2020.00578
36. Yun T, Li H, Chang PC, Lin MF, Carroll A, McLean CY. Accurate, scalable cohort variant calls using DeepVariant and GLnexus. *Bioinformatics*. (2021) 36:5582-9. doi: 10.1093/bioinformatics/btaa1081
37. Steinfeldt J, Buergel T, Loock L, Kittner P, Ruyoga G, Belzen JU, et al. Neural network-based integration of polygenic and clinical information: development and validation of a prediction model for 10-year risk of major adverse cardiac events in the UK Biobank cohort. *Lancet Digit Heal*. (2022) 4:e84-94. doi: 10.1016/S2589-7500(21)00249-1
38. Mieth B, Rozier A, Rodriguez JA, Höhne MMC, Görnitz N, Müller KR. DeepCOMBI: explainable artificial intelligence for the analysis and discovery in genome-wide association studies. *NAR Genom Bioinform*. (2021) 3:lqab065. doi: 10.1093/nargab/lqab065
39. Aoun A, Darwish F, Hamod N. The influence of the gut microbiome on obesity in adults and the role of probiotics, prebiotics, and synbiotics for weight loss. *Prev Nutr Food Sci*. (2020) 25:113–23. doi: 10.3746/pnf.2020.25.2.113
40. Davis CD. The gut microbiome and its role in obesity. *Nutr Today*. (2016) 51:167–74. doi: 10.1097/NT.0000000000000167
41. Oh M, Zhang L. DeepMicro: deep representation learning for disease prediction based on microbiome data. *Sci Rep*. (2020) 10:6026. doi: 10.1038/s41598-020-63159-5
42. Liang Q, Bible PW, Liu Y, Zou B, Wei L. DeepMicrobes: taxonomic classification for metagenomics with deep learning. *NAR Genom Bioinform*. (2020) 2:lqaa009. doi: 10.1093/nargab/lqaa009
43. Kopylova E, Noé L, Touzet H. SortMeRNA: fast and accurate filtering of ribosomal RNAs in metatranscriptomic data. *Bioinformatics*. (2012) 28:3211–7. doi: 10.1093/bioinformatics/bts611
44. Bokulich NA, Kaehler BD, Rideout JR, Dillon M, Bolyen E, Knight R, et al. Optimizing taxonomic classification of marker-gene amplicon sequences with QIIME 2's q2-feature-classifier plugin. *Microbiome*. (2018) 6:90. doi: 10.1186/s40168-018-0470-z
45. Mahé F, Rognes T, Quince C, de Vargas C, Dunthorn M. Swarm: robust and fast clustering method for amplicon-based studies. *PeerJ*. (2014) 2:e593. doi: 10.7717/peerj.593
46. Bolyen E, Rideout JR, Dillon MR, Bokulich NA, Abnet CC, Al-Ghalith GA, et al. Reproducible, interactive, scalable and extensible microbiome data science using QIIME 2. *Nat Biotechnol*. (2019) 37:852–57. doi: 10.1038/s41587-019-0209-9
47. Zhu Q, Jiang X, Zhu Q, Pan M, He T. Graph Embedding deep learning guides microbial biomarkers' identification. *Front Genet*. (2019) 10:1182. doi: 10.3389/fgene.2019.01182
48. Wang Y, Bhattacharya T, Jiang Y, Qin X, Wang Y, Liu Y, et al. A novel deep learning method for predictive modeling of microbiome data. *Briefings Bioinformatics*. (2020) 22:bbaa073. doi: 10.1093/bib/bbaa073
49. Sharma D, Paterson AD, Xu W. TaxoNN: ensemble of neural networks on stratified microbiome data for disease prediction. *Bioinformatics*. (2020) 36:4544–50. doi: 10.1093/bioinformatics/btaa542
50. LaPierre N, Ju CJT, Zhou G, Wang W. MetaPheno: a critical evaluation of deep learning and machine learning in metagenome-based disease prediction. *Methods*. (2019) 166:74–82. doi: 10.1016/j.ymeth.2019.03.003
51. Jasner Y, Belogolovski A, Ben-Itzhak M, Koren O, Louzoun Y. Microbiome preprocessing machine learning pipeline. *Front Immunol*. (2021) 12:677870. doi: 10.3389/fimmu.2021.677870

Conflict of Interest: The authors declare that the research was conducted in the absence of any commercial or financial relationships that could be construed as a potential conflict of interest.

Publisher's Note: All claims expressed in this article are solely those of the authors and do not necessarily represent those of their affiliated organizations, or those of the publisher, the editors and the reviewers. Any product that may be evaluated in this article, or claim that may be made by its manufacturer, is not guaranteed or endorsed by the publisher.

frontiers | Frontiers in Nutrition

REVIEW
published: 18 July 2022
doi: 10.3389/fnut.2022.932670

The Role of Branched-Chain Amino Acids and Branched-Chain α-Keto Acid Dehydrogenase Kinase in Metabolic Disorders

Chuang Du[1,2,3,4], Wen-Jie Liu[1,2,3], Jing Yang[1,2,3], Shan-Shan Zhao[1,2,3,5] and Hui-Xin Liu[1,2,3]**

[1] Institute of Life Sciences, China Medical University, Shenyang, China, [2] Health Sciences Institute, China Medical University, Shenyang, China, [3] Liaoning Key Laboratory of Obesity and Glucose/Lipid Associated Metabolic Diseases, China Medical University, Shenyang, China, [4] Department of Gastroenterology, Shengjing Hospital of China Medical University, Shenyang, China, [5] Department of Gynecology, Cancer Hospital of China Medical University, Liaoning Cancer Hospital & Institute, Shenyang, China

OPEN ACCESS

Edited by:
Qutuba G. Karwi,
University of Alberta, Canada

Reviewed by:
Man Ren,
Anhui Science and Technology University, China
Elżbieta Supruniuk,
Medical University of Bialystok, Poland
Jerry Raymond Colca,
Metabolic Solutions Development Company, United States

***Correspondence:**
Shan-Shan Zhao
shanshan0313@126.com
Hui-Xin Liu
liuhx@cmu.edu.cn

Specialty section:
This article was submitted to Nutrition and Metabolism, a section of the journal Frontiers in Nutrition

Received: 30 April 2022
Accepted: 16 June 2022
Published: 18 July 2022

Citation:
Du C, Liu W-J, Yang J, Zhao S-S and Liu H-X (2022) The Role of Branched-Chain Amino Acids and Branched-Chain α-Keto Acid Dehydrogenase Kinase in Metabolic Disorders. Front. Nutr. 9:932670. doi: 10.3389/fnut.2022.932670

Branched-chain amino acids (BCAAs), composed of leucine, isoleucine, and valine, are important essential amino acids in human physiology. Decades of studies have revealed their roles in protein synthesis, regulating neurotransmitter synthesis, and the mechanistic target of rapamycin (mTOR). BCAAs are found to be related to many metabolic disorders, such as insulin resistance, obesity, and heart failure. Also, many diseases are related to the alteration of the BCAA catabolism enzyme branched-chain α-keto acid dehydrogenase kinase (BCKDK), including maple syrup urine disease, human autism with epilepsy, and so on. In this review, diseases and the corresponding therapies are discussed after the introduction of the catabolism and detection methods of BCAAs and BCKDK. Also, the interaction between microbiota and BCAAs is highlighted.

Keywords: branched-chain amino acids, branched-chain α-keto acid dehydrogenase kinase, metabolic disorders, microbiota, MALDI-MSI

INTRODUCTION

Branched-chain amino acids (BCAAs) account for about 35% of essential amino acids in most mammals, which cannot be synthesized by mammals themselves, and the functional R group makes them vital components of most proteins (1). BCAAs, composed of leucine, isoleucine, and valine, are not synthesized in animals but in plants, bacteria, and fungi. They have become popular study subjects since their discovery in the mid-nineteenth century. All BCAA members play important roles in nutrient sensing and cellular signaling, especially leucine, which acts directly by activating the mammalian/mechanistic targets of rapamycin complex 1 (mTORC1) (2). BCAAs have been studied due to their beneficial role in promoting protein synthesis in muscle during physical training and under conditions of negative energy balance, such as syndromes of cachexia and aging. Moreover, continuous accumulation in BCAAs from circulation is reported in patients with insulin resistance, obesity, type 2 diabetes, as well as heart diseases (3).

BRANCHED-CHAIN AMINO ACID METABOLISM

In BCAAs metabolism, the first step is BCAAs' transforming into branched-chain α-ketoacids (BCKAs) under the catalyzation of branched-chain aminotransferases (BCATs; **Figure 1**). The

corresponding BCKAs of leucine, isoleucine, and valine are α-ketoisocaproate (KIC), α-keto-β-methylvalerate (KMV), and α-ketoisovalerate (KIV) (4). Two different genes which encode BCATs are responsible for this process: BCAT1 is mostly expressed in the brain and encodes a cytoplasmic protein, at the same time, BCAT2 is widely expressed and encodes a mitochondrial protein (1). This step is a reversible transamination reaction, that largely occurs in skeletal muscle. After BCKAs are released back into circulation, they are oxidatively decarboxylated to acyl-CoA mainly in the liver. The branched-chain α keto-acid dehydrogenase (BCKDH) complex is an important enzyme that catalyzes this irreversible and rate-controlling process in BCAA catabolism. Although the liver and other tissues (such as adipose and muscle) all possess BCKDH and are able to carry out the catabolism of BCKAs, the liver is reported as the highest metabolic efficiency organ in the body in the oxidative decarboxylation of BCKAs (5). BCKAs covalently bind to a coenzyme A group and lose CO_2 in an oxidative decarboxylation process catalyzed by BCKDH (1). The BCKDH complex consists of three parts, namely, E1, E2, and E3. BCKDH converts KIC to isovaleryl-CoA (IV-CoA), KMV to α-methylbutyryl-CoA (MB-CoA), and KIV to isobutyryl-CoA (IB-CoA). *BCKDHA* and *BCKDHB* genes encode E1, which exists as an α2/β2 heterotetramer, and its role is a thiamin-dependent decarboxylase. The *DBT* gene encodes E2, which acts as a lipoate-dependent dihydrolipoyl transacylase, transferring the acyl groups to coenzyme A. The *DLD* gene encodes E3, which is a FAD-dependent dihydrolipoyl dehydrogenase and functions in transferring the released electrons to NAD^+ (1). BCKDH kinase (BCKDK) suppresses the activity of BCKDH by adding phosphate to three residues of BCKDHA. BCKAs especially the KIC allosterically regulate BCKDK. If the BCKAs are at high concentration, BCKAs will inhibit the activity of BCKDK, preventing BCAAs from running out when they are at low concentration (6). However, BCKDK also seems to be regulated by the BCKDH complex, the details of the mechanism need to be studied (6). The dephosphorylation process which activates the BCKDH complex is catalyzed by mitochondrial phosphatase 2C (PP2Cm). After the decarboxylation of BCKAs catalyzed by BCKDH, the following catabolism step is similar to the oxidation of fatty acid, every reaction is unique to the three BCAAs, and the mitochondrial matrix is the only site these reactions take place (**Figure 2**). In the end, the carbons from BCAA catabolism are either released as CO_2 or enter the tricarboxylic acid (TCA) cycle (1). Except for complete oxidation, the BCAA intermediates also underwent degradation through gluconeogenesis, lipogenesis, ketogenesis, or cholesterol synthesis pathway (7).

DETECTION METHODS OF BRANCHED-CHAIN AMINO ACIDS AND BRANCHED-CHAIN α-KETO ACID DEHYDROGENASE KINASE

Nowadays, there is a great progress in the detection of amino acids at very low concentrations in complex matrixes, including liquid chromatography-mass spectrometry (LC-MS) and capillary electrophoresis-mass spectrometry (CE-MS) (6, 8, 9). Liquid chromatography and tandem mass spectrometry appear to be the major methods for detecting plasma BCAAs nowadays (10–13). Also, there are other improved LC-MS methods, including isotope dilution liquid chromatography tandem mass spectrometry (ID-LC/MS/MS) and high-performance liquid chromatography with electrospray ionization mass spectrometry (LC-ESI-MS) (14, 15). Due to the significant biological role that BCAAs and BCKAs play in metabolism, being able to measure them at the same time has become an important topic. A liquid chromatography-electrospray ionization-tandem mass spectrometry (LC-$ESI^{\pm}$-MS/MS) method makes it possible to investigate BCAAs accompanied by BCKAs in human serum simultaneously (10). The CE-MS method (9, 16–18) is a valuable alternative for detecting BCAA concentrations. This method is widely used in the quantification of BCAAs in fluids and food, also, it has a wide application in pharmaceutical quality control (16).

Recently, a novel method of matrix-assisted laser desorption ionization-mass spectrometry imaging (MALDI-MSI) has been used to analyze BCAAs localization in tissues, especially in the brain. Many researches have demonstrated that the derivatization reagents such as 4-(anthracen-9-yl)-2-fluoro-1-methylpyridin-1-ium iodide (FMP-10), 2,4-diphenyl-pyranylium tetrafluoroborate (DPP), 2,3-diphenyl-pyranylium tetrafluoroborate (DPP-TFB), and 2,4,6-trimethylpyrylium (TMP) can promote amino metabolites detection in MALDI-MSI (19–21). This technique can simultaneously locate and quantify BCAAs in tissue sections, giving researchers credible information when studying the spatial distribution and quantity of BCAAs. Also, this technique makes it possible to study the impact of medication intervention on BCAAs.

The detection methods for BCKDK are quite simple. Real-time quantitative PCR, western blot, and immunohistochemical assay are used to analyze the expression of BCKDK. The activity of BCKDH also represents BCKDK function, and it can be measured by scintigraphy (22). The phosphorylation rate of BCKDH represents BCKDK function as well. At the same time, the function of BCKDK in glucose metabolism can be measured by the uptake amount of glucose, the production level of lactate, the oxygen consumption rate in the cell, the extracellular acidification rate, and reactive oxygen species (23, 24).

MICROBIOTA AND BRANCHED-CHAIN AMINO ACID-ASSOCIATED METABOLIC DISORDER

Food nutrients are regarded as the main nutrition supply for humans and other mammals. However, the gut microbiota has been reported to play an important role in modulating the utilization of numerous necessary nutrition for the host. Increasing evidence shows that obesity and many metabolic disorders may be related to the circulating BCAA pool, which can be affected by gut microbiota (25). Given the same protein proportion in high-fat diets (HFD) and normal

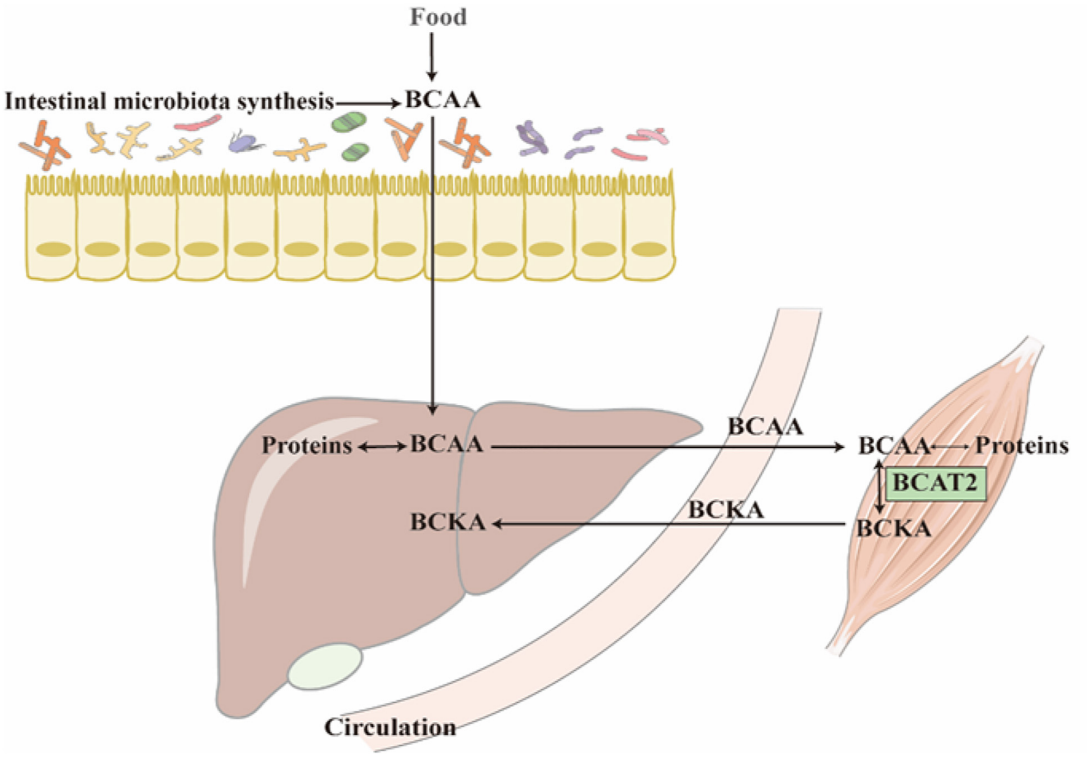

FIGURE 1 | Most of the BCAAs come from protein decomposition and food absorption. The reversible transamination reaction of BCAAs catabolism mostly occurs in skeletal muscle. After BCKAs are released back into circulation, most of them are oxidatively decarboxylated to acyl-CoA in the liver.

control diets (NCD), bacterial metabolism is considered to be the source of high levels of serum BCAAs in HFD. In diet-induced obese (DIO) mice which are treated with luffa administration, the relative abundances of *g-Enterortabdus*, *g-Eubacterium-xylanophilum*-group, and *g-Butyricicoccus* were found to be increased in 16S rRNA gene sequencing (26). Also, in dietary luffa-treated DIO mice, the mRNA expression of the enzymes that catalyze BCAA the catabolism to decrease BCAA levels is upregulated in tissues such as the liver, adipose, and colon (26). Gut microbiota is altered in patients with stable heart failure, through the use of metagenomic analysis. Patients with heart failure have lower plasma essential amino acid levels than healthy controls. The lack of *Eubacterium* and *Prevotella* leads to the decreased biosynthesis of essential amino acids (especially BCAAs and histidine) in patients with heart failure, on account of the reduced abundance of microbial genes related to essential amino acid biosynthesis (27). *Prevotella-copri* is lipopolysaccharide-producing bacteria, making it related to low-grade inflammation and the synthesis of BCAAs (28).

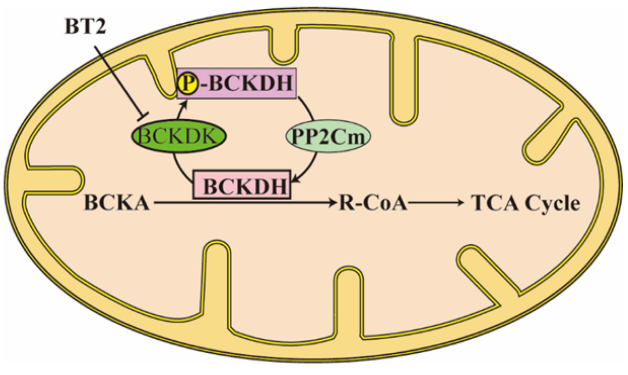

FIGURE 2 | A brief schematic of BCKA catabolism, and the enzymes that regulate this process.

Branched chain amino acids have potential effects on lipid composition. BCAAs metabolize into acetyl coenzyme A and propionyl coenzyme A, which are substrates for lipid synthesis. Excess carbon produced by catabolism of BCAA may lead to an increase in the rate of adipogenesis (29). Research has reported that fat accumulation in the liver was reduced after BCAAs supplementation in a rat experiment. The supplementation of BCAA will lead to the proliferation of *R. flavefaciens* which synthesized and released acetic acid into the portal vein, so that the expression of fatty-acid synthase (FAS) and acetyl-CoA carboxylase (ACC) in the liver is downregulated, reducing the occurrence of non-alcoholic fatty liver disease (NAFLD) (30).

Generally, individuals with obesity are prone to having gut microbiota dysbiosis with higher levels of circulating BCAAs and BCKAs compared with lean individuals. It is reported that gavage with *Bacteroides spp*. reduced the defects in BCAA catabolism

of brown adipose tissue (BAT) caused by obesity and protected mice from obesity. The supplementation of *Bacteroides spp.* alters gut microbiota composition and reduces the levels of BCAA and BCKA in BAT, proving the beneficial effect of *Bacteroides spp.* in the catabolism of BCAA in BAT (31). Many studies that are targeted at microbiota intervention have suggested that regulating the BCAAs can be achieved by changing the gut microbiota, thus showing a promising therapeutic prospect. Some key findings focused on BCAAs and microbiota are summarized in **Table 1**.

ROLE OF BRANCHED-CHAIN AMINO ACIDS AND BRANCHED-CHAIN α-KETO ACID DEHYDROGENASE KINASE IN METABOLIC DISORDERS

Obesity, Insulin Resistance, and Type 2 Diabetes Mellitus

Concentrations of plasma BCAAs, BCKAs, and carnitine esters, which derive from BCAAs metabolites are reported to be elevated in insulin resistance (IR), obesity, and type 2 diabetes mellitus (T2DM) patients and mice. And the circulating levels of BCAA and BCKA show an obvious correlation with body weight in mice as well as humans. Apart from the higher amount of food intake, the decreased metabolism of BCAAs contributes to another important aspect of obesity (42). It has been proven that the translation of BCAAs metabolism enzymes in adipose and liver is inhibited in obese mice, and the increased expression of BCKDK leads to the increased phosphorylation of BCKDH E1α and impaired activity of BCKDH in the liver (5, 43, 44). At the same time, BCKDK inhibitor treatment of diet-induced obese mice can inhibit weight gain and reduce the BCAAs and BCKAs concentrations in plasma (31). It is proposed that BCKDK promotes the occurrence of obesity by inhibiting BCAAs metabolism in obese animals. There are other studies pointing out that the elevated BCAAs in plasma might be related to impaired insulin action since it will increase protein catabolism in obese animals (31, 42). It is proposed that inflammation can down-regulate BCAA catabolism and lipogenesis in visceral adipose tissue partly through the NF-κB pathway, and endoplasmic reticulum stress can also down-regulate the BCAA metabolism pathway (45).

Muscle is reported as the earliest detectable tissue under insulin resistance abnormality, and the dysfunction of β-cell in the pancreas is widely accepted as the main pathophysiologic factor that drives T2DM (28, 46). It has been reported that elevated plasma BCAAs and BCKAs concentrations are early signs of insulin resistance in clinical studies (2). However, the level of BCAAs is not consistent with IR in different obesity-induced IR studies. In different tissues, the increase of circulating BCKAs is found to be better correlated with the severity of IR and T2DM, making BCKAs more effective and reliable biomarkers for IR (47–53). Accumulation of BCKAs is also an indicator of glucose intolerance and cardiac insufficiency and diabetes (54). The clearance of BCKAs is catalyzed by BCKDH, which is regulated by the inhibitory phosphorylation of BCKDK, suggesting BCKDK might be an important enzyme regulating this process.

BCAAs and BCKAs are reported to be involved in multiple IR pathways, including mTOR, insulin receptor substrate 1 (IRS1) pathway, fatty acid oxidation, and c-Jun NH2 terminal kinase (55–58). Activation of the mTORC1 pathway by leucine via Rag GTPases is considered to be an important mechanism of the impaired insulin signaling pathway. When activated, the tyrosine residues of insulin receptor substrates 1 and 2 (IRS1 and IRS2) were phosphorylated by insulin receptors, binding them to PI3K, causing AKT and protein kinase C (PKC) activated (59), those downstream effectors regulate glucose metabolism by phosphorylating downstream proteins in a cell-specific manner. AKT is considered a major and universal node in insulin signal transduction (60). It has been demonstrated that serum BCKAs inhibits insulin signaling by inhibiting AKT phosphorylation. Treatment with rapamycin, an mTOR inhibitor, showed a recovery in AKT2 phosphorylation and a moderate recovery of AKT1 phosphorylation suggesting that BCKAs inhibited AKT phosphorylation is dependent on mTOR (50, 59). Moreover, BCKAs have been proved to directly activate mTORC1, then activate S6K1 to phosphorylate the serine residue of insulin receptor substrate (IRS), preventing insulin receptors from binding to IRS and functioning (50).

Furthermore, it is proposed that activated mTORC1 can induce IR by directly promoting IRS1/2 degradation. However, in ob/ob mice given a low-protein diet, BCAAs supplementation causes insulin impairment without enhancing the activity of mTORC1. So that the activation of mTORC1 is not the only regulatory way of BCAA catabolism affecting insulin sensitivity (47). There are other ways leading to IR caused by BCAAs catabolic defects, such as increased synthesis and uptake of fatty acids due to BCAAs metabolic disorders. BCKDK can not only regulate BCAAs metabolism with BCAA as substrate but also phosphorylate ATP-Citrate Lyase (ACL), a critical enzyme in fatty acid synthesis from the beginning, and regulate the *de novo* formation pathway of fat, thus regulating the content of fatty acids (22). The metabolite of the valine, 3-HIB, may also cause insulin resistance through increasing muscle fatty acid usage (61). BCAAs supplementation to a normal diet does not affect mTOR activity while adding BCAAs to a high-fat diet increases mTOR activity in animal experiments. This proved that the existence of fatty acids promotes the activation of mTOR by BCAA and promotes the occurrence of IR. Abnormal BCAAs metabolism leads to the toxic stock of BCAAs metabolites, which triggers the dysfunction of mitochondria and stress signaling related to insulin resistance and T2DM. An example is JNK, which is associated with insulin resistance (62, 63).

Cardiovascular Disease

As mentioned above, BCAAs are found to be increased in the failing heart. It is proposed that cardiac BCAAs oxidation is decreased in insulin resistance. A study showed that BCAAs

TABLE 1 | Summary of the interaction between microbiota and BCAA levels in different experimental settings from the recent studies.

Model	Treatment	Finding	Microbiome composition	Changes of BCAA	Refs
Mice	HFD, luffa gavage	Dietary luffa reduced higher circulating BCAA and upregulated BCAA catabolizing enzymes. In germ-free-mimic mice, dietary *luffa* did not influence BCAA catabolism when mice are fed HFD and formed DIO.	Decreased relative abundances of *g_Enterortabdus*, *g_Eubacterium_xylanophilum_group* and *g_Butyricicoccus*.	Decreased circulating BCAA levels.	(26)
Human	Stable heart failure patients	The depletion of *Eubacterium* and *Prevotella* cause the decreased abundance of microbial genes which are related to BCAAs biosynthesis in the heart failure patients.	Decreased *Eubacterium* and *Prevotella.*	Decreased circulating BCAA levels.	(27)
Rat	HFD, BCAA supplementation	BCAA supplementation caused the proliferation of R. *flavefaciens,* and the increased level of acetic acid subsequently inhibit lipogenesi-srelated genes expression, and avoid fat accumulation in the liver.	Increased R. *flavefaciens.*	Increased BCAA levels.	(30)
Mice	HFD, *bacteroides spp.* gavage	Supplementation of *Bacteroides spp.* reduced the defects in BCAA catabolism of BAT and avoid obesity in mice.	Supplementation of *Bacteroides spp.*	Reduced BCAA and BCKA levels in brown adipose tissue.	(31)
Human	T2DM patients	Intestinal dysbiosis characterized as an elevated abundance in *Prevotella copri*. was found in T2DM patients.	Increased *Prevotella copri* abundance in T2DM patients.	Increased serum BCAA levels.	(32)
Mice	HFD, PMFE gavage	PMFE gavage increased the abundance of commensal bacterium Bacteroides ovatus. In HFD mice, BCAA levels were decreased after gavaging with Bacteroides ovatus, and alleviated metabolic syndrome was relieved.	Increased abundance of *Bacterium Bacteroides ovatus*.	Decreased serum BCAA levels.	(33)
Human	Patients with lung cancer	The effect of gut microbiota on serum BCAAs concentration was prone to affected by the combinational influence of various bacteria, rather than individual microbial species. *Prevotella copri* and *Lactobacillus gasseri*. have positive correlation with BCAAs levels in non-cachectic patients.	*Prevotella copri* and *Lactobacillus gasseri* level increased in non-cachectic patients.	Increased serum BCAA levels in non-cachectic patients.	(34)
Mice	HFD, oral doses of ginsenoside Rb1 (200 mg/kg/day)	Rb1 supplementation decreased levels of BCAAs, and improved HFD induced insulin resistance.	19 genera showed strong correlation with serum BCAAs, Eubacterium corprostanoligenes was correlated with leucine and isoleucine simultaneously.	Rb1 supplementation decreased serum BCAA levels.	(35)
Mice	HFD, Prevotella *copri* gavage	The major bacteria that connect BCAA synthesis and insulin resistance are *Prevotella copri* and *bacteroides vulgatus.*	*Prevotella copri* gavage.	Increased circulating levels of BCAAs.	(28)
Mice	Normal diet, intermittent leucine-deficient food every other day	Leucine deficiency can change gut microbiome composition. Lack of leucine intermittently elevates *Bacteroidetes* and reduces *Firmicutes* at phylum level. Also, *Bacteroides, Alloprevotella and Rikenellaceae RC9* was elevated, *Lachnospiraceae* was reduced at genus level in leucine deficiency.	*Bacteroides, Alloprevotella and Rikenellaceae RC9* was increased, *Lachnospiraceae* was reduced.	Intermittent leucine deficiency.	(36)
Mice	Dietay supplementation BCAAem	The BCAAem supplemented group showed gut microbiota changes and lower serum concentrations of lipopolysaccharide-binding protein.	The abundance of *Akkermansia* and *Bifidobacterium* increased, *Enterobacteriaceae* decreased.	Increased BCAA levels.	(37)
Mice	HFD/STZ-induced T2DM mice, SF-Alg gavage	SF-Alg increased some benign bacteria, and decreased harmful bacteria. Meanwhile, SF-Alg dramatically decreased BCAAs in the colon of T2DM mice.	Beneficial bacteria such as *Lactobacillus*, *Bacteroides*, *Akkermansia Alloprevotella*, *Weissella* and *Enterorhabdus* were increased, deleterious bacteria (*Turicibacter* and *Helicobacter*) were decreased.	BCAAs decreased in the colon.	(38)
Mice	HFD, AB23A gavage	AB23A gavage decreased the abundance of the *Firmicutes*/*Bacteroidaeota* ratio and *Actinobacteriota*/*Bacteroidaeota* ratio, and significantly reduced serum lipopolysaccharide and BCAA levels.	*Firmicutes*/*Bacteroidaeota* ratio decreased and *Actinobacteriota*/*Bacteroidaeota* ratio decreased.	Decreased serum BCAA levels.	(39)
Rat	T2DM rats, SSJIBL	SSJIBL elevated the abundance of *Escherichia coli* and *Ruminococcus gnavus* in gut, and decreased *Prevotella copri* level, as well as the levels of serum BCAA.	Elevated abundance of gut *Escherichia coli* and *Ruminococcus gnavus*, reduction in *Prevotella copri*.	Decreased serum BCAA levels.	(40)
Human	Chronic haemodialysis patients, BCAA supplementation	The BCAA and glycine supplementation did not change faecal microbiota composition and microbial diversity, however, *L. paracasei* and *B. dentium* were reduced in abundance level.	Decreased abundance of *L. paracasei* and *B. dentium*.	Increased BCAA levels.	(41)

HFD, high-fat diet; BCAA, branched-chain amino acid; DIO, diet-induce obesity; T2DM, type 2 diabetes mellitus; BCAAem, BCAA-enriched mixture; STZ, streptozotocin; SF-Alg, Sargassum fusiforme alginate; AB23A, Alisol B 23-acetate; SSJIBL, side-to-side jejunoileal bypass plus proximal loop ligation.

oxidation dedicated about one percentage of ATP production in heart ATP production, however, the main sources of heart ATP production are glucose and fatty acid oxidation. This suggests that cardiac insulin resistance is not due to the increased oxidation of BCAAs, which inhibits glucose and fatty acid oxidation (64). However, it is not clear whether BCAAs result in heart failure and mediate cardiac insulin resistance. In a permanent myocardial infarction (MI) model, utilizing coronary artery ligation, BCAAs catabolism was damaged seriously in the myocardium. This leads to an obvious elevation in BCAAs levels and activates mTOR signaling, exacerbating cardiac dysfunction and remodeling (65). It has been reported that BCAA levels were increased in dilated cardiomyopathy (DCM) hearts, accompanied by a decreased expression of mitochondrial BCAT2 and total expression of BCKDH compared to non-failing control. Also, phosphorylation of BCKDH and expression of cardiac PP2Cm were reduced in the DCM hearts, with an unchanged expression of BCKDK. It is reported that in heart failure patients, KLF15 expression is inhibited through the TAK1/P38MAPK axis, thus inhibiting BCAA catabolism, which leads to BCAAs accumulated in the heart. Also, increasing the oxidation rate of BCAAs has proved a practicable way to improve the contractile function of failing hearts in mice. After injecting BCKDK inhibitor, there is an increase in the activity of BCKDH and oxidation of BCAAs and the% ejection fraction (%EF) of TAC mouse increased significantly in transverse aortic constriction (TAC) surgery as heart failure mouse models. The results suggest that lowering cardiac BCAA levels by increasing the BCAA oxidation rate might offer a novel therapeutic way of heart failure treatment (66).

Exercise Damage

BCAAs are believed to increase muscle mass and limit exercise damage, so they are often utilized as nutritional supplements after exercise by some athletes and people with exercise habits regardless of their practice level. To investigate whether BCAAs supplements are beneficial, 11 studies described tests performed on humans who took BCAAs supplementation orally as a nutritional strategy were included, and a systematic review was published by some researchers, providing a comprehensive analysis of the effects of BCAAs supplementation on muscle damage induced by exercise. The result is quite neutral because the positive effect study numbers was equal to the no effect ones. What's more, the studies which reported BCAAs supplementation had a positive effect on muscle damage, appeared to be of low quality. Most of the high-quality studies suggest there is no significant effect of BCAAs supplementation. This systematic review proposed that whether BCAAs supplementation is beneficial in muscle damage is uncertain. But under certain circumstances, supplying BCAAs might lessen the exercise-induced muscle damage. Under these circumstances, the experiment subjects are asked to take BCAAs supplementation at a dosage greater than 200 mg/kg/day, starting 1 week before exercise, and with a time duration longer than 10 days (67). To investigate whether BCAAs supplementation is needed to prevent exercise-induced muscle damage, there are more experiments with a larger sample size that needs to be done in the future.

Nervous System Diseases

As an important subgroup of essential amino acids, BCAAs in particular leucine, play an important role in the stimulation of protein synthesis, and cellular signaling. Some nervous system diseases are found to be related to be lack of BCAAs caused by mutations in the gene *BCKDK*. In a colony of Sprague–Dawley rats, there is a new mutant with the characteristics of hindlimb splaying, seizures, and brain weight decreasing. Mutations in the gene *Bckdk* are found in those rats (68). A study first reported that *Bckdk*$^{-/-}$ mice displayed repetitive hind limb flexion and extension when hung by the tail and eventually developed epileptic seizures (69). By studying those consanguineous families with autism, epilepsy, and intellectual disability, researchers have found mutations in the inactivating gene *BCKDK*. Patients with homozygous *BCKDK* mutations show decreasing messenger RNA and protein of *BCKDK* and plasma BCAAs. *Bckdk* knock-out mice have abnormal amino acid profiles in the brain and neurobehavioral deficits that respond to dietary BCAA supplementation (70). Another study discovered two novel mutations in the gene *BCKDK* of two children who are not related to each other, and their body fluids' BCAA levels were decreased. Also, their delay in development and abnormal neurobehaviors were partially corrected after BCAA supplementation in a rich-protein diet (71).

Also, *BCKDK* and BCAAs are found to be related to energy metabolism in Huntington's disease, which has the characteristics of progressive dysfunction in activity and cognition, with the symptoms of speech cessation, swallowing problems, walking difficulties, and losing independence, and dementia attack in the end. By measuring the blood of Huntington's disease gene carriers and healthy controls in metabolites and gene expression changes, 6 statistically significant mRNA transcripts were found, and *BCKDK* was 1.34-fold higher in gene transcription level than healthy controls (72).

In maple syrup urine disease (MSUD) patients, accumulation of BCAAs and BCKAs are found due to the deficiency of branched-chain α-keto acid dehydrogenase caused by some certain inborn error of metabolism. It is proposed that the toxic accumulation of BCAAs and BCKAs can lead to apoptosis in glial cells and neurons with dosage and time-dependent pattern (73). Destroying the metabolism of brain energy is another mechanism. Pyruvate dehydrogenase, α-ketoglutarate dehydrogenase and the mitochondrial respiration chain are all inhibited by the accumulating BCKAs and leucine (74).

Treatment Targeting Branched-Chain α-Keto Acid Dehydrogenase Kinase and Branched-Chain Amino Acids

The therapeutic way of treating BCKDK deficiency is to restore the normal BCAA levels in patient fluids currently (75). The supplementation of BCAAs is quite important in nervous system diseases with mutations in the gene *BCKDK*. Nowadays, the research focus is mainly on decreasing the circulation BCAAs by inhibiting BCKDK or other methods.

The mitochondrial BCKDH is negatively regulated by reversible phosphorylation, and recent studies have found a novel

BCKDK inhibitor, compound 3,6-dichlorobenzo[b]thiophene-2-carboxylic acid (BT2) can reduce the concentrations of BCAA *in vivo*. BT2 binds to BCKDK and leads to helix movements in the N-terminal domain, causing the dissociation of BCKDK from the BCKDH along with accelerated degradation of the released kinase *in vivo* (54, 76). When DIO mice were administered BT2 by oral gavage, serum BCAA and BCKA concentrations in the BT2 group showed a remarkable reduction compared with those in the control group after 4 weeks of BT2 treatment. Although the food intake amount of a high-fat diet appeared no difference in the two groups, BT2 treatment can obviously inhibit the weight gain compared with control (31). It is proposed that when wild-type mice were treated with BT2 at a dosage of 20 mg/kg/day for 1 week, it will result in almost completely dephosphorylated and maximally activated BCKDH in the heart, muscle, kidneys, and liver with a decrease in serum BCAA concentrations (76).

Similar to BT2, another BCKDK inhibitor (s)-α-chlorophenylpropionic acid [(S)-CPP] is believed to achieve the same effect of reducing plasma BCAA concentrations. (S)-CPP binds to the N-terminal domain in a unique allosteric site, causing helix movements in BCKDK. These conformational changes are transferred to the lipoyl-binding pocket, which prevents BCKDK from binding to the BCKDH core to remove its activity (77).

There is also an easily available drug in the clinic found useful in improving BCAAs catabolism. Pyridostigmine has been widely used and tested in the clinic for the treatment of myasthenia gravis. Recently, some studies have revealed that pyridostigmine inhibits cholinesterase to increase acetylcholine levels, leading to an improvement in cardiac function in rats with cardiovascular diseases. At the same time, the cardiac function of normal rats was not affected. Also, pyridostigmine was found to promote BCAAs catabolism by enhancing vagal activity and attenuating intestinal barrier injury and gut bacteria dysbiosis in diabetic cardiomyopathy mice. Pyridostigmine was also found to enhance cardiac BCAAs catabolism by upregulating BCAT2 and PP2Cm and downregulating p-BCKDHA/BCKDHA and BCKDK (78).

Nowadays, insulin sensitizer therapy such as thiazolidinediones is found to improve insulin sensitivity and reduce serum BCAAs (79–81). A study reported that thiazolidinediones (in this experiment, rosiglitazone was used) treated mice had lower circulating BCAA and showed upregulated BCAT as well as BCKDH activities compared with those treated with placebo, independently of diet. They hypothesized that rosiglitazone could reduce IRS1 serine phosphorylation in skeletal muscle dependent on mTORC1 and thus reduce insulin resistance throughout the body (79).

CONCLUSION

The homeostasis of BCAAs is critical in health and disease. Like essential amino acids, BCAAs participate in protein synthesis, regulating neurotransmitter synthesis, providing energy support, and acting as nitrogen donors. The accumulation and insufficiency of BCAAs play critical roles in different metabolic disorders (**Figure 3**). Lacking BCAAs and BCKDK mutations may cause severe neurological disorders and growth retardation.

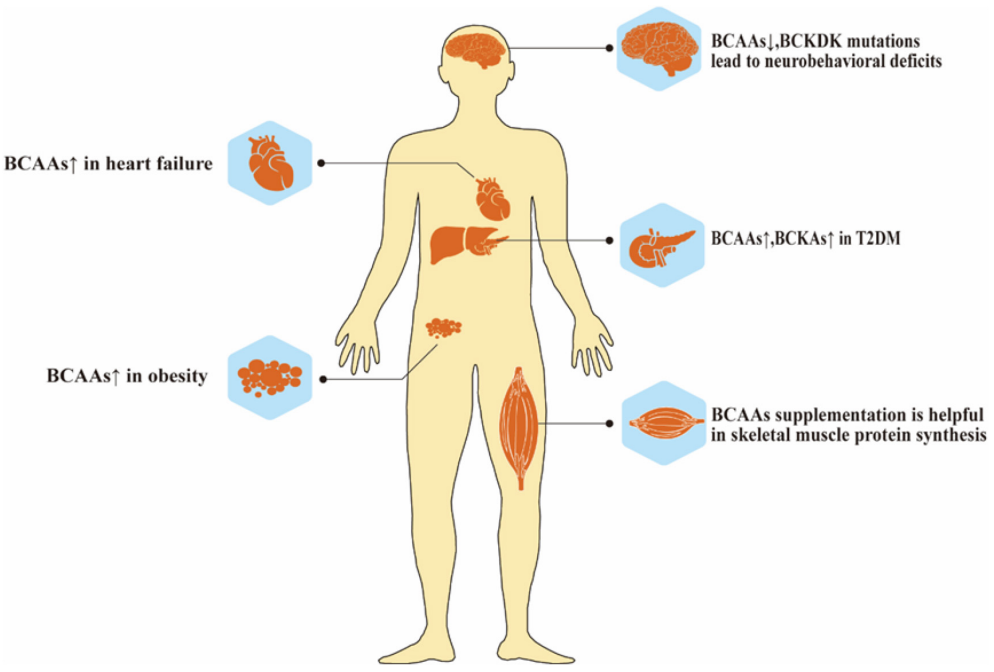

FIGURE 3 | Role of BCAAs metabolism in health. Abnormal elevation or deficiency of BCAAs lead to many diseases, such as neurobehavioral deficits, heart failure, T2DM and obesity.

However, insulin resistance, obesity, heart failure, and even cancer are all associated with the accumulation of excess BCAAs. BCKDK, as an important enzyme affecting the metabolism of BCAA, is now recognized as a new therapeutic target for treating metabolic disorders caused by BCAA accumulation. Certain microbiota may also affect BCAA metabolism, and further studies are needed in this area. Apart from introducing diseases related to BCAAs and BCKDK, this review has also offered information about some novel detection methods of BCAAs, the interaction between BCAAs and microbiota, and BCKDK inhibitors, facilitating the researchers to get a comprehensive understanding of studies on BCAAs.

AUTHOR CONTRIBUTIONS

All authors listed have made a substantial, direct, and intellectual contribution to the work, and approved it for publication.

FUNDING

This research received financial support from the General Project of the Liaoning Provincial Department of Education under grant no. LJKZ0758. China Medical University and Chinese Academic of Science partnership grant no. HZHB2022009.

REFERENCES

1. Neinast M, Murashige D, Arany Z. Branched chain amino acids. *Annu Rev Physiol.* (2019) 81:139–64. doi: 10.1146/annurev-physiol-020518-114455
2. Lynch CJ, Adams SH. Branched-chain amino acids in metabolic signalling and insulin resistance. *Nat Rev Endocrinol.* (2014) 10:723–36. doi: 10.1038/nrendo.2014.171
3. White PJ, Newgard CB. Branched-chain amino acids in disease. *Science.* (2019) 363:582–3. doi: 10.1126/science.aav0558
4. Holeèek M. Branched-chain amino acids in health and disease: metabolism, alterations in blood plasma, and as supplements. *Nutr Metab.* (2018) 15:33. doi: 10.1186/s12986-018-0271-1
5. Shin AC, Fasshauer M, Filatova N, Grundell LA, Zielinski E, Zhou JY, et al. Brain insulin lowers circulating BCAA levels by inducing hepatic BCAA catabolism. *Cell Metab.* (2014) 20:898–909. doi: 10.1016/j.cmet.2014.09.003
6. Maguolo A, Rodella G, Giorgetti A, Nicolodi M, Ribeiro R, Dianin A, et al. A gain-of-function mutation on BCKDK gene and its possible pathogenic role in branched-chain amino acid metabolism. *Genes.* (2022) 13:233. doi: 10.3390/genes13020233
7. Supruniuk E, Zebrowska E, Chabowski A. Branched chain amino acids-friend or foe in the control of energy substrate turnover and insulin sensitivity? *Crit Rev Food Sci Nutr*. (2021) 1–39. doi: 10.1080/10408398.2021.1977910 [Epub ahead of print].
8. Ferré S, González-Ruiz V, Guillarme D, Rudaz S. Analytical strategies for the determination of amino acids: past, present and future trends. *J Chromatogr B Analyt Technol Biomed Life Sci.* (2019) 1132:121819. doi: 10.1016/j.jchromb.2019.121819
9. Desiderio C, Iavarone F, Rossetti DV, Messana I, Castagnola M. Capillary electrophoresis-mass spectrometry for the analysis of amino acids. *J Sep Sci.* (2010) 33:2385–93. doi: 10.1002/jssc.201000171
10. Li R, Liu P, Liu P, Tian Y, Hua Y, Gao Y, et al. A novel liquid chromatography tandem mass spectrometry method for simultaneous determination of branched-chain amino acids and branched-chain α-keto acids in human plasma. *Amino Acids.* (2016) 48:1523–32. doi: 10.1007/s00726-016-2212-5
11. Le TT, Shafaei A, Genoni A, Christophersen C, Devine A, Lo J, et al. Development and validation of a simple LC-MS/MS method for the simultaneous quantitative determination of trimethylamine-N-oxide and branched chain amino acids in human serum. *Anal Bioanal Chem.* (2019) 411:1019–28. doi: 10.1007/s00216-018-1522-8
12. Ten Have GAM, Jansen L, Schooneman MG, Engelen M, Deutz NEP. Metabolic flux analysis of branched-chain amino and keto acids (BCAA, BCKA) and β-hydroxy β-methylbutyric acid across multiple organs in the pig. *Am J Physiol Endocrinol Metab.* (2021) 320:E629–40. doi: 10.1152/ajpendo.00384.2020
13. Wang M, Yang R, Dong J, Zhang T, Wang S, Zhou W, et al. Simultaneous quantification of cardiovascular disease related metabolic risk factors using liquid chromatography tandem mass spectrometry in human serum. *J Chromatogr B Analyt Technol Biomed Life Sci.* (2016) 100:144–51. doi: 10.1016/j.jchromb.2015.12.019
14. Yang R, Dong J, Guo H, Li H, Wang S, Zhao H, et al. Rapid and precise measurement of serum branched-chain and aromatic amino acids by isotope dilution liquid chromatography tandem mass spectrometry. *PLoS One.* (2013) 8:e81144. doi: 10.1371/journal.pone.0081144
15. Rebane R, Oldekop ML, Herodes K. Comparison of amino acid derivatization reagents for LC-ESI-MS analysis. Introducing a novel phosphazene-based derivatization reagent. *J Chromatogr B Analyt Technol Biomed Life Sci.* (2012) 904:99–106. doi: 10.1016/j.jchromb.2012.07.029
16. Piestansky J, Matuskova M, Cizmarova I, Olesova D, Mikus P. Determination of branched-chain amino acids in food supplements and human plasma by a CE-MS/MS method with enhanced resolution. *Int J Mol Sci.* (2021) 22:8261. doi: 10.3390/ijms22158261
17. Soga T, Kakazu Y, Robert M, Tomita M, Nishioka T. Qualitative and quantitative analysis of amino acids by capillary electrophoresis-electrospray ionization-tandem mass spectrometry. *Electrophoresis.* (2004) 25:1964–72. doi: 10.1002/elps.200305791
18. Hirayama A, Soga T. Amino acid analysis by capillary electrophoresis-mass spectrometry. *Methods Mol Biol.* (2012) 828:77–82. doi: 10.1007/978-1-61779-445-2_8
19. Shariatgorji M, Nilsson A, Källback P, Karlsson O, Zhang X, Svenningsson P, et al. Pyrylium salts as reactive matrices for MALDI-MS imaging of biologically active primary amines. *J Am Soc Mass Spectrom.* (2015) 26:934–9. doi: 10.1007/s13361-015-1119-9
20. Esteve C, Tolner EA, Shyti R, van den Maagdenberg AM, McDonnell LA. Mass spectrometry imaging of amino neurotransmitters: a comparison of derivatization methods and application in mouse brain tissue. *Metabolomics.* (2016) 12:30. doi: 10.1007/s11306-015-0926-0
21. Shariatgorji R, Nilsson A, Fridjonsdottir E, Strittmatter N, Dannhorn A, Svenningsson P, et al. Spatial visualization of comprehensive brain neurotransmitter systems and neuroactive substances by selective in situ chemical derivatization mass spectrometry imaging. *Nat Protoc.* (2021) 16:3298–321. doi: 10.1038/s41596-021-00538-w
22. White PJ, McGarrah RW, Grimsrud PA, Tso SC, Yang WH, Haldeman JM, et al. The BCKDH kinase and phosphatase integrate BCAA and lipid metabolism via regulation of ATP-citrate lyase. *Cell Metab.* (2018) 27:1281–93.e7. doi: 10.1016/j.cmet.2018.04.015
23. Zhang W, Wu Y, Fan W, Chen H, Du H, Rao J. The pattern of plasma BCAA concentration and liver Bckdha gene expression in GK rats during T2D progression. *Animal Model Exp Med.* (2018) 1:305–13. doi: 10.1002/ame2.12038
24. Wang Y, Xiao J, Jiang W, Zuo D, Wang X, Jin Y, et al. BCKDK alters the metabolism of non-small cell lung cancer. *Transl Lung Cancer Res.* (2021) 10:4459–76. doi: 10.21037/tlcr-21-885
25. Gojda J, Cahova M. Gut microbiota as the link between elevated BCAA serum levels and insulin resistance. *Biomolecules.* (2021) 11:1414. doi: 10.3390/biom11101414
26. Zhang L, Yue Y, Shi M, Tian M, Ji J, Liao X, et al. Dietary *Luffa cylindrica (L.)* roem promotes branched-chain amino acid catabolism in the circulation system via gut microbiota in diet-induced obese mice. *Food Chem.* (2020) 320:126648. doi: 10.1016/j.foodchem.2020.126648
27. Hayashi T, Yamashita T, Takahashi T, Tabata T, Watanabe H, Gotoh Y, et al. Uncovering the role of gut microbiota in amino acid metabolic disturbances

in heart failure through metagenomic analysis. *Front Cardiovasc Med.* (2021) 8:789325. doi: 10.3389/fcvm.2021.789325
28. Pedersen HK, Gudmundsdottir V, Nielsen HB, Hyotylainen T, Nielsen T, Jensen BA, et al. Human gut microbes impact host serum metabolome and insulin sensitivity. *Nature.* (2016) 535:376–81. doi: 10.1038/nature18646
29. Dimou A, Tsimihodimos V, Bairaktari E. The critical role of the branched chain amino acids (BCAAs) catabolism-regulating enzymes, branched-chain aminotransferase (BCAT) and branched-chain alpha-keto acid dehydrogenase (BCKD), in human pathophysiology. *Int J Mol Sci.* (2022) 23:4022. doi: 10.3390/ijms23074022
30. Iwao M, Gotoh K, Arakawa M, Endo M, Honda K, Seike M, et al. Supplementation of branched-chain amino acids decreases fat accumulation in the liver through intestinal microbiota-mediated production of acetic acid. *Sci Rep.* (2020) 10:18768. doi: 10.1038/s41598-020-75542-3
31. Yoshida N, Yamashita T, Osone T, Hosooka T, Shinohara M, Kitahama S, et al. *Bacteroides* spp. promotes branched-chain amino acid catabolism in brown fat and inhibits obesity. *iScience.* (2021) 24:103342. doi: 10.1016/j.isci.2021.103342
32. Medina-Vera I, Sanchez-Tapia M, Noriega-López L, Granados-Portillo O, Guevara-Cruz M, Flores-López A, et al. A dietary intervention with functional foods reduces metabolic endotoxaemia and attenuates biochemical abnormalities by modifying faecal microbiota in people with type 2 diabetes. *Diabetes Metab.* (2019) 45:122–31. doi: 10.1016/j.diabet.2018.09.004
33. Zeng SL, Li SZ, Xiao PT, Cai YY, Chu C, Chen BZ, et al. Citrus polymethoxyflavones attenuate metabolic syndrome by regulating gut microbiome and amino acid metabolism. *Sci Adv.* (2020) 6:eaax6208. doi: 10.1126/sciadv.aax6208
34. Ni Y, Lohinai Z, Heshiki Y, Dome B, Moldvay J, Dulka E, et al. Distinct composition and metabolic functions of human gut microbiota are associated with cachexia in lung cancer patients. *Isme J.* (2021) 15:3207–20. doi: 10.1038/s41396-021-00998-8
35. Yang X, Dong B, An L, Zhang Q, Chen Y, Wang H, et al. Ginsenoside Rb1 ameliorates glycemic disorder in mice with high fat diet-induced obesity via regulating gut microbiota and amino acid metabolism. *Front Pharmacol.* (2021) 12:756491. doi: 10.3389/fphar.2021.756491
36. Wei S, Zhao J, Wang S, Huang M, Wang Y, Chen Y. Intermittent administration of a leucine-deprived diet is able to intervene in type 2 diabetes in db/db mice. *Heliyon.* (2018) 4:e00830. doi: 10.1016/j.heliyon.2018.e00830
37. Yang Z, Huang S, Zou D, Dong D, He X, Liu N, et al. Metabolic shifts and structural changes in the gut microbiota upon branched-chain amino acid supplementation in middle-aged mice. *Amino Acids.* (2016) 48:2731–45. doi: 10.1007/s00726-016-2308-y
38. Liu J, Wu S, Cheng Y, Liu Q, Su L, Yang Y, et al. *Sargassum fusiforme* alginate relieves hyperglycemia and modulates intestinal microbiota and metabolites in type 2 diabetic mice. *Nutrients.* (2021) 13:2887. doi: 10.3390/nu13082887
39. Xia F, Xiang S, Chen Z, Song L, Li Y, Liao Z, et al. The probiotic effects of AB23A on high-fat-diet-induced non-alcoholic fatty liver disease in mice may be associated with suppressing the serum levels of lipopolysaccharides and branched-chain amino acids. *Arch Biochem Biophys.* (2021) 714:109080. doi: 10.1016/j.abb.2021.109080
40. Tan C, Zheng Z, Wan X, Cao J, Wei R, Duan J. The role of gut microbiota and amino metabolism in the effects of improvement of islet β-cell function after modified jejunoileal bypass. *Sci Rep.* (2021) 11:4809. doi: 10.1038/s41598-021-84355-x
41. Genton L, Pruijm M, Teta D, Bassi I, Cani PD, Gaïa N, et al. Gut barrier and microbiota changes with glycine and branched-chain amino acid supplementation in chronic haemodialysis patients. *J Cachexia Sarcopenia Muscle.* (2021) 12:1527–39. doi: 10.1002/jcsm.12781
42. She P, Van Horn C, Reid T, Hutson SM, Cooney RN, Lynch CJ. Obesity-related elevations in plasma leucine are associated with alterations in enzymes involved in branched-chain amino acid metabolism. *Am J Physiol Endocrinol Metab.* (2007) 293:E1552–63. doi: 10.1152/ajpendo.00134.2007
43. Lackey DE, Lynch CJ, Olson KC, Mostaedi R, Ali M, Smith WH, et al. Regulation of adipose branched-chain amino acid catabolism enzyme expression and cross-adipose amino acid flux in human obesity. *Am J Physiol Endocrinol Metab.* (2013) 304:E1175–87. doi: 10.1152/ajpendo.00630.2012
44. White PJ, McGarrah RW, Herman MA, Bain JR, Shah SH, Newgard CB. Insulin action, type 2 diabetes, and branched-chain amino acids: a two-way street. *Mol Metab.* (2021) 52:101261. doi: 10.1016/j.molmet.2021.101261
45. Burrill JS, Long EK, Reilly B, Deng Y, Armitage IM, Scherer PE, et al. Inflammation and ER stress regulate branched-chain amino acid uptake and metabolism in adipocytes. *Mol Endocrinol.* (2015) 29:411–20. doi: 10.1210/me.2014-1275
46. Taylor R. Type 2 diabetes: etiology and reversibility. *Diabetes Care.* (2013) 36:1047–55. doi: 10.2337/dc12-1805
47. Zhou M, Shao J, Wu CY, Shu L, Dong W, Liu Y, et al. Targeting BCAA catabolism to treat obesity-associated insulin resistance. *Diabetes.* (2019) 68:1730–46. doi: 10.2337/db18-0927
48. Chen T, Ni Y, Ma X, Bao Y, Liu J, Huang F, et al. Branched-chain and aromatic amino acid profiles and diabetes risk in Chinese populations. *Sci Rep.* (2016) 6:20594. doi: 10.1038/srep20594
49. Tai ES, Tan ML, Stevens RD, Low YL, Muehlbauer MJ, Goh DL, et al. Insulin resistance is associated with a metabolic profile of altered protein metabolism in Chinese and Asian-Indian men. *Diabetologia.* (2010) 53:757–67. doi: 10.1007/s00125-009-1637-8
50. Biswas D, Dao KT, Mercer A, Cowie AM, Duffley L, El Hiani Y, et al. Branched-chain ketoacid overload inhibits insulin action in the muscle. *J Biol Chem.* (2020) 295:15597–621. doi: 10.1074/jbc.RA120.013121
51. Felig P, Wahren J, Hendler R, Brundin T. Splanchnic glucose and amino acid metabolism in obesity. *J Clin Invest.* (1974) 53:582–90. doi: 10.1172/jci107593
52. Chevalier S, Marliss EB, Morais JA, Lamarche M, Gougeon R. Whole-body protein anabolic response is resistant to the action of insulin in obese women. *Am J Clin Nutr.* (2005) 82:355–65. doi: 10.1093/ajcn.82.2.355
53. Kadota Y, Toyoda T, Kitaura Y, Adams SH, Shimomura Y. Regulation of hepatic branched-chain α-ketoacid dehydrogenase complex in rats fed a high-fat diet. *Obes Res Clin Pract.* (2013) 7:e439–44. doi: 10.1016/j.orcp.2013.07.003
54. East MP, Laitinen T, Asquith CRM. BCKDK: an emerging kinase target for metabolic diseases and cancer. *Nat Rev Drug Discov.* (2021) 20:498. doi: 10.1038/d41573-021-00107-6
55. Yue SJ, Liu J, Wang AT, Meng XT, Yang ZR, Peng C, et al. Berberine alleviates insulin resistance by reducing peripheral branched-chain amino acids. *Am J Physiol Endocrinol Metab.* (2019) 316:E73–85. doi: 10.1152/ajpendo.00256.2018
56. Um SH, D'Alessio D, Thomas G. Nutrient overload, insulin resistance, and ribosomal protein S6 kinase 1. S6K1. *Cell Metab.* (2006) 3:393–402. doi: 10.1016/j.cmet.2006.05.003
57. Tremblay F, Brûlé S, Hee Um S, Li Y, Masuda K, Roden M, et al. Identification of IRS-1 Ser-1101 as a target of S6K1 in nutrient- and obesity-induced insulin resistance. *Proc Natl Acad Sci U.S.A.* (2007) 104:14056–61. doi: 10.1073/pnas.0706517104
58. Krebs M, Brunmair B, Brehm A, Artwohl M, Szendroedi J, Nowotny P, et al. The mammalian target of rapamycin pathway regulates nutrient-sensitive glucose uptake in man. *Diabetes.* (2007) 56:1600–7. doi: 10.2337/db06-1016
59. Ong PS, Wang LZ, Dai X, Tseng SH, Loo SJ, Sethi G. Judicious Toggling of mTOR Activity to combat insulin resistance and cancer: current evidence and perspectives. *Front Pharmacol.* (2016) 7:395. doi: 10.3389/fphar.2016.00395
60. Sharma M, Dey CS. AKT ISOFORMS-AS160-GLUT4: the defining axis of insulin resistance. *Rev Endocr Metab Disord.* (2021) 22:973–86. doi: 10.1007/s11154-021-09652-2
61. Harris LLS, Smith GI, Patterson BW, Ramaswamy RS, Okunade AL, Kelly SC, et al. Alterations in 3-Hydroxyisobutyrate and FGF21 metabolism are associated with protein ingestion-induced insulin resistance. *Diabetes.* (2017) 66:1871–8. doi: 10.2337/db16-1475
62. Newgard CB, An J, Bain JR, Muehlbauer MJ, Stevens RD, Lien LF, et al. A branched-chain amino acid-related metabolic signature that differentiates obese and lean humans and contributes to insulin resistance. *Cell Metab.* (2009) 9:311–26. doi: 10.1016/j.cmet.2009.02.002
63. Sun H, Olson KC, Gao C, Prosdocimo DA, Zhou M, Wang Z, et al. Catabolic defect of branched-chain amino acids promotes heart failure. *Circulation.* (2016) 133:2038–49. doi: 10.1161/circulationaha.115.020226
64. Fillmore N, Wagg CS, Zhang L, Fukushima A, Lopaschuk GD. Cardiac branched-chain amino acid oxidation is reduced during insulin resistance in

the heart. *Am J Physiol Endocrinol Metab.* (2018) 315:E1046–52. doi: 10.1152/ajpendo.00097.2018
65. Wang W, Zhang F, Xia Y, Zhao S, Yan W, Wang H, et al. Defective branched chain amino acid catabolism contributes to cardiac dysfunction and remodeling following myocardial infarction. *Am J Physiol Heart Circ Physiol.* (2016) 311:H1160–9. doi: 10.1152/ajpheart.00114.2016
66. Uddin GM, Zhang L, Shah S, Fukushima A, Wagg CS, Gopal K, et al. Impaired branched chain amino acid oxidation contributes to cardiac insulin resistance in heart failure. *Cardiovasc Diabetol.* (2019) 18:86.
67. Fouré A, Bendahan D. Is Branched-chain amino acids supplementation an efficient nutritional strategy to alleviate skeletal muscle damage? a systematic review. *Nutrients.* (2017) 9:1047. doi: 10.3390/nu9101047
68. Zigler JS Jr, Hodgkinson CA, Wright M, Klise A, Sundin O, Broman KW, et al. A spontaneous missense mutation in branched chain keto acid dehydrogenase kinase in the rat affects both the central and peripheral nervous systems. *PLoS One.* (2016) 11:e0160447. doi: 10.1371/journal.pone.0160447
69. Joshi MA, Jeoung NH, Obayashi M, Hattab EM, Brocken EG, Liechty EA, et al. Impaired growth and neurological abnormalities in branched-chain alpha-keto acid dehydrogenase kinase-deficient mice. *Biochem J.* (2006) 400:153–62. doi: 10.1042/bj20060869
70. Novarino G, El-Fishawy P, Kayserili H, Meguid NA, Scott EM, Schroth J, et al. Mutations in BCKD-kinase lead to a potentially treatable form of autism with epilepsy. *Science.* (2012) 338:394–7. doi: 10.1126/science.1224631
71. García-Cazorla A, Oyarzabal A, Fort J, Robles C, Castejón E, Ruiz-Sala P, et al. Two novel mutations in the BCKDK (branched-chain keto-acid dehydrogenase kinase) gene are responsible for a neurobehavioral deficit in two pediatric unrelated patients. *Hum Mutat.* (2014) 35:470–7. doi: 10.1002/humu.22513
72. Krzysztoń-Russjan J, Zielonka D, Jackiewicz J, Kuśmirek S, Bubko I, Klimberg A, et al. A study of molecular changes relating to energy metabolism and cellular stress in people with Huntington's disease: looking for biomarkers. *J Bioenerg Biomembr.* (2013) 45:71–85. doi: 10.1007/s10863-012-9479-3
73. Jouvet P, Rustin P, Taylor DL, Pocock JM, Felderhoff-Mueser U, Mazarakis ND, et al. Branched chain amino acids induce apoptosis in neural cells without mitochondrial membrane depolarization or cytochrome c release: implications for neurological impairment associated with maple syrup urine disease. *Mol Biol Cell.* (2000) 11:1919–32. doi: 10.1091/mbc.11.5.1919
74. Burrage LC, Nagamani SC, Campeau PM, Lee BH. Branched-chain amino acid metabolism: from rare Mendelian diseases to more common disorders. *Hum Mol Genet.* (2014) 23:R1–8. doi: 10.1093/hmg/ddu123
75. Oyarzabal A, Bravo-Alonso I, Sánchez-Aragó M, Rejas MT, Merinero B, García-Cazorla A, et al. Mitochondrial response to the BCKDK-deficiency: some clues to understand the positive dietary response in this form of autism. *Biochim Biophys Acta.* (2016) 1862:592–600. doi: 10.1016/j.bbadis.2016.01.016
76. Tso SC, Gui WJ, Wu CY, Chuang JL, Qi X, Skvora KJ, et al. Benzothiophene carboxylate derivatives as novel allosteric inhibitors of branched-chain α-ketoacid dehydrogenase kinase. *J Biol Chem.* (2014) 289:20583–93. doi: 10.1074/jbc.M114.569251
77. Tso SC, Qi X, Gui WJ, Chuang JL, Morlock LK, Wallace AL, et al. Structure-based design and mechanisms of allosteric inhibitors for mitochondrial branched-chain α-ketoacid dehydrogenase kinase. *Proc Natl Acad Sci U.S.A.* (2013) 110:9728–33. doi: 10.1073/pnas.1303220110
78. Yang Y, Zhao M, He X, Wu Q, Li DL, Zang WJ. Pyridostigmine protects against diabetic cardiomyopathy by regulating vagal activity. Gut microbiota, and branched-chain amino acid catabolism in diabetic mice. *Front Pharmacol.* (2021) 12:647481. doi: 10.3389/fphar.2021.647481
79. Blanchard PG, Moreira RJ, Castro É, Caron A, Côté M, Andrade ML, et al. PPARγ is a major regulator of branched-chain amino acid blood levels and catabolism in white and brown adipose tissues. *Metabolism.* (2018) 89:27–38. doi: 10.1016/j.metabol.2018.09.007
80. Irving BA, Carter RE, Soop M, Weymiller A, Syed H, Karakelides H, et al. Effect of insulin sensitizer therapy on amino acids and their metabolites. *Metabolism.* (2015) 64:720–8. doi: 10.1016/j.metabol.2015.01.008
81. Iwasa M, Ishihara T, Mifuji-Moroka R, Fujita N, Kobayashi Y, Hasegawa H, et al. Elevation of branched-chain amino acid levels in diabetes and NAFL and changes with antidiabetic drug treatment. *Obes Res Clin Pract.* (2015) 9:293–7. doi: 10.1016/j.orcp.2015.01.003

Conflict of Interest: The authors declare that the research was conducted in the absence of any commercial or financial relationships that could be construed as a potential conflict of interest.

Publisher's Note: All claims expressed in this article are solely those of the authors and do not necessarily represent those of their affiliated organizations, or those of the publisher, the editors and the reviewers. Any product that may be evaluated in this article, or claim that may be made by its manufacturer, is not guaranteed or endorsed by the publisher.

frontiers | Frontiers in Nutrition

TYPE Mini Review
PUBLISHED 29 July 2022
DOI 10.3389/fnut.2022.922051

OPEN ACCESS

EDITED BY
Ju-Sheng Zheng,
Westlake University, China

REVIEWED BY
Jie Yin,
Hunan Agricultural University, China
Xin Zhang,
China Agricultural University, China

*CORRESPONDENCE
Tongxing Song
songtongxing@mail.hzau.edu.cn

†These authors have contributed equally to this work and share first authorship

SPECIALTY SECTION
This article was submitted to Nutrition and Metabolism, a section of the journal Frontiers in Nutrition

RECEIVED 17 April 2022
ACCEPTED 06 June 2022
PUBLISHED 29 July 2022

CITATION
Xie J, Shi S, Liu Y, Wang S, Rajput SA and Song T (2022) Fructose metabolism and its role in pig production: A mini-review. *Front. Nutr.* 9:922051. doi: 10.3389/fnut.2022.922051

Fructose metabolism and its role in pig production: A mini-review

Jiahao Xie[1†], Shiyi Shi[1†], Yucheng Liu[1], Shaoshuai Wang[1], Shahid Ali Rajput[2] and Tongxing Song[1*]

[1]Department of Animal Nutrition and Feed Science, College of Animal Science and Technology, Huazhong Agricultural University, Wuhan, China, [2]Faculty of Veterinary and Animal Sciences, Muhammad Nawaz Shareef University of Agriculture Multan, Multan, Pakistan

Epidemiological studies have shown that excessive intake of fructose is largely responsible for the increasing incidence of non-alcoholic fatty liver, obesity, and diabetes. However, depending on the amount of fructose consumption from diet, the metabolic role of fructose is controversial. Recently, there have been increasing studies reporting that diets low in fructose expand the surface area of the gut and increase nutrient absorption in mouse model, which is widely used in fructose-related studies. However, excessive fructose consumption spills over from the small intestine into the liver for steatosis and increases the risk of colon cancer. Therefore, suitable animal models may be needed to study fructose-induced metabolic changes. Along with its use in global meat production, pig is well-known as a biomedical model with an advantage over murine and other animal models as it has similar nutrition and metabolism to human in anatomical and physiological aspects. Here, we review the characteristics and metabolism of fructose and summarize observations of fructose in pig reproduction, growth, and development as well as acting as a human biomedical model. This review highlights fructose metabolism from the intestine to the blood cycle and presents the critical role of fructose in pig, which could provide new strategies for curbing human metabolic diseases and promoting pig production.

KEYWORDS

fructose, pig production, biomedical model, intestine, liver

Introduction

Overwhelming evidence has established a strong causal link between excessive fructose intake and metabolic diseases (1). For instance, non-alcoholic-fatty liver disease (NAFLD) is currently the most prevalent liver disease worldwide (2), and excessive consumption of fructose intake is considered to boost diseases (3–5). However, the role of fructose is multifactorial. Diets low in fructose increase the length of the intestines and the height of intestinal villi (6), contributing to weight gain and promoting growth, which suggests the potential and beneficial role of fructose with appropriate concentration. But excessive fructose consumption spills over from the small intestine into the liver, causing steatosis and increasing the risk of colon cancer (7–12). Therefore, it is necessary to clarify the critical role of fructose metabolism and its relationship with metabolic diseases.

Animal models are widely employed for studying fructose-induced metabolic changes. Mice fed a high fructose diet (HFD), such as high fructose corn syrup (HFCS), and conditional genetic mouse models help to address fructose-induced metabolic disorders (13, 14). Notably, pig is well-known as a biomedical model because pig is more similar to human. As omnivores, humans and pigs have a large number of similarities in anatomy, physiology, metabolism, and pathology, e.g., they have similar gastrointestinal anatomy and function, pancreas morphology, and metabolic regulation (15). In addition, pork accounts for more than one-third of meat produced worldwide (16), but there are still some problems such as low growth efficiency in the pig industry.

Currently, some important reviews have summarized the progress in the research on fructose metabolism (11, 17–24). However, fructose consumption and its metabolic role in pig are still poorly understood. Hence, this review will focus on the characteristics and metabolism of fructose and its applications in pig reproduction, growth, and development. The review will also highlight the pig biomedical models in fructose metabolism.

Characteristics and beneficial function of fructose in physiology

Characteristics of fructose: A low glycemic sugar

Fructose has been traditionally viewed as a simple 6-carbon monosaccharide found widely in fruit, honey, and some vegetables (17). Over the past few decades, the consumption of soft drinks, especially carbonated drinks, has increased significantly, which are sweetened with sweeteners containing a high percentage of fructose (25, 26).

Fructose is added to beverages and foods in the form of sucrose (50% fructose) or the industrial product high fructose corn syrup (usually 55% fructose) (17). Both fructose and glucose are well absorbed from the intestine into the blood cycle. Admittedly, glucose, not fructose, is the predominant circulating sugar in animals (17), which reflects the innate differences in mammalian glucose and fructose metabolism in circulating blood levels. The normal fasting blood glucose concentration in peripheral blood is 5 mM, while under fasting conditions, the circulating concentration of fructose is about 0.02 mM (27, 28). Early studies reported the average plasma fructose concentration of fructose-fed mice was 1.5 mM, while that of starch-fed mice was 0.23 mM (29). Furthermore, glucose is the main fuel for most tissues and cell types. In contrast, the fructose ingested from sucrose is quickly removed by intestines and liver, converted into glucose and its polymer storage form, glycogen, or fatty acids, and stored in the form of triglycerides in the liver (17). It is of note that fructose has a low glycemic index. Several pieces of evidence have established that the hyperglycemic effect of fructose is much weaker than glucose (30). Thus, the difference between fructose and glucose may suggest the unique role, metabolism, and biological function of fructose.

Fructose functions as a growth-promotor in mouse model

Due to the decreased concentration gradient of fructose in intestine, namely "first-pass" effect, the fructose is potentially related to regulating intestinal growth and development (31). Strikingly, gavaging of 15% fructose for $<$ 3 months will increase the energy intake, weight gain, and growth of mice (32, 33). Similar results are found by feeding mice with 30% fructose solution for 8 weeks (34). However, when mice were fed with 60% fructose for 6 weeks, the incidence of insulin resistance increased (35). Another study reports that 60% of fructose gavage increases cholesterol, triglycerides, blood glucose levels, and liver lipid peroxidation (36). Interestingly, an administration of low concentration of fructose (∼15%) gavaging for 30 weeks results in obesity and liver cirrhosis (37). These observations provide evidence that appropriate dose and time of fructose treatment may enhance the length of the small intestine and its absorption of nutrition, indicating the complexity of metabolic flux.

Cellular metabolism of fructose with normal and excessive consumption in intestine and liver

Digestion and absorption of fructose from lumen to intestine

Following oral ingestion, fructose travels through the gastrointestinal tract into the small intestine, where it is passively absorbed from the intestinal lumen mainly by the hexose transporter SLC2A5, also known as GLUT5, and expressed at the brush border of the intestinal epithelium, as shown in Figure 1. GLUT5 is a facilitative transporter, which means that the transport of fructose into intestinal cells is proportional to the concentration gradient across the luminal membrane of intestinal cells (38). Although the expression of GLUT5 is responsible for intestinal fructose absorption, it is also expressed in other tissues and cell types, including skeletal muscle, pre-adipocytes, prostate, spermatozoa, and erythrocytes (39–42). However, the importance of fructose transport to these tissues is poorly understood. Exceeding the clearance capacity of the small intestine, excessive fructose escapes the small intestine and reaches the large intestine and liver (1).

10.3389/fnut.2022.922051

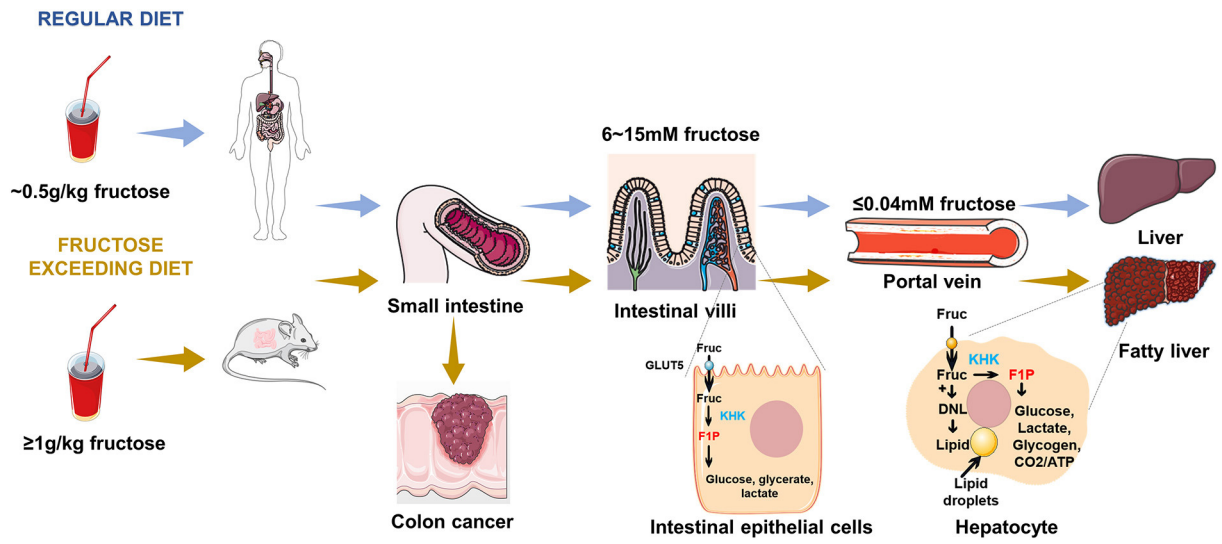

FIGURE 1
Fructose metabolism in the gut and liver. Following ingestion of fructose, fructose is absorbed into intestinal epithelial enterocytes. Under fasting conditions, the fructose concentration in the small intestine is in the range of 6 ~ 15 mM, while fructose concentration in the portal vein is < 0.04 mM. A portion of this fructose is phosphorylated by KHK within enterocyte and is converted to glucose, lactate, glycerate, and other organic acids, which transport from the portal vein to the liver. Fructose reaching the liver is efficiently extracted by hepatocytes and phosphorylated by KHK, where it can be used for glucose production, lipogenesis, glycogen synthesis, and energetic purposes. An excessive fructose diet can lead to colon cancer, fatty liver, and other related metabolic diseases.

Fructose metabolism in intestinal epithelial cell

The small intestine is the major and first site for fructose metabolism, as shown in Figure 1 (1). Fructose concentration in peripheral plasma is typically about 0.04 mM, which is consistent with the data reported by the previous studies (27, 28, 43–45). By contrast, the concentration of fructose in the intestine (6 to 15 mM) is higher than peripheral plasma (39, 46). This observation provides evidence that dietary fructose metabolism started in small intestinal epithelial cells, and was formed by ketohexokinase (KHK) phosphorylation to form a fructose-1-phosphate (F1P), which accumulated in cells with high levels (1, 47). Much of the fructose is metabolized to lactate, alanine, glycerate, and other organic acids within the intestine. The small intestine fully express glucoisomerase to efficiently convert fructose into circulating glucose (1, 48, 49), which is the mechanism of maintaining liver health. Low doses of fructose(~0.5 g/kg) are 90% cleared by the intestine (1), but high doses of fructose (≥1 g/kg), exceeding intestinal fructose absorption and clearance, results in fructose reaching both the liver and colon, where it may cause disease by impacting hepatic function or microbial composition (1).

Fructose metabolism in hepatocyte

It has been assumed that the liver is another vital site of dietary fructose metabolism (47, 50–52). In a more recent study, it was reported that the liver is able to extract 70% of the oral fructose load, whereas the liver extracts only 10% to 35% of the oral glucose load (53, 54). A small fraction of the carbon in ingested fructose is converted into glucose by the liver and enters the systemic circulation. These observations demonstrate that the rapid clearance of fructose in the blood is largely mediated by the effective extraction of the liver (21). When fructose reaches the liver from the portal vein, fructokinase phosphorylates fructose to fructose-1-phosphate, which can be converted to glycerol-3-phosphate for synthesis of glycerol or metabolized to acetyl-CoA and incorporated into fatty acids through *de novo* lipogenesis preferentially (55). In fact, fructose is converted to fatty acids at a higher rate in the liver than glucose (56). The entry of fructose into the lipogenic process may contribute to fructose-induced hyperlipidemia, particularly the marked increase in postprandial triglyceride levels (57, 58). Pathologically, recent studies have confirmed that NAFLD is commonly associated with excessive fructose intake (4, 59). Based on the cellular metabolism and function of fructose in the intestine and liver, investigations are required for in-depth study.

Fructose consumption and metabolic roles in pigs

At present, most of the studies on fructose are from mouse model, which is widely used but not well-accorded with human diseases, so we have chosen to focus on another greater model than murine: pigs. Pig is a more suitable biomedical model for humans than mouse (60). The anatomical and physiological similarities between pigs and humans suggests pig model to be an important tool for medical research, providing important models for human therapies (61). In addition, pig production plays an important role in farming systems worldwide (62) and the large-scale pig industry is developing rapidly all over the world to satisfy the growing requirement of consumers (63). However, there are still some problems that are difficult to solve at present, for example, postnatal growth retardation (PGR) is common in piglets, which are prone to developing chronic disease (64). Therefore, we further summarized the roles of fructose in pig production and pig biomedical models for human metabolic diseases.

Fructose in reproductive performance of pigs

Reproductive performance has a great influence on sow productivity and production profit (65). As mentioned in Table 1, McCracken (70) gave pre-pubertal gilts dietary treatments containing 35% fructose for 9 weeks, and found that the size of the reproductive tract had increased but the pregnancy rate decreased. It was also observed that fructose can increase litter size of primiparous sows but had no effect on individual weight and milk yield (67). However, there are different views that the milk yield of sows fed with a fructose diet increased significantly on day 14 and day 21 during a 22-d lactation, implying that fructose might be used to increase total yield of milk during lactation (66), but the dose and concentration need to be further studied. In fact, there is increasing clinical evidence that fructose contributes to elongated estrous cycles and hyperandrogenemia, accompanied by decreased LH concentrations and an increase in the number of follicles and in the level of luteal phase progesterone (68). Mechanically, Ossabaw pigs fed with fructose have increased transcript levels and dysfunctional steroidogenic enzymes in the ovarian delta 4 steroidogenic pathway, leading to hyperandrogenemia (69). However, the detailed mechanism of how fructose affects the reproduction functions of pigs needs further investigation.

Fructose metabolism in growth and development of pigs

Despite the controversial role of fructose in reproduction, fructose is the most abundant hexose sugar in pig embryos, indicating a specific function of fructose in embryo development. It has also been shown to be the principal blood sugar in the ungulate fetus (81–83). In fetal pig blood, the concentration of fructose is higher than glucose (84). Gluconeogenesis rarely occurs in the placenta and embryo of pigs (85). It means that glucose and fructose in maternal blood must be transported to the uterine cavity to ensure the use of glucose and fructose in the placenta and fetus. In pigs, glucose and fructose are transported from the maternal vascular system to the placental vascular system through multiple cell layers in a SLC2A-dependent manner (74, 75). Notably, intraperitoneal injection of sugars containing uniformly labeled carbon (UL14C) into pigs shows that glucose may act as a precursor of fructose and convert to fructose in porcine endometrium and placenta (71, 74). Due to the high concentration of fructose, a partial amount of fructose is involved in the synthesis of nucleic acids, thereby providing substrate for anabolic functions necessary for fetal growth and development (72). In a more recent study, it is reported that fructose can be used as an alternative energy source by embryos that express enzymes to promote fructose to enter the glycolysis pathway for metabolism (74). Moreover, it was observed that fructose is mediated *via* hexosamine biosynthesis pathway to stimulate mTOR cell signaling, which can promote embryonic/fetal growth and development (73). Thus, it is of importance to better understand the critical role of fructose in the placenta and embryo.

Pig acts as a human biomedical model for fructose-induced metabolic disorders

Animal biomedical models play a central role in human medical research and developing new therapeutical strategies (61). Pig biomedical models for human reproduction have greatly advanced our understanding of the basic science of fertilization and pregnancy, as well as metabolic diseases including NAFLD (61). Although there are several factors that may lead to NAFLD, excessive consumption of fructose is considered to be a key factor in the formation of the disease (3–5). A recent study reported that juvenile Ossabaw swine fed a high-fat, high-fructose, high-cholesterol diet, containing 17.8% HFCS, can develop obesity and have serious effects on liver, blood lipids, microflora, and a NAFLD phenotype (76). Furthermore, a high-fructose and high-fat diet (HFF) interfered with the skeletal muscle metabolism of Iberian piglets after feeding for 10 weeks (78). Mechanically, there

TABLE 1 Role of fructose in pigs.

	Subject	Fructose dose or markers	Duration	Outcome	Ref
Reproduction	25 Hampshire x Yorkshire x Large White sows	24%	3 weeks	The milk yield of sows fed with a fructose diet increased significantly on the day 14 and day 21.	(66)
	45 crossbred sows and 36 gilts	20%	4 weeks	Fructose can increase litter size of primiparous sows but have no effect on individual weight and milk yield.	(67)
	9 multiparous Ossabaw female pigs	8.9%	8 months	Fructose contributes to elongating estrous cycles and hyperandrogenemia, accompanied by decreasing LH concentrations and increasing the number of follicles and the level of luteal phase progesterone.	(68)
	19 nulliparous Ossabaw miniature pigs	8.9%	8 months	Obese Ossabaw pigs have increased transcript levels and function of ovarian enzymes in the delta 4 steroidogenic pathway.	(69)
	Female crossbred pigs	35%	9 weeks	Fructose consumption increases reproductive tract size but reduces reproductive capabilities.	(70)
Development	16 crossbred fetal pigs	^{14}C-fructose	–	Glucose acts as a precursor of fructose and converts to fructose in porcine endometrium and placenta.	(71)
	8 fetal pigs from two primiparous crossbred Yorkshire x Hampshire gilts	^{14}C-fructose	–	Fructose is involved in the synthesis of nucleic acid and provides a substrate for the synthetic metabolic function needed for fetal growth and development.	(72)
	An established mononuclear porcine trophectoderm cell line from day 12 pig conceptuses	–	–	Fructose is mediated by the hexosamine biosynthesis pathway to stimulate mTOR cell signaling, proliferation of porcine trophectoderm cells, and synthesis of hyaluronic acid, a significant glycosaminoglycan in the pregnant uterus.	(73)
	8-month-old crossbred gilts	–	–	Conversion of glucose to fructose is present at the uterine-placental interface of pigs.	(74)
	8-month-old crossbred gilts	^{14}C-fructose	–	Glucose and fructose transporters are precisely regulated in a spatial-temporal pattern along the uterine-placental interface of pigs to maximize hexose sugar transport to the pig conceptus/placenta.	(75)
Biomedical model	Juvenile female Ossabaw swine	4.45%	16 weeks	Pigs become obese, with adverse effects on liver, blood lipids, microflora, and a NAFLD phenotype.	(76)
	Female Göttingen Minipigs	20%	20 weeks	Fructose produces potential lipogenesis through precursors that can be used for DNL, leading to fat accumulation and liver steatosis.	(77)
	13-day old Iberian pigs	10 g fructose and 20.6 g fat	9 weeks	Fructose interferes with skeletal muscle metabolism and reduces fat metabolism in piglets.	(78)
	Male Danish Landrace × Yorkshire × Duroc pigs	60%	4 weeks	No macrovesicular steatosis or hepatocyte ballooning.	(79)
	Iberian pigs	64%	16 weeks	Increase of butyric acid synthesis, triglyceridemia, and subcutaneous fat deposition in young Iberian pigs. No differences in histological markers of NAFLD.	(80)

10.3389/fnut.2022.922051

is increasing clinical evidence to show that fructose produces potential lipogenesis through precursors that can be used for *de novo* lipogenesis (DNL), leading to fat accumulation and liver steatosis (77, 86).

However, it has been reported recently that a high-fructose diet does not induce NAFLD. Some studies demonstrate that, compared with a sucrose-enriched diet, histological markers of NAFLD in Iberian pigs showed no significant increase in the fructose group (80). Feeding castrated male Danish Landrace-Yorkshire-Duroc pigs with 60% fructose for 4 weeks showed no steatosis or hepatocyte ballooning in the liver, providing evidence that short-term feeding with a high-fructose diet may not induce NAFLD in pigs (79). Collectively, breed and age of pigs might be factors that protect pigs from the development of steatosis.

Conclusion and perspective

Over the last decade, studies have illustrated the role of fructose and its metabolic mechanism. However, the functional effect of fructose *in vivo* remains controversial, and there is no conclusion on the specific healthy use of fructose. Moreover, its different roles in pigs are challenging and worthy of exploration. In piglets, PGR is also prevalent in pig production (64). From the perspective of the effect of fructose, it indicates that fructose might have a potential growth-promoting effect. Besides, taking the safe thresholds for sugar consumption into account will be a matter of concern in nutrition and the detailed mechanism of how fructose affects the reproduction functions of pigs warrants further investigation. Hopefully, better understanding of the complex role of fructose may open new avenues for curbing human metabolic diseases and improve pig production.

Author contributions

TS designed this review, helped with writing and revising of the manuscript, and provided critical feedback. JX and SS conceptualized the topic, researched and analyzed the literature, and composed and revised the manuscript. YL, SW, and SR helped draft the manuscript. All authors approve the final version of the manuscript, ensure the accuracy and integrity of the work, and agree to be accountable for all aspects of the work.

Funding

This work was supported by grants from the National Natural Science Foundation of China (32102561), the Chinese Fundamental Research Funds for the Central Universities (2662019QD022), the Student Research Funds of Huazhong Agricultural University (S202110504033), National Innovation and Entrepreneurship Training Program for Undergraduate (202210504008), and the State Key Laboratory for Managing Biotic and Chemical Threats to the Quality and Safety of Agro-products (2021DG700024-KF202214).

Acknowledgments

We would like to thank all the members of Adipo-mystery group.

Conflict of interest

The authors declare that the research was conducted in the absence of any commercial or financial relationships that could be construed as a potential conflict of interest.

Publisher's note

References

1. Jang C, Hui S, Lu W, Cowan AJ, Morscher RJ, Lee G, et al. The small intestine converts dietary fructose into glucose and organic acids. *Cell Metab.* (2018) 27:351–61. e3. doi: 10.1016/j.cmet.2017.12.016

2. Adams LA, Lindor KD. Nonalcoholic fatty liver disease. *Ann Epidemiol.* (2007) 17:863–9. doi: 10.1016/j.annepidem.2007.05.013

3. Ishimoto T, Lanaspa MA, Rivard CJ, Roncal-Jimenez CA, Orlicky DJ, Cicerchi C, et al. High-Fat and high-sucrose (Western) diet induces steatohepatitis that is dependent on fructokinase. *Hepatology.* (2013) 58:1632–43. doi: 10.1002/hep.26594

4. Lim JS, Mietus-Snyder M, Valente A, Schwarz J-M, Lustig RH. The role of fructose in the pathogenesis of Nafld and the metabolic syndrome. *Nat Rev Gastroenterol Hepatol.* (2010) 7:251–64. doi: 10.1038/nrgastro.2010.41

5. Basaranoglu M, Basaranoglu G, Bugianesi E. Carbohydrate intake and nonalcoholic fatty liver disease: fructose as a weapon of mass destruction. *Hepatobiliary Surg Nutr.* (2015) 4:109.

6. Taylor SR, Ramsamooj S, Liang RJ, Katti A, Pozovskiy R, Vasan N, et al. Dietary fructose improves intestinal cell survival and nutrient absorption. *Nature.* (2021) 597:263–7. doi: 10.1038/s41586-021-03827-2

7. Joh H-K, Lee DH, Hur J, Nimptsch K, Chang Y, Joung H, et al. simple sugar and sugar-sweetened beverage intake during adolescence and risk of colorectal cancer precursors. *Gastroenterology.* (2021) 161:128–42. e20. doi: 10.1053/j.gastro.2021.03.028

8. Tasevska N, Jiao L, Cross AJ, Kipnis V, Subar AF, Hollenbeck A, et al. Sugars in diet and risk of cancer in the Nih-Aarp diet and health study. *Int J cancer.* (2012) 130:159–69. doi: 10.1002/ijc.25990

9. Bostick RM, Potter JD, Kushi LH, Sellers TA, Steinmetz KA, McKenzie DR, et al. Sugar, meat, and fat intake, and non-dietary risk factors for colon cancer incidence in iowa women (United States). *Cancer Cause Control.* (1994) 5:38–52. doi: 10.1007/BF01830725

10. Meyerhardt JA, Sato K, Niedzwiecki D, Ye C, Saltz LB, Mayer RJ, et al. Dietary glycemic load and cancer recurrence and survival in patients with stage iii colon cancer: findings from Calgb 89803. *J Natl Cancer Inst.* (2012) 104:1702–11. doi: 10.1093/jnci/djs399

11. Jang C, Wada S, Yang S, Gosis B, Zeng X, Zhang Z, et al. The small intestine shields the liver from fructose-induced steatosis. *Nature Metab.* (2020) 2:586–93. doi: 10.1038/s42255-020-0222-9

12. Goncalves MD, Lu C, Tutnauer J, Hartman TE, Hwang S-K, Murphy CJ, et al. High-Fructose corn syrup enhances intestinal tumor growth in mice. *Science.* (2019) 363:1345–9. doi: 10.1126/science.aat8515

13. Deol P, Evans JR, Dhahbi J, Chellappa K, Han DS, Spindler S, et al. Soybean oil is more obesogenic and diabetogenic than coconut oil and fructose in mouse: potential role for the liver. *PLoS ONE.* (2015) 10:e0132672. doi: 10.1371/journal.pone.0132672

14. Lozano I, Van der Werf R, Bietiger W, Seyfritz E, Peronet C, Pinget M, et al. High-Fructose and high-fat diet-induced disorders in rats: impact on diabetes risk, hepatic and vascular complications. *Nutr Metab.* (2016) 13:1–13. doi: 10.1186/s12986-016-0074-1

15. Aigner B, Renner S, Kessler B, Klymiuk N, Kurome M, Wünsch A, et al. Transgenic pigs as models for translational biomedical research. *J Mol Med.* (2010) 88:653–64. doi: 10.1007/s00109-010-0610-9

16. VanderWaal K, Deen J. Global trends in infectious diseases of swine. *Proc Nat Acad Sci.* (2018) 115:11495–500. doi: 10.1073/pnas.1806068115

17. Herman MA, Birnbaum MJ. Molecular aspects of fructose metabolism and metabolic disease. *Cell Metab.* (2021) 33:2329–54. doi: 10.1016/j.cmet.2021.09.010

18. Krause N, Wegner A. Fructose metabolism in cancer. *Cells.* (2020) 9:2635. doi: 10.3390/cells9122635

19. Nakagawa T, Lanaspa MA, San Millan I, Fini M, Rivard CJ, Sanchez-Lozada LG, et al. Fructose contributes to the warburg effect for cancer growth. *Cancer Metab.* (2020) 8:1–12. doi: 10.1186/s40170-020-00222-9

20. Febbraio MA, Karin M. "Sweet Death": fructose as a metabolic toxin that targets the gut-liver axis. *Cell Metab.* (2021) 33:2316–28. doi: 10.1016/j.cmet.2021.09.004

21. Hannou SA, Haslam DE, McKeown NM, Herman MA. Fructose metabolism and metabolic disease. *J Clin Invest.* (2018) 128:545–55. doi: 10.1172/JCI96702

22. Gonzalez JT, Betts JA. Dietary fructose metabolism by splanchnic organs: size matters. *Cell Metab.* (2018) 27:483–5. doi: 10.1016/j.cmet.2018.02.013

23. Federico A, Rosato V, Masarone M, Torre P, Dallio M, Romeo M, et al. The role of fructose in non-alcoholic steatohepatitis: old relationship and new insights. *Nutrients.* (2021) 13:1314. doi: 10.3390/nu13041314

24. Jiang H, Lin Q, Ma L, Luo S, Jiang X, Fang J, et al. Fructose and fructose kinase in cancer and other pathologies. *J Genetics Genomics.* (2021) 48:531–9. doi: 10.1016/j.jgg.2021.06.006

25. Park YK, Yetley EA. Intakes and food sources of fructose in the United States. *Am J Clin Nutr.* (1993) 58:737S—47S. doi: 10.1093/ajcn/58.5.737S

26. Wang P, Wu T, Fu Q, Liao Q, Li Y, Huang T, et al. Maternal high-fructose intake activates myogenic program in fetal brown fat and predisposes offspring to diet-induced metabolic dysfunctions in adulthood. *Front Nutr.* (2022) 9:848983. doi: 10.3389/fnut.2022.848983

27. Chen Y, Lin H, Qin L, Lu Y, Zhao L, Xia M, et al. Fasting serum fructose levels are associated with risk of incident type 2 diabetes in middle-aged and older Chinese population. *Diabetes Care.* (2020) 43:2217–25. doi: 10.2337/dc19-2494

28. Francey C, Cros J, Rosset R, Crézé C, Rey V, Stefanoni N, et al. the extra-splanchnic fructose escape after ingestion of a fructose–glucose drink: an exploratory study in healthy humans using a dual fructose isotope method. *Clinical Nutr ESPEN.* (2019) 29:125–32. doi: 10.1016/j.clnesp.2018.11.008

29. Klein AV, Kiat H. The mechanisms underlying fructose-induced hypertension: a review. *J Hypertens.* (2015) 33:912. doi: 10.1097/HJH.0000000000000551

30. Lee BM, Lee SK, Kim HS. Inhibition of oxidative DNA damage, 8-Ohdg, and carbonyl contents in smokers treated with antioxidants (Vitamin E, Vitamin C, B-Carotene and Red Ginseng). *Cancer Lett.* (1998) 132:219–27. doi: 10.1016/S0304-3835(98)00227-4

31. Schaefer EJ, Gleason JA, Dansinger ML. Dietary fructose and glucose differentially affect lipid and glucose homeostasis. *J Nutr.* (2009) 139:1257S—62S. doi: 10.3945/jn.108.098186

32. Jürgens H, Haass W, Castaneda TR, Schürmann A, Koebnick C, Dombrowski F, et al. Consuming fructose-sweetened beverages increases body adiposity in mice. *Obes Res.* (2005) 13:1146–56. doi: 10.1038/oby.2005.136

33. Nunes PM, Anastasiou D. *Fructose in the Diet Expands the Surface of the Gut and Promotes Nutrient Absorption*. Nature Publishing Group. (2021) 597:180–2. doi: 10.1038/d41586-021-02195-1

34. Volynets V, Spruss A, Kanuri G, Wagnerberger S, Bischoff SC, Bergheim I. Protective effect of bile acids on the onset of fructose-induced hepatic steatosis in mice. *J Lipid Res.* (2010) 51:3414–24. doi: 10.1194/jlr.M007179

35. Mellor K, Ritchie RH, Meredith G, Woodman OL, Morris MJ, Delbridge LM. High-fructose diet elevates myocardial superoxide generation in mice in the absence of cardiac hypertrophy. *Nutrition.* (2010) 26:842–8. doi: 10.1016/j.nut.2009.08.017

36. Rivera EC, Yamakawaa CK, Garciaa MH, Geraldoa VC, Rossella CE, Filhob RM, et al. A procedure for estimation of fermentation kinetic parameters in fed-batch bioethanol production process with cell recycle. *Chemical Eng.* (2013) 32:1369–74. doi: 10.3303/CET1332229

37. Mastrocola R, Collino M, Rogazzo M, Medana C, Nigro D, Boccuzzi G, et al. Advanced Glycation end products promote hepatosteatosis by interfering with scap-srebp pathway in fructose-drinking mice. *Am J Physiol Gastrointest Liver Physiol.* (2013) 305:G398–407. doi: 10.1152/ajpgi.00450.2012

38. Cori CF. The rate of absorption of hexoses and pentoses. *Proceedings Soc Experiment Biol Med.* (1925) 22:497–9. doi: 10.3181/00379727-22-239

39. Burant C, Takeda J, Brot-Laroche E, Bell G, Davidson N. Fructose transporter in human spermatozoa and small intestine is glut5. *J Biol Chem.* (1992) 267:14523–6. doi: 10.1016/S0021-9258(18)42067-4

40. Concha II, Velásquez FV, Martinez JM, Angulo C, Droppelmann A, Reyes AM, et al. Human erythrocytes express glut5 and transport fructose. *Blood.* (1997) 89:4190–5. doi: 10.1182/blood.V89.11.4190

41. Kayano T, Burant C, Fukumoto H, Gould G, Fan Y, Eddy R, et al. Human facilitative glucose transporters isolation, functional characterization, and gene localization of cdnas encoding an isoform (glut5) expressed in small intestine, kidney, muscle, and adipose tissue and an unusual glucose transporter pseudogene-like sequence (glut6). *J Biol Chem.* (1990) 265:13276–82. doi: 10.1016/S0021-9258(19)38295-X

42. Reinicke K, Sotomayor P, Cisterna P, Delgado C, Nualart F, Godoy A. Cellular distribution of glut-1 and glut-5 in benign and malignant human prostate tissue. *J Cell Biochem.* (2012) 113:553–62. doi: 10.1002/jcb.23379

43. Sugimoto K, Kawasaki T, Tomoda M, Nakagawa K, Hayashi S, Inui H, et al. Lowering of postprandial hyperfructosemia in humans by eucalyptus leaf extract: a randomized, double-blind, placebo-controlled crossover study. *Food Sci Technol Res.* (2010) 16:509–12. doi: 10.3136/fstr.16.509

44. Wahjudi PN, Patterson ME, Lim S, Yee JK, Mao CS, Lee W-NP. Measurement of glucose and fructose in clinical samples using gas chromatography/mass spectrometry. *Clin Biochem.* (2010) 43:198–207. doi: 10.1016/j.clinbiochem.2009.08.028

45. Preston GM, Calle RA. Elevated serum sorbitol and not fructose in type 2 diabetic patients. *Bio Insights.* (2010) 5:S4530. doi: 10.4137/BMI.S4530

46. Douard V, Ferraris RP. Regulation of the fructose transporter glut5 in health and disease. *Am J Physiol Endocrinol Metab.* (2008) 295:E227–37. doi: 10.1152/ajpendo.90245.2008

47. Miller M, Craig JW, Drucker WR, Woodward Jr H. The metabolism of fructose in man. *Yale J Biol Med.* (1956) 29:335.

48. BISMUT H, HERS HG, Van Schaftingen E. Conversion of fructose to glucose in the rabbit small intestine: a reappraisal of the direct pathway. *Eur J Biochem.* (1993) 213:721–6. doi: 10.1111/j.1432-1033.1993.tb17812.x

49. Ginsburg V, Hers H. On the Conversion of Fructose to Glucose by Guinea Pig Intestine. *Biochim Biophys Acta.* (1960) 38:427–34. doi: 10.1016/0006-3002(60)91278-6

50. Herman RH, Stifel FB, Greene HL, Herman YF. Intestinal metabolism of fructose. *Acta Med Scand.* (1972) 192:19–25. doi: 10.1111/j.0954-6820.1972.tb05315.x

51. Froesch E. Fructose metabolism in adipose tissue. *Acta Med Scand.* (1972) 192:37–46. doi: 10.1111/j.0954-6820.1972.tb05317.x

52. Mirtschink P, Krishnan J, Grimm F, Sarre A, Hörl M, Kayikci M, et al. Hif-Driven Sf3b1 induces Khk-C to enforce fructolysis and heart disease. *Nature.* (2015) 522:444–9. doi: 10.1038/nature14508

53. Lam P. Effects of consuming dietary fructose versus glucose on de novo lipogenesis in overweight and obese human subjects. *Berkeley Sci J.* (2011) 15:1–3. doi: 10.5070/BS3152011589

54. Tappy L, Lê K-A. Does fructose consumption contribute to non-alcoholic fatty liver disease? *Clin Res Hepatol Gastroenterol.* (2012) 36:554–60. doi: 10.1016/j.clinre.2012.06.005

55. Frayn KN, Kingman SM. Dietary sugars and lipid metabolism in humans. *Am J Clin Nutr.* (1995) 62:250S−61S. doi: 10.1093/ajcn/62.1.250S

56. Aoyama Y, Yoshida A, Ashida K. Effect of dietary fats and fatty acids on the liver lipid accumulation induced by feeding a protein-repletion diet containing fructose to protein-depleted rats. *J Nutr.* (1974) 104:741–6. doi: 10.1093/jn/104.6.741

57. Imamura F, O'Connor L, Ye Z, Mursu J, Hayashino Y, Bhupathiraju SN, et al. Consumption of sugar sweetened beverages, artificially sweetened beverages, and fruit juice and incidence of type 2 diabetes: systematic review, meta-analysis, and estimation of population attributable fraction. *BMJ.* (2015) 351:h3576. doi: 10.1136/bmj.h3576

58. de Koning L, Malik VS, Kellogg MD, Rimm EB, Willett WC, Hu FB. Sweetened beverage consumption, incident coronary heart disease, and biomarkers of risk in men. *Circulation.* (2012) 125:1735–41. doi: 10.1161/CIRCULATIONAHA.111.067017

59. Jensen VS, Hvid H, Damgaard J, Nygaard H, Ingvorsen C, Wulff EM, et al. Dietary fat stimulates development of nafld more potently than dietary fructose in sprague–dawley rats. *Diabetol Metab Syndr.* (2018) 10:1–13. doi: 10.1186/s13098-018-0307-8

60. Bassols A, Costa C, Eckersall PD, Osada J, Sabria J, Tibau J. The pig as an animal model for human pathologies: a proteomics perspective. *PROTEOMICS–Clin Appli.* (2014) 8:715–31. doi: 10.1002/prca.201300099

61. Lunney JK, Van Goor A, Walker KE, Hailstock T, Franklin J, Dai C. Importance of the pig as a human biomedical model. *Science Trans Med.* (2021) 13:eabd5758. doi: 10.1126/scitranslmed.abd5758

62. Zhang Y-g, Yin Y-l, Fang J, Wang Q. Pig production in subtropical agriculture. *J Sci Food Agric.* (2012) 92:1016–24. doi: 10.1002/jsfa.4679

63. Thomas R, Singh V, Gupta VK. Current status and development prospects of India's pig industry. *Indian J Animal Sci.* (2021) 91:255–68.

64. Qi M, Tan B, Wang J, Li J, Liao S, Yan J, et al. Small intestinal transcriptome analysis revealed changes of genes involved in nutrition metabolism and immune responses in growth retardation piglets. *J Anim Sci.* (2019) 97:3795–808. doi: 10.1093/jas/skz205

65. Engblom L, Stalder KJ, Mabry JW. *Culling, Mortality and Lifetime Production among Us Sows.* Iowa State University Animal Industry Report (2010).

66. White C, Head H, Bachman K, Bazer F. Yield and composition of milk and weight gain of nursing pigs from sows fed diets containing fructose or dextrose. *J Anim Sci.* (1984) 59:141–50. doi: 10.2527/jas1984.591141x

67. Campbell W, Brendemuhl J, Bazer F. Effect of fructose consumption during lactation on sow and litter performance and sow plasma constituents. *J Anim Sci.* (1990) 68:1378–88. doi: 10.2527/1990.6851378x

68. Newell-Fugate AE, Taibl JN, Clark SG, Alloosh M, Sturek M, Krisher RL. Effects of diet-induced obesity on metabolic parameters and reproductive function in female ossabaw minipigs. *Comp Med.* (2014) 64:44–9.

69. Newell-Fugate AE, Taibl JN, Alloosh M, Sturek M, Bahr JM, Nowak RA, et al. Effects of obesity and metabolic syndrome on steroidogenesis and folliculogenesis in the female ossabaw mini-pig. *PLoS ONE.* (2015) 10:e0128749. doi: 10.1371/journal.pone.0128749

70. McCracken VL. *The Effects of Dietary Fructose and Fat on the Reproductive Parameters of Prepubertal and Pregnant Gilts.* Virginia Tech (2015) 1–106.

71. White C, Piper E, Noland P. Conversion of glucose to fructose in the fetal pig. *J Anim Sci.* (1979) 48:585–90. doi: 10.2527/jas1979.483585x

72. White C, Piper E, Noland P, Daniels L. Fructose utilization for nucleic acid synthesis in the fetal pig. *J Anim Sci.* (1982) 55:73–6. doi: 10.2527/jas1982.55173x

73. Kim J, Song G, Wu G, Bazer FW. Functional roles of fructose. *Proc Nat Acad Sci.* (2012) 109:E1619–E28. doi: 10.1073/pnas.1204298109

74. Steinhauser CB, Landers M, Myatt L, Burghardt RC, Vallet JL, Bazer FW, et al. Fructose synthesis and transport at the uterine-placental interface of pigs: cell-specific localization of Slc2a5, Slc2a8, and components of the polyol pathway. *Biolo Reproduct.* (2016) 95:108. doi: 10.1095/biolreprod.116.142174

75. Kramer AC, Steinhauser CB, Gao H, Seo H, McLendon BA, Burghardt RC, et al. Steroids regulate Slc2a1 and Slc2a3 to deliver glucose into trophectoderm for metabolism via glycolysis. *Endocrinology.* (2020) 161:bqaa098. doi: 10.1210/endocr/bqaa098

76. Panasevich MR, Meers GM, Linden MA, Booth FW, Perfield JW, Fritsche KL, et al. High-Fat, high-fructose, high-cholesterol feeding causes severe nash and cecal microbiota dysbiosis in juvenile ossabaw swine. Am J Physiol Endocrinol Metab. (2018) 314:E78–92. doi: 10.1152/ajpendo.00015.2017

77. Curtasu MV, Tafintseva V, Bendiks ZA, Marco ML, Kohler A, Xu Y, et al. Obesity-Related metabolome and gut microbiota profiles of juvenile göttingen minipigs—long-term intake of fructose and resistant starch. *Metabolites.* (2020) 10:456. doi: 10.3390/metabo10110456

78. Spooner HC, Derrick SA, Maj M, Manjarín R, Hernandez GV, Tailor DS, et al. High-Fructose, high-fat diet alters muscle composition and fuel utilization in a juvenile iberian pig model of non-alcoholic fatty liver disease. *Nutrients.* (2021) 13:4195. doi: 10.3390/nu13124195

79. Schmidt NH, Svendsen P, Albarrán-Juárez J, Moestrup SK, Bentzon JF. High-Fructose feeding does not induce steatosis or non-alcoholic fatty liver disease in pigs. *Sci Rep.* (2021) 11:1–10. doi: 10.1038/s41598-021-82208-1

80. Maj M, Harbottle B, Thomas PA, Hernandez GV, Smith VA, Edwards MS, et al. Consumption of high-fructose corn syrup compared with sucrose promotes adiposity and increased triglyceridemia but comparable nafld severity in juvenile iberian pigs. *J Nutr.* (2021) 151:1139–49. doi: 10.1093/jn/nxaa441

81. Bacon J, Bell D. Fructose and Glucose in the Blood of the Foetal Sheep. *Biochem J.* (1948) 42:397. doi: 10.1042/bj0420397

82. Bacon J, Bell D. The identification of fructose as a constituent of the foetal blood of the sheep. *Biochem J.* (1946) 40:xlii.

83. Barklay H, Haas P, Huggett ASG, King G, Rowley D. The Sugar of the foetal blood, the amniotic and allantoic fluids. *J Physiol.* (1949) 109:98. doi: 10.1113/jphysiol.1949.sp004373

84. Huggett ASG. Carbohydrate metabolism in the placenta and foetus. *Br Med Bull.* (1961) 17:122–6. doi: 10.1093/oxfordjournals.bmb.a069885

85. Fowden AL, Forhead AJ, Silver M, MacDonald A. Glucose, lactate and oxygen metabolism in the fetal pig during late gestation. *Exp Physiol.* (1997) 82:171–82. doi: 10.1113/expphysiol.1997.sp004006

86. Jegatheesan P, De Bandt JP. Fructose and Nafld: the multifaceted aspects of fructose metabolism. *Nutrients.* (2017) 9:230. doi: 10.3390/nu9030230

Advantages of publishing in Frontiers

OPEN ACCESS
Articles are free to read for greatest visibility and readership

FAST PUBLICATION
Around 90 days from submission to decision

HIGH QUALITY PEER-REVIEW
Rigorous, collaborative, and constructive peer-review

TRANSPARENT PEER-REVIEW
Editors and reviewers acknowledged by name on published articles

Frontiers
Avenue du Tribunal-Fédéral 34
1005 Lausanne | Switzerland

Visit us: www.frontiersin.org
Contact us: frontiersin.org/about/contact

REPRODUCIBILITY OF RESEARCH
Support open data and methods to enhance research reproducibility

DIGITAL PUBLISHING
Articles designed for optimal readership across devices

FOLLOW US
@frontiersin

IMPACT METRICS
Advanced article metrics track visibility across digital media

EXTENSIVE PROMOTION
Marketing and promotion of impactful research

LOOP RESEARCH NETWORK
Our network increases your article's readership